DOC.20070306.0037

QA: QA

ANL-EBS-MD-000045 REV 03

March 2007

In-Drift Precipitates/Salts Model

Prepared for:
U.S. Department of Energy
Office of Civilian Radioactive Waste Management
Office of Repository Development
1551 Hillshire Drive
Las Vegas, Nevada 89134-6321

Prepared by:
Sandia National Laboratories
OCRWM Lead Laboratory for Repository Systems
1180 Town Center Drive
Las Vegas, Nevada 89144

Under Contract Number
DE-AC04-94AL85000

DISCLAIMER

This report was prepared as an account of work sponsored by an agency of the United States Government. Neither the United States Government nor any agency thereof, nor any of their employees, nor any of their contractors, subcontractors or their employees, makes any warranty, express or implied, or assumes any legal liability or responsibility for the accuracy, completeness, or any third party's use or the results of such use of any information, apparatus, product, or process disclosed, or represents that its use would not infringe privately owned rights. Reference herein to any specific commercial product, process, or service by trade name, trademark, manufacturer, or otherwise, does not necessarily constitute or imply its endorsement, recommendation, or favoring by the United States Government or any agency thereof or its contractors or subcontractors. The views and opinions of authors expressed herein do not necessarily state or reflect those of the United States Government or any agency thereof.

QA: QA

In-Drift Precipitates/Salts Model

ANL-EBS-MD-000045 REV 03

March 2007

Sandia National Laboratories

Model Signature Page/Change History

Complete only applicable items.

1. Total Pages: 358

2. Type of Mathematical Model

☒ Process Model ☐ Abstraction Model ☐ System Model

Describe Intended Use of Model

The intended use of this model is to estimate, within an appropriate level of confidence, the effects of evaporation and deliquescence on the chemical evolution of water and precipitated minerals within the repository during the postclosure period.

3. Title

In-Drift Precipitates/Salts Model

4. DI (including Rev. No.):

ANL-EBS-MD-000045 REV 03

	Printed Name	Signature	Date
5. Originator	Paul Mariner	for Geoff Freeze	3/1/07
6. Independent Technical Reviewer	Laura Price	for Palmer Vaughn	3/1/07
7. Checker	David Shields		3/1/07
8. QCS/Lead Lab QA Reviewer	Steve Schuermann	for per telecon Ronald J. Stevens	3/1/07
9. Responsible Manager/Lead	Ernest Hardin		3/1/07
10. Responsible Manager	Geoff Freeze For Paul R Dixon		3-1-07

11. Remarks

Change History

12. Revision No.	13. Description of Change
REV 00	Initial Issue.
REV 00 / ICN 01	ICN to incorporate discussion affirming the application of this AMR and its calculations to backfill and no backfill scenarios. This ICN includes modifications resulting from changes in AP-3.10Q procedures and data qualification status.
REV 00 / ICN 02	ICN to qualify previously unqualified technical products.

REV 00 / ICN 03	ICN to improve transparency, incorporate model enhancements, document newly discovered model limitations, and qualify model enhancements used in calculations performed for the SSPA. This ICN affects Sections 1 through 8. Affected pages (except those for table of contents, table of figures, and table of tables) are identified by vertical change bars in the margin indicating the locations of the changes. Changes can be found on pages 1-15, 19-23, 25-27, 29, 31-38, 41, 42, 44, 45, 47-50, 52, 54, 56, 58, 62, 66, 69, 70, 72-74, 82, 93-100, and 102-106.
REV 01	Revision to qualify and document major improvements to the In-Drift Precipitates/Salts model. These improvements include the use of a new software version of EQ3/6 (version 8.0) and a new Pitzer database, which together are designed to predict aqueous chemical reactions in highly concentrated brines. These changes are extensive and required a full revision of the document.
REV 01 / ICN 01	ICN to extend validation range to higher temperature and ionic strength. Changes bars in the margins mark changes from REV 01. Attachment II in REV 01, "MINTEQA2 Mineral Occurrence Database," was removed because it is reference material that can be found in the TIC. For the remaining three attachments, there are no changes from REV 01 (except for headers, footers, and renumbering due to removal of the mineral database attachment).
REV 02	Minor rewriting and clarifications to address transparency and data traceability comments resulting from Regulatory Integration Team Phase I evaluation and to address CR 2049.
REV 03	Revision to improve the Pitzer thermodynamic database, augment the validation, reanalyze model uncertainty, and address several condition reports (6489, 6731, 6770, 7143, and 7721). A large portion of the model documentation has been revised and the changes were too extensive to use change bars.

ACKNOWLEDGMENTS

Several key contributions to this document must be acknowledged. One is the Pitzer thermodynamic database developed and documented in Appendix I. Carlos Jove-Colon with the assistance of Tom Wolery, Joseph Rard, Ananda Wijesinghe, Russell Jarek, and Kate Helean developed the Pitzer database and provided the documentation included in Section 4.1.1 and Appendix I. Another key contribution is the mineral suppression methodology presented in Section 6.6.2.6. This methodology was developed by Darren Jolley with the assistance of Richard Metcalf. In addition, Tom Wolery contributed the theoretical validation for predicting pH at high temperature and high ionic strength in Section 7.5.1. Tom Wolery, with the assistance of Joseph Rard, Ananda Wijesinghe, and Carlos Jove-Colon, also produced DTN: LL031106231032.007, a compilation and reduction of salt solubilities and vapor pressures in binary and ternary systems.

The work presented in this document was supported by the Office of Repository Design as part of the Civilian Radioactive Waste Management Program, managed by the U.S. Department of Energy.

INTENTIONALLY LEFT BLANK

CONTENTS

Page

CONTENTS (Continued)

Page

CONTENTS (Continued)

Page

INTENTIONALLY LEFT BLANK

FIGURES

Page

FIGURES (Continued)

Page

FIGURES (Continued)

Page

FIGURES (Continued)

Page

FIGURES (Continued)

Page

INTENTIONALLY LEFT BLANK

TABLES

Page

TABLES (Continued)

Page

ACRONYMS AND ABBREVIATIONS

100x	concentration factor of 100
C_i	concentration of component *i*
CF	concentration factor
CR	condition report
DF	dilution factor
DTN	data tracking number
EBS	Engineered Barrier System
f_{CO2}	carbon dioxide fugacity
f_{O2}	oxygen fugacity
FEPs	features, events, and processes
gm	gram
IAP	ion activity product
IDPS	in-drift precipitates/salts
IS	ionic strength
kg	kilogram
L	liter
mg	milligram
mL	milliliter
molal	moles per kilogram of water
NBS	National Bureau of Standards
Q^d	discharge rate (rate of flow out of cell)
Q^e	net evaporation rate (net of evaporation [positive] and condensation [negative])
Q^s	incoming seepage rate
R^{es}	relative evaporation rate (Q^e/Q^s)
RH	relative humidity
RH_d	deliquescence point or deliquescence relative humidity of a solution or mineral assemblage in *RH* units
S_m	Suppression flag for mineral *m*
T	temperature
TSPA	total system performance assessment
TSPA	Total System Performance Assessment for the License Application
TSPA-SR	Total System Performance Assessment for the Site Recommendation
TWP	technical work plan
YMP	Yucca Mountain Project
YMRP	*Yucca Mountain Review Plan, Final Report*

INTENTIONALLY LEFT BLANK

1. PURPOSE

This report documents the development and validation of the in-drift precipitates/salts (IDPS) process model. The IDPS process model is a geochemical model designed to predict the postclosure effects of evaporation and deliquescence on the chemical composition of water within the Engineered Barrier System (EBS) in support of the total system performance assessment (TSPA). Application of the model in support of TSPA is documented in *Engineered Barrier System: Physical and Chemical Environment* (BSC 2005 [DIRS 175083]).

The technical work plan (TWP) for this report is *Technical Work Plan for: Revision of Model Reports for Near-Field and In-Drift Water Chemistry* (SNL 2007 [DIRS 179287]). It calls for a revision of the previous version of the IDPS model report (BSC 2004 [DIRS 169863]) to update the thermodynamic database, augment the validation, reanalyze model uncertainty, and address several condition reports (CRs) (CR-6489, CR-6731, CR-6770, CR-7143, and CR-7721). Note that there is a small deviation from the TWP. In the TWP it notes that CR-6752 will be resolved in this document, by the update to the thermodynamic database. This is erroneous; CR-6752 does not apply to this thermodynamic database, thus it has not been addressed by this document.

The intended use of the IDPS model is to estimate, within an appropriate level of confidence, the effects of evaporation, deliquescence, and potential environmental conditions on the presence and composition of water and salts occurring within the drift during the postclosure period. Specifically, the intended use is as follows:

- To estimate, within an appropriate level of confidence, the effects of evaporation and deliquescence on the presence and composition of water occurring within the repository during the postclosure period (i.e., effects on pH, ionic strength, deliquescence relative humidity, total concentrations of dissolved components in the system containing Na-K-H-Mg-Ca-Al-Cl-F-NO_3-SO_4-Br-CO_3-SiO_2-CO_2-O_2-H_2O, and concentrations of the following aqueous species that potentially affect acid neutralizing capacity: HCO_3^-, CO_3^{2-}, OH^-, H^+, HSO_4^-, Ca^{2+}, Mg^{2+}, $CaHCO_3^+$, $MgHCO_3^+$, $HSiO_3^-$, and $MgOH^+$)

- To estimate, within an appropriate level of confidence, mineral precipitation resulting from the evaporation of water occurring within the repository during the postclosure period (specifically, minerals of the system containing Na-K-H-Mg-Ca-Al-Cl-F-NO_3-SO_4-Br-CO_3-SiO_2-CO_2-O_2-H_2O)

- To provide a means for abstracting these effects into a set of lookup tables that provide input to downstream models used for performance assessment.

The presence and composition of liquid water in the drift depend upon relative humidity, temperature, incoming water composition, in-drift gas composition, and relative rates of evaporation and seepage. In downstream applications of this model, intended input values for these parameters are abstracted results from thermal-hydrological-chemical models, water sample measurements, dust leachate samples, and values used in sensitivity and uncertainty analyses that encompass the expected ranges of these parameters.

The IDPS model is a quasi-equilibrium model. All reactions proceed to equilibrium except for a number of suppressed minerals in the thermodynamic database not expected to form under repository conditions within the modeling timeframe. These minerals are listed in Table 6-3 along with references that document why these minerals are not expected to form. The IDPS model developed in this report simulates evaporation to highly concentrated brines for potential water compositions of the system containing Na-K-H-Mg-Ca-Al-Cl-F-NO_3-SO_4-Br-CO_3-SiO_2-CO_2-O_2-H_2O for temperatures between 20°C and 140°C, total pressures in the atmospheric range, and relative humidity between 0% and 100%. The model applies to oxidizing conditions only.

A number of thermodynamic parameters in the Pitzer database have values that have not been determined or verified for the entire temperature range. In these cases, the known values are used to approximate the values for the remainder of the temperature range. Although such treatment contributes to uncertainty in model outputs, the model validation test cases indicate that the model, with its associated uncertainty, is valid for its intended use. For more details on the limitations and uncertainities associated with this report, refer to Section 8.4.

2. QUALITY ASSURANCE

The Quality Assurance Program has been determined to apply to the development of this document, as discussed in *Technical Work Plan for: Revision of Model Reports for Near-Field and In-Drift Water Chemistry* (SNL 2007 [DIRS 179287]), because it involves activities that provide data used to assess the potential dispersion of radioactive materials from the repository. This model provides bases for predicting performance of engineered barriers that are important to the demonstration of compliance with the postclosure performance objective prescribed in 10 CFR 63.113 [DIRS 173273]. Thus, it is classified as "Safety Category (SC)" with regard to importance to waste isolation as defined in LS-PRO-0203, *Q-List and Classification of Structures, Systems, and Components*. This document was developed as directed in Section 1.2.2 of the TWP (SNL 2007 [DIRS 179287]). The TWP was prepared in accordance with SCI-PRO-002, *Planning for Science Activities.* The methods used to control the electronic management of data were implemented as required by IM-PRO-002, *Control of the Electronic Management of Information*. This document was prepared in accordance with SCI-PRO-006, *Models*, and IM-PRO-003, *Software Management*, and reviewed in accordance with SCI-PRO-003, *Document Review*.

INTENTIONALLY LEFT BLANK

3. USE OF SOFTWARE

3.1 QUALIFIED SOFTWARE

All qualified software discussed in this document was obtained from Software Configuration Management in accordance with IM-PRO-003. This software was used in the operating environments for which it was baselined.

3.1.1 EQ3/6 Version 8.0

EQ3/6 Version 8.0 (EQ3/6 V8.0 [DIRS 162228], STN: 10813-8.0-00) was installed and used on IBM-compatible computers using the Microsoft Windows 2000 operating system. This software was selected because it was the best software available for implementing the model developed in this report. There are no limitations of the software within the range of application of the model as established in Section 8.4. This software is appropriate for the application and was used only within the range of model validation in accordance with IM-PRO-003. No macros or software routines were developed for, or used by, this software.

3.1.2 GetEQData Version 1.0.1

GetEQData Version 1.0.1 (GetEQData V1.0.1 [DIRS 161900], STN: 10809-1.0.1-00) was installed and used on IBM-compatible computers using the Microsoft Windows 2000 operating system. This software was selected because it was the only available software for extracting data from EQ3/6 output files. There are no relevant limitations of the software. This software is appropriate for the application and was used only within the range of validation in accordance with IM-PRO-003. No other macros or software routines were developed for, or used by, this software. GetEQData is itself a macro for Microsoft Excel.

3.1.3 SUPCRT92 Version 1.0

SUPCRT92 Version 1.0 (SUPCRT92 V1.0 [DIRS 153218], STN: 10058-1.0-00) installed and used using the Microsoft Windows NT operating system. Microsoft Windows NT is a qualified operating system for this code. Details on how the SUPCRT92 calculations were used in this report are provided in Sections I-5, I-5.1, I-5.2, and I-5.3 of Appendix I. This software is appropriate for the Windows NT application and was used only within the range of validation in accordance with IM-PRO-003. No macros or software routines were developed for, or used by, this software.

3.2 EXEMPT SOFTWARE

Microsoft Excel 2000, a commercially available spreadsheet software package, was installed and used on IBM-compatible computers using the Microsoft Windows 2000 or Microsoft Windows XP operating system. This software was used to tabulate results, visually display results, and perform the algebraic equations documented in Section 6.6.3.5, Appendix I, and elsewhere. This software was selected because it is the standard Yucca Mountain Project (YMP) software used for performing these tasks. There are no limitations of the software relevant to these tasks. Hand calculations and visual inspection of these tabulations, charts, and equations confirm that

the spreadsheet applications provided correct results. Except for GetEQData listed above (which is an Excel macro), no macros or software routines were developed for, or used by, this software, and consequently it is an exempt software application in accordance with Section 2.0 of IM-PRO-003.

Output data tracking numbers (DTNs) containing Excel spreadsheets include:

- DTN: LL031106231032.007
- DTN: MO0701SPAPTZER.001
- DTN: SN0611T0509206.006
- DTN: SN0702T0509206.008
- DTN: MO0701EQ36IDPS.000
- DTN: SN0611T0509206.007.

4. INPUTS

4.1 DIRECT INPUT

This report is a revision of a previously developed and validated IDPS model (BSC 2004 [DIRS 169863]). Data inputs used to develop the IDPS model and associated Pitzer thermodynamic database (Output DTN: SN0609T0502404.012) are presented in Sections 4.1.1 and 4.1.2. After reviewing a wide range of data, these data were found to be the most reliable and appropriate sources of information and data available for developing the model. Section 4.1.1 focuses on data constants in the Pitzer database (Output DTN: SN0609T0502404.012), and Section 4.1.2 focuses on variable model parameters and values for these parameters used in model validation.

Independent data used to validate and demonstrate the IDPS model are presented in Section 4.4. A subset of the independent data in Section 4.4 is also used in Section 7.2 to estimate uncertainties. While it is preferable to have an additional independent set to estimate uncertainties (independent of the data used to validate the model), such data were not available. Per SCI-PRO-006, Attachment 2, these data do not belong in Section 4.1 because they were not used to develop the model.

4.1.1 Data

A Pitzer thermodynamic database (Output DTN: SN0609T0502404.012) is developed in this report for use in the IDPS model. The IDPS model is designed to predict the evolution of water in the drift caused by changing environmental conditions. To predict salt precipitation, deliquescence, and aqueous concentrations in brines, a Pitzer database is needed. This database is developed for the system Na-K-H-Mg-Ca-Al-Cl-F-NO_3-SO_4-Br-CO_3-SiO_2-CO_2-O_2-H_2O, which generally encompasses the most abundant ions in natural ground waters. It is designed for temperatures ranging from 0°C to 200°C, a broader range than that of the IDPS model (20°C to 140°C). The smaller range for the IDPS model is primarily due to the smaller temperature range of the independent set of model validation data.

Qualification of data for use in the present report is achieved within this report under the provisions of SCI-PRO-006. A principal technical product of this report is an EQ3/6 Pitzer data file that is qualified for use elsewhere, particularly for use in *Engineered Barrier System: Physical and Chemical Environment* (BSC 2005 [DIRS 175083]).

The development of the Pitzer database (Output DTN: SN0609T0502404.012) is discussed in detail in Appendix I. The sources of direct input data used in the development of the Pitzer database are listed in Table 4-1. Uncertainty associated with these data is also addressed in Appendix I. In general, the input data (in the form of all the numerical values used to develop the present model) are far too numerous to list in Section 4.1.1 of this report or even in Appendix I. The actual direct input numerical values are contained in the many supporting spreadsheets located in Output DTN: MO0701SPAPTZER.001. Binary and ternary Pitzer temperature-dependent interaction coefficients are presented in Tables 4-2 and 4-3. Each interaction coefficient is generally treated as a temperature function, which has its own coefficients (see Appendix I for details). These temperature coefficients comprise the actual set

of data. They are too numerous to reproduce in Tables 4-2 and 4-3. Uncertainty in the values of the coefficients (the interaction coefficients or the temperature coefficients used to calculate them) is difficult to assess given the multiple sources of data and the series of refitting and conversions conducted in the retrieval of coefficient data. Confidence in the retrieved Pitzer parameter coefficients for a given electrolyte is demonstrated by comparing osmotic coefficient data, whether from the source used in the parameter retrieval or that obtained elsewhere, with that computed from the Pitzer equations and the regressed parameter coefficients. Testing of the retrieved coefficients upon refitting/conversion was performed by comparing predictions using the Pitzer equations with the osmotic coefficient data used in the parameter regression serving as a confirmation exercise. Further confidence is then established by comparing the predictions with osmotic coefficient data not used in the parameter retrieval. The fitting error analyses and comparisons of these predictions are reported in the spreadsheets referenced in Appendix I and pertain only to the original sources where the fitted coefficients were derived.

The Debye-Hückel A_φ parameter is also an intrinsic part of any Pitzer model. This is also treated by the use of a temperature function. The representation used in the IDPS model is based on that given by Greenberg and Møller (1989 [DIRS 152684]). However, the data were refitted to a different temperature function, the same one used in the IDPS model for the Pitzer interaction coefficients. This refitting of A_φ was repeated in each of the refittings for each set of binary interaction parameters, not because it needed to be repeated, but because this functionality was built into the spreadsheet template for binary coefficient refitting. The model of Greenberg and Møller (1989 [DIRS 152684]) was in fact used as the "core" of the database developed in the present report, and for the sake of thermodynamic consistency, it was appropriate to use their data for the A_φ parameter as a direct input for the expanded model.

Table 4-1 summarizes the input sources used in constructing the Pitzer database (Output DTN: SN0609T0502404.012) and lists selected factors used to justify qualification of the data. These sources are demonstrated in this section and/or in Appendix I to be justified for intended use for the specific application per SCI-PRO-006, Section 6.2.1(K). In all cases, the extent to which the data demonstrate the properties of interest is in their entirety. Reliability of data source, qualifications of personnel or organizations generating the data, prior uses of the data, and/or availability of corroborating data are described in this section and/or Appendix I to justify qualification of the data for the intended use.

The data taken from these sources is in general not provided on a source by source basis, but rather on a data subset by data subset basis. For example, Table 4-2 summarizes the binary Pitzer parameter groupings, each of which is identified by a pair of aqueous species, usually ions (e.g., "$Na^+ - Cl^-$"). Appendix I discusses the binary Pitzer parameter groupings in Section I-4.4, presenting the case for each grouping in a subsection named after the species pair (e.g., "Ions: "$Na^+ - Cl^-$"). These discussions are presented in a pseudo-alphabetic ordering. Thus, the discussions for "$Na^+ - Cl^-$" and "$K^+ - Cl^-$", for both of which the input data are taken from Greenberg and Møller (1989 [DIRS 152684]), do not appear in a common grouping within Section I-4.4. Furthermore, the ternary Pitzer parameter groupings are similarly identified by similar species pairs (e.g., "$K^+ - Na^+$") and triplets (e.g., "$Na^+ - K^+ - Cl^-$") listed in Table 4-3, and the corresponding justifications for the individual groupings of this type are given in Section I-4.5 in subsections labeled accordingly (e.g., "Ions: $K^+ - Na^+$" and "Ions: "$Na^+ - K^+ - Cl^-$"). The input data for these particular examples are also taken from Greenberg and Møller

(1989 [DIRS 152684]). Additional Pitzer data used "as-is" (not requiring conversion to the Pitzer parameter temperature function used in the present model) are described in detail in Section I-4.6 and their usage is justified therein.

Table 4-1 also summarizes the input sources for single-phase mineral thermodynamic data, solubility data, and solubility product constant data (including related data necessary to compute equilibrium constants, such as standard state thermodynamic data for water and aqueous species). Note that the report by Greenberg and Møller (1989 [DIRS 152684]) is also a source of such data. The detailed justifications of these input data are presented in Section I-5.

In addition, Table 4-1 summarizes the sources of the various equations and mathematical relationships employed in the developed Pitzer model. The use of these mathematical elements does not require specific justification under the procedures governing the development of the present model. However, it is noted that the cited sources include works by the late Professor Kenneth S. Pitzer (Pitzer 1973 [DIRS 152738]; 1991 [DIRS 152709]), who promulgated the model that bears his name. These works, which contain equations and data used are widely and accepted throughout the scientific, and have proven to be reliable, and therefore are suitable for the intended use in this report.

The sources listed in Table 4-1 include several major works on the subject of Pitzer's equations. Pitzer's article entitled "Thermodynamics of Electrolytes. I. Theoretical Basis and General Equations" (Pitzer 1973 [DIRS 152738]) is a classic in the field of physical chemistry and the original paper describing the basic Pitzer model. The study by Harvie et al. (1984 [DIRS 118163]) is another classic paper containing the first extensive application of the Pitzer model to aqueous geochemical systems at 25°C. Pabalan and Pitzer (1987 [DIRS 162147]; 1987 [DIRS 162096]) and Greenberg and Møller (1989 [DIRS 152684]) also produced three notable papers describing application to systems of geochemical interest extending to high temperature. A number of the other sources are books that are de facto handbooks in the field of aqueous geochemistry or related disciplines, including works by Barin and Platzki (1995 [DIRS 157865]) (a two-volume compendium of thermodynamic data based on calorimetry), Linke (1965 [DIRS 166191]) (the second volume in a two-volume set of solubility data, of which Linke (1958 [DIRS 166192]) is the first volume), and Robie and Hemingway (1995 [DIRS 153683]) (a compendium of mineral thermodynamic data published by the U.S. Geological Survey). Data from the Linke volumes were primarily used for validation (see Table 4-5 in Section 4.4). Only the data for thermonatrite on p. 915 of the second volume (Linke 1965 [DIRS 166191]) was used in the actual development of the present model. Some non-Pitzer thermodynamic data were taken from data0.ymp.R2 and data0.ymp.R4, both of which are YMP non-Pitzer databases (DTNs: MO0302SPATHDYN.000.[DIRS 161756] and SN0410T0510404.002 [DIRS 172712], respectively) developed for other applications within the YMP. The remaining input sources, which are generally not as widely used in the construction of the Pitzer database, are addressed in Appendix I.

Table 4-1. Input Sources for Pitzer Database

Type of Input	Source	Qualifications
Pitzer ion interaction coefficients and/or osmotic coefficient data; Debye-Hückel A_φ parameter	Archer 2000 [DIRS 162065]	Reliable source; prior uses of the data (Section I-2)
	Clegg and Brimblecombe 1990 [DIRS 162067]	Reliable source; prior uses of the data (Section I-4.4.7)
	Clegg and Brimblecombe 1990 [DIRS 162089]	Reliable source; availability of corroborating data (Section I-4.5.16)
	Clegg et al. 1996 [DIRS 162068]	Reliable source; prior uses of the data (Section I-4.4.21)
	Felmy et al. 1994 [DIRS 162111]	Reliable source; availability of corroborating data (Sections I-4.4.7, I-4.5.16)
	Felmy et al. 1994 [DIRS 162112]	Reliable source; availability of corroborating data (Section I-4.4.26)
	Greenberg and Møller 1989 [DIRS 152684]	Reliable source; prior uses of the data (Section 4.1.1)
	He and Morse 1993 [DIRS 162090]	Reliable source; prior uses of the data (Section I-2)
	Holmes and Mesmer 1992 [DIRS 162076]	Reliable source; prior uses of the data (Section I-4.4.5 and I-4.4.6)
	Holmes and Mesmer 1983 [DIRS 162073]	Reliable source; prior uses of the data (Sections I-4.4.3 and I-4.4.13)
	Holmes and Mesmer 1994 [DIRS 162078]	Reliable source; prior uses of the data (Section I-2)
	Holmes and Mesmer 1998 [DIRS 162083]	Reliable source; availability of corroborating data (Sections I-4.4.8, I-4.4.11, I-4.4.12, I-4.4.16)
	Holmes et al. 1987 [DIRS 162075]	Reliable source; prior uses of the data (Section I-4.4.4); availability of corroborating data (Section I-4.4.4)
	Konigsberger et al. 1999 [DIRS 168345]	Reliable source; prior uses of the data (Section 4.1.1, Table I-2)
	Oakes et al. 2000 [DIRS 162102]	Reliable source; prior uses of the data (Section I-2)
	Peiper and Pitzer 1982 [DIRS 162097]	Reliable source; prior uses of the data (Section 4.1.1)
	Pabalan and Pitzer 1987 [DIRS 162096]	Reliable source; prior uses of the data (Section I-2)
	Pabalan and Pitzer 1987 [DIRS 162147]	Reliable source; prior uses of the data (Section I-2)
	Pitzer 1991 [DIRS 152709]	Reliable source; prior uses of the data (Section 4.1.1)
	Sterner et al. 1998 [DIRS 162116]	Reliable source; prior uses of the data (Section I-.4.4.1)
	Thiessen and Simonson 1990 [DIRS 162108]	Reliable source; prior uses of the data (Section I-4.4.22)

Table 4-1. Input Sources for Pitzer Database (Continued)

Type of Input	Source	Qualifications
Pitzer ion interaction coefficients and/or osmotic coefficient data; Debye-Hückel A_φ parameter (continued)	Corti 1990 [DIRS 178211]	Reliable source; availability of corroborating data (Section I-4.5.16)
	Rumpf and Maurer 1993 [DIRS 178223]	Reliable source; availability of corroborating data (Section I-4.5.16)
	Rumpf et al 1994 [DIRS 178222]	Reliable source; availability of corroborating data (Section I-4.5.16)
	Rard et al. 2004 [DIRS 173816]	Reliable source; availability of corroborating data (Section I.4.4.2)
	Baes et al 1993 [DIRS 168318]	Reliable source; availability of corroborating data (Sections I.4.4.5, I.4.4.6, I.4.4.25, and, I.4.5.15)
	Wijesinghe and Rard 2005 [DIRS 176847]	Reliable source; availability of corroborating data (Sections I-4.4.17 and I-4.4.2)
Single-phase mineral thermodynamic data, mineral solubility data, and solubility product constants	Barin and Platzki 1995 [DIRS 157865]	Reliable source; prior uses of the data (Section 4.1.1)
	Greenberg and Møller 1989 [DIRS 152684]	Reliable source; prior uses of the data (Sections 4.1.1, I-4.4.9, I-4.4.10, I-4.4.18, and I-4.4.19)
	Harvie et al. 1984 [DIRS 118163]	Reliable source; prior uses of the data (Section 4.1.1)
	Linke 1965 [DIRS 166191], p. 915	Reliable source; prior uses of the data (Section 4.1.1)
	Meisingset and Grønvold 1986 [DIRS 162094]	Reliable source; availability of corroborating data (Section I-5.1)
	Pabalan and Pitzer 1987 [DIRS 162096]	Reliable source; prior uses of the data (Sections 4.1.1 and I-2)
	Pitzer and Oakes 1994 [DIRS 163583]	Reliable source; availability of corroborating data (Section I-5.1)
	Pitzer and Shi 1993 [DIRS 163582]	Reliable source; availability of corroborating data (Section I-5.1)
	Robie and Hemingway 1995 [DIRS 153683], pp. 23, 27, 53, and 55	Reliable source; prior uses of the data (Section 4.1.1)
	DTN: SN0410T0510404.002 [DIRS 172712]	Product output
	DTN: SN0410T0510404.001 [DIRS 172759]	Product output
	DTN: MO0302SPATHDYN.000 [DIRS 161756]	Product output
Equations and theoretical relations	Garrels and Christ 1990 [DIRS 144877]	Reliable source; prior use (Section I-3.2.1)
	Møller 1988 [DIRS 152695]	Reliable source; prior use (Section I-2)
	Pitzer 1991 [DIRS 152709]	Reliable source; prior use (Section 4.1.1)
	Pitzer 1973 [DIRS 152738]	Reliable source; prior use (Section 4.1.1)
	Rard and Wijesinghe 2003 [DIRS 162327]	Reliable source; prior use (Section I-2)

NOTE: Additional input sources used to estimate model uncertainties are noted in Table 4-5 (Section 4.4).

Table 4-2. Binary Pitzer Ion Interaction Coefficients

Ions	Coefficient Name	Coefficient Type	Coefficient Units	Coefficient Source	Source DIRS #	Coefficient Use in This Report
$Na^+ – Cl^-$	$\beta^{(0)}$, $\beta^{(1)}$, and $C^{(\phi)}$	Binary	kg/mol, kg/mol, and $(kg/mol)^2$ respectively	Greenberg and Møller 1989	152684	Appendix I
$Na^+ – SO_4^{2-}$	$\beta^{(0)}$, $\beta^{(1)}$, and $C^{(\phi)}$	Binary	kg/mol, kg/mol, and $(kg/mol)^2$ respectively	Greenberg and Møller 1989	152684	Appendix I
$Na^+ – HSO_4^-$	$\beta^{(0)}$, $\beta^{(1)}$, and $C^{(\phi)}$	Binary	kg/mol, kg/mol, and $(kg/mol)^2$ respectively	Holmes and Mesmer 1994	162078	Appendix I
$Na^+ – OH^-$	$\beta^{(0)}$, $\beta^{(1)}$, and $C^{(\phi)}$	Binary	kg/mol, kg/mol, and $(kg/mol)^2$ respectively	Pabalan and Pitzer 1987	162147	Appendix I
$Na^+ – NO_3^-$	$\beta^{(0)}$, $\beta^{(1)}$, and $C^{(\phi)}$	Binary	kg/mol, kg/mol, and $(kg/mol)^2$ respectively	Wijesinghe and Rard 2005	176847	Appendix I
$Na^+ – CO_3^-$	$\beta^{(0)}$, $\beta^{(1)}$, and $C^{(\phi)}$	Binary	kg/mol, kg/mol, and $(kg/mol)^2$ respectively	He and Morse 1993	162090	Appendix I
$Na^+ – HCO_3^-$	$\beta^{(0)}$, $\beta^{(1)}$, and $C^{(\phi)}$	Binary	kg/mol, kg/mol, and $(kg/mol)^2$ respectively	He and Morse 1993	162090	Appendix I
$Na^+ – Br^-$	$\beta^{(0)}$, $\beta^{(1)}$, and $C^{(\phi)}$	Binary	kg/mol, kg/mol, and $(kg/mol)^2$ respectively	Holmes and Mesmer 1998	162083	Appendix I
$Na^+ – AlO_2^-$	$\beta^{(0)}$, $\beta^{(1)}$, and $C^{(\phi)}$	Binary	kg/mol, kg/mol, and $(kg/mol)^2$ respectively	Felmy et al. 1994	162112	Appendix I
$H^+ – Cl^-$	$\beta^{(0)}$, $\beta^{(1)}$, and $C^{(\phi)}$	Binary	kg/mol, kg/mol, and $(kg/mol)^2$ respectively	Holmes et al. 1987	162075	Appendix I
$AlO_2^- – NO_3^-$	$\beta^{(0)}$, $\beta^{(1)}$, and $C^{(\phi)}$	Binary	kg/mol, kg/mol, and $(kg/mol)^2$ respectively	Felmy et al. 1994	162112	Appendix I
$AlO_2^- – OH^-$	$\beta^{(0)}$, $\beta^{(1)}$, and $C^{(\phi)}$	Binary	kg/mol, kg/mol, and $(kg/mol)^2$ respectively	Felmy et al. 1994	162112	Appendix I
$H^+ – NO_3^-$	$\beta^{(0)}$, $\beta^{(1)}$, and $C^{(\phi)}$	Binary	kg/mol, kg/mol, and $(kg/mol)^2$ respectively	Felmy et al. 1994; Clegg and Brimblecombe 1990	162111 162067	Appendix I
$H^+ – SO_4^{2-}$	$\beta^{(0)}$, $\beta^{(1)}$, and $C^{(\phi)}$	Binary	kg/mol, kg/mol, and $(kg/mol)^2$ respectively	Holmes and Mesmer 1992	162076	Appendix I
$H^+ – HSO_4^-$	$\beta^{(0)}$, $\beta^{(1)}$, and $C^{(\phi)}$	Binary	kg/mol, kg/mol, and $(kg/mol)^2$ respectively	Holmes and Mesmer 1992	162076	Appendix I
$K^+ – Cl^-$	$\beta^{(0)}$, $\beta^{(1)}$, and $C^{(\phi)}$	Binary	kg/mol, kg/mol, and $(kg/mol)^2$ respectively	Greenberg and Møller 1989	152684	Appendix I

Table 4-2. Binary Pitzer Ion Interaction Coefficients (Continued)

Ions	Coefficient Name	Coefficient Type	Coefficient Units	Coefficient Source	Source DIRS #	Coefficient Use in This Report
$K^+ – SO_4^{2-}$	$\beta^{(0)}$, $\beta^{(1)}$, and $C^{(\phi)}$	Binary	kg/mol, kg/mol, and $(kg/mol)^2$ respectively	Greenberg and Møller 1989	152684	Appendix I
$K^+ – Br^-$	$\beta^{(0)}$, $\beta^{(1)}$, and $C^{(\phi)}$	Binary	kg/mol, kg/mol, and $(kg/mol)^2$ respectively	Holmes and Mesmer 1998	162083	Appendix I
$Ca^{++} – Cl^-$	$\beta^{(0)}$, $\beta^{(1)}$, and $C^{(\phi)}$	Binary	kg/mol, kg/mol, and $(kg/mol)^2$ respectively	Sterner et al. 1998	162116	Appendix I
$Ca^{++} – SO_4^{2-}$	$\beta^{(0)}$, $\beta^{(1)}$, and $C^{(\phi)}$	Binary	kg/mol, kg/mol, and $(kg/mol)^2$ respectively	Greenberg and Møller 1989	152684	Appendix I
$Ca^{++} – NO_3^-$	$\beta^{(0)}$, $\beta^{(1)}$, and $C^{(\phi)}$	Binary	kg/mol, kg/mol, and $(kg/mol)^2$ respectively	Wijesinghe and Rard 2005	176847	Appendix I
$Li^+ – Cl^-$	$\beta^{(0)}$, $\beta^{(1)}$, and $C^{(\phi)}$	Binary	kg/mol, kg/mol, and $(kg/mol)^2$ respectively	Holmes and Mesmer 1983	162073	Appendix I
$Li^+ – Br^-$	$\beta^{(0)}$, $\beta^{(1)}$, and $C^{(\phi)}$	Binary	kg/mol, kg/mol, and $(kg/mol)^2$ respectively	Holmes and Mesmer 1998	162083	Appendix I
$Mg^{++} – SO_4^{2-}$	$\beta^{(0)}$, $\beta^{(1)}$, and $C^{(\phi)}$	Binary	kg/mol, kg/mol, and $(kg/mol)^2$ respectively	Pabalan and Pitzer 1987	162096	Appendix I
$Mg^{++} – Cl^-$	$\beta^{(0)}$, $\beta^{(1)}$, and $C^{(\phi)}$	Binary	kg/mol, kg/mol, and $(kg/mol)^2$ respectively	Pabalan and Pitzer 1987	162096	Appendix I
$Cs^+ – Br^-$	$\beta^{(0)}$, $\beta^{(1)}$, and $C^{(\phi)}$	Binary	kg/mol, kg/mol, and $(kg/mol)^2$ respectively	Holmes and Mesmer 1998	162083	Appendix I
$Cs^+ – Cl^-$	$\beta^{(0)}$, $\beta^{(1)}$, and $C^{(\phi)}$	Binary	kg/mol, kg/mol, and $(kg/mol)^2$ respectively	Holmes and Mesmer 1983	162073	Appendix I
$NH_4^+ – SO_4^{2-}$	$\beta^{(0)}$, $\beta^{(1)}$, and $C^{(\phi)}$	Binary	kg/mol, kg/mol, and $(kg/mol)^2$ respectively	Clegg et al. 1996	162068	Appendix I
$NH_4^+ – Cl^-$	$\beta^{(0)}$, $\beta^{(1)}$, and $C^{(\phi)}$	Binary	kg/mol, kg/mol, and $(kg/mol)^2$ respectively	Thiessen and Simonson 1990	162108	Appendix I
$Na^+ – CrO_4^{2-}$	θ	Binary	kg/mol	Pitzer 1991	152709	Appendix I
$Na^+ – F^-$	θ	Binary	kg/mol	Pitzer 1991	152709	Appendix I

Table 4-2. Binary Pitzer Ion Interaction Coefficients (Continued)

Ions	Coefficient Name	Coefficient Type	Coefficient Units	Coefficient Source	Source DIRS #	Coefficient Use in This Report
$Na^+ – HPO_4^{2-}$	θ	Binary	kg/mol	Pitzer 1991	152709	Appendix I
$Na^+ – I^-$	θ	Binary	kg/mol	Pitzer 1991	152709	Appendix I
$Na^+ – K^+$	θ	Binary	kg/mol	Greenberg and Møller 1989	152684	Appendix I
$Na^+ – Ca^{++}$	θ	Binary	kg/mol	Greenberg and Møller 1989	152684	Appendix I
$K^+ – Ca^{++}$	θ	Binary	kg/mol	Greenberg and Møller 1989	152684	Appendix I
$Mg^+ – Na^{++}$	θ	Binary	kg/mol	Pabalan and Pitzer 1987	162096	Appendix I
$CaCl_2(aq)\_CaCl_2(aq)$	θ	Binary	kg/mol	Sterner et al. 1998	162116	Appendix I
$CaCl_2(aq)\_Cl^-$	θ	Binary	kg/mol	Sterner et al. 1998	162116	Appendix I
$Cl^- – SO_4^{2-}$	θ	Binary	kg/mol	Greenberg and Møller 1989	152684	Appendix I
$Cl^- – CO3^{2-}$	θ	Binary	kg/mol	Peiper and Pitzer 1982	162097	Appendix I
$Cl^- – HCO3^-$	θ	Binary	kg/mol	Peiper and Pitzer 1982	162097	Appendix I
$HSO_4^- – SO_4^{2-}$	θ	Binary	kg/mol	Holmes and Mesmer 1992	162076	Appendix I
$Ca^{++} – H^-$	θ	Binary	kg/mol	Pitzer 1991	152709	Appendix I
$Ca^{++} –K^+$	θ	Binary	kg/mol	Pitzer 1991	152709	Appendix I
$Ca^{++} – Br^-$	θ	Binary	kg/mol	Pitzer 1991	152709	Appendix I
$Ca^{++} – HSO_4^-$	θ	Binary	kg/mol	Pitzer 1991	152709	Appendix I
$Ca^{++} – Na^+$	θ	Binary	kg/mol	Pitzer 1991	152709	Appendix I
$Ca^{++} – HCO_3^-$	θ	Binary	kg/mol	Pitzer 1991	152709	Appendix I
$Ca^{++} – HSO_3^-$	θ	Binary	kg/mol	Pitzer 1991	152709	Appendix I
$Ca^{++} – I^-$	θ	Binary	kg/mol	Pitzer 1991	152709	Appendix I
$Ca^{++} – Mg^{++}$	θ	Binary	kg/mol	Pitzer 1991	152709	Appendix I
$Cs^+ – H^+$	θ	Binary	kg/mol	Pitzer 1991	152709	Appendix I
$Cs^+ – I^-$	θ	Binary	kg/mol	Pitzer 1991	152709	Appendix I
$Cl^- – HSO_4^-$	θ	Binary	kg/mol	Pitzer 1991	152709	Appendix I

Table 4-2. Binary Pitzer Ion Interaction Coefficients (Continued)

Ions	Coefficient Name	Coefficient Type	Coefficient Units	Coefficient Source	Source DIRS #	Coefficient Use in This Report
$Cl^- – NO_3^-$	θ	Binary	kg/mol	Pitzer 1991	152709	Appendix I
$Cs^+ – NO_3^-$	θ	Binary	kg/mol	Pitzer 1991	152709	Appendix I
$Cs^+ – OH^-$	θ	Binary	kg/mol	Pitzer 1991	152709	Appendix I
$Cs^+ – SO_4^-$	θ	Binary	kg/mol	Pitzer 1991	152709	Appendix I
$Cs^+ – F^-$	θ	Binary	kg/mol	Pitzer 1991	152709	Appendix I
$Cs^+ – K^+$	θ	Binary	kg/mol	Pitzer 1991	152709	Appendix I
$Cs^+ – Li^+$	θ	Binary	kg/mol	Pitzer 1991	152709	Appendix I
$Cs^+ – Na^+$	θ	Binary	kg/mol	Pitzer 1991	152709	Appendix I
$H^+ – Br^-$	θ	Binary	kg/mol	Pitzer 1991	152709	Appendix I
$H^+ – I^-$	θ	Binary	kg/mol	Pitzer 1991	152709	Appendix I
$H^+ – K^+$	θ	Binary	kg/mol	Pitzer 1991	152709	Appendix I
$H^+ – Li^+$	θ	Binary	kg/mol	Pitzer 1991	152709	Appendix I
$H^+ – Mg^{++}$	θ	Binary	kg/mol	Pitzer 1991	152709	Appendix I
$H^+ – Na^+$	θ	Binary	kg/mol	Pitzer 1991	152709	Appendix I
$H^+ – NH_4^+$	θ	Binary	kg/mol	Pitzer 1991	152709	Appendix I
$H^+ – Sr^{++}$	θ	Binary	kg/mol	Pitzer 1991	152709	Appendix I
$K^+ – Li^+$	θ	Binary	kg/mol	Pitzer 1991	152709	Appendix I
$K^+ – CO_3^{2-}$	θ	Binary	kg/mol	Pitzer 1991	152709	Appendix I
$K^+ – HCO_3^-$	θ	Binary	kg/mol	Pitzer 1991	152709	Appendix I
$K^+ – CrO_4^{2-}$	θ	Binary	kg/mol	Pitzer 1991	152709	Appendix I
$K^+ – F^-$	θ	Binary	kg/mol	Pitzer 1991	152709	Appendix I
$K^+ – HPO_4^{2-}$	θ	Binary	kg/mol	Pitzer 1991	152709	Appendix I
$K^+ – HSO_4^-$	θ	Binary	kg/mol	Pitzer 1991	152709	Appendix I
$K^+ – I^-$	θ	Binary	kg/mol	Pitzer 1991	152709	Appendix I

Table 4-2. Binary Pitzer Ion Interaction Coefficients (Continued)

Ions	Coefficient Name	Coefficient Type	Coefficient Units	Coefficient Source	Source DIRS #	Coefficient Use in This Report
$K^+ – NO_3^-$	θ	Binary	kg/mol	Pitzer 1991	152709	Appendix I
$K^+ – Mg^{++}$	θ	Binary	kg/mol	Pitzer 1991	152709	Appendix I
$K^+ – Na^+$	θ	Binary	kg/mol	Pitzer 1991	152709	Appendix I
$K^+ – OH^-$	θ	Binary	kg/mol	Pitzer 1991	152709	Appendix I
$Li^+ – I^-$	θ	Binary	kg/mol	Pitzer 1991	152709	Appendix I
$Li^+ – NO_3^-$	θ	Binary	kg/mol	Pitzer 1991	152709	Appendix I
$Li^+ – OH^-$	θ	Binary	kg/mol	Pitzer 1991	152709	Appendix I
$Li^+ – SO_4^{2-}$	θ	Binary	kg/mol	Pitzer 1991	152709	Appendix I
$Li^+ – Na^+$	θ	Binary	kg/mol	Pitzer 1991	152709	Appendix I
$Mg^{++} – Br^-$	θ	Binary	kg/mol	Pitzer 1991	152709	Appendix I
$Mg^{++} – HCO_3^-$	θ	Binary	kg/mol	Pitzer 1991	152709	Appendix I
$Mg^{++} – HSO_4^-$	θ	Binary	kg/mol	Pitzer 1991	152709	Appendix I
$Mg^{++} – I^-$	θ	Binary	kg/mol	Pitzer 1991	152709	Appendix I
$Mg^{++} – NO_3^-$	θ	Binary	kg/mol	Rard et al. 2004	173816	Appendix I
$Sr^{++} – Br^-$	θ	Binary	kg/mol	Pitzer 1991	152709	Appendix I
$Sr^{++} – Cl^-$	θ	Binary	kg/mol	Pitzer 1991	152709	Appendix I
$Sr^{++} – I^-$	θ	Binary	kg/mol	Pitzer 1991	152709	Appendix I
$Sr^{++} – NO_3^-$	θ	Binary	kg/mol	Pitzer 1991	152709	Appendix I
$Br^{++} – Cl^-$	θ	Binary	kg/mol	Pitzer 1991	152709	Appendix I
$Br^{++} – OH^-$	θ	Binary	kg/mol	Pitzer 1991	152709	Appendix I
$Cu^+ – HSO_4^-$	θ	Binary	kg/mol	Beas et al. 1993	168318	Appendix I
$Cu^+ – H^-$	θ	Binary	kg/mol	Beas et al. 1993	168318	Appendix I
$MgOH^- – Cl^-$	θ	Binary	kg/mol	Pitzer 1991	152709	Appendix I
$NH4^+ – Br^-$	θ	Binary	kg/mol	Pitzer 1991	152709	Appendix I

Table 4-2. Binary Pitzer Ion Interaction Coefficients (Continued)

Ions	Coefficient Name	Coefficient Type	Coefficient Units	Coefficient Source	Source DIRS #	Coefficient Use in This Report
$NH4^+ – HCO_3^-$	θ	Binary	kg/mol	Pitzer 1991	152709	Appendix I
$NH4^+ – I^-$	θ	Binary	kg/mol	Pitzer 1991	152709	Appendix I
$NH4^+ – NO_3^-$	θ	Binary	kg/mol	Pitzer 1991	152709	Appendix I
$CO_3^{2-} – HCO_3^-$	θ	Binary	kg/mol	Pitzer 1991	152709	Appendix I
$CO_3^{2-} – SO_4^{2-}$	θ	Binary	kg/mol	Pitzer 1991	152709	Appendix I
$HCO_3^{2-} – SO_4^{2-}$	θ	Binary	kg/mol	Pitzer 1991	152709	Appendix I
$SiO_2 – H^+$	λ	Binary	kg/mol	Felmy et al. 1994	162111	Appendix I
$SiO_2 – NO_3^-$	λ	Binary	kg/mol	Felmy et al. 1994	162111	Appendix I
$SiO_2 – Na^+$	λ	Binary	kg/mol	Felmy et al. 1994	162111	Appendix I
$SiO_2 – Cl^-$	λ	Binary	kg/mol	Felmy et al. 1994	162111	Appendix I
$SiO_2 – SO_4^{2-}$	λ	Binary	kg/mol	Felmy et al. 1994	162111	Appendix I
$SiO_2 – Mg^{++}$	λ	Binary	kg/mol	Felmy et al. 1994	162111	Appendix I
$O_2(aq) – Na^+$	λ	Binary	kg/mol	Clegg and Brimblecombe 1990	162089	Appendix I
$O_2(aq) – K^+$	λ	Binary	kg/mol	Clegg and Brimblecombe 1990	162089	Appendix I
$O_2(aq) – Mg^{++}$	λ	Binary	kg/mol	Clegg and Brimblecombe 1990	162089	Appendix I
$O_2(aq) – Ca^{++}$	λ	Binary	kg/mol	Clegg and Brimblecombe 1990	162089	Appendix I
$O_2(aq) – Al^{+++}$	λ	Binary	kg/mol	Clegg and Brimblecombe 1990	162089	Appendix I
$O_2(aq) – Cl^-$	λ	Binary	kg/mol	Clegg and Brimblecombe 1990	162089	Appendix I
$O_2(aq) – Br^-$	λ	Binary	kg/mol	Clegg and Brimblecombe 1990	162089	Appendix I
$O_2(aq) – OH^-$	λ	Binary	kg/mol	Clegg and Brimblecombe 1990	162089	Appendix I
$O_2(aq) – SO_4^{2-}$	λ	Binary	kg/mol	Clegg and Brimblecombe 1990	162089	Appendix I
$O_2(aq) – H^+$	λ	Binary	kg/mol	Clegg and Brimblecombe 1990	162089	Appendix I
$O_2(aq) – Li^+$	λ	Binary	kg/mol	Clegg and Brimblecombe 1990	162089	Appendix I
$O_2(aq) – NH_4^+$	λ	Binary	kg/mol	Clegg and Brimblecombe 1990	162089	Appendix I

Table 4-2. Binary Pitzer Ion Interaction Coefficients (Continued)

Ions	Coefficient Name	Coefficient Type	Coefficient Units	Coefficient Source	Source DIRS #	Coefficient Use in This Report
$O_2(aq) – Ba^{++}$	λ	Binary	kg/mol	Clegg and Brimblecombe 1990	162089	Appendix I
$O_2(aq) – I^-$	λ	Binary	kg/mol	Clegg and Brimblecombe 1990	162089	Appendix I
$O_2(aq) – NO_3^-$	λ	Binary	kg/mol	Clegg and Brimblecombe 1990	162089	Appendix I
$O_2(aq) – HCO_3^-$	λ	Binary	kg/mol	Clegg and Brimblecombe 1990	162089	Appendix I
$O_2(aq) – CO_3^{2-}$	λ	Binary	kg/mol	Clegg and Brimblecombe 1990	162089	Appendix I
$CO_2(aq) – Ca^{++}$	λ	Binary	kg/mol	Corti 1990	178211	Appendix I
$CO_2(aq) – Cl^-$	λ	Binary	kg/mol	Corti 1990	178211	Appendix I
$CO_2(aq) – K+$	λ	Binary	kg/mol	Corti 1990	178211	Appendix I
$CO_2(aq) – Mg^{++}$	λ	Binary	kg/mol	Corti 1990	178211	Appendix I
$CO_2(aq) – Na^+$	λ	Binary	kg/mol	Corti 1990	178211	Appendix I
$CO_2(aq) – H^+$	λ	Binary	kg/mol	He and Morse 1993	162090	Appendix I
$CO_2(aq) – SO_4^{2-}$	λ	Binary	kg/mol	Rumpf and Maurer 1993	178223	Appendix I

Table 4-3. Ternary Pitzer Ion Interaction Coefficients

Ions	Coefficient Name	Coefficient Type	Coefficient Units	Coefficient Source	Source DIRS #	Coefficient Use in This Report
$CO_2(aq) – Na^+ – Cl^-$	ζ	Ternary	kg/mol	Corti 1990	178211	Appendix I
$CO_2(aq) – Na^+ – SO_4^{2-}$	ζ	Ternary	kg/mol	Corti 1990	178211	Appendix I
$O_2(aq) – Na^+ – Cl^-$	ζ	Ternary	kg/mol	Clegg and Brimblecombe 1990	162089	Appendix I
$O_2(aq) – Na^+ – Br^-$	ζ	Ternary	kg/mol	Clegg and Brimblecombe 1990	162089	Appendix I
$O_2(aq) – Na^+ – NO_3^-$	ζ	Ternary	kg/mol	Clegg and Brimblecombe 1990	162089	Appendix I
$O_2(aq) – Na^+ – SO_4^{2-}$	ζ	Ternary	kg/mol	Clegg and Brimblecombe 1990	162089	Appendix I
$O_2(aq) – Al^{+++} – Cl^-$	ζ	Ternary	kg/mol	Clegg and Brimblecombe 1990	162089	Appendix I
$O_2(aq) – Al^{+++} – SO_4^{2-}$	ζ	Ternary	kg/mol	Clegg and Brimblecombe 1990	162089	Appendix I
$O_2(aq) – Ba^{++} – Cl^-$	ζ	Ternary	kg/mol	Clegg and Brimblecombe 1990	162089	Appendix I
$O_2(aq) – NH_4^+ – SO_4^{2-}$	ζ	Ternary	kg/mol	Clegg and Brimblecombe 1990	162089	Appendix I
$O_2(aq) – K^+ – Cl^-$	ζ	Ternary	kg/mol	Clegg and Brimblecombe 1990	162089	Appendix I
$O_2(aq) – K^+ – Br^-$	ζ	Ternary	kg/mol	Clegg and Brimblecombe 1990	162089	Appendix I
$O_2(aq) – K^+ – OH^-$	ζ	Ternary	kg/mol	Clegg and Brimblecombe 1990	162089	Appendix I
$O_2(aq) – K^+ – I^-$	ζ	Ternary	kg/mol	Clegg and Brimblecombe 1990	162089	Appendix I
$O_2(aq) – K^+ – NO_3^-$	ζ	Ternary	kg/mol	Clegg and Brimblecombe 1990	162089	Appendix I
$O_2(aq) – K^+ – SO_4^{2-}$	ζ	Ternary	kg/mol	Clegg and Brimblecombe 1990	162089	Appendix I
$O_2(aq) – H^+ – Cl^-$	ζ	Ternary	kg/mol	Clegg and Brimblecombe 1990	162089	Appendix I
$O_2(aq) – Li^+ – Cl^-$	ζ	Ternary	kg/mol	Clegg and Brimblecombe 1990	162089	Appendix I
$O_2(aq) – Mg^{++} – Cl^-$	ζ	Ternary	kg/mol	Clegg and Brimblecombe 1990	162089	Appendix I
$O_2(aq) – Mg^{++} – SO_4^{2-}$	ζ	Ternary	kg/mol	Clegg and Brimblecombe 1990	162089	Appendix I
$O_2(aq) – Ca^{++} – Cl^-$	ζ	Ternary	kg/mol	Clegg and Brimblecombe 1990	162089	Appendix I
$O_2(aq) – Ca^{++} – NO_3^-$	ζ	Ternary	kg/mol	Clegg and Brimblecombe 1990	162089	Appendix I
$O_2(aq) – Na^+ – OH^-$	ζ	Ternary	kg/mol	Clegg and Brimblecombe 1990	162089	Appendix I
$O_2(aq) – Na^+ – HCO_3^-$	ζ	Ternary	kg/mol	Clegg and Brimblecombe 1990	162089	Appendix I
$O_2(aq) – Na^+ – CO_3^{2-}$	ζ	Ternary	kg/mol	Clegg and Brimblecombe 1990	162089	Appendix I

Table 4-3. Ternary Pitzer Ion Interaction Coefficients (Continued)

Ions	Coefficient Name	Coefficient Type	Coefficient Units	Coefficient Source	Source DIRS #	Coefficient Use in This Report
$Cl^- – OH^- – Na^+$	ζ	Ternary	kg/mol	Pabalan and Pitzer 1987	162096	Appendix I
$Na^+ – K^+ – Cl^-$	ψ	Ternary	kg/mol	Pabalan and Pitzer 1987	162096	Appendix I
$Na^+ – K^+ – SO_4^{2-}$	ψ	Ternary	kg/mol	Greenberg and Møller 1989	152684	Appendix I
$Na^+ – Ca^{++} – Cl^-$	ψ	Ternary	kg/mol	Greenberg and Møller 1989	152684	Appendix I
$Na^+ – Ca^{++} – SO_4^{2-}$	ψ	Ternary	kg/mol	Greenberg and Møller 1989	152684	Appendix I
$Na^+ – Mg^{++} – Cl^-$	ψ	Ternary	kg/mol	Pabalan and Pitzer 1987	162096	Appendix I
$Na^+ – Cl^- – SO_4^2$	ψ	Ternary	kg/mol	Greenberg and Møller 1989	152684	Appendix I
$Na^+ – OH^- – SO_4^{2-}$	ψ	Ternary	kg/mol	Pabalan and Pitzer 1987	162096	Appendix I
$Na^+ – Cl^- – HCO_3^-$	ψ	Ternary	kg/mol	Peiper and Pitzer 1982; Konigsberger et al. 1999	162097 168345	Appendix I
$Na^+ – HSO_4^- – SO_4^{2-}$	ψ	Ternary	kg/mol	Holmes and Mesmer 1994	162078	Appendix I
$H – HSO_4^- – SO_4^{2-}$	ψ	Ternary	kg/mol	Holmes and Mesmer 1994; Baes et al. 1993	162078 168318	Appendix I
$K^+ – Ca^{2+} – Cl^-$	ψ	Ternary	kg/mol	Greenberg and Møller 1989	152684	Appendix I
$K^+ – Mg^{2+} – Cl^-$	ψ	Ternary	kg/mol	Pabalan and Pitzer 1987	162096	Appendix I
$K^+ – Cl^- – SO_4^{2-}$	ψ	Ternary	kg/mol	Greenberg and Møller 1989	152684	Appendix I
$Ca^{++} – Cl^- – SO_4^{2-}$	ψ	Ternary	kg/mol	Greenberg and Møller 1989	152684	Appendix I
$Cu^+ – H^- – HSO_4^-$	ψ	Ternary	kg/mol	Beas et al. 1993	168318	Appendix I
$Na^+ – Cl^- – OH^-$	ψ	Ternary	kg/mol	Pabalan and Pitzer 1987	162096	Appendix I
$Mg^{++} – Na^+ – Cl^-$	ψ	Ternary	kg/mol	Pabalan and Pitzer 1987	162096	Appendix I
$Mg^{++} – Cl^- – SO_4^{2-}$	ψ	Ternary	kg/mol	Pabalan and Pitzer 1987	162096	Appendix I
$Na^+ – AlO_2^- – NO_3^-$	ψ	Ternary	kg/mol	Felmy et al. 1994	162112	Appendix I
$Na^+ – AlO_2^- – OH^-$	ψ	Ternary	kg/mol	Felmy et al. 1994	162112	Appendix I
$Na^+ – HSO_4^- – SO_4^{2-}$	ψ	Ternary	kg/mol	Felmy et al. 1994	162112	Appendix I
$SiO_2(aq) – H^+ – NO_3^-$	ψ	Ternary	kg/mol	Felmy et al. 1994	162112	Appendix I
$SiO_2(aq) – Mg^{2+} – Cl^-$	ψ	Ternary	kg/mol	Felmy et al. 1994	162112	Appendix I
$SiO_2(aq) – Na^+ – Cl^-$	ψ	Ternary	kg/mol	Felmy et al. 1994	162112	Appendix I

4.1.2 Parameters

The variable input parameters important to the IDPS model are summarized in Table 4-4. The modeled incoming seepage includes the following components: Na, K, Ca, Mg, Cl, F, CO_3, SO_4, NO_3, SiO_2, Al, H, H_2O, and potentially Br. The input for hydrogen (H) is the pH of the incoming water. pH is the negative logarithm of the activity of the hydrogen ion. Input values for the aqueous component concentrations are acquired directly from water sample analyses or are qualified technical product output from geochemical model simulations. Values for T, RH, f_{CO2}, and f_{O2} are selected by the user of the IDPS model to cover the expected ranges of these parameters for the systems being modeled (Section 6.6.2.4). The approximate atmospheric value for f_{O2} ($10^{-0.7}$ bars) limits the model to oxidizing conditions and inhibits the components from reducing to lower oxidation states. The actual value of f_{O2} has little effect on the model results when it is above $10^{-9.0}$ bars, as can be demonstrated by running the model at a f_{O2} value of $10^{-9.0}$ bars. Though f_{O2} in the drift could decrease markedly during the thermal period, oxidizing conditions will prevail for nearly the entire regulatory period (BSC 2005 [DIRS 175083], Section 6.7). Consequently, the IDPS model is used in TSPA only for oxidizing conditions, achieved by setting f_{O2} at approximately atmospheric for all simulations.

Use of the IDPS model is demonstrated in an example in Section 6.7. This example demonstrates how the IDPS model is used to produce technical product output. The input data for this example are introduced in Section 4.4. They are not introduced here because (1) they are not used to develop the IDPS model and (2) the results from this example are not directly used in performance assessment. Model calculations used in support of TSPA are documented elsewhere, such as in *Engineered Barrier System: Physical and Chemical Environment* (BSC 2005 [DIRS 175083]).

Table 4-4. IDPS Model Input Parameters

Parameter Name	Parameter Description	Parameter Units	Parameter Source Range	Parameter Use in this Report
C_i^s	Concentration or activity of each modeled component *i* in the incoming seepage	mass/volume, moles/mass, or moles/volume (or pH for the hydrogen ion activity)	Predicted or measured major ion composition of a starting water of the system Na-K-H-Mg-Ca-Al-Cl-F-Br-NO_3-SO_4-CO_3-SiO_2-CO_2-O_2-H_2O	Section 4.4, Section 6.6.2.1, Section 6.7, Sections 7.1 to 7.3
T	Temperature	degrees Celsius	20 to 140	Section 4.4, Section 6.6.2.4, Section 6.7, Sections 7.1 to 7.3
RH	Relative humidity	non-dimensional or percentage	0 to 100	Section 4.4, Section 6.6.2.4, Section 6.7, Sections 7.1 to 7.3
f_{CO2}	Fugacity of carbon dioxide	bars	0 to 1	Section 4.4, Section 6.6.2.4, Section 6.7, Sections 7.1 to 7.3
f_{O2}	Fugacity of oxygen	bars	$10^{-0.7}$ (this value is chosen to represent a range of oxidizing conditions from $10^{-9.0}$ to 1, as explained in Section 4.1.2)	Section 4.4, Section 6.6.2.4, Section 6.7, Sections 7.1 to 7.3
R^{es} (or Q^e/Q^s)	Relative evaporation rate	non-dimensional	–99 to 1	Section 6.6.2.5, Section 6.7, Sections 7.1 to 7.3
S_m	Suppression flag for mineral *m*	Boolean	True or False	Section 6.6.2.6, Section 6.7, Sections 7.1 to 7.3

4.2 CRITERIA

Project Requirements Document (Canori and Leitner 2003 [DIRS 166275]) contains one criterion that is relevant to the work documented in this report: PRD-002/T-015 Requirements for Performance Assessment. See 10 CFR 63.114 [DIRS 173273] for complete requirement text. Work described in this report supports PRD-002/T-015, but more specific criteria exist in *Yucca Mountain Review Plan, Final Report* (YMRP) (NRC 2003 [DIRS 163274]). Selected YMRP acceptance criteria are presented in order to supplement or clarify the Project Requirements Document citation.

YMRP acceptance criteria (NRC 2003 [DIRS 163274]) applicable to this report are identified in Section 3.2 of *Technical Work Plan for: Revision of Model Reports for Near-Field and In-Drift Water Chemistry* (SNL 2007 [DIRS 179287]). The criteria are those established for the quantity and chemistry of water contacting engineered barriers and waste forms, as presented in Section 2.2.1.3.3.3 of the YMRP (NRC 2003 [DIRS 163274]) and also in 10 CFR 63.114(a)-(c) and (e)-(g) [DIRS 173273]. These criteria are presented in the following subsections, and an assessment of how these criteria are addressed is provided in Sections 8.5.1 through 8.5.5.

4.2.1 Acceptance Criterion 1 – System Description and Model Integration Are Adequate

(1) Total system performance assessment adequately incorporates important design features, physical phenomena, and couplings, and uses consistent and appropriate assumptions throughout the quantity and chemistry of water contacting engineered barriers and waste forms abstraction process.

(2) The abstraction of the quantity and chemistry of water contacting engineered barriers and waste forms uses assumptions, technical bases, data, and models, that are appropriate and consistent with other related U.S. Department of Energy abstractions.

(3) Important design features, such as waste package design and material selection, drip shield, ground support, thermal loading strategy, and degradation processes, are adequate to determine the initial and boundary conditions for calculations of the quantity and chemistry of water contacting engineered barriers and waste forms.

(5) Sufficient technical bases and justification are provided for total system performance assessment assumptions and approximations for modeling coupled thermal-hydrologic-mechanical-chemical effects on seepage and flow, the waste package chemical environment, and the chemical environment for radionuclide release. The effects of distribution of flow on the amount of water contacting the engineered barriers and waste forms are consistently addressed, in all relevant abstractions.

(6) The expected ranges of environmental conditions within the waste package emplacement drifts, inside the breached waste packages, and contacting the waste forms and their evolution with time are identified.

(8) Adequate technical bases are provided, including activities such as independent modeling, laboratory or field data, or sensitivity studies, for inclusion of any thermal-hydrologic-mechanical-chemical couplings and features, events, and processes.

(9) Performance-affecting processes that have been observed in thermal-hydrologic tests and experiments are included into the performance assessment.

(10) Likely modes for container corrosion (Section 2.2.1.3.1 of the Yucca Mountain Review Plan) are identified and considered in determining the quantity and chemistry of water entering the engineered barriers and contacting waste forms. For example, the model abstractions consistently address the role of parameters, such as pH, carbonate concentration, and the effect of corrosion on the quantity and chemistry of water contacting engineered barriers and waste forms.

(12) Guidance in NUREG–1297 (Altman et al. 1988 [DIRS 103597]) and NUREG–1298 (Altman et al. 1988 [DIRS 103750]), or other acceptable approaches, is followed.

4.2.2 Acceptance Criterion 2 – Data Are Sufficient for Model Justification

(1) Geological, hydrological, and geochemical values used in the license application are adequately justified. Adequate description of how the data were used, interpreted, and appropriately synthesized into the parameters is provided.

(2) Sufficient data were collected on the characteristics of the natural system and engineered materials to establish initial and boundary conditions for conceptual models of thermal-hydrologic-mechanical-chemical coupled processes, that affect seepage and flow and the waste package chemical environment.

(4) Sufficient information to formulate the conceptual approach(es) for analyzing water contact with the drip shield, engineered barriers, and waste forms is provided.

4.2.3 Acceptance Criterion 3 – Data Uncertainty Is Characterized and Propagated through the Model Abstraction

(1) Models use parameter values, assumed ranges, probability distributions, and bounding assumptions that are technically defensible, reasonably account for uncertainties and variabilities, and do not result in an under-representation of the risk estimate.

(2) Parameter values, assumed ranges, probability distributions, and bounding assumptions used in the total system performance assessment calculations of quantity and chemistry of water contacting engineered barriers and waste forms are technically defensible and reasonable, based on data from the Yucca Mountain region (e.g., results from large block and drift-scale heater and niche tests), and a combination of techniques that may include laboratory experiments, field measurements, natural analog research, and process-level modeling studies.

(3) Input values used in the total system performance assessment calculations of quantity and chemistry of water contacting engineered barriers (e.g., drip shield and waste package) are consistent with the initial and boundary conditions and the assumptions of the conceptual models and design concepts for the Yucca Mountain site. Correlations between input values are appropriately established in the U.S. Department of Energy total system performance assessment. Parameters used to define initial conditions, boundary conditions, and computational domain in sensitivity analyses involving coupled thermal-hydrologic-mechanical-chemical effects on seepage and flow, the waste package chemical environment, and the chemical environment for radionuclide release, are consistent with available data. Reasonable or conservative ranges of parameters or functional relations are established.

(4) Adequate representation of uncertainties in the characteristics of the natural system and engineered materials is provided in parameter development for conceptual models, process-level models, and alternative conceptual models. The U.S. Department of Energy may constrain these uncertainties using sensitivity

analyses or conservative limits. For example, the U.S. Department of Energy demonstrates how parameters used to describe flow through the engineered barrier system bound the effects of excavation-induced changes.

4.2.4 Acceptance Criterion 4 – Model Uncertainty Is Characterized and Propagated through the Model Abstraction

(1) Alternative modeling approaches of features, events, and processes are considered and are consistent with available data and current scientific understanding, and the results and limitations are appropriately considered in the abstraction.

(2) Alternative modeling approaches are considered and the selected modeling approach is consistent with available data and current scientific understanding. A description that includes a discussion of alternative modeling approaches not considered in the final analysis and the limitations and uncertainties of the chosen model is provided.

(3) Consideration of conceptual model uncertainty is consistent with available site characterization data, laboratory experiments, field measurements, natural analog information and process-level modeling studies; and the treatment of conceptual model uncertainty does not result in an under-representation of the risk estimate.

(4) Adequate consideration is given to effects of thermal-hydrologic-mechanical-chemical coupled processes in the assessment of alternative conceptual models.

4.2.5 Acceptance Criterion 5 – Model Abstraction Output Is Supported by Objective Comparisons

(3) Accepted and well-documented procedures are used to construct and test the numerical models that simulate coupled thermal-hydrologic-mechanical-chemical effects on seepage and flow, waste package chemical environment, and the chemical environment for radionuclide release. Analytical and numerical models are appropriately supported. Abstracted model results are compared with different mathematical models, to judge robustness of results.

4.3 CODES, STANDARDS, AND REGULATIONS

10 CFR 63 [DIRS 173273]. Energy: Disposal of High-Level Radioactive Wastes in a Geologic Repository at Yucca Mountain, Nevada.

4.4 VALIDATION AND DEMONSTRATION DATA

Data used to validate the IDPS model, demonstrate its use, and estimate model uncertainties are presented in this section. These data are independent of IDPS model development and therefore are not presented in Sections 4.1.1 or 4.1.2.

Table 4-5 lists the sources of these independent data, the specific tables where the data are presented (or identified in further detail), and how and where the data are used in this report.

Data used to validate a model are considered "indirect inputs." Data used to estimate model uncertainty are "direct inputs" because estimated model uncertainties (Table 7-10) are used in support of TSPA. These data are not "directly used to develop the model," so in accordance with SCI-PRO-006, they are not introduced in Section 4.1. Data used solely for validation or demonstration are not direct inputs because outputs having these data as sources are not used directly or indirectly in TSPA calculations. Some data listed in Table 4-5 (from McCaffrey et al. 1987 [DIRS 164481], for seawater evaporation; and from Linke 1965 [DIRS 166191], pp. 127 to 128, 482 to 483, and 976 to 978; and Linke 1958 [DIRS 166192], p. 573, for mutual solubilities of salt minerals) are treated as both indirect inputs (for validation use) and as direct inputs (for the purpose of estimating uncertainties to use in TSPA).

Qualification of the data in the Linke sources is justified per Section 6.2.1(K) of SCI-PRO-006 for use within the report based on reliability of the data source, extent to which the data demonstrate the properties of interest, and prior uses of the data. As explained in Section 4.1.1, the Linke volumes are essentially de facto handbooks in the field of aqueous geochemistry. These volumes are identified in Section 4.1.1 in support of a specific data set from Linke (1965 [DIRS 166191], p. 915) used only for model development. Qualification of the McCaffrey et al. (1987 [DIRS 164481]) data is justified per Section 6.2.1(K) of SCI-PRO-006 for use within the report based on the extent to which the data demonstrate the properties of interest. The reliability of this source is supported by its publication in a refereed scientific journal. This paper is highly relevant to the validation of the IDPS model and estimates of model uncertainty because it is the only source of pH and ionic strength measurements found in the literature for a naturally evaporating brine. Results from McCaffrey et al. (1987 [DIRS 164481]) and the Linke volumes used in estimating uncertainty are summarized in Tables 7-9 and 7-10.

Table 4-5. Data Used for Model Validation, Model Demonstration, and Estimation of Model Uncertainties

Data	Tables	Use in Report
Chemistry handbook data for binary salt systems (Lide 2000 [DIRS 162229]; Dean 1992 [DIRS 100722]; Weast and Astle 1981 [DIRS 100833])	Tables 4-6, 4-7, and 4-11	Validation
Non-handbook data for binary salt systems (Linke 1965 [DIRS 166191]; Linke 1958 [DIRS 166192]; Dutrizac 2002 [DIRS 166148]; Moore et al. 1997 [DIRS 166150]; Kracek 1928 [DIRS 122125]; Greenspan 1977 [DIRS 104945]; Dingemans and Dijkgraaf 1948 [DIRS 166149]; Grønvold and Meisingset 1983 [DIRS 162069]; Robie and Hemingway 1995 [DIRS 153683])	Tables 4-8, 4-9, 4-10, and 4-11	Validation
Salt solubilities in ternary systems (Linke 1965 [DIRS 166191]; de Lima and Pitzer 1983 [DIRS 162110]; Linke 1958 [DIRS 166192])	Table 4-12	Validation
Salt solubilities in ternary systems involving both Cl and NO_3 (Linke 1965 [DIRS 166191], pp. 127 to 128, 482 to 483, 976 to 978; Linke 1958 [DIRS 166192], p. 573) (This source is suitable for use in estimating IDPS model uncertainty because it provides data that demonstrate the properties of interest and it is a reliable source of data; see Section 4.1.1.)	Table 4-12	Validation and Uncertainty Estimation
Temperature dependence of carbon dioxide solubility in pure water (Lide 2006 [DIRS 178081] p. 8-85).	Table 4-13	Validation
Solubility of calcite in pure water at fixed partial pressure of carbon dioxide (Linke 1958 [DIRS 166192] p. 539).	Table 4-14	Validation

Table 4-5. Data Used for Model Validation, Model Demonstration, and Estimation of Model Uncertainties (Continued)

Data	Tables	Use in Report
Temperature dependence of calcite solubility in calcite-CO_2-(NaCl,KCl,$CaCl_2$)-(gypsum) systems (Wolf et al. 1989 [DIRS 177633]).	Tables 4-15, 4-16, 4-17, and 4-18	Validation
Dependence of calcite solubility in three different brines at 0.0004 atm CO_2(g) (He and Morse 1993 [DIRS 162090] p. 3543)	Table 4-19	Validation
Laboratory evaporation data for synthetic average J-13 well water (Rosenberg et al. 1999 [DIRS 125338]; DTN: LL991008104241.042 [DIRS 120489])	Tables 4-20 and 4-21	Validation
Laboratory evaporation data for synthetic 100x J-13 well water (BSC 2001 [DIRS 155640]; DTN: LL000202905924.117 [DIRS 144913])	Table 4-22	Validation
Laboratory evaporation data for synthetic Topopah Spring Tuff pore water (Rosenberg et al. 1999 [DIRS 125339]; DTN: LL991008004241.041 [DIRS 120487])	Table 4-23	Validation
Laboratory evaporation data for synthetic Topopah Spring Tuff pore water at 95°C (Alai et al. 2005 [DIRS 176811]; DTN: LL030106923121.018 [DIRS 177573], DTN: LL030107023121.019 [DIRS 177574], DTN: LL030107123121.020 [DIRS 177575], DTN: LL030408523121.028 [DIRS 177576]) (These data are qualified.)	Table 4-24	Validation and Uncertainty Estimation
Seawater evaporation data (McCaffrey et al. 1987 [DIRS 164481]) (This source is suitable for use in estimating IDPS model uncertainty because it provides data that demonstrate the properties of interest and it is a reliable source of data.)	Table 4-25	Validation and Uncertainty Estimation
Average in situ composition of water from well J-13 (Harrar et al. 1990 [DIRS 100814]; DTN: MO0006J13WTRCM.000 [DIRS 151029])	Table 4-26	Demonstration

Table 4-6. Handbook Aqueous Solubilities of Na, K, Ca, Mg, and Al Salts

Salt	Aqueous Solubility at 25°C (mass percent of solute)	Aqueous Solubility at 100°C (mass percent of solute)
NaCl	26.45	28.05
KCl	26.22	36.05
$CaCl_2$	44.83	59.94
$MgCl_2$	35.90	42.15
$NaHCO_3$	9.32	19.10
$KHCO_3$	26.6	40.45 at 70°C
Na_2CO_3	23.5	30.09
K_2CO_3	52.7	61.0
NaF	3.97	4.82
KF	50.4	60.0 at 80°C
CaF_2	0.0016	Not reported above 25°C
MgF_2	0.013	Not reported above 25°C

Table 4-6. Handbook Aqueous Solubilities of Na, K, Ca, Mg, and Al Salts (Continued)

Salt	Aqueous Solubility at 25°C (mass percent of solute)	Aqueous Solubility at 100°C (mass percent of solute)
Na_2SO_4	21.94	29.67
K_2SO_4	10.7	19.3
$CaSO_4$	0.205	0.163
$MgSO_4$	26.3	33.3
NaBr	48.6	54.9
KBr	40.4	50.8
$CaBr_2$	61.0	73.0 at 60°C
$MgBr_2$	50.6	55.7
$NaNO_3$	47.7	63.8
KNO_3	27.7	70.8
$Ca(NO_3)_2$	59.0	78.5
$Mg(NO_3)_2$	41.6	72.0

Source: Lide 2000 [DIRS 162229], pp. 8-102 to 8-110.

Table 4-7. Handbook Equilibrium Relative Humidity for Saturated Aqueous Solutions in Contact with an Excess of Solid-Phase Salts

Salt	Equilibrium Relative Humidity (%)	Temperature of Measurement (°C)
NaCl	76.4	80
KCl	79.5	80
$MgCl_2 \cdot 6H_2O$	33.0	25
$Na_2CO_3 \cdot 10H_2O$	87[a]	24.5
$K_2CO_3 \cdot 2H_2O$	42	40
NaF	96.6[a]	100
KF	22.9[a]	100
$Na_2SO_4 \cdot 10H_2O$	93[a]	20
K_2SO_4	96	60
$NaNO_3$	65.5	80
KNO_3	82	60
KNO_3, $NaNO_3$, and NaCl	30.49[a]	16.39

Source: Dean 1992 [DIRS 100722], p. 11.6.

[a] Weast and Astle 1981 [DIRS 100833], p. E-44.

Table 4-8 Sources of Additional Aqueous Solubility Data for Na, K, Ca, and Mg Salts as a Function of Temperature

Salt [a]	Source
NaCl	Linke 1965 [DIRS 166191], p. 959
KCl	Linke 1965 [DIRS 166191], p. 114
$CaCl_2$	Linke 1958 [DIRS 166192], p. 565
$MgCl_2$	Linke 1965 [DIRS 166191], p. 480
NaBr	Linke 1965 [DIRS 166191], p. 831
KBr	Linke 1965 [DIRS 166191], p. 12
$CaBr_2$	Linke 1958 [DIRS 166192], p. 503
$MgBr_2$	Linke 1965 [DIRS 166191], p. 444
NaF	Linke 1965 [DIRS 166191], p. 1029-1030
KF	Linke 1965 [DIRS 166191], p. 202
$NaNO_3$	Linke 1965 [DIRS 166191], p. 1069
KNO_3	Linke 1965 [DIRS 166191], p. 250
$Ca(NO_3)_2$	Linke 1958 [DIRS 166192], p. 616
$Mg(NO_3)_2$	Linke 1965 [DIRS 166191], p. 511
Na_2SO_4	Linke 1965 [DIRS 166191], p. 1122
K_2SO_4	Linke 1965 [DIRS 166191], p. 296
$CaSO_4$	Linke 1958 [DIRS 166192], pp. 660 to 662; Dutrizac 2002 [DIRS 166148]
Na_2CO_3	Grønvold and Meisingset 1983 [DIRS 162069]; Robie and Hemingway 1995 [DIRS 153683], pp. 26
K_2CO_3	Linke 1965 [DIRS 166191], p. 81; Moore et al. 1997 [DIRS 166150]
$NaHCO_3$	Linke 1965 [DIRS 166191], p. 947
$KHCO_3$	Linke 1965 [DIRS 166191], p. 102

[a] Potential hydration states not shown.

Table 4-9. Sources of Additional Vapor Pressure Data for Several Salt Solutions as a Function of Temperature

Salt [a]	Source
NaCl	Kracek 1928 [DIRS 122125], p. 369
KCl	Kracek 1928 [DIRS 122125], p. 373
$CaCl_2$	Kracek 1928 [DIRS 122125], p. 368
$MgCl_2$	Kracek 1928 [DIRS 122125], pp. 367 to 368
KNO_3	Kracek 1928 [DIRS 122125], p. 373
$Ca(NO_3)_2$	Kracek 1928 [DIRS 122125], p. 368
Na_2SO_4	Kracek 1928 [DIRS 122125], pp. 371 to 372

[a] Potential hydration states not shown.

Table 4-10. Equilibrium *RH* of Saturated Aqueous Solutions of Selected Pure Salts as a Function of Temperature

Temperature (°C)	KF	$MgCl_2$	K_2CO_3	$Mg(NO_3)_2$	$NaNO_3$	NaCl	KCl	KNO_3	K_2SO_4
0	N/R	33.66%	43.13%	60.35%	N/R	75.51%	88.61%	96.33%	98.77%
5	N/R	33.60%	43.13%	58.86%	78.57%	75.65%	87.67%	96.27%	98.48%
10	N/R	33.47%	43.14%	57.36%	77.53%	75.67%	86.77%	95.96%	98.18%
15	N/R	33.30%	43.15%	55.87%	76.46%	75.61%	85.92%	95.41%	97.89%
20	N/R	33.07%	43.16%	54.38%	75.36%	75.47%	85.11%	94.62%	97.59%
25	30.85%	32.78%	43.16%	52.89%	74.25%	75.29%	84.34%	93.58%	97.30%
30	27.27%	32.44%	43.17%	51.40%	73.14%	75.09%	83.62%	92.31%	97.00%
35	24.59%	32.05%	N/R	49.91%	72.06%	74.87%	82.95%	90.79%	96.71%
40	22.68%	31.60%	N/R	48.42%	71.00%	74.68%	82.32%	89.03%	96.41%
45	21.46%	31.10%	N/R	46.93%	69.99%	74.52%	81.74%	87.03%	96.12%
50	20.80%	30.54%	N/R	45.44%	69.04%	74.43%	81.20%	84.78%	95.82%
55	20.60%	29.93%	N/R	N/R	68.15%	74.41%	80.70%	N/R	N/R
60	20.77%	29.26%	N/R	N/R	67.35%	74.50%	80.25%	N/R	N/R
65	21.18%	28.54%	N/R	N/R	66.64%	74.71%	79.85%	N/R	N/R
70	21.74%	27.77%	N/R	N/R	66.04%	75.06%	79.49%	N/R	N/R
75	22.33%	26.94%	N/R	N/R	65.56%	75.58%	79.17%	N/R	N/R
80	22.85%	26.05%	N/R	N/R	65.22%	76.29%	78.90%	N/R	N/R
85	23.20%	25.11%	N/R	N/R	65.03%	N/R	78.68%	N/R	N/R
90	23.27%	24.12%	N/R	N/R	65.00%	N/R	78.50%	N/R	N/R
95	N/R	23.07%	N/R	N/R	N/R	N/R	N/R	N/R	N/R
100	N/R	21.97%	N/R	N/R	N/R	N/R	N/R	N/R	N/R

Source: Greenspan 1977 [DIRS 104945].

NOTE: N/R = not reported.

Table 4-11. Selected Vapor Pressure Data for Saturated Aqueous $NaNO_3$ Solutions and Pure Water as a Function of Temperature

Temperature (°C)	$NaNO_3$ Solution Vapor Pressure (bar)	Vapor Pressure of Pure Water (mm Hg) [a]	Temperature (°C)	$NaNO_3$ Solution Vapor Pressure (bar)	Vapor Pressure of Pure Water (mm Hg) [a]
10.0	0.0095	9.209	80.0	0.2852	355.1
15.0	0.0128	12.788	85.0	0.3412	433.6
20.0	0.0173	17.535	90.0	0.4052	525.76
25.0	0.0232	23.756	95.0	0.4781	633.9
30.0	0.0305	31.824	100.0	0.5606	760.00
35.0	0.0399	42.175	105.0	0.6534	906.07
40.0	0.0515	55.324	110.0	0.7570	1074.56
45.0	0.0656	71.88	115.0	0.8719	1267.98
50.0	0.0831	92.51	120.0	0.9989	1489.14
55.0	0.1043	118.04	125.0	1.1386	1740.93
60.0	0.1296	149.38	130.0	1.2906	2026.16
65.0	0.1596	187.54	140.0	1.6332	2710.92
70.0	0.1952	233.7	145.0	1.8239	3116.76
75.0	0.2368	289.1	150.0	2.0265	3570.48

Source: Dingemans and Dijkgraaf 1948 [DIRS 166149].

[a] Weast and Astle 1981 [DIRS 100833], pp. D-168 to D-169.

NOTE: 1 bar = 750.062 mm Hg (Weast and Astle 1981 [DIRS 100833], p. F-283).

Table 4-12. Sources of Salt Solubilities in Ternary Systems as a Function of Temperature

Salts [a]	Source
NaCl–KCl	Linke 1965 [DIRS 166191], pp. 146 to 148
NaCl–$NaNO_3$	Linke 1965 [DIRS 166191], pp. 976 to 978
NaCl–Na_2SO_4	de Lima and Pitzer 1983 [DIRS 162110]
NaCl–$MgCl_2$	Linke 1965 [DIRS 166191], p. 489; de Lima and Pitzer 1983 [DIRS 162110]
NaCl–Na_2CO_3	Linke 1965 [DIRS 166191], pp. 931 to 932
$NaNO_3$–KNO_3	Linke 1965 [DIRS 166191], pp. 262 to 263
$NaNO_3$–$Ca(NO_3)_2$	Linke 1958 [DIRS 166192], p. 621
$NaNO_3$–Na_2SO_4	Linke 1965 [DIRS 166191], p. 1076
Na_2CO_3–$NaHCO_3$	Linke 1965 [DIRS 166191], pp. 926 to 927
KCl–KNO_3	Linke 1965 [DIRS 166191], pp. 127 to 128
KCl–$MgCl_2$	Linke 1965 [DIRS 166191], pp. 141 to 143
K_2CO_3–K_2SO_4	Linke 1965 [DIRS 166191], p. 89
$CaCl_2$–$Ca(NO_3)_2$	Linke 1958 [DIRS 166192], p. 573
$CaSO_4$–Na_2SO_4	Linke 1958 [DIRS 166192], pp. 676 to 677
$CaSO_4$–K_2SO_4	Linke 1958 [DIRS 166192], pp. 671 to 672
$MgCl_2$–$Mg(NO_3)_2$	Linke 1965 [DIRS 166191], pp. 482 to 483

[a] Potential hydration states not shown.

Table 4-13. Temperature Dependence of Carbon Dioxide Solubility in Pure Water

Temperature (°C)	CO_2 (aq) at 0.05 bar CO_2 (g) (1,000x mole fraction)	CO_2 (aq) at 0.1 bar CO_2 (g) (1,000x mole fraction)
0	0.067	0.135
5	0.056	0.113
10	0.048	0.096
15	0.041	0.082
20	0.035	0.071
25	0.031	0.062
30	0.027	0.054
35	0.024	0.048
40	0.022	0.043
45	0.020	0.039
50	0.018	0.036
55	0.016	0.033
60	0.015	0.030
65	0.014	0.028
70	0.013	0.026
75	0.012	0.025

Table 4-13. Temperature Dependence of Carbon Dioxide Solubility in Pure Water (Continued)

Temperature (°C)	CO_2 (aq) at 0.05 bar CO_2 (g) (1,000x mole fraction)	CO_2 (aq) at 0.1 bar CO_2 (g) (1,000x mole fraction)
80	0.012	0.023
85	0.011	0.022
90	0.011	0.021
95	0.010	0.020
100	0.010	0.020

Source: Lide 2006 [DIRS 178081], p. 8-85.

Table 4-14. Solubility of Calcite in Pure Water at Fixed Partial Pressure of Carbon Dioxide

Partial Pressure of CO_2 (atm)	Calcite Solubility at 25°C (mmolal)
0.00032	0.53
0.001	0.78
0.01	1.7
0.1	3.9
Temperature (°C)	**Solubility Ratio[a]**
0	1.8
10	1.4
20	1.1
25	1
30	0.9
50	0.6

Source: Linke 1958 [DIRS 166192] p. 539.
[a] Ratio of the solubility at the given temperature to that at 25°C.

Table 4-15. Temperature Dependence of Calcite Solubility in NaCl-Calcite-Gypsum-CO_2-H_2O System

Temp (°C)	Ca (mmolal)	$\sum CO_2$ (mmolal)	Alkalinity (mmolal)	CO_2 (g) (kPa)	NaCl (molal)
25	15.6	2.26	2.03	0.93	0.00
25	29.0	2.21	2.00	0.93	0.21
25	38.5	2.23	2.00	0.93	0.54
25	N/R	2.18	N/R	0.93	1.08
25	49.6	2.18	1.98	0.93	1.16
25	54.6	2.03	1.90	0.93	2.12
25	56.8	1.99	1.80	0.93	2.30
25	58.5	1.56	1.47	0.94	3.60
25	52.8	1.22	1.16	0.94	5.02
25	45.8	1.10	1.01	0.94	6.14
60	15.5	0.91	0.72	0.78	0.00

Table 4-15. Temperature Dependence of Calcite Solubility in NaCl-Calcite-Gypsum-CO_2-H_2O System (Continued)

Temp (°C)	Ca (mmolal)	$\sum CO_2$ (mmolal)	Alkalinity (mmolal)	CO_2 (g) (kPa)	NaCl (molal)
60	15.5	0.86	0.68	0.78	0.00
60	15.4	N/R	0.72	0.78	0.00
60	27.4	1.01	0.89	0.78	0.20
60	37.0	0.98	0.82	0.78	0.51
60	46.1	0.88	0.77	0.78	1.03
60	55.3	0.74	0.61	0.79	2.08
60	57.6	0.67	0.52	0.81	4.00
60	53.8	0.59	0.48	0.82	5.05
60	47.0	0.55	0.40	0.83	6.33

Source: Wolf et al. 1989 [DIRS 177633], p. 293.

NOTE: N/R = not reported.

Table 4-16. Temperature Dependence of Calcite Solubility in KCl-Calcite-CO_2-H_2O System

Temp (°C)	Ca (mmolal)	$\sum CO_2$ (mmolal)	Alkalinity (mmolal)	CO_2 (g) (kPa)	KCl (molal)
25	1.65	3.56	3.19	0.93	0.00
25	2.30	5.00	4.61	0.93	0.10
25	2.90	N/R	6.09	0.93	0.26
25	3.39	7.44	7.15	0.93	0.76
25	3.70	7.66	7.64	0.93	1.11
25	3.72	7.73	7.69	0.93	1.72
25	3.69	7.87	N/R	0.93	2.16
25	3.74	7.72	7.71	0.93	2.33
25	3.32	7.03	6.81	0.93	4.05
25	3.15	6.65	6.44	0.93	4.81
25	3.23	N/R	6.50	0.93	4.81
60	1.29	3.04	2.46	0.77	0.23
60	1.50	3.09	2.88	0.77	0.45
60	1.99	3.99	3.63	0.78	1.04
60	2.04	3.62	3.74	0.78	2.00
60	2.01	3.82	3.59	0.79	4.49
60	1.79	N/R	3.25	0.80	5.14
60	1.60	3.19	3.01	0.81	5.89

Source: Wolf et al. 1989 [DIRS 177633], pp. 293 to 294.

NOTE: N/R = not reported.

Table 4-17. Temperature Dependence of Calcite Solubility in KCl-Calcite-Gypsum-CO_2-H_2O System

Temp (°C)	Ca (mmolal)	$\sum CO_2$ (mmolal)	Alkalinity (mmolal)	CO_2 (g) (kPa)	KCl (molal)
25	16.2	2.32	2.09	0.94	0.00
25	33.0	2.35	2.12	0.94	0.30
25	38.6	2.33	2.15	0.94	0.45
25	55.6	2.31	2.22	0.94	1.36
25	59.5	2.11	2.12	0.94	2.13
25	57.4	2.04	1.98	0.94	3.05
25	57.0	1.95	1.96	0.94	3.55
25	52.4	1.63	1.68	0.94	4.80
60	23.8	N/R	N/R	0.76	0.11
60	29.5	N/R	N/R	0.76	0.23
60	37.8	0.93	0.76	0.77	0.48
60	50.1	1.00	0.82	0.77	1.03
60	60.6	1.22	1.00	0.77	1.94
60	56.9	1.01	0.83	0.78	3.06
60	54.1	0.86	N/R	0.79	3.98
60	52.7	0.96	0.74	0.79	4.63
60	N/R	0.84	0.59	0.80	5.84

Source: Wolf et al. 1989 [DIRS177633], p. 294.

NOTE: N/R = not reported.

Table 4-18. Temperature Dependence of Calcite Solubility in $CaCl_2$-Calcite-CO_2-H_2O System

Temp (°C)	$\sum CO_2$ (mmolal)	Alkalinity (mmolal)	CO_2 (g) (kPa)	$CaCl_2$ (molal)
25	3.58	N/R	0.94	0.00
25	1.33	1.15	0.94	0.10
25	1.30	1.09	0.94	0.10
25	1.21	0.98	0.94	0.27
25	1.11	0.99	0.94	0.32
25	1.02	0.88	0.94	0.53
25	0.84	0.75	0.94	1.16
25	0.81	0.72	0.94	1.37
25	0.78	0.68	0.94	1.72
25	0.63	0.63	0.94	2.39
25	0.66	0.64	0.94	2.45
25	0.55	0.56	0.94	3.04
60	1.64	1.49	0.77	0.00
60	1.65	1.51	0.77	0.00
60	1.69	1.55	0.77	0.00
60	1.69	1.54	0.77	0.00
60	1.78	1.51	0.77	0.00

Table 4-18. Temperature Dependence of Calcite Solubility in $CaCl_2$-Calcite-CO_2-H_2O System (Continued)

Temp (°C)	∑CO_2 (mmolal)	Alkalinity (mmolal)	CO_2 (g) (kPa)	$CaCl_2$ (molal)
60	0.69	0.54	0.77	0.02
60	0.57	0.49	0.77	0.04
60	0.57	0.47	0.77	0.08
60	0.59	0.43	0.77	0.08
60	0.55	0.47	0.77	0.13
60	0.55	0.43	0.77	0.17
60	0.50	0.34	0.77	0.42
60	0.50	0.37	0.77	0.43
60	0.51	0.44	0.78	0.60
60	0.42	0.34	0.78	0.85
60	0.49	0.39	0.78	0.88
60	0.46	0.42	0.79	1.80
60	0.50	0.40	0.80	1.82
60	0.47	N/R	0.81	2.76

Source: Wolf et al. 1989 [DIRS 177633], p. 294.

NOTE: N/R = not reported.

Table 4-19. Temperature Dependence of Calcite Solubility in Three Different Brines at 0.0004 atm CO_2(g)

Temp (°C)	Ca (molal)	Alkalinity (molal as HCO_3)	Brine	Na (molal)	K (molal)	Mg (molal)	Cl (molal)	SO_4 (molal)
0.00	0.03844	0.00101	Colbey 12	1.103	0.012	0.010	1.137	0.0387
25.00	0.03854	0.00054	Colbey 12	1.103	0.012	0.010	1.137	0.0387
50.00	0.03857	0.00037	Colbey 12	1.103	0.012	0.010	1.137	0.0387
75.00	0.03841	0.00026	Colbey 12	1.103	0.012	0.010	1.137	0.0387
90.00	0.03836	0.00021	Colbey 12	1.103	0.012	0.010	1.137	0.0387
0.00	0.02154	0.00140	Colbey 18	1.592	0.019	0.175	1.915	0.0457
25.00	0.02153	0.00074	Colbey 18	1.592	0.019	0.175	1.915	0.0457
50.00	0.02147	0.00051	Colbey 18	1.592	0.019	0.175	1.915	0.0457
75.00	0.02136	0.00048	Colbey 18	1.592	0.019	0.175	1.915	0.0457
90.00	0.02135	0.00045	Colbey 18	1.592	0.019	0.175	1.915	0.0457
0.00	0.65454	0.00012	Kennedy 1	3.438	0.132	0.037	4.954	0.0
25.00	0.65484	0.00009	Kennedy 1	3.438	0.132	0.037	4.954	0.0
50.00	0.65413	0.00007	Kennedy 1	3.438	0.132	0.037	4.954	0.0
75.00	0.65404	0.00006	Kennedy 1	3.438	0.132	0.037	4.954	0.0
90.00	0.65401	0.00007	Kennedy 1	3.438	0.132	0.037	4.954	0.0

Source: He and Morse 1993 [DIRS 162090], p. 3543.

Table 4-20. Water Chemistry Data from Experimental J-13 Well Water Evaporation of Rosenberg et al. (1999 [DIRS 125338])

Constituent	Units	Synthetic J-13 Well Water for evap1	Evaporated Synthetic J-13 Well Water for evap1 (Reported Concentration Factor: 956)	Synthetic J-13 Well Water for evap4	Evaporated Synthetic J-13 Well Water for evap4 (Reported Concentration Factor: 157)
Ca	mg/kg	6.4	29.86	5.3	1.2
Mg	mg/kg	2.2	0.14	2.1	0.05
Na	mg/kg	46	44,082	45.4	5,298
K	mg/kg	5.3	4,792	4.9	560
SiO_2	mg/kg	11.3	18,008	10	999
NO_3	mg/kg	8.0	5,532	8.0	1,050
HCO_3	mg/kg	108	24,878	103	4,295
Cl	mg/kg	6.9	4,835	7.5	849
F	mg/kg	2.2	1,550	2.4	247
SO_4	mg/kg	18.1	12,926	19	2,162
pH	pH	7.84	N/R	8.33	10.18

Source: DTN: LL991008104241.042 [DIRS 120489], Tables S00004_001 ["evap1"] and S00004_004 ["evap4"].

NOTE: "evap1" and "evap4" refer to the two evaporation cases for which data are shown in this table.
N/R = not reported.

Table 4-21. pH Data from Experimental J-13 Well Water Evaporation of Rosenberg et al. (1999 [DIRS 125338])

Reported Concentration Factor	pH
1	8.46
1	8.65
1.05	9.04
1.29	9.43
1.6	9.58
2.41	9.67
6.08	9.67
6.37	9.77
7.59	9.79
11.6	9.95
12.6	10
15.3	10.03
20.9	10.08
25.2	10.09
34.4	10.12
52.1	10.18
104	10.18
157	10.18

Source: DTN: LL991008104241.042 [DIRS 120489], Table S00004_003.

Table 4-22. Water Chemistry Data from Experimental 100x J-13 Well Water (BSC 2001 [DIRS 155640])

Constituent	Units	Synthetic 100x J-13 Well Water	Evaporated Synthetic 100x J-13 Well Water
Ca	mg/L	5	36
Mg	mg/L	2	0
Na	mg/L	4,032	76,314
K	mg/L	513	10,832
NO_3	mg/L	732	14,085
CO_3 (as HCO_3)	mg/L	4,142	54,614
Cl	mg/L	730	14,419
F	mg/L	208	3,630
SO_4	mg/L	1,632	29,783
pH	pH	N/R	N/R

Source: DTN:LL000202905924.117 [DIRS 144913], Table S00134_002.

NOTE: N/R = not reported. "100x" J-13 Well Water is an approximate synthetic equivalent of J-13 Well Water concentrated by a factor of 100. It is subject to mineral precipitation relative to the unconcentrated water. Also, in general, even in the absence of such precipitation, it is difficult to prepare "concentrated" synthetic waters that exactly match the specified concentration factor for all dissolved components. Therefore, deviations are to be expected.

Table 4-23. Water Chemistry Data from Topopah Spring Tuff Pore Water Evaporation Experiment of Rosenberg et al. (1999 [DIRS 125339])

Constituent	Units	Synthetic Pore Water	Evaporated Synthetic Pore Water (Reported Concentration Factor: 1243x)
Ca	mg/kg	57.2	15,629
Mg	mg/kg	11.7	5,478
Na	mg/kg	8.2	5,961
K	mg/kg	4.2	2,779
SiO_2	mg/kg	9.8	513
NO_3	mg/kg	11.0	Not measured
HCO_3	mg/kg	16.2	<35
Cl	mg/kg	78.0	53,084
F	mg/kg	2.3	<577
SO_4	mg/kg	81.7	2,077
pH	pH	7.68	6 to 6.5[a]

Source: DTN: LL991008004241.041 [DIRS 120487], Table S00002_002.

[a] Estimated from pH paper.

Table 4-24. Water Chemistry Data from 95°C Evaporation Based on Experiments by Alai et al. (2005 [DIRS 176811])

Sample	pH	C (mg/kg)	Ca (mg/kg)	Mg (mg/kg)	Si (mg/kg)	Na (mg/kg)	K (mg/kg)	F^- (mg/kg)	Cl^- (mg/kg)	NO_3^- (mg/kg)	SO_4^{2-} (mg/kg)
FEC9 Initial Solution	9.65	9.52	63.09	24.64	39.03	65.31	6.86	1.13	115.42	21.89	118.40
FEC9-1	N/R	3.73	50.23	15.74	25.86	69.84	6.36	N/D	117.22	24.43	177.27
FEC9-2	N/R	2.95	65.76	7.56	17.59	71.48	6.75	N/D	126.24	24.61	186.80
FEC9-3	N/R	1.39	76.55	6.21	17.04	84.51	7.79	N/D	144.02	27.77	213.77
FEC9-4	7.94	N/D	92.70	7.17	19.56	101.64	9.62	N/D	180.43	32.66	269.08
FEC9-5	7.18	N/D	124.40	9.37	24.86	136.27	13.16	N/D	246.99	42.96	358.51
FEC9-6	7.57	N/D	174.43	13.55	32.21	212.01	20.11	N/D	355.17	71.00	435.84
FEC9-7	7.15	N/D	420.68	59.86	56.07	961.04	95.58	N/D	1715.03	316.16	856.03
FEC12 Initial Solution	7.52	2.85	196.28	14.93	38.98	264.50	20.79	N/D	349.35	86.17	450.23
FEC12-1	8.6	1.91	187.64	14.67	38.79	252.48	22.73	N/D	346.91	81.82	445.27
FEC12-2	8.29	N/D	204.71	14.67	40.88	276.35	22.06	N/D	380.69	86.38	490.83
FEC12-3	7.91	N/D	217.26	14.97	42.44	293.30	26.16	N/D	404.54	89.79	519.82
FEC12-4	7.87	N/D	261.28	17.16	49.58	351.67	30.06	N/D	483.07	104.37	619.63
FEC12-5	7.59	N/D	299.42	19.74	57.32	399.66	34.74	N/D	571.74	118.52	733.49
FEC12-6	7.19	N/D	369.91	24.12	70.78	494.35	44.71	N/D	674.36	141.47	861.84
FEC12-7	7.61	N/D	465.92	30.63	88.89	622.26	55.49	N/D	878.35	180.69	1121.06
FEC12-8	7.47	N/D	703.88	46.37	133.69	946.55	88.61	N/D	1337.75	273.04	1686.87
FEC12-9	7.32	N/D	892.08	108.72	219.93	2388.30	219.18	N/D	3438.87	689.94	2229.13
FEC13 Initial Solution	8.91	N/A	984.90	47.44	45.30	2655.30	233.16	N/D	3913.24	713.20	2369.10
FEC13-1	7.69	2.29	861.43	25.41	62.23	2520.01	253.11	N/D	3673.84	723.66	2133.78
FEC13-2	7.07	N/D	816.73	21.58	79.59	3106.64	343.63	N/D	4514.17	1005.53	2162.54
FEC13-3	6.99	N/D	806.94	23.48	93.57	3551.67	488.38	N/D	5329.13	1220.95	2291.96
FEC13-4	6.4	N/D	1067.36	36.82	116.93	5342.15	514.13	N/D	6968.52	1758.83	2641.75
FEC13-5	6.21	N/D	1129.60	61.79	174.35	10136.08	965.39	N/D	12568.95	2755.90	3012.90
FEC13-6	6.34	N/D	1295.26	81.76	177.18	13579.10	1543.86	N/D	18498.13	4363.83	3920.42
FEC13-7	N/A	N/A	1562.73	144.69	164.21	24459.44	2529.91	N/D	32602.68	7407.33	5199.70
FEC14 Initial Solution	9.2	1.14	1526.00	47.50	6.06	26120.00	2920.20	N/D	34570.00	7568.00	5306.00

Table 4-24. Water Chemistry Data from 95°C Evaporation Based on Experiments by Alai et al. (2005 [DIRS 176811]) (Continued)

Sample	pH	C (mg/kg)	Ca (mg/kg)	Mg (mg/kg)	Si (mg/kg)	Na (mg/kg)	K (mg/kg)	F^- (mg/kg)	Cl^- (mg/kg)	NO_3^- (mg/kg)	SO_4^{2-} (mg/kg)
FEC14-1	8.076	2.16	1502.64	42.29	8.03	23745.76	2849.49	N/D	35569.00	7560.40	5147.11
FEC14-2	7.82	1.91	1560.31	43.22	5.07	28355.77	3286.61	N/D	41265.33	8728.80	5495.45
FEC14-3	7.476	1.80	1582.88	45.89	3.87	31384.29	3704.44	N/D	46709.21	9807.63	5769.02
FEC14-4	7.899	1.62	1604.16	48.92	3.11	35927.98	4196.48	N/D	52933.06	11037.26	6045.48
FEC14-5	7.772	1.43	1441.55	58.53	2.54	46833.81	5433.50	N/D	67693.84	14536.17	5963.89
FEC14-6	7.946	1.67	1285.14	68.23	2.00	58547.10	6853.68	N/D	84816.01	17946.98	6094.84
FEC14-7	7.376	1.40	859.27	89.04	1.31	81355.19	9354.63	N/D	118357.80	24771.17	6134.05
FEC14-8	6.87	1.08	536.62	107.69	0.90	104956.33	11904.63	N/D	152147.77	31899.97	6624.71
FEC14-9	6.971	2.34	327.93	136.84	0.58	109976.25	16720.12	N/D	155665.47	45055.42	8159.11
FEC14-10	7.322	2.08	267.57	142.63	0.35	110927.67	20577.06	N/D	151939.13	57400.04	8480.66

Source: DTNs: LL030106923121.018 [DIRS 177573] (file: *LL030106923121.018,FEC13.xls*, tab: "TDMS Data Experiment FEC13"); LL030107023121.019 [DIRS 177574] (file: *LL030107023121.019.FEC9.xls*, tab: "TDMS Data Experiment FEC9"); LL030107123121.020 [DIRS 177575] (file: *L030107123121.020,FEC12.xls*, tab: "TDMS Data Experiment FEC12"); LL030408523121.028 [DIRS 177576] (file: *FEC14.apr20.xls*, tab: "TDMS Data Experiment FEC14").

NOTE: N/R = not reported; N/A = not analyzed; N/D = not detected.

Table 4-25. Sample Data for Evaporated Seawater

Brine	*T* (°C)	Den.[a] (mg/cm^3)	pH	*IS*	Deg. of Ev.[b]	Total Concentration (molal)						
						Cl	Br	SO_4	Mg	Ca	K	Na
w63	28.4	1024	8.19	0.72	0.95	0.579	0.000883	0.0294	0.0520	0.00987	0.0107	0.497
w64		1024		0.73	0.98	0.585	0.000917	0.0303	0.0541	0.00985	0.0111	0.497
w49	28.6	1028	8.12	0.75	1.10	0.594	0.000931	0.0305	0.0604	0.0108	0.0120	0.506
w53	29.9	1028	8.15	0.83	1.17	0.649	0.00099	0.0339	0.0642	0.0118	0.0132	0.582
w57	30.0	1040	8.33	1.21	1.75	0.947	0.00149	0.0518	0.0965	0.0192	0.0179	0.839
w54	32.6	1050	8.43	1.5	2.26	1.21	0.00177	0.0615	0.124	0.0210	0.0219	1.01
w55	29.6	1060	8.53	1.79	2.68	1.44	0.00224	0.0781	0.147	0.0247	0.0266	1.22
w52	30.4	1075	8.35	2.23	3.16	1.79	0.00285	0.0956	0.174	0.0316	0.0348	1.60
w56	31.4	1088	8.11	2.48	3.53	2.03	0.00305	0.110	0.194	0.0401	0.0392	1.71
w51	30.2	1103	8.14	2.98	4.36	2.49	0.00375	0.123	0.240	0.0325	0.0468	2.16
w50	29.8	1141	7.85	3.95	6.07	3.50	0.00536	0.138	0.334	0.0171	0.0623	2.93
w58	32.3	1151	7.70	4.41	6.91	3.87	0.00584	0.156	0.381	0.0185	0.0723	3.36
w48	28.8	1181	7.60	5.37	8.45	4.90	0.00733	0.184	0.466	0.0123	0.0905	4.17
w59	32.6	1181	7.56	5.39	8.62	4.90	0.00722	0.175	0.475	0.0121	0.0877	4.21
w61	32.1	1187	7.53	5.46	9.03	4.90	0.00757	0.190	0.498	0.0107	0.0914	4.22
w46	33.2	1215	7.42	6.25	10.5	5.67	0.00880	0.205	0.579	0.00610	0.112	5.00
w62	34.1	1215	7.43	6.34	11.0	5.88	0.00938	0.232	0.604	0.00581	0.109	4.83
w37	29.5	1220	7.41	6.49	12.6	5.91	0.0108	0.254	0.691	0.00433	0.115	4.70
w43	32.5	1220	7.45	6.68	13.2	5.75	0.0119	0.274	0.728	0.00352	0.152	5.02
w35	28.9	1224	7.44	6.88	15.1	6.04	0.0127	0.287	0.830		0.157	4.74
w42	32.8	1224	7.34	6.94	16.4	5.82	0.0138	0.314	0.904		0.180	4.67
w44	31.9	1225	7.40	6.96	17.6	5.72	0.0146	0.328	0.968		0.190	4.48
w34	31.8	1231	7.25	7.27	20.1	5.98	0.0167	0.381	1.11		0.208	4.14
w32	32.0	1231	7.28	7.34	20.4	6.01	0.0174	0.399	1.13		0.212	4.13
w33	30.7	1236	7.22	7.75	23.4	6.08	0.0195	0.446	1.29		0.249	4.11
w30	31.4	1239	7.28	7.61	23.6	5.98	0.0208	0.417	1.30		0.242	3.96
w28	32.4	1239	7.13	7.87	25.4	6.08	0.0195	0.478	1.40		0.253	3.81
w41	32.7	1242	7.22	7.84	26.8	5.85	0.0230	0.450	1.48		0.278	3.72
w45	35.1	1249	7.06	8.42	31.4	5.92	0.0264	0.600	1.73		0.33	3.32
w38	29.6	1254	7.12	8.65	32.8	5.96	0.0287	0.678	1.81		0.339	3.17
w36	29.9	1254	7.03	8.64	34.0	5.83	0.0282	0.632	1.87		0.342	3.19
w40	32.1	1260	7.00	9.01	36.8	5.89	0.0299	0.694	2.03		0.379	3.06
w39	32.6	1260	6.99	9.33	39.4	5.93	0.0331	0.776	2.17		0.402	2.83
36#1				9.29	40.4	5.86	0.0343	0.753	2.23		0.417	2.63
40#1				9.47	43.5	5.74	0.0356	0.796	2.39		0.443	2.31
36#2				9.81	44.8	6.03	0.0384	0.849	2.47		0.449	2.27
40#2				10.1	48.9	5.80	0.0401	0.895	2.70		0.495	1.96
36#3				11.3	58.1	6.10	0.0482	1.11	3.20		0.591	1.37
40#3				11.4	58.6	6.26	0.0481	1.09	3.23		0.588	1.50
40#4				11.9	63.6	6.23	0.0518	1.19	3.50		0.637	1.16
39#1				12.7	66.2	6.62	0.0590	1.21	3.91		0.632	0.842
36#4				13.0	69.2	6.47	0.0598	1.35	3.99		0.754	0.712
40#5				12.3	72.9	7.13	0.0661	0.966	3.76		0.782	0.825
40#6				12.3	78.8	7.38	0.0716	0.763	3.98		0.712	0.545
39#6				12.2	87.9	7.50	0.0777	0.679	4.03		0.565	0.413
39#2				11.8	87.9	6.89	0.0748	0.703	3.96		0.348	0.553
39#3				12.4	93.3	7.50	0.0773	0.664	4.20		0.311	0.500
36#5				12.8	97.1	7.80	0.0828	0.713	4.27		0.597	0.428
39#4				9.53	98.1	5.99	0.0774	0.366	3.35		0.125	0.169

Source: McCaffrey et al. 1987 [DIRS 164481], Tables 1 through 3.

[a] Density of sample.
[b] Degree of evaporation (equivalent to concentration factor, relative to seawater).

Table 4-26. Average Composition of Water from Well J-13

Constituent	Units	Average J-13 Well Water Concentration
Al	mg/L	0.028 [a]
Ca	mg/L	13.0
Mg	mg/L	2.01
Na	mg/L	45.8
K	mg/L	5.04
Si	mg/L	28.5
NO_3	mg/L	8.78
Alkalinity (as HCO_3)	mg/L	128.9
Cl	mg/L	7.14
F	mg/L	2.18
SO_4	mg/L	18.4
Lab pH	standard units	7.41
Field pH	standard units	6.9 and 7.1 [b]
Temperature	Celsius	31 [b]
O_2 (aq)	mg/L	5.5 to 5.7 [b]

Source: DTN: MO0006J13WTRCM.000 [DIRS 151029].

[a] Mean detected value in Table 4-2 (Harrar et al. 1990 [DIRS 100814], p 4.3).
[b] Harrar et al. 1990 [DIRS 100814], p 4.9.

5. ASSUMPTIONS

This section addresses the assumptions built into the IDPS model. There are no upstream assumptions relevant to the IDPS model.

5.1 AIR–WATER INTERFACE

Assumption: The air–water interface is flat.

Basis: Curvature at the air-water interface, such as the curvature of a water droplet or the curvature of a meniscus of water in a pore, affects vapor pressure near the air–water interface (Neiburger et al. 1983 [DIRS 178080], pp. 121 and 122; Walton 1994 [DIRS 127454], Figure 2; Koorevaar et al. 1983 [DIRS 125329], pp. 67 to 68). However, this effect is expected to be small in the drift. According to the Kelvin equation, a radius of curvature on the order of one micron or smaller is needed to alter the vapor pressure by more than 105 (Neiburger et al. 1983 [DIRS 178080], p. 121). Thus, capillary forces under dry conditions (in the range of negative 500-m water pressure head) have a limited effect on H_2O activity in solution (Walton 1994 [DIRS 127454], pp. 3480 to 3481). Because of the limited effect of interface curvature on vapor pressure and the likelihood that the average air–water interface curvature in the drift will be much larger than one micron, this assumption is justified.

Confirmation Status: No further confirmation is required.

Use in the Model: This assumption is used throughout.

5.2 EQUILIBRIUM CONDITIONS

Assumption: The system is in a state of local metastable equilibrium. All aqueous and gas constituents in the model achieve and maintain local equilibrium, and most mineral phases achieve and maintain local equilibrium upon saturation. Several slow-forming and unlikely minerals identified in Section 6.6.2.6 will not precipitate upon saturation or supersaturation. The model can be used, however, to make steady-state non-equilibrium predictions with respect to relative humidity, provided the appropriate inputs are used (Section 6.6.3.3).

Basis: Most chemical reactions included in the model occur rapidly compared to the modeling timeframe. Redox reactions, which generally are not rapid, are not included in the model. Similarly, certain mineral precipitation reactions are not expected to be rapid enough to occur to a considerable degree for the anticipated applications of the model. Mineral precipitation reactions that fall into this category are suppressed, as explained in Section 6.6.2.6, permitting the formation of metastable mineral phases in the model.

Confirmation Status: No further confirmation is required.

Use in the Model: This assumption is used throughout.

INTENTIONALLY LEFT BLANK

6. MODEL DISCUSSION

6.1 MODELING OBJECTIVES

The objective of the IDPS model is to predict the effects of evaporation and deliquescence on the chemical evolution of potential aqueous solutions and mineral deposition within the repository. Specific details of these objectives are described in Section 1. The data used to develop the model are identified in Section 4.1. Data used to demonstrate the model (Section 6.7) are presented in Table 4-26 in Section 4.4. Data used in validation are addressed in Section 7.

In addition to the modeling objectives, five CRs are addressed:

- CR-6489: *Sensitivity studies on form of sepiolite used in ANL-EBS-MD-000074, Rev. 00*. This concern is addressed in Table 6-3.

- CR-6731: *Discrepancy in thermodynamic data for phosphate species*. This concern is addressed in Appendix I.

- CR-6770: *Integrated effect of uncertainties on the implementation of localized corrosion in TSPA has not been evaluated.* This concern is not addressed because integrated effects on downstream models cannot be determined until the downstream models are fully developed.

- CR-7143: *RIT action items associated with AMR ANL-EBS-MD-000045 Precipitates and Salts Analysis*. Review of YMRP criteria is addressed in Section 4.2. In addition, the order of the validation simulations in this report was rearranged to improve flow.

- CR-7721: *Revision of Pitzer interaction parameters for carbonate species.* This concern is addressed in Section 7.1.3 and Appendix I.

6.2 FEATURES, EVENTS, AND PROCESSES INCLUDED IN MODEL

The comprehensive list of features, events, and processes (FEPs) potentially relevant to postclosure performance of the Yucca Mountain repository are summarized in DTN: MO0407SEPFEPLA.000 [DIRS 170760]. The approach for developing an initial list of FEPs, in support of total system performance assessment for the site recommendation (TSPA-SR) (CRWMS M&O 2000 [DIRS 153246]), was documented in *The Development of Information Catalogued in REV00 of the YMP FEP Database* (Freeze et al. 2001 [DIRS 154365]). The initial FEP list contained 328 FEPs, of which 176 were included in TSPA-SR models (CRWMS M&O 2000 [DIRS 153246], Tables B-9 through B-17). To support TSPA, the FEP list was re-evaluated in accordance with the Enhanced FEP Plan (BSC 2002 [DIRS 158966], Section 3.2). Table 6-1 provides a list of FEPs that are included in TSPA models described in this model document. For each of these FEPs, the implementation in TSPA is described in this model document. Details of the implementations are summarized here in the table, including specific references to sections within this document.

Table 6-1 includes all FEP numbers associated with this report and FEPs identified in the TWP (SNL 2007 [DIRS 179287]), Table 3). The TWP (SNL 2007 [DIRS 179287], Table 3) gives the description of the associated FEPS, whereas Table 6-1 below gives the location in this report where the FEP is described.

Table 6-1. TSPA FEPs Included in the IDPS Model

FEP Number	FEPs Subject	Section Where Discussed
2.1.09.01.0A	Chemical characteristics of water in drifts	This model document provides a partial treatment of this FEP in Section 6.6.3.5. The relevant parameters and ranges for this model are listed in Table 4-4. The IDPS model is designed to perform in-drift water chemistry calculations that provide detail required for predicting interactions of water chemistry with in-drift materials. Further disposition of this FEP is addressed in *Engineered Barrier System: Physical and Chemical Environment* (BSC 2005 [DIRS 175083]). The IDPS model lookup table output includes boundary values, abstraction output, and supplemental calculations, as defined in Section 6.6.3.5. Boundary values include temperature, the fugacities of carbon dioxide and oxygen, and the reaction progress. Abstraction output includes pH, activity of water, ionic strength, mass of solvent water remaining, total concentrations of each element, concentrations of select aqueous species that potentially contribute to acid-neutralizing capacity, and amounts of solids precipitating in a given EQ6 simulation. Supplemental calculations include relative humidity, concentration factor, relative evaporation rate, and dilution factor.
2.1.09.28.0A, 2.1.09.28.0B	Localized corrosion on waste package outer surface due to deliquescence/Localized corrosion on drip shield surface due to deliquescence	This model document provides a partial treatment of these FEPs in Section 6.4. The IDPS model is used in *Engineered Barrier System: Physical and Chemical Environment* (BSC 2005 [DIRS 175083]) to predict the composition of water on the waste package and/or drip shield resulting from the deliquescence of salts and dust deposited on these surfaces. The IDPS model lookup table output includes boundary values, abstraction output, and supplemental calculations, as defined in Section 6.6.3.5. Boundary values include temperature, the fugacities of carbon dioxide and oxygen, and the reaction progress. Abstraction output includes pH, activity of water, ionic strength, mass of solvent water remaining, total concentrations of each element, concentrations of select aqueous species that potentially contribute to acid-neutralizing capacity, and amounts of solids precipitating in a given EQ6 simulation. Supplemental calculations include relative humidity, concentration factor, relative evaporation rate, and dilution factor.

Table 6-1. TSPA FEPs Included in Model (Continued)

FEP Number	FEPs Subject	Section Where Discussed
2.1.09.06.0B	Reduction-oxidation potential in drifts	This model document provides a partial treatment of this FEP in Section 4.1.2. The IDPS model is only validated for oxidizing conditions. Oxidizing conditions prevail as long as the equilibrium fugacity of oxygen does not fall far below 10^{-9} bars. Above 10^{-9} bars, the model is insensitive to the value of the fugacity of oxygen; thus, the fugacity in the model is typically set at the approximate atmospheric value of $10^{-0.7}$ bars. The IDPS model lookup table output includes boundary values, abstraction output, and supplemental calculations, as defined in Section 6.6.3.5. Boundary values include temperature, the fugacities of carbon dioxide and oxygen, and the reaction progress. Abstraction output includes pH, activity of water, ionic strength, mass of solvent water remaining, total concentrations of each element, concentrations of select aqueous species that potentially contribute to acid-neutralizing capacity, and amounts of solids precipitating in a given EQ6 simulation. Supplemental calculations include relative humidity, concentration factor, relative evaporation rate, and dilution factor.
2.1.09.07.0B	Reaction kinetics in EBS	This model document provides a partial treatment of this FEP in Section 5.2. In the IDPS model, all aqueous and gas constituents achieve and maintain local equilibrium, and most mineral phases achieve and maintain local equilibrium upon saturation. Most chemical reactions included in the model occur rapidly compared to the modeling timeframe. Redox reactions, which generally are not rapid, are not included in the model. Similarly, certain mineral precipitation reactions are not expected to be rapid enough to occur to a considerable degree for the anticipated applications of the model. Mineral precipitation reactions that fall into this category are suppressed, as explained in Section 6.6.2.6, permitting the formation of metastable mineral phases in the model. Reaction rates themselves are not included in the model because the model is used to develop lookup tables that provide water compositions that are independent of time, i.e., at metastable equilibrium.
2.1.11.08.0A	Thermal effects on chemistry and microbial activity in the EBS	This model document provides a partial treatment of this FEP in Section 6.6.3.5. The IDPS model performs in-drift water chemistry calculations that provide detail required for predicting thermal effects on water chemistry. This model is not used to predict the thermal effects on microbial activity. The IDPS model lookup table output includes boundary values, abstraction output, and supplemental calculations, as defined in Section 6.6.3.5. Boundary values include temperature, the fugacities of carbon dioxide and oxygen, and the reaction progress. Abstraction output includes pH, activity of water, ionic strength, mass of solvent water remaining, total concentrations of each element, concentrations of select aqueous species that potentially contribute to acid-neutralizing capacity, and amounts of solids precipitating in a given EQ6 simulation. Supplemental calculations include relative humidity, concentration factor, relative evaporation rate, and dilution factor.

6.3 SALTS/PRECIPITATES PROCESSES

6.3.1 Evaporation, Relative Humidity, and Salt Precipitation

Within a drift environment, water exists primarily in two phases, liquid and vapor. Because these two phases are in contact with one another throughout time (except when all liquid water vaporizes), Brownian motion causes water molecules to exchange constantly between the two phases. According to the Maxwell-Boltzmann law, a fraction of the molecules in one phase has the energy required to make the transformation to the other phase, and vice versa, for as long as both phases exist (Mahan 1975 [DIRS 125331], pp. 131 to 139).

Under equilibrium conditions, there is no net movement of water molecules from one phase to the other, i.e., the non-zero evaporation rate equals the non-zero condensation rate. For liquid water to be in equilibrium with the vapor phase, the partial pressure of water vapor must equal the saturation vapor pressure of the liquid water.

Relative humidity (*RH*) is the ratio, expressed in percent, of the measured water vapor pressure and the saturated water vapor pressure at the same temperature and total pressure. In porous media or on solid surfaces, the curvature of the air-water interface can affect the saturated water vapor pressure at the interface. However, the effect of curvature is small and is assumed negligible for the IDPS model (Assumption 5.1).

Dissolved salts in water also decrease the saturation water vapor pressure because they reduce the chemical activity of water in the solution. The chemical activity of the water molecule, *a(w)*, is a function of the mole fraction of water in the aqueous solution and is equivalent to the equilibrium relative humidity of the solution (Kinsman 1976 [DIRS 100769], p. 274). As a result, brines reach liquid-vapor equilibrium, and thus stability, at relative humidity values below 100%. This effect on brine stability is included in the IDPS model.

Based on *RH* measurements from the single heater test (Tsang 1999 [DIRS 124334], Section 2.2.2), the *RH* within the potential drift is expected to fall below 99% for many years during the pre- and postclosure periods. As a result, dilute ground water in the unsaturated zone, having an activity of water greater than 0.99, is not expected to be at liquid-vapor equilibrium within the drift during this time. For any dilute ground water that resides or flows into the drift during this period, there is a net transfer of liquid water to the vapor phase that results in increasing concentrations of dissolved salts in the remaining liquid water. If the vaporization rate is rapid compared to the flux of liquid water flowing into the drift, brines will develop within the drift. In addition, if the *RH* is sufficiently low, dissolved salts will precipitate until either a more stable brine develops or all free liquid water evaporates, adsorbs, and/or is incorporated in hydrated salts.

6.3.2 Formation and Chemistry of Brines and Salt Precipitates

As water evaporates from solution, dissolved solids concentrate until they become supersaturated with respect to a solid phase, whereupon, assuming conditions are favorable and precipitation is sufficiently rapid, the solid phase will precipitate. If the solid phase is a binary salt and the normalities of the two reactants are not equal, the reactant having the lower normality will become depleted in solution while the reactant with higher normality will continue to concentrate

(Eugster and Hardie 1978 [DIRS 100743], pp. 243 to 247; Eugster and Jones 1979 [DIRS 123175], pp. 614 to 629). This mechanism is known as a chemical divide (Drever 1988 [DIRS 118564], pp. 235 to 236). A chemical divide determines which reactant concentrations are predominantly controlled by the solubility of a precipitating phase (i.e., those that become depleted in solution) and which reactant concentrations are only partially controlled by a precipitating phase (i.e., those that continue to concentrate in solution despite partial precipitation). It should be noted that the resulting evaporative evolution depends on how close the normalities of the reactants are. If they are close, both reactants will maintain fairly constant concentrations as evaporation and precipitation continue. Eventually, however, the normalities of the reactants will diverge, with the predominant reactant concentrating and the lesser reactant depleting.

The chemical divide during evaporative precipitation is demonstrated by thermodynamic calculations and studies of saline lakes and sabkhas (hardpan salt playas). Garrels and Mackenzie (1967 [DIRS 123636]) thermodynamically simulated the evaporative evolution of Sierra Nevada spring water into a strongly alkaline sodium carbonate brine observed in natural saline lakes in the western United States. In these calculations, calcite precipitated first, depleting the aqueous calcium concentration. Calcite precipitation is an important evolutionary step because the chemical divide for calcium and carbonate determines whether the evaporating water becomes carbonate poor or carbonate rich (Eugster and Hardie 1978 [DIRS 100743], p. 244). In this case, the water became carbonate rich. Next in the calculations, precipitation of sepiolite depleted the magnesium concentration. Continued evaporation resulted in a sodium carbonate brine with a pH near 10 (Garrels and Mackenzie 1967 [DIRS 123636], p. 239).

Studies of saline lakes in the western United States show that alkaline sodium carbonate brines, such as the brine derived by Garrels and Mackenzie (1967 [DIRS 123636]), are common (Eugster and Hardie 1978 [DIRS 100743], p. 240). Many of these same alkaline brines occur in volcanic terrain and have high silica content (Jones et al. 1967 [DIRS 123170]). These waters are also enriched in chloride, sulfate, and to some extent potassium. Studies of naturally occurring brines indicate that potassium is largely removed during evaporative precipitation. The likely mechanisms for this removal are ion exchange reactions on clay minerals, silicate gels, and volcanic glass (Eugster and Hardie 1978 [DIRS 100743], p. 246).

In the late stage of evaporation, the highly soluble components precipitate. In carbonate-rich brines, these salts include, but are not limited to, salts of Na, Cl, SO_4, CO_3, and SiO_2 (Eugster and Hardie 1978 [DIRS 100743], p. 244). The predominant dissolved components in carbonate-poor brines, such as brines resulting from the evaporation of seawater, are Na, Ca, Mg, Cl, and SO_4 (Eugster and Hardie 1978 [DIRS 100743], p. 244). Other dissolved components observed to become enriched in some brines include K, F, Br, Sr, PO_4, and B (Eugster and Hardie 1978 [DIRS 100743], pp. 239 to 241). NO_3, although it is highly soluble, is not mentioned (and perhaps not investigated) in these studies.

The sequence of salt precipitation by evaporation depends on the chemistry of the solution and the environment. The relative and total activities of the dissolved salt species and the solubilities of the solid salt phases determine when a dissolved species becomes supersaturated, when it begins to precipitate, which other species precipitate with it, and which species continue to concentrate in the remaining solution.

The aqueous solubilities of various combinations of binary Na, K, Ca, and Mg salts at 25°C and 100°C (or temperatures near 100°C) are presented in Table 4-6 (Section 4.1). Each value represents the maximum amount of the specified salt that can be dissolved into pure water at the given temperature. These handbook values are useful in assessing semi-quantitatively the relative solubilities of different salts in aqueous solutions containing many different dissolved salts. For example, Table 4-6 indicates that sulfate salts and sodium fluoride are some of the least soluble of these salts.

In naturally occurring brines, high sulfate concentrations are attributed to the dissolution of gypsum in geologic strata or the oxidation of sulfides such as pyrite (Eugster and Hardie 1978 [DIRS 100743], p. 243). In a carbonate-poor (calcium-rich) brine, such as a brine derived from the evaporation of seawater, sulfate precipitates as gypsum or anhydrite before halite precipitates (Kinsman 1976 [DIRS 100769], p. 275). In carbonate-rich alkaline brines, sulfate precipitates as a sodium salt (Eugster and Hardie 1978 [DIRS 100743], p. 246). Based on the data in Table 4-6, sulfate salts would be expected to precipitate prior to halite or other more soluble salts, given approximately equal molar concentrations of sulfate and chloride in the solution.

Another indication of the likely sequence of salt precipitation is evident in the comparison of hygroscopic properties, i.e., the abilities of different brines or salts to absorb water from the air. Deliquescence is the process of dissolution of a solid by absorbing moisture from the air. This process is the reverse of evaporation to dryness and can be modeled as such. Table 4-7 lists literature values of the equilibrium relative humidity of aqueous solutions saturated with a given salt. Lower values in this table imply lower chemical activities of H_2O (see previous section) and therefore higher salt solubilities. This relationship is apparent when comparing the values in Tables 4-6 and 4-7.

For evaporating seawater, when the chemical activity of H_2O falls below 0.93 due to net evaporation of water into air having an *RH* less than 93%, sodium sulfate precipitates (Kinsman 1976 [DIRS 100769], p. 273). In this same water, when the chemical activity of H_2O falls below 0.77 (*RH* less than about 77%), halite precipitates (Kinsman 1976 [DIRS 100769], pp. 274 to 275). Thus, as water evaporates, the chemical activity of water in the brine decreases, forcing less hygroscopic, less soluble salts to precipitate before more hygroscopic, more soluble salts. This sequence is consistent with the properties listed in Tables 4-6 and 4-7 for sodium sulfate and halite.

The sequence of precipitation reactions for a given water upon evaporation can often be reliably predicted using a quantitative evaporation simulation that assumes control by thermodynamic equilibrium or metastable equilibrium. Such a simulation can be performed using a code like EQ3/6. An evaporation simulation is a series of incremental steps in which a small amount of water is removed (or evaporated) at the beginning of a step and the remaining solution is re-equilibrated at the end of the step. If the ion activity product of a salt exceeds the solubility equilibrium constant of the precipitation reaction, the salt will begin to precipitate, assuming the rate of the reaction is sufficiently rapid (Stumm and Morgan 1996 [DIRS 125332], pp. 351 to 359). Insensibly slow precipitation reactions on the time scale of interest can be censored by instructing the code to suppress the reactions, in which case other (metastable) minerals may precipitate instead. For example, amorphous silica may form if quartz is suppressed. In a batch evaporation simulation, an early precipitated mineral may later redissolve as a more lately

precipitated phase competes with it for common chemical components. An evaporation simulation often achieves a final (eutectic) state in which the composition of the last remaining aqueous solution is fixed by a combination of mineral and gas equilibria.

Evaporative precipitation generally results in the precipitation of dissolved components from solution. One exception is carbonate because it can both precipitate and degas. Degassing of carbon dioxide in alkaline brines is represented by the reaction:

$$2HCO_3^- = CO_3^{2-} + CO_2 + H_2O \qquad \text{(Eq. 6.3.2-1)}$$

This reaction causes the pH to rise (Drever 1988 [DIRS 118564], p. 244). The pH rise is enhanced by the decrease in carbon dioxide solubility as salinity increases (Eugster and Jones 1979 [DIRS 123175], p. 614). Carbonate precipitation includes calcite during the early stages of evaporation and various sodium carbonate salts at later stages (Jones et al. 1977 [DIRS 123192], p. 64; Eugster and Hardie 1978 [DIRS 100743], pp. 244 to 246).

For silica, wetting and drying cycles can be responsible for the precipitation observed in alkaline brines. At Lake Magadi in Kenya, complete evaporation causes the formation of silica crusts that do not easily dissolve during the following wetting cycle because of slow kinetics. As a result, only the most soluble salts (e.g., salts of Na, K, Cl, and SO_4) dissolve into the recharged interstitial waters (Eugster and Hardie 1978 [DIRS 100743], pp. 245 to 246).

6.3.3 Potential Brines and Salt Precipitates at Yucca Mountain

A number of simulations and experimental studies have been performed to directly assess evaporative precipitation effects within and near the repository in Yucca Mountain. In these studies, water entering the drift is predicted to have variable composition as a function of time as a result of the boiling/condensation and reaction of both heated and condensed waters with minerals and gases in the fractures of the host rocks (Arthur and Murphy 1989 [DIRS 100699]; Glassley 1994 [DIRS 100741]; Murphy 1993 [DIRS 100804]; Wilder 1996 [DIRS 100792]; Lichtner and Seth 1996 [DIRS 100771]; Glassley 1997 [DIRS 100742]; Hardin 1998 [DIRS 100123], Section 6.2.2). These reacted, or thermally perturbed, fluid compositions could flow down fracture pathways and enter potential emplacement drifts where they could undergo reaction with introduced materials or evaporate, depositing salts (Glassley 1994 [DIRS 100741]; Murphy and Pabalan 1994 [DIRS 100805]; Wilder 1996 [DIRS 100792]; Lichtner and Seth 1996 [DIRS 100771]). The salts deposited and brines that occur within the drifts would depend on the volume, composition, and extent of evaporation of water seeping into the drift over time from the unsaturated zone.

As temperature increases, a number of changes could affect the geochemical behavior of the near-field environment. Mineral stabilities and phase equilibria are temperature dependent, and the rates at which reactions occur generally increase at higher temperatures. Both continuous reactions (such as the gradual dehydration or shift in cation composition of a solid phase) and discontinuous reactions (such as the disappearance of a phase outside of its stability range) occur as temperature increases (Glassley 1994 [DIRS 100741]; Murphy 1993 [DIRS 100804]; Hardin 1998 [DIRS 100123], Sections 5 and 6).

The increased temperatures are predicted to vaporize much of the water in the near-field as an above-boiling zone forms within the drift and in the near-field (Glassley 1994 [DIRS 100741]). This transition would increase the capacity of the system to transport moisture as volatiles and would result in precipitation of dissolved solids from boiling fluids in the near-field. Condensation of water in cooler regions in three dimensions above the repository horizon could dissolve new material, which could be transported through fractures back down into the boiling zone with subsequent boiling and phase precipitation.

Mineral precipitates including salts will form in the drift and near-field due to boiling and evaporation of water. Water undergoing boiling or evaporation or reacting with precipitated salts is predicted to become concentrated in a number of dissolved constituents either in close proximity to, or within, potential emplacement drifts (Hardin 1998 [DIRS 100123], Section 6.2.2). The evolving compositions of these fluids can be predicted by geochemical mass-transfer calculations for simplified systems designed to simulate the vaporization that would occur within a thermally perturbed repository environment. Results from two such calculations (Murphy and Pabalan 1994 [DIRS 100805]; Wilder 1996 [DIRS 100792]; Hardin 1998 [DIRS 100123], Section 6.2.2) are discussed here.

In one calculation (Wilder 1996 [DIRS 100792]; Hardin 1998 [DIRS 100123], Section 6.2.2), J-13 water is predicted to evaporate/boil along a temperature rise from ambient to 95°C at equilibrium with atmospheric gases. This calculation represents 95% evaporation. The second set of calculations (Murphy and Pabalan 1994 [DIRS 100805]) starts with a synthetic J-13 water evaporatively evolved at 75°C (heated J-13 water that has reacted with tuff) and heats it instantaneously to 100°C in equilibrium with atmospheric oxygen and the calculated CO_2 fugacity (this latter parameter value is higher than atmospheric values and was derived from a coupled reactive transport calculation in which both gas and fluid flow were calculated). The compositions resulting from this second set are reported to about 99.6% evaporation. Even though the results of these two calculations are not directly comparable because they represent different compositional systems and different controls on the gas phase, they appear to be roughly consistent. Relative to ambient compositions, these fluids, in general, have high ionic strength values (greater than 1 molal stoichiometric ionic strength for the 99.6% evaporated case); high concentrations of alkalis, chloride, sulfate, and other ligands (F^-, and HCO_3^-); and have high pH (around 9.5).

Because mineral precipitation occurs throughout these calculations (calcite, silica polymorphs, etc.), these compositions do not represent simply concentrated ambient values, but are selectively concentrated. In both sets of calculations, the dissolved Ca content is low (<50 mg/kg) because calcite precipitation removes Ca from the fluid. However, concentrations of elements that do not precipitate in the calculations are orders of magnitude higher than at ambient conditions. For example, at the 99% and 99.6% evaporation points, chloride concentrations are about 100 times and about 250 times higher, respectively, than the average value for J-13 water (Murphy and Pabalan 1994 [DIRS 100805]).

Modeling results of water evaporation indicate that resultant composition may be profoundly affected by the gas phase assumed to be in equilibrium with the evaporating water and by whether the system behaves as open to the atmosphere or in a closed manner (Wilder 1996 [DIRS 100792]; Hardin 1998 [DIRS 100123], Section 6.2.2). In an open system with a fixed

partial pressure of carbon dioxide, J-13 well water evolves to a pH above 9.5 at high degrees of evaporation. Alternatively, in a closed system, the pH falls below 6.8 after a similar extent of evaporation. The results are sensitive to the constraints on CO_2 fugacity (Murphy and Pabalan 1994 [DIRS 100805]), with different solid phases precipitating for lower CO_2 fugacities. When refluxed water is nearly completely evaporated, more calcite precipitates in an open system compared to a closed system (Murphy and Pabalan 1994 [DIRS 100805]). These results emphasize the need to have a model that incorporates consistently the evolution of near-field gas composition and the need to have such constraints defined for each scenario.

In another modeling study, Lichtner and Seth (1996 [DIRS 100771]) used a multiphase, multicomponent, non-isothermal reactive transport code to simulate the evolution, vaporization, and condensation of groundwater through the vertical centerline of the repository during the boiling period. This type of code does not fix local gas fugacities within the grid block, but evaluates them based on multiphase reactions. Their results predict that in the vicinity of the repository, the pH will rise to about 10 and chloride concentration will increase to approximately 100 mg/L in the vicinity of the drift. This predicted pH rise suggests that the repository will behave more like an open system than a closed system with respect to carbon dioxide. Lichtner and Seth (1996 [DIRS 100771]) indicate that a tenfold increase in J-13 fluid concentrations (for elements that do not precipitate in this range) could be a reasonable water composition entering the drift through fractures during the boiling period. Quartz and calcite were predicted to dissolve where water was predicted to condense and to precipitate where water was predicted to evaporate (Lichtner and Seth 1996 [DIRS 100771]).

6.4 BASE-CASE CONCEPTUAL MODEL

The conceptual model for the IDPS model incorporates a set of processes that affect the chemical aqueous composition of water in the repository. These processes, illustrated in Figure 6-1, include evaporation, condensation, deliquescence, exchange of gases with the atmosphere, and salt precipitation and dissolution.

The conceptual model asserts that the controlling variables in the chemical evolution of water within the drift are (1) the drift conditions (specifically, relative humidity, temperature, and gas fugacities) and (2) the starting composition of the water or dust. Interaction of seepage water (or deliquesced water) with EBS materials is not simulated in the base-case IDPS model because the IDPS model focuses on processes associated with evaporative evolution. The effects of EBS material degradation on the evolution of water in the drift is simulated in other models, such as in *Engineered Barrier System: Physical and Chemical Environment* (BSC2005 [DIRS 175083]). The base-case conceptual model also does not consider steady-state flow-through conditions. However, a steady-state flow-through model is discussed in Section 6.6.3.3 and included in the IDPS model output as an alternative conceptual model (Section 6.6.3.5, Table 6-2).

The IDPS conceptual model is based on processes expected to occur within the repository over its lifetime. In the early years, high temperatures and low values of relative humidity are expected to generate dry conditions as water boils away or evaporates completely. Seepage water that enters the drift during this period is expected to vaporize quickly, depositing its dissolved, nonvolatile constituents as salts and minerals.

In addition to these potential salt deposits, dust produced by excavation and construction activities is expected to settle onto the drip shield and waste package surface. Deliquescent salts in the dust can absorb water, resulting in the formation of brines that may be corrosive to these surfaces.

Over time, temperature will fall and relative humidity will rise. At some point, the relative humidity will rise to a point at which the most soluble salts will deliquesce. For pure sodium nitrate at 100°C, the deliquescence relative humidity is around 65% (Table 4-7). Thus, if sodium nitrate is the most soluble and hygroscopic salt deposited from the evaporation of incoming seepage water, wet conditions will persist whenever the relative humidity exceeds 65%. The deliquescence relative humidity for a given salt assemblage will depend on the concentrations of the various salts in the system. If a calcium chloride salt is the most soluble and hygroscopic salt deposited, the critical relative humidity would be around 22% (BSC 2001 [DIRS 155640], p. 29) or lower depending on the abundance of additional soluble components.

As the relative humidity continues to rise with time, the activity of water rises and precipitated salts dissolve either completely or to saturation. For example, halite will dissolve into an initial sodium nitrate brine to maintain saturation with respect to halite. Because the concentration of sodium is already high in the sodium nitrate brine, little halite will dissolve before halite saturation is reached. As the mole fraction of water rises due to increasing relative humidity, the sodium concentration effectively becomes more dilute, allowing for additional halite dissolution. Eventually, this effective dilution process exhausts the halite in the system at a relative humidity near the deliquescence relative humidity for halite, approximately 76% at 80°C (Table 4-7).

In the conceptual model, the effects of relative humidity and temperature on evaporation and dilution processes are reversible. Because the conceptual model is an equilibrium model in which the relative humidity controls the extent of evaporation or dilution, the complete evaporative evolution of the aqueous solution to a final mineral assemblage describes in reverse the deliquescence and sequential dissolution of the mineral assemblage that produces the original incoming water composition. Thus, given the incoming seepage water composition, temperature, and the fugacities of O_2 (always set at atmospheric, as explained in Section 4.1.2) and CO_2, the conceptual model allows a single evaporation calculation to provide predictions of aqueous and mineral compositions for the full range of relative humidity potentially encountered under the specified conditions, regardless of whether relative humidity is rising or falling.

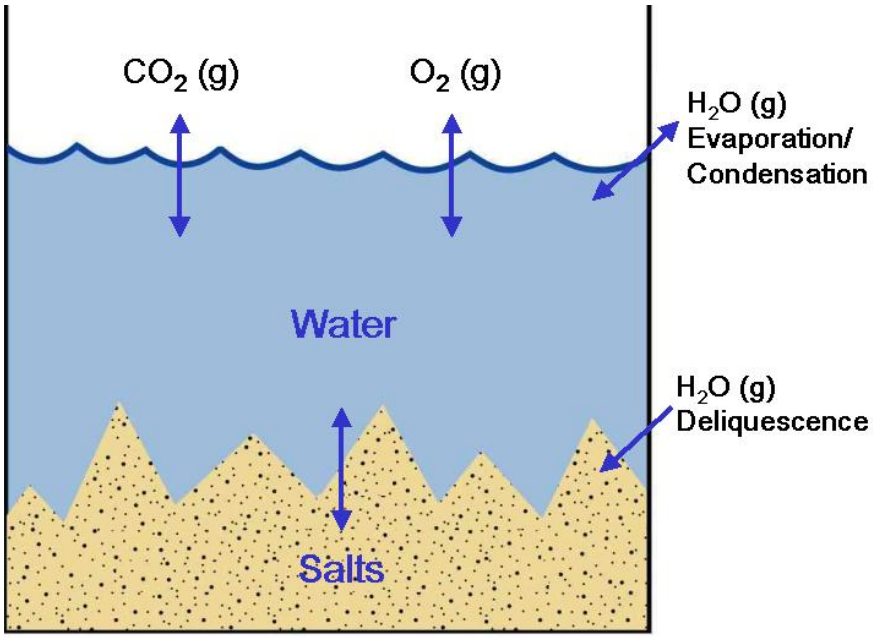

Figure 6-1. Processes Simulated by the IDPS Model

6.5 CONSIDERATION OF ALTERNATIVE CONCEPTUAL MODELS

Uncertainties in the conceptual model arise from an incomplete understanding of system processes. This type of uncertainty is addressed in part by identifying, developing, and evaluating alternative conceptual models.

Table 6-2 lists six alternative conceptual models for the IDPS model, each of which is defined by a unique set of equations. Five of the six are not utilized because they either are not as realistic as the IDPS model, do not provide the types of outputs requested of the IDPS model, or do not cover the necessary ranges of applicability. The one that is utilized, the steady-state alternative conceptual model, is incorporated directly into the IDPS model lookup table output files. Details of the key assumptions of these alternative conceptual models and the associated screening assessments are presented in Table 6-2.

Table 6-2. Alternative Conceptual Models Considered

Alternative Conceptual Model	Key Assumptions	Screening Assessment and Basis
Ion Association Model	Non-ideal ion interaction can be adequately modeled using an ion association approach, such as the Davies equation or B-dot equation.	This model was not utilized because it cannot be used at the high ionic strengths of extensively evaporated natural waters. The IDPS model utilizes a Pitzer ion interaction model, which can be used at high ionic strength and low ionic strength. At low ionic strength, ion association and ion interaction models provide nearly identical results, as illustrated in Section 7.3.
Steady-State Model	The flow-through of incoming seepage water is too rapid to allow local equilibrium with respect to *RH* (Section 6.6.3.3, Figure 6-3).	This model is included in the current IDPS model (Section 6.6.3.3) and cross-referenced in the model lookup tables (Section 6.6.3.5). It can be implemented if two parameter values are determined prior to use: (1) the relative evaporation rate (R^{es}) at the location being modeled, and (2) the composition of the incoming water (or the approximate concentration factor of an incoming water).
Simplified Binary Salt Model	Evaporative evolution of a potential incoming ground water can be approximated by completely precipitating components of lowest normality upon chemical saturation with respect to binary salts as evaporation occurs.	This model is a predecessor to the IDPS model (CRWMS M&O 1998 [DIRS 100358]). Unlike the IDPS model, it does not account for CO_2 dissolution or degassing or the effects of pH, ionic strength, and incomplete depletion of dissolved solids. Also, the simplified binary salt model cannot be used to predict all of the IDPS model outputs, such as pH and concentrations of aqueous species that potentially contribute to acid-neutralizing capacity.
SNORM (Bodine and Jones 1986 [DIRS 162352])	An equilibrium normative salt assemblage at complete evaporation can be predicted from an aqueous solution composition without predicting the evaporative evolution of the aqueous solution.	This model was not utilized because predicting the evaporative evolution of the aqueous solution is the primary modeling objective. SNORM cannot predict the evaporative evolution of the aqueous solution. SNORM also is not capable of making predictions at temperatures other than 25°C or making predictions involving silica or aluminum.
Kinetic Model	Slow reactions are to be modeled using kinetic rate equations.	Kinetic rate equations are not utilized in the IDPS model because the IDPS model is designed to produce model abstractions that are necessarily independent of time. Slow redox reactions are excluded from the IDPS model and sufficiently slow mineral precipitation reactions are prevented by suppression (Section 6.6.2.6). Thus, the IDPS model is a quasi-equilibrium model.
Closed System Model with respect to CO_2	Carbonate exchange with the gas phase via CO_2 degassing or dissolution results in a corresponding increase or decrease of CO_2 in the gas phase.	A closed system with respect to CO_2 is not implemented in the IDPS model because the expected volume ratio of air to water in the drift is so large that CO_2 degassing from, or dissolution into, seepage water in the drift will negligibly affect the CO_2 fugacity compared to the uncertainty in the input value for CO_2 fugacity. A closed system might be appropriate in a wetter climate; however, RH would be ~100% and little or no evaporation would occur. To address this issue further, the IDPS model is used to quantify the output uncertainty resulting from the uncertainty in CO_2 fugacity in *Engineered Barrier System: Physical and Chemical Environment* (BSC2005 [DIRS 175083]).

6.6 MODEL FORMULATION FOR BASE-CASE MODEL

The mathematical IDPS model is designed to simulate the conceptual model. As detailed in Section 1, the intended use of this model is to estimate and tabulate, within an appropriate level of confidence (as defined in Section 7), the effects of evaporative processes and potential environmental conditions on the pH, ionic strength, deliquescence relative humidity, and chemical compositions of water and minerals on the drip shield or other location within the drift during the postclosure period.

The current IDPS model covers two predominant regimes. The first regime occurs at low relative humidity ($RH < 98\%$) where the solubilities of "soluble" salts begin to control the water chemistry. In this regime, incoming seepage water either evaporates completely (e.g., during the boiling period), thereby precipitating all dissolved solids of the seepage water, or it evaporates to a stable brine (e.g., during the early cool-down period). This regime also includes the realm of deliquescence, which occurs when temperature falls and *RH* rises to a level at which a hygroscopic salt is no longer stable in solid form. This first regime generally requires the use of Pitzer equations because the ionic strength of water in equilibrium with the relative humidity ($RH < 98\%$) is generally around 1 molal or higher. This model regime is simulated using the geochemical code EQ3/6 v8.0 and the Pitzer database developed in Appendix I.

In the second regime, *RH* is 98% or higher. In this regime, the steady-state water composition can be more precisely controlled by the ratio of the rates of evaporation and seepage (Q^e/Q^s). This ratio is always less than one in this regime. If it were not, steady-state conditions would either be dry (if *RH* were sufficiently low) or consist of a steady-state brine, either of which is simulated in the first regime. This regime is also simulated using the geochemical code EQ3/6 v8.0. However, the thermodynamic database for this regime can either be the Pitzer database developed in Appendix I or the data0.ymp.R4 thermodynamic database (DTN: SN0410T0510404.002 [DIRS 172712]). While the Pitzer equations are generally not required for this regime, they are accurate at low ionic strengths for major ion chemistry, as shown in Section 7.3.

6.6.1 Mathematical Description of Base-Case Model

The IDPS model uses the code EQ3/6 v8.0 to execute the mathematical formulation of the conceptual model. A general description of the IDPS mathematical model is presented below. A full discussion of the relevant equations is presented in the appendices of the EQ3/6 v8.0 user's manual (SNL 2003 [DIRS 162494]).

EQ3/6 consists of two primary codes, EQ3NR and EQ6. EQ3NR is a speciation-solubility code designed to predict equilibrium aqueous species concentrations and to compute the degree of disequilibrium with respect to mineral phases, oxidation-reduction reactions, and various other phases and reactions. EQ6 is a companion code that takes the results of EQ3NR simulations and performs reaction path calculations, such as evaporation, mineral precipitation, and mineral dissolution.

The governing equations consist primarily of mass balance and mass action equations. Mass balance equations ensure that the total mass of each chemical component (e.g., Na, K, Ca, Mg,

Cl, SO_4, etc.) is conserved, and mass action equations ensure that each chemical reaction involving these components achieves equilibrium, if equilibrium is desired.

The total mass of each component in solution is distributed among all possible aqueous species involving the component and other components in the simulated system. The aqueous mass balance equation for each component is the cumulative mass of the component among all aqueous species multiplied by the appropriate stoichiometric coefficients. For example, the aqueous mass balance equation for F would be:

$$m_{T,F} = m_{F^-} + m_{HF(aq)} + 2m_{HF_2^-} + \ldots \quad \text{(Eq. 6.6.1-1)}$$

where $m_{T,F}$ is the total molality of F and m_i is the individual molality of each aqueous species i in the model. The set of species for a given component includes one basis species and a number of other species, equal to the number of reactions in the database involving the component. For F, the basis species is F^-. All other species involving F are determined from reactions involving the basis species F^-.

The reactions of the basis species are represented by mass action equations. For the chemical reaction:

$$HF_2^- = 2\,F^- + H^+ \quad \text{(Eq. 6.6.1-2)}$$

where "=" denotes a reversible reaction, the mass action equation is:

$$K_{HF_2^-} = \frac{a_{F^-}^2 a_{H^+}}{a_{HF_2^-}} \quad \text{(Eq. 6.6.1-3)}$$

where K_i is the equilibrium constant of species i and a_i is the thermodynamic activity. The equilibrium constant for each species is provided by the thermodynamic database. At equilibrium, the value of the term on the right-hand side of this equation equals the equilibrium constant.

The thermodynamic activity a_i is related to the molal concentration m_i by the equation:

$$a_i = m_i \gamma_i \quad \text{(Eq. 6.6.1-4)}$$

where γ_i is the activity coefficient. The activity coefficient is used to correct for non-ideal behavior that occurs when the aqueous solution is not dilute. Calculation of the activity coefficient depends on the model chosen. For the Pitzer ion interaction model, Pitzer equations are used, as described in Appendix I.

Substituting Equation 6.6.1-4 into Equation 6.6.1-3 gives:

$$K_{HF_2^-} = \frac{m_{F^-}^2 \gamma_{F^-}^2 m_{H^+} \gamma_{H^+}}{m_{HF_2^-} \gamma_{HF_2^-}} \quad \text{(Eq. 6.6.1-5)}$$

This equation shows how the molalities of the reactants and products relate to the reaction equilibrium constant and the mass action equation.

Each mass action equation can be solved for the molality of the non-basis species (e.g., HF_2^-). The resulting functions can then be substituted into the mass balance equations to generate equations in which the only unknowns are the molalities of the basis species. Doing this for each component generates a set of *n* equations and *n* unknowns, which is solved in EQ3/6 using variations of the Newton-Raphson iteration method (SNL 2003 [DIRS 162494]). The solution to these equations provides basis species concentrations that are then used to calculate the concentrations of each non-basis species via the mass action equations. By solving this set of equations simultaneously, the code can calculate equilibrium concentrations for each included chemical reaction while also maintaining mass balance for each component.

In some cases, the total component concentration is not an input. For example, the total hydrogen concentration is not a convenient measurement or bound for an aqueous model. Instead, another parameter, such as pH, is often used as the input value. The activity of the basis species H^+ can be directly computed from the pH using the equation:

$$a_{H^+} = 10^{-\mathrm{pH}} \qquad \text{(Eq. 6.6.1-6)}$$

This value can then be converted to molality using the relation given in Equation 6.6.1-4. Thus, the molality of the basis species H^+ becomes a known value, and the total hydrogen mass balance equation is no longer needed to constrain the system.

In the case of a fixed fugacity of carbon dioxide, the activity of the carbonate basis species HCO_3^- can be determined explicitly from the pH and the equilibrium constant relating HCO_3^- to carbon dioxide. The relevant chemical reaction in the Pitzer database (data0.ypf.R2) developed in Appendix I (Output DTN: SN0609T0502404.012) is:

$$CO_2(g) + H_2O = HCO_3^- + H^+ \qquad \text{(Eq. 6.6.1-7)}$$

which has an associated equilibrium constant $K_{CO_2(g)}$. The mass action equation for this reaction is:

$$K_{CO_2(g)} = \frac{a_{HCO_3^-} a_{H^+}}{a_{CO_2(g)} a_{H_2O}} \qquad \text{(Eq. 6.6.1-8)}$$

When the pH is known, the activity of the hydrogen ion is determined directly from Equation 6.6.1-6. The activity of carbon dioxide is equivalent to the known fixed fugacity. Thus, the only two unknowns in Equation 6.6.1-8 are the activities of HCO_3^- and H_2O.

In dilute solutions (e.g., ionic strength less than 0.1 molal), the activity of H_2O is approximately one, and Equation 6.6.1-8 can be solved directly for the activity of HCO_3^-. Another way to solve for the activity of HCO_3^- is to allow equilibrium with a fixed relative humidity because at equilibrium the activity of H_2O is equivalent to the relative humidity. However, because relative humidity is an output of the titration and not an input, the activity of H_2O must be determined

based on the molalities of all other aqueous species in solution. For EQ3/6, the equation used to calculate the activity of H_2O and its derivation can be found in the EQ3/6 user's manual (SNL 2003 [DIRS 162494], pp. B-28 to B-29). After estimating the activity of H_2O, solving Equation 6.6.1-8 for the activity of HCO_3^-, and converting the HCO_3^- activity to molality using Equation 6.6.1-4, the molality of the carbonate basis species HCO_3^- is no longer an unknown. As a result, the total dissolved carbonate molality mass balance equation is no longer a constraint on the system, and the total molality of dissolved carbonate becomes an output of the model instead of an input.

In the IDPS model, the fugacity of carbon dioxide is fixed in the EQ6 input file. Because EQ6 is a reaction path code and the solution is previously equilibrated using EQ3NR, EQ6 effectively adds or subtracts dissolved carbon dioxide to bring the solution into equilibrium with the fixed fugacity. When CO_2(aq) is added to the solution, it acts like an acid according to the reaction in Equation 6.6.1-7. In accordance with Le Chatelier's principle, the increase in reactants results in an increase in products such that the overall effect on the system is minimized. Thus, addition of CO_2(aq) results in an increase in HCO_3^- and H^+, implying a decrease in pH. Subtraction of CO_2(aq) has the opposite effect. In effect, EQ6 titrates (or "de-titrates") the solution with dissolved carbon dioxide until the fixed fugacity of carbon dioxide is achieved.

Evaporation of water is also a process that is simulated using EQ6. For evaporation, H_2O is incrementally removed from solution. Each incremental removal of H_2O causes the total molalities of the aqueous components to change. As a result, the IDPS model system must be re-equilibrated after each incremental removal of H_2O (i.e., the set of n equations and n unknowns must be solved again using revised total molalities of components). In this way, the evolution of the solution can be predicted as evaporation occurs.

Mineral precipitation also affects the total molalities of aqueous components. Mineral precipitation occurs in EQ6 when the solution becomes supersaturated with respect to a mineral phase. As an example, the anhydrite mineral reaction is presented:

$$CaSO_4(s) = Ca^{2+} + SO_4^{2-} \qquad \text{(Eq. 6.6.1-9)}$$

The corresponding mass action equation is:

$$K_{CaSO_4(s)} = \frac{a_{Ca^{2+}} a_{SO_4^{2-}}}{a_{CaSO_4(s)}} \qquad \text{(Eq. 6.6.1-10)}$$

The mass action equation for a mineral phase does not constrain the model unless the ion activity product (IAP) equals or potentially exceeds the equilibrium constant. The IAP is the term on the right-hand side of the mass action equation as presented in Equation 6.6.1-10. By convention, the activity of a pure solid phase is always one; thus, only the activities of aqueous basis species are important to the IAP.

If the solution to the set of n equations and n unknowns indicates that the IAP of a mineral exceeds the mineral's equilibrium constant, then either the solution will be supersaturated with respect to the mineral or the code will precipitate the mineral. In the IDPS model, suppressed

minerals are allowed to supersaturate while unsuppressed minerals are required to precipitate to saturation. Thus, only unsuppressed mineral phases can constrain the IDPS model system.

Precipitation of a mineral phase moves a portion of the masses of the mineral components from the aqueous phase to the solid phase. This process requires adjustments to the total dissolved concentrations of the precipitating aqueous components and their corresponding mass balance equations. The exact amount of precipitation is determined by iteration. At equilibrium, the IAP for the precipitating mineral equals the mineral equilibrium constant, and the total masses of the mineral's components are conserved between the aqueous and solid phases.

6.6.2 Base-Case Model Inputs and Boundary Conditions

6.6.2.1 Seepage Water Composition

The elements in the model include Na, K, Ca, Mg, Cl, F, C, S, N, Br, Si, Al, H, and O. Except for H and O, the incoming seepage water composition (C_i^s) for each element is defined by the total aqueous concentration of the corresponding basis species. For the Pitzer database, the corresponding basis species are Na^+, K^+, Ca^{2+}, Mg^{2+}, Cl^-, F^-, HCO_3^-, SO_4^{2-}, NO_3^-, Br^-, SiO_2(aq), and Al^{3+}. O and H are found in several of these basis species, but their elemental totals are almost entirely accounted for in the 1 kg of water solvent used to initialize each EQ3/6 simulation. Defining the mass of solvent is necessary for calculating the corresponding masses of the other components from their input concentrations. In addition, the negative log of the activity of the hydrogen ion is defined by entering the pH of the incoming seepage water.

6.6.2.2 Time Period Modeled

The IDPS model is applied to discrete time periods when all inputs are fairly constant. Although inputs are varied during these time periods over their ranges of uncertainty, they are not varied as a function of time. Because the model is an equilibrium model, time itself is not an input.

6.6.2.3 Locations Modeled

The IDPS model can be used to describe evaporative processes at any location where evaporative or condensation processes occur. Possible locations are on the drip shield and on the waste package surface.

6.6.2.4 Temperature, Gas Composition, and Relative Humidity

Temperature, gas composition, and relative humidity in the drift environment will change over time. The thermodynamic database is designed for a temperature range from 0°C to 200°C (though only validated for 20°C to 140°C in the IDPS model). Discrete values are chosen for temperature and the fugacities of oxygen and carbon dioxide. The fugacity of oxygen is set at atmospheric for all applications. Relative humidity, however, is varied over the entire range from 100% to the deliquescence relative humidity below which no water solvent remains. Because relative humidity is not an identified input or output parameter in EQ3/6, the activity of water is the actual parameter that is allowed to vary over this range. The activity of water is

equivalent to the relative humidity at equilibrium (Section 6.3.1). To evaporate a given water to the lowest relative humidity possible, an input value of 0 is entered for the final activity of water.

6.6.2.5 Relative Evaporation Rate

Relative evaporation rate can potentially become important under steady-state flow-through conditions. The relative evaporation rate (R^{es}) [units: nondimensional] is defined by the equation:

$$R^{es} = \frac{Q^e}{Q^s} \qquad \text{(Eq. 6.6.2.5-1)}$$

where Q^e is the steady-state net evaporation rate [units: volume/time] and Q^s is the incoming seepage rate [units: volume/time]. As explained in Section 6.6.3.3, seepage rates that exceed net evaporation rates can create flow-through conditions that generate a steady-state sustained disequilibrium between the relative humidity and the activity of water in the solution.

The model is designed for a range of R^{es} from –99 to 1. Negative values indicate condensation of water vapor. At steady state, the net evaporation rate cannot exceed the seepage rate (i.e., R^{es} cannot exceed 1) without achieving dry conditions.

R^{es} can be directly related to the concentration factor (*CF*) [units: nondimensional] of a conservative ion in the starting water. A conservative ion is an ion that does not precipitate and therefore concentrates in proportion to the concentration factor of the water. For example, if R^{es} is 0.9, then at steady state, the incoming water will evolve to a steady state in which the concentration of a conservative ion is 10 times the incoming concentration, i.e., a *CF* of 10. This relationship is described by the following equation:

$$CF = \frac{1}{1 - R^{es}} \qquad \text{(Eq. 6.6.2.5-2)}$$

Alternatively, a value of –99 for R^{es} is equivalent to *CF* of 0.01. Concentration factors less than one indicate condensation of water vapor. Defining a dilution factor (*DF*) [units: nondimensional] as the inverse of *CF*:

$$DF = \frac{1}{CF} \qquad \text{(Eq. 6.6.2.5-3)}$$

it would follow that the *DF* would be 100 for a R^{es} value of –99, implying that the original starting water is diluted 100-fold by the condensation of pure water vapor.

Because R^{es} is related to *CF* by Equation 6.6.2.5-2, the effects of R^{es} can be assessed by using EQ3/6 to subtract or add a sufficient amount of pure water to achieve the *CF* corresponding to the R^{es} desired. One additional equation is needed for this because *CF* must be calculated from the EQ3/6 output, and there are no conservative ions that stay conservative for the entire range of concentration factors. Therefore, the best estimate of *CF* is provided by the relative amount of solvent water remaining (or accumulating) at each stage of evaporation (or condensation).

Each EQ3/6 simulation is designed to begin with 1 kg of water solvent. Dividing the original amount of water solvent (1 kg) by the amount of water solvent in the system at any point during evaporation or condensation defines the *CF* for the IDPS model. That is:

$$CF = \frac{M^{o}_{H2O}}{M_{H2O}} \qquad \text{(Eq. 6.6.2.5-4)}$$

where M^{o}_{H2O} is the original mass of water solvent in the system (1 kg) and M_{H2O} is the mass of water solvent after evaporation or condensation.

6.6.2.6 Mineral Suppressions

To understand the technical basis for why minerals are included in, or excluded from, applications of the IDPS model, such as applications documented in *Engineered Barrier System: Physical and Chemical Environment* (BSC 2005 [DIRS 175083]), it is important to establish a framework for the selection of suppressed minerals. This framework is established in the subsections below for the anticipated geochemical boundary conditions at Yucca Mountain.

6.6.2.6.1 Geochemical Modeling Methodology

Generally, a reaction path geochemical equilibrium model is constructed using the steps outlined in Figure 6-2. First, a conceptual model is defined where the chemical system and state are defined. Constructing a first-order model tests this system and state. A first-order model generally simulates complete thermodynamic equilibrium. Results of the first-order model are compared with independent experimental, natural analogue, or other modeling data to ensure that the model is reasonable for the system. If mineral phases are predicted to occur that are not appropriate for the system or timeframe being analyzed, then the precipitation/dissolution reactions involving these minerals should be suppressed.

Below is a brief summary of the importance of kinetics in determining whether a mineral phase should be suppressed. Detailed discussions of various aspects of this modeling methodology are documented elsewhere (Bethke 1996 [DIRS 162270]; Smith and Missen 1991 [DIRS 161602]; Van Zeggeren and Storey 1970 [DIRS 161603]).

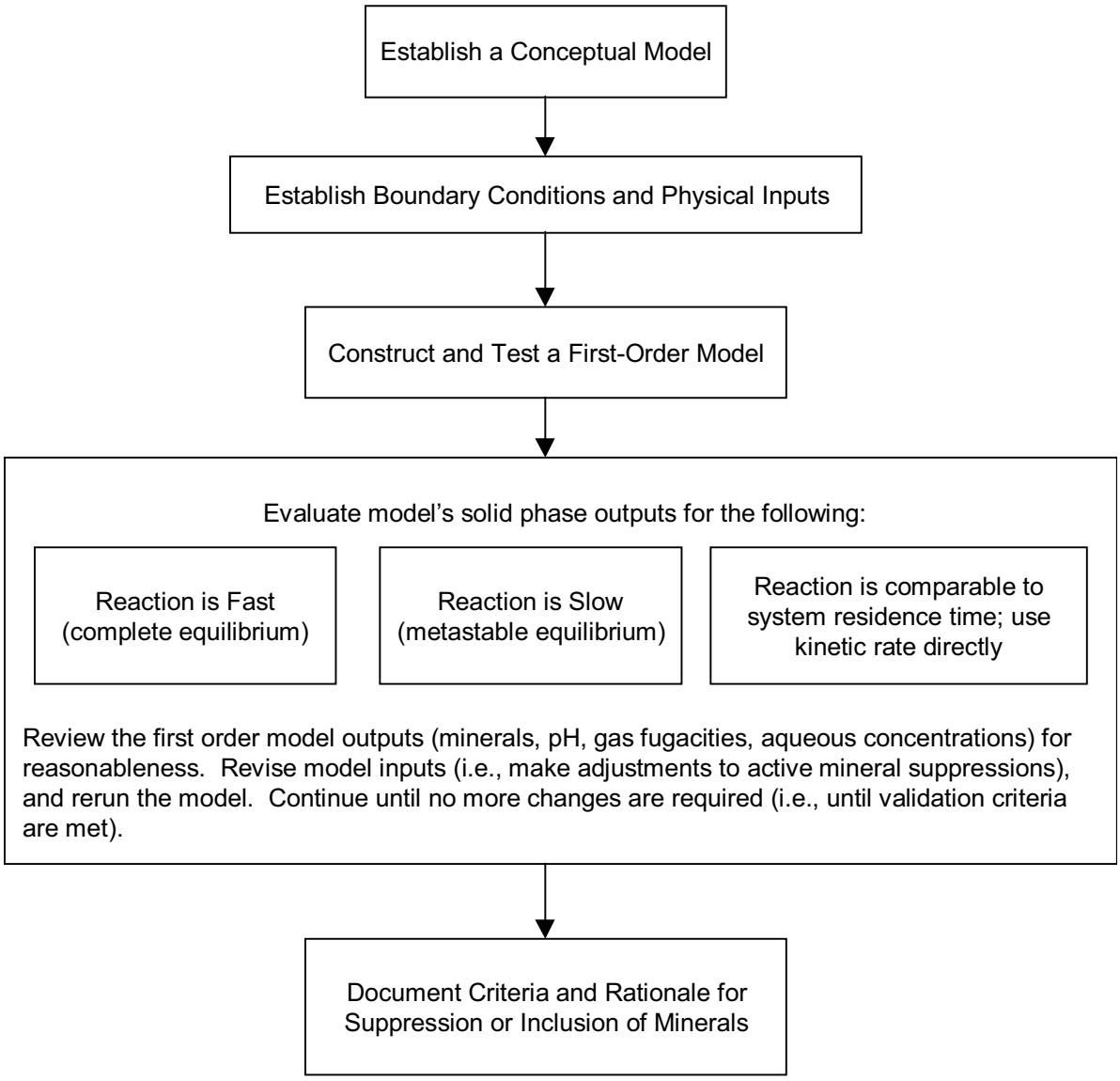

Figure 6-2. General Process Required for a Valid Technical Basis for Mineral Suppression or Inclusion in Geochemical Equilibrium Modeling

6.6.2.6.2 Metastable Equilibrium

The IDPS model is designed to predict long-term chemical processes occurring within the repository drift. "Long-term" for this model can vary from weeks to millennia, consistent with the abstracted time periods that the model is designed to simulate. While relatively short-term occurrences, such as a drop of water falling onto the drip shield, can cause a sporadic divergence from equilibrium for a short time period, a metastable local equilibrium approach is adopted for this model (Assumption 5.2). This approach generally represents the long-term processes that the model is designed to simulate.

An equilibrium reaction path model relies upon a thermodynamic database that contains the standard state and equation-of-state thermo-chemical properties of the different chemical species in a system to determine the chemical reaction equilibria as functions of the changing conditions. In addition to the homogeneous reactions that occur within each phase (e.g., water, gas, solid), there are heterogeneous reactions that involve more than one phase, such as mineral precipitation and degassing of volatile constituents from the aqueous phase.

Most of the reactions in the IDPS model are rapid relative to the timeframe of the modeling period; therefore, most reactions are allowed to reach local equilibrium. However, there are several minerals in the thermodynamic database that are not expected to form under the expected conditions of the repository. These minerals typically require high pressures or high temperatures (i.e., greater than 200°C) in order to achieve the kinetic rates of formation that would produce a considerable mass within the modeling timeframe. In this case, the system can be described by metastable equilibrium. Metastable equilibrium occurs when one or more chemical reactions proceed toward equilibrium at a rate that is so small on the time scale of interest that the system cannot produce a considerable quantity of the product (Bethke 1996 [DIRS 162270], Chapter 2). The rates of nucleation or growth of some minerals frequently fall into this category. This state of metastable equilibrium can be simulated in the IDPS model by suppressing slow reactions.

The pressure in the repository will remain near atmospheric, and the temperature at the drift wall will not likely rise above 200°C (BSC 2005 [DIRS 172862]). These conditions would prevent many minerals in the database from forming at a rate that would produce a considerable mass. By suppressing a mineral that falls into this category, the IDPS model does not allow the mineral to precipitate, allowing for potential supersaturation of that phase. The ability to suppress minerals, therefore, is necessary for equilibrium models that simulate systems in which metastable phases are more likely to occur. By suppressing unlikely minerals, slow kinetic processes can be qualitatively accounted for without knowing the precise kinetic rates of the dissolution or precipitation reactions.

6.6.2.6.3 Mineral Suppression Criteria

The Pitzer thermodynamic database developed in Appendix I contains more than 250 minerals, but only a small number of these are expected to require suppression. It is unnecessary to identify *a priori* every one of the 250-plus minerals that should be suppressed for the IDPS model. The limited range of chemical compositions of the waters likely to occur within the drift dictates that a large number of these minerals will never achieve a chemical potential favoring

precipitation. Preliminary IDPS model simulations for more than 40 different observed and predicted water compositions at Yucca Mountain have been evaporated to dryness, yet fewer than 40 minerals have become saturated or supersaturated with respect to the aqueous composition. Of these, 13 are identified for suppression in the IDPS model (Section 6.6.2.6.4).

A methodology was developed to identify mineral phases to suppress in the IDPS model. Five criteria were developed to assist in determining the justification for suppression in the model in order to account for the kinetic or metastable equilibrium arguments stated above. An affirmative answer to any one of these criteria can be used to justify suppression of the mineral. This methodology used to categorize the minerals in Table 6-3 and Table 6-4 is recommended for categorizing additional minerals when they are initially predicted to precipitate in IDPS model applications. These five criteria, which are not mutually exclusive, are presented below.

Criterion 1. Is the mineral of interest unreasonable for the defined chemical system of the model?

If the mineral lies outside or beyond the defined chemical system of the model, then there is no reason to allow the mineral to precipitate. For example, if the reactions between rainwater and a soil derived from the weathering of mafic minerals were being modeled, a clay mineral that is known to form exclusively from authigenic minerals that are felsic in composition would not be expected. For another example, minerals known only to form at high temperature or pressure would not be expected to form in a low temperature, low pressure system.

These determinations can be made using reference sources such as *Manual of Mineralogy* (Klein and Hurlbut 1999 [DIRS 124293]), *Optical Mineralogy* (Kerr 1977 [DIRS 161606]) or another appropriate reference source that discusses the petrology or mineralogy of a given system or analogue system. One source that could be of use is a resource for the MINTEQA2 software code (Wadley and Buckley 1997 [DIRS 162329]). This source discusses the mineral forms at ambient temperature and pressure and gives comments on their occurrence or formation.

Criterion 2. Is the mineral precipitation or dissolution reaction so slow for the given system that the reaction hardly progresses at all during the timeframe of interest?

When a reaction is much slower than the residence time (for example, 100 times slower than the residence time), the reaction hardly progresses within the modeling timeframe. In this case, suppressing the mineral reaction provides results that would be nearly identical to the results of a kinetic model of the same system.

One of the most commonly suppressed minerals in EBS geochemical modeling is quartz. When precipitation initiates, amorphous phases will tend to form first, and then a process of mineral recrystallization will take place (Langmuir 1997 [DIRS 100051], p. 55). Because precipitation of quartz and other crystalline silica phases is kinetically limited at low temperature and pressure, amorphous silica is generally the metastable phase allowed to precipitate in EBS models. If instead the conceptual model were to account for a longer system residence time or higher temperatures, then the modeler would allow quartz or one of its polymorphs to precipitate.

Criterion 3. Is analytical or natural analogue information available that warrants additional mineral suppressions?

A geochemical modeler can often find information or data from the relevant literature used to develop the conceptual model. This information often comes from analytical data or natural analogue information and could warrant the suppression or inclusion of minerals that might otherwise be dispositioned differently based on an analysis using Criteria 1 and 2. In these instances, the analytical or analogue data justify their use. This criterion allows for additional mineral suppressions that permit the formation of metastable phases observed to occur in the laboratory or natural analogue.

Criterion 4. Do minerals need to be suppressed to test overall model uncertainty or sensitivity due to reported uncertainty in the supporting literature, database, or conceptual model?

For minerals whose potential occurrence is uncertain, simulations can be performed with and without suppressing the minerals to evaluate the sensitivity of the output to these minerals.

Criterion 5. Does the suppression of a mineral whose occurrence is highly uncertain drive the resulting chemical output to a more or less conservative modeling result?

A sensitivity analysis could reveal whether suppression of an uncertain potential mineral results in a more conservative output than inclusion of the mineral, or *vice versa*. If so, the more conservative choice could potentially be justified.

6.6.2.6.4 Mineral Suppressions for the IDPS Model

Relevant natural analogues for mineral assemblages in the IDPS and physical and chemical environment conceptual models are the evaporative mineral assemblages observed by Eugster and Hardie (1978 [DIRS 100743]) and Papke (1976 [DIRS 162274]) in the saline lakes and playa deposits of the western United States. The minerals from these types of evaporitic environments reflect the mineral assemblages that could form in a low-temperature, low-pressure, in-drift environment where the activity of water is below 0.99 and the solution compositions are comparable.

Table 6-3 provides a listing of the minerals that are suppressed in the IDPS model. This list is documented in Output DTN: SN0610T0509206.001. Many of the minerals that have been allowed to precipitate are listed in Table 6-4.

Table 6-3. Mineral Suppressions Included in the IDPS Model

Mineral	Formula	Criterion Selected	Rationale	References
Cristobalite (alpha)	SiO_2	Criterion 2	Cristobalite forms at temperatures greater than 1,470°C. At standard temperatures and pressures, cristobalite will slowly convert to quartz.	Krauskopf 1979 [DIRS 105909], Figure 14-1
Dolomite	$CaMg(CO_3)_2$	Criterion 2	Although dolomite is a common mineral in evaporite deposits from springs derived from carbonate and tuffaceous waters in southern Nevada at Yucca Mountain, its growth mechanism is slow when compared to the precipitation of calcite and Mg-bearing minerals.	Vaniman et al. 1992 [DIRS 107066]
Glaserite	$NaK_3(SO_4)_2$	Criterion 4	Although glaserite is a mineral that is expected to form in evaporitic type deposits, the thermodynamic data in the Pitzer database are questionable.	Suppressed, subject to sensitivity analysis
Magnesite	$MgCO_3$	Criterion 2	Magnesite is commonly associated with metamorphic mineral assemblages such as schist. There are instances where magnesite is associated with salt deposits, yet it is uncertain that it can form under standard temperatures and pressures, as magnesite could be associated with the diagenesis of buried salt deposits. Because it is slow to form and laboratory evaporation experiments are short, this phase is suppressed in the validation simulations.	Klein and Hurlbut 1999 [DIRS 124293], p. 408; Langmuir 1997 [DIRS 100051], p. 195; Eugster and Hardie 1978 [DIRS 100743] Suppressed, subject to sensitivity analysis
Maximum Microcline	$KAlSi_3O_8$	Criterion 1	Microcline is generally associated with the formation of granite, syenite and gneiss at high temperature and pressure. Although it is often found as a common mineral in sandstone or arkose, the occurrence in these instances is detrital and not authigenic.	Kerr 1977 [DIRS 161606], p. 306
Quartz	SiO_2	Criterion 2	Amorphous silica is at metastable equilibrium with respect to quartz at low temperatures and pressures. This is also evidenced by the precipitation of opal-CT (an amorphous silica phase) as opposed to quartz in evaporated carbonate and tuffaceous waters of southern Nevada.	Langmuir 1997 [DIRS 100051]; Vaniman et al. 1992 [DIRS 107066]

Table 6-3. Mineral Suppressions Included in the IDPS Model (Continued)

Mineral	Formula	Criterion Selected	Rationale	References
Sepiolite	$Mg_4Si_6O_{15}(OH)_2$: $6H_2O$	Criterion 2	Unlike the poorly ordered form of sepiolite (represented in the database by Sepiolite(am)) this crystalline form requires several years to form at 25°C. Precipitation of sepiolite is common in conjunction with calcite precipitation in calcrete deposits. Sepiolite is a common fracture-lining mineral above the basal vitrophyre of the Topopah Spring Member at Yucca Mountain and is known to commonly precipitate from evaporation of either carbonate-source or tuff-source waters in southern Nevada. However, because it is slow to form and laboratory evaporation experiments are short, this phase is suppressed in the validation simulations. This approach addresses the concern raised in CR-6489.	Kent and Kastner 1985 [DIRS 162345], p. 1124; Hay and Wiggens 1980 [DIRS 162281]; Carlos et al. 1995 [DIRS 105213]; Vaniman et al. 1992 [DIRS 107066]; Jones 1983 [DIRS 162331]
Talc	$Mg_3Si_4O_{10}(OH)_2$	Criterion 1	Talc is characteristically associated with low-grade metamorphic rock and hydrothermal alteration of ultramafic rocks.	Klein and Hurlbut 1999 [DIRS 124293], p. 514
Ca-saponite Mg-saponite Na-saponite H-saponite K-saponite	$Ca_{0.165}Mg_3Al_{0.33}Si_{3.67}O_{10}(OH)_2$ $Mg_{3.165}Al_{0.33}Si_{3.67}O_{10}(OH)_2$ $Na_{0.33}Mg_3Al_{0.33}Si_{3.67}O_{10}(OH)_2$ $H_{0.33}Mg_3Al_{0.33}Si_{3.67}O_{10}(OH)_2$ $K_{0.33}Mg_3Al_{0.33}Si_{3.67}O_{10}(OH)_2$	Criterion 1	Saponite is a smectite clay. Smectite clays are commonly associated with fracture linings at Yucca Mountain. However, saponitic clays are associated with the weathering of basalt and not rhyolitic tuffs. Saponite also does not generally form independently from its associated parent material.	Krauskopf 1979 [DIRS 105909]; Carlos et al. 1995 [DIRS 105213]; Deer et al 1966 [DIRS 102773]; Borchardt 1995 [DIRS 156639]

Table 6-4. Minerals Allowed to Precipitate in the IDPS Model

Mineral	Formula	Rationale for Inclusion	References
Anhydrite	$CaSO_4$	Anhydrite is associated with evaporite deposits in Nevada playas.	Papke 1976 [DIRS 162274], Table 1; Kerr 1977 [DIRS 161606], p. 221
Antigorite (am)	$Mg_3Si_2O_5(OH)_4$	Precipitates readily upon supersaturation. This phase controls Mg concentration in <100°C basaltic ground waters of Iceland.	Gunnarsson et al. 2005 [DIRS 176844]
Arcanite	K_2SO_4	Arcanite is a highly soluble mineral belonging to the Mascagnite group and can be precipitated in the laboratory from the slow evaporation of water solutions. This mineral is related to thenardite and should have similar properties.	Palache et al. 1951 [DIRS 162280], pp. 398 to 400
Burkeite	$Na_6CO_3(SO_4)_2$	Burkeite is a saline mineral associated with Na-CO_3-SO_4-Cl brines.	Eugster and Hardie 1978 [DIRS 100743], Table 3
Calcite	$CaCO_3$	Calcite is a common evaporite mineral formed from evaporated waters of southern Nevada.	Vaniman et al. 1992 [DIRS 107066]
Carnallite	$KMgCl_3{:}6H_2O$	Carnallite is associated with evaporite deposits in Nevada playas.	Papke 1976 [DIRS 162274], Table 1; Kerr 1977 [DIRS 161606], p. 221
Celadonite	$KMgAlSi_4O_{10}(OH)_2$	Although its occurrence is generally associated with hydrothermally altered mafic volcanic rocks and with illite–chlorite minerals, celadonite is also found as an authigenic silicate mineral in saline, alkaline, nonmarine environments such as playa deposits.	Li et al. 1997 [DIRS 159034]; Hay 1966 [DIRS 105965]
Fluorite	CaF_2	Fluorite is associated with evaporite deposits in Nevada playas.	Papke 1976 [DIRS 162274], Table 1
Glauberite	$Na_2Ca(SO_4)_2$	Glauberite is associated with evaporite deposits in Nevada playas.	Papke 1976 [DIRS 162274], Table 1
Gypsum	$CaSO_4{:}2H_2O$	Gypsum is associated with evaporite deposits in Nevada playas.	Papke 1976 [DIRS 162274], Table 1; Kerr 1977 [DIRS 161606], p. 221
Halite	NaCl	Halite is associated with evaporite deposits in Nevada playas.	Papke 1976 [DIRS 162274], Table 1; Kerr 1977 [DIRS 161606], p. 221

Table 6-4. Minerals Allowed to Precipitate in the IDPS Model (Continued)

Mineral	Formula	Rationale for Inclusion	References
Huntite	$CaMg_3(CO_3)_4$	Huntite is a Mg carbonate mineral associated with cave and evaporite deposits as well as with meteoric (low-temperature) dissolution, and reprecipitation of calcite, dolomite, or magnesite. Huntite will precipitate instead of calcite when Mg^{2+} is concentrated in solutions with respect to Ca^{2+}.	Faust 1953 [DIRS 162282]; Walling et al. 1995 [DIRS 162283], p. 360
Kieserite	$MgSO_4:H_2O$	Kieserite is an evaporite mineral commonly found in salt deposits. Often it is associated with halite or carnallite.	Palache et al. 1951 [DIRS 162280], pp. 477 to 479
Kogarkoite	Na_3SO_4F	Kogarkoite has been shown to form in water upon mixing Na_2SO_4 with NaF at temperatures ranging from 17°C to 35°C.	Linke 1965 p. 1033 [DIRS 166191]
Nahcolite	$NaHCO_3$	Nahcolite is a saline mineral associated with Na-CO_3-Cl brines.	Eugster and Hardie 1978 [DIRS 100743], Table 3
Natrite	Na_2CO_3	Natrite is a highly soluble carbonate mineral associated with shortite, pirssonite, and gaylussite. These three minerals are also associated with the precipitation of trona, calcite, and montmorillonite, and are found in clay beds that have deposited in borax lakes.	Fleischer and Pabst 1983 [DIRS 162284]; Palache et al. 1951 [DIRS 162280]
Niter	KNO_3	Niter is associated with evaporite deposits in Nevada playas.	Papke 1976 [DIRS 162274], Table 1
Pentasalt (Gorgeyite)	$K_2Ca_5(SO_4)_6:H_2O$	Gorgeyite (or goergeyite) occurs in association with glauberite, halite, and polyhalite in salt deposits.	Fleischer and Efremov 1954 [DIRS 162312]
Phillipsite	$K_{0.7}Na_{0.7}Ca_{1.1}Al_{3.6}Si_{12.4}O_{32}: 12.6H_2O$	Phillipsite is a zeolite mineral commonly associated with evaporite deposits.	Hay 1966 [DIRS 105965]
Sellaite	MgF_2	Sellaite is the Mg analogue to fluorite that forms in evaporite deposits.	Palache et al. 1951 [DIRS 162280], pp. 37 to 39
Sepiolite (am)	$Mg_4Si_6O_{15}(OH)_2: 6H_2O$	Precipitation of sepiolite is common in conjunction with calcite precipitation in calcrete deposits. Sepiolite is a common fracture-lining mineral above the basal vitrophyre of the Topopah Spring member at Yucca Mountain. Sepiolite is also known to commonly form on evaporation of either carbonate-source or tuff-source waters in southern Nevada. Poorly crystallized sepiolite precipitates readily at low temperature (~25°C) in alkaline solutions.	Hay and Wiggens 1980 [DIRS 162281]; Carlos et al. 1995 [DIRS 105213]; Vaniman et al. 1992 [DIRS 107066]; Jones 1983 [DIRS 162331]; Wollast et al. 1968 [DIRS 162340]; Kent and Kastner 1985 [DIRS 162345]

Table 6-4. Minerals Allowed to Precipitate in the IDPS Model (Continued)

Mineral	Formula	Rationale for Inclusion	References
SiO_2(am)	SiO_2	Literature evidence suggests that amorphous silica is at metastable equilibrium with respect to quartz at low temperatures and pressures. This is also evidenced by precipitation of opal-CT as opposed to quartz in evaporated carbonate and tuffaceous waters of southern Nevada.	Langmuir 1997 [DIRS 100051]; Vaniman et al. 1992 [DIRS 107066]
Soda Niter	$NaNO_3$	Soda Niter is associated with evaporite deposits in Nevada playas.	Papke 1976 [DIRS 162274], Table 1
Stellerite	$Ca_2Al_4Si_{14}O_{36}$:$14H_2O$	Stellerite is a zeolite mineral commonly associated with fracture linings at Yucca Mountain.	Carlos et al. 1995 [DIRS 105213]
Sylvite	KCl	Sylvite is associated with evaporite deposits in Nevada playas.	Papke 1976 [DIRS 162274], Table 1; Kerr 1977 [DIRS 161606], p. 221
Syngenite	$K_2Ca(SO_4)_2$:H_2O	Syngenite is associated with salt deposits (especially halite) and is known to be precipitated in cavities created by volcanic action. It precipitates at room temperatures from solutions that contain K_2SO_4.	Palache et al. 1951 [DIRS 162280], pp. 442 to 444
Thenardite	Na_2SO_4	Thenardite is associated with evaporite deposits in Nevada playas.	Papke 1976 [DIRS 162274], Table 1
Trona	$Na_3H(CO_3)_2$:$2H_2O$	Trona is associated with evaporite deposits in Nevada playas.	Papke 1976 [DIRS 162274], Table 1

6.6.3 Summary of Computational Model

6.6.3.1 Preparation of Starting Water

The IDPS model starting water is the incoming seepage water or other aqueous solution subjected to evaporation by the IDPS model. For validation or other analyses, starting waters can include synthesized waters used in laboratory evaporation experiments, hypothetical dilute binary solutions of soluble salts, and compositions of water samples collected from the site.

To prepare these starting waters for evaporation, it is usually important to charge balance them. Evaporation will result in precipitation of minerals and degassing of carbon dioxide. Because the minerals and carbon dioxide are neutrally charged, each of these processes removes an equivalent amount of positive and negative charge from the solution. Thus, if the starting water is not charge balanced prior to evaporation, the percent charge balance error (*%CBE*) can increase to unacceptable levels after much of the dissolved solids have precipitated or degassed. If, however, evaporation is minimal and *%CBE* remains within acceptable limits for the simulation, then foregoing charge balancing can be justified on the grounds of honoring the data.

Charge balance can be achieved in EQ3/6 by identifying the dissolved component that has the largest normality and selecting the option to add or subtract this component to achieve charge balance. When charge balancing with a single component, choosing the component with the largest molality minimizes the percentage adjustment of a component concentration. However, a side effect of choosing only one component to adjust is that the concentration of the component could change by many times the *%CBE* and the ratios of this component to each of the other components (to both cations and anions) will change even more. Because the ratios of the components define a water type (Section 6.3.2), this side effect has the potential to bias evaporation calculations. An alternative to this approach is to spread the charge adjustment among several components. For example, adjusting the concentrations of all major cations by $-\%CBE$ and all major anions by $+\%CBE$ will balance the charge, maintain the major anion/anion and cation/cation ratios, and limit the changes in major anion/cation ratios to no more than two times the *%CBE*.

For starting waters in which information is missing or specific measurements are known to be biased, highly uncertain, or below detection limits, other approaches can be justified for charge balancing. Justifiable approaches might include correcting for an identified bias, fixing the fugacity of carbon dioxide to atmospheric values, preventing supersaturation of readily precipitated minerals, or other methods.

6.6.3.2 Simple Evaporation

Evaporative concentration of dissolved solids in solution can be performed using EQ3/6. Water, the designated reactant, is incrementally removed from the solution while the remaining solution is maintained at equilibrium. Depending on mineral saturation indices and interaction with the gas phase, removal of water causes the dissolved ions to concentrate, precipitate, and/or degas.

A simple evaporation mode is used in the IDPS model to predict the evolution of a given water composition at a given temperature and carbon dioxide fugacity as it evaporates. For this mode, there is no solution flowing into the cell and no solution flowing out, as depicted in the

conceptual model illustrated in Figure 6-1 (Section 6.4). The simulation begins with a given starting water composition, the solution is equilibrated with the fixed gas fugacities, all supersaturated unsuppressed minerals are allowed to precipitate, and water is incrementally removed from the system. In EQ3/6 v8.0, "H2O" is declared the aqueous species reactant, and the rate constant (rk1) is set at −1.0. The concentration factor of the evolving solution is calculated from Equation 6.6.2.5-4.

These reactions can be simulated to an ionic strength of about 1 molal using traditional ion activity correction equations such as the B-dot equation (SNL 2003 [DIRS 162494], p. B-32). However, with EQ3/6 v8.0 and the Pitzer database in Appendix I, evaporation for the system Na-K-H-Mg-Ca-Al-Cl-F-NO_3-SO_4-Br-CO_3-SiO_2-CO_2-O_2-H_2O can proceed until there is essentially no free water remaining.

In the simple evaporation mode, the activity of water decreases as water evaporates. Because this mode assumes equilibrium conditions at all times (Assumption 5.2), the resulting activity of water after each incremental decrease in solvent determines the equilibrium relative humidity. As evaporation proceeds to its extreme, the model produces a complete sweep of equilibrium results down to the relative humidity of the dryout point of the solution. In the opposite direction, the model predicts equilibrium results for condensation of water added to an initial seepage water. Condensation predictions can be obtained for dilution factors of 100 or more. Together, the evaporation and condensation results can then be tabulated in a set of lookup tables so that the equilibrium composition can be identified or interpolated for any given equilibrium relative humidity (Section 6.6.3.5).

6.6.3.3 Representation of Steady-State Evaporation with Flow-Through

The IDPS model abstraction for TSPA simulates discrete time intervals in which the seepage rate of water flowing into the drift can be modeled as a constant. If the seepage rate exceeds the evaporation rate, then a steady-state condition can develop such that some of the water will evaporate from the assigned control volume (e.g., a pool) and some will flow out of it. Such a steady-state condition is represented in Figure 6-3. This mode is implemented using results from the simple evaporation mode.

In the simple evaporation mode, the total volume (or mass) of water within the cell (or control volume) decreases with evaporation. This is not the case for the steady-state flow-through mode. In the steady-state flow-through mode, the total volume (or mass) of water in the cell is maintained. At steady state, the flux of water seeping into the cell (Q^s) is equivalent to the sum of the evaporation flux (Q^e) and the flux of water flowing out of the cell (Q^d) (Figure 6-3). As a result, the water composition within the cell will reach a steady-state concentration factor that depends only on the incoming water composition and the relative evaporation rate, R^{es}, as described by Equation 6.6.2.5-2.

For example, from Equation 6.6.2.5-2, a *CF* of 10 implies a R^{es} value of 0.9. This implies that if R^{es} equals 0.9, a conservative constituent in the incoming seepage water will reach a steady-state concentration in the cell that is a factor of 10 higher than the incoming seepage concentration. Thus, whether the incoming seepage undergoes simple evaporation to achieve the *CF* or steady-state flow-through evaporation, there is a unique and identical resulting water

composition and mineral assemblage at the *CF*. The differences between the steady-state result and the equilibrium result at the *CF* are only in the amount of water and total amount of mineral precipitation that accumulate in the control volume.

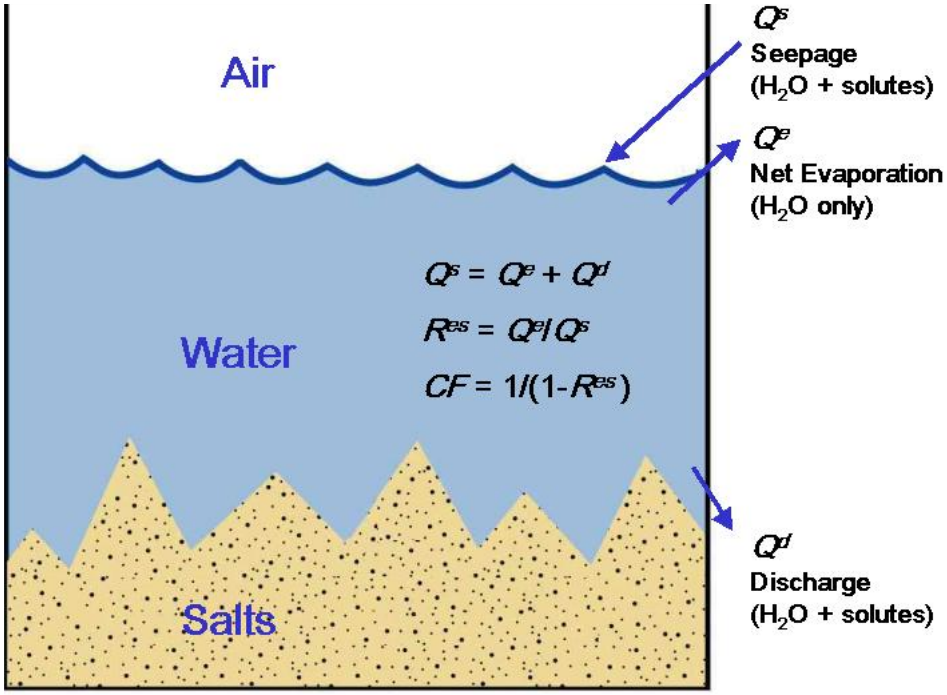

Figure 6-3. Representation of Steady-State Flow-Through for the IDPS Model

In the IDPS model abstractions for TSPA, the time required to reach equilibrium or steady state is negligible compared to the abstraction timeframes to which a given incoming seepage is applied. For simple evaporation, water evaporates quickly when the relative humidity is considerably below 100%. For flow-through conditions, steady-state compositions are nearly achieved after as few as 10 cell flushes (i.e., after the total volume of incoming seepage exceeds 10 cell volumes). Because abstraction timeframes are long compared to the time required for equilibrium evaporation of static water, or 10 cell flushes under flow-through conditions, equilibrium or steady-state assumptions provide reasonable evaporation predictions.

It is possible for steady-state conditions to develop that will prevent equilibrium with *RH*. For example, if the evaporation rate is one half of the seepage rate (i.e., R^{es} equals 0.5), Equation 6.6.2.5-2 dictates that conservative ions will reach a steady-state concentration that is twice the incoming concentration (*CF* equals 2). If the incoming seepage water is dilute, the steady-state activity of water at a *CF* of 2 could be around 0.999 or higher. If this is the case and the relative humidity in the drift is much lower than 99.9%, then steady-state conditions would prevent equilibrium with *RH*.

6.6.3.4 Model Input Files

Two EQ3/6 input files are required to represent the IDPS model. The first is the EQ3NR input file used to define the starting water, as described in Section 6.6.3. The second is the EQ6 input

file used to evaporate the starting water. The EQ3NR pickup file, produced by EQ3NR, must be appended to the corresponding EQ6 input file to initialize the EQ6 simulation. The general formats of these input files are documented in Output DTN: SN0610T0509206.001.

6.6.3.5 Model Output

Application of the IDPS model generates EQ3/6 output files that describe the boundary conditions, equilibrium calculations, and effects of evaporation, condensation, and dust deliquescence on water composition and precipitation of solids. These output files contain much more information than is used in downstream modeling. Lookup tables are generated to summarize the outputs important to the TSPA.

Three types of model output are tabulated in the lookup tables: boundary values, abstraction output, and supplemental calculations. The first two types of output are directly provided in the EQ6 output files. The third type, supplemental calculations, consists of simple algebraic manipulations of the EQ6 output.

Boundary values include temperature, the fugacities of carbon dioxide and oxygen, and the reaction progress. These values are, for all practical purposes, input values. The reaction progress is a measure of the extent of evaporation or condensation that has occurred for a set of equilibrium output values.

Abstraction output includes all EQ6 calculations for the aqueous output variables of direct or indirect interest in the TSPA. It includes the pH, activity of water, ionic strength, mass of solvent water remaining, total concentrations of each element, concentrations of select aqueous species that potentially contribute to acid-neutralizing capacity, and amounts of solids precipitating in a given EQ6 simulation. Although some of this information is not directly used in support of TSPA, this information is useful in understanding how a starting water chemically evolves for a given set of boundary conditions. Direct outputs in support of TSPA are pH, ionic strength, concentrations of Cl and NO_3, the Cl:NO_3 mole ratio, and the deliquescence relative humidity. There is only one value for the deliquescence relative humidity in each table. It is the lowest relative humidity in the table, located in the last row.

Supplemental calculations include lookup table calculations for relative humidity (*RH*), concentration factor (*CF*), relative evaporation rate (R^{es} or Q^e/Q^s), and dilution factor (*DF* or $1 - Q^e/Q^s$). These calculations support the base case equilibrium model (Figure 6-1) and steady-state alternative conceptual model (Figure 6-3). *RH* is calculated by multiplying the activity of water by 100%. *CF* is calculated using Equation 6.6.2.5-4. R^{es} (or Q^e/Q^s) is calculated from an algebraic manipulation of Equation 6.6.2.5-2. Solving Equation 6.6.2.5-2 for R^{es} gives:

$$R^{es} = 1 - \frac{1}{CF} \qquad \text{(Eq. 6.6.3.5-1)}$$

Finally, the dilution factor (*DF* or $1 - Q^e/Q^s$) is calculated by subtracting Q^e/Q^s from one. The value of $(1 - Q^e/Q^s)$ is equivalent to the dilution factor (*DF*) defined in Equation 6.6.2.5-3. This calculation is useful for plotting and visually comparing the results of various EQ6 simulations.

In addition, plotting evaporative evolution as a function of $(1 - Q^e/Q^s)$ generally linearizes the results. This is useful when interpolations must be made because linear interpolation of linearized data can increase the accuracy of interpolations. An example lookup table is presented in Appendix II based on a demonstration in Section 6.7.2.

6.7 DEMONSTRATION OF BASE-CASE MODEL

An example application of the IDPS model is presented in this section to demonstrate how the model is used to produce lookup tables for the TSPA. For this demonstration, an average in situ J-13 well water is used as the incoming seepage composition.

The composition of in situ J-13 well water used in the demonstration is summarized in Table 4-26. This composition originates from a report by Harrar et al. (1990 [DIRS 100814]), in which sample data for individual dissolved components in well J-13 water were compiled and averaged. These averages are documented in DTN: MO0006J13WTRCM.000 [DIRS 151029]. For this example, pH is set at 7.0, which is the average of the two field-measured pH values (6.9 and 7.1) reported by Harrar et al. (1990 [DIRS 100814], p. 4.9). Similarly, for this example, dissolved oxygen is set at 5.6 mg/L, which is within the 5.5 to 5.7 mg/L range reported by Harrar et al. (1990 [DIRS 100814], p. 4.9). The initial temperature is set at 31°C, corresponding to the approximate down-hole temperature (Harrar et al. 1990 [DIRS 100814], p. 4.9). This demonstration is not directly used in performance assessment.

6.7.1 Evaporation of Average In Situ J-13 Well Water

Average in situ J-13 water (summarized in Table 4-26 and described in Section 6.7 above) was evaporated using the IDPS model. For this simulation, EQ3/6 v8.0 and the Pitzer thermodynamic database, data0.ypf.R2 (Output DTN: SN0609T0502404.012, developed in Appendix I), were the code and database used to execute the IDPS model. Because EQ3/6 uses SiO_2 (aq) as the basis species, the input value for Si (28.5 mg/L) was converted to an equivalent amount of SiO_2 (aq) (61.0 mg/L). This conversion required multiplying the input value for Si by the ratio of the molecular weight of SiO_2 (aq) (60.0843 gm/mole) to the atomic weight of Si (28.0855 gm/mole). The molecular weight of SiO_2 (aq) is the sum of the atomic weights of one mole of Si (28.0855 gm/mole) and two moles of atomic oxygen (15.9994 gm/mole). These atomic weights are those provided in the "elements" section of the Pitzer database (Output DTN: SN0609T0502404.012). The temperature for the evaporation was reset at 70°C and the carbon dioxide fugacity was fixed at 10^{-3} bars. The results are documented in Output DTN: SN0611T0509206.006.

Figures 6-4 and 6-5 show the predicted evolution of pH, ionic strength (*IS*), and total concentrations of aqueous constituents as a function of equilibrium *RH* and concentration factor (*CF*). In the model, *RH* reflects the equilibrium activity of water, and *CF* reflects the ratio of the original and remaining masses of H_2O in solution (Equation 6.6.2.5-4). These results show that more than 99% of the H_2O is evaporated before the equilibrium *RH* falls below 99%.

As shown in Figure 6-5, in the early stages of evaporation, Cl, F, K, Na, N, and S concentrate in a linear manner such that the concentration at a given *CF* equals the starting equilibrium concentration multiplied by *CF*. This linear relationship implies conservative behavior (i.e., the

total masses of these components are conserved within the evaporating solution). Departures from conservative behavior are caused by heterogeneous reactions such as precipitation or degassing. At a *CF* around 1100, which corresponds to an equilibrium *RH* of about 95%, F begins to depart from the linear trend. Beyond this point, Cl, K, and N continue to concentrate in a conservative manner until Cl departs from this trend at a *CF* around 26,000. K and N continue to concentrate linearly until the simulation is complete at a *CF* around 50,000 (*RH* around 57%).

Figures 6-6 and 6-7 show the predicted accumulations of precipitating minerals. At the start, calcite, amorphous antigorite, and celadonite are predicted to precipitate. As the solution evaporatively concentrates by a factor of about 7, silica begins to precipitate. At a *CF* of about 1,100, fluorite begins to precipitate, which corresponds to the point at which F departs from the linear trend (Figure 6-5). Further evaporation results in precipitation of kogarkoite, natrite, thenardite, and eventually halite.

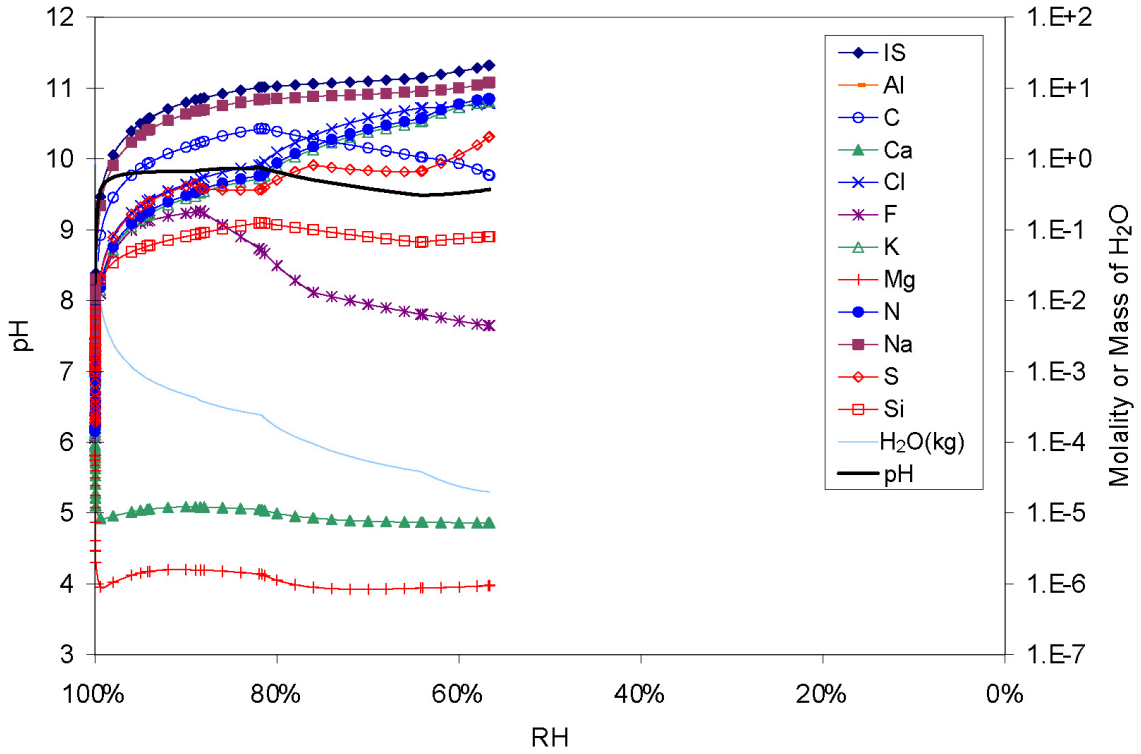

Output DTN: SN0611T0509206.006, file : *j13c3t7e.xls*.

Figure 6-4. Example Aqueous Composition Evaporation Predictions vs. *RH*

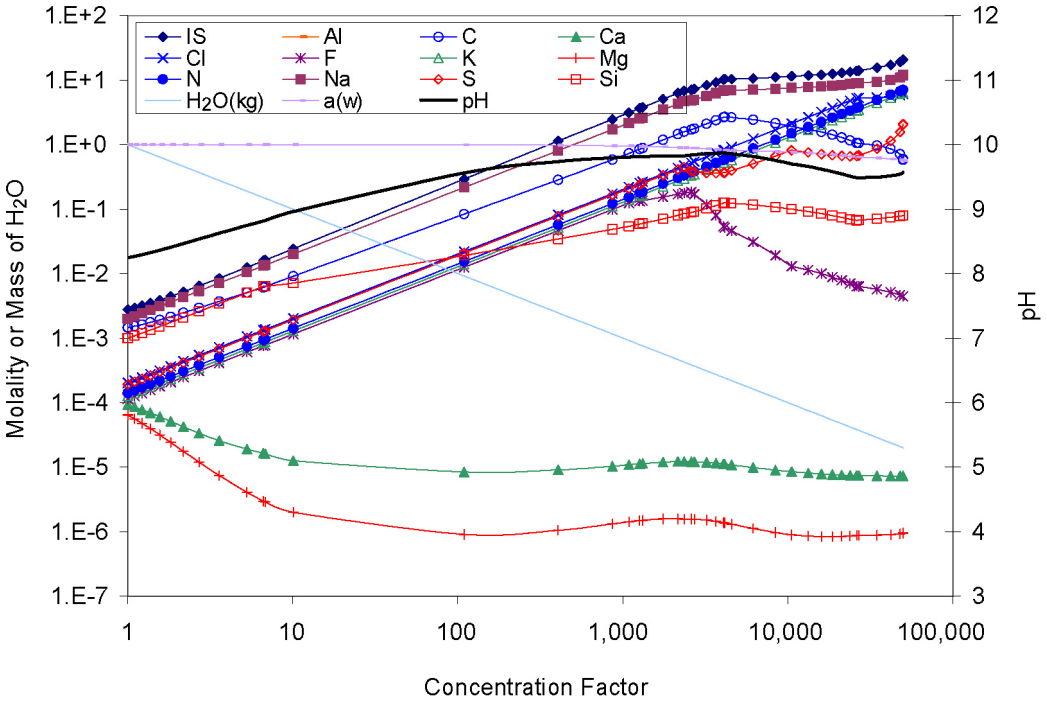

Output DTN: SN0611T0509206.006, file : *j13c3t7e.xls*.

Figure 6-5. Example Aqueous Composition Evaporation Predictions vs. *CF*

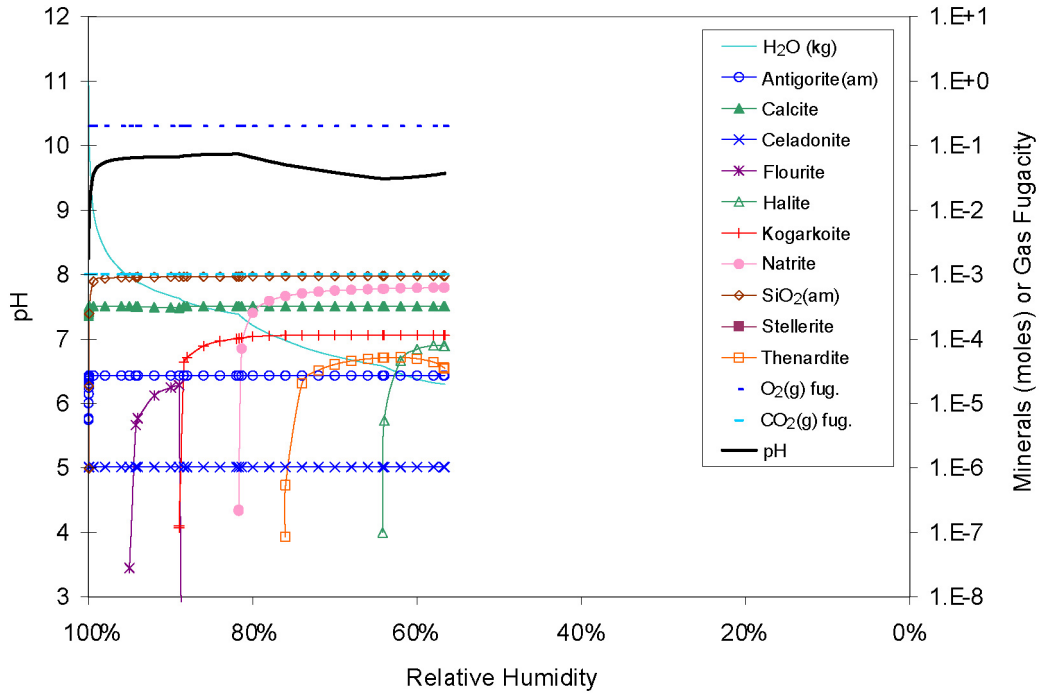

Output DTN: SN0611T0509206.006, file : *j13c3t7e.xls*.

Figure 6-6. Example Mineral Precipitation Evaporation Predictions vs. *RH*

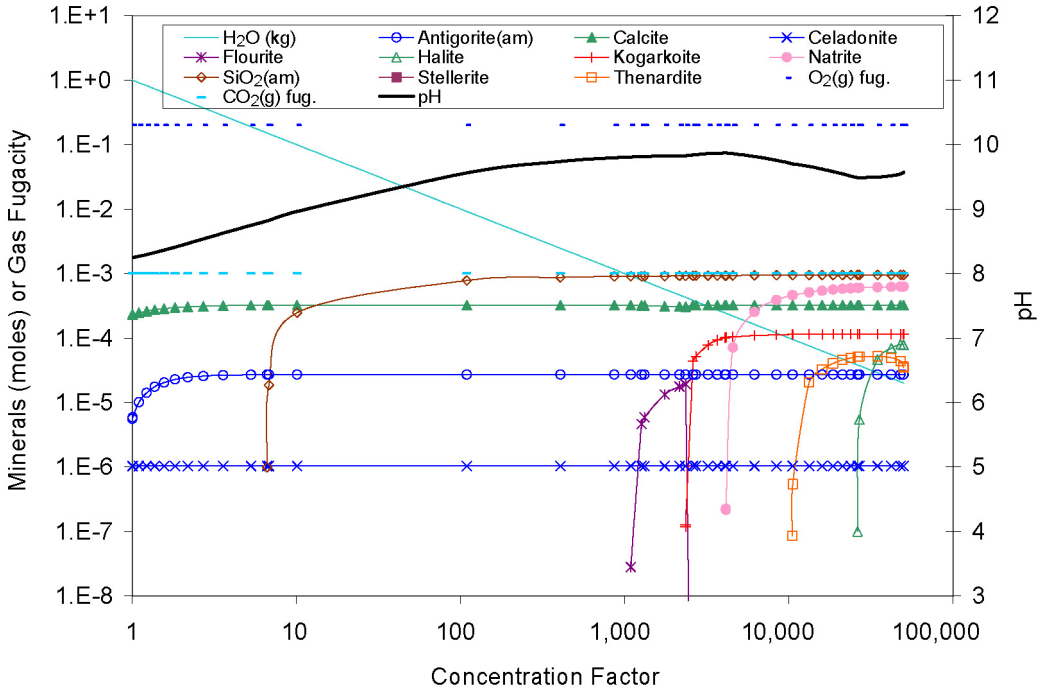

Output DTN: SN0611T0509206.006, file : *j13c3t7e.xls*.

Figure 6-7. Example Mineral Precipitation Evaporation Predictions vs. *CF*

6.7.2 Resulting Model Lookup Tables

As described in Section 6.6.3.5, the IDPS model outputs that are important to the TSPA include boundary conditions, abstraction output, and supplemental calculations. Each evaporation or condensation lookup table is specific to a defined set of boundary conditions. These tables provide snapshots of the output parameter values as the water incrementally evolves due to evaporation or condensation given the defined boundary conditions. Each snapshot is defined by a unique equilibrium *RH*, *CF*, and Q^e/Q^s.

An example lookup table is provided in Appendix II. Appendix II is the lookup table associated with the evaporative concentration of the average in situ J-13 well water presented in Section 6.7.1. This lookup table is documented in Output DTN: SN0611T0509206.006 (file: *j13c3t7e.xls*).

The evaporation lookup table is divided into sections by column. The first three columns are supplemental spreadsheet calculations for concentration factor (*CF*), relative evaporation rate (Q^e/Q^s), and dilution factor (*DF*). These calculations are described in Section 6.6.3.5. The next column is the equilibrium *RH*, calculated by multiplying the activity of water (in column 11) by 100%. The rest of the columns are filled using GetEQData Version 1.0.1. Columns 5 through 8 show reaction progress and the boundary conditions for the starting water, i.e., the temperature and the fugacities of oxygen and carbon dioxide. Columns 9 through 24 show reaction progress, pH, activity of water, ionic strength, mass of H_2O in the reactor, and the total concentrations of the aqueous components. Columns 25 through 38 present reaction progress, mass of H_2O in the reactor, and the concentrations of potential acid-neutralizing species. Finally, columns 39

through 56 are reserved to show the amounts of minerals accumulated in the reactor. The top three rows in these spreadsheets provide a visual check that the correct type of information was entered into each column. The values in the lookup tables may be used to define response surfaces so that interpolations or extrapolations may be obtained for precise input values not provided in the tables.

INTENTIONALLY LEFT BLANK

7. VALIDATION

The IDPS model is a geochemical model designed to predict the postclosure effects of evaporation and deliquescence on the chemical composition of water within the EBS in support of TSPA. This section documents the validation of the IDPS model. Validation is used to generate confidence that the model is appropriate and adequate for the intended use. All data used in the validation are identified in Section 4.4. Section 2.2 of the TWP (SNL 2007 [DIRS 179287]), describes the model validation activities for the IDPS model. The IDPS model is used to represent chemical conditions in the drift, particularly at the drip shield and waste package surfaces. It supports TSPA (indirectly) and is used to evaluate: (1) the chemical environment for waste package and drip shield corrosion, and (2) chemical conditions for radionuclide transport from the waste package to the drift wall. The model is associated with moderate impact on dose estimates. The IDPS, in accordance with Attachment 3 of SCI-PRO-002, has been assigned Level II validation, as discussed in Sections 2.2.2.2 through 2.2.2.4 of the TWP (SNL 2007 [DIRS 179287]). According to SCI-PRO-002 (Attachment 3), the criteria for Level II validation include listed criteria (1) through (6) during development, and two post-development model validation method. Honoring the requirements defined in that procedure, the following steps are adopted for building confidence into the models. As per Section 2.2.2.2 of the TWP (SNL 2007 [DIRS 179287]), two approaches to validation of a model are to be used: (1) validation during model development to establish scientific basis and accuracy for intended use, and (2) validation after model development to support the scientific basis of the model. These approaches and how they were used in the development of the IDPS model are explained below.

Confidence Building during Model Development

As per Section 2.2.2.2 of the TWP (SNL 2007 [DIRS 179287]), development of the model will be documented in accordance with the requirements of SCI-PRO-006. Confidence building (model validation) includes the following requirements:

(1) Selection of appropriate input parameters and/or input data, assumptions, simplifications and physical principles, consistent with the intended use of the model, and discussion of how the selections build confidence.

Data inputs used to develop the IDPS model and associated Pitzer thermodynamic database are presented in Section 4.1. After reviewing a wide range of data, these data were found to be the most reliable and appropriate sources of information and data available for developing the model.

(2) Description of important future state (aleatory), parameter (epistemic), and alternative model uncertainties and how they are represented, commensurate with the intended use of the model.

Uncertainties relevant to the IDPS model are addressed in detail in Section 7.5. Uncertainties are largely determined from comparisons of model predictions of solubilities to independent solubility measurements and from comparisons of the results of evaporation experiments to model predictions. For pH in saline and

brackish water, uncertainties are estimated based on theoretical arguments (Section 7.5.1). The uncertainties presented in Section 7.5 are the overall estimated model uncertainties for the specified output parameters, i.e., they represent the combined uncertainties of aleatory, epistemic, and alternative model uncertainties.

(3) Demonstration that model predictions adequately represent the range of possible outcomes, consistent with important uncertainties and modeling assumptions, conceptualizations, and implementation.

There is high confidence that the range of possible outcomes is adequately represented by the model because the model accurately predicts the general evaporative evolution of synthetic Topopah Spring tuff pore water (Sections 7.2.3 and 7.2.4) and J-13 well water (Sections 7.2.1 and 7.2.2). In addition, it accurately predicts the evaporative evolution of seawater to a highly concentrated brine (Section 7.2.5). Additional confidence that the range of the model is adequate over the potential range of application is demonstrated in Sections 7.1 and 7.2 by the model's ability to predict the solubility of a complete spectrum of soluble salts that could potentially dominate brines generated in the EBS.

(4) Documentation of steps taken to ensure that chosen simulation conditions span the range of intended use, and that such conditions avoid inconsistent results, or that any inconsistencies are adequately explained and demonstrated to have little impact on results.

The range of possible simulation conditions is defined in Section 4.1.2 (Table 4-4) and also in Section 8.4.

Confidence Building after Model Development

As per Section 2.2.2.2 of the TWP (SNL 2007 [DIRS 179287]), development of the model will be documented in accordance with the requirements of SCI-PRO-006, Section 6.3.2. For validation after model development, Section 6.3.2 of SCI-PRO-006 requires that at least one of nine different listed methods be used for model validation. The post-development methods used to validate the IDPS model are:

After development, the IDPS model will achieve the required validation by the following methods:

(1) SCI-PRO-006, Section 6.3.2 (1st bullet): Corroboration of model results with data acquired from the laboratory, field experiments, analog studies, or other relevant observations, not previously used to develop or calibrate the model

For model validation, independent experimental data, showing the combined effects of temperature and relative humidity on water compositions and the effects of complex multi-component systems, as well as independent salt solubility data, were compared to model predictions. These comparisons, presented in Section 7.1, build a high degree of confidence in the model and support its scientific basis.

(2) SCI-PRO-006, Section 6.3.2 (3rd bullet):Corroboration of model results with relevant information published in refereed journals or literature provided that data used to develop and calibrate a model shall not be used to validate a model

For model validation, independent information published in refereed journals or literature, showing the combined effects of temperature and relative humidity on water compositions and the effects of complex multi-component systems, as well as independent salt solubility data, were compared to model predictions. These comparisons, presented in Section 7.2, build a high degree of confidence in the model and support its scientific basis.

(3) SCI-PRO-006, Section 6.3.2 (5th bullet): Technical review, as planned in the TWP (SNL 2007 [DIRS 179287], Section 2.2.2.4).

For model validation, an independent technical reviewer was chosen by group manager of the NFE team. This review was conducted in accordance with SCI-PRO-006, Attachment 4. Documentation to support this technical review is included in Appendix III.

Additional model validation was completed as follows:

(4) SCI-PRO-006, Section 6.3.2 (2nd bullet): Corroboration of model results with other model results (alternative model) obtained from the implementation of other independent mathematical models developed for similar or comparable intended use/purpose.

Additional validation of the model was attained by comparing model results at low ionic strengths (below 1 molal) to results using the qualified data0.ymp.R5 database. This comparison is presented in Section 7.3.

As stated in Section 2.2.2.2 of the TWP (SNL 2007 [DIRS 179287]), the post-development validation of the IDPS model will be performed by comparing model results with measured evaporation test results (Method 1), by comparing model results with data published in handbooks and technical literature (Method 2), and by performing an independent expert technical review (Method 3), as allowed by SCI-PRO-006, Section 6.3.2. Sections 7.1 through 7.3 present model validation simulations to compare with the results of multi-component evaporation experiments, sample data for evaporated seawater, handbook aqueous solubilities and deliquescence relative humidity values of simple salts, and predictions using an alternative mathematical model and database. These sections focus primarily on validating the aqueous outputs of the IDPS model. Section 7.4 draws upon these model validation simulations to document how the IDPS model is validated for mineral outputs. Section 7.5 summarizes the results of the simulations and their implications. Appendix III contains the independent expert technical review.

The experimental data used as validation cases may not be fully representative of possible in-drift conditions. Variations may occur in regard to water compositions, temperatures, and other environmental variables such as the partial pressure of CO_2. Because of this, the validation was conducted using a suite of test data collected under a variety of laboratory conditions

involving aqueous solutions of various chemistries. The validation cases chosen include cases representative of or similar to potential repository conditions, such as evaporation test data for Yucca Mountain groundwater compositions. However, the cases used here also include others to provide tests of the general modeling capability that do not represent and may not be similar to potential conditions in the repository. These cases include data for the solubility of single salt minerals as a function of temperature and data for the evaporation of seawater under normal earth surface conditions. These cases build confidence that the model is free of conceptual or numerical errors, and add confidence to the use of the model when a set of validation data spanning the complete range of potential conditions for the application of interest is unavailable.

Quantitative validation criteria for the IDPS model and their justification are provided in Section 2.2.2.4 of the TWP (SNL 2007 [DIRS 179287]). These criteria are interpreted and/or summarized in Table 7-1. The order-of-magnitude criterion for predicting concentrations is used for all aqueous species except slowly-equilibrating ones, for which the criterion is two orders of magnitude. These validation criteria are reasonable because high degrees of evaporation can cause species concentrations to change by many orders of magnitude. Ionic strength is a function of dissolved concentrations; therefore, the order-of-magnitude criterion is extended to ionic strength. The validation criterion for pH, i.e., prediction of experimental results within one pH unit, is consistent with the order-of-magnitude criterion because one pH unit is equivalent to an order-of-magnitude change in the activity of the hydrogen ion. The IDPS model is also used to predict deliquescence relative humidity (RH_d). The TWP sets a validation criterion of ±15% (*RH* units). In this report, this criterion is lowered to ±10% (*RH* units), which is equivalent to ±0.1 in units of activity of water. This criterion is justified because differences larger than this generally indicate a lack of reliable data to validate or constrain the model.

The IDPS model, in much of its range of application, is considerably more accurate than the validation criteria require. This is can be demonstrated, for example, in its prediction of sodium chloride (NaCl) solubility in water over a temperature range of 0°C to 200°C. The data required to develop the model for sodium chloride are abundant and accurate (to within a few percent or better), and the uncertainty in the sodium chloride data set used for validation is generally accurate and available. In addition, the assumption of rapid chemical equilibrium is valid. On the other hand, the broad range of criteria in Table 7-1 is appropriate in the validation of the IDPS model for several reasons. The data available to develop some parts of the model may be more limited or less accurate than for other parts. This may also be the case for the validation data set, particularly data sets associated with complex, more difficult tests or with more complex chemistries. Also, the assumption of rapid chemical equilibrium is not always applicable for a number of slow-reacting chemical components, species, or minerals.

The equilibrium assumption works well for strongly ionic components, species, and minerals (i.e., usually salt minerals). It breaks down when covalent bonding is involved because kinetic limitations are more likely to become evident. A good example is the precipitation of quartz (SiO_2). Evaporation of a silica-containing water is likely to result in the formation of metastable amorphous silica instead of quartz. Often, suppressing the precipitation of a mineral with known kinetic difficulties and allowing a metastable mineral to form produces a more accurate model. However, in some cases the kinetics may be such that neither assumption of stable equilibrium nor simple metastable equilibrium improves the model.

Table 7-1. Model Validation Criteria

Category of Model Output	Related Components	Related ANC Species	Related Minerals	Experimental Agreement for Aqueous Components and ANC Species	Experimental Agreement for Minerals
pH	H	H^+, OH^-	N/A	pH within 1 pH unit; Concentration within 1 order of magnitude (factor of 10)	N/A
Ionic Strength	Al, Br, Ca, CO_3, Cl, F, K, Mg, Na, NO_3, SiO_2, SO_4	N/A	N/A	Concentration within 1 order of magnitude (factor of 10)	N/A
Deliquescence Relative Humidity (RH_d)	H_2O	N/A	Highly soluble minerals in the system Al-Br-Ca-CO_3-Cl-F-K-Mg-Na-NO_3-SO_4-SiO_2-H-H_2O at potential repository temperatures and pressures	Activity of water within 0.1 of deliquescence relative humidity (RH_d)	Solubility within 1 order of magnitude (factor of 10)
Aqueous concentrations of rapidly equilibrated components and their associated ANC species and minerals	Al, Br, CO_3, Cl, F, K, Na, NO_3, SO_4	HCO_3^-, CO_3^{2-}, HSO_4^-	Unsuppressed potential minerals of the system Al-Br-CO_3-Cl-F-K-Na-NO_3-SO_4-H-H_2O at potential repository temperatures and pressures	Concentration within 1 order of magnitude (factor of 10)	Solubility within 1 order of magnitude (factor of 10)
Aqueous concentrations of less rapidly equilibrated components and their associated ANC species and minerals	Ca, Mg, SiO_2	Ca^{2+}, Mg^{2+}, $CaHCO_3^+$, $MgHCO_3^+$, $MgOH^+$, $HSiO_3^-$	Unsuppressed potential Ca, Mg, and SiO_2 minerals of the system Al-Br-Ca-CO_3-Cl-F-K-Mg-Na-NO_3-SO_4-SiO_2-H-H_2O at potential repository temperatures and pressures	Concentration within 2 orders of magnitude (factor of 100)	Equilibrium solubility within 1 order of magnitude (factor of 10)

NOTE: ANC = acid-neutralizing capability; N/A = not applicable.

Because of the factors discussed above, the validation criteria used here do not necessarily imply large uncertainties in the model outputs. Uncertainties must be individually assessed for the specific applications of the model. In addition, large differences between model predictions and experimental results may not be due to model uncertainty but rather to errors or uncertainty in experimental data or how the data are reported. Experimental uncertainties complicate assessments of model validation and model uncertainty. Often, experimental errors and uncertainties are not quantifiable from published reports. Considerable uncertainties are inherent in methods used to measure or control pH and relative humidity in equilibrium with concentrated salt solutions, especially at high temperature (e.g., Section 7.5.1). As a result, model uncertainties, such as those estimated in Section 7.5, cannot be separated from experimental uncertainty with a high degree of confidence. Thus, the model uncertainties estimated in this report account for both model uncertainties and experimental uncertainties.

Of all the IDPS model output parameters developed and validated in this report, the specific output parameters developed in support of the TSPA are pH, ionic strength, concentrations of Cl and NO_3, the Cl:NO_3 molal ratio, and deliquescence relative humidity (RH_d). TSPA uses pH, Cl, NO_3, and the Cl:NO_3 molal ratio to predict initiation of corrosion of waste package materials. Initiation of localized corrosion is enhanced by high Cl concentrations in the absence of high NO_3 concentrations; hence the importance of the Cl:NO_3 molal ratio. TSPA predicts colloid stability in the invert using IDPS model predictions of pH and ionic strength in the invert. Radionuclide solubility in the invert under diffusive flux conditions is also predicted by TSPA using IDPS model predictions of pH in the invert. The remaining output parameter, RH_d, defines the *RH* below which liquid water cannot persist for the given conditions. Liquid water is required for corrosion and aqueous diffusion. Model uncertainties associated with these output parameters are evaluated and determined in Section 7.5 for propagation into the TSPA. In addition, fluoride concentration model uncertainty is evaluated in Section 7.5. IDPS model predictions of fluoride concentration are not currently used in TSPA but could potentially be used in future calculations to help predict radionuclide solubility in the waste package or invert. Although this report provides the model uncertainties for each of these parameters, it does not determine the nominal predicted values. The nominal predictions for TSPA are derived in *Engineered Barrier System: Physical and Chemical Environment* (BSC 2005 [DIRS 175083]), where the IDPS model is applied.

7.1 EVAPORATION OF SIMPLE SALT SOLUTIONS

Dilute salt solutions were evaporated to assess whether the IDPS model can accurately predict the deliquescence points and aqueous solubilities of salts in simple systems. Solubilities and deliquescence points of binary salts are predicted and compared to literature values in Section 7.1.1, and solubilities of salts in ternary systems are predicted and compared to literature values in Section 7.1.2. Section 7.1.3 addresses the solubility of carbon dioxide and carbonate in simple systems.

Validation comparisons in these simple systems assess the differences between measured and predicted salt solubilities. These comparisons are useful for evaluating model validation and uncertainty when the solution has reached saturation with respect to one or more salts in the system. It is important to note that these comparisons do not allow assessment of uncertainty in solutions that are undersaturated with respect to these salts. At solution concentrations below the measured and predicted solubilities, the model will accurately and precisely predict the effects of evaporation on aqueous salt concentrations.

7.1.1 Binary Salt Systems

In this report a binary salt system is defined as a mixture of pure water and one salt made up of one cation component and one anion component. To demonstrate model validation for predicting aqueous solubilities and deliquescence relative humidity values of individual salts in binary systems, IDPS model simulations were performed to compare against independent data from the literature.

Two sets of literature values are used in these comparisons. The first set is from various chemistry handbook sources. These data are compared to IDPS model predictions in

Section 7.1.1.1. The second set of values comes from non-handbook sources and extends to temperatures above 100°C. These values are compared to IDPS model predictions in Section 7.1.1.2.

7.1.1.1 Comparisons to Chemistry Handbook Data

7.1.1.1.1 Aqueous Solubilities

Table 4-6 lists temperature-dependent solubility values for individual salts in units of mass percent of solute (w_i) as provided in the *CRC Handbook of Chemistry and Physics* (Lide 2000 [DIRS 162229], pp. 8-102 to 8-110). These solubilities are converted to molal concentrations (C_i) in Table 7-2 using the following equation:

$$C_i = \frac{1000 \dfrac{w_i}{100\%}}{MW_i \left(1 - \dfrac{w_i}{100\%} \right)} \qquad \text{(Eq. 7.1-1)}$$

where MW_i is the molecular weight (in grams per mole) of salt i (Lide 2000 [DIRS 162229], p. 8-102).

The EQ3/6 evaporations begin with a 0.0001 molal solution of the particular salt whose solubility is to be estimated. Because the pH of pure water can be affected by the salt dissolved in it and by the temperature, the starting solution is charge balanced on the hydrogen ion. The salt components added to the pure water are inherently charge balanced; thus, charge balancing on the hydrogen ion in these systems reflects a true equilibration process. For evaporations involving carbonate, a closed system is prescribed. An evaporation simulation is complete when the solution reaches saturation with respect to the salt components.

The results of the simulations are documented in Output DTN: MO0701EQ36IDPS.000 and displayed in Table 7-3, Figure 7-1, and Figure 7-2. The table provides the predicted solubilities, relative error with respect to handbook values, and the specific mineral phase that reached saturation at the given temperature. The comparison shows that for every salt in the table, the IDPS model predicted solubility within a factor of 10 of handbook values. Most predictions are within 20%. The implications of these results are discussed in Section 7.2 as applicable.

Three nitrate salts did not reach saturation in the calculations before their simulations became unstable and terminated: $Ca(NO_3)_2$ (100°C), $Mg(NO_3)_2$ (25°C and 100°C), and KNO_3 (100°C). In IDPS model applications, these errors could only happen at low relative humidity (e.g., below 50%) and for those incoming waters whose chemical divides allow extensive concentration of the components of these salts. In the event that one or more of these salts does become concentrated in an application, using the end of the simulation as the maximum solubility is not expected to introduce unacceptable errors compared to the validation criteria. The absolute limit for the concentration of these salts is an ionic strength of 100 molal, which causes EQ6 to terminate the simulation. Thus, however the simulations terminate, the predicted maximum concentrations of these salt components would remain well within one order of magnitude of the actual salt solubilities, meeting validation criteria. For example, for $Mg(NO_3)_2$ at 25°C, the EQ6

evaporation terminates at a Mg concentration of 14.4 molal (Table 7-3). This concentration is only three times the measured solubility at this temperature (Table 7-2). Early termination of a simulation like this is not considered non-convergence because the simulation converges to a satisfactory end point, as defined by the validation criteria.

Table 7-2. Unit Conversion of Chemistry Handbook Aqueous Solubilities of Na, K, Ca, and Mg Salts

Salt	Molecular Weight (gram/mole)	Aqueous Solubility at 25°C		Aqueous Solubility at 100°C	
		Mass Percent of Solute (%)	(molal)	Mass Percent of Solute (%)	(molal)
NaCl	58.44	26.45	6.153	28.05	6.671
KCl	74.55	26.22	4.767	36.05	7.562
$CaCl_2$	110.98	44.83	7.322	59.94	13.482
$MgCl_2$	95.21	35.90	5.882	42.15	7.653
$NaHCO_3$	84.01	9.32	1.22	19.10	2.81
$KHCO_3$	100.12	26.6	3.62	40.45 at 70°C	6.78 at 70°C
Na_2CO_3	105.99	23.5	2.90	30.09	4.06
K_2CO_3	138.21	52.7	8.06	61.0	11.32
NaF	41.99	3.97	0.985	4.82	1.206
KF	58.10	50.4	17.5	60.0 at 80°C	25.8 at 80°C
CaF_2	78.07	0.0016	0.00020	Not reported above 25°C	Not reported above 25°C
MgF_2	62.30	0.013	0.0021	Not reported above 25°C	Not reported above 25°C
Na_2SO_4	142.04	21.94	1.979	29.67	2.970
K_2SO_4	174.26	10.7	0.688	19.3	1.372
$CaSO_4$	136.14	0.205	0.0151	0.163	0.0120
$MgSO_4$	120.37	26.3	2.96	33.3	4.15
NaBr	102.89	48.6	9.19	54.9	11.83
KBr	119.00	40.4	5.70	50.8	8.68
$CaBr_2$	199.89	61.0	7.82	73.0 at 60°C	13.53 at 60°C
$MgBr_2$	184.11	50.6	5.56	55.7	6.83
$NaNO_3$	84.99	47.7	10.7	63.8	20.7
KNO_3	101.10	27.7	3.79	70.8	23.98
$Ca(NO_3)_2$	164.09	59.0	8.77	78.5	22.25
$Mg(NO_3)_2$	148.31	41.6	4.80	72.0	17.34

Output DTN: MO0701EQ36IDPS.000, files: *Salts25.zip* (*Salt solubilities at 25C v4.xls*) and *Salts100.zip* (*Salt solubilities at 100C v4.xls*).

Source: Lide 2000 [DIRS 162229], pp. 8-102 to 8-110.

Table 7-3. Comparison of Model Predictions to Chemistry Handbook Aqueous Solubilities

Salt	Aqueous Solubility at 25°C			Aqueous Solubility at 100°C		
	Predicted (molal)	Relative Error (%)	Mineral	Predicted (molal)	Relative Error (%)	Mineral
NaCl	6.17	0.3	Halite	6.63	−0.6	Halite
KCl	4.87	2.1	Sylvite	7.52	−0.6	Sylvite
$CaCl_2$	7.62	4.1	Antarcticite	13.60	0.8	$CaCl_2:2H_2O$
$MgCl_2$	5.46	−7.3	Bischofite	7.62	−0.4	Bischofite
$NaHCO_3$	0.81	−34.0	Nahcolite	2.35	−16.5	Nahcolite
$KHCO_3$	4.19	15.8	Kalicinite	4.93 at 70°C	−27.4	Kalicinite
Na_2CO_3	2.68	−7.6	Natron	3.43	−15.4	Natrite
K_2CO_3	8.36	3.7	$K_2CO_3:1.5H_2O$	9.54	−15.7	K_2CO_3
NaF	1.37	38.8	Villiaumite	1.34	11.0	Villiaumite
KF	18.77	7.3	Carobbite	16.64 at 80°C	−35.6	Carobbite
CaF_2	0.00030	48.6	Fluorite	0.00033	Not applicable	Fluorite
MgF_2	0.00051	−75.6	Sellaite	0.00028	Not applicable	Sellaite
Na_2SO_4	2.05	3.5	Mirabilite	2.98	0.5	Thenardite
K_2SO_4	0.69	0.3	Arcanite	1.33	−3.0	Arcanite
$CaSO_4$	0.014	−6.5	Gypsum	0.00567	−52.7	Anhydrite
$MgSO_4$	2.65	−10.7	Epsomite	3.70	−10.9	Kieserite
NaBr	10.45	13.7	NaBr	10.99	−7.1	NaBr
KBr	5.23	−8.1	KBr	8.77	1.1	KBr
$CaBr_2$	14.16	81.0	$CaBr_2$	12.64 at 60°C	−6.5	$CaBr_2$
$MgBr_2$	16.27	192.5	$MgBr_2$	13.02	90.6	$MgBr_2$
$NaNO_3$	10.90	1.5	Soda Niter	20.72	−0.1	Soda Niter
KNO_3	2.74	−27.7	Niter	>16.3[a]	> −32.2	None
$Ca(NO_3)_2$	8.80	0.4	$Ca(NO_3)_2:4H_2O$	>18.4[a]	> −17.5	None
$Mg(NO_3)_2$	>14.4	>200.4	None	>13.7[a]	> −20.8	None

Output DTN: MO0701EQ36IDPS.000, files: *Salts25.zip* (*Salt solubilities at 25C v4.xls*) and *Salts100.zip* (*Salt solubilities at 100C v4.xls*).

[a] Concentration at the minimum activity of water achieved in the simulation.

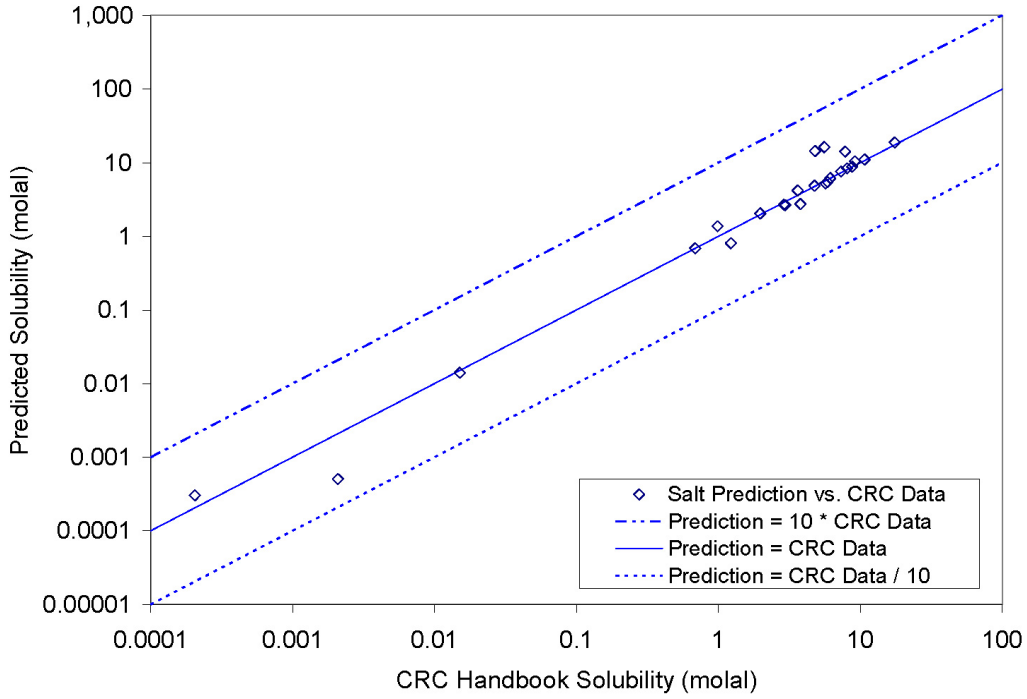

Output DTN: MO0701EQ36IDPS.000, file: *Salts25.zip*, *Salt solubilities at 25C v4.xls*.

Figure 7-1. Predicted vs. Chemistry Handbook Mineral Solubilities at 25°C

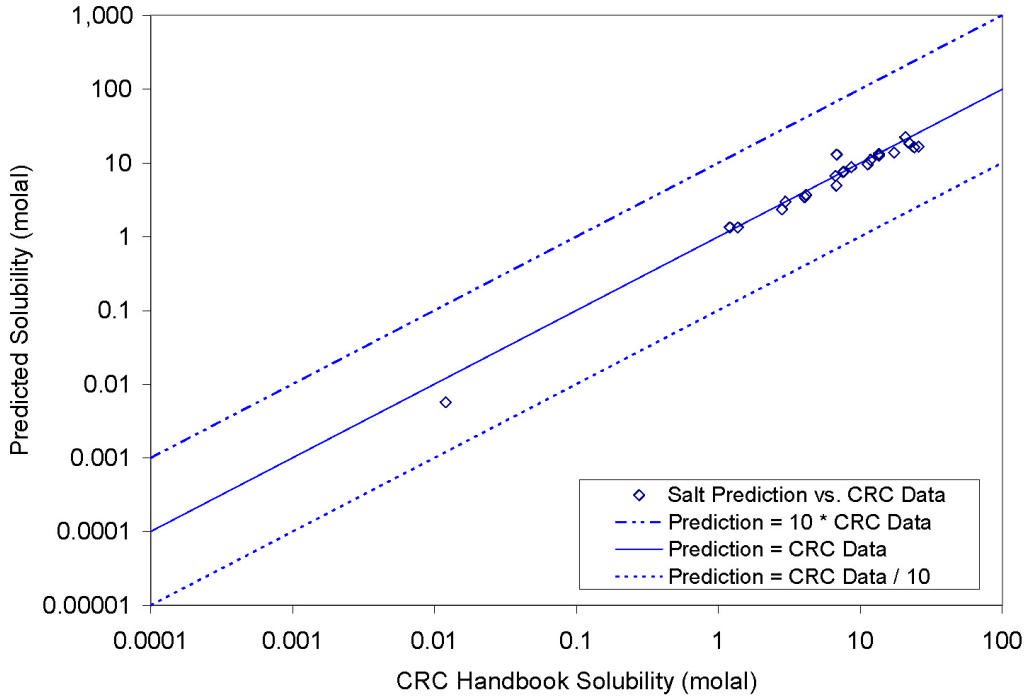

Output DTN: MO0701EQ36IDPS.000, file: *Salts100.zip*, *Salt solubilities at 100C v4.xls*.

Figure 7-2. Predicted vs. Chemistry Handbook Mineral Solubilities at 100°C

7.1.1.1.2 Deliquescence Relative Humidity

To demonstrate model validation for predicting the deliquescence relative humidity (RH_d) of simple salts, the same approach as in Section 7.1.1.1.1 was used. The IDPS model was used to evaporate dilute binary solutions (0.0001 molal) of Na, K, Ca, and Mg salts from Table 4-7 to mineral saturation at temperatures listed in the table. Predicted RH_d values were then compared to those reported in Table 4-7.

The results of the simulations are documented in Output DTN: MO0701EQ36IDPS.000 and displayed in Table 7-4. This table lists the predicted deliquescence relative humidity values, the error with respect to handbook values, and the specific mineral phases that reached saturation in the evaporations. The comparison shows that the largest predicted difference in the value of the deliquescence relative humidity is 5.1% (in *RH* percentage units), which is well within the model validation criterion of 10% (Table 7-1). The implications of these results are discussed in Section 7.5 as applicable.

Table 7-4. Model Predictions of Equilibrium Relative Humidity for Saturated Aqueous Solutions in Contact with an Excess of Solid-Phase Salts

Salt	Predicted Equilibrium Relative Humidity (or Deliquescence Point) (%*RH*)	Temperature (°C)	Difference Compared to Handbook Values Listed in Table 4-7 (%*RH*)	Precipitating Mineral
NaCl	74.7	80	–1.7	Halite
KCl	77.0	80	–2.5	Sylvite
$MgCl_2 \cdot 6H_2O$	37	25	4.0	Bischofite
$Na_2CO_3 \cdot 10H_2O$	90	24.5	3.0	Natron
$K_2CO_3 \cdot 2H_2O$	37.8	40	–4.2	$K_2CO_3 \cdot 1.5H_2O$
NaF	96.1	100	–0.5	Villiaumite
KF	28.0	100	5.1	Carobbite
$Na_2SO_4 \cdot 10H_2O$	95.6	20	2.6	Mirabilite
K_2SO_4	96.4	60	0.4	Arcanite
$NaNO_3$	61.6	80	–3.9	Soda Niter
KNO_3	77.9	60	–4.1	Niter

Output DTN: MO0701EQ36IDPS.000, file: *Linke binary1.zip*, *Deliq RH Uncert r3.xls*.

7.1.1.2 Comparisons to Non-Handbook Data

7.1.1.2.1 Aqueous Solubilities

Aqueous solubilities of salts over a broad range of temperature for binary systems are compiled and documented in Output DTN: LL031106231032.007. These data, summarized in Table 4-8, are from Linke (1965 [DIRS 166191]; 1958 [DIRS 166192]), except where noted.

As in Section 7.1.1.1, each IDPS model evaporation begins with a 0.0001 molal solution of the particular salt whose solubility is to be estimated. Because the pH of pure water can be affected

by the dissolved salt and by temperature, the starting solution is charge balanced on the hydrogen ion. The salt components added to the pure water are inherently charge balanced; thus, charge balancing on the hydrogen ion in these systems reflects a true equilibration process. For evaporations involving carbonate, a closed system is prescribed. An evaporation simulation is complete when the solution reaches saturation with respect to the salt components.

The only difference in these model evaporation simulations compared to those in Section 7.1.1.1 is that the species O_2(aq) is suppressed. The presence of O_2(aq) hinders the ability of EQ6 to reach convergence in some cases. For example, suppression of this species allows KNO_3 to reach saturation at high temperature. O_2(aq) does not directly affect the IDPS model system because the system does not include redox reactions. Termination of model simulations before mineral saturations are reached is not considered non-convergence because the simulations do converge to a satisfactory end point, as defined by the validation criteria.

The results of the simulations are documented in Output DTN: MO0701EQ36IDPS.000. Figures 7-3 through 7-24 compare the aqueous solubilities documented by Linke (1965 [DIRS 166191]; 1958 [DIRS 166192]) to model predictions as a function of temperature from 25°C to 140°C. These figures also contain model predictions of RH_d (marked as DRH in the figures) as well as measurements of RH_d where available (see Section 7.1.1.2.2). The implications of these results are discussed in Section 7.5 as applicable.

As shown in the figures, the salt solubility model predictions are within a factor of 2 of measurements for most of the salts evaluated. Occasionally, the model does not reach mineral saturation at some temperatures (e.g., Figures 7-5, 7-8, 7-19, 7-20, 7-21, 7-23, and 7-24). In these instances, the aqueous concentrations at the lowest *RH* achieved are operationally defined as the model predictions of the salt solubilities. Regardless, the model predictions are always within a factor of 10 of measured solubilities (in accordance with model validation criteria in Table 7-1) and are usually within a factor of 3. These uncertainties are captured and propagated in the model uncertainty estimates assessed in Section 7.5. Model bias in predicting output parameters used in TSPA, such as Cl and NO_3 concentrations, is addressed in Section 7.5.4, where all relevant comparisons in Sections 7.1 and 7.2 are summarized and evaluated as a whole.

The differences between model predictions and measured data do not necessarily reflect model uncertainty (or bias) alone because there is some uncertainty associated with the measured data. Uncertainty in solubility measurements is apparent in Figures 7-5, 7-10, 7-23, and 7-24, where multiple data are provided for the same approximate temperature.

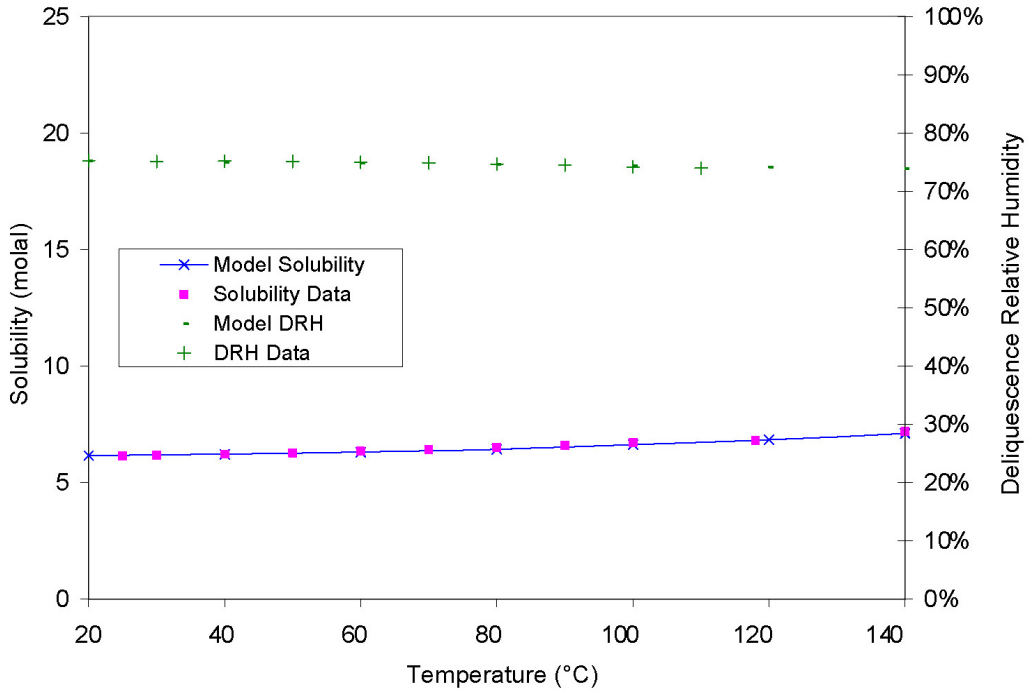

Output DTN: MO0701EQ36IDPS.000, file: *Linke binary2.zip*, *naclev.xls*.

Figure 7-3. Solubility and Deliquescence *RH* Predictions vs. Data for NaCl

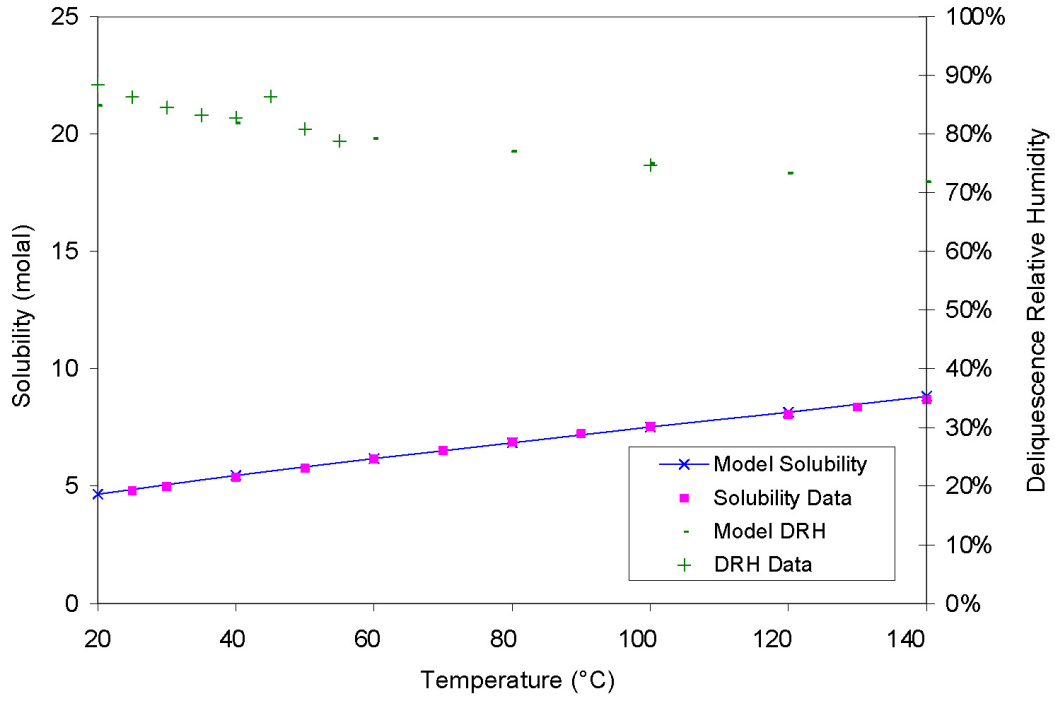

Output DTN: MO0701EQ36IDPS.000, file: *Linke binary1.zip*, *kclev.xls*.

Figure 7-4. Solubility and Deliquescence *RH* Predictions vs. Data for KCl

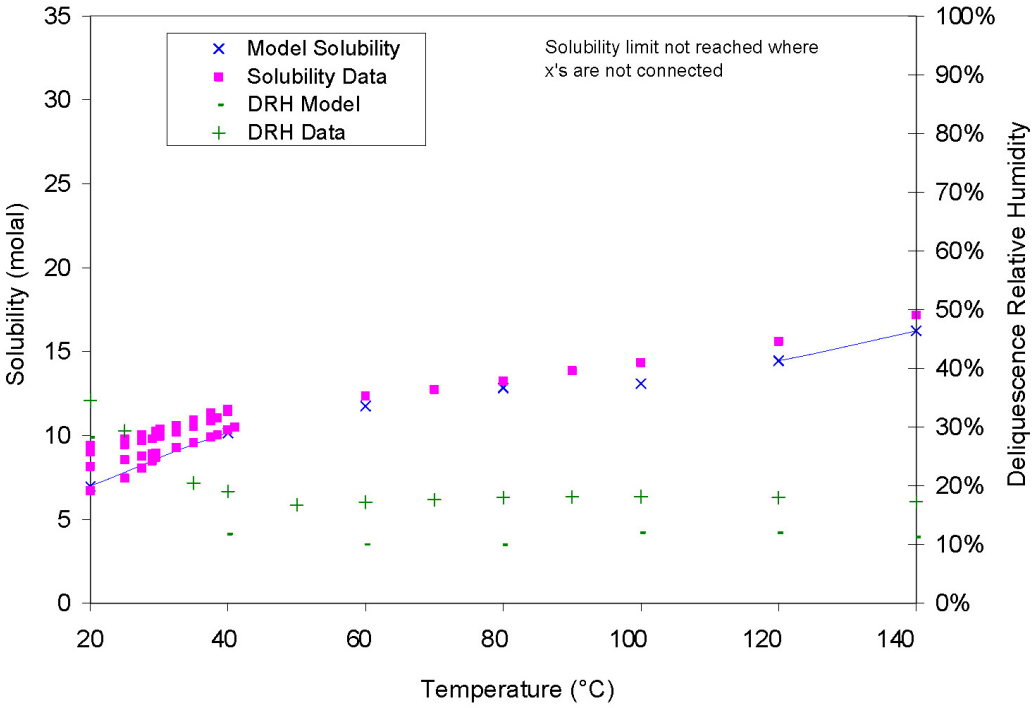

Output DTN: MO0701EQ36IDPS.000, file: *Linke binary1.zip*, *cacl2ev.xls*.

Figure 7-5. Solubility and Deliquescence *RH* Predictions vs. Data for $CaCl_2$

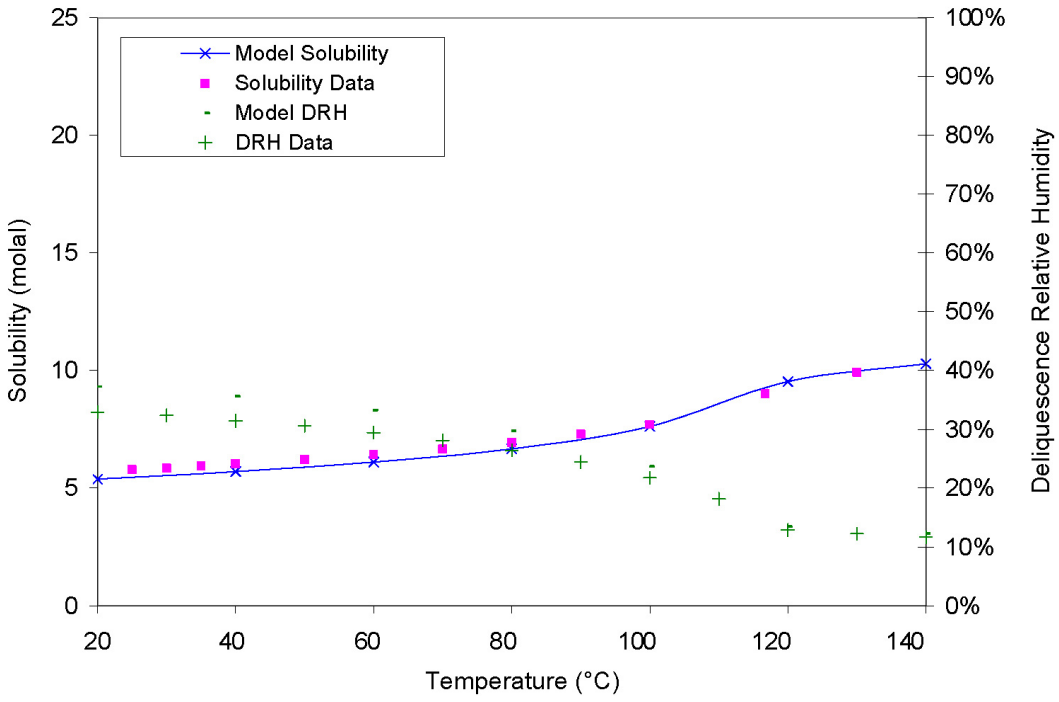

Output DTN: MO0701EQ36IDPS.000, file: *Linke binary1.zip*, *mgcl2ev.xls*.

Figure 7-6. Solubility and Deliquescence *RH* Predictions vs. Data for $MgCl_2$

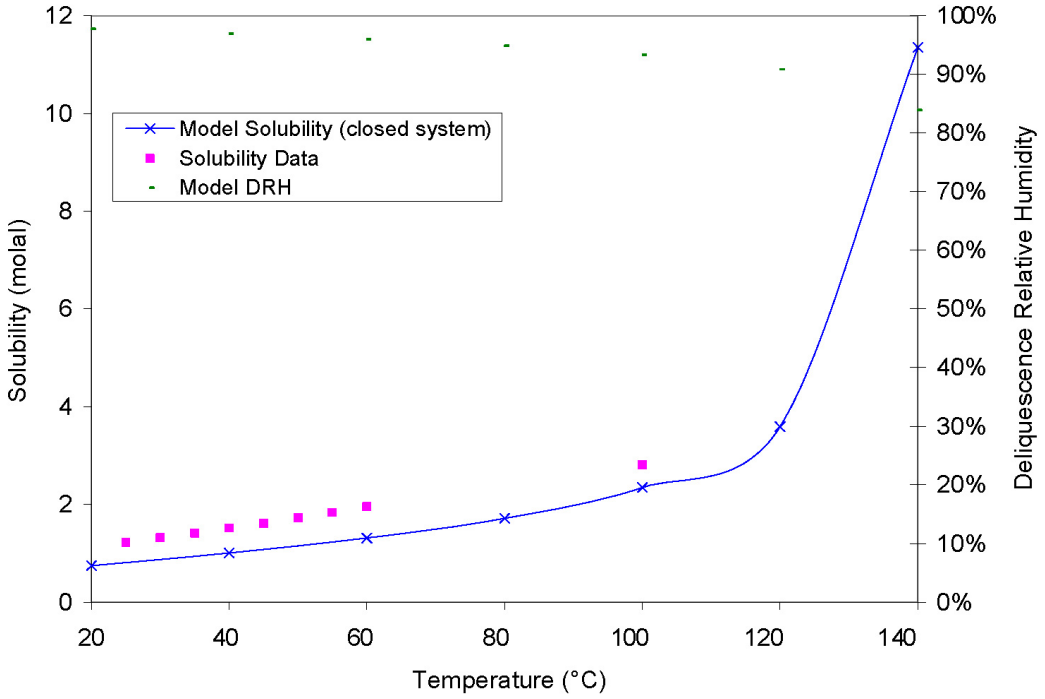

Output DTN: MO0701EQ36IDPS.000, file: *Linke binary2.zip*, *nahco3xev.xls*.

Figure 7-7. Solubility and Deliquescence *RH* Predictions vs. Solubility Data for $NaHCO_3$

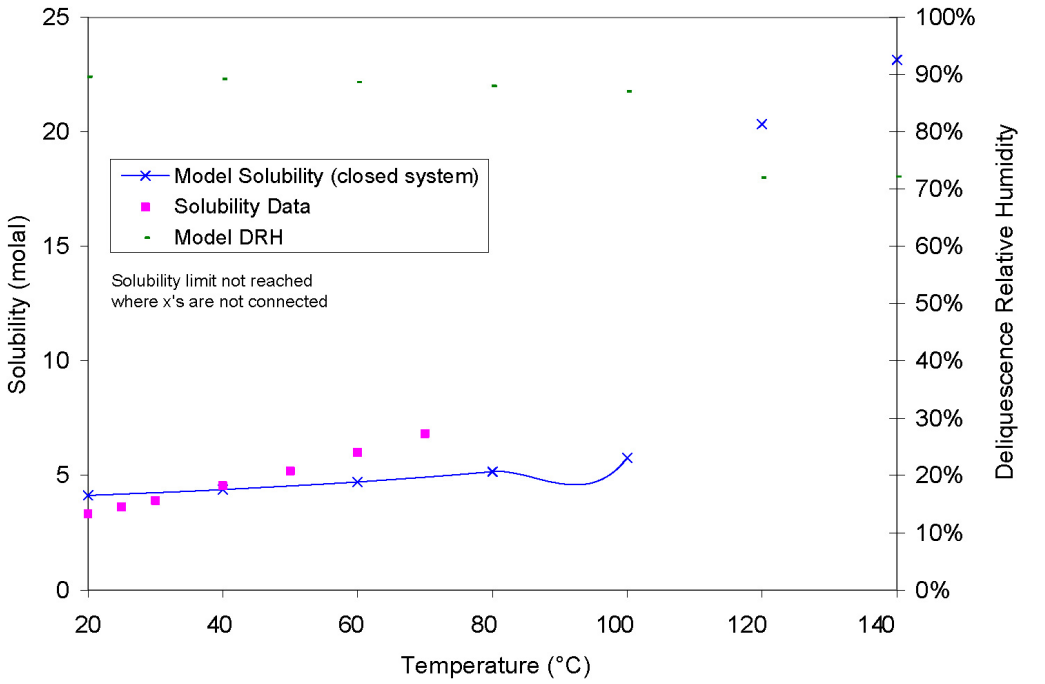

Output DTN: MO0701EQ36IDPS.000, file: *Linke binary1.zip*, *khco3ev.xls*.

Figure 7-8. Solubility and Deliquescence *RH* Predictions vs. Solubility Data for $KHCO_3$

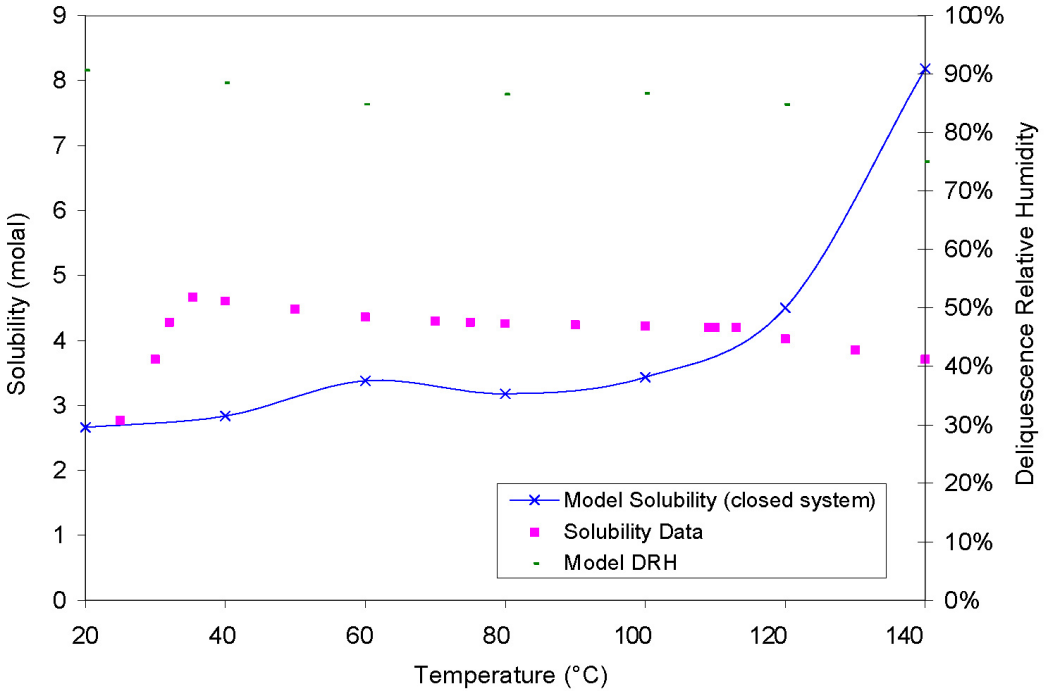

Output DTN: MO0701EQ36IDPS.000, file: *Linke binary2.zip*, *na2co3xev.xls*.

Figure 7-9. Solubility and Deliquescence *RH* Predictions vs. Solubility Data for Na_2CO_3

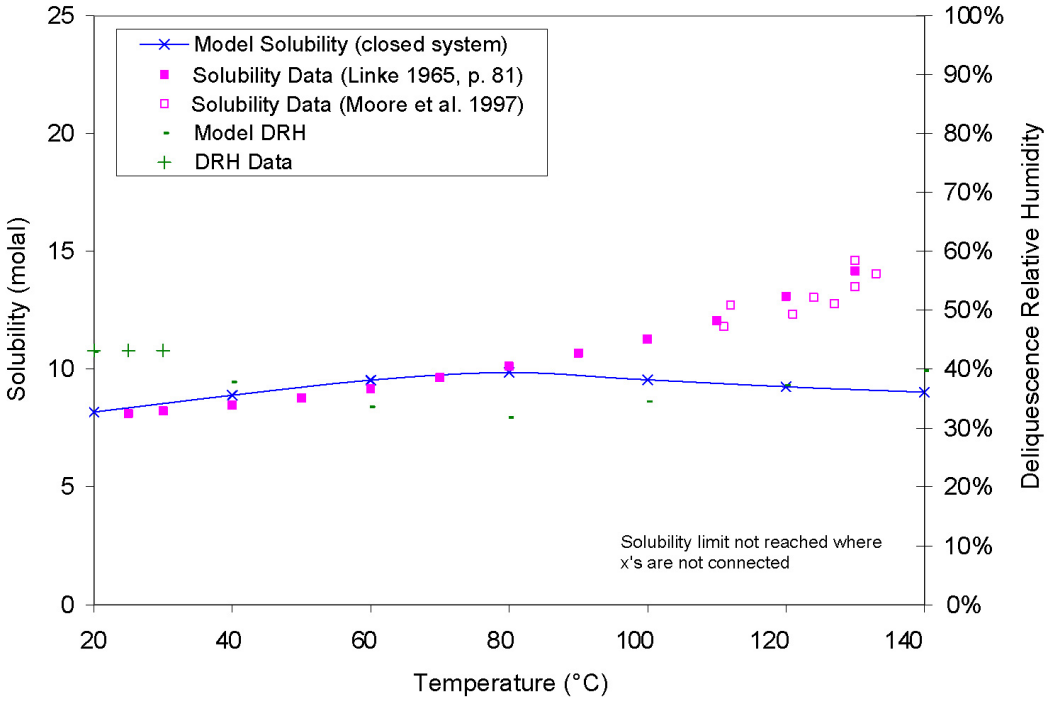

Output DTN: MO0701EQ36IDPS.000, file: *Linke binary1.zip*, *k2co3ev.xls*.

Figure 7-10. Solubility and Deliquescence *RH* Predictions vs. Data for K_2CO_3

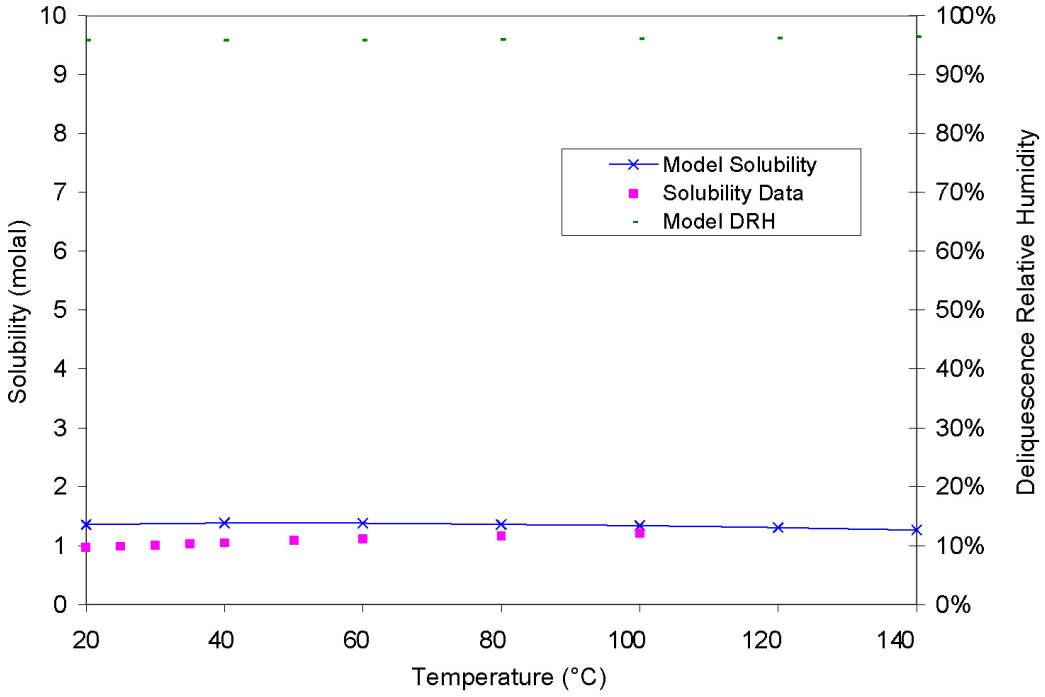

Output DTN: MO0701EQ36IDPS.000, file: *Linke binary2.zip*, *nafev.xls*.

Figure 7-11. Solubility and Deliquescence *RH* Predictions vs. Solubility Data for NaF

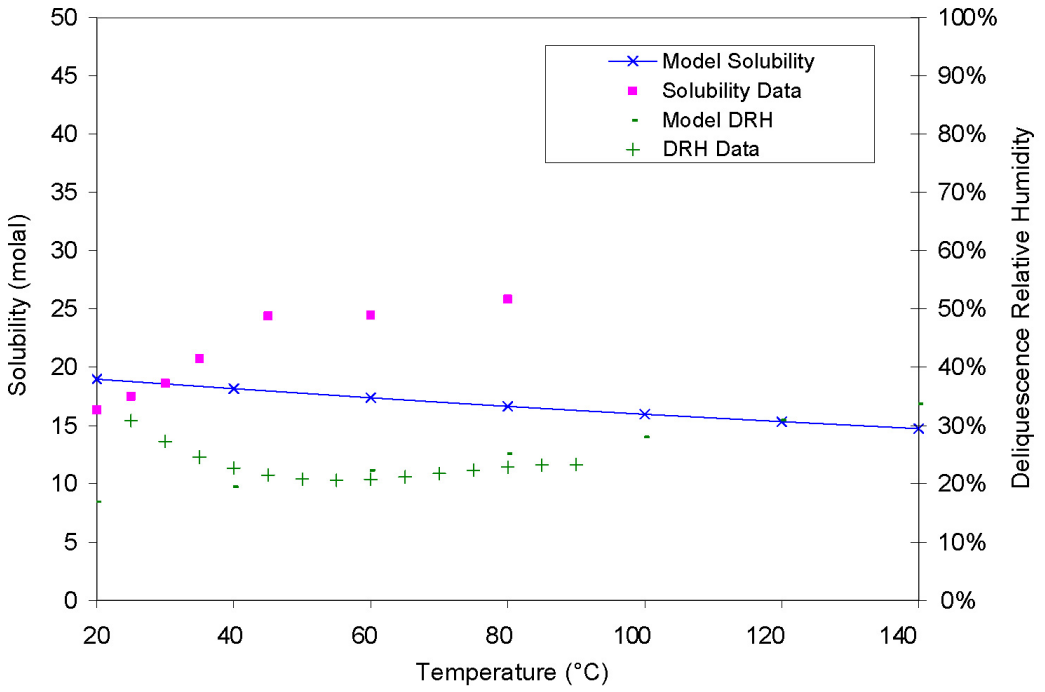

Output DTN: MO0701EQ36IDPS.000, file: *Linke binary1.zip*, *kfev.xls*.

Figure 7-12. Solubility and Deliquescence *RH* Predictions vs. Data for KF

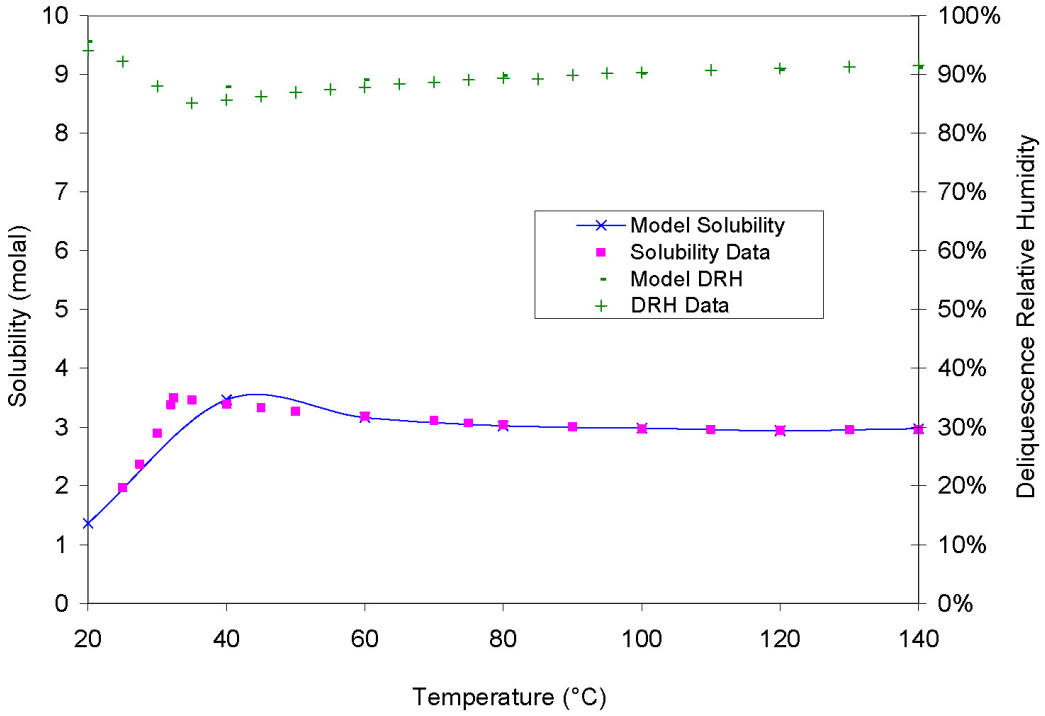

Output DTN: MO0701EQ36IDPS.000, file: *Linke binary2.zip*, *na2so4ev.xls*.

Figure 7-13. Solubility and Deliquescence *RH* Predictions vs. Data for Na_2SO_4

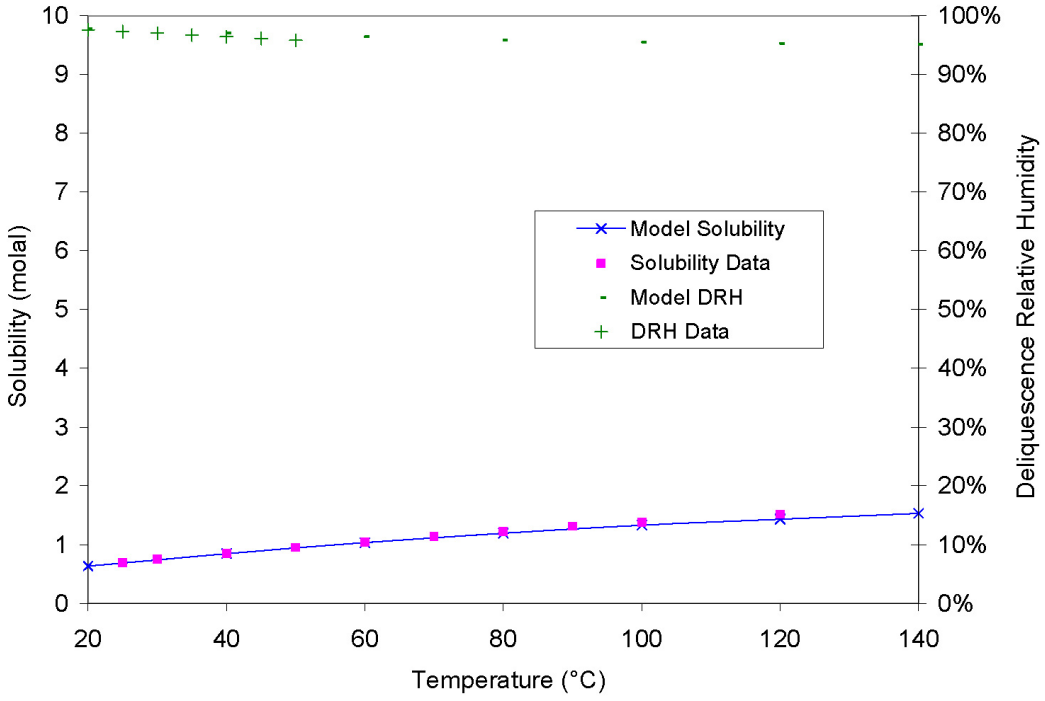

Output DTN: MO0701EQ36IDPS.000, file: *Linke binary1.zip*, *k2so4ev.xls*.

Figure 7-14. Solubility and Deliquescence *RH* Predictions vs. Data for K_2SO_4

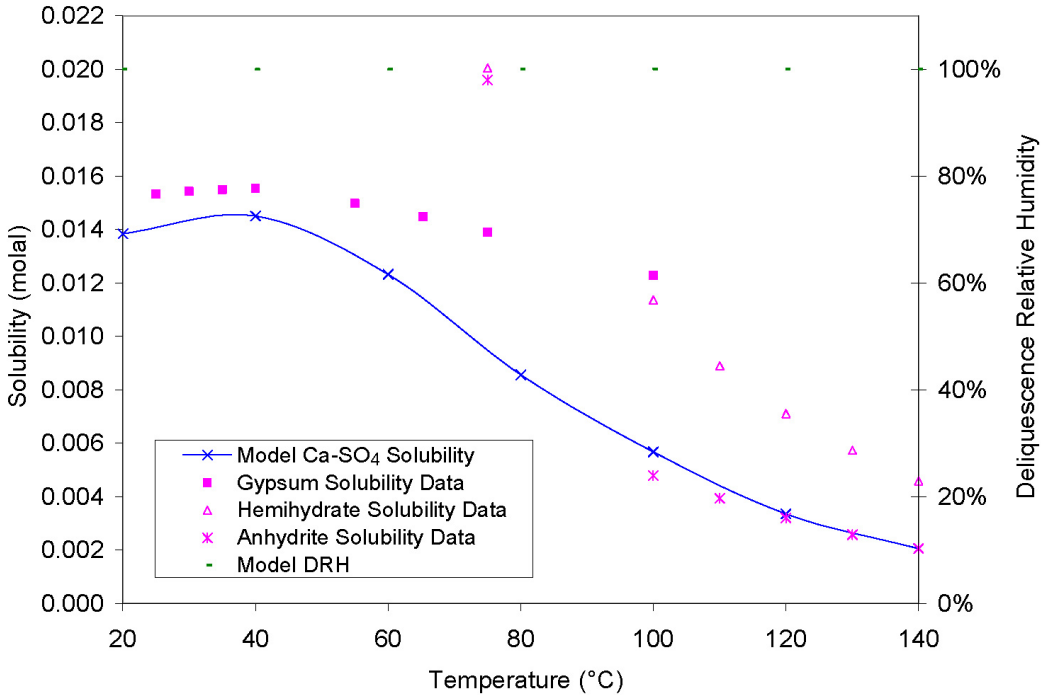

Output DTN: MO0701EQ36IDPS.000, file: *Linke binary1.zip*, *caso4ev.xls*.

Figure 7-15. Solubility and Deliquescence *RH* Predictions vs. Solubility Data for $CaSO_4$

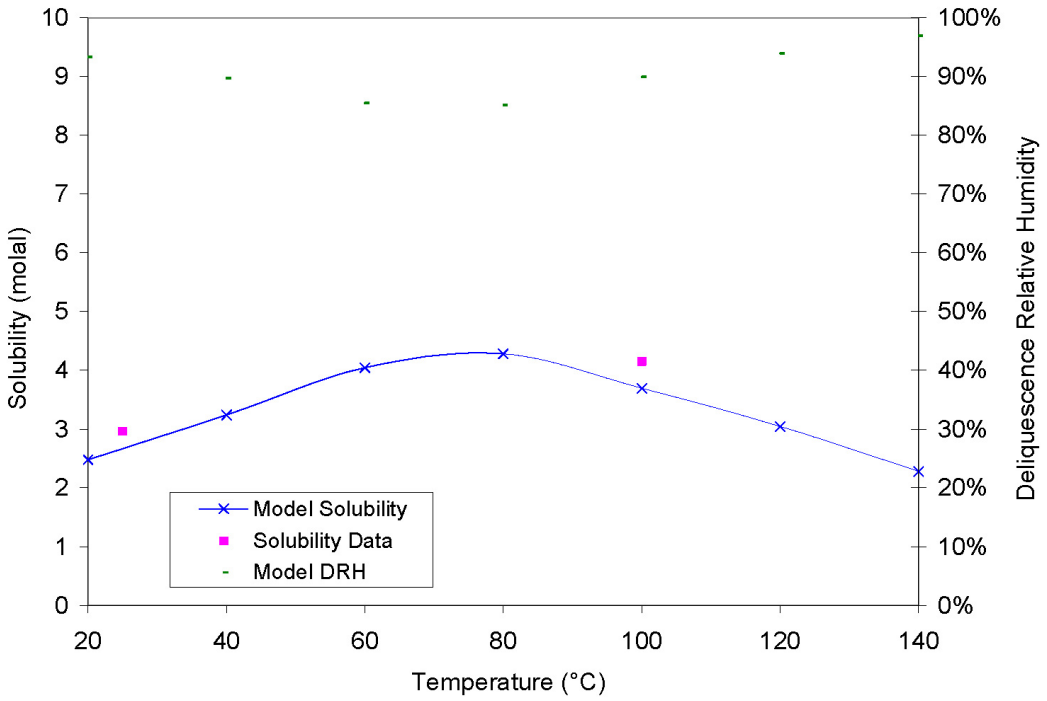

Output DTN: MO0701EQ36IDPS.000, file: *Linke binary2.zip*, *mgso4ev.xls*.

Figure 7-16. Solubility and Deliquescence *RH* Predictions vs. Solubility Data for $MgSO_4$

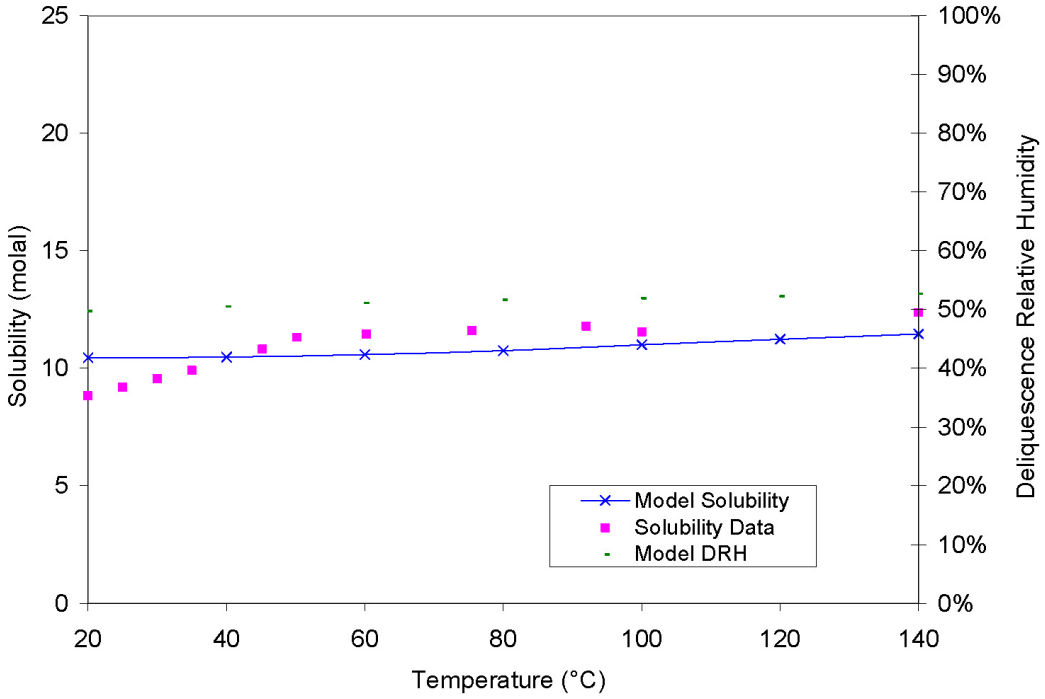

Output DTN: MO0701EQ36IDPS.000, file: *Link binary2.zip*, *nabrev.xls*.

Figure 7-17. Solubility and Deliquescence *RH* Predictions vs. Solubility Data for NaBr

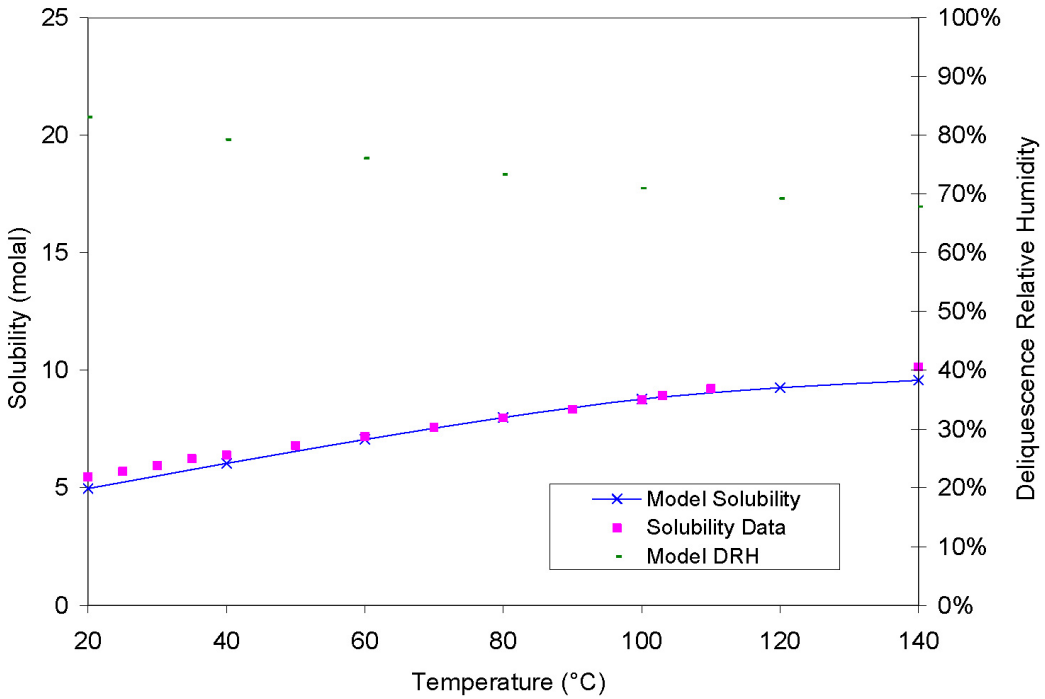

Output DTN: MO0701EQ36IDPS.000, file: *Linke binary1.zip*, *kbrev.xls*.

Figure 7-18. Solubility and Deliquescence *RH* Predictions vs. Solubility Data for KBr

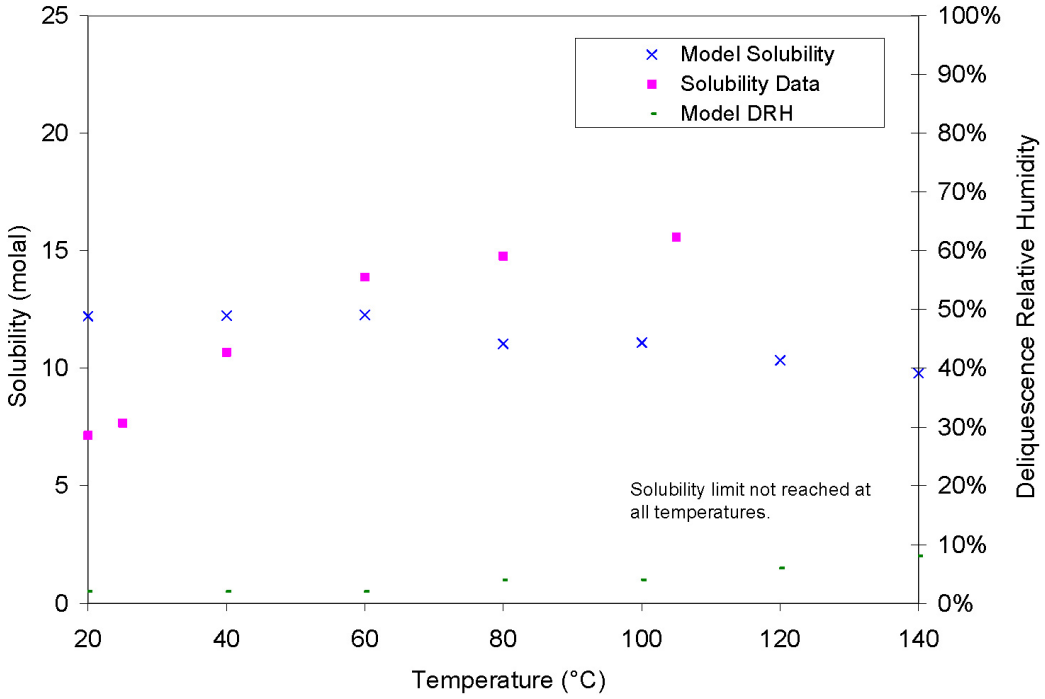

Output DTN: MO0701EQ36IDPS.000, file: *Linke binary1.zip*, *cabr2ev.xls*.

Figure 7-19. Solubility and Deliquescence *RH* Predictions vs. Solubility Data for $CaBr_2$

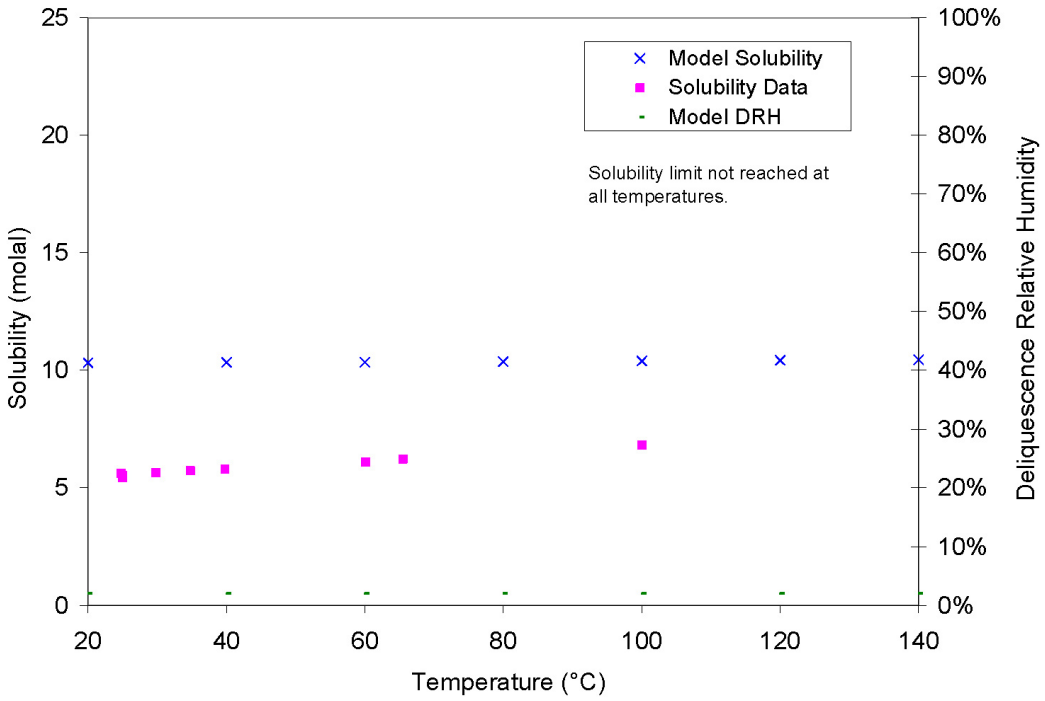

Output DTN: MO0701EQ36IDPS.000, file: *Linke binary2.zip*, *mgbr2ev.xls*.

Figure 7-20. Solubility and Deliquescence *RH* Predictions vs. Solubility Data for $MgBr_2$

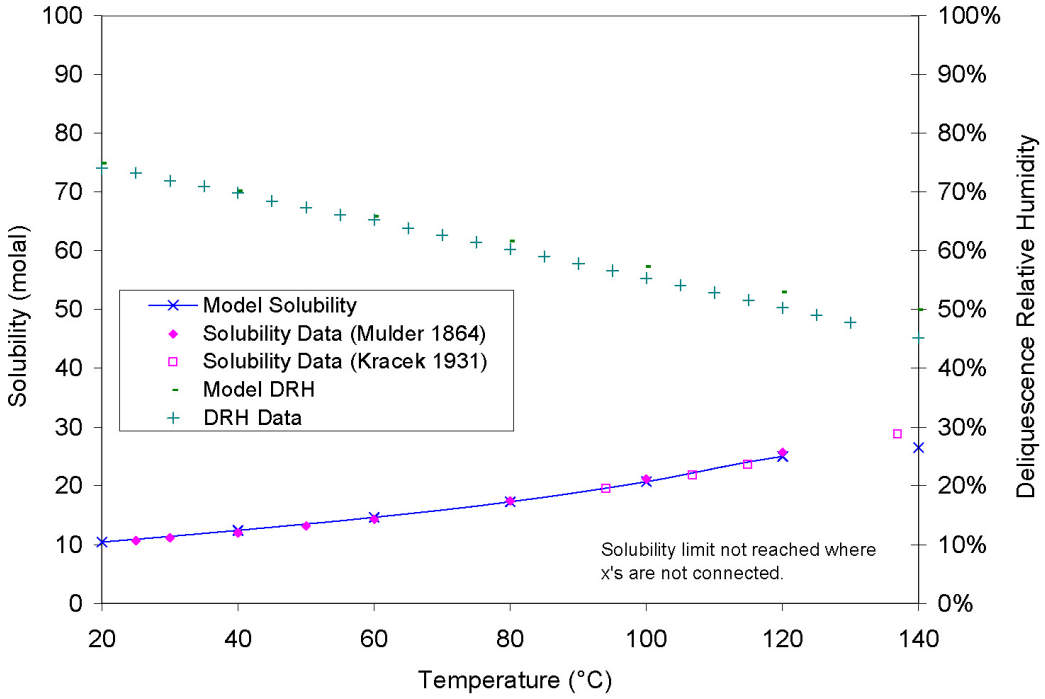

Output DTN: MO0701EQ36IDPS.000, file: *Linke binary2.zip*, *nano3ev.xls*.

NOTE: Data sources of (Mulder 1864) and (Kracek 1931) are cited in the reference Linke (1965 [DIRS 166191]), pp. 1069 and 1070

Figure 7-21. Solubility and Deliquescence *RH* Predictions vs. Data for $NaNO_3$

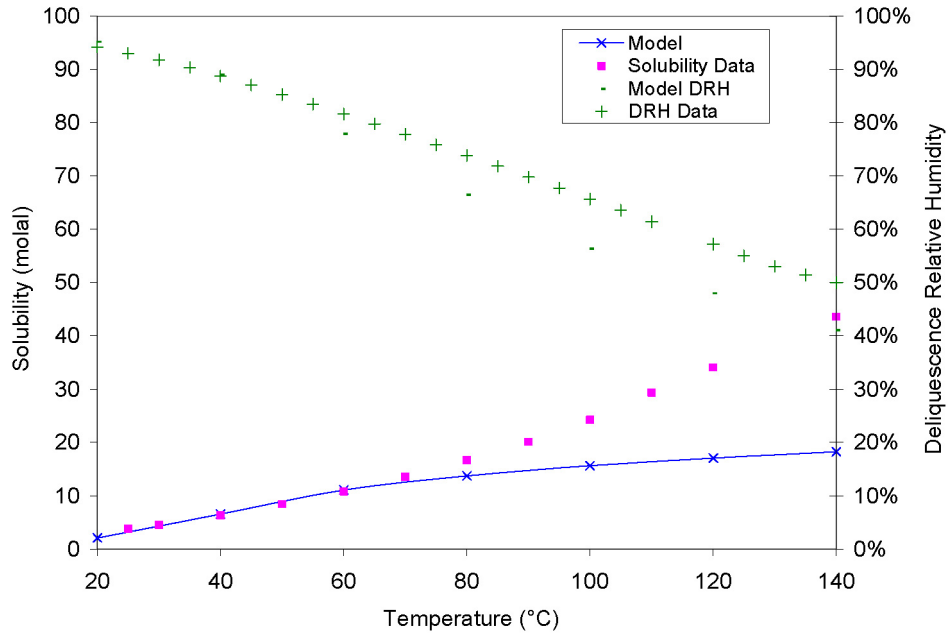

Output DTN: MO0701EQ36IDPS.000, file: *Linke binary1.zip*, *kno3ev.xls*.

Figure 7-22. Solubility and Deliquescence *RH* Predictions vs. Data for KNO_3

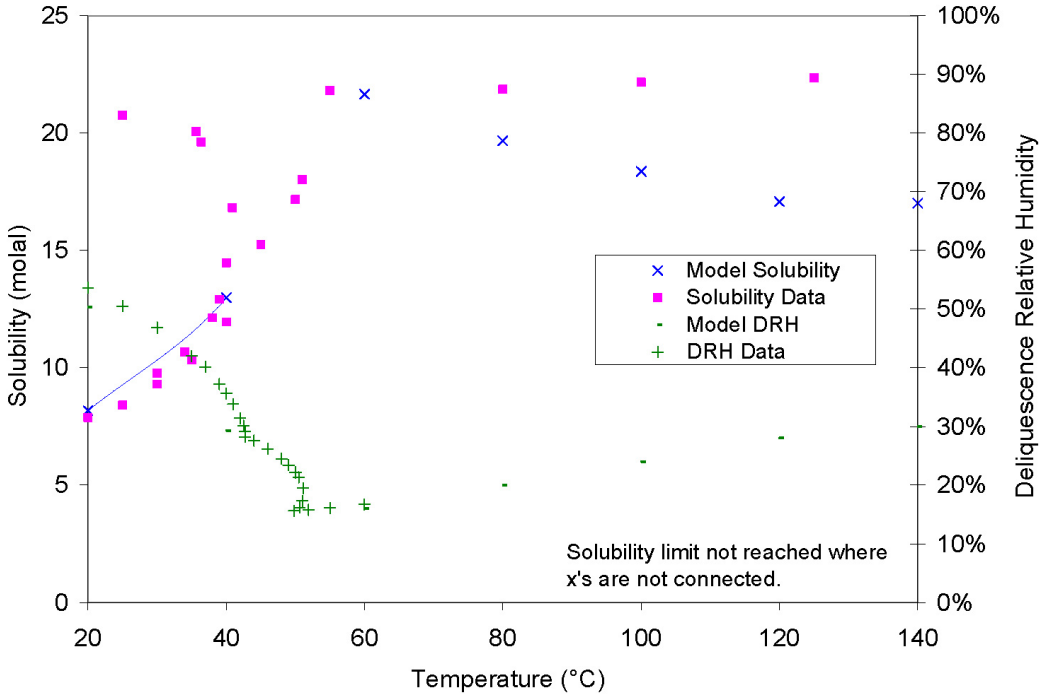

Output DTN: MO0701EQ36IDPS.000, file: *Linke binary1.zip*, *kcano32ev.xls*.

Figure 7-23. Solubility and Deliquescence *RH* Predictions vs. Data for $Ca(NO_3)_2$

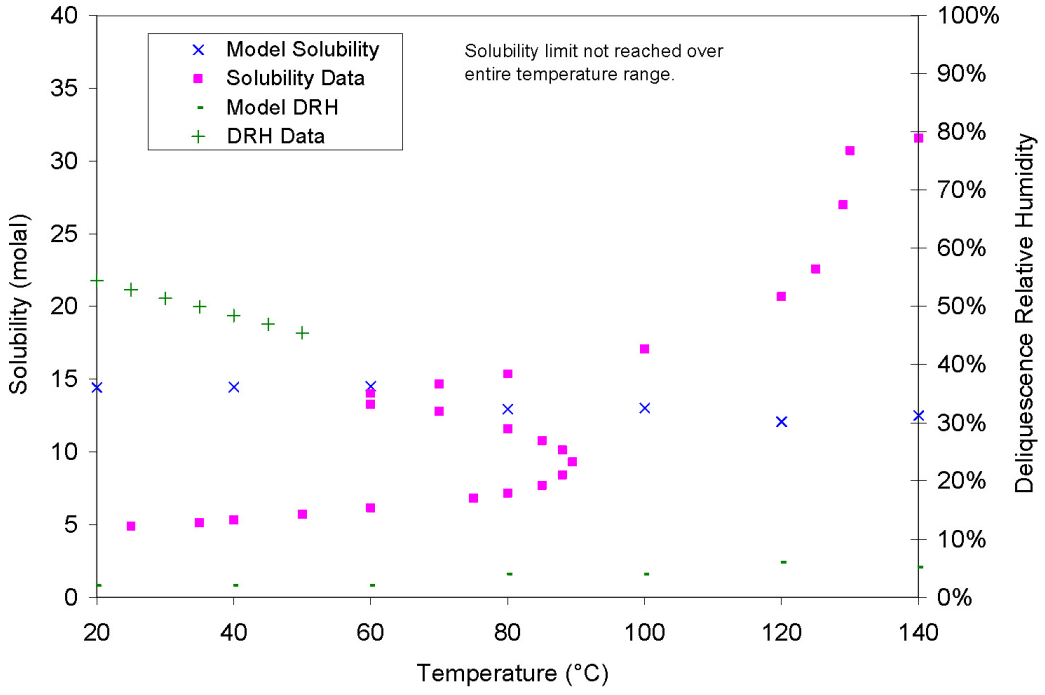

Output DTN: MO0701EQ36IDPS.000, file: *Linke binary2.zip*, *mgno32ev.xls*.

Figure 7-24. Solubility and Deliquescence *RH* Predictions vs. Data for $Mg(NO_3)_2$

7.1.1.2.2 Deliquescence Relative Humidity

Non-handbook sources of deliquescence relative humidity (RH_d) values used in the IDPS model validation are summarized in Tables 4-9 through 4-11 in Section 4.4. Data referenced in Tables 4-9 and 4-11 are reduced and compiled in Output DTN: LL031106231032.007. Data from Greenspan (1977 [DIRS 104945]) are listed in Table 4-10. These data sets are used in this section to compare to values of RH_d predicted by the IDPS model.

RH_d values are computed from vapor pressures of saturated salt solutions ($P_{solution}$) using the following equation:

$$RH_d = \frac{P_{solution}}{P_{H2O}} \quad \text{(Eq. 7.1-2)}$$

where P_{H2O} is the vapor pressure of pure water. Values for P_{H2O} as a function of temperature for saturated $NaNO_3$ solutions are listed in Table 4-11.

The IDPS model predictions of RH_d are presented in the figures of Section 7.1.1.2.1. RH_d (marked as DRH in the graphs) is plotted as a function of temperature. Where available, RH_d measurements are included in the figures for comparison.

As shown in the figures, the RH_d predictions are within 5% in *RH* units for most of the salts with RH_d measurements. The differences generally increase with decreasing RH_d. For several salts whose RH_d values are less than about 60%, differences between predictions and measurements can be greater than 5% in *RH* units (e.g., Figure 7-12, Figure 7-22, and Figure 7-23). Results are documented in Output DTN: MO0701EQ36IDPS.000, and implications are discussed in Section 7.5.

7.1.2 Ternary Salt Systems

Ternary salt systems are mixtures of pure water and two different salts having a common cation or anion. To demonstrate model validation for predicting aqueous solubilities in ternary systems, IDPS model simulations were performed to compare against data reported by Linke (1965 [DIRS 166191]; 1958 [DIRS 166192]) and de Lima and Pitzer (1983 [DIRS 162110]). The specific data used from these sources are listed in Table 4-12. Also, atomic weights for the elements were taken from DTN: SN0302T0510102.002 [DIRS 162572]. These data are reduced and compiled in Output DTN: LL031106231032.007.

Two types of ternary systems are simulated. If both salts are at saturation in the data set, the IDPS model evaporations are simulated to the eutectic end points. Similar to the approach in Section 7.1.1.2.1, the simulations begin with a 0.0001 molal solution of each salt in the system. Because the pH of pure water can be affected by the dissolved salt and by temperature, the starting solution is charge balanced on the hydrogen ion. The salt components added to the pure water are inherently charge balanced; thus, charge balancing on the hydrogen ion in these systems reflects a true equilibration process. For evaporations involving carbonate, a closed system is prescribed. An evaporation simulation is complete when the solution reaches saturation with respect to both salts.

If only one salt is at saturation in the ternary system being simulated, then the simulations start with a solution that is saturated only with respect to that salt. The undersaturated salt is then incrementally added to the solution to cover the range of aqueous concentrations of the undersaturated salt in the data set. As the undersaturated salt is added, the salt at saturation is allowed to precipitate or dissolve to maintain aqueous saturation.

The results of the simulations are documented in Output DTN: MO0701EQ36IDPS.000. Figures7-25 through 7-53 compare data to model predictions over a temperature range from 20°C to 140°C in Output DTN: LL031106231032.007. For the isothermal ternary systems in which only one solid phase salt is present in the system, model predictions and measurements of the aqueous concentrations of the saturated salt are plotted against the concentrations of the undersaturated salt. The implications of these results are discussed in Section 7.5.

The figures show small differences between predictions and measurements for some ternary systems and larger differences for others. In some cases, differences are small at lower temperatures and large at high temperatures, such as in ternary systems involving $NaNO_3$ or KNO_3 (e.g., Figures 7-26, 7-28, 7-29, and 7-33). These differences correlate with differences observed in the binary systems (e.g., Figure 7-21). Although model predictions often indicate a bias in one direction or another, the bias is almost always within the uncertainty limits of the model validation criteria. Model bias in predicting output parameters important to TSPA, such as concentrations of Cl and NO_3 and the $Cl:NO_3$ molar ratio, is addressed in Section 7.5 where all relevant comparisons in Sections 7.1 and 7.2 are summarized and evaluated as a whole.

Except for two cases, all predictions are within a factor of 10 of the measurements (in accordance with model validation criteria shown in Table 7-1) and are usually within a factor of 3. One exception is the underprediction of Na solubility in the $Na\text{-}Ca\text{-}NO_3$ system (Figure 7-40). The total nitrate and calcium concentrations are within the range of measurements but the sodium concentration is far below measurements. The other exception is the $Cl:NO_3$ ratio in the $Mg\text{-}Cl\text{-}NO_3$ system (Figure 7-53). The model underpredicts this ratio by more than a factor of ten at 20°C. These two systems have predicted RH_d values between 4% and 30%.

The uncertainties that appear in the comparisons are captured and propagated into model uncertainty estimates in Section 7.5. Potential model bias as it might relate to conservatism is also addressed in Section 7.5.

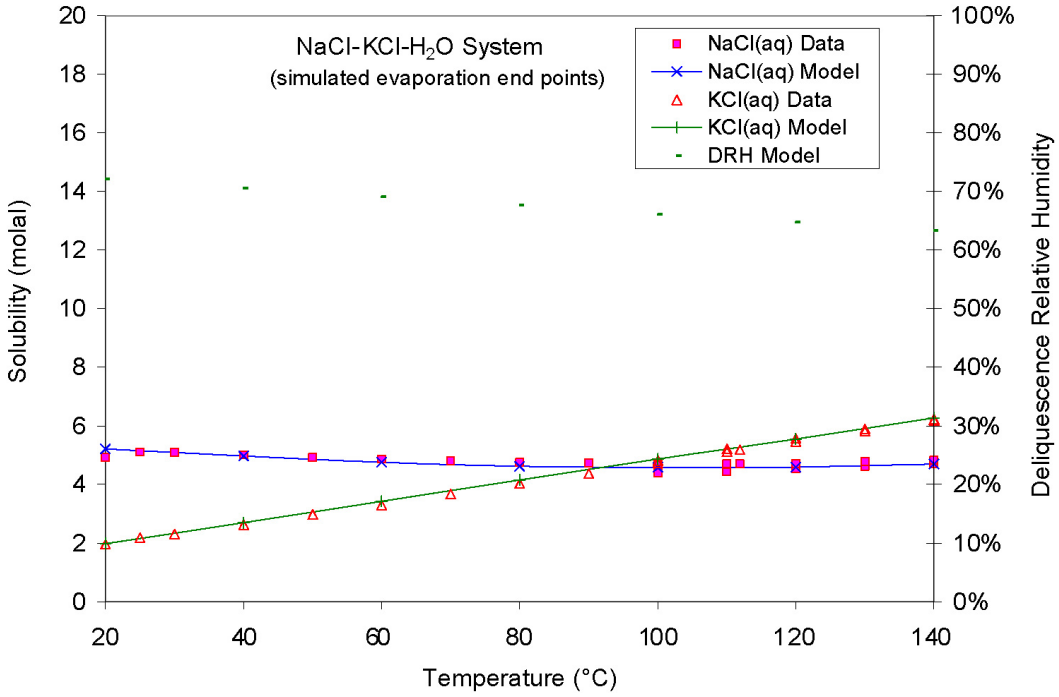

Output DTN: MO0701EQ36IDPS.000, file: *Linke ternary2.zip*, *nakclev.xls*.

Figure 7-25. Model Predictions vs. Data for Na-K-Cl Eutectic System

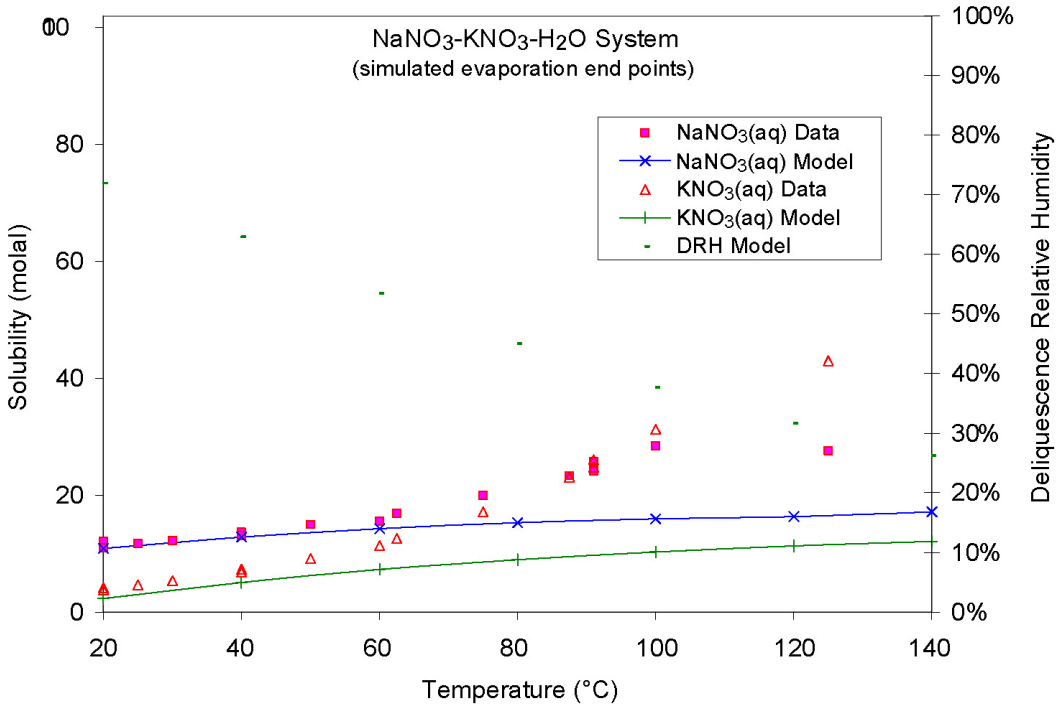

Output DTN: MO0701EQ36IDPS.000, file: *Linke ternary2.zip*, *naknev.xls*.

Figure 7-26. Model Predictions vs. Data for Na-K-NO_3 Eutectic System

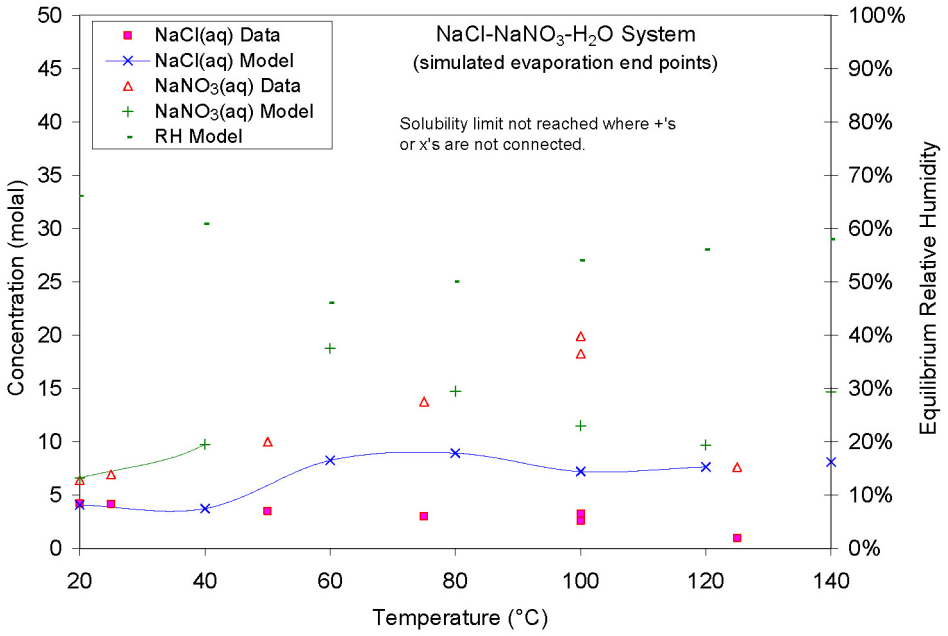

Output DTN: MO0701EQ36IDPS.000, file: *Linke ternary2.zip*, *naclnev.xls*.

Figure 7-27. Model Predictions vs. Data for Na-Cl-NO_3 Eutectic System

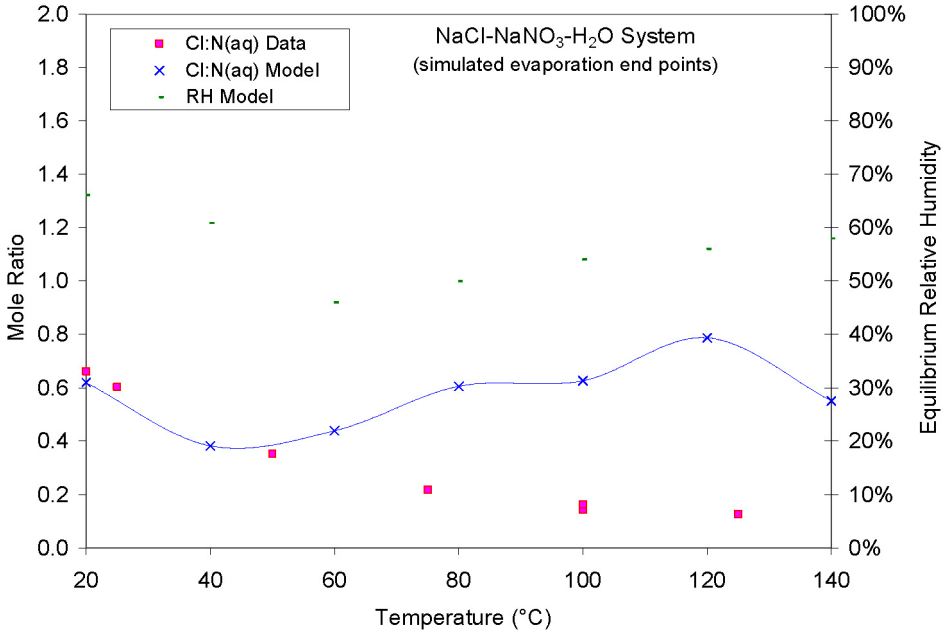

Output DTN: MO0701EQ36IDPS.000, file: *Linke ternary2.zip*, *naclnev.xls*.

Figure 7-28. Cl:NO_3 Mole Ratio Predictions vs. Data for Na-Cl-NO_3 Eutectic System

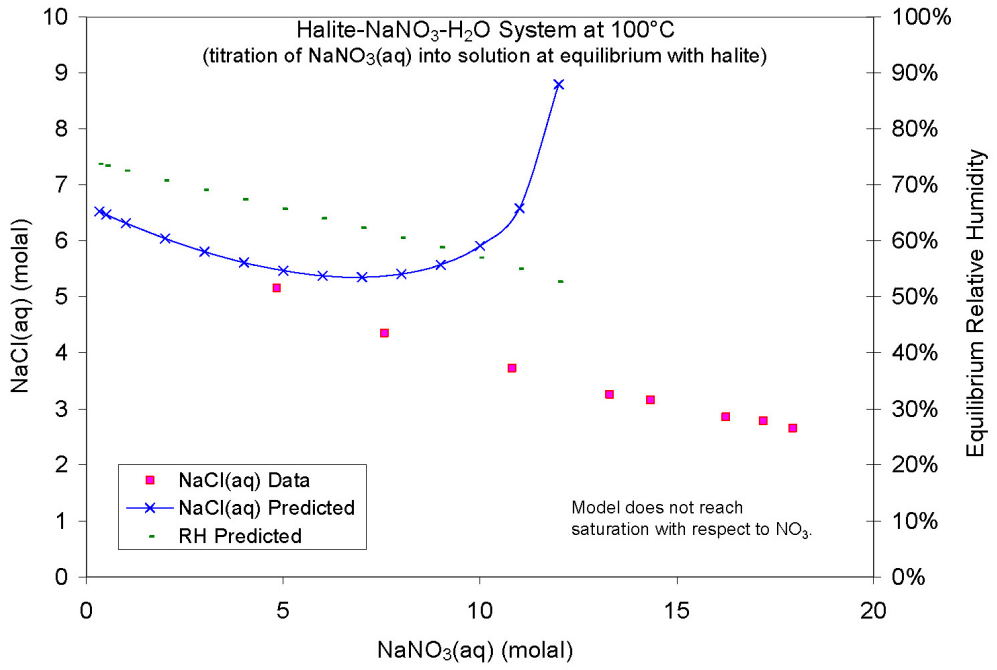

Output DTN: MO0701EQ36IDPS.000, file: *Linke ternary2.zip*, *nacln100.xls*.

Figure 7-29. NaCl Solubility Predictions vs. Data as a Function of $NaNO_3$ Concentration at 100°C

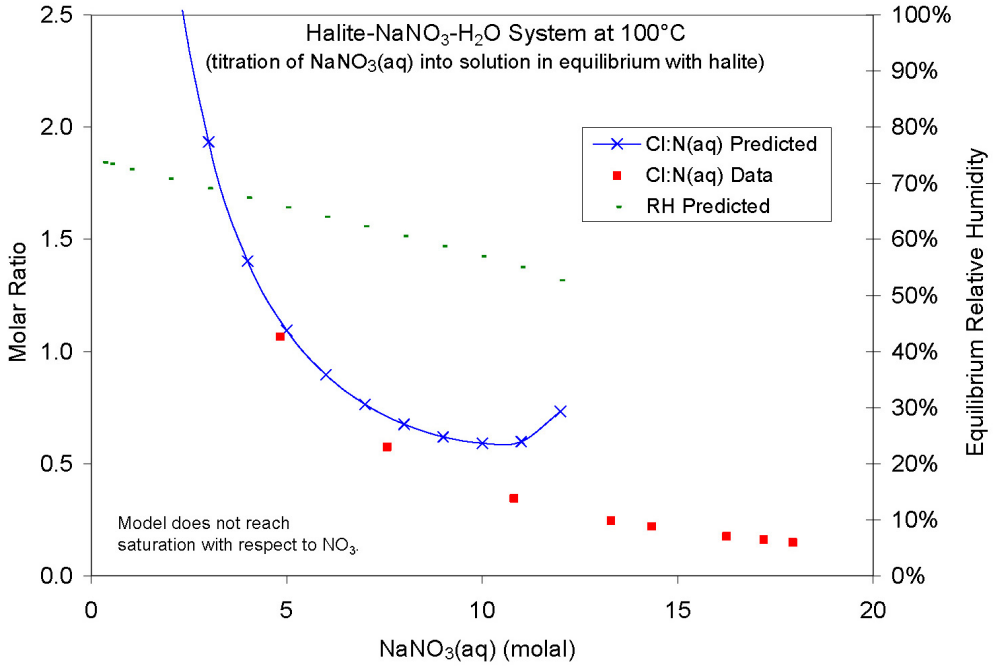

Output DTN: MO0701EQ36IDPS.000, file: *Linke ternary2.zip*, *nacln100.xls*.

Figure 7-30. Cl:NO_3 Mole Ratio Predictions at NaCl Saturation vs. Data as a Function of $NaNO_3$ Concentration at 100°C

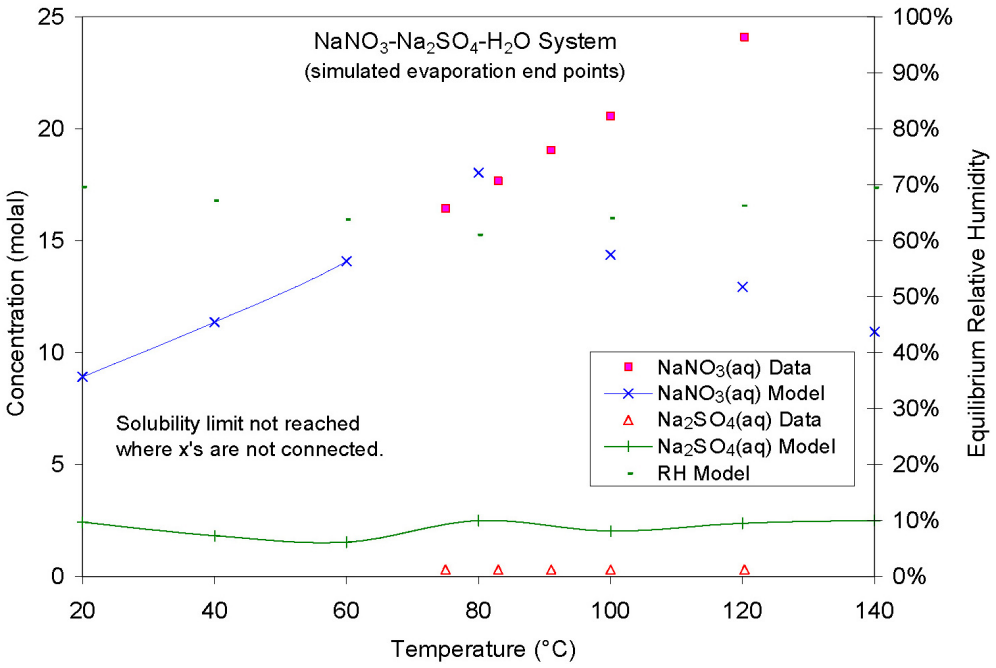

Output DTN: MO0701EQ36IDPS.000, file: *Linke ternary2.zip*, *nansev.xls*.

Figure 7-31. Model Predictions vs. Data for Na-NO_3-SO_4 Eutectic System

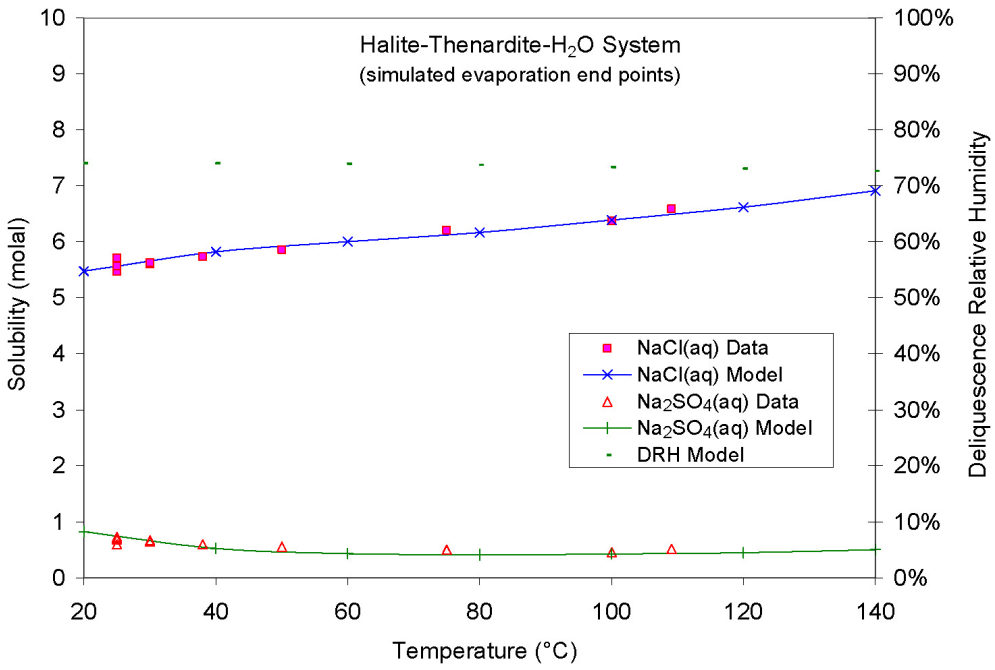

Output DTN: MO0701EQ36IDPS.000, file: *Linke ternary2.zip*, *naclsev.xls*.

Figure 7-32. Model Predictions vs. Data for Na-Cl-SO_4 Eutectic System

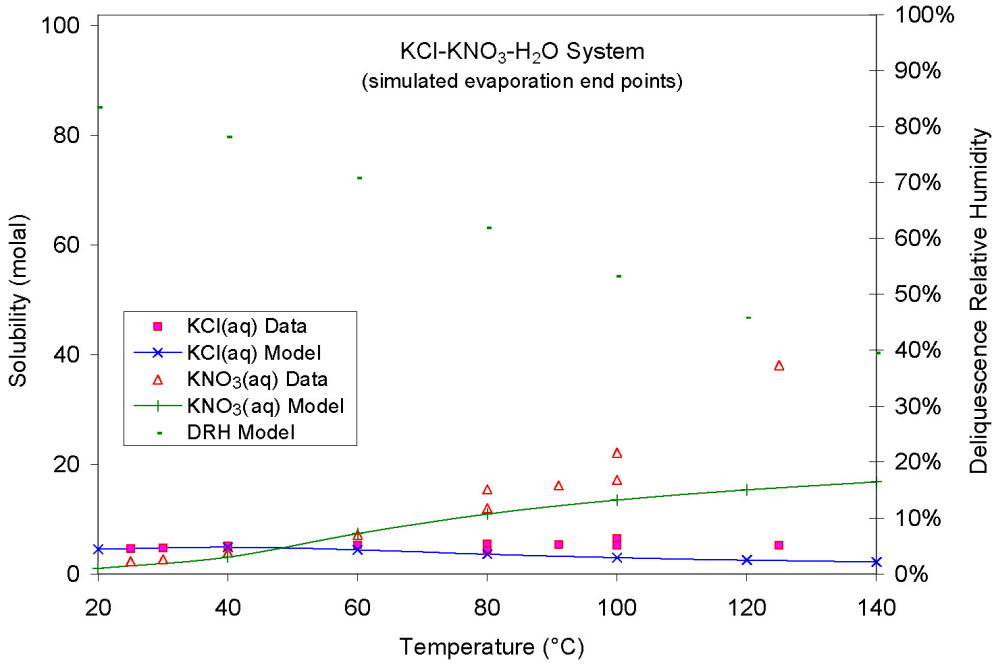

Output DTN: MO0701EQ36IDPS.000, file: *Linke ternary1.zip*, *kclnev.xls*.

Figure 7-33. Model Predictions vs. Data for K-Cl-NO_3 Eutectic System

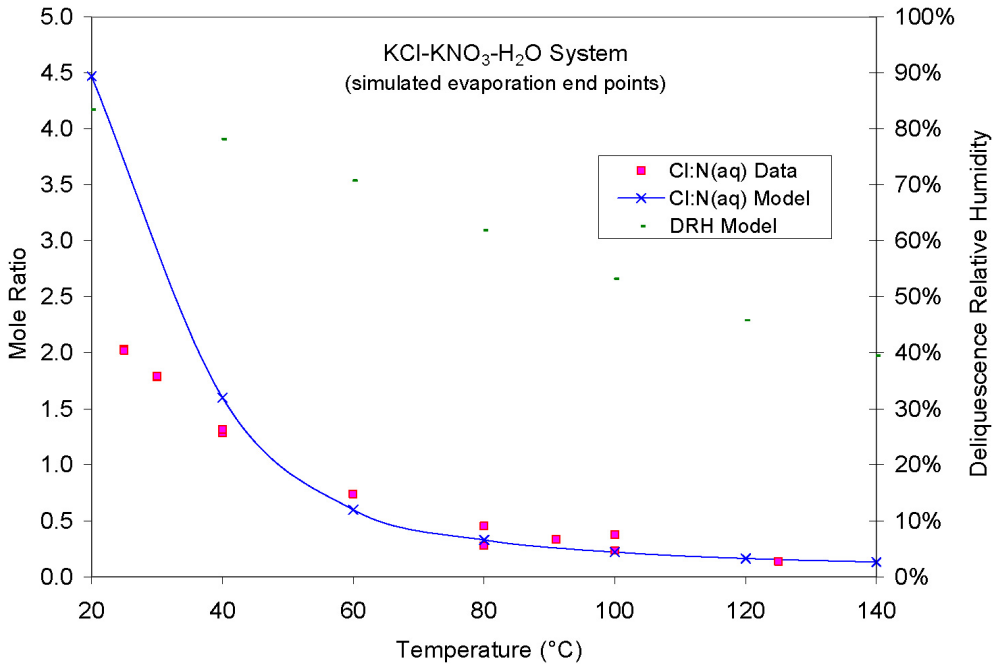

Output DTN: MO0701EQ36IDPS.000, file: *Linke ternary1.zip*, *kclnev.xls*.

Figure 7-34. Cl:NO_3 Mole Ratio Predictions vs. Data for K-Cl-NO_3 Eutectic System

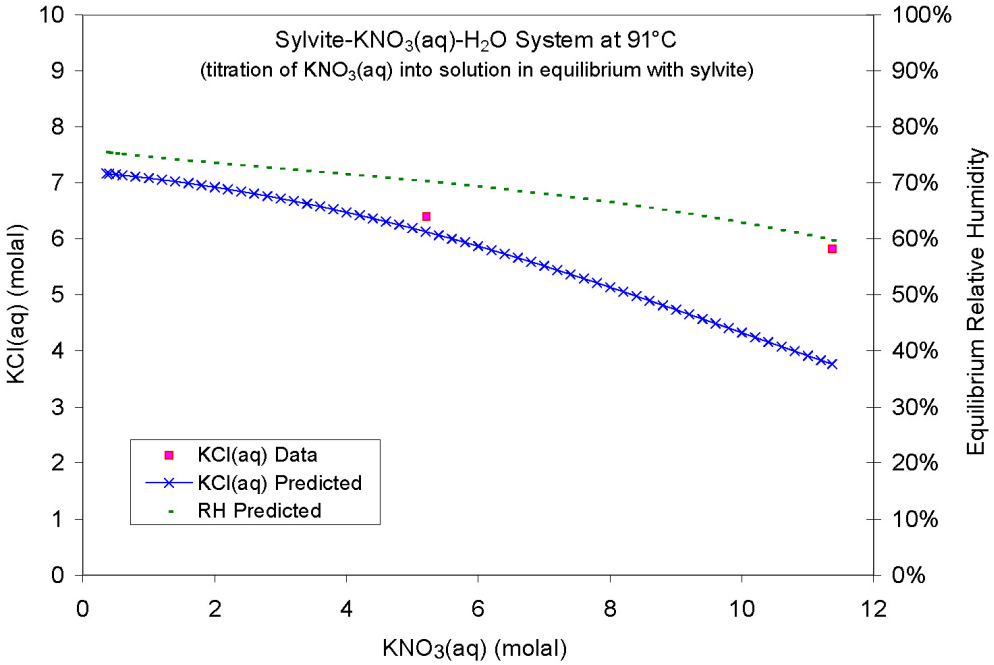

Output DTN: MO0701EQ36IDPS.000, file: *Linke ternary1.zip*, *kcln91.xls*.

Figure 7-35. KCl Solubility Predictions vs. Data as a Function of KNO_3 Concentration at 91°C

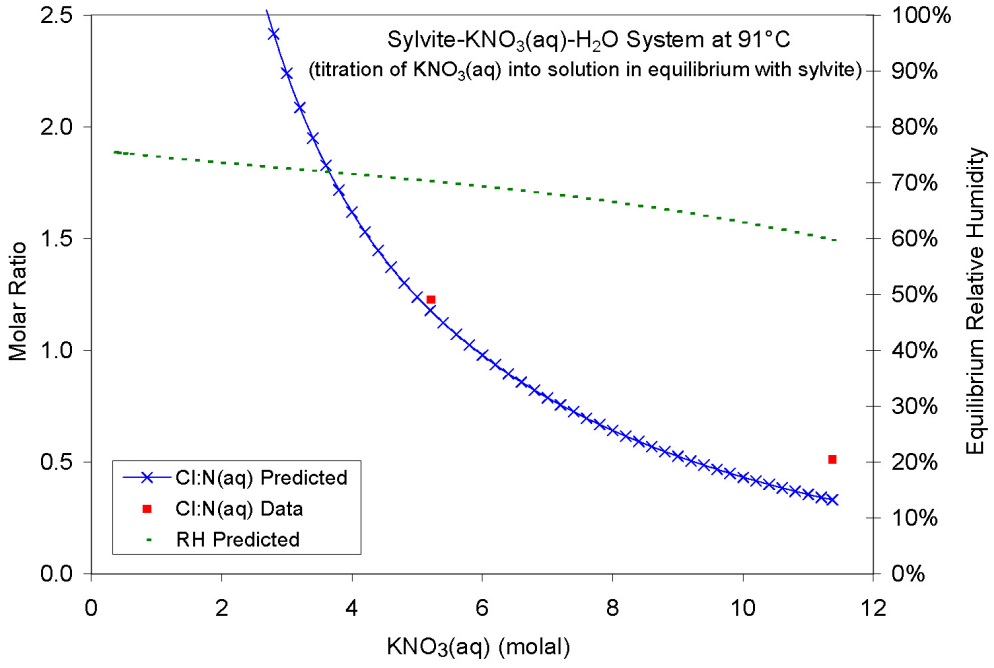

Output DTN: MO0701EQ36IDPS.000, file: *Linke ternary1.zip*, *kcln91.xls*.

Figure 7-36. Cl:NO_3 Mole Ratio Predictions at KCl Saturation vs. Data as a Function of KNO_3 Concentration at 91°C

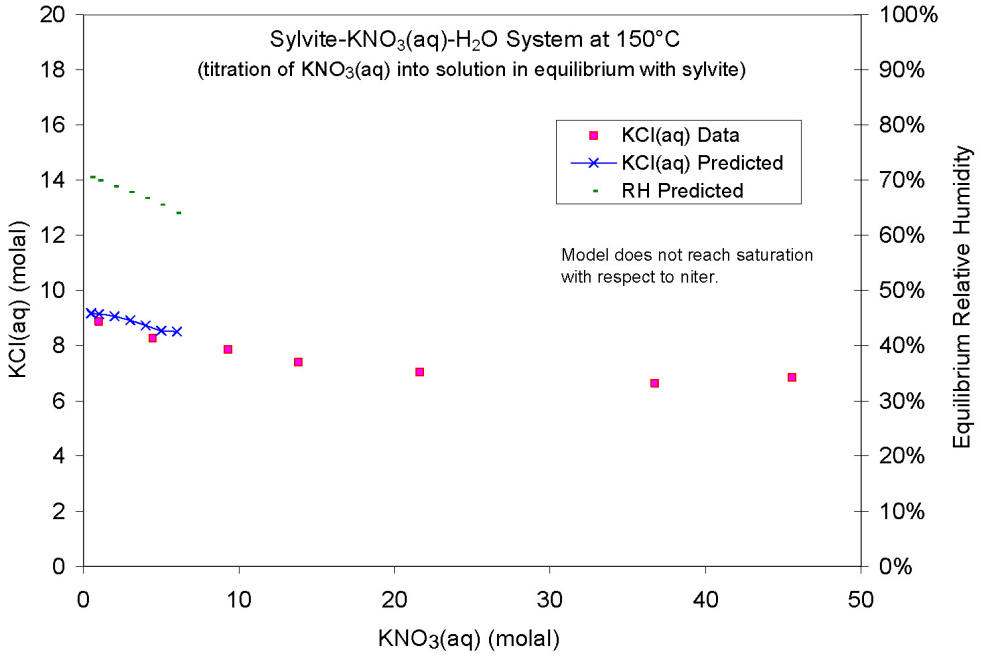

Output DTN: MO0701EQ36IDPS.000, file: *Linke ternary1.zip*, *kcln150.xls*.

Figure 7-37. KCl Solubility Predictions vs. Data as a Function of KNO_3 Concentration at 150°C

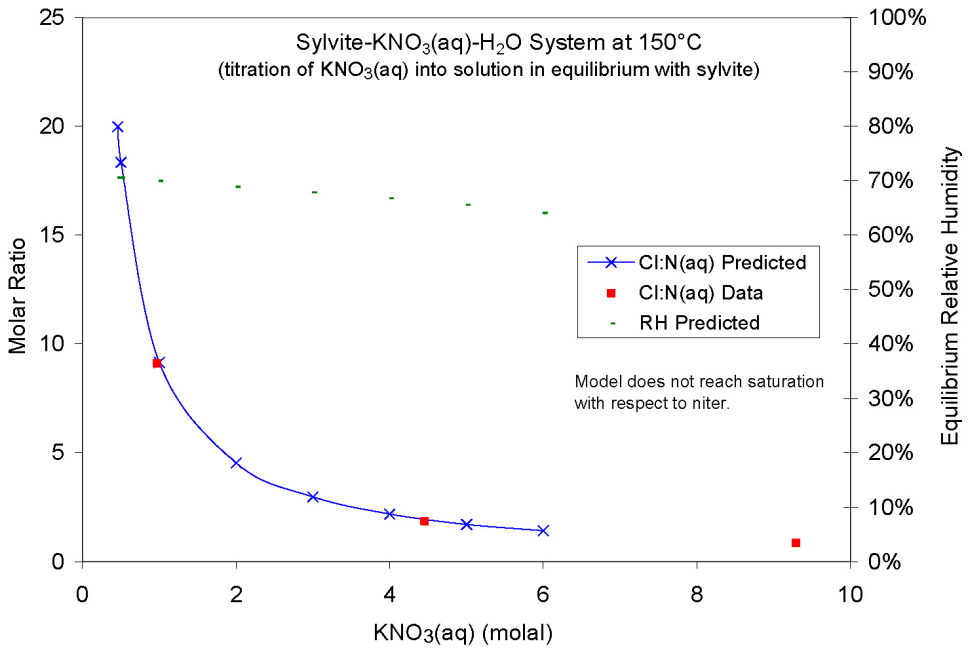

Output DTN: MO0701EQ36IDPS.000, file: *Linke ternary1.zip*, *kcln150.xls*.

Figure 7-38. Cl:NO_3 Mole Ratio Predictions at KCl Saturation vs. Data as a Function of KNO_3 Concentration at 150°C

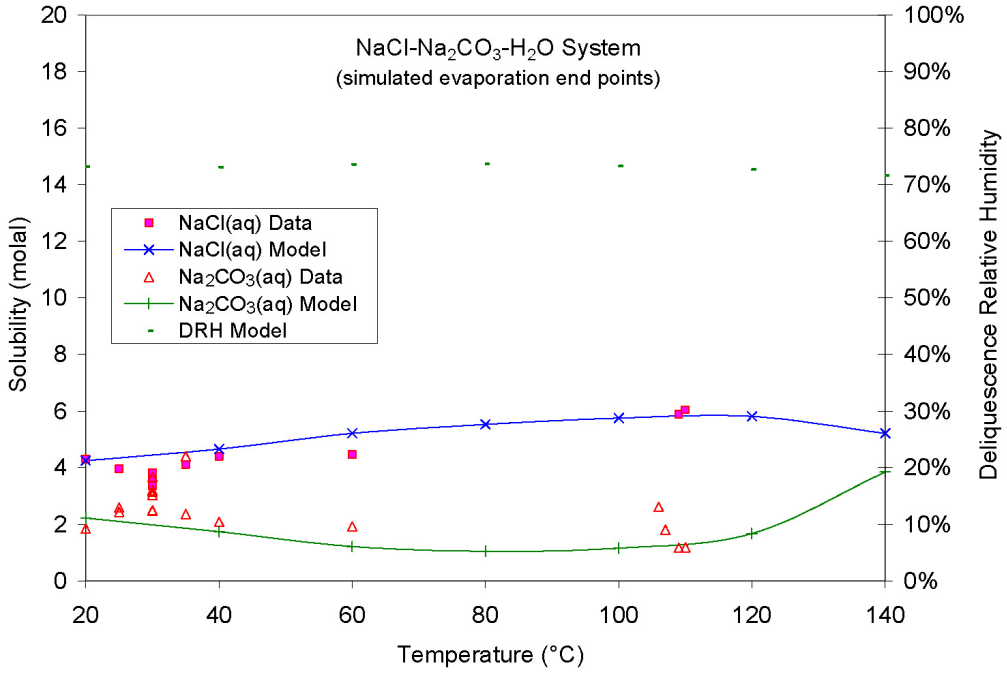

Output DTN: MO0701EQ36IDPS.000, file: *Linke ternary2.zip*, *naclcxev.xls*.

Figure 7-39. Model Predictions vs. Data for Na-Cl-CO_3 Eutectic System

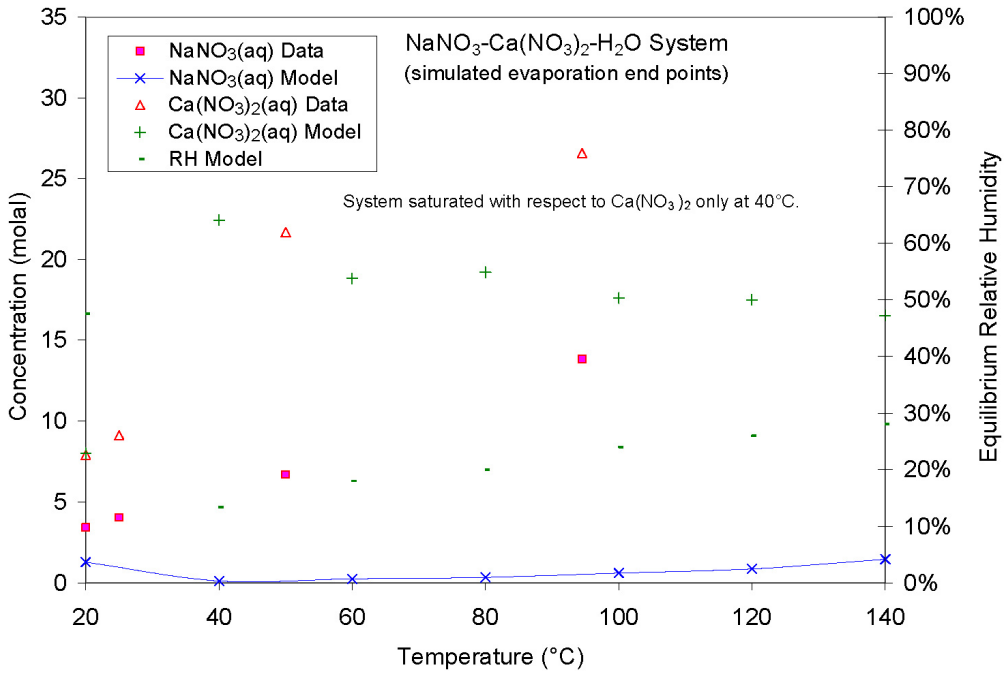

Output DTN: MO0701EQ36IDPS.000, file: *Linke ternary1.zip*, *nacanev.xls*.

Figure 7-40. Model Predictions vs. Data for Na-Ca-NO_3 Eutectic System

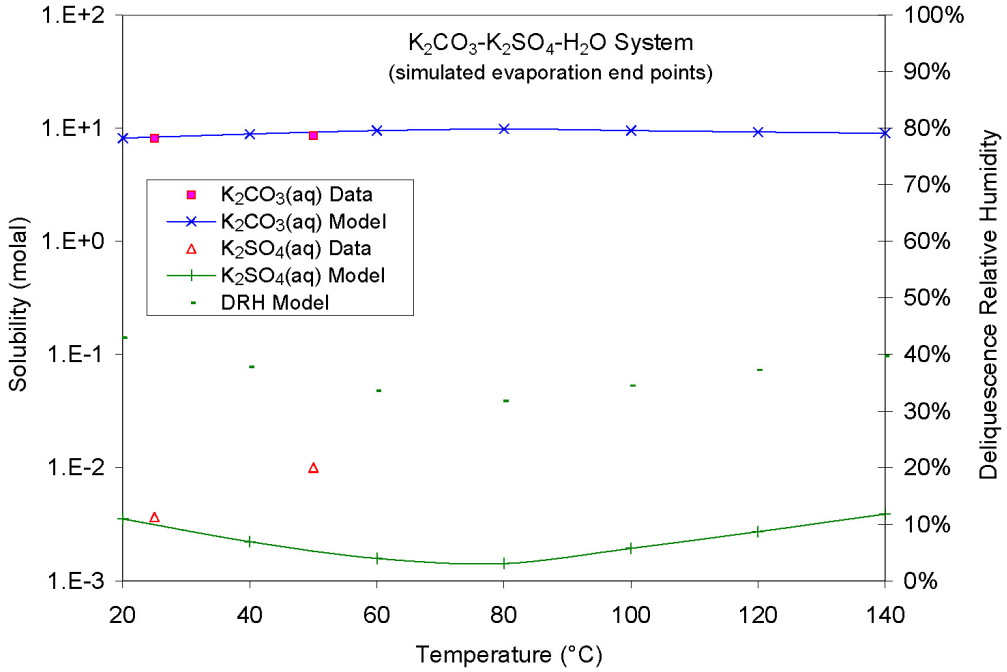

Output DTN: MO0701EQ36IDPS.000, file: *Linke ternary1.zip*, *kcsev.xls*.

Figure 7-41. Model Predictions vs. Data for K-CO_3-SO_4 Eutectic System

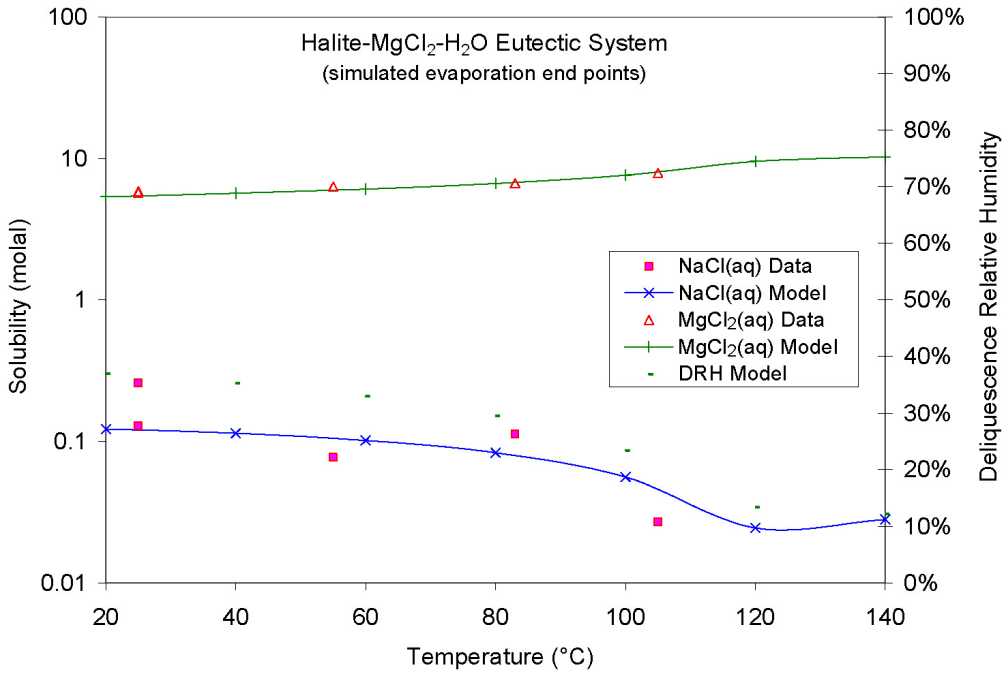

Output DTN: MO0701EQ36IDPS.000, file: *Linke ternary2.zip*, *namgclev.xls*.

Figure 7-42. Model Predictions vs. Data for Na-Mg-Cl Eutectic System

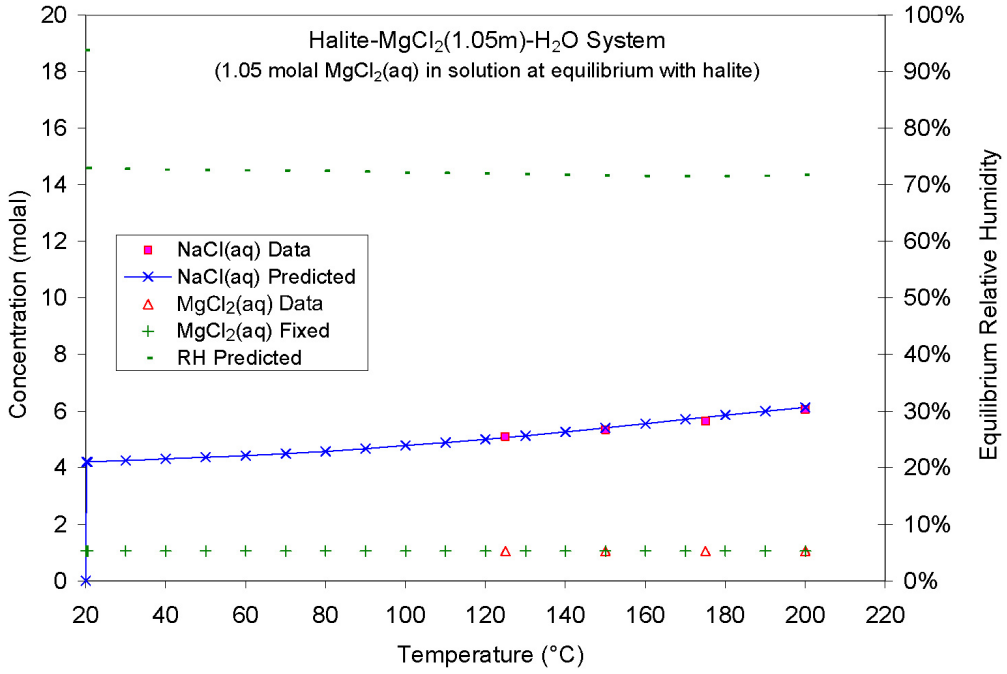

Output DTN: MO0701EQ36IDPS.000, file: *Linke ternary2.zip*, *namgcl1.xls*.

Figure 7-43. NaCl Solubility Predictions vs. Data in the Presence of 1.05 Molal $MgCl_2$

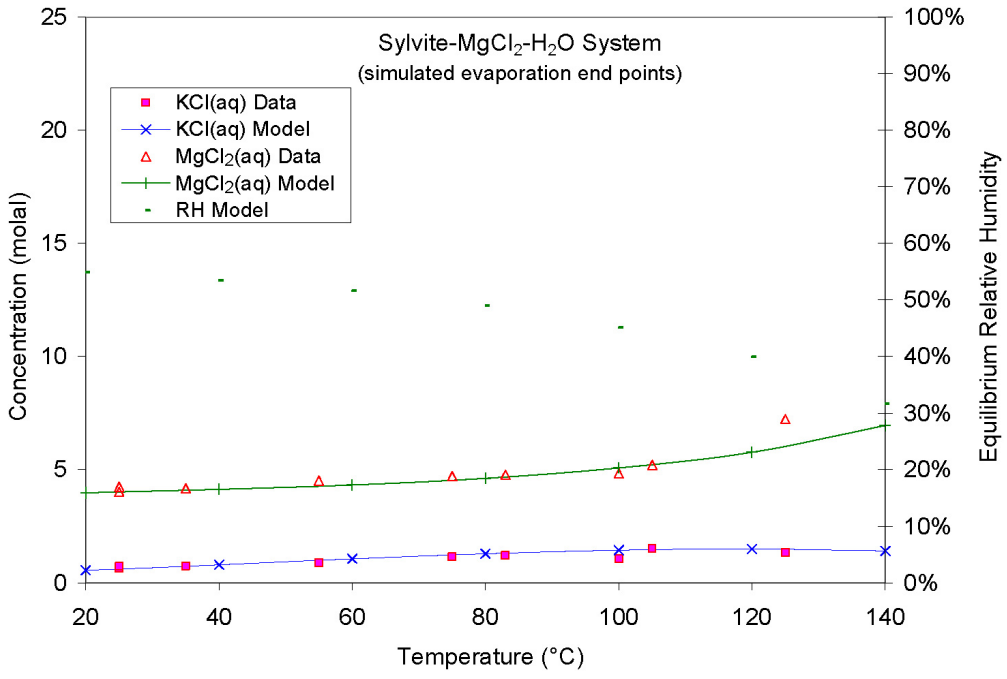

Output DTN: MO0701EQ36IDPS.000, file: *Linke ternary1.zip*, *kmgclev.xls*.

Figure 7-44. Model Predictions vs. Data for K-Mg-Cl Eutectic System

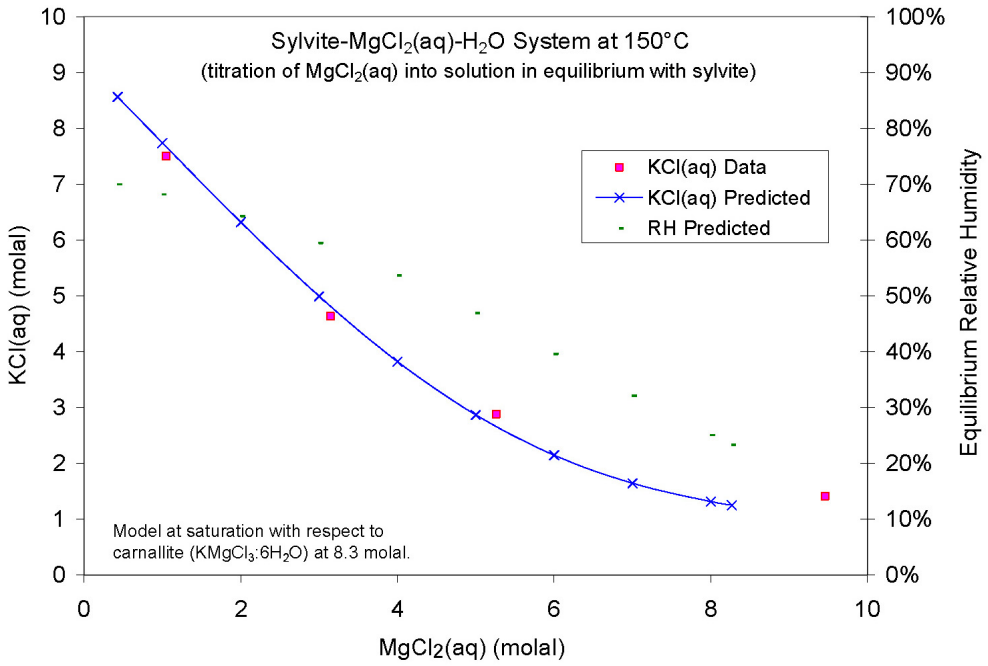

Output DTN: MO0701EQ36IDPS.000, file: *Linke ternary1.zip*, *kmgcl150.xls*.

Figure 7-45. KCl Solubility Predictions vs. Data as a Function of $MgCl_2$ Concentration at 150°C

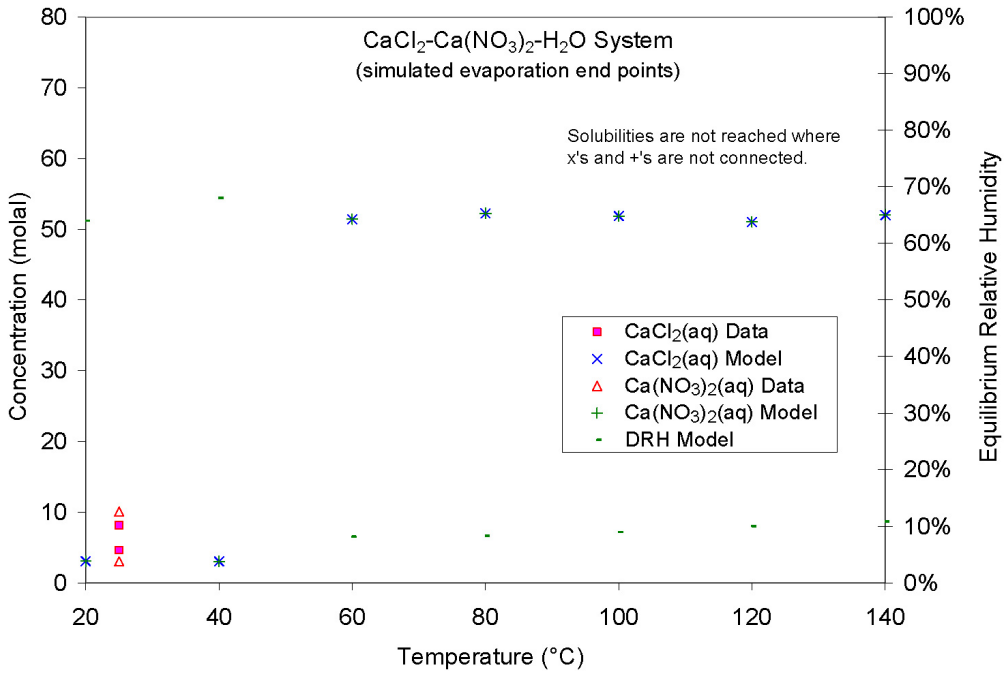

Output DTN: MO0701EQ36IDPS.000, file: *Linke ternary1.zip*, *caclnev.xls*.

Figure 7-46. Model Predictions vs. Data for Ca-Cl-NO_3 Eutectic System

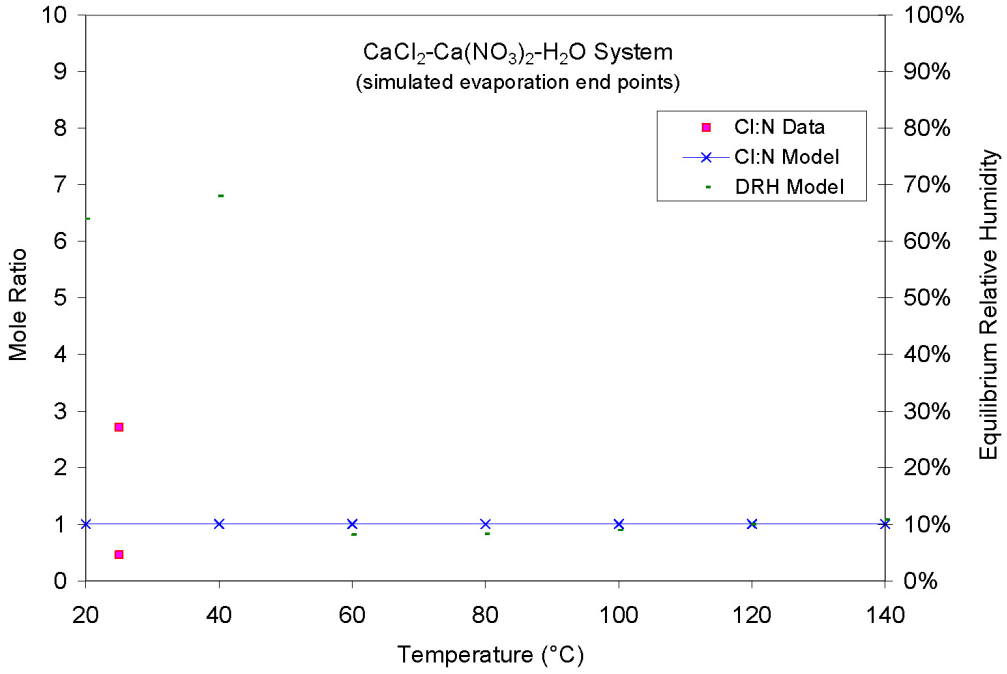

Output DTN: MO0701EQ36IDPS.000, file: *Linke ternary1.zip*, *kcln91.xls*.

Figure 7-47. $Cl:NO_3$ Mole Ratio Predictions vs. Data for Ca-Cl-NO_3 Eutectic System

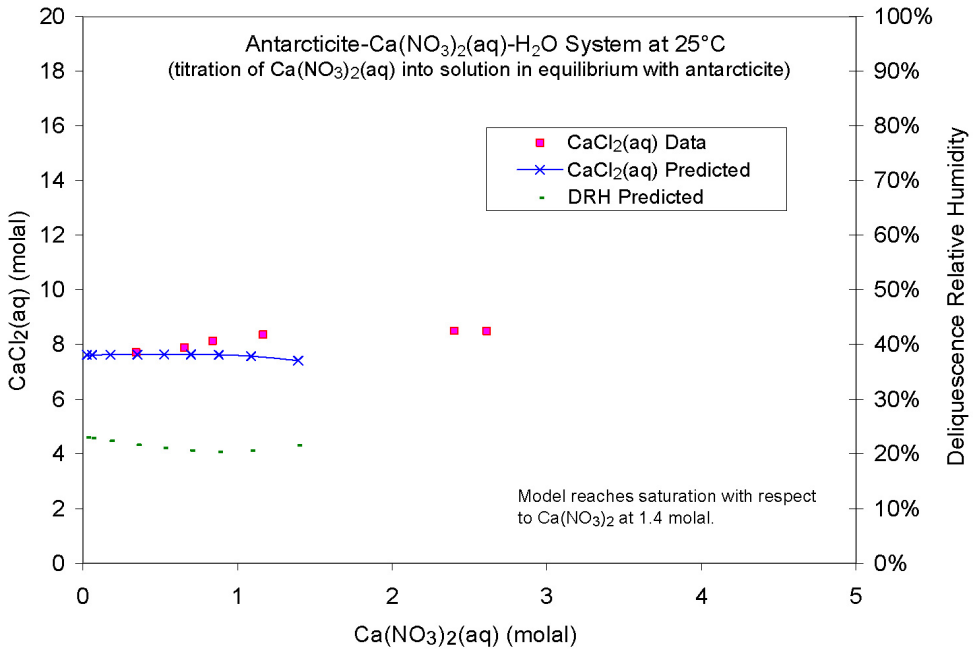

Output DTN: MO0701EQ36IDPS.000, file: *Linke ternary1.zip*, *cacln25n.xls*.

Figure 7-48. $Ca(NO_3)_2$ Solubility Predictions vs. Data as a Function of $CaCl_2$ Concentration at 25°C

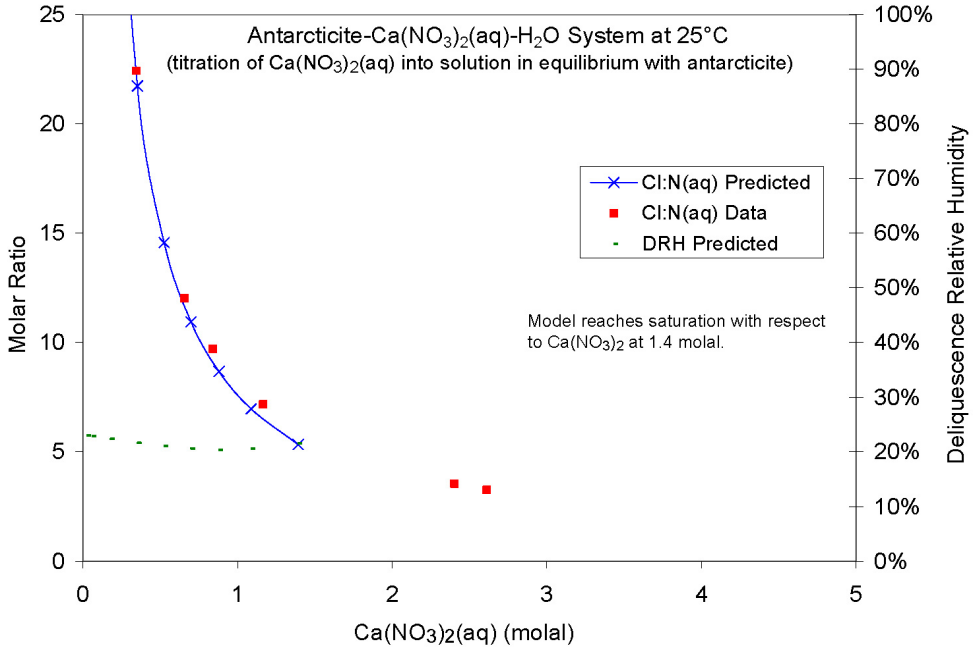

Output DTN: MO0701EQ36IDPS.000, file: *Linke ternary1.zip*, *cacln25n.xls*.

Figure 7-49. Cl:NO $_3$ Mole Ratio Predictions at $Ca(NO_3)_2$ Saturation vs. Data as a Function of $CaCl_2$ Concentration at 25°C

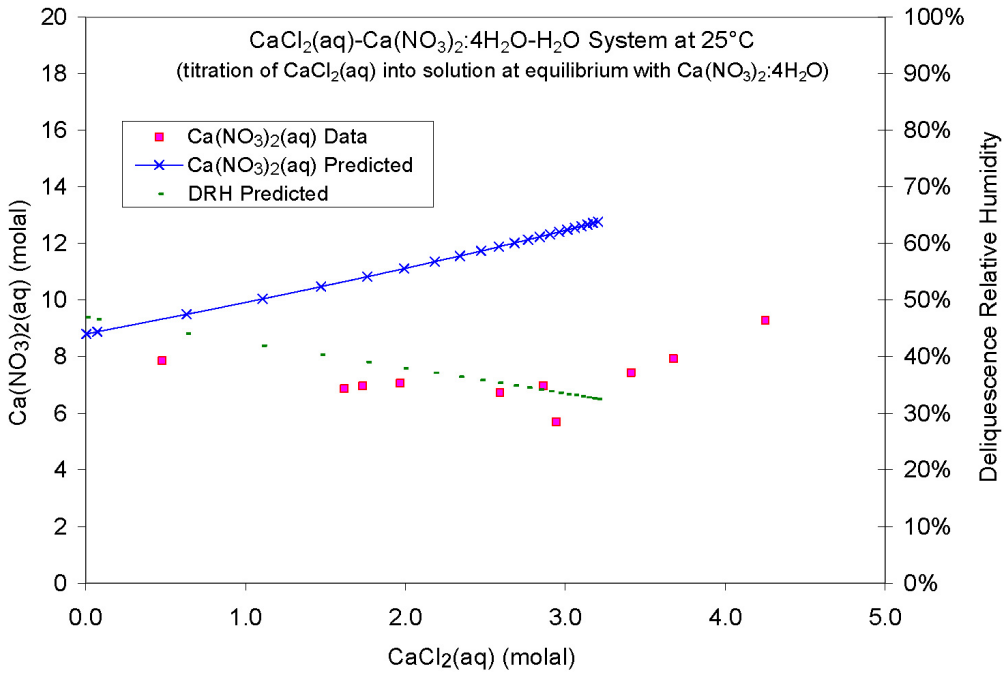

Output DTN: MO0701EQ36IDPS.000, file: *Linke ternary1.zip*, *cacln25n.xls*.

Figure 7-50. $CaCl_2$ Solubility Predictions vs. Data as a Function of $Ca(NO_3)_2$ Concentration at 25°C

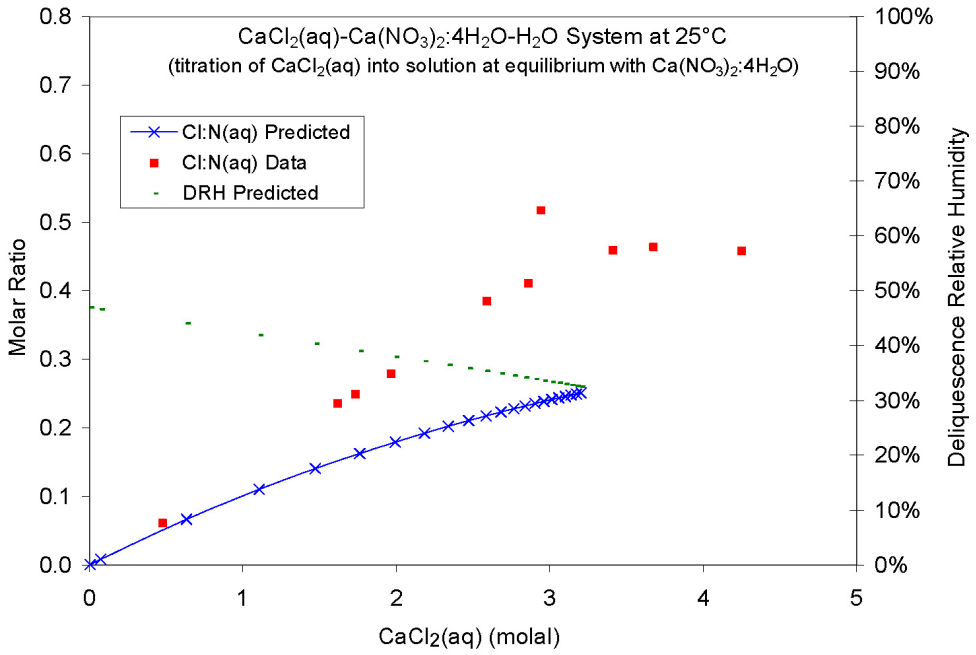

Output DTN: MO0701EQ36IDPS.000, file: *Linke ternary1.zip*, *cacln25.xls*.

Figure 7-51. Cl:NO_3 Mole Ratio Predictions at $CaCl_2$ Saturation vs. Data as a Function of $Ca(NO_3)_2$ Concentration at 25°C

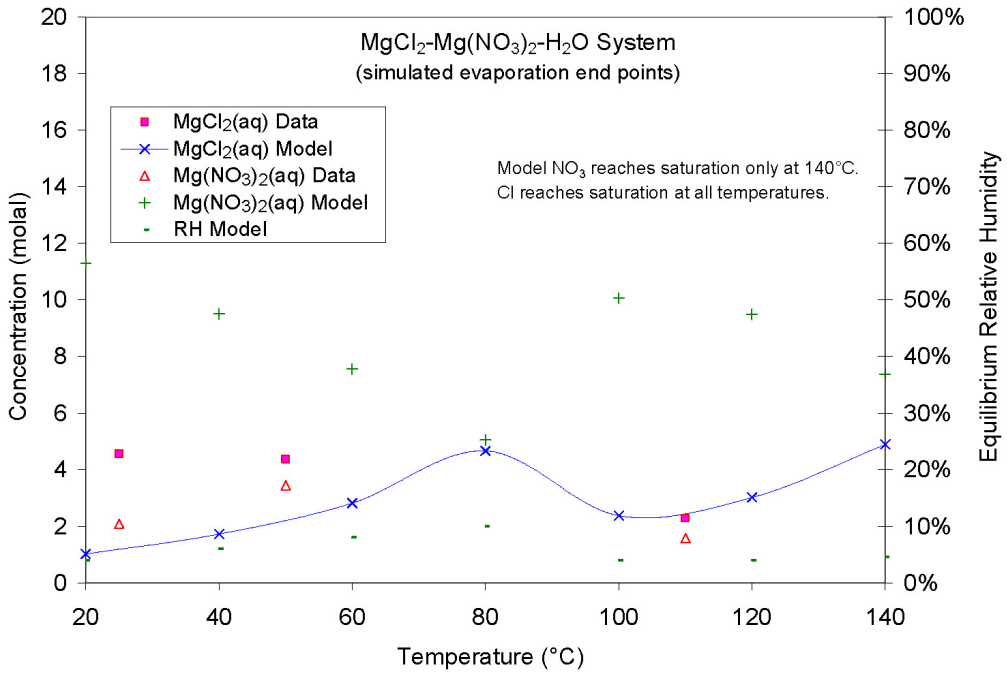

Output DTN: MO0701EQ36IDPS.000, file: *Linke ternary1.zip*, *mgclnev.xls*.

Figure 7-52. Model Predictions vs. Data for Mg-Cl-NO_3 Eutectic System

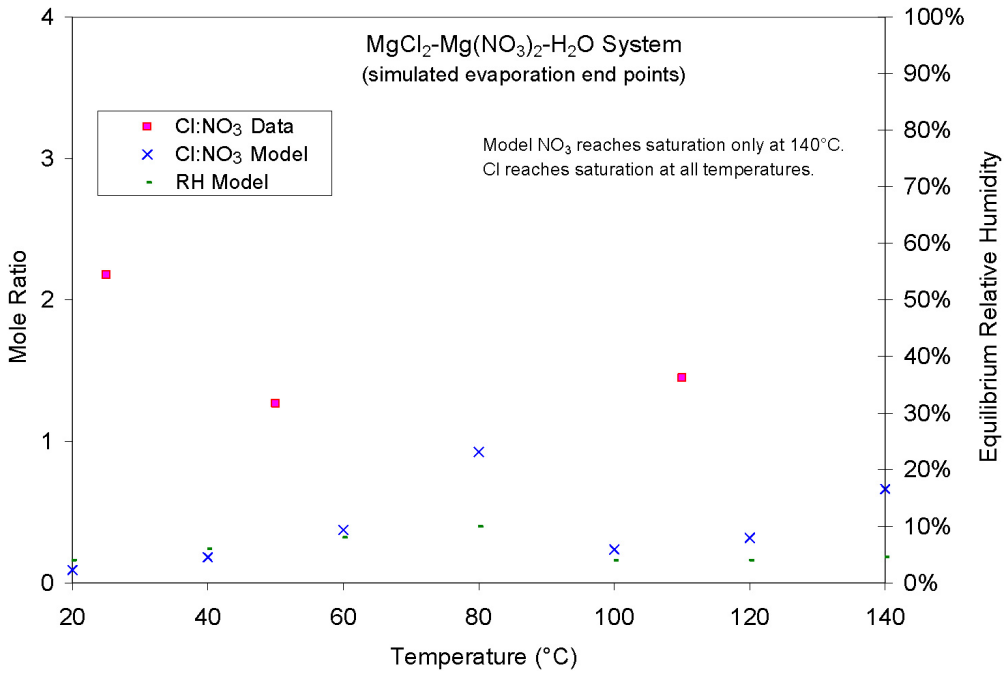

Output DTN: MO0701EQ36IDPS.000, file: *Linke ternary1.zip*, *mgclnev.xls*.

Figure 7-53. $Cl:NO_3$ Mole Ratio Predictions vs. Data for Mg-Cl-NO_3 Eutectic System

7.1.3 Calcite and Carbon Dioxide

Although calcite and carbon dioxide are not soluble salts, they are important players in the evaporative evolution of natural waters. Natural waters are often at saturation with respect to calcite because of the low solubility of calcite and the abundance of calcium, calcite, and carbonate in geologic media (Stumm and Morgan 1996 [DIRS 125332], Figure 4.15). Calcite will usually be one of the first minerals to precipitate upon evaporation (Section 6.3.2). Such is the case for Yucca Mountain ground waters (e.g., Figure 6-7). Carbon dioxide is important because calcite solubility is strongly related to the partial pressure of carbon dioxide. At pH values less than 10, calcite solubility increases in proportion to the cube root of the carbon dioxide partial pressure (Stumm and Morgan 1996 [DIRS 125332], p. 191).

The subsections below investigate the validity of the IDPS model to predict the solubility of calcite and carbon dioxide in simple and multicomponent systems. Sections 7.1.3.1 and 7.1.3.2 examine simple systems in the absence of electrolytes, while Section 7.1.3.3 examines calcite solubility in brines. Section 7.1.3 was added to help address CR-7721.

7.1.3.1 Carbon Dioxide Solubility in Pure Water

The solubility of carbon dioxide in pure water is a function of temperature and the partial pressure of carbon dioxide. Handbook data are presented in Table 4-13 for a temperature range of 0°C to 100°C and CO_2 partial pressures of 0.05 and 0.1 bar. These data are converted to molal concentrations in Table 7-5 by dividing the 1000x mole fractions by 1,000 times the molecular weight of water (18.015 g/mol). This approximation is acceptable because the mole fraction of CO_2 in the solution is very small compared to that of water. These conversions

are documented in file: Ca-CO3-CO2.zip, *Solubility_Ca-CO3-CO2_V1.02 ckd.xls* in Output DTN: MO0701EQ36IDPS.000.

Table 7-5. Solubility of Carbon Dioxide in Pure Water Converted to Molality

Temperature (°C)	CO_2 (aq) at 0.05 bar CO_2 (g) (molal)	CO_2 (aq) at 0.1 bar CO_2 (g) (molal)
0	0.00372	0.00749
5	0.00311	0.00627
10	0.00266	0.00533
15	0.00228	0.00455
20	0.00194	0.00394
25	0.00172	0.00344
30	0.00150	0.00300
35	0.00133	0.00266
40	0.00122	0.00239
45	0.00111	0.00216
50	0.00100	0.00200
55	0.00089	0.00183
60	0.00083	0.00167
65	0.00078	0.00155
70	0.00072	0.00144
75	0.00067	0.00139
80	0.00067	0.00128
85	0.00061	0.00122
90	0.00061	0.00117
95	0.00056	0.00111
100	0.00056	0.00111

NOTE: Solubilities converted to molalities from 1000x mole fractions in Table 4-13.

EQ3/6 simulations using the IDPS Pitzer database were performed to compare CO_2 solubility calculations to the handbook data. The input files are called *co2.3i*, *co2-1.6i*, and *co2-13.6i*. The EQ6 simulations, *co2-1.6i* and *co2-13.6i*, have fixed CO_2 partial pressures of 0.05 and 0.1 bar and spanned a temperature range of 0°C to 140°C. Outputs are compiled and charted in spreadsheet *Ca-CO3-CO2.zip,co2.xls* in Output DTN: MO0701EQ36IDPS.000.

Figure 7-54 shows that there is nearly perfect agreement between the handbook data and model CO_2 solubility predictions in this simple system. More complex systems involving fixed CO_2 partial pressures are simulated in subsequent sections.

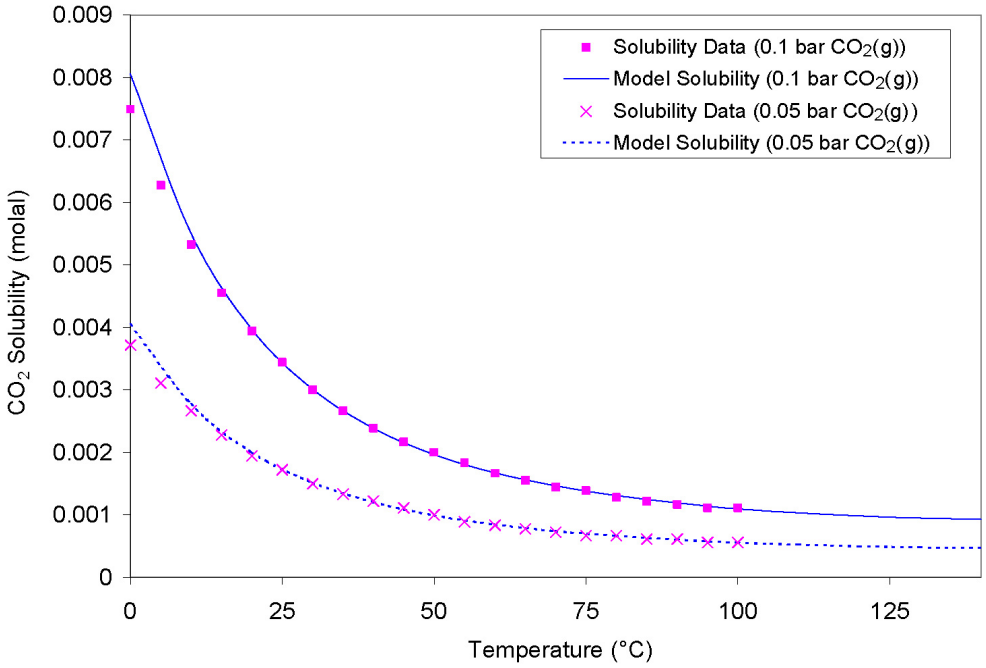

Output DTN: MO0701EQ36IDPS.000, file: *Ca-CO3-CO2.zip*, *co2.xls*.

Figure 7-54. CO_2 Solubility Prediction vs. Handbook Data

7.1.3.2 Calcite Solubility in Pure Water

As in the case of CO_2 solubility, the solubility of calcite in pure water is a function of temperature and the partial pressure of CO_2. Solubility data are presented in Table 4-14 for a temperature range of 0°C to 50°C and CO_2 partial pressures of 0.00032 and 0.1 atm. These data are converted to molal concentrations at each temperature in Table 7-6 by multiplying the millimolal values in Table 4-14 by 1,000 times the solubility ratio. These calculations are documented in file *Ca-CO3-CO2.zip*, *Solubility_Ca-CO3-CO2_V1.02 ckd2.xls* in Output DTN: MO0701EQ36IDPS.000 .

Table 7-6. Solubility of Calcite in Pure Water as a Function of Temperature and CO_2 Partial Pressure

Temperature (°C)	Calcite Solubility at 0.00032 atm CO_2 (g) (molal)	Calcite Solubility at 0.001 atm CO_2 (g) (molal)	Calcite Solubility at 0.01 atm CO_2 (g) (molal)	Calcite Solubility at 0.1 atm CO_2 (g) (molal)
0	0.00095	0.00140	0.00306	0.00702
10	0.00074	0.00109	0.00238	0.00546
20	0.00058	0.00086	0.00187	0.00429
25	0.00053	0.00078	0.00170	0.00390
30	0.00048	0.00070	0.00153	0.00351
50	0.00032	0.00047	0.00102	0.00234

NOTE: Solubilities converted to molalities from Table 4-14.

For these validation simulations, the EQ6 input files are called *cXX-YYY.6i*, where *XX* is 10 times the log of the CO_2 partial pressure and -*YYY* is the temperature (°C) (e.g., *c35-020.6i* is for a CO_2 partial pressure of $10^{-3.5}$ bar and a temperature of 20°C). Each of these simulations is an application of the IDPS model. Dilute solutions of $CaCO_3$ are evaporated at constant temperature and CO_2 partial pressure until the eutectic point is reached. In this case, the eutectic point is reached when the concentrations of calcium and carbonate become saturated with respect to calcite.

Calcite solubility predictions are compared to the handbook data in Figure 7-55. Predictions are generally lower than handbook solubilities but well within validation criteria. Outputs are compiled and charted in file *Ca-CO3-CO2.zip*, *caco3-ev.xls*. All inputs and outputs for these simulations are documented in Output DTN: MO0701EQ36IDPS.000.

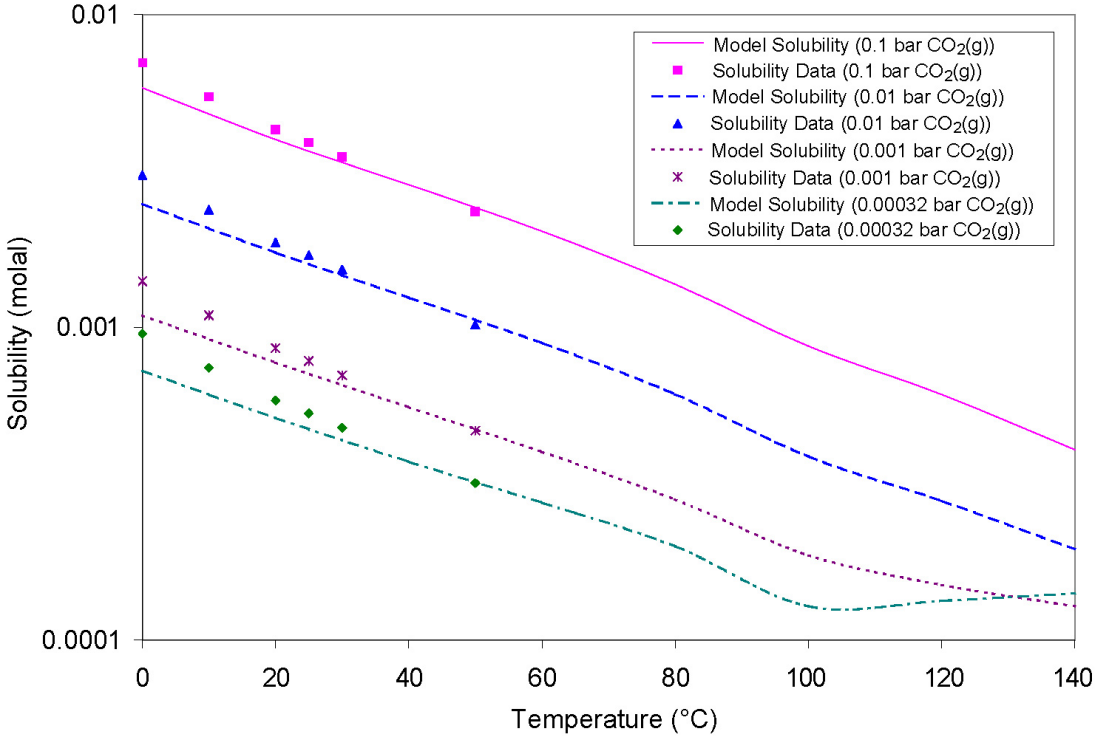

Output DTN: MO0701EQ36IDPS.000, file: *Ca-CO3-CO2.zip*, *caco3-ev.xls*.

Figure 7-55. Calcite Solubility Prediction vs. Handbook Data

7.1.3.3 Calcite Solubility in Brines

In saline waters, dissolved calcium and carbonate, like other electrolytes, do not exhibit ideal behavior. The IDPS model uses the Pitzer equations of EQ3/6 and the Pitzer ion-interaction coefficients of the IDPS Pitzer database to predict the effects of electrolyte concentrations on aqueous complexation and mineral solubilities. In the following two sections, calcite solubility in brines is examined and compared to IDPS model predictions.

7.1.3.3.1 Calcite-CO_2-(NaCl,KCl,$CaCl_2$)-(Gypsum)

The solubility of calcite was studied by Wolf et al. (1989 [DIRS 177633]) at different temperatures and at CO_2 partial pressures around 1 kPa (~ 0.01 atm). In these experiments, calcite or both calcite and gypsum were equilibrated with NaCl, KCl, or $CaCl_2$ solutions at concentrations from 0 to 6.33 molal. The solutions were stirred magnetically and equilibrated with a stream of nitrogen gas containing 1.00% ± 0.02% CO_2. Equilibration times were approximately eight days, after which aqueous samples were collected, filtered, and analyzed for total alkalinity, total calcium, and total carbonate. The 25°C and 60°C results of these experiments are presented in Tables 4-15 through 4-18.

The experiments were simulated using EQ3/6 and the IDPS Pitzer database by titrating NaCl, KCl, and $CaCl_2$ into solutions containing calcite or both calcite and gypsum. The results are compared to the data in Figures 7-56 through 7-63. The NaCl-Calcite-CO_2-H_2O system is not presented because the data from this system was used in the development of the Pitzer database.

The model predictions are generally within 10% of measurements except at high KCl concentrations in the KCl-Gypsum-Calcite-CO_2-H_2O system (Figures 7-60 and 7-61). The divergence of the predictions from the measurements is due to the precipitation of pentasalt or syngenite in the simulations. These minerals apparently do not form in the eight-day experiments; otherwise the trajectories of the data would mimic those of the simulations. Because the experiments do not begin with sulfate in solution, the only sulfate source is the gypsum that must first dissolve to form the syngenite or pentasalt, a process that is likely to be too slow to be of consequence in the experimental timeframe.

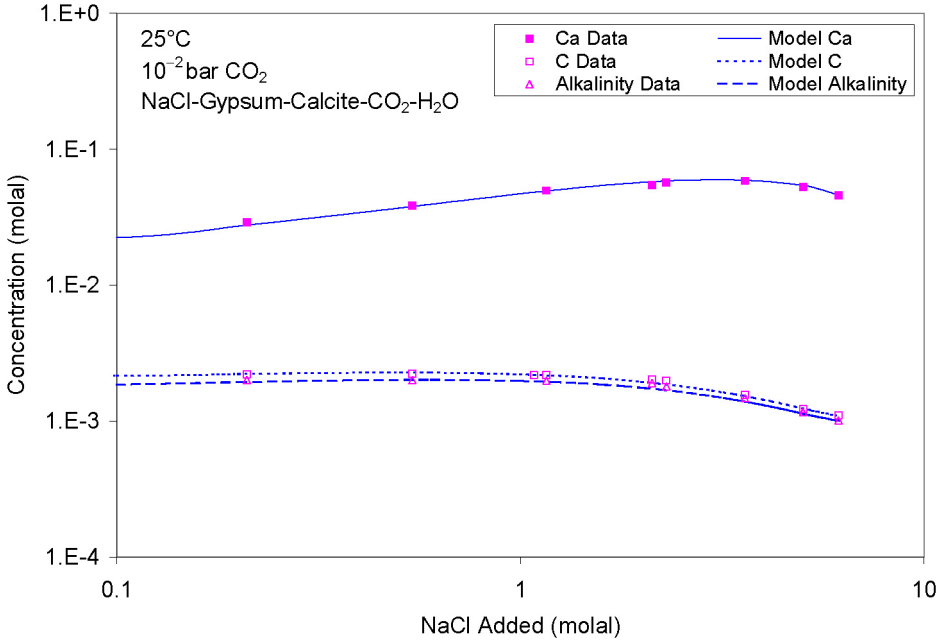

Output DTN: MO0701EQ36IDPS.000, file: *Ca-CO3-CO2.zip*, *Calcite Wolf et al NaCl gyp r1.xls*.

Figure 7-56. Predicted vs. Measured Concentrations for Calcite Solubility Experiments in System NaCl-Gypsum-Calcite-CO_2-H_2O at 25°C (Wolf et al. 1989 [DIRS 177633])

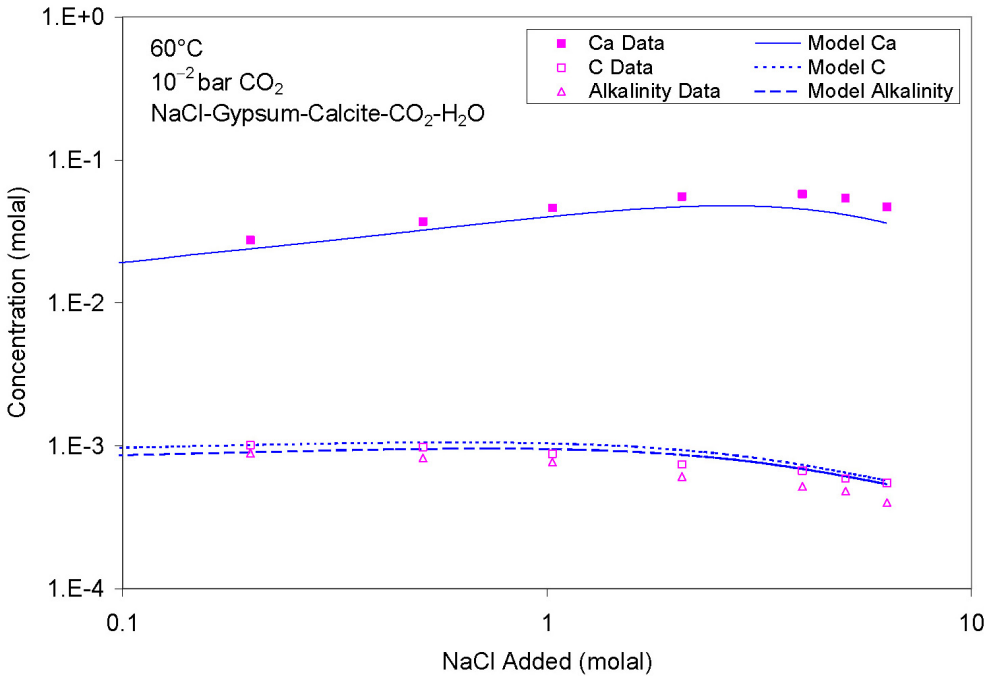

Output DTN: MO0701EQ36IDPS.000, file: *Ca-CO3-CO2.zip*, *Calcite Wolf et al NaCl gyp r1.xls*.

Figure 7-57. Predicted vs. Measured Concentrations for Calcite Solubility Experiments in System NaCl-Gypsum-Calcite-CO_2-H_2O at 60°C (Wolf et al. 1989 [DIRS 177633])

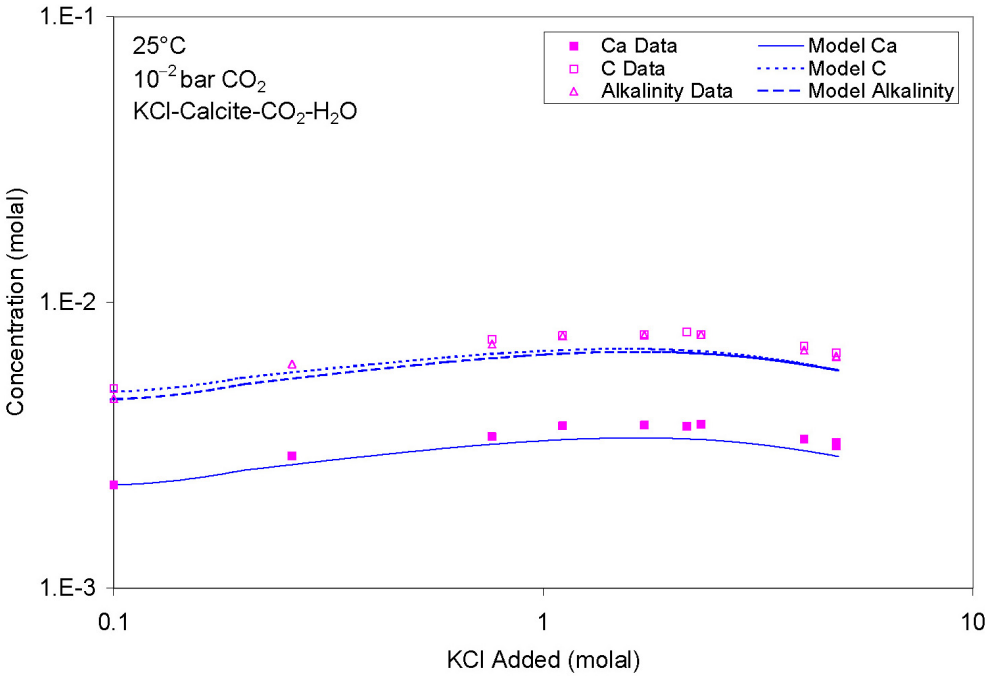

Output DTN: MO0701EQ36IDPS.000, file: *Ca-CO3-CO2.zip*, *Calcite Wolf et al KCl r1.xls*.

Figure 7-58. Predicted vs. Measured Concentrations for Calcite Solubility Experiments in System KCl-Calcite-CO_2-H_2O at 25°C (Wolf et al. 1989 [DIRS 177633])

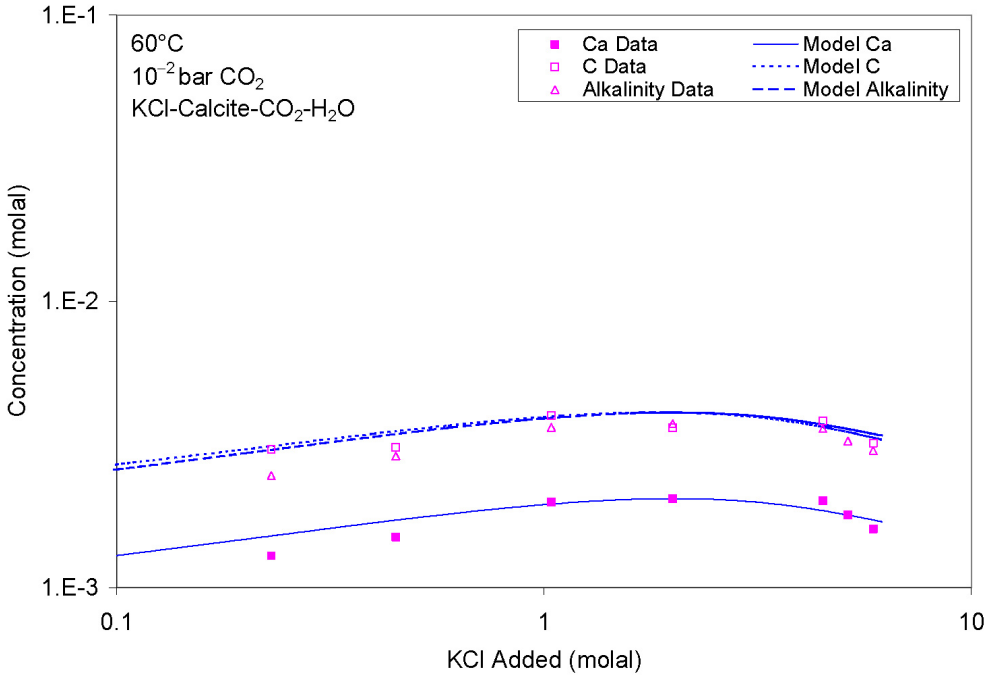

Output DTN: MO0701EQ36IDPS.000, file: *Ca-CO3-CO2.zip*, *Calcite Wolf et al KCl r1.xls*.

Figure 7-59. Predicted vs. Measured Concentrations for Calcite Solubility Experiments in System KCl-Calcite-CO_2-H_2O at 60°C (Wolf et al. 1989 [DIRS 177633])

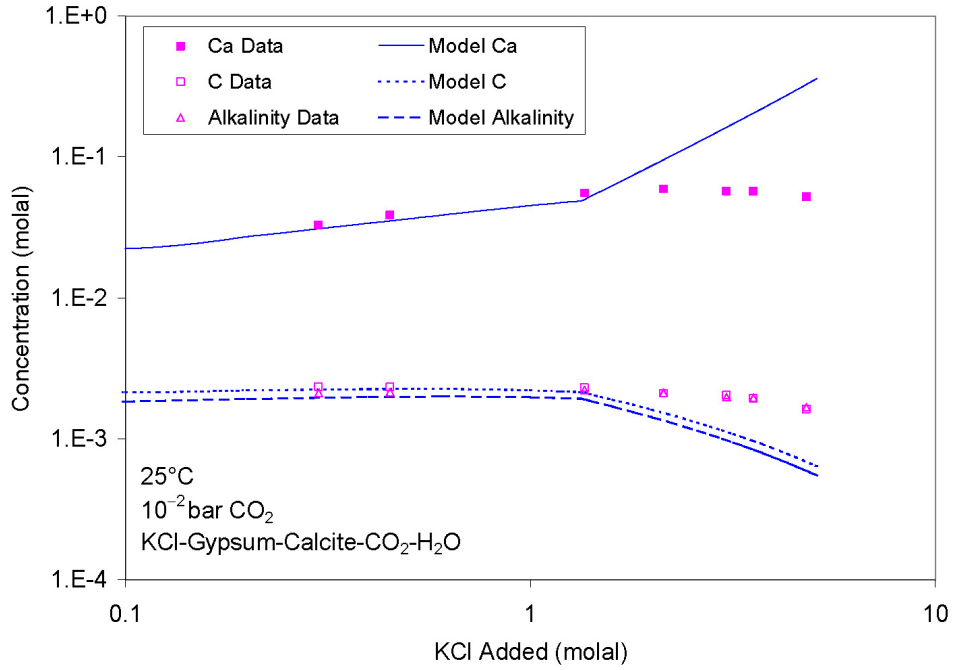

Output DTN: MO0701EQ36IDPS.000, file: *Ca-CO3-CO2.zip*, *Calcite Wolf et al KCl gyp r1.xls*.

Figure 7-60. Predicted vs. Measured Concentrations for Calcite Solubility Experiments in System KCl-Gypsum-Calcite-CO_2-H_2O at 25°C (Wolf et al. 1989 [DIRS 177633])

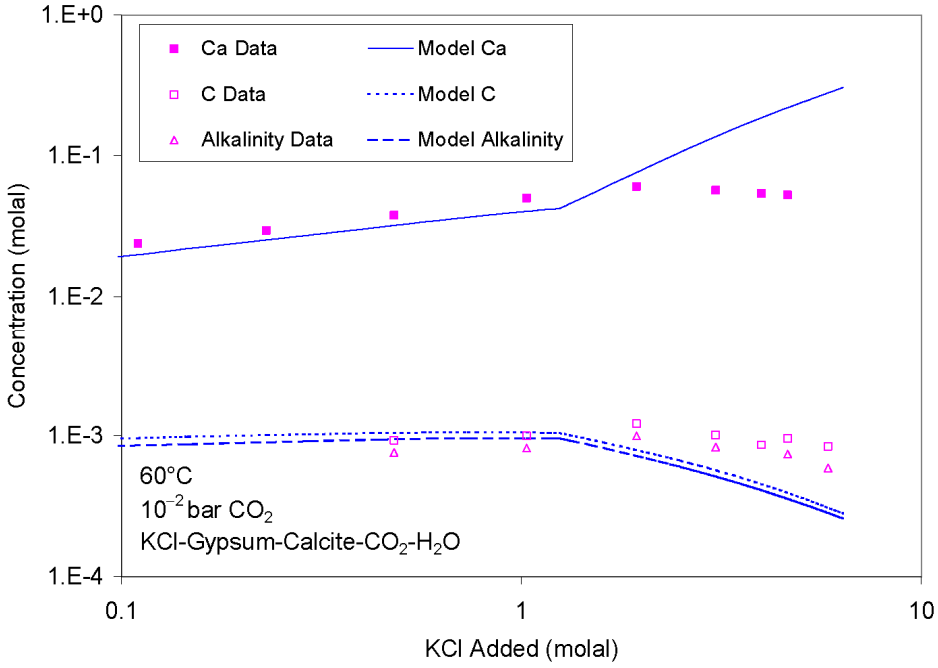

Output DTN: MO0701EQ36IDPS.000, file: *Ca-CO3-CO2.zip*, *Calcite Wolf et al KCl gyp r1.xls*.

Figure 7-61. Predicted vs. Measured Concentrations for Calcite Solubility Experiments in System KCl-Gypsum-Calcite-CO_2-H_2O at 60°C (Wolf et al. 1989 [DIRS 177633])

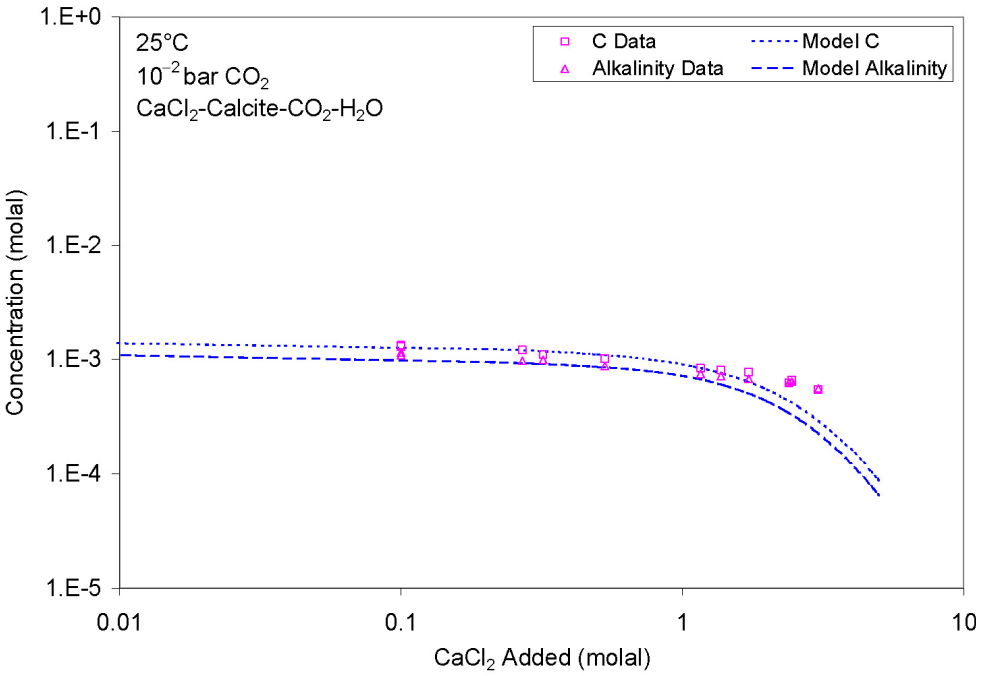

Output DTN: MO0701EQ36IDPS.000, file: *Ca-CO3-CO2.zip*, *Calcite Wolf et al CaCl2 r1.xls*.

Figure 7-62. Predicted vs. Measured Concentrations for Calcite Solubility Experiments in System $CaCl_2$-Calcite-CO_2-H_2O at 25°C (Wolf et al. 1989 [DIRS 177633])

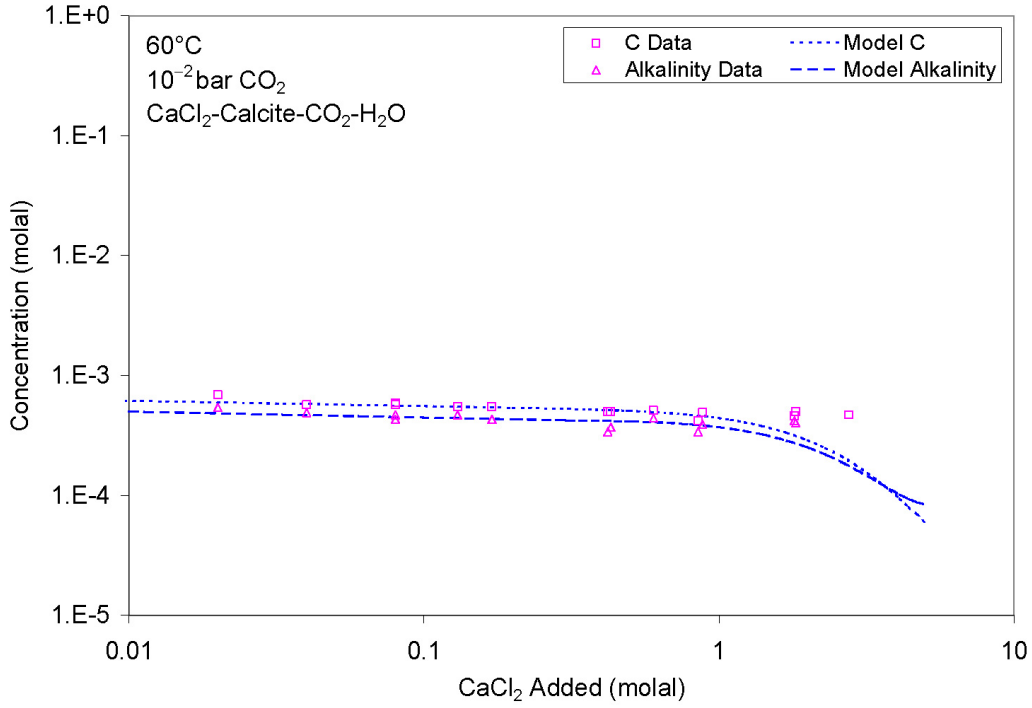

Output DTN: MO0701EQ36IDPS.000, file: *Ca-CO3-CO2.zip*, *Calcite Wolf et al CaCl2 r1.xls*.

Figure 7-63. Predicted vs. Measured Concentrations for Calcite Solubility Experiments in System $CaCl_2$-Calcite-CO_2-H_2O at 60°C (Wolf et al. 1989 [DIRS 177633])

7.1.3.3.2 Calcite-CO_2-Na-Ca-Mg-K-Cl-(SO_4)

He and Morse (1993 [DIRS 162090]) studied calcite solubility in aqueous Na-K-Ca-Mg-Cl-SO_4 solutions. This work involved a number of experiments, some of which were used to derive Pitzer ion-interaction parameters, which were ultimately adopted for the IDPS Pitzer database (Tables 4-2 and 4-3). Another set of experiments presented in the same study involved measuring calcite solubility in three different synthetic brines. These additional experiments were used to test the derived database and Pitzer parameters. Because they were performed independently from the experiments used to derive the Pitzer parameters, the results from these experiments are used here as a validation exercise. The three brines, called Colbey 12, Colbey 18, and Kennedy 1, are presented in Table 4-19 along with the measured calcium and carbonate solubilities in these brines.

The specific experiments simulated are the experiments in which calcite solubility was approached from undersaturation. These experiments were conducted in open systems with a partial pressure of CO_2 of approximately 0.0004 atm. The experiments that approached equilibrium from supersaturation involved partial pressures of CO_2 near 1 atm, which is far beyond the required range of the IDPS model.

In each experiment, six grams of reagent grade calcite was stirred into 200 grams of synthetic brine for a period of between six hours and one week depending on the temperature and CO_2 conditions. After the equilibration periods, 100 mL of solution was sampled, filtered, weighed, and analyzed for total alkalinity, total calcium, and total carbonate.

The experimental endpoints were simulated using the IDPS Pitzer database by equilibrating the three brines with excess calcite over the temperature range of the experiments and fixing the partial pressure of CO_2 at approximately 0.0004 atm. Results within the temperature range of the IDPS model are compared to the data in Figures 7-64 and 7-65.

The IDPS model predicts that huntite ($CaMg_3(CO_3)_4$) will precipitate in the Colbey 18 experiments above a temperature of 37°C. Huntite is generally not suppressed in the IDPS model because the model is designed to simulate processes that occur over many months or years. Because the experiments simulated here lasted from six hours to one week, there likely was not time for an appreciable amount of huntite to precipitate if indeed the solution was supersaturated with respect to huntite. The effect of allowing or suppressing huntite is shown in the figures. Allowing huntite to precipitate increases the calcite solubility. This increase is not observed in the experiments, suggesting that huntite did not precipitate in the experiments.

Model predictions are within a factor of three or less of the measurements when huntite formation is suppressed. When it is not suppressed, the difference can be as high as a factor of five. Thus, these results satisfy validation criteria with or without huntite suppression.

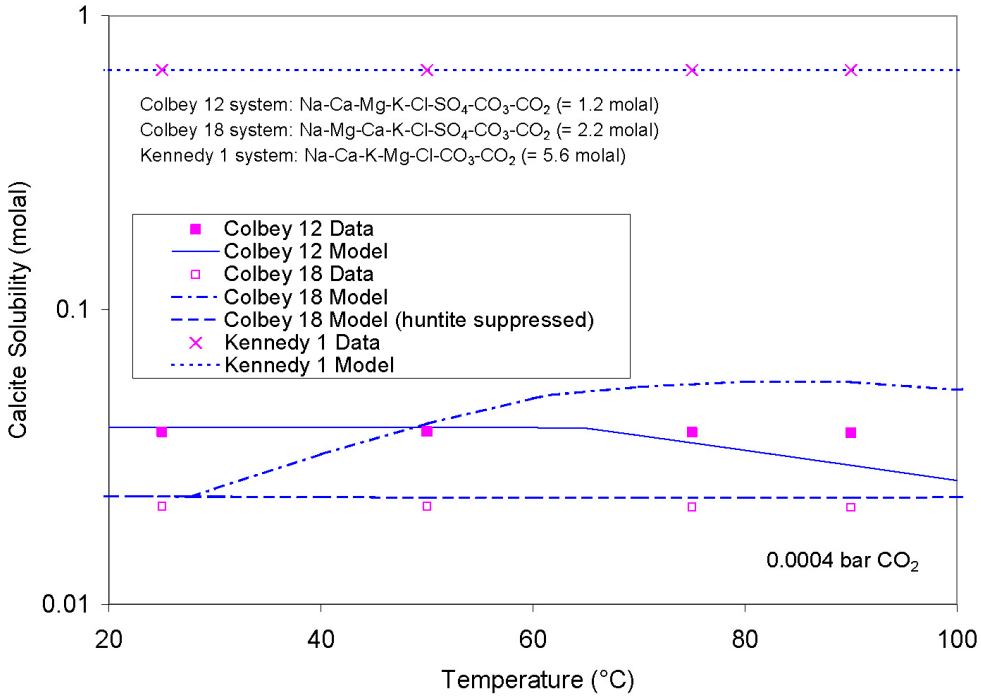

Output DTN: MO0701EQ36IDPS.000, file: *Ca-CO3-CO2.zip*, *Calcite He and Morse r2.xls*.

Figure 7-64. Predicted vs. Measured Calcite Solubility in Three Synthetic Brines (He and Morse 1993 [DIRS 162090])

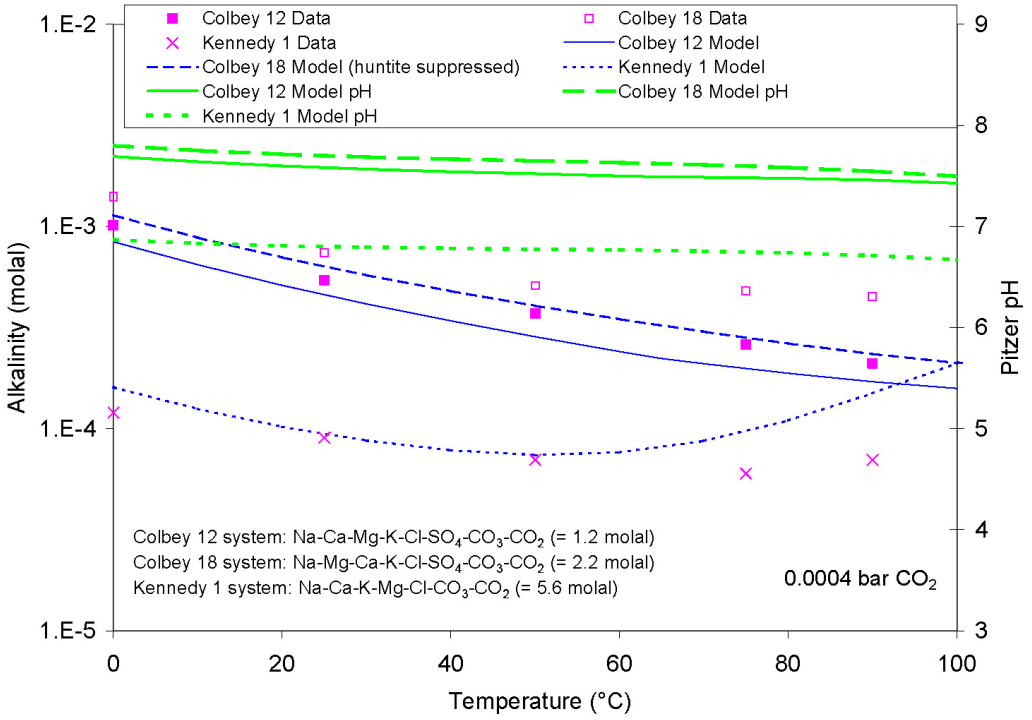

Output DTN: MO0701EQ36IDPS.000, file: *Ca-CO3-CO2.zip*, *Calcite He and Morse r2.xls*.

Figure 7-65. Predicted vs. Measured Alkalinity in Calcite Solubility Experiments of Three Synthetic Brines (He and Morse 1993 [DIRS 162090])

7.2 VALIDATION USING EVAPORATION DATA

Several sources of evaporation data are relevant to the validation of the model. They include studies by Rosenberg et al. (1999 [DIRS 125338]; 1999 [DIRS 125339]), Alai et al. (2005 [DIRS 176811]), and McCaffrey et al. (1987 [DIRS 164481]), and the report *Environment on the Surfaces of the Drip Shield and Waste Package Outer Barrier* (BSC 2001 [DIRS 155640]). These data are presented in Tables 4-20 through 4-25 in Section 4.4.

7.2.1 Evaporation of Average J-13 Well Water at 85°C

Rosenberg et al. (1999 [DIRS 125338]) evaporated synthetic J-13 well water in a beaker that was open to the atmosphere and maintained at a constant elevated temperature of 85°C. In the experiment named evap1, synthetic average J-13 well water was evaporated without contact with tuff or other non-precipitated rock material. The experiment began with 30 liters of synthetic average J-13 well water with a measured composition as shown in Table 4-20. A peristaltic pump was used to pump this water into a 1-liter Pyrex beaker at a constant rate while a hot plate was used to maintain a water temperature of 85°C to evaporate the water. Water samples were collected after the 30 liters had been evaporated to approximately 30 mL. Results of this experiment are also included in Table 4-20. The solids that had accumulated at this stage were identified by x-ray diffraction to be amorphous silica, aragonite, and calcite. Analysis of solids after complete evaporation indicated the additional presence of halite, niter, thermonatrite, and possibly gypsum, anhydrite, and hectorite.

In a similar synthetic J-13 well water evaporation experiment (named evap4), the pH of the evaporating water was monitored intermittently during the evaporation (Rosenberg et al. 1999 [DIRS 125338]). The experiment used approximately the same J-13 starting solution as evap1 (Table 4-20). The pH measurements are presented in Table 4-21 as a function of the reported concentration factor. There is some uncertainty associated with the pH measurements. Details of the pH measurement procedure are not reported. Measuring pH at high temperature and/or in saline conditions requires special methods (Section 7.5.1), which may or may not have been adopted. The reported concentration factor was measured as the ratio of the initial water mass divided by the measured water mass at the time of analysis.

The results of these evaporation experiments were modeled using the IDPS model and Pitzer database. Total aqueous concentrations, pH, ionic strength (*IS*), and mineral precipitation predictions are plotted in Figures 7-66 and 7-67. Comparisons of measurements and predictions are plotted in Figures 7-68 and 7-69. Modeling results are documented in Output DTN: SN0702T0509206.008 .

The final concentration factors (*CF* values) reported for evap1 and evap4 are 956 and 157, respectively. These *CF* values are too high based on the mean measured *CF* values of Na, K, Cl, and NO_3, which are 814 for evap1 and 119 for evap4 (file *j13n1pitpH.xls* in Output DTN: SN0702T0509206.008). These components should have concentrated conservatively in these experiments for the following reasons:

1. Na, K, Cl, and NO_3 should not reach aqueous solubility limits in these experiments. The aqueous solubilities of these components (Table 7-2) are much higher than the maximum aqueous concentrations observed in the experiments (Table 4-20).

2. Minerals containing Na, K, Cl, and NO_3 were not identified by x-ray diffraction at the reported *CF* values (Rosenberg et al. 1999 [DIRS 125338], p. 6).

3. No other processes have been identified that could explain the large losses of Na, K, Cl, and NO_3 that would be needed to achieve the final aqueous concentrations at the reported *CF* values.

For the reported *CF* of 157 (evap4), the losses of Na, K, Cl, and NO_3 (e.g., by precipitation, adsorption to solids, or other process) would need to be 26%, 27%, 28%, and 16%, respectively. For the reported *CF* of 956 (evap1), they would need to be 0%, 5%, 27% and 28%.[1] For evap3, a similar experiment discussed in Section 7.2.3, the reported concentration factors would have required losses of Na, K, and Cl of 42% to 47%. However, as in evap1 and evap4, these salts should have concentrated conservatively (Section 7.2.3) and were not found in the analyzed precipitate.

Adsorption might account for some loss of these ions, but the small amount of precipitated solids in the beaker cannot possibly provide enough adsorption capacity to cause more than a negligible change in the aqueous concentrations of Na, K, Cl, and NO_3. This is clear from a comparison of

[1] Although the required losses of Na and K at the reported *CF* of 956 tend to corroborate the reported *CF*, they are inconsistent with: (1) the 27% and 28% losses of Cl and NO_3 that also would be required, and (2) the 26% and 27% losses of Na and K that would be needed at the much lower reported *CF* of 157.

the predicted mineral accumulation at these *CF* values (Figure 7-67) to the concentrations of these ions in solution at the same *CF* values (Figure 7-66).

The reported *CF* values for evap1 and evap4 were calculated from bulk mass measurements (Rosenberg et al. 1999 [DIRS 125338], p. 3). This method by itself is insufficient because it will not confirm that all 30 liters of the synthesized J-13 water were delivered to the beaker during the experiment. For example, it is not clear whether some of this water was removed for analysis from each of the three batches of J-13 water prepared and analyzed. Also, there might have been an undetected slow leak or a spill that could have prevented a significant portion of the J-13 from entering the beaker. One way to confirm the amount of water delivered to the beaker is to measure the total masses of salts delivered to the beaker to estimate mass balance errors; however, elemental analysis and total abundances of precipitated salts were not performed.

The report also does not document how the density of the final solution was factored into the calculation of the reported concentration factors. Without this information and without measurements to assess mass balance, there is no way to confirm the reported *CF* values. Therefore, the most reliable indicators of the actual *CF* values achieved in these experiments are the observed *CF* values of Na, K, Cl, and NO_3. Because these components should have concentrated conservatively for the reasons given above, they are the best indicators of the true quantity of J-13 water delivered to the beaker and therefore the best indicators of the actual *CF* values. Thus, for the validation simulations, the mean *CF* values of Na, K, Cl, and NO_3 are used to estimate the actual *CF* values (814 for evap1 and 119 for evap4). The differences between these *CF* values and the reported values (956 and 157) are small compared to the factor-of-ten precision required for aqueous concentrations in the validation criteria. Consequently, the issues involving the *CF* are too small to conclude that the experimental data are not of sufficient quality for validation purposes.

As shown in Figure 7-68, the modeled evaporation results approximate the Na, F, HCO_3, Cl, K, NO_3, SO_4, and SiO_2 concentrations within a factor of 10 or better when compared to the laboratory measurements. Ca and Mg predictions are within a factor of 100 of the measurements. The differences in the predicted and measured aqueous concentrations are within the acceptable range of the model validation criteria listed in Table 7-1.

Figure 7-69 shows general agreement between the laboratory measured pH and modeled pH in evap4. The predicted pH is largely controlled by the fugacity of carbon dioxide, which is fixed at $10^{-3.4}$ bars to approximate the laboratory condition of a beaker open to the atmosphere.

The discrepancies between the predicted and measured Si, Ca, and Mg concentrations and pH may be due to errors or uncertainty in the Pitzer thermodynamic database, kinetic limitations of precipitation reactions, and/or analytical errors such as incomplete removal of small particles of minerals containing these elements from the aqueous samples. If errors and uncertainty in the database and analytical measurements can be ruled out, the relatively short laboratory experiments could have produced sustained supersaturated conditions for calcite. Calcite is perpetually supersaturated in surface seawater where evaporation is an ongoing process (Drever 1988 [DIRS 118564], pp. 71 to 72) and has been shown to be supersaturated in laboratory evaporation experiments (Krauskopf and Bird 1995 [DIRS 101702], p. 72). Precipitation of calcite when the pH is below 10 results in the release of a proton from the bicarbonate ion:

$$Ca^{2+} + HCO_3^- = CaCO_3(s) + H^+ \quad \text{(Eq. 7.2.1-1)}$$

Thus, slow precipitation of calcite could also explain why the model predicts lower pH than observed.

The fixed carbon dioxide fugacity is another possible explanation for the observed discrepancies in pH. In a solution that is boiling or evaporating from a beaker, it is possible that the atmospheric partial pressure of carbon dioxide is below atmospheric values because of an increased partial pressure of water vapor and a net flux of vapor flowing out of the beaker. If this was the case, the actual carbon dioxide fugacity would have been lower and pH predictions would have been higher.

At a concentration factor of 814 (*CF* 814) in evap1 (i.e., reported *CF* 956), precipitation of amorphous silica (SiO_2 (am)), aragonite ($CaCO_3$), and calcite ($CaCO_3$) was identified in the experiment. These minerals cannot account for the loss of Mg, whose concentration decreases by more than a factor of 10 rather than increases by a factor of 956. At this stage the model predicts precipitation of calcite and amorphous antigorite. Precipitation of amorphous antigorite ($Mg_3Si_2O_5(OH)_4$) would be consistent with the reported precipitation of amorphous silica, if the loss of Mg was accounted for in the observed mineral assemblage at *CF* 814.

Upon complete evaporation, the following minerals were observed: amorphous silica, aragonite, calcite, halite, niter, thermonatrite, gypsum, anhydrite, and hectorite. The last three minerals were not positive matches. These minerals do not account for the precipitation of Mg or F (except for the possible occurrence of hectorite). In comparison, the following minerals were predicted by the IDPS model to precipitate: calcite, fluorite, halite, natrite, amorphous antigorite, kogarkoite, amorphous silica, and thenardite. Although the predicted phases may not perfectly match the actual phases that precipitate in the experiment, their predicted precipitation accurately accounts for mass balance and produces a scenario that is consistent with the observed evaporative evolution of the solution to *CF* 814.

Ionic strength was not directly measured in these experiments. Instead, a "measured" ionic strength was estimated from the reported evaporated water compositions using EQ3NR. This was done by entering the reported water compositions and instructing the code to maintain any charge imbalances while it equilibrated the solutions. These EQ3NR calculations did not permit precipitation of potentially supersaturated minerals and did not equilibrate the solution with fixed partial pressures. Such heterogeneous reactions would alter the water compositions from the measured concentrations. Thus, the results provided estimated "measured" values of ionic strength, as the data0.ypf database would calculate them. These calculations are documented in Output DTN: SN0702T0509206.008 and are summarized in Table 7-7. The results indicate that predictions are within 12% or less of "measured" ionic strength. "Measured" ionic strength was not estimated at a concentration factor of 814 because pH was not measured at this concentration factor. Ionic strength can be highly sensitive to pH.

Table 7-7. Calculation of "Measured" Ionic Strength in Average J-13 Well Water Evaporation Experiment

Concentration Factor	EQ3NR Input/Output Filenames	Measured Ionic Strength[a] (molal)	Predicted Ionic Strength[b] (molal)
1	j13n1is.3i, j13n1is.3o	2.97E-03	2.62E-03
119[c]	j13n157i.3i, j13n157i.3o	3.28E-01	3.53E-01

[a] Output DTN: SN0702T0509206.008, files: *j13n1is.3o* and *j13n157i.3o*.
[b] Output DTN: SN0702T0509206.008, file: *j13n1pitpH.xls*.
[c] Reported concentration factor is 157.

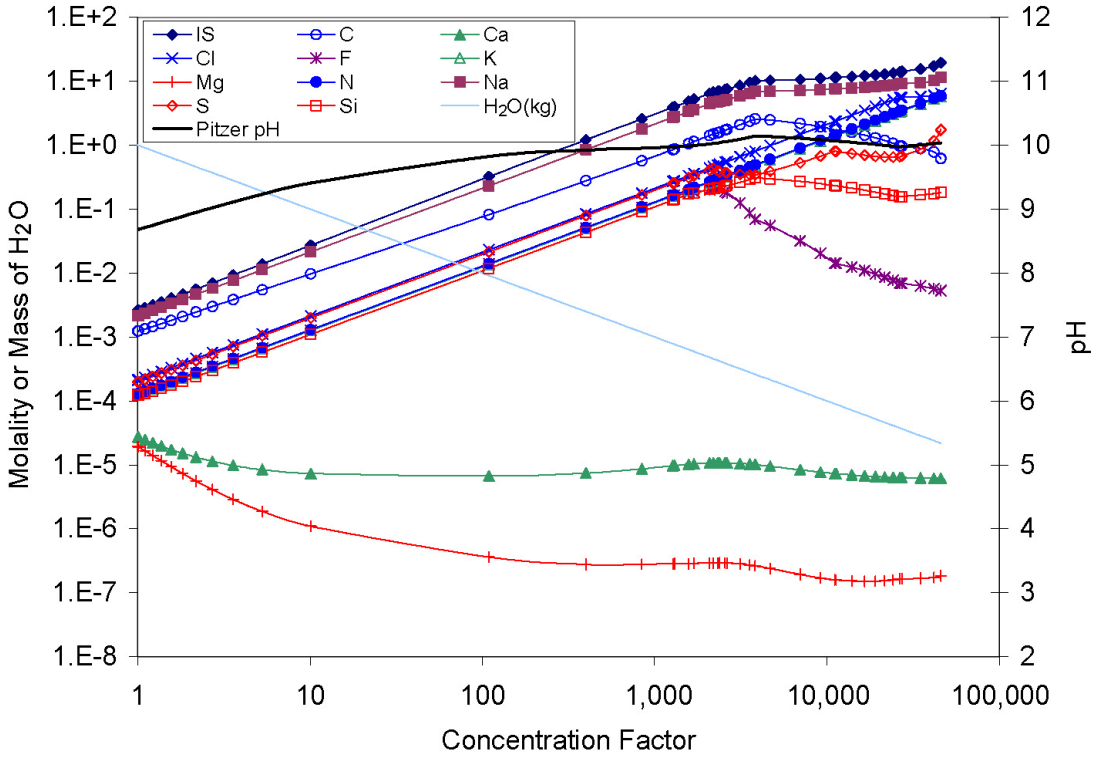

Output DTN: SN0702T0509206.008, file: *j13n1pitpH.xls*.

Figure 7-66. Predicted Aqueous Evolution of Synthetic J-13 Water for Evaporation Experiments of Rosenberg et al. (1999 [DIRS 125338])

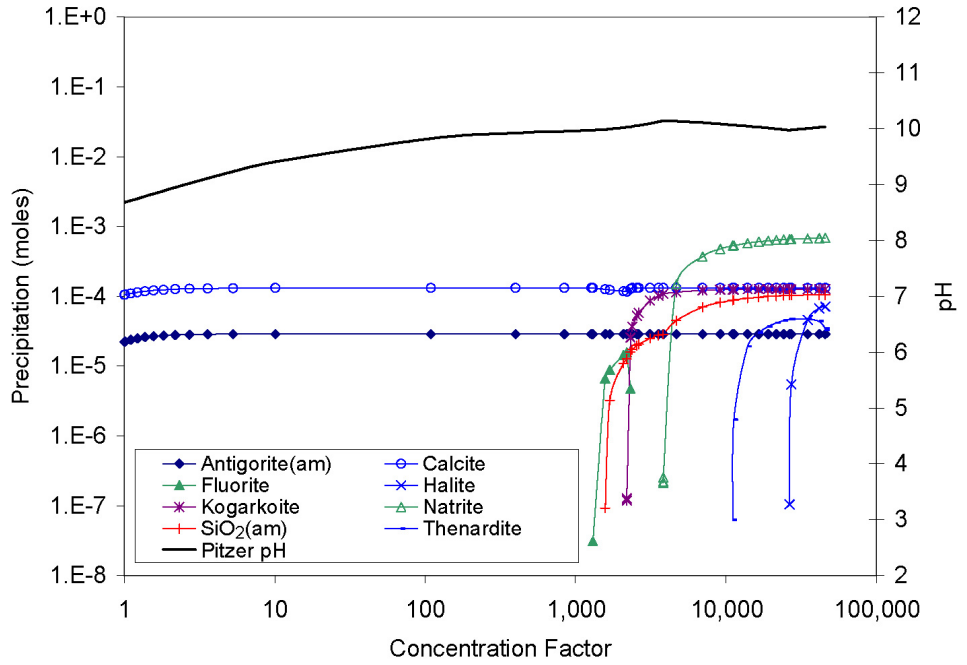

Output DTN: SN0702T0509206.008, file: *j13n1pitpH.xls*.

Figure 7-67. Predicted Mineral Evolution of Synthetic J-13 Water for Evaporation Experiments of Rosenberg et al. (1999 [DIRS 125338])

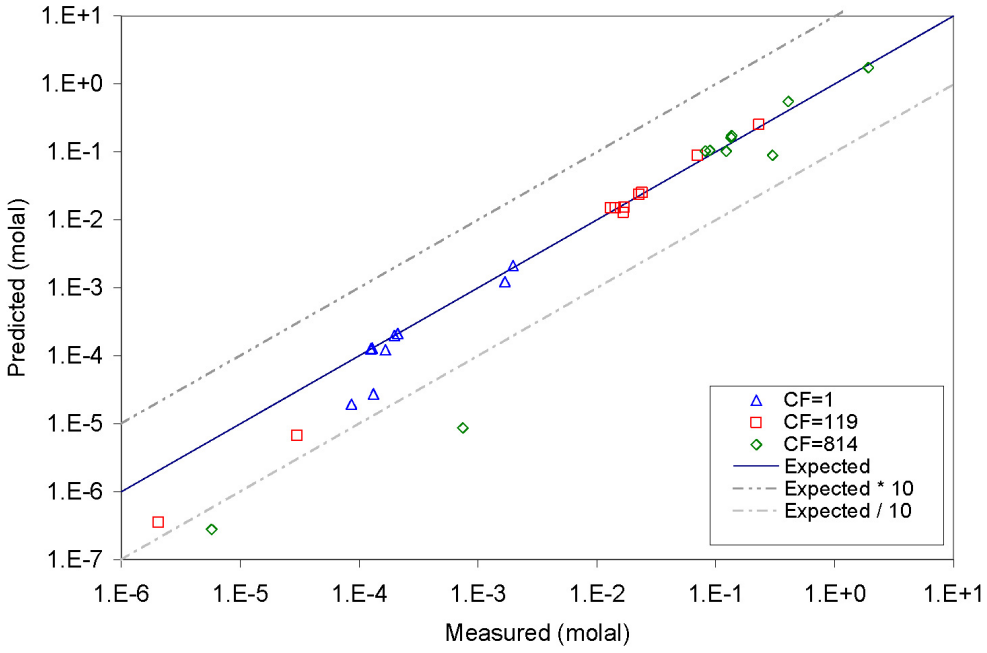

Output DTN: SN0702T0509206.008, file: *j13n1pitpH.xls*.

Figure 7-68. Predicted vs. Measured Concentrations for Synthetic J-13 Water Evaporation Experiments of Rosenberg et al. (1999 [DIRS 125338])

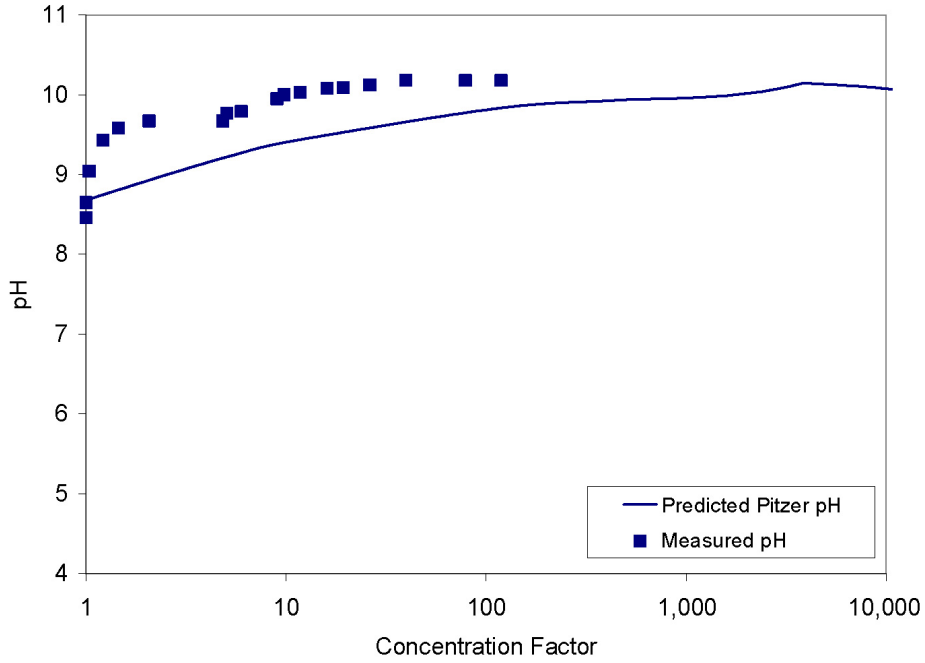

Output DTN: SN0702T0509206.008, file: *j13n1pitpH.xls*.

Figure 7-69. Predicted vs. Measured pH Values for Synthetic J-13 Water Evaporation Experiments of Rosenberg et al. (1999 [DIRS 125338])

7.2.2 Evaporation of 100x Average J-13 Well Water at 90°C and 85% Relative Humidity

In another synthetic J-13 well water evaporation experiment, a synthetic 100-times concentrated (100x) average J-13 well water was dripped through a column of heated tuff into a Teflon beaker (BSC 2001 [DIRS 155640], pp. 6 to 16). In this experiment (called Batch 1), the beaker was open to the atmosphere and maintained at a constant temperature of 90°C and relative humidity of 85%. The solution was then allowed to evaporate to a volume of approximately 5% of the original volume, based on the concentration factors reported (the actual volume or mass decrease in the solution was not reported). The starting and final solution compositions are displayed in Table 4-22. The recipe for the synthetic 100x J-13 well water did not include Si, Al, or Fe, likely because these components have limited solubility or are minor constituents (Al and Fe). A 100x concentration of these components cannot be prepared without making adjustments, such as raising the pH to an unrealistic value. A true 100x J-13 water can only be realistically derived by evaporating unconcentrated J-13 in a container open to a fixed fugacity of carbon dioxide and allowing supersaturated minerals to precipitate from solution during the process (as was done in Rosenberg et al. 1999 [DIRS 125338]).

The results of these evaporation experiments were modeled using the IDPS model and the Pitzer database. Predictions of total aqueous concentrations, pH, ionic strength, and mineral precipitation upon evaporation are documented in Output DTN: SN0702T0509206.008 and plotted in Figures 7-70 and 7-71. Measurements and predictions are compared in Figure 7-72. No pH measurements were reported. Dissolved Si was not measured after this solution was passed through the column of heated tuff or after subsequent evaporation. Thus, Si was not included in the EQ6 evaporation simulation.

Figure 7-72 shows that the predictions closely approximate the Na, F, Cl, K, NO_3, HCO_3, and SO_4 concentrations when compared to the laboratory measurements. To compare the results to the data, the reported nitrate concentration factor of 20.7 is used to represent the concentration factor of the solution. However, because the original concentration factor of the synthesized 100x J-13 water is defined as 100, the final concentration factor is represented here as 2,070 (100×20.7). As shown in the figures, the agreement between the Na, F, Cl, K, HCO_3, and SO_4 measurements and predictions indicate that the concentration factor of the solution is well represented by the nitrate concentration factor.

The model underestimates Ca and Mg by about 1 to 2 orders of magnitude when compared to the laboratory measurements. Two of several possible explanations for these underestimates are errors or uncertainties in the Pitzer database and/or analytical measurements. The concentration factor of 100 represents the starting water prior to the water flowing through the column of crushed tuff. According to the EQ3/6 calculations, this starting water is supersaturated with respect to calcite and huntite. No pH measurements were reported, so pH was predicted by EQ3/6 based on heterogeneous equilibrium with respect to an atmospheric carbon dioxide fugacity of $10^{-3.4}$ bars. Thus, other potential explanations for the underestimates of Ca and Mg are that predictions of pH might be higher than actual, the actual carbon dioxide fugacity might be considerably lower than atmospheric, and/or the precipitation of calcite and huntite is not rapid enough to achieve equilibrium in the laboratory experiment. At a concentration factor of around 2,070, the model predicts additional precipitation of Ca and Mg minerals fluorite and sellaite, as shown in Figure 7-71. Precipitation of these minerals could also be kinetically limited in the experiment. Laboratory analysis of the precipitates was not performed.

In a solution that is boiling or evaporating from a beaker, it is possible that the atmospheric partial pressure of carbon dioxide is below atmospheric values because of an increased partial pressure of water vapor and a net flux of vapor flowing out of the beaker. If this were the case, the actual carbon dioxide fugacity would have been lower and the pH predictions would have been higher.

Calcite can be supersaturated by as much as a factor of two when calcium and carbonate concentrations are slowly increased in laboratory experiments (Krauskopf and Bird 1995 [DIRS 101702], p. 72). This phenomenon may partly explain why measured Ca concentrations in this evaporation experiment (and the one in the previous section) are larger than the predicted values. Because the model assumes equilibrium for calcite due to the long periods of time that the model is designed to simulate for TSPA, it is understandable that the model might under-predict the Ca concentration in a short-term laboratory evaporation experiment. Regardless, the model cannot be invalidated for its intended use simply because the prediction of Ca in a short-term experiment falls slightly outside the validation criteria approximated in Table 7-1. If calcite were allowed to supersaturate in the simulation due to the slow kinetics of calcite precipitation and the short-term experiment, Ca predictions would have fallen within the approximated validation criteria. Alternatively, if the evaporation experiment had been conducted over a longer period of time, on the scale of the time periods that the IDPS model is designed to simulate for TSPA, calcite precipitation would have had time to progress towards equilibrium, resulting in a Ca concentration closer to the value predicted by the IDPS model.

Ionic strength was not directly measured in these experiments and cannot be accurately estimated without pH measurements. Thus, "measured" ionic strength was not estimated for this experiment using EQ3NR, as was done for the data in Sections 7.2.1 and 7.2.3.

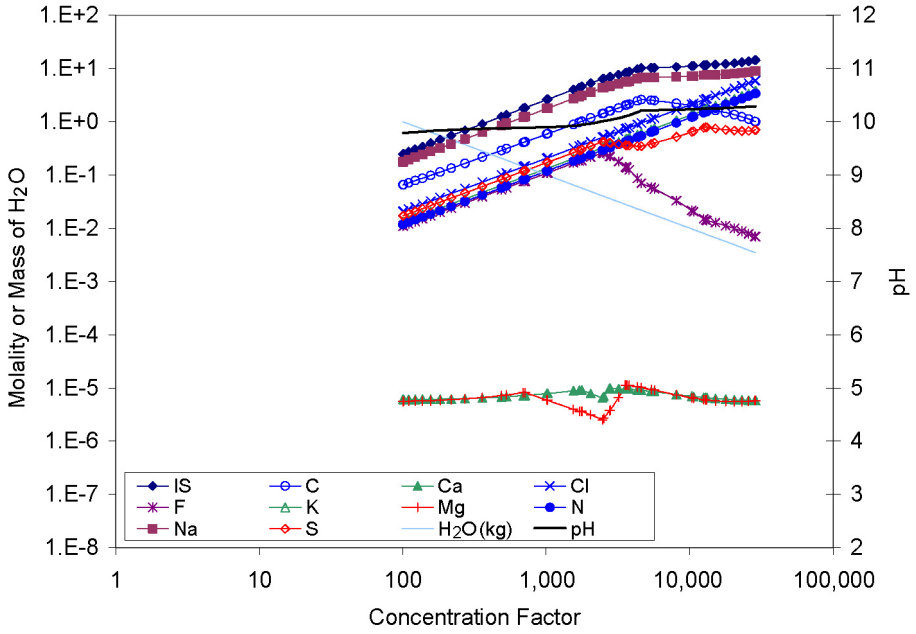

Output DTN: SN0702T0509206.008, file: *j13b1 v3.xls*.

Figure 7-70. Predicted Aqueous Evolution of 100x Synthetic J-13 Water for Evaporation Experiments (BSC 2001 [DIRS 155640])

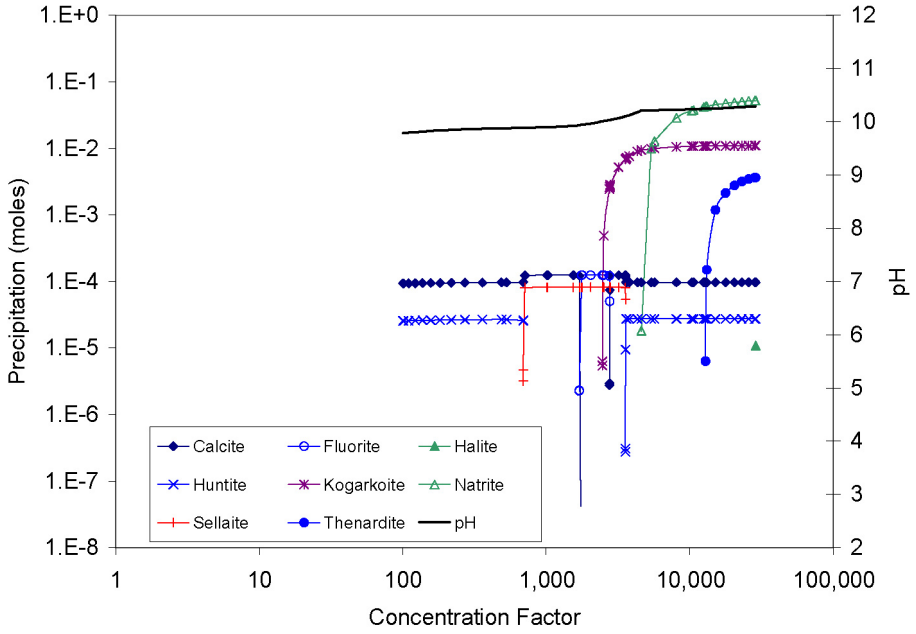

Output DTN: SN0702T0509206.008, file: *j13b1 v3.xls*.

Figure 7-71. Predicted Mineral Evolution of 100x Synthetic J-13 Water for Evaporation Experiments (BSC 2001 [DIRS 155640])

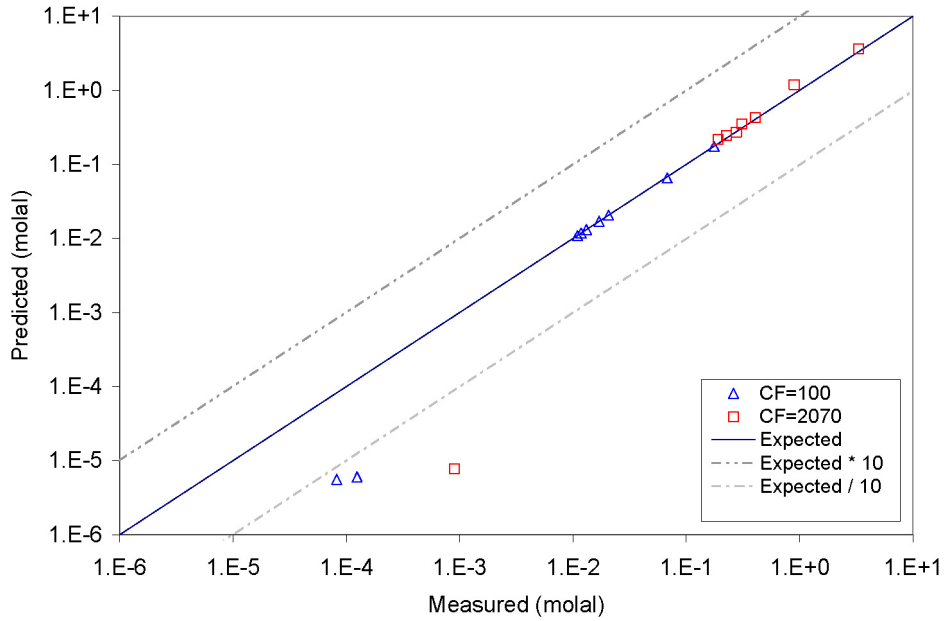

Output DTN: SN0702T0509206.008, file: *j13b1 v3.xls*.

Figure 7-72. Predicted vs. Measured Concentrations for 100x Synthetic J-13 Water Evaporation Experiments (BSC 2001 [DIRS 155640])

7.2.3 Evaporation of Topopah Spring Tuff Pore Water at 75°C

Synthetic Topopah Spring Tuff pore water was evaporated in an experiment reported by Rosenberg et al. (1999 [DIRS 125339]). The experiment, named evap3, was performed following the same procedures as in a second study by Rosenberg et al. (1999 [DIRS 125338]) presented in Section 7.2.1, except that the temperature was maintained at 75°C. Both the starting and final solutions are provided in Table 4-23. The final solution was reported to have an approximate concentration factor of 1243 ± 10%. An x-ray diffraction analysis at this concentration factor detected gypsum. After complete evaporation, tachyhydrite was also detected.

These evaporation experiments were simulated using the IDPS model and the Pitzer database. Predictions of total aqueous concentrations, pH, ionic strength, and mineral precipitation upon evaporation are documented in Output DTN: SN0702T0509206.008 and plotted in Figure 7-73 and Figure 7-74. These predictions are compared to the measurements in Figures 7-75 and 7-76.

As in the J-13 experiments presented in Section 7.2.1, the reported concentration factor of this experiment is not consistent with the *CF* values of ions that should concentrate conservatively. The solution at the reported *CF* value of 1243 (Table 4-23) is not saturated with respect to any Na, K, Cl, or NO_3 minerals (Table 7-2). The results of the simulation (Figures 7-73 and 7-74) corroborate the expected conservative behavior of these ions. For these reasons, the actual concentration factor of this experiment is estimated from the mean *CF* value of Na, K, Cl, and NO_3 in solution. This approach is explained and justified in Section 7.2.1.

The *CF* values of Na, K, and Cl in this experiment are 727, 662, and 681 (computed from Table 4-23). (The concentration of NO_3 was not measured in the final solution, so a *CF* value could not be determined for NO_3.) If the *CF* value actually were 1,243 as reported, then 42%, 47%, and 45% of Na, K, and Cl would have been precipitated, adsorbed, or otherwise lost from solution (Output DTN: SN0702T0509206.008, file: *tspw3pitpH.xls*). If these losses were to the solid phase, they would have dominated the solid phase. However, to the contrary, these salts were not identified in the mineral analysis at the reported *CF* value. Therefore, the reported *CF* value of 1,243 is much too high, and the mean *CF* value of Na, K, and Cl (690) is adopted here as the actual value. This difference is less than a factor of two, which is small compared to the factor-of-ten precision required for aqueous concentrations in the validation criteria. Consequently, the issues involving the *CF* are too small to conclude that the experimental data are not of sufficient quality for validation purposes.

Figure 7-75 shows that the modeled results closely approximate the measured Na, Mg, Ca, Cl, and K concentrations. At a concentration factor of 690, modeled results underestimate the measured SO_4 and Si concentrations by approximately 0.5 order of magnitude. Final NO_3, HCO_3, and F laboratory data are not reported (Rosenberg et al. 1999 [DIRS 125339]).

Figure 7-76 shows close agreement between the laboratory measured pH and predicted pH. Unlike the observations in the J-13 evaporation experiments, the pH decreased with increasing evaporation, resulting in a value around 6.3 by the end of the experiment. The predicted pH is largely controlled by the fugacity of carbon dioxide, which is fixed at $10^{-3.4}$ bars to approximate the laboratory condition of a beaker open to the atmosphere. There is some uncertainty associated with the pH measurements because details of the pH measurement procedure are not reported. Measuring pH at high temperature and high ionic strength requires special methods (Section 7.5.1), which may or may not have been adopted.

Gypsum was identified by x-ray diffraction in the laboratory experiment at the 690 concentration factor. In contrast, the model predicted calcite, sepiolite, and anhydrite precipitation at *CF* 690. Anhydrite ($CaSO_4$) is predicted to be more stable than gypsum ($CaSO_4{:}2H_2O$) at the 75°C temperature of the experiment. However, the short term of the experiment may have prevented a perceivable accumulation of anhydrite. Other potential explanations for the difference are potential inaccuracies in experimental measurements or the Pitzer database. Regardless of the difference, either mineral provides a good explanation why the aqueous Ca and SO_4 concentrations at *CF* 690 are not nearly 690 times their initial concentrations (Table 4-23).

Mass balance suggests that gypsum could not be the only mineral precipitating at *CF* 690. As indicated in Table 4-23, the Si concentration did not nearly increase by a *CF* of 690, nor did HCO_3. Thus, some Si and C likely precipitated, which is consistent with the calcite, amorphous silica, and amorphous antigorite precipitation that the IDPS model independently predicted based on aqueous solubilities.

Upon complete evaporation, the only other mineral identified to precipitate was tachyhydrite. The relative amounts of gypsum and tachyhydrite in the final mineral assemblage were not measured. The minerals predicted by the IDPS model to precipitate upon complete evaporation are displayed in Figure 7-74. No precipitation was identified in the experiment that contained Na, K, CO_3, F, Si, or NO_3. Mass balance indicates that these components should be there.

Without quantitative and nearly complete information on the composition of precipitation in an experiment, experimental measurements and model predictions of mineral assemblages cannot be easily corroborated.

Ionic strength was not directly measured in these experiments. However, a "measured" ionic strength was estimated from the reported evaporated water compositions using EQ3NR, as described in Section 7.2.1. These calculations are also documented in Output DTN: SN0702T0509206.008 and are summarized in Table 7-8. Because of the correction to the concentration factor (from 1,243 to 690), the ionic strength predictions are within 2% of "measured" ionic strength.

Table 7-8. Calculation of "Measured" Ionic Strength in Topopah Spring Tuff Pore Water Evaporation Experiment

Concentration Factor	EQ3NR Input/Output Filenames	Measured Ionic Strength[a] (molal)	Predicted Ionic Strength[b] (molal)
1	tspw3is.3i, tspw3is.3o	6.73E-03	6.60E-03
690[c]	tsp1243i.3i, tsp1243i.3o	2.17E+00	2.12E+00

[a] Output DTN: SN0702T0509206.008, files: *tspw3is.3o* and *tsp1243i.3o*.
[b] Output DTN: SN0702T0509206.008, file: *tspw3pitpH.xls*.
[c] Reported concentration factor of 1,243.

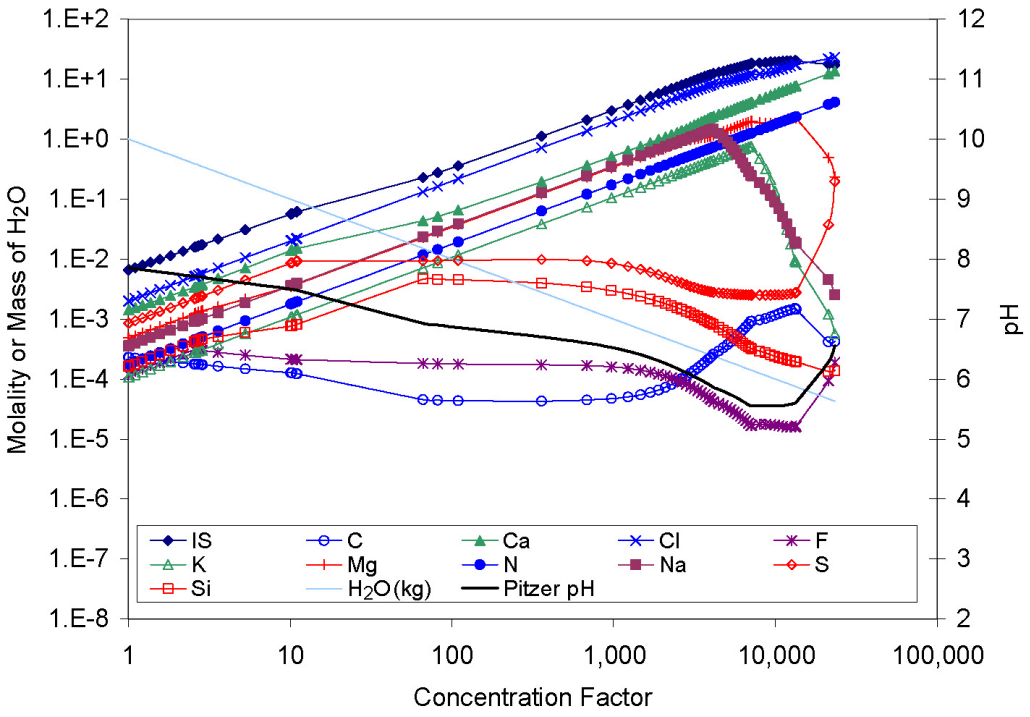

Output DTN: SN0702T0509206.008, file: *tspw3pitpH.xls*.

Figure 7-73. Predicted Aqueous Evolution of Synthetic Topopah Spring Tuff Pore Water for Evaporation Experiments of Rosenberg et al. (1999 [DIRS 125339])

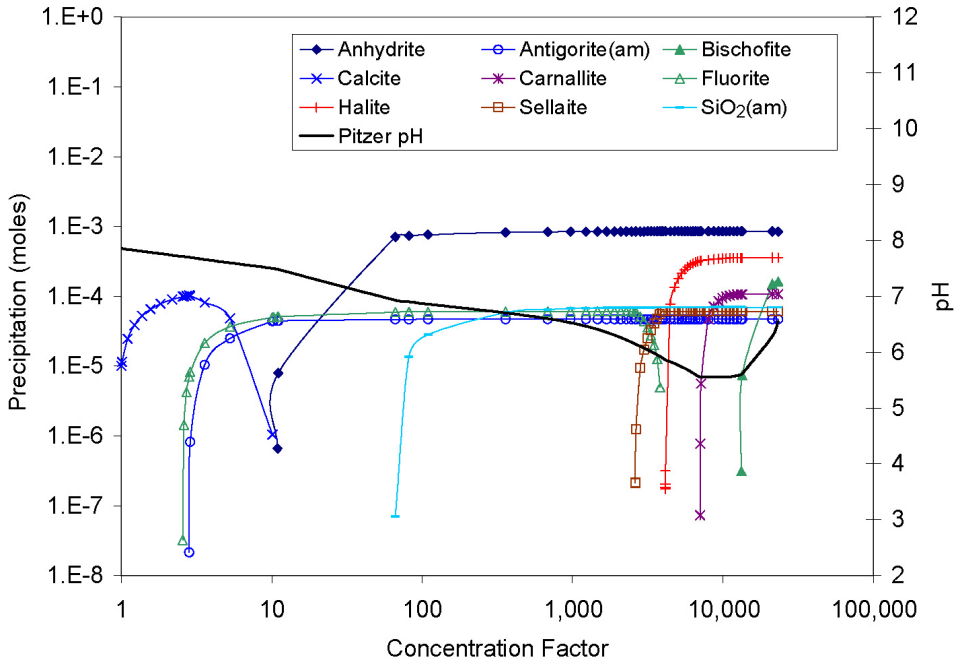

Output DTN: SN0702T0509206.008, file: *tspw3pitpH.xls*.

Figure 7-74. Predicted Mineral Evolution of Synthetic Topopah Spring Tuff Pore Water for Evaporation Experiments of Rosenberg et al. (1999 [DIRS 125339])

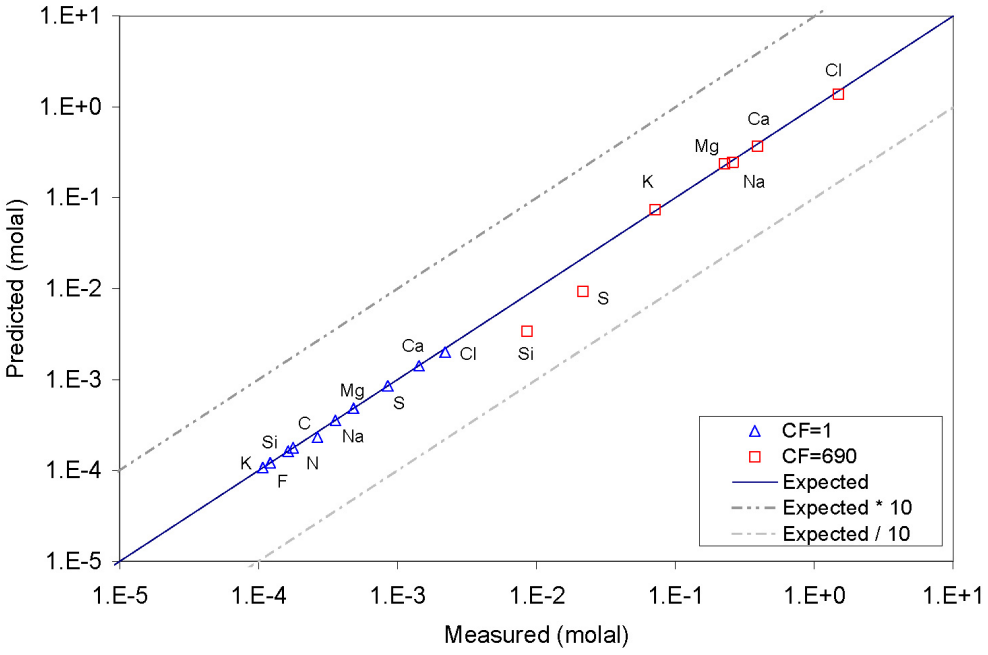

Output DTN: SN0702T0509206.008, file: *tspw3pitpH.xls*.

Figure 7-75. Predicted vs. Measured Concentrations for Synthetic Topopah Spring Tuff Pore Water from Evaporation Experiments of Rosenberg et al. (1999 [DIRS 125339])

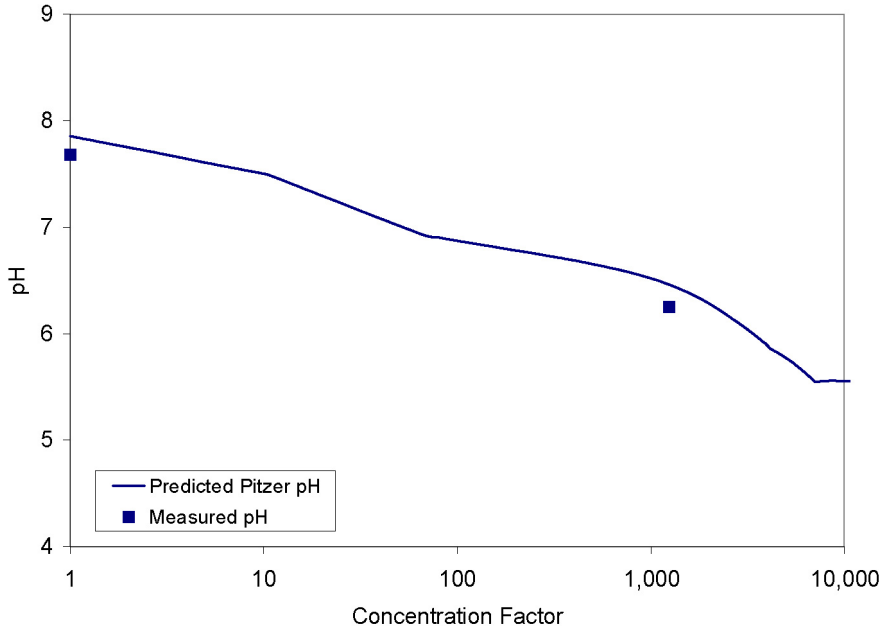

Output DTN: SN0702T0509206.008, file: *tspw3pitpH.xls*.

Figure 7-76. Predicted vs. Measured pH Values for Synthetic Topopah Spring Tuff Pore Water from Evaporation Experiments of Rosenberg et al. (1999 [DIRS 125339])

7.2.4 Evaporation of Topopah Spring Tuff Pore Water at 95°C

Alai et al. (2005 [DIRS 176811]) evaporated synthetic Topopah Spring Tuff water at 95°C in a series of four experiments. These experiments, named FEC 9, 12, 13, and 14, are referred to as legs 1, 2, 3, and 4. The data from these experiments are documented in the following DTNs:

- LL030106923121.018 [DIRS 177573] (file: *LL030106923121.018, FEC13.xls*, tab: "TDMS Data Experiment FEC13")
- LL030107023121.019 [DIRS 177574] (file: *LL030107023121.019.FEC9.xls*, tab: "TDMS Data Experiment FEC9")
- LL030107123121.020 [DIRS 177575] (file: *L030107123121.020, FEC12.xls*, tab: "TDMS Data Experiment FEC12")
- LL030408523121.028 [DIRS 177576] (file: *FEC14.apr20.xls*, tab: "TDMS Data Experiment FEC14").

The composition of the starting water of each successive leg approximated the aqueous composition at the end of the previous leg. The solutions were constantly stirred, and atmospheric air was constantly streamed over the solutions. During each leg, the solution was sampled and analyzed for pH and dissolved solids. After the final aqueous sample was collected, the evaporations were allowed to proceed to dryness whereupon precipitated salts were analyzed by powder x-ray diffraction. Salts that accumulated during each leg were not included at the beginning of the subsequent leg.

Each leg was evaporated to a concentration factor (*CF*) of between 9 and 15. In the analysis presented here, the *CF* value along each leg was estimated by the mean of the *CF* values of conservative ions. For legs 1 through 3, the conservative ions used to determine the leg *CF* values were Na, K, Cl, and NO_3. In leg 4, halite precipitates, so only K and NO_3 concentrations were used.

IDPS model simulations were performed for each leg separately. These simulations were not combined into a continuous evaporation because the starting solutions for legs 2, 3, and 4 did not perfectly replicate the final solutions of legs 1, 2, and 3 and precipitated minerals were not included in the subsequent legs. Thus, each leg has a distinctly different composition and trajectory upon evaporation.

Table 4-24 provides the evaporation data from the experiment. Aqueous samples were analyzed after they were cooled to room temperature. The pH was measured using a combination electrode designed for ionic strengths as high as 0.1 molal. For solutions exceeding the ionic strength limit (primarily legs 3 and 4), pH measurements were not corrected for ionic strength and are not included in the figures. Total dissolved carbon was measured by an infrared carbon analyzer. Total dissolved Ca, Mg, Si, and Na was measured by an inductively coupled plasma-atomic emission spectrometer. Total dissolved K was measured by atomic absorption spectrophotometer and F^-, Cl^-, NO_3^- and SO_4^{2-} by an ion chromatograph. These data are converted to molal concentrations in spreadsheets *FEC9bsum PitpH r1.xls*, *FEC12bsum PitpH r1.xls*, *FEC13bsum PitpH r1.xls*, and *FEC14bsum PitpH r1.xls* in Output DTN: MO0701EQ36IDPS.000 and are plotted in Figures 7-77 through 7-92.

The input and output files of the IDPS model simulations are also included in Output DTN: MO0701EQ36IDPS.000 . The starting water compositions in these simulations are the "initial solution" compositions presented in Table 4-24. The fugacity of carbon dioxide was set at $10^{-3.4}$ bar to simulate the stream of air passed over the solutions. The temperature of the simulations was raised to 95°C prior to evaporation. Results are compared to measurements in Figures 7-77 through 7-92.

As shown in the figures, IDPS model simulations predict pH within a pH unit and dissolved salt concentrations within a factor of ten or better (except for Si in leg 4). More precisely, most pH values are predicted within a half pH unit, and most dissolved salt concentrations are predicted within a factor of two. Note that only the pH values measured at ionic strengths less than 0.1 molal are plotted because measurements at ionic strengths above 0.1 molal are uncorrected for ionic strength.

The dissolved constituents that show the most notable differences between predictions and measurements are Si, C, Ca, and Mg. Of these, only the differences for Si exceed a factor of ten, which occurs in leg 4 where the differences reach a factor of 73 (Figure 7-91). The validation criteria allow for a factor of 100 for the difference between predicted and measured concentrations of Ca, Mg, and Si (Table 7-1). The differences may be due to errors or uncertainty in the Pitzer thermodynamic database and/or kinetic limitations errors.

Ionic strength was not directly measured in these experiments. Instead, a "measured" ionic strength was estimated from the reported evaporated water compositions using EQ3NR in the

same manner described in Section 7.2.1. The results provide estimated "measured" values of ionic strength, as the IDPS model and Pitzer database would calculate them. These calculations are documented in Output DTN: MO0701EQ36IDPS.000 and are plotted in Figures 7-77, 7-81, 7-85, and 7-89 as "IS data." The results indicate that predicted ionic strength is always within 50% of "measured" values and usually within 10%. The largest differences (near 50%) are observed in leg 4 when the ionic strength exceeds 5 molal; however, these differences are small compared to validation criteria.

The minerals observed in the experiments were those that accumulated after the solutions were completely evaporated to dryness. For each leg, halite (NaCl) and anhydrite ($CaSO_4$) precipitated (DTNs: LL030106923121.018 [DIRS 177573]; LL030107023121.019 [DIRS 177574]; LL030107123121.020 [DIRS 177575]; LL030408523121.028 [DIRS 177576]). In addition, bassanite ($2CaSO_4:H_2O$) was found in legs 2 and 4 and niter (KNO_3) and soda niter ($NaNO_3$) were found in leg 4 (DTN: LL030408523121.028 [DIRS 177576]). Niter and soda niter also likely precipitated in the first three legs after complete evaporation, but their quantities would have been much smaller and were likely below detection limits. Amorphous minerals cannot be identified by x-ray diffraction and therefore were not identified in the experiments. Thus, amorphous antigorite and amorphous silica, which were predicted to precipitate in each leg, might have precipitated in the experiments but could not have been observed using the methods employed.

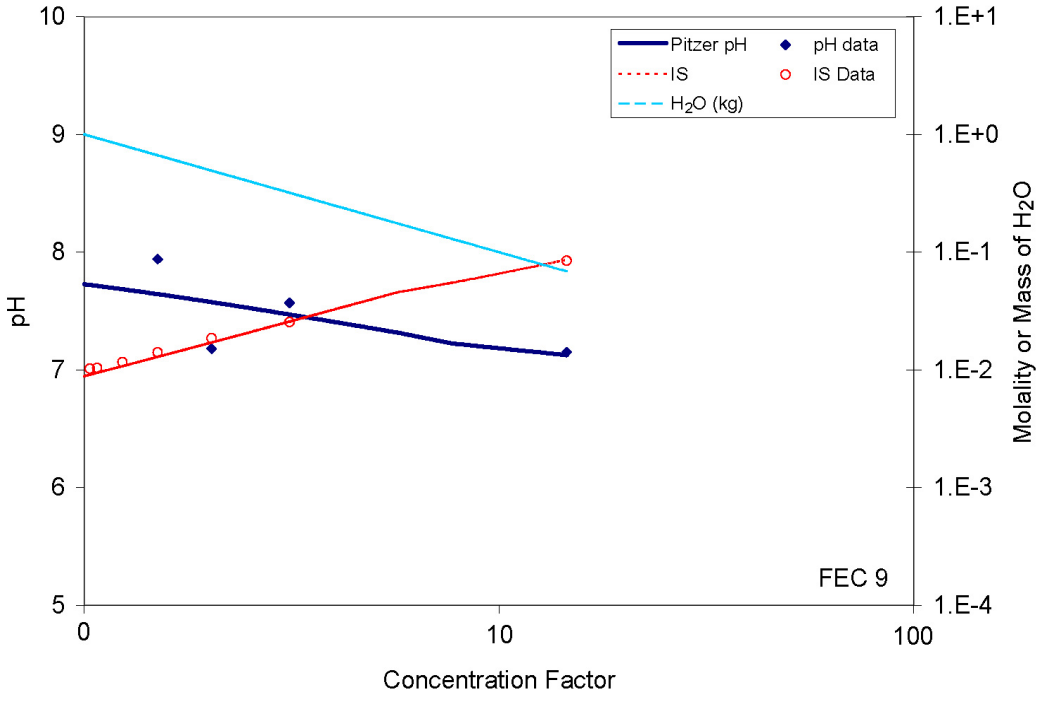

Output DTN: MO0701EQ36IDPS.000, file: *Topopah95.zip*, *FEC9bsum PitpH r1.xls*.

Figure 7-77. Predicted vs. Measured pH and Ionic Strength for Leg 1 of Evaporation Based on Experiments in Alai et al. (2005 [DIRS 176811])

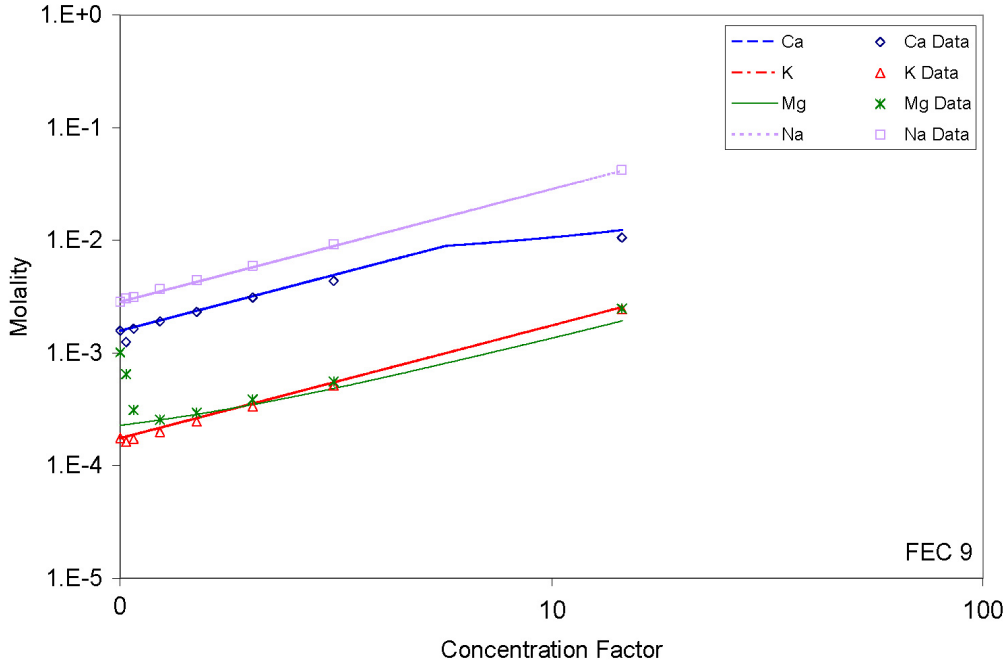

Output DTN: MO0701EQ36IDPS.000, file: *Topopah95.zip*, *FEC9bsum PitpH r1.xls*.

Figure 7-78. Predicted vs. Measured Cations for Leg 1 of Evaporation Based on Experiments in Alai et al. (2005 [DIRS 176811])

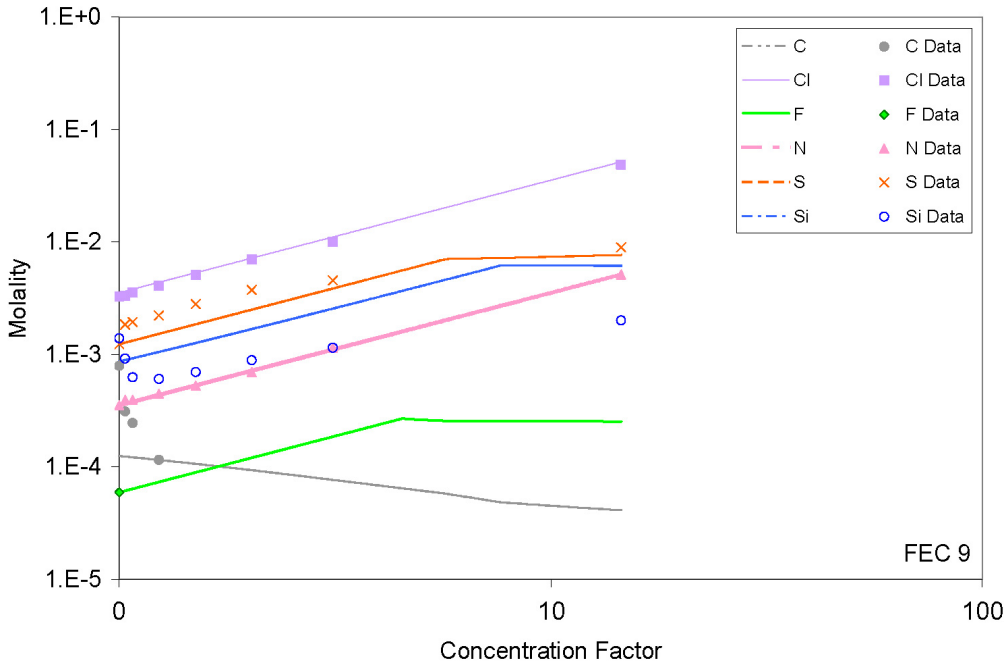

Output DTN: MO0701EQ36IDPS.000, file: *Topopah95.zip*, *FEC9b sum PitpH r1.xls*.

NOTE: N, S, and C represent the total aqueous concentrations of nitrate, sulfate, and carbonate.

Figure 7-79. Predicted vs. Measured Anions and Si for Leg 1 of Evaporation Based on Experiments in Alai et al. (2005 [DIRS 176811])

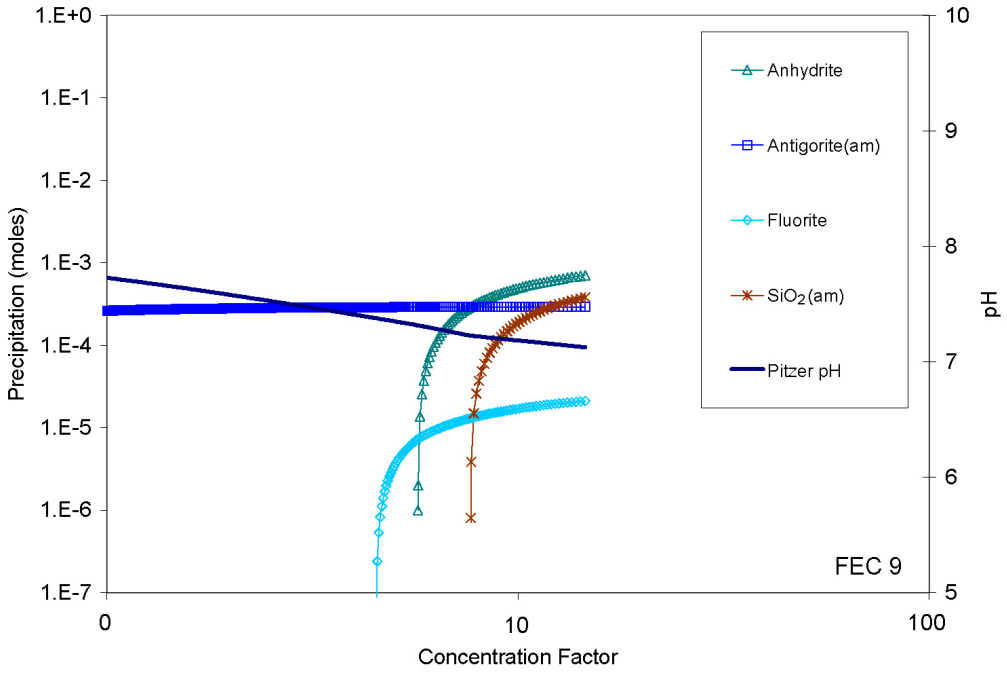

Output DTN: MO0701EQ36IDPS.000, file: *Topopah95.zip*, *FEC9bsum PitpH r1.xls*.

Figure 7-80. Predicted Mineral Evolution for Leg 1 of Evaporation Based on Experiments in Alai et al. (2005 [DIRS 176811])

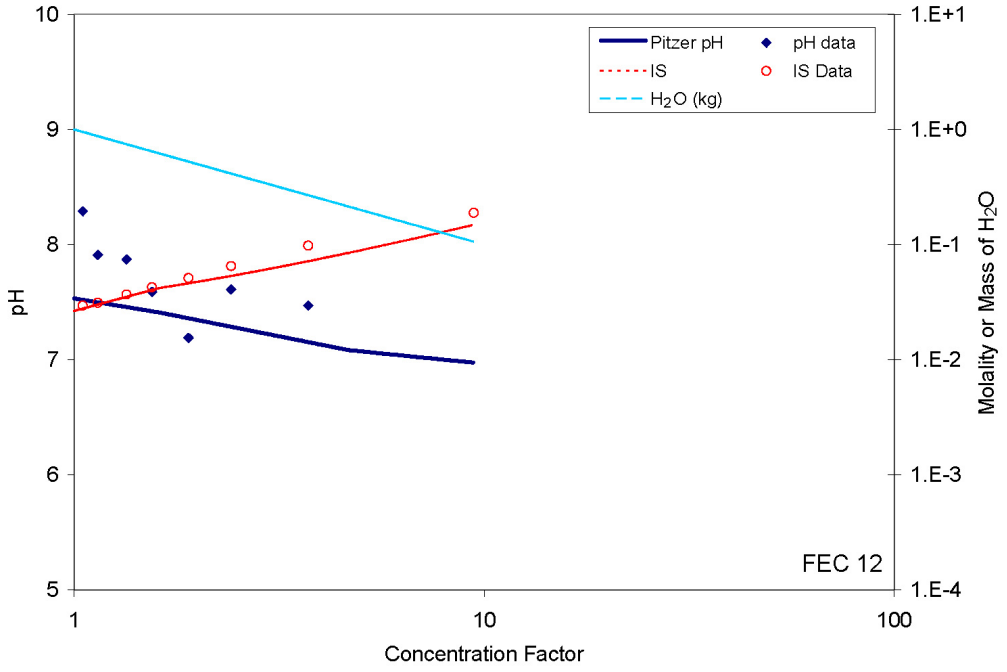

Output DTN: MO0701EQ36IDPS.000, file: *Topopah95.zip*, *FEC12bsum PitpH r1.xls*.

Figure 7-81. Predicted vs. Measured pH and Ionic Strength for Leg 2 of Evaporation Based on Experiments in Alai et al. (2005 [DIRS 176811])

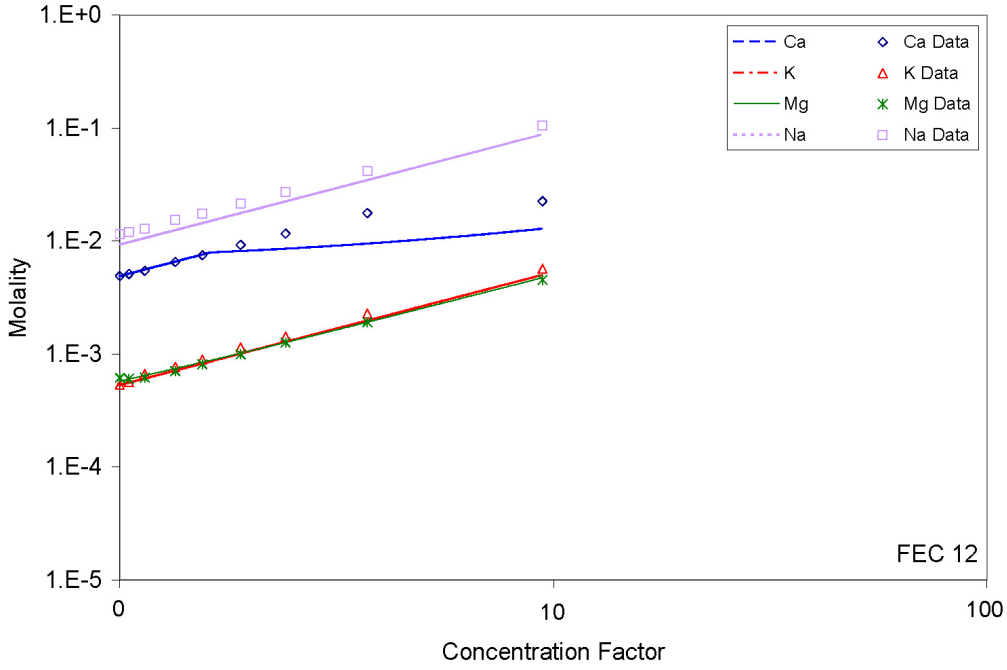

Output DTN: MO0701EQ36IDPS.000, file: *Topopah95.zip*, *FEC12bsum PitpH r1.xls*.

Figure 7-82. Predicted vs. Measured Cations for Leg 2 of Evaporation Based on Experiments in Alai et al. (2005 [DIRS 176811])

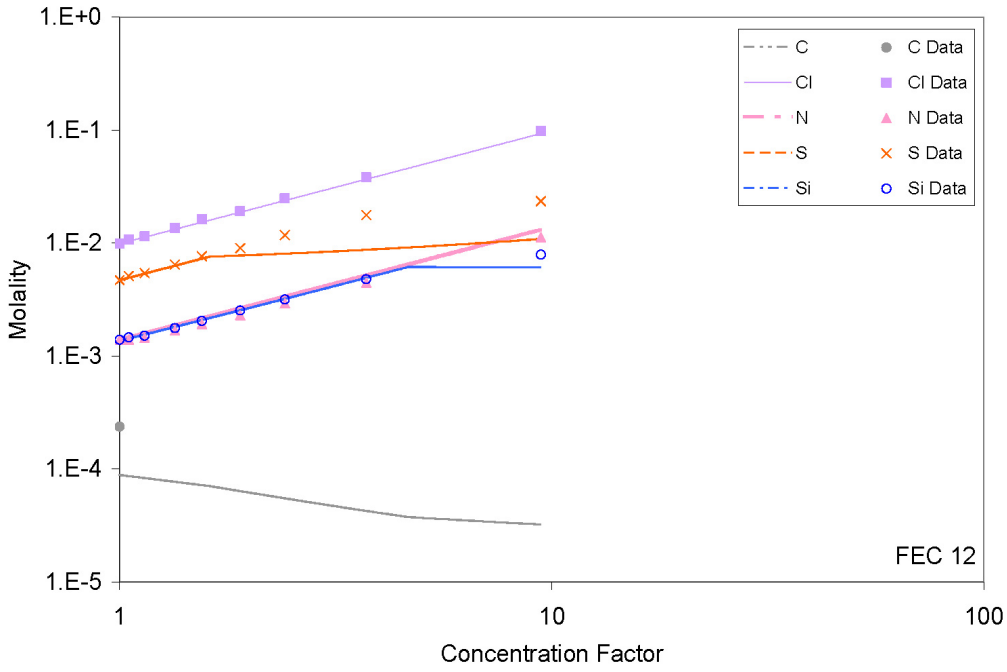

Output DTN: MO0701EQ36IDPS.000, file: *Topopah95.zip*, *FEC12bsum PitpH r1.xls*.

NOTE: N, S, and C represent the total aqueous concentrations of nitrate, sulfate, and carbonate

Figure 7-83. Predicted vs. Measured Anions and Si for Leg 2 of Evaporation Based on Experiments in Alai et al. (2005 [DIRS 176811])

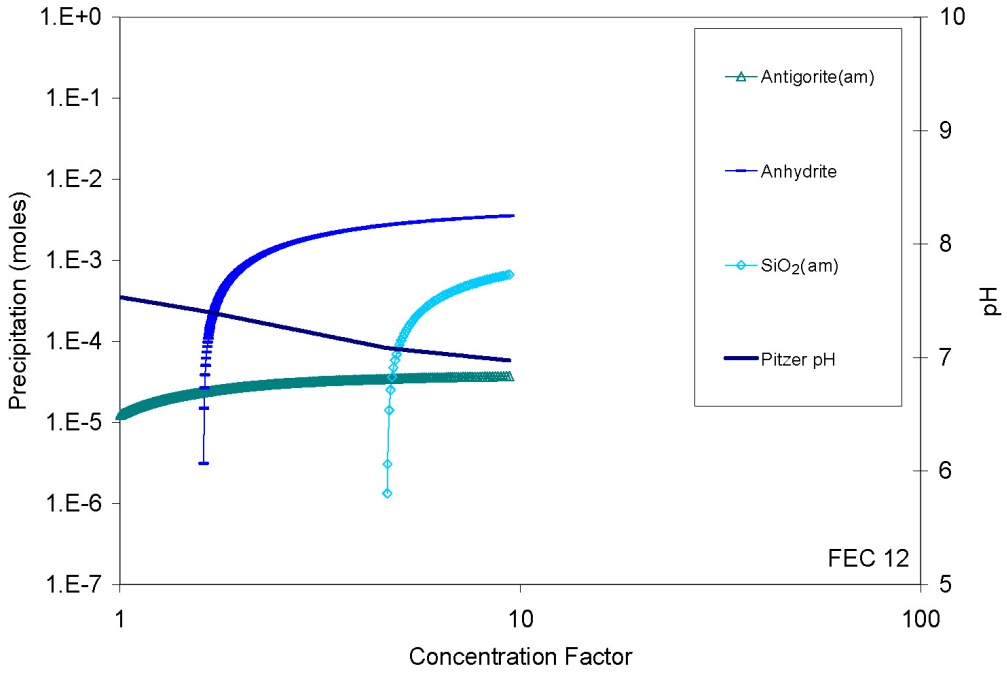

Output DTN: MO0701EQ36IDPS.000, file: *Topopah95.zip*, *FEC12bsum PitpH r1.xls*.

Figure 7-84. Predicted Mineral Evolution for Leg 2 of Evaporation Based on Experiments in Alai et al. (2005 [DIRS 176811])

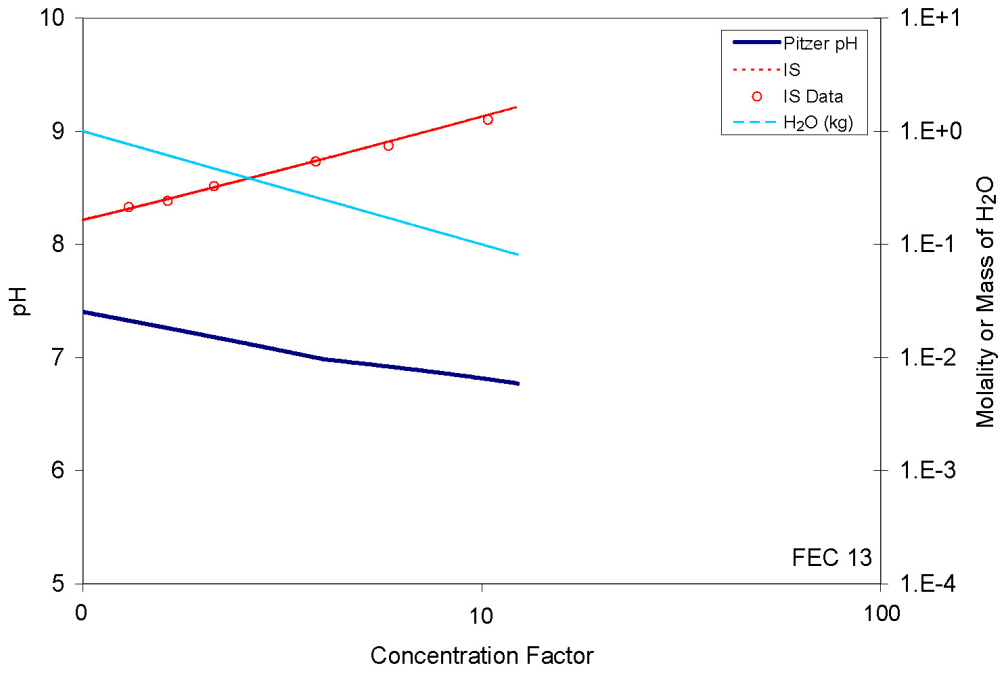

Output DTN: MO0701EQ36IDPS.000, file: *Topopah95.zip*, *FEC13bsum PitpH r1.xls*.

Figure 7-85. Predicted vs. Measured pH and Ionic Strength for Leg 3 of Evaporation Based on Experiments in Alai et al. (2005 [DIRS 176811])

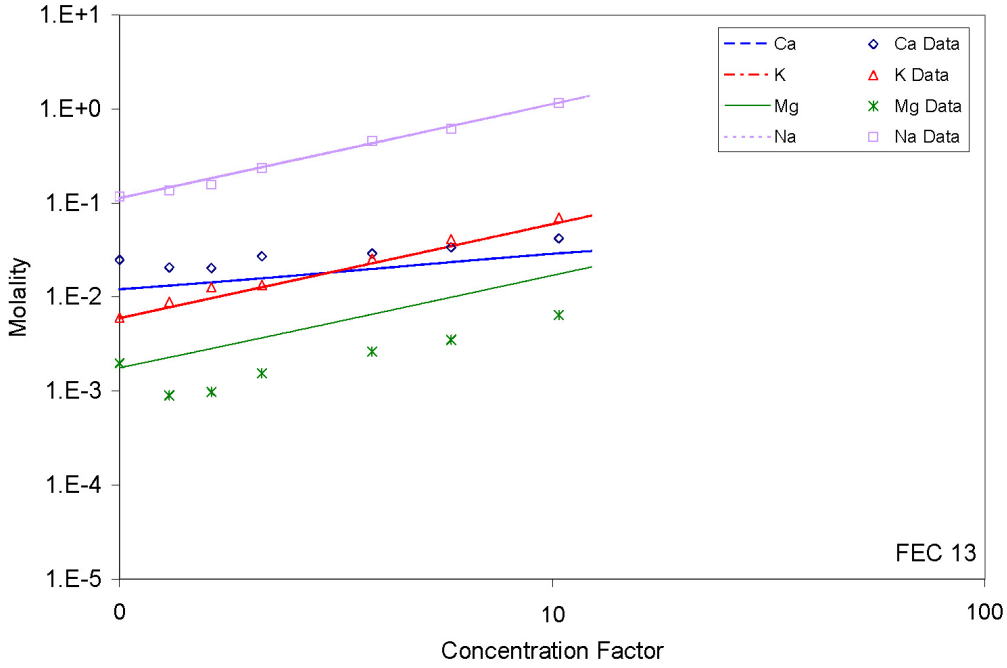

Output DTN: MO0701EQ36IDPS.000, file: *Topopah95.zip*, *FEC13bsum PitpH r1.xls*.

Figure 7-86. Predicted vs. Measured Cations for Leg 3 of Evaporation Based on Experiments in Alai et al. (2005 [DIRS 176811])

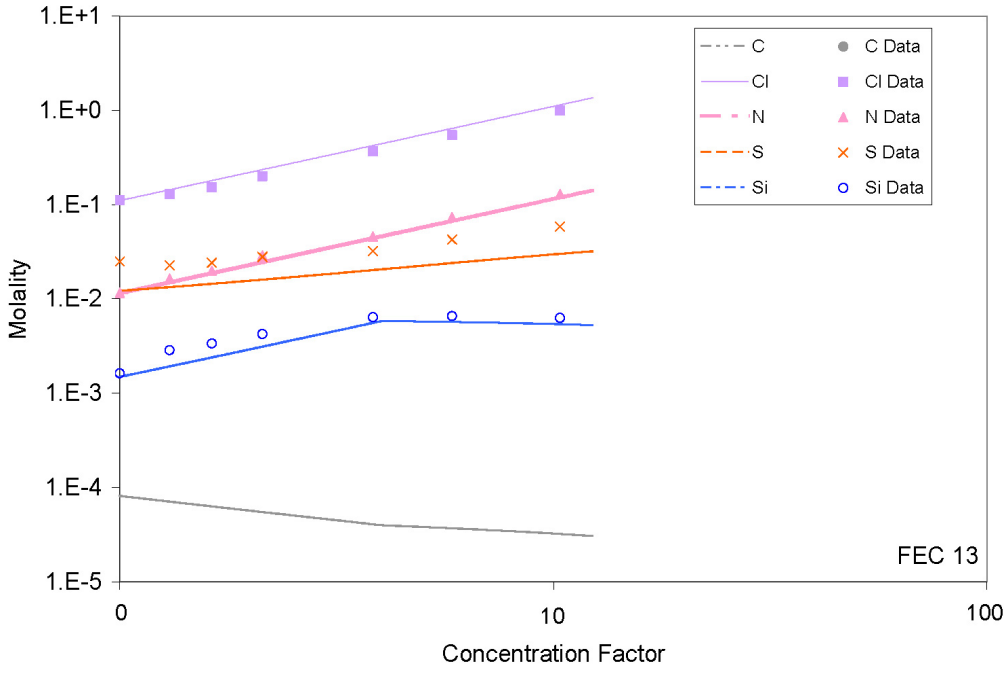

Output DTN: MO0701EQ36IDPS.000, file: *Topopah95.zip*, *FEC13bsum PitpH r1.xls*.

NOTE: N, S, and C represent the total aqueous concentrations of nitrate, sulfate, and carbonate.

Figure 7-87. Predicted vs. Measured Anions and Si for Leg 3 of Evaporation Based on Experiments in Alai et al. (2005 [DIRS 176811])

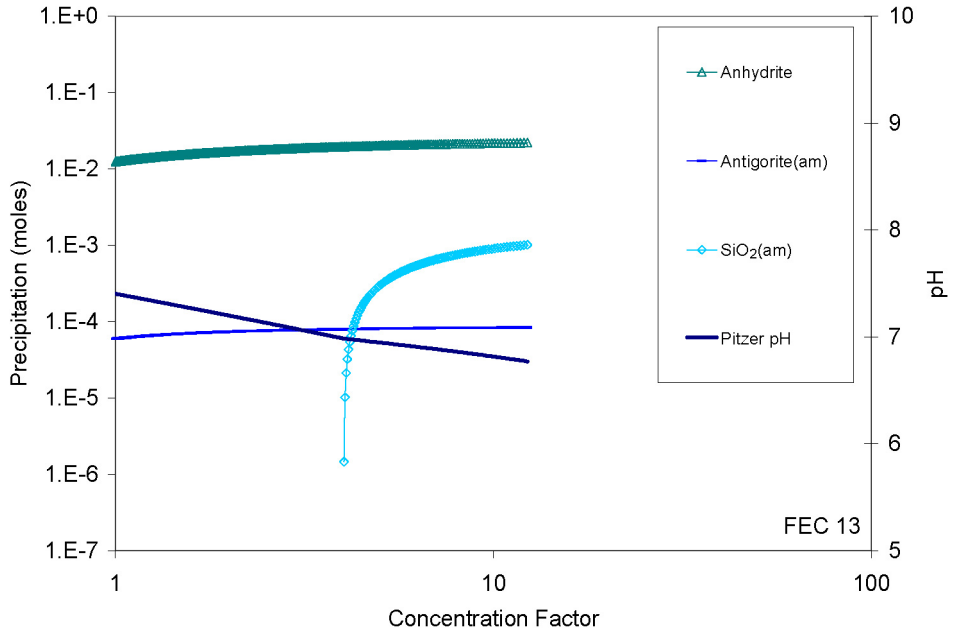

Output DTN: MO0701EQ36IDPS.000, file: *Topopah95.zip*, *FEC13bsum PitpH r1.xls*.

Figure 7-88. Predicted Mineral Evolution for Leg 3 of Evaporation Based on Experiments in Alai et al. (2005 [DIRS 176811])

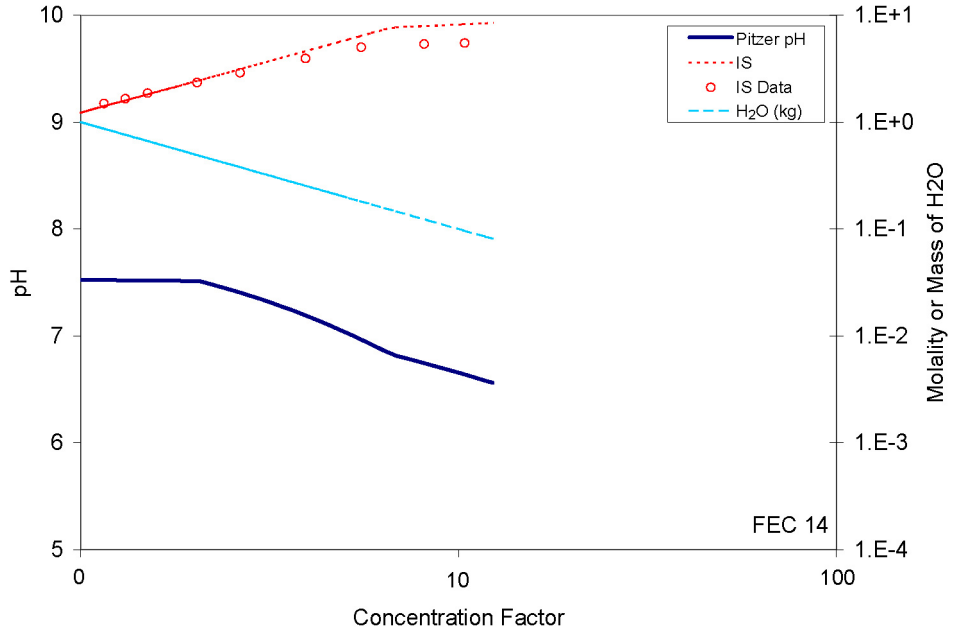

Output DTN: MO0701EQ36IDPS.000, file: *Topopah95.zip*, *FEC14bsum PitpH r1.xls*.

Figure 7-89. Predicted vs. Measured pH and Ionic Strength for Leg 4 of Evaporation Based on Experiments in Alai et al. (2005 [DIRS 176811])

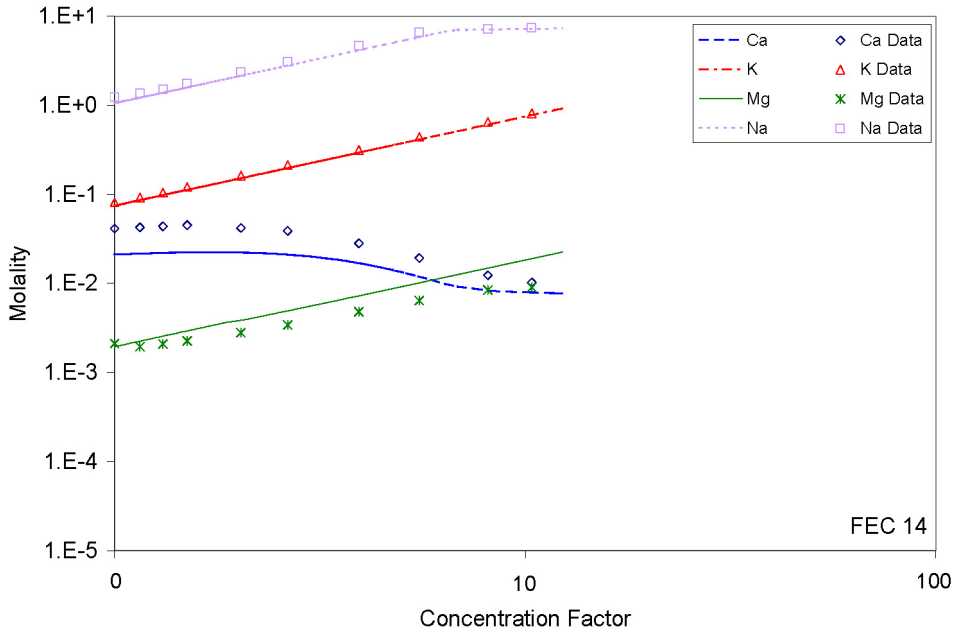

Output DTN: MO0701EQ36IDPS.000, file: *Topopah95.zip*, *FEC14bsum PitpH r1.xls*.

Figure 7-90. Predicted vs. Measured Cations for Leg 4 of Evaporation Based on Experiments in Alai et al. (2005 [DIRS 176811])

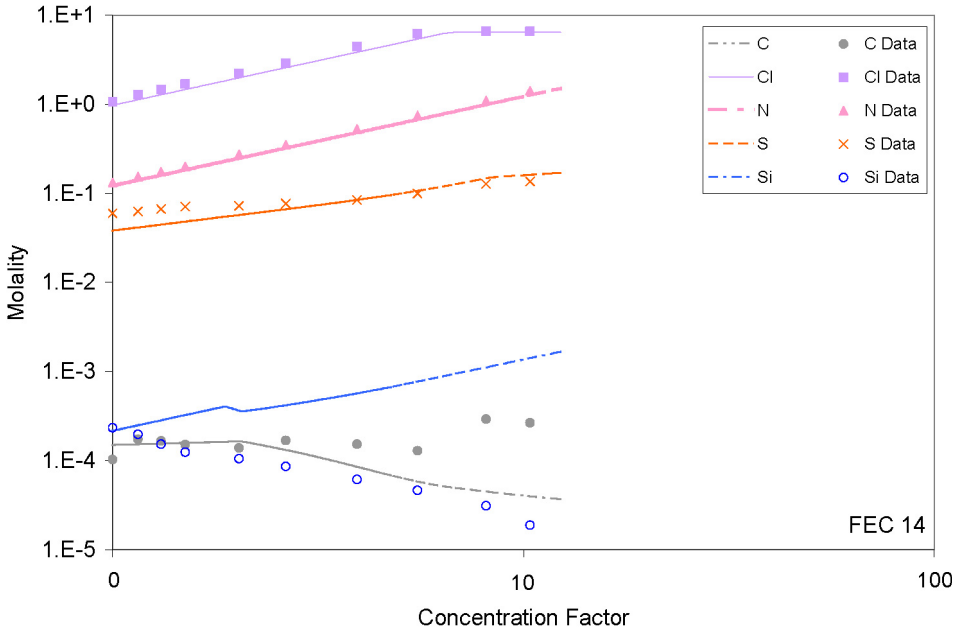

Output DTN: MO0701EQ36IDPS.000, file: *Topopah95.zip*, *FEC14bsum PitpH r1.xls*.

Figure 7-91. Predicted vs. Measured Anions and Si for Leg 4 of Evaporation Based on Experiments in Alai et al. (2005 [DIRS 176811])

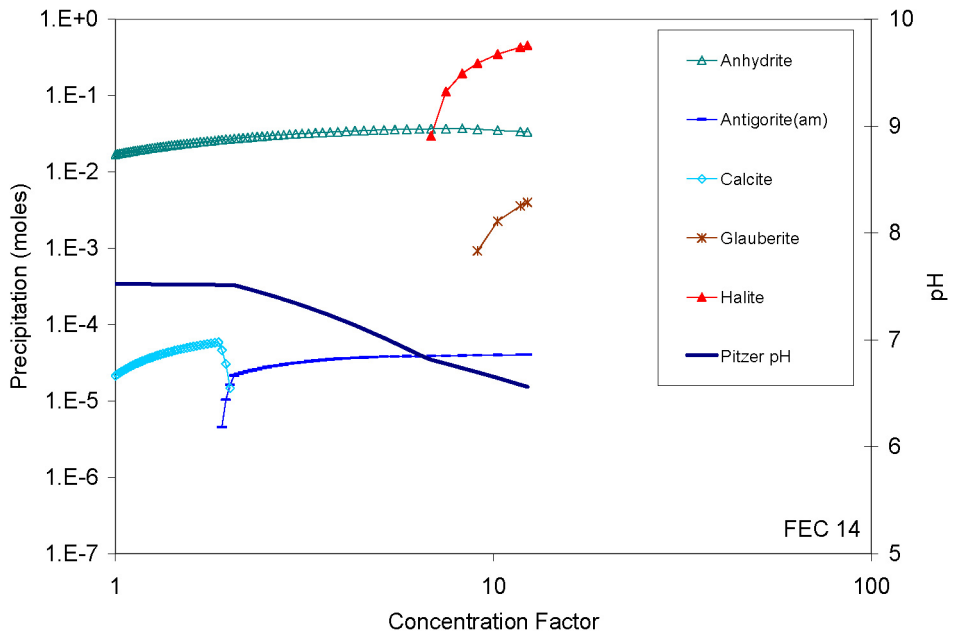

Output DTN: MO0701EQ36IDPS.000, file: *Topopah95.zip*, *FEC14bsum PitpH r1.xls*.

Figure 7-92. Predicted Mineral Evolution for Leg 4 of Evaporation Based on Experiment in Alai et al. (2005 [DIRS 176811])

7.2.5 Seawater Evaporation

The Morton Bahamas solar salt production facility on Great Inagua Island in the Bahamas provides an excellent example of evaporative chemical evolution of natural multicomponent water. At this plant, seawater is evaporatively concentrated in a sequence of reservoirs to precipitate table salt (halite). This production process results in a final brine with a concentration factor near 40 with respect to seawater. One of the primary advantages of this data set compared to samples taken from saline lakes is that these reservoirs are not subject to large mixing effects from streams and rivers. In addition, the reservoirs are shallow and open to the atmosphere, facilitating equilibrium conditions with respect to atmospheric partial pressures of carbon dioxide and oxygen. Thus, the major processes affecting the evolution of seawater at the plant are the same processes incorporated in the IDPS model.

McCaffrey et al. (1987 [DIRS 164481]) sampled and analyzed the chemical compositions of the evolving seawater at the plant. Three of the most concentrated samples were evaporated even further in the laboratory. The data for both the reservoir samples and the laboratory evaporation experiments are presented in Table 4-25. The samples in the table that start with a "w" were collected directly from the plant reservoirs while the remainder were artificially evaporated from samples w36, w39, and w40. The reported degree of evaporation is equivalent to the concentration factors of conservative components. For degrees of evaporation up to 70, the concentration factor for Mg was used to determine degree of evaporation. Beyond 70, the concentration factor of lithium was used.

The IDPS model was used to simulate the seawater evaporation at the plant. The results are documented in Output DTN: MO0701EQ36IDPS.000. Sea intake water (sample w63) was used

as the starting water. This sample, collected at the plant intake, had a degree of evaporation slightly less than seawater, perhaps because it was composed of seawater mixed with a small amount of fresh water from a nearby stream. In the simulation, the temperature was fixed at 31.25°C, the average value of the reservoir samples. To balance the charge, the model decreased the Cl concentration by about 1.5%. The partial pressures of carbon dioxide and oxygen were set approximately at atmospheric values, $10^{-3.5}$ and $10^{-0.7}$ bars, respectively. Because carbonate was not measured, the concentration of dissolved carbonate was set at heterogeneous equilibrium with the partial pressure of carbon dioxide. Finally, the minerals listed in Table 6-3 were suppressed.

It is important to note that the laboratory evaporation experiments were closed to the atmosphere. These experiments resulted in the samples in Table 4-25 that have degrees of evaporation greater than 40. These samples were derived by placing samples of w36, w39, and w40 in uncovered teflon vials and sealing them in desiccation chambers containing $CaCl_2$ crystals, a desiccant (McCaffrey et al. 1987 [DIRS 164481], p. 931). Sealing the desiccation chambers does not allow for exchange of oxygen and carbon dioxide with the atmosphere. This could have caused partial pressure deviations from atmospheric values. Changes in carbon dioxide partial pressure affects pH, which in turn has the potential to affect which minerals precipitate. No pH values were measured for these samples. Differences, however, between aqueous concentration measurements and IDPS predictions are small (as shown below) and suggest that gas fugacities did not depart markedly from atmospheric and/or did not play a major role in the evaporative evolution of the water samples. The data from the desiccation chambers are included in the validation because they provide increased confidence in the ability of the IDPS model to predict the effects of evaporation in highly saline multicomponent water samples.

The IDPS model predictions are compared to sample measurements in Figures 7-93, 7-94, and 7-95. These figures show that the IDPS model predictions are highly accurate. Comparison of the predicted mineral precipitation in Figure 7-96 to the dissolved concentrations confirms that halite precipitation begins to control the concentrations of Na and Cl at a degree of evaporation around 10. Degree of evaporation relative to seawater was calculated from the IDPS model output by multiplying the IDPS concentration factor (*CF*) by 0.95, the degree of evaporation of the sea intake water used as the starting water for the evaporation. The *CF* calculated by the IDPS model reflects the degree of evaporation relative to the intake water.

Like halite, other minerals that control the evaporative concentration of the dissolved components are revealed by the trajectories of their concentrations in the figures. For example, McCaffrey et al. (1987 [DIRS 164481], p. 935) found that gypsum ($CaSO_4 \cdot 2H_2O$) begins to precipitate at a degree of evaporation around 3.8. This explains the decrease in Ca concentrations at this degree of evaporation. The IDPS model predicts that gypsum starts precipitating at a degree of evaporation of around 3.7 and is immediately replaced by anhydrite ($CaSO_4$). From that point until the degree of evaporation reaches about 10, anhydrite is the predicted controlling phase for Ca. Above a degree of evaporation of 10 but below about 57, glauberite ($Na_2Ca(SO_4)_2$) replaces anhydrite as the controlling phase for Ca in the simulation. The differences between the minerals predicted to precipitate and those observed to precipitate may be due to several factors, such as errors in the equilibrium constants of the minerals, nonequilibrium conditions (e.g., mineral supersaturation), errors in boundary conditions (e.g., the partial pressure of carbon dioxide), and sampling error. The end result, however, is that the

model predicts the Ca concentrations within 50% of measurements to a degree of evaporation of 10 and within a factor of 3 for all measurements (Figure 7-93).

Figure 7-93 shows that measured K concentrations begin to decrease sharply after concentrations reach approximately 80 times that of seawater. McCaffrey et al. (1987 [DIRS 164481], p. 935) did not determine the K-bearing phases precipitating at this degree of evaporation. In the IDPS model simulation, precipitation of polyhalite ($K_2MgCa_2(SO_4)_4 \cdot 2H_2O$) begins to control K concentrations starting around concentrations 45 times that of seawater. This difference results in a maximum overestimation of K by a factor of about five at a degree of evaporation around 73.

In the analysis that follows here and after, the most concentrated sample plotted in the graphs is ignored because it is an outlier. Ignoring this last data point is justified for two reasons. First, the trends established by the last data point are not supported by the trends of the preceding 48 data points. Second, as water evaporates from solution, the total molality of dissolved components in the solution cannot decrease. To the contrary, the total molality of this outlier markedly decreases.

Model predictions of Na, Mg, Cl, Br, and SO_4 compare well with sample concentrations for the entire range of measurements. Ignoring the outlier, the largest overestimate is a factor of about 2.3 for Na at a degree of evaporation of 87.9. The largest underestimate is a factor of about 0.45 for SO_4 at a degree of evaporation of 69.2. The marked decrease in SO_4 measurements above this degree of evaporation is due to the precipitation of one or more magnesium sulfates (McCaffrey et al. 1987 [DIRS 164481], p. 935). The largest differences between predictions and measurements for Mg, Cl, and Br are approximately –23%, 12%, and 12%, respectively, relative to the measurements. These differences do not consider the outlier identified above.

Figure 7-95 shows good agreement between measurements and predictions for pH and ionic strength. The largest difference observed for pH is approximately 0.79 pH units. However, there is some uncertainty associated with the pH measurements. Measuring pH at high ionic strength requires special methods (Section 7.5.1), which may or may not have been used. Thus, the differences between model predictions and experimental measurements could partly (or largely) be a result of experimental error. For ionic strength, the largest difference is approximately 15%, except for the outlier at the highest degree of evaporation.

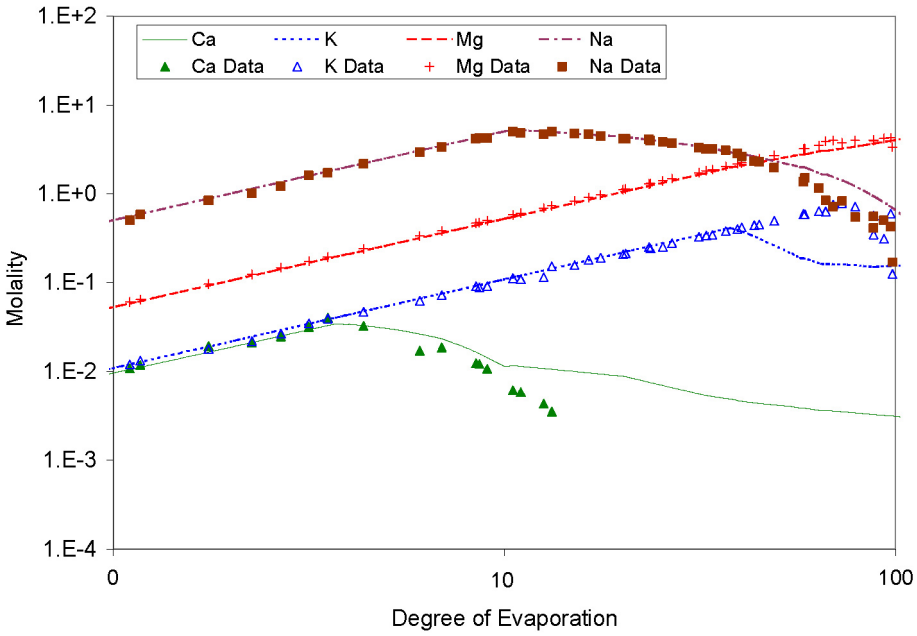

Output DTN: MO0701EQ36IDPS.000, file: *Seawater.zip*, *inagua r2.xls*.
Source: McCaffrey et al. 1987 [DIRS 164481].

Figure 7-93. Predicted vs. Measured Ca, K, Mg, and Na Concentrations from Evaporation of Inagua Seawater

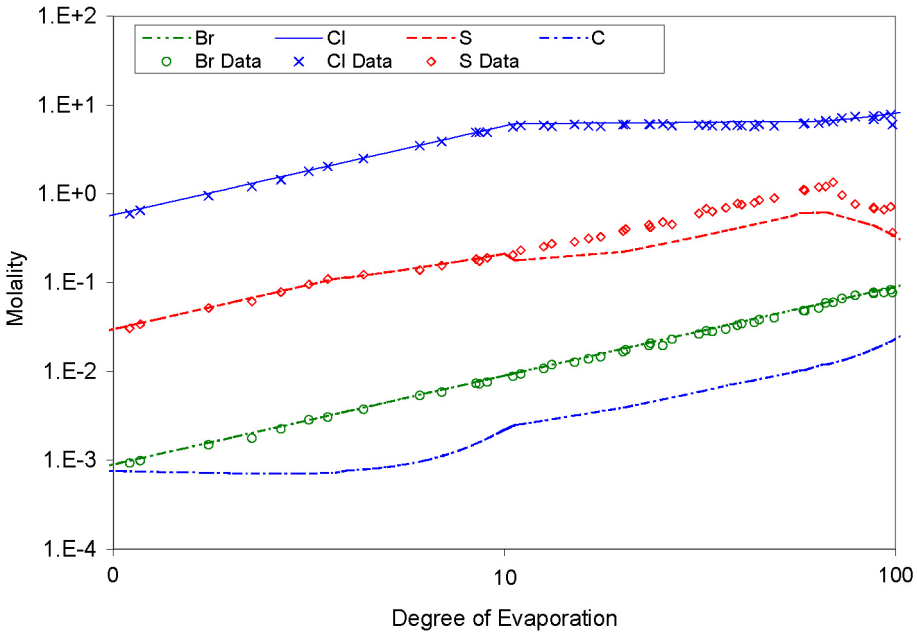

Output DTN: MO0701EQ36IDPS.000, file: *Seawater.zip*, *inagua r2.xls*.

Source: McCaffrey et al. 1987 [DIRS 164481].

NOTE: There is no data for C located in the source (McCaffrey et al. 1987 [DIRS 164481]).

Figure 7-94. Predicted vs. Measured Br, Cl, and SO_4 Concentrations from Evaporation of Inagua Seawater

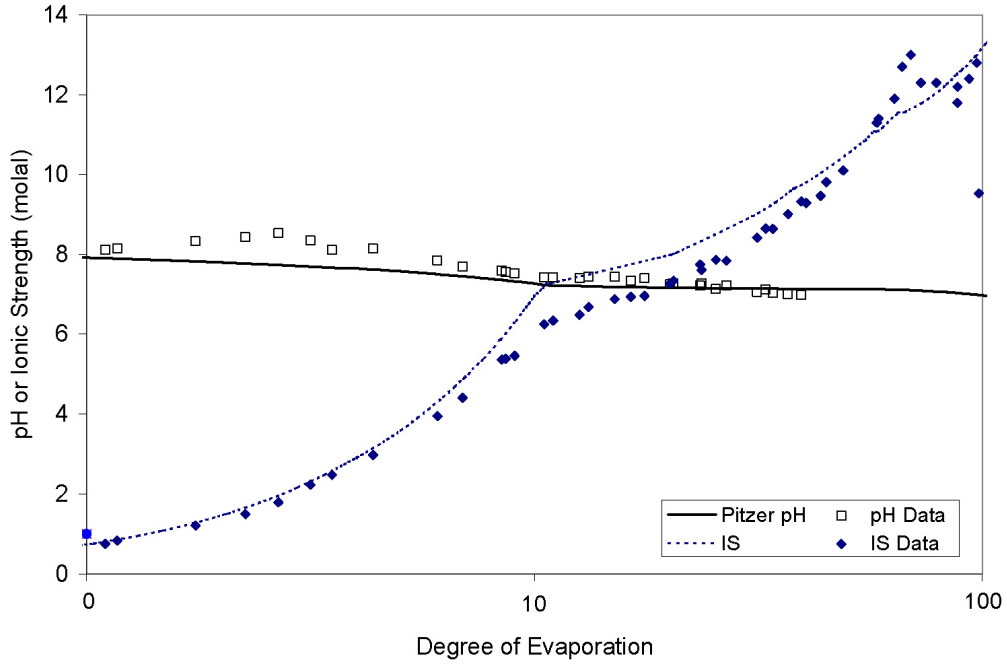

Output DTN: MO0701EQ36IDPS.000, file: *Seawater.zip*, *inagua r2.xls*.

Source: McCaffrey et al. 1987 [DIRS 164481].

Figure 7-95. Predicted vs. Measured pH and Ionic Strength from Evaporation of Inagua Seawater

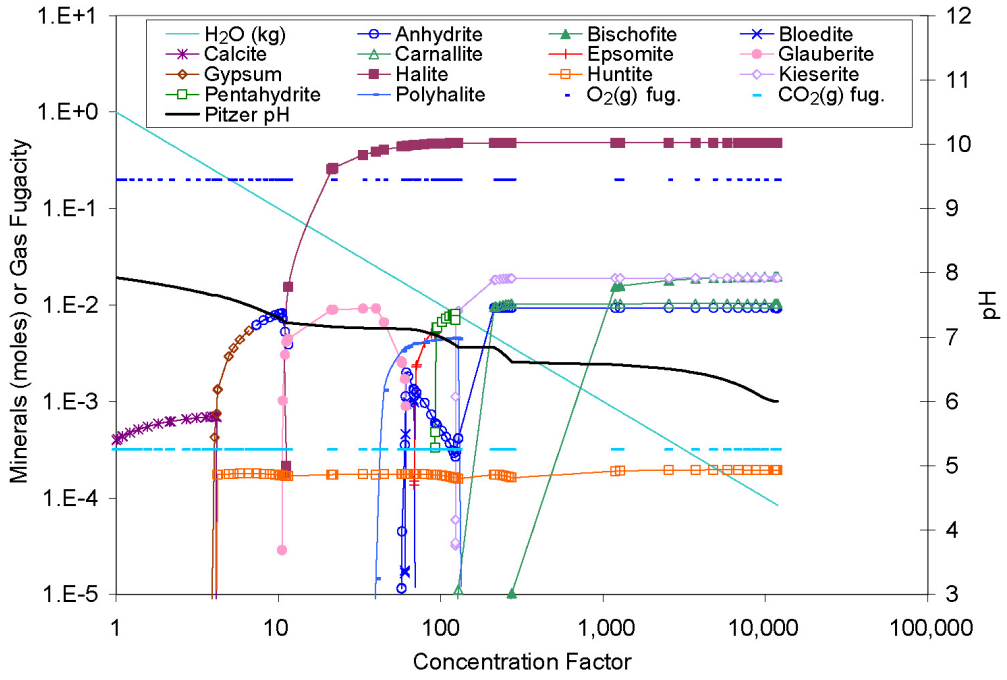

Output DTN: MO0701EQ36IDPS.000, file: *Seawater.zip*, *inagua r2.xls*.

Figure 7-96. Predicted Mineral Precipitation from Evaporation of Inagua Seawater

7.3 COMPARISON OF PITZER AND DATA0.YMP.R5 DATABASE PREDICTIONS

The model was further validated by comparing model predictions, using the Pitzer database, to those generated using the data0.ymp.R5 thermodynamic database (DTN: SN0612T0502404.014 [DIRS 178850]). The J-13 example water in Section 6.7 was evaporated to an ionic strength of 1 molal using the data0.ymp.R5 database. The B-dot equation option was chosen for calculating the activity coefficients. This option is generally valid for solutions having ionic strength values up to 1 molal (SNL 2003 [DIRS 162494], Section B.2.1).

The results of this comparison are documented in Output DTN: SN0702T0509206.008 (file: *j13.ymp.xls*). Evaporating this J-13 water to an ionic strength of 1 molal using the data0.ymp.R5 database (DTN: SN0612T0502404.014 [DIRS 178850]) and B-dot equation results in a concentration factor of about 413.

Two sets of results were generated using the data0.ymp.R5 database (DTN: SN0612T0502404.014 [DIRS 178850]). In the first set, only the minerals in Table 6-3 were suppressed from forming. The results for this set are compared to the Pitzer database predictions in Figures 7-97 and 7-98. Because the data0.ymp.R5 database contains many more minerals than the Pitzer database, three minerals not included in the Pitzer database (tridymite, phlogopite, and dolomite-ord) precipitated in this set of results. These minerals are not predicted to form under the conditions of the repository. Tridymite is only stable at temperatures between 870°C and 1,470°C at atmospheric pressure (Klein and Hurlbut 1999 [DIRS 124293], p. 530), and dolomite formation is slow (Vaniman et al. 1992 [DIRS 107066]). Despite these differences in the predicted mineral precipitation, the comparisons in Figures 7-97 and 7-98 show strong agreement between the two databases in the values of the aqueous output parameters.

In the second set of data0.ymp.R5 results, only the minerals that precipitated in the Pitzer results (calcite, amorphous antigorite, amorphous silica, and celadonite) were allowed to precipitate. The results for this set are compared to the Pitzer database predictions in Figures 7-99 and 7-100. Except for Si, these results are almost identical to the Pitzer results.

These simulations demonstrate that the IDPS model produces similar aqueous output (up to an ionic strength of 1 molal) regardless of whether the Pitzer database (Output DTN: SN0609T0502404.012) or the data0.ymp.R5 database (DTN: SN0612T0502404.014 [DIRS 178850]) is used. As a result, the calculations for each aqueous output parameter in this example fall within model validation specifications.

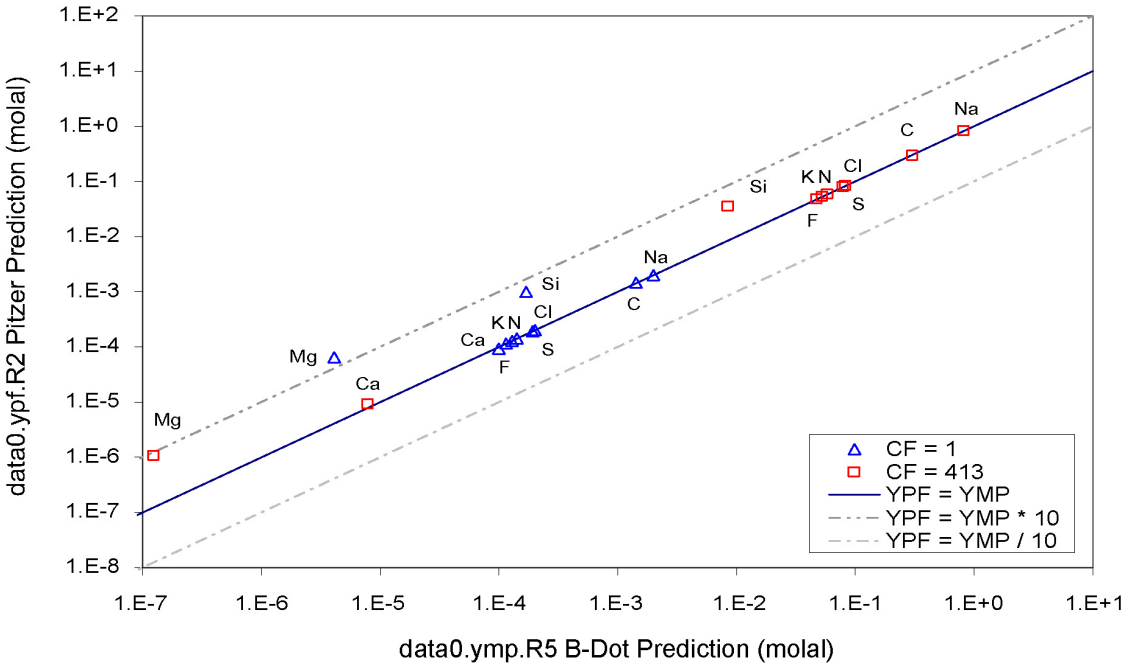

Output DTN: SN0702T0509206.008, file: *j13 ymp.xls*.

NOTE: "YPF" in the legend indicates data0.ypf.R2; "YMP" indicates data0.ymp.R5.

Figure 7-97. Pitzer vs. Set 1 data0.ymp.R5 Aqueous Predictions for Average In Situ J-13 Well Water at 70°C and CO_2(g) Fugacity of 10^{-3} Bars

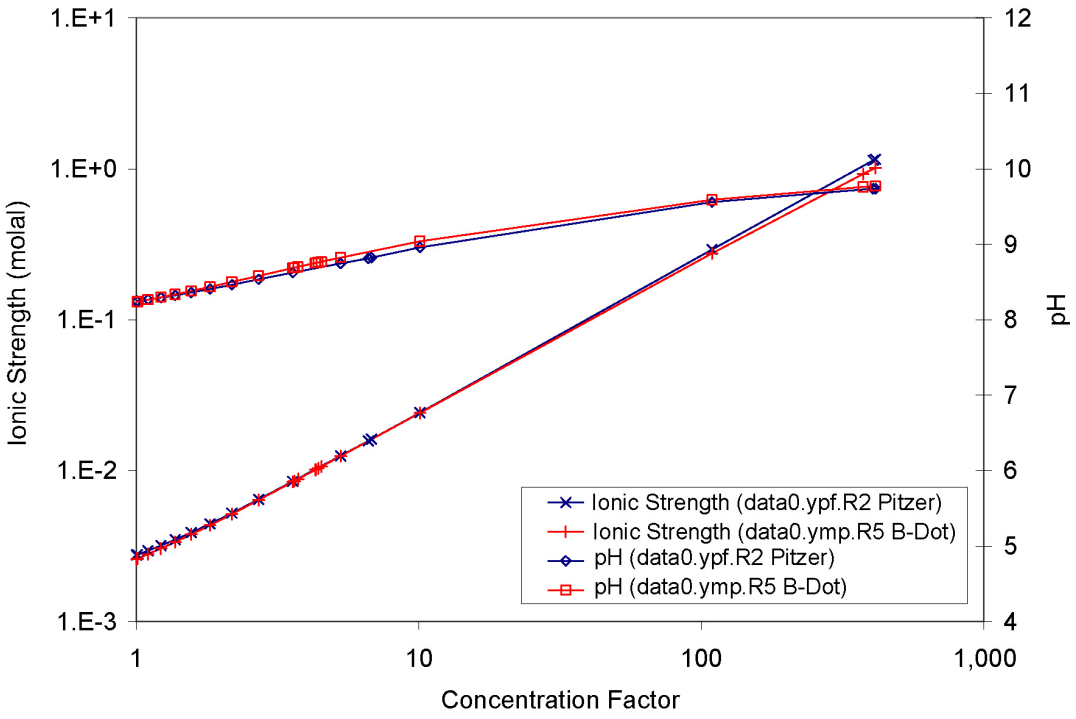

Output DTN: SN0702T0509206.008, file: *j13 ymp.xls*.

Figure 7-98. Pitzer vs. Set 1 data0.ymp.R5 pH and Ionic Strength Predictions for Average In Situ J-13 Well Water at 70°C and CO_2(g) Fugacity of 10^{-3} Bars

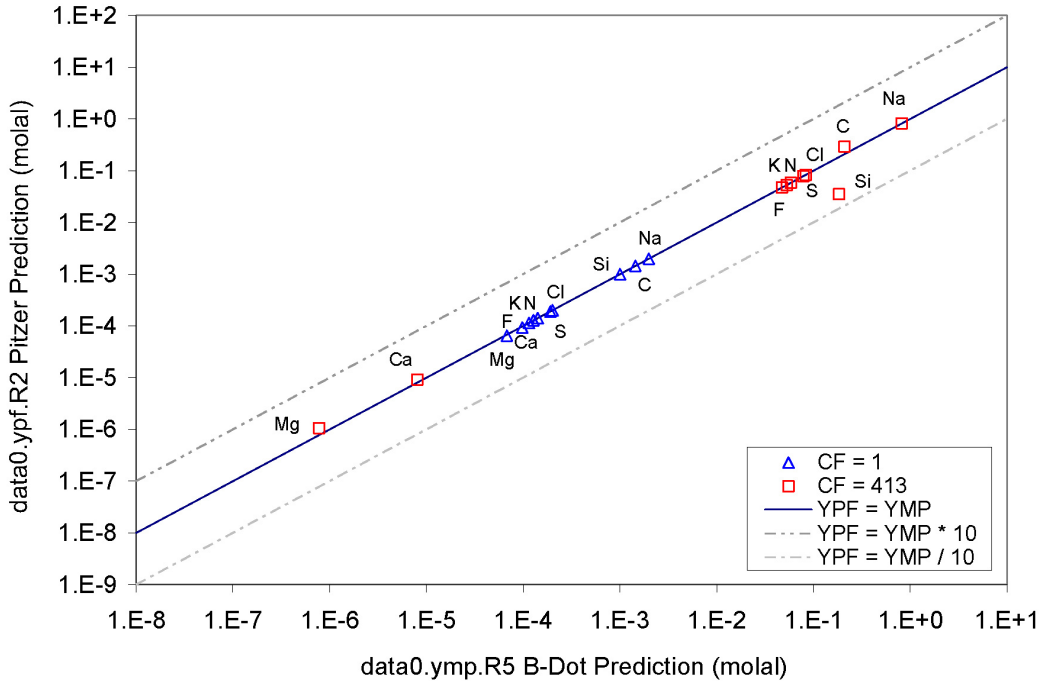

Output DTN: SN0702T0509206.008, file: *j13 ymp.xls*.

NOTE: "YPF" in the legend indicates data0.ypf.R2; "YMP" indicates data0.ymp.R5.

Figure 7-99. Pitzer vs. Set 2 data0.ymp.R5 Aqueous Predictions for Average In Situ J-13 Well Water at 70°C and CO_2(g) Fugacity of 10^{-3} Bars

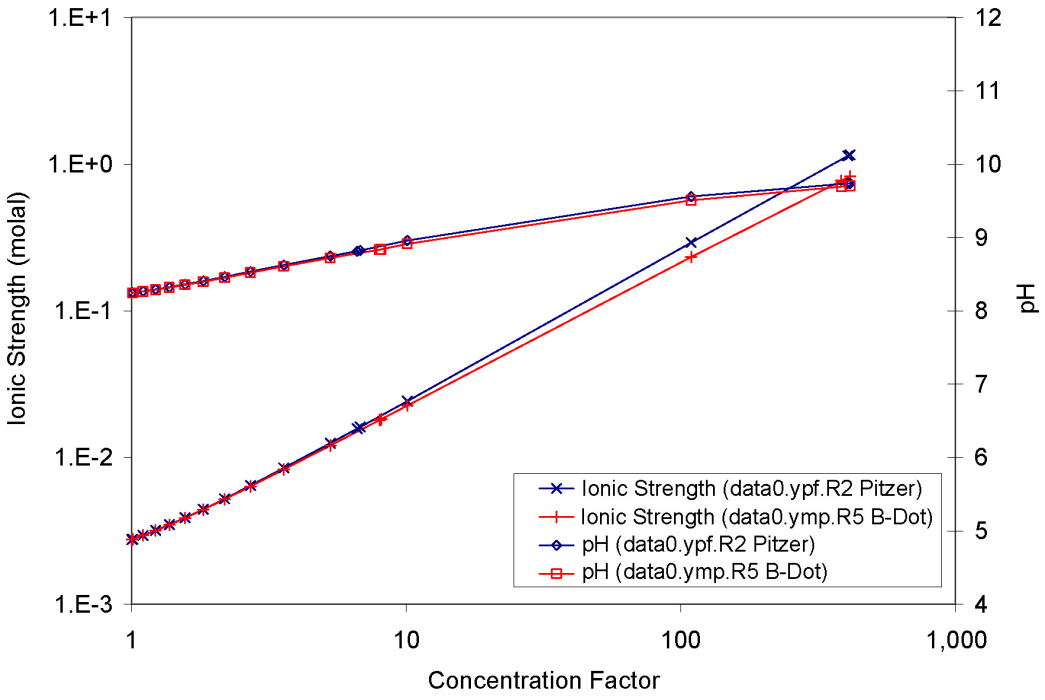

Output DTN: SN0702T0509206.008, file: *j13 ymp.xls*.

Figure 7-100. Pitzer vs. Set 2 data0.ymp.R5 pH and Ionic Strength Predictions for Average In Situ J-13 Well Water at 70°C and CO_2(g) Fugacity of 10^{-3} Bars

7.4 VALIDATION FOR MINERAL OUTPUTS

A major feature of the IDPS model is the selection of minerals that are allowed (or not allowed) to precipitate upon saturation. Each mineral that precipitates creates a new chemical divide that has important consequences for the evolution of the aqueous phase (Section 6.3). Thus, mineral precipitation in the model determines the aqueous evolution of the evaporating solution. In the IDPS model, the minerals allowed to precipitate are those in the thermodynamic database that are not suppressed in the input file. The codependence of the evolving aqueous and mineral phases is imposed by the conservation of mass. At all times, the total mass of each component in the system is the sum of the masses of the component in the mineral and aqueous phases. Precipitation transfers a portion of the component mass from the aqueous to the mineral phase such that the total mass in the system remains constant. There are two components, however, whose masses do not remain constant in the system described by the IDPS model. They are water, which is incrementally removed by evaporation, and carbonate, which exchanges with the atmosphere via degassing and dissolution of carbon dioxide. Removal of water or carbonate (via carbon dioxide) does not affect the total masses of other components in the system.

Because the IDPS model imposes conservation of mass, the fact that the IDPS model predicts aqueous evolution within specified model validation criteria (Sections 7.1 through 7.3) validates the IDPS model for predicting bulk compositions of precipitated minerals. The bulk mineral composition is the set of the total masses of each elemental component in the total precipitation. While model validation for predicting the bulk mineral composition does not imply that the model accurately predicts exactly which minerals precipitate, this line of reasoning implies that the minerals predicted by the model to precipitate were adequate for predicting the evaporative evolution of the aqueous phase.

For TSPA, it is the latter conclusion that is paramount—that the minerals predicted by the model to precipitate are adequate for predicting the composition of the aqueous phase. The minerals themselves do not affect performance of the repository. It is the potential aqueous solution that can be produced by deliquescence or dissolution of these minerals that is important to TSPA in predicting corrosion initiation and radionuclide mobility. Thus, predicting the specific mineral assemblage that would be generated by evaporation of a given water is not required. What is required, however, is predicting a mineral assemblage that will generate sufficiently accurate aqueous solutions upon deliquescence or dissolution. As Sections 7.1 through 7.3 show, the mineral assemblages predicted by the model accomplish this criterion, thereby validating the mineral outputs for their intended use.

This model validation argument is not as easily applied to the carbonate minerals because total carbonate in the system is not constant. The fixed partial pressure of carbon dioxide largely controls the mass of dissolved carbonate. If the solution becomes momentarily supersaturated with a non-suppressed carbonate mineral, that mineral is allowed to precipitate, thereby quantitatively transferring carbonate from the aqueous phase to the mineral phase. This loss of carbonate from the aqueous phase in turn permits additional dissolution of carbon dioxide. The code iterates on these mass transfers until equilibrium is attained.

Validating the open-system IDPS model for carbonate minerals requires that the model adequately predict not only the aqueous evolution of dissolved carbonate but also the evolution

of pH. Removal and addition of carbonate from the aqueous phase via precipitation, dissolution, and degassing of carbon dioxide have important consequences on the evolution of pH. As shown in Section 7.2, the pH and carbonate concentrations are predicted within specifications in the open-system laboratory evaporation tests on synthesized J-13 and Topopah Spring tuff pore water and in the Inagua seawater evaporation reservoirs.

The evaporation simulations of dilute salt solutions in Section 7.1, which include carbonate minerals, add to the validation of the IDPS model for mineral outputs. In essentially each of these evaporations, the solubility of the mineral phase was predicted within a factor of 10 and usually within 20% (Table 7-3, Figures 7-1 and 7-2). For a few salts, the solubility was never reached by the model at one or more temperatures tested; however, the potential impact of these salts on IDPS model results is negligible. These particular salts are highly soluble and their precipitation in the IDPS model is not required to predict evaporative evolution within the uncertainty limitations prescribed by the model validation criteria. For additional verification of the accuracy of mineral solubility predictions, the reader is referred to the Pitzer database appendix.

7.5 VALIDATION SUMMARY AND ESTIMATED UNCERTAINTIES

This section addresses the validation of the IDPS model for temperatures from 20°C to 140°C by comparing the results of the validation simulations to the validation criteria in Table 7-1. In addition, this section evaluates the uncertainty associated with selected IDPS model output parameters. The selected parameters include pH, ionic strength, F concentration, Cl concentration, NO_3 concentration, the Cl:NO_3 mole ratio, and deliquescence relative humidity (RH_d).

Table 7-9 summarizes the maximum differences observed for selected parameters between model predictions and experimental data for the multi-component evaporation simulations in Section 7.2. RH_d was not measured for these systems. For these data sets, only the evaporated seawater samples and leg 4 of the pore water evaporation at 95°C have predicted equilibrium *RH* values below 91%. The seawater samples have predicted equilibrium *RH* values as low as about 54% for Cl and ionic strength measurements and as low as 68% for pH measurements (Figure 7-95). Leg 4 of the pore water experiment at 95°C reaches a predicted equilibrium *RH* of 71%.

Differences between measurements and model predictions of Cl, NO_3, and the Cl:NO_3 mole ratio were also compiled for the ternary systems in Section 7.1.2 that involve both Cl and NO_3. The results are plotted in Figure 7-101 as a function of equilibrium *RH*. Also included in this figure are predictions and measurements from leg 4 of the TSw pore water experiment at 95°C. These differences are documented in Output DTN: SN0611T0509206.007. The plot shows differences in both directions. Positive differences indicate that the model predictions are higher than measurements, and negative differences indicate the model predictions are lower than measurements.

Uncertainty in IDPS model predictions is strongly correlated with equilibrium *RH*, as illustrated in Figure 7-101. There is a strong theoretical basis for this relationship. As *RH* decreases, solubility limits are reached that have important consequences on the concentrations of Cl, NO_3,

and the Cl:NO_3 mole ratio. If the model starts to precipitate Cl or NO_3 phases at *RH* above or below the *RH* that is consistent with measurements, then deviations begin to occur between model predictions and measurements as *RH* decreases further. In addition, the EQ3/6 code and Pitzer database have calculation uncertainties that can become considerable at low *RH,* and the reliability and availability of experimental data decrease. The only available data relevant to the system below an *RH* of about 50% are data for Ca, Mg, and some K salts; the solubilities of Na salts inhibit Na from staying in solution in the binary and ternary systems at *RH* below 50%.

Table 7-9. Maximum Differences between Predictions and Measurements for pH, Ionic Strength, Cl, F, NO_3, and the Cl:NO_3 Ratio

Evaporation Simulation	pH (pH units)	Ionic Strength (RPD[a])	Cl (RPD)	F (RPD)	NO_3 (RPD)	NO_3:Cl Ratio (RPD)	Cl:NO_3 Ratio (RPD)
J-13 Evaporation Experiment (Section 7.2.1)	−0.79	−12%	26%	14% [b]	18%	−14%	16%
100x J-13 Evaporation Experiment (Section 7.2.2)	N/M [c]	N/E [d]	5%	26% [e]	8%	3%	-3%
Topopah Spring Tuff Pore Water Evaporation Experiment at 75°C (Section 7.2.3)	0.17	−2%	−9%	N/E [f]	N/M [c]	N/M [c]	N/M [c]
Topopah Spring Tuff Pore Water Evaporation Experiments at 95°C (Section 7.2.4)	−0.68	50%	−12%	N/E [f]	20%	−8%	9%
Seawater Evaporation (Section 7.2.5	−0.79	15% [g]	10% [g]	N/M [c]	N/M [c]	N/M [c]	N/M [c]

[a] RPD (relative percent difference) = 100% * ([predicted concentration] − [measured concentration]) / [measured concentration].
[b] Based on one data point.
[c] N/M = not measured.
[d] N/E = not estimated, pH needed for estimate.
[e] This value ignores the sample with the highest degree of evaporation as justified in Section 7.2.5.
[f] Although these data sets include F as a component in the initial solution composition before evaporation, no F concentration was measured (or the concentration was below detection limits after dilution) at the end of the experiment.
[g] Based on two data points.

NOTE: Calculated from Output DTNs: SN0702T0509206.008 and MO0701EQ36IDPS.000. Values can be checked semi-quantitatively from the graphs and tables in the sections referenced in column 1.

Validation comparisons in the binary and ternary systems in Section 7.1 assess the differences between measured and predicted salt solubilities. These comparisons are useful for evaluating model validation and uncertainty when the solution has reached saturation with respect to one or all salts in the systems. These comparisons are essentially worst case scenarios for the IDPS model because they only reveal differences between predictions and measurements in highly

concentrated solutions. In contrast, they do not provide uncertainty information for solutions that are undersaturated with respect to these salts. At solution concentrations below the measured and predicted solubilities of these salts, the model will accurately and precisely predict the effects of evaporation and condensation on aqueous salt concentrations.

Figure 7-101 reveals the possibility of model bias when salinities are high and *RH* is below about 70%. Specifically, the figure shows that for certain *RH* ranges there is potential bias in predicting Cl and NO_3 concentrations and Cl:NO_3 mole ratios in systems saturated with Cl and/or NO_3 salts. However, considering the small sample size and the statistically nonrepresentative distribution of data points in this chart, a clear bias in the results of specific applications of the IDPS model in TSPA cannot be reliably predicted and justified.

Below an *RH* of 20%, a potentially significant bias appears where predictions of the Cl:NO_3 mole ratio tend to far exceed measurements. This *RH* range only has data from the Mg-Cl-NO_3 system (Figures 7-52 and 7-53). This apparent bias suggests that model predictions of the Cl:NO_3 mole ratio are likely nonconservative in this system (i.e., biased toward predicting a less corrosive brine).

Estimates of IDPS model uncertainties for Cl, F, NO_3, and the Cl:NO_3 mole ratio are presented in Table 7-10 along with estimated model uncertainties for pH, ionic strength, and RH_d. The estimates for Cl, NO_3, and the Cl:NO_3 mole ratio are largely based on the plot in Figure 7-101 while the estimates for F are based on Figure 7-102 (see Section 7.5.8). In the subsections that follow, each validation criterion is compared to the results of the simulations. Where applicable, the results are also compared to the estimated model uncertainties listed in Table 7-10.

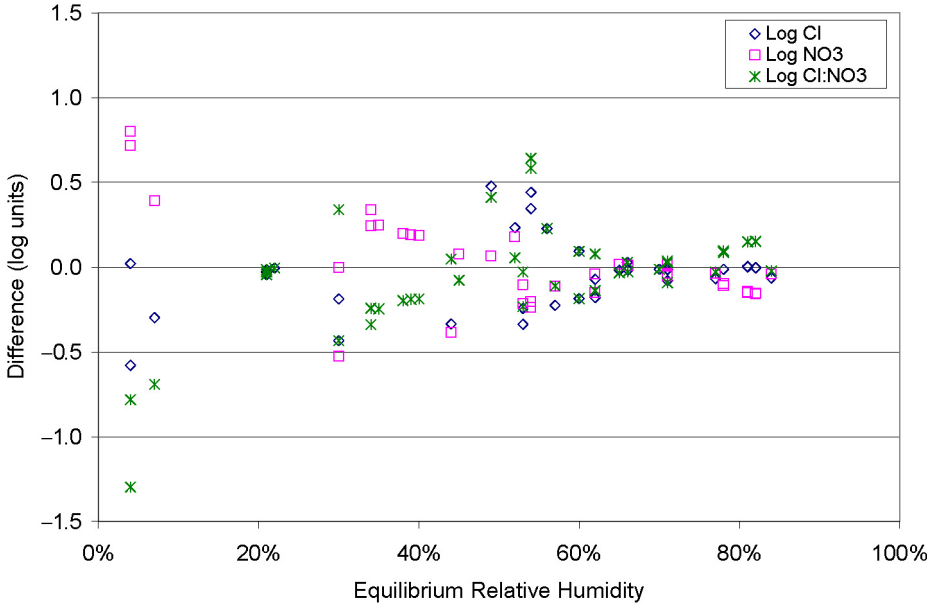

Output DTN: SN0611T0509206.007.

Figure 7-101. Differences between Measurements and Model Predictions for Ternary Systems and Leg 4 of the Pore Water Evaporation Experiment at 95°C

Table 7-10. Estimated IDPS Model Uncertainties for Temperatures between 20°C and 140°C

Parameter[a]	Units	*RH* Range 100% to 85%	*RH* Range 85% to 65%	*RH* Range 65% to 40%	*RH* Range 40% to 20%	*RH* Range 20% to 0%
pH	pH units	±1	±1	±2	±2	±2
Ionic Strength	log molal	±0.1	N/A [b]	N/A [b]	N/A [b]	N/A [b]
Cl	log molal	±0.0	±0.1	±0.4	±0.5	±0.7
F	log molal	±0.5 [c]	±0.5	±0.5	±0.5	±0.5
NO_3	log molal	±0.0	±0.2	±0.4	±0.5	±0.9
Cl:NO_3	log mole ratio	±0.0	±0.2	±0.5	±0.5	±1.4
RH_d	%RH units	±5%	±10%	±10% [d]	±15% [d]	±15% [d]

Output DTN: SN0611T0509206.007.

[a] The uncertainties of these parameters can be described with a triangular distribution with the most likely uncertainty defined as ±0% and the maximum and minimum uncertainties defined by the values in this table. The uncertainties for pH represent uncertainties in the evaporative evolution of pH in unbuffered systems. The uncertainty in pH may be reduced by considering pH buffering reactions in specific systems.

[b] Not applicable to TSPA. Prediction of ionic strength is for colloids model. At *RH* below 85%, ionic strength is greater than 1 molal, which is far above the critical ionic strength where colloids are unstable.

[c] The exception for this estimated uncertainty is for a model simulation of a solution saturated with respect to sellaite (MgF_2). The model simulation underestimates the total soluble F, probably because there is experimental uncertainty in the solubility of MgF_2 given by (Lide 2000 [DIRS 162229]). See Section 7.5.8 for a discussion of uncertainty in experimental determinations of sellaite solubility.

[d] The exception for this estimated uncertainty is for a brine with a large $Mg(NO_3)_2$ component. IDPS model predictions in binary $Mg(NO_3)_2$ systems operationally provide RH_d values that are much lower than reported measurements. Because the validation criterion for the IDPS model is to predict RH_d within ±10% *RH* (Table 7-1), the IDPS model is not valid for predicting RH_d below 40% or when $Mg(NO_3)_2$ is a large component of the brine at *RH* below 65%.

7.5.1 pH

The IDPS model validation criterion for pH is to predict pH within one pH unit (Table 7-1). In each of the simulations in which pH data are available, pH is predicted within 0.79 pH unit or less (Figures 7-69, 7-76, 7-81, 7-85, and 7-95). The maximum pH differences in each of the multi-component evaporation data sets are summarized in Table 7-9.

The set of validation data contains pH measurements to temperatures as high as 95°C (Figures 7-81 and 7-85) and activities of water as low as 0.68 (water activity used to make Figure 7-95). The pH measurements of samples at ionic strengths greater than 0.1 molal (Figures 7-69, 7-76, and 7-95) may or may not have been adjusted for ionic strength and therefore may not be highly accurate. The scientific literature appears to be devoid of reported measured pH values for concentrated salt solutions at temperatures above 100°C and/or at high ionic strengths. Consequently, the validation of the pH aspect of the IDPS model and Pitzer database at such temperatures and ionic strengths cannot be accomplished in the same manner as at lower temperatures and lower ionic strengths. A different, less-direct approach must be taken. Before proceeding to that, however, the nature of pH and pH measurement are briefly reviewed to provide context for the problem. In brief, there are two problematic aspects, one associated with elevated temperature, the other with concentrated salt solutions (high ionic strength).

The measurement of pH in dilute solutions above 100°C in a manner analogous to measurement at lower temperatures is possible but relatively infrequent. Special electrodes must be utilized.

A pressurized apparatus is often required to keep water in a liquid phase. In situ measurement then requires integration of the electrodes into the pressurized apparatus. An additional difficulty is the lack of widely accepted calibration buffers for use in high temperature measurement, though this is a relatively minor impediment from a technical standpoint.

One approach to obtaining high-temperature values for dilute solutions is to measure the pH of quenched solutions, then use a geochemical modeling code such as EQ3/6 to "correct" such quench values to the original temperature (cf. Knauss et al. 1985 [DIRS 143694]; Knauss et al. 1985 [DIRS 100150]). A closely related approach is to use the modeling code to compute the elevated temperature pH of buffer solutions to be used in experiments, such as in studies of mineral dissolution kinetics (cf. Knauss and Wolery 1986 [DIRS 160184]; Knauss and Wolery 1988 [DIRS 133140]). If all the relevant acid-base equilibria are properly represented with respect to the applicable temperature range, either approach should give reliable results. It must be noted that the use of either approach requires avoiding mass transfer (e.g., mineral precipitation or degassing of volatiles such as CO_2). Such mass transfer may occur during the quenching process (when quench pH is measured) or in heating of a buffer to elevated temperature. A quenched sample may be diluted into pure water prior to pH measurement to minimize such problems, with correction for this in the modeling code calculation. Such dilution intrinsically increases the uncertainty in the calculated result. However, it may be necessary to obtain an acceptable result.

Of all the potentially relevant acid-base equilibria, a key one for any aqueous system is that for the acid-base dissociation of water:

$$H_2O_{(l)} = H^+ + OH^- \qquad \text{(Eq. 7.5.1-1)}$$

for which the mass-action equation can be written as:

$$\log K_w = -pH - pOH - \log a_w \qquad \text{(Eq. 7.5.1-2)}$$

where K_w is the equilibrium constant for the reaction as written above, $pH = -\log a_{H^+}$ (negative logarithm of the thermodynamic activity of H^+), $pOH = -\log a_{OH^-}$ (analogous to pH), and a_w is the thermodynamic activity of water (which has a value near unity in dilute solutions). Traditionally, "neutral pH" at any temperature is defined as $-1/2 \log K_w$ and the nominal maximum pH as $-\log K_w$. At 25°C, $\log K_w$ has a value of −13.9951 (the negative of the value for the reverse reaction taken from data0.ypf.R0 (DTN: SN0302T0510102.002 [DIRS 162572]). Hence the traditional neutral pH at this temperature has a value close to 7.0 and the nominal maximum pH is 14. The dielectric constant of water decreases as temperature is increased, creating a medium that is much less favorable for ionization reactions (cf. Helgeson and Kirkham 1974 [DIRS 157904]). This decrease is particularly notable between 25°C and 100°C. At 100°C, $\log K_w$ has a value of −12.2551 (also from data0.ypf.R0), implying a neutral pH close to 6.13 and a nominal maximum pH of 12.26. At 150°C, $\log K_w$ has a value of −11.6308 (again from data0.ypf.R0), implying a neutral pH close to 5.82 and a nominal maximum pH of 11.63. These results imply that a solution with a pH of 8 at 100°C is more alkaline than one with a pH of 8 at 25°C because the pOH is lower for the former.

The measurement and reporting of pH in most of the modern scientific and technical literature are consistent with the "NBS" pH scale. A scale is required because (at least by thermodynamic methods) ionic activities can only be observed in combinations corresponding to electrical neutrality. Some kind of arbitrary convention to allow a "splitting" is required. For standard state Gibbs energies of the aqueous ions, such a splitting convention sets that quantity for H^+ equal to zero. Ionic activities are related to molalities and activity coefficients by the relation:

$$a_i = m_i \gamma_i \qquad \text{(Eq. 7.5.1-3)}$$

where a_i is the activity of the *i*th ion, m_i is the molality of that ion, and γ_i is the corresponding activity coefficient. Individual ionic molalities are observable; individual ionic activity coefficients are not. A splitting convention for ionic activity coefficients is tantamount to one for ionic activities, and hence also tantamount to defining a scale for pH. In fact, pH scales are generally defined by adopting some expression for the activity coefficient of some ion. In the case of the National Bureau of Standards (NBS) pH scale, this is the Bates-Guggenheim equation (e.g., Bates 1973 [DIRS 166051]):

$$\log \gamma_{Cl^-} = \frac{-A_{\gamma,10}\sqrt{I}}{1+1.5\sqrt{I}} \qquad \text{(Eq. 7.5.1-4)}$$

where $A_{\gamma,10}$ is the Debye-Hückel "A" parameter and *I* is the ionic strength. Results for any set of model equations for ionic activity coefficients can be rescaled for consistency with this definition (cf. Knauss et al. 1990 [DIRS 166144]; Wolery 1992 [DIRS 100836], p. 43). This in fact is done in EQ3/6, which by default reports pH and ionic activities and activity coefficients on an extended NBS scale.

The Bates-Guggenheim equation is a simple "extended" Debye-Hückel equation that is consistent with the Debye-Hückel limiting law:

$$\log \gamma_i = -A_{\gamma,10} z_i^2 \sqrt{I} \qquad \text{(Eq. 7.5.1-5)}$$

where z_i is the electrical charge number of the *i*th ion. This applies accurately only in the limit of dilute aqueous solutions. One would expect the Bates-Guggenheim equation to be realistic (in some absolute sense) with respect to higher but still relatively low ionic strength (e.g., less than about 0.1 molal). However, one would also expect the Bates-Guggenheim equation to become highly inaccurate in some absolute sense at high ionic strength. If one applies this convention to highly concentrated salt solutions, the usual understanding of numbers for pH as corresponding to solutions that are acidic, neutral, or alkaline may no longer apply. For example, at 25°C, a pH value of 7 might be acidic or alkaline instead of neutral.

If one were to desire that the pH numbers for concentrated solutions correspond to their commonly accepted implications of solution character, one would be forced to consider alternative pH scales. One alternative would be to use the raw single-ion form of Pitzer's equations (no rescaling). That is also consistent with the limiting law; hence it is also consistent with the NBS pH scale at sufficiently low ionic strength. This alternative contains its own

splitting convention, which is discussed for example by Wolery (1992 [DIRS 100836], pp. 44 to 61). A second alternative, the "Mesmer" scale (cf. Mesmer 1991 [DIRS 166053]), is based on the convention:

$$\log a_{H^+} = \log m_{H^+} \qquad \text{(Eq. 7.5.1-6)}$$

This is equivalent to setting $\log \gamma_{H^+} = 0$. The Mesmer convention is not consistent with the limiting law. Therefore, it is also not consistent with the NBS pH scale at low ionic strength. It does have the advantage that the molality of the hydrogen ion in concentrated salt solutions can sometimes be determined experimentally. EQ3/6 (and various other geochemical modeling codes) typically allow code users to deal with any of several pH scales, including those discussed here.

The measurement of pH in concentrated salt solutions at any temperature is another problem. The standard method for measuring pH at low temperature using a specific ion electrode (specific to H^+) in combination with a reference electrode (commonly Ag/AgCl) is really designed for use in dilute solutions only. The NBS pH scale was originally recommended for application to solutions having a maximum ionic strength of 0.1 molal (e.g., Bates 1973 [DIRS 166051]). This is commonly exceeded in the treatment of natural waters including brackish waters and seawater (which has an ionic strength of approximately 0.7 molal). The problem with the standard measurement method is that at high ionic strengths the method is increasingly affected by a liquid junction potential error (e.g., Baes and Mesmer 1986 [DIRS 100702]). The liquid junction potential is associated with the reference electrode. This potential is non-zero in dilute solutions; however, it is approximately constant for any solution with relatively low ionic strength and therefore effectively zeroed out in the standard calibration process. However, it takes on different values in more concentrated solutions. There is no generally accepted model for correcting liquid junction potential errors. Such corrections are sometimes attempted, but they involve relatively severe approximations and it is not clear if the results are better or worse.

Knauss et al. (1990 [DIRS 166144]) proposed elimination of the liquid junction potential by replacing the standard reference electrode with another specific ion electrode, such as one specific to the chloride ion. The parameter measured would then be not pH but pH + pCl. Such an approach is generally feasible. However, there are no "standard" calibration buffer solutions for this type of measurement. In essence, one must compute compositions for possible calibration buffers using a modeling code such as EQ3/6 and a model for concentrated aqueous salt solutions, based for example on Pitzer's equations. EQ3/6 is capable of taking a quantity such as pH + pCl in place of pH, and computing a thermodynamic model of the aqueous solution that includes a value for the pH on whichever pH scale is desired (Wolery 1992 [DIRS 100836], pp. 19 to 21). This general approach appears to have been used only at low temperatures.

The above discussion should give the impression that pH cannot be measured in practice in the absence of a thermodynamic model for ionic activities and activity coefficients. That is in fact the correct impression, because without such a model (at least covering some small number of chemical components) it is not possible to develop calibration buffers to define in an operational sense what the pH is. In essence, pH measurement is based on a procedure which at a more

basic level attempts to measure the difference between the pH in a water sample and the pH in a calibration buffer (though in standard practice two calibration buffer solutions bracketing the expected sample pH are to be used). Thus, the pH is basically a model construct. The activity of the hydrogen ion is likewise a model construct.

Nothing more is added by other methods to measure the pH. For example, pH paper works by color changes of dyes in the paper. The dyes are buffers with their own thermodynamic properties. The pH values assigned to the color changes are calibrated against other, standard pH buffers. The expected response of the dyes will likely only occur for relatively dilute solutions. At high ionic strength, the color responses may be altered by interactions with ions other than the hydrogen ion. In general, pH paper is only intended to be used in dilute solutions (and at low temperatures).

In essence, one accepts the pH because one accepts the accuracy of the thermodynamic models for buffer-electrolyte systems, at least the key ones associated with the principal operational standards (as represented for example in commercial pH calibration buffer solutions). The acceptance of these thermodynamic models is based on their consistency with observations of speciation and solubilities. Here the observations of speciation may be tied to potentiometric or spectroscopic measurements. The pH as measured in standard practice is useful for correlating such data (at least in dilute solutions). That is the basic justification for defining and using this parameter.

Consequently, the pH aspect of the high-temperature IDPS model and Pitzer database above 100°C can be validated even in the absence of any direct pH measurements. It is only necessary to show that the model does a reasonable job of predicting things that depend on or strongly correlate with the pH. Here the focus will be on solubilities, as the relevant data are more readily available than other types of data that correlate with pH. Consider the case of portlandite ($Ca(OH)_2$). The dissolution reaction can be written as:

$$Ca(OH)_{2(c)} + 2H^+ = Ca^{2+} + 2H_2O \qquad \text{(Eq. 7.5.1-7)}$$

The corresponding mass action equation can be written as:

$$\log K = \log a_{Ca^{2+}} + 2\log a_w + 2pH \qquad \text{(Eq. 7.5.1-8)}$$

The solubility of portlandite is more directly obtained by recasting this as:

$$\log m_{Ca^{2+}} = \log K - \left\{\log \gamma_{Ca^{2+}} + 2\log a_w\right\} - 2pH \qquad \text{(Eq. 7.5.1-9)}$$

(other potential dissolved calcium species that might contribute to the solubility are ignored here). Clearly, the calculated solubility of this mineral is strongly correlated with pH, such that a change of 0.5 pH unit would change the calculated solubility by one log unit.

If there were no uncertainties in the equilibrium constant or the activity coefficient model (which determines the activity coefficient of the calcium ion and the activity of water), an uncertainty of one log unit in the solubility would imply an uncertainty of 0.5 unit in the pH. Other

uncertainties in the right hand side of the above equation must be addressed. The uncertainty in log *K* for such a reaction is likely relatively small, in the range 0.005 to 0.1 unit. The remaining quantity in braces $\{\log\gamma_{Ca^{2+}} + 2\log a_w\}$ is a function of the activity coefficient model (here the high-temperature Pitzer model). The uncertainty is potentially highly variable, depending on the total aqueous solution composition. Portlandite itself (and many other common minerals whose solubilities correlate strongly with pH) is sparingly soluble. In a two-aqueous-electrolyte system such as $Ca(OH)_2$-NaCl-H_2O (where the other electrolyte is highly soluble and there is no common ion), the activity of water would depend almost entirely on the concentration of the second, more soluble electrolyte over most of the compositional range, and the activity coefficient of the calcium ion would depend mainly on the generalized ionic strength and the interactions of this ion with the sodium and chloride ions. In such a simple system, the activity coefficient model could carry relatively little uncertainty. One would therefore expect that pH values calculated from the model would carry uncertainties that correlate mainly with uncertainties in the solubility of the sparingly soluble mineral.

To the extent that systems meeting the above criteria are available, one can say that the uncertainty in calculated pH correlates with uncertainty in solubility. The exact degree of correlation depends on the charge of the cation in the sparingly soluble electrolyte. In the above example, that cation is divalent and a one log unit uncertainty in calculated solubility correlates with an uncertainty of 0.5 unit in the pH. If one substituted a trivalent ion, such as Al^{3+}, the one log unit uncertainty in calculated solubility correlates with 0.33 unit in the pH. The correlation is less favorable for monovalent cations such as Na^+ and K^+ (one log unit in the solubility correlating to one pH unit). In addition, highly soluble compounds give rise to concentrated brines that have additional uncertainties associated with calculated ion activity coefficients. For example, as evaporation occurs and salts precipitate, small amounts of NaOH and KOH can concentrate to large proportions. The additional uncertainties in the contributions from the activity coefficient model therefore increase the overall pH uncertainty for highly concentrated brines to approximately two units.

The carbonate systems in Section 7.1 also meet the criteria above for a strong correlation between pH and solubility. In all cases simulated, the solubilities of the carbonate salts are predicted within a factor of 10 and usually within a factor of 2 (Figures 7-7, 7-8, 7-9, 7-10, 7-39, and 7-41).

The pH uncertainty cannot be defined in a highly quantitative manner because there are high temperature and/or high ionic strength solubility data for relatively few of the sorts of systems described above that are ideal for constraining uncertainty in pH. However, the uncertainty in calculated solubilities for such pH-correlative systems probably does not differ much from that in such results for non-pH-correlative systems. Overall, this validation study has indicated that the uncertainty in calculated solubilities in the temperature range of interest is generally better than one log unit, and in some cases much better. This indicates that a reasonable estimate of maximum error in pH in all but the most concentrated solutions is one pH unit, and for the most concentrated solutions (e.g., equilibrium *RH* less than 65%), two pH units (Table 7-10). A triangular distribution for this uncertainty is justified because smaller errors in pH predictions have larger frequency and all predictions are within the established uncertainty limits. These

uncertainties are comparable to, and perhaps smaller than, uncertainties that may apply to reported pH measurements in high-ionic strength solutions at high temperature.

IDPS model uncertainty in predicting pH can be substantially reduced by considering the pH buffering reactions in a particular system. The analysis above and the pH uncertainties in Table 7-10 assume poorly buffered systems. However, aqueous reactions, mineral dissolution, and/or a fixed partial pressure of CO_2 can strongly buffer pH. The pH buffering capacity of a given system can be quantified by titrating the system with acid or base and noting the change in pH as a function of acid or base added.

7.5.2 Ionic Strength

The model validation criterion for ionic strength is to predict ionic strength within a factor of 10 (Table 7-1). In each of the multi-component evaporation simulations in Section 7.2, ionic strength is predicted within 50% or less (Table 7-7, Table 7-8, and Figure 7-95).

The estimated model uncertainty for ionic strength at *RH* values above 85% is plus or minus 0.1 in log units (Table 7-10). This value is approximately equivalent to an uncertainty of plus or minus 30%. The maximum difference between measured and predicted ionic strength in the seawater samples is approximately 15%, except for an outlier at the highest degree of evaporation (Figure 7-95). Considering the accuracy in the predicted seawater ionic strength and the maximum difference observed in the laboratory evaporation experiments at equilibrium *RH* values above 85%, the estimated plus or minus 0.1 model uncertainty in log units for ionic strength at *RH* values above 85% is supported and justified.

At *RH* less than 85%, ionic strength is greater than 1 molal, as suggested in the data used to construct Figures 6-4 and 7-95. Ionic strength outputs of the IDPS model are used as input to the colloids model in TSPA. At ionic strengths above 0.05 molal, colloids are unstable (BSC 2004 [DIRS 170025], Section 6.3.1) and do not affect repository performance. Thus, uncertainties for ionic strength predictions are not required by TSPA at the high ionic strengths that occur at *RH* values below 85%.

7.5.3 Deliquescence Relative Humidity

The model validation criterion for deliquescence relative humidity (RH_d) is to predict RH_d within 10% in *RH* units (Table 7-1). In each of the deliquescence simulations in Sections 7.1.1.1.2 and 7.1.1.2.2, the predicted RH_d is within 10% *RH* of available measurements, except for $Mg(NO_3)_2$ for all temperatures (Figure 7-24) and for KF at 25°C (Figure 7-12). The large *RH* difference between predictions and measurements of RH_d for $Mg(NO_3)_2$ indicates that the model is not valid for predicting RH_d when $Mg(NO_3)_2$ is a major component of the brine.

As presented in Table 7-10 and supported by the results in Sections 7.1.1.1.2 and 7.1.1.2.2, the estimated model uncertainty for RH_d is plus or minus 5% in *RH* units when RH_d predictions are 85% or higher. From 40% to 85%, the model uncertainty for RH_d is estimated to be plus or minus 10% in *RH* units for systems that do not contain major quantities of $Mg(NO_3)_2$. Below 40% *RH*, the IDPS model cannot be validated for predicting RH_d with the available data because the uncertainty is greater than validation criteria established in Table 7-1. Any

prediction of RH_d at low *RH* (i.e., below 40% *RH* or when $Mg(NO_3)_2$ is a major component of the brine) will require information outside this report.

7.5.4 Al, Br, CO_3, Cl, K, Na, NO_3, and SO_4

The model validation criterion for Al, Br, CO_3, Cl, K, Na, NO_3, and SO_4 is to predict the total concentrations of these components within a factor of 10 (Table 7-1). Of these components, only Cl and NO_3 predictions are used in downstream models in the TSPA. However, Al, Br, CO_3, K, Na, and SO_4 can potentially contribute directly or indirectly to IDPS model predictions of Cl and NO_3 (Section 6.3.2), and each of the components can potentially affect predictions of pH, ionic strength, and RH_d.

In each of the multi-component evaporation experiments in Section 7.2, the total concentrations of Br, CO_3, Cl, Na, NO_3, and SO_4 are predicted within a factor of 3 or less (Figures 7-68, 7-72, 7-75, 7-78, 7-79, 7-82, 7-83, -86, 7-87, 7-90, 7-91, 7-93, and 7-94) with two exceptions. The first exception is for CO_3, which is underpredicted by as much as a factor of 7 in the most concentrated samples of leg 4 of the pore water experiments at 95°C, and the second exception is the outlier in the seawater evaporation data, which can be ignored as explained in Section 7.2.5. The factor of 3 is readily confirmed in the first three figures because a line drawn at a factor of 3.16 would plot equidistantly between lines drawn at factors of 1 and 10 (i.e., $10^{1/2} = 3.16$). Al was not evaluated because of a lack of evaporation data involving Al. K was predicted within a factor of 3 or less in all cases except the later stages of the seawater evaporation, where K predictions differed from measurements by nearly a factor of 5 (Figure 7-93) as explained in Section 7.2.5.

For the simple salt systems evaluated in Section 7.1, model predictions of Br, CO_3, Cl, K, Na, NO_3, and SO_4 solubilities were almost always within a factor of 10 and nearly always within a factor of 3. In the Na-Ca-NO_3 ternary system, the dissolved $NaNO_3$ concentration (and associated Na concentration) was not predicted within a factor of 10 (Figure 7-40); however, the total dissolved NO_3 concentration was predicted within a factor of 3.

The ability of the model to predict solubilities of Br, CO_3, Cl, K, Na, NO_3, and SO_4 within a factor of 10 or better in nearly every validation simulation indicates that the model is valid for its intended use. Because Cl and NO_3 are the only components in this group that are model outputs used directly or indirectly in TSPA calculations, only the estimation of model uncertainty associated with Cl and NO_3 is addressed below.

The maximum differences in predictions and measurements for Cl and NO_3 in each of the Section 7.2 evaporation data sets are summarized in Table 7-9. At the temperatures of the experiments, Cl and NO_3 should concentrate conservatively until halite precipitates. In multi-component aqueous systems, halite should not precipitate until the activity of water falls to around 0.7 or lower (e.g., Figure 6-6).

The seawater samples and samples from leg 4 of the pore water evaporation experiment at 95°C achieve much higher salinities and lower activities of water than the other evaporation experiments (Figure 7-95). Thus, Cl does not concentrate conservatively in these evaporations except during the early stages. At a seawater concentration factor of about 10, the activity of

water falls to approximately 0.7, whereupon halite begins to precipitate, as indicated by the plateau of the Cl concentration curve in Figure 7-94. In leg 4 of the pore water evaporation experiment at 95°C, the data and model both show that Cl concentrations level off when halite begins precipitating at an equilibrium relative humidity around 72%. The maximum difference between measured and predicted Cl in these high ionic strength waters is approximately 10% to 12%. NO_3 was not measured in the seawater study.

The estimated model uncertainties for Cl and NO_3 are presented in Table 7-10 as a function of *RH*. Above 85% *RH*, Cl and NO_3 should not precipitate, as implied in Figure 7-101 by the absence of data points at *RH* greater than 85%. Instead, Cl and NO_3 should simply concentrate conservatively as water evaporates whenever the *RH* is between 100% and 85%. Thus, the model uncertainty in Cl and NO_3 predictions is set at zero for *RH* between 100% and 85%.

As *RH* decreases below 85%, the model uncertainty in Cl and NO_3 increases, as indicated in Table 7-10 and Figure 7-101. Between 85% and 60% *RH*, the concentrations of these anions can be controlled by the solubilities of Na and K salts of Cl and NO_3 (e.g., Figures 7-3, 7-4, 7-21, and 7-22). The estimated model uncertainties in Cl and NO_3 predictions in this *RH* range consider effects of other dissolved components, such as SO_4 (Figures 7-31 and 7-32), CO_3 (Figure 7-39), and the effects of ternary systems involving both Cl and NO_3 (Figure 7-101).

It would be difficult to justify any model biases based on Figure 7-101 because the data in Figure 7-101 are patchy, largely uncorroborated, and not necessarily representative of the more complex systems predicted to occur in the repository. In addition, potential bias is generally system-specific. The various ternary systems are unevenly dispersed across Figure 7-101, and the sizes of the data sets for each system are unequal. For example, most of the data shown at 24% *RH* and in the 45% to 55% *RH* range are for the Ca-Cl-NO_3 system (Figures 7-46 through 7-51). The data for the Na-Cl-NO_3 system are confined to the 50% to 70% *RH* range (Figures 7-27 through 7-30). While Cl and NO_3 concentrations show some potential biases in these systems, it is not known whether they would persist in more complex systems (i.e., systems involving more than three components). The contribution of experimental error in these data sets is also unknown but could be large, as suggested in Figure 7-46. For this reason and the unavailability of a sufficient set of corroborating data for multi-component systems, potential bias in predicting Cl and NO_3 concentrations is not quantified. Instead, the potential bias is subsumed in the estimates of model uncertainty for these parameters (Table 7-10).

Below 60% *RH*, uncertainties in Cl and NO_3 predictions increase markedly. In this low *RH* range, Cl and NO_3 concentrations can be controlled by the solubilities of Ca and Mg salts (e.g., Figures 7-5, 7-6, 7-23, and 7-24). In addition, when temperatures are above approximately 90°C in this *RH* range, NO_3 concentrations can be controlled by the solubility of KNO_3 (Figure 7-22). The larger differences between predictions and measurements shown in these figures justify the higher estimated model uncertainties in Cl and NO_3 predictions at these low *RH* values (Table 7-10). The uncertainty estimates in Cl and NO_3 predictions in this *RH* range consider effects of Na (Figures 7-40 and 7-42) and K (Figures 7-44 and 7-45) and the effects of ternary systems involving both Cl and NO_3 (Figure 7-48).

7.5.5 Ca, Mg, and SiO_2

The model validation criterion for Ca, Mg, and SiO_2 is to predict the total concentrations of these components within a factor of 100 (Table 7-1). The larger validation range for Ca, Mg, and SiO_2 recognizes the importance of kinetic limitations in the precipitation of Ca, Mg, and SiO_2 minerals. Equilibrium in the short timeframes of laboratory experiments may not be attained with respect to Ca, Mg, or SiO_2 species and minerals; however, they may be nearly or completely attained in the repository timeframes that the IDPS model is intended to simulate. Thus, the differences observed between IDPS model predictions and laboratory measurements may be due to slow formation of Ca, Mg, and SiO_2 minerals in short-term evaporation experiments. For Ca and Mg, whose solubilities are strongly affected by pH and total carbonate, differences may also be due to errors in the presumed values of carbon dioxide fugacity during the experiments and/or to errors in the predicted pH value. These effects are discussed in more detail in Section 7.2.2. As a result, the larger uncertainty in the predicted concentrations of Ca, Mg, and SiO_2 is reflected in the validation criteria for these outputs.

The model validation criterion for Ca, Mg, and SiO_2 is met in nearly every validation simulation in Section 7.2 (Figures 7-68, 7-72, 7-75, 7-78, 7-79, 7-82, 7-83, 7-86, 7-87, 7-90, 7-91, and 7-93). The one exception is for Ca in the 100x J-13 evaporation experiment (Figure 7-72). The Ca concentration predicted by the IDPS model was slightly more than two orders of magnitude lower than the measured concentration. This exception may be due to the importance of slow calcite precipitation in the short-term laboratory evaporation experiments (Section 7.2.2). Processes that are only important in the short term do not fall into the scope of the intended use of the IDPS model.

In the binary evaporation simulations in Section 7.1, Ca and Mg solubilities are predicted within a factor of 10 and usually within a factor of 2 (Table 7-3, Figures 7-5, 7-6, 7-15, 7-16, 7-19, 7-20, 7-23, and 7-24). In the ternary systems, they are always predicted within a factor of 10 and usually within a factor of 2 (Figures 7-40, 7-42, 7-44, 7-46, 7-48, 7-50, and 7-52).

7.5.6 Minerals

Because the IDPS model imposes the principle of conservation of mass, the fact that the IDPS model predicts aqueous evolution within specified model validation criteria validates the IDPS model for predicting bulk compositions of precipitated minerals. While model validation for predicting the bulk mineral composition does not imply that the model accurately predicts the exact minerals observed to precipitate in laboratory evaporation experiments (and for various reasons, it often does not, as explained in Section 7.4), this line of reasoning implies that the minerals predicted by the model to precipitate are adequate for predicting the evaporative evolution of the aqueous phase. This is important because the minerals themselves do not affect the performance of the repository. It is the potential aqueous solution produced by deliquescence or dissolution of these minerals that is important in predicting corrosion initiation and radionuclide mobility.

7.5.7 Cl:NO_3 Ratio

Model validation criteria were not established for the Cl:NO_3 ratio because criteria were already established for Cl and NO_3 separately (Table 7-1). However, the uncertainty in the Cl:NO_3 ratio is an important consideration in corrosion calculations. Consequently, uncertainty in the Cl:NO_3 ratio due to IDPS model uncertainty was estimated for propagation in TSPA (Table 7-10).

The maximum differences in predictions and measurements for the Cl:NO_3 mole ratio in the evaporation data sets in Section 7.2 are summarized in Table 7-9. They are less than 20%. The model uncertainties presented in Table 7-10 as a function of *RH* are estimated based on the results in Figure 7-101. Above 85% *RH*, Cl and NO_3 should not precipitate, as implied in Figure 7-101 by the absence of data points at *RH* greater than 85%. Instead, Cl and NO_3 should concentrate conservatively as water evaporates whenever the *RH* is between 100% and 85%. Thus, the model uncertainty in the Cl:NO_3 mole ratio predictions is set at zero for *RH* between 100% and 85%.

As *RH* decreases below 85%, the model uncertainty in Cl and NO_3 predictions increases, as indicated in Table 7-10 and Figure 7-101. Between 85% and 60% *RH*, the concentrations of Cl and NO_3 can be controlled by the solubilities of Na and K salts (e.g., Figures 7-3, 7-4, 7-21, and 7-22). The estimated model uncertainties in this *RH* range consider effects of ternary systems involving both Cl and NO_3 (Figure 7-101).

The results displayed in Figure 7-101 show no consistent bias across the *RH* range in predicting the Cl:NO_3 mole ratio. The data as a whole in Figure 7-101 are patchy, largely uncorroborated, and not necessarily representative of the more complex systems predicted to occur in the repository. The experimental error in these data sets is also unknown but could be large, as suggested in Figure 7-46. For these reasons, potential bias is not quantified for predicting the Cl:NO_3 mole ratio. Instead, the potential bias is subsumed in the estimates of model uncertainty for this ratio (Table 7-10). Bias and its potential effect on conservatism are discussed at the beginning of Section 7.5 where Figure 7-101 is introduced.

Below 60% *RH*, uncertainties in Cl and NO_3 predictions increase markedly. In this low *RH* range, Cl and NO_3 concentrations can be controlled by the solubilities of Ca and Mg salts (e.g., Figure 7-5, Figure 7-6, 7-23, and 7-24). In addition, when temperatures are above approximately 90°C in this *RH* range, NO_3 concentrations can be controlled by the solubility of KNO_3 (Figure 7-22). Regardless of which salt controls NO_3 concentrations below 60% *RH*, NO_3 solubility is high. The larger differences between predictions and measurements shown in these figures justify the larger estimated model uncertainties in Cl:NO_3 mole ratio predictions at these low *RH* values (Table 7-10). The uncertainty estimates in Cl:NO_3 mole ratio predictions in this *RH* range consider effects of ternary systems involving both Cl and NO_3 (Figure 7-101).

7.5.8 F Concentration

The model validation criterion for F is to predict the total concentration within a factor of 10 (Table 7-1). Differences between measurements and model predictions of F were compiled for the binary and ternary systems in Sections 7.1.1 and 7.1.2 that involve F. The results are plotted in Figure 7-102 as a function of equilibrium *RH*. These differences are documented in Output

DTN: SN0611T0509206.007. The plot shows differences in both directions. Positive differences indicate that the model predictions are higher than measurements, and negative differences indicate the model predictions are lower than measurements.

The results displayed in Figure 7-102 show no consistent bias across the *RH* range in predicting the F concentration. The differences from KF saturated systems are clustered in the 10% to 30% *RH* region. Differences from the NaF system are clustered at ~96% *RH* while the differences from the MgF_2 and CaF_2 systems are near 100% *RH*. The data as a whole in Figure 7-102 are not necessarily representative of the more complex systems predicted to occur in the repository.

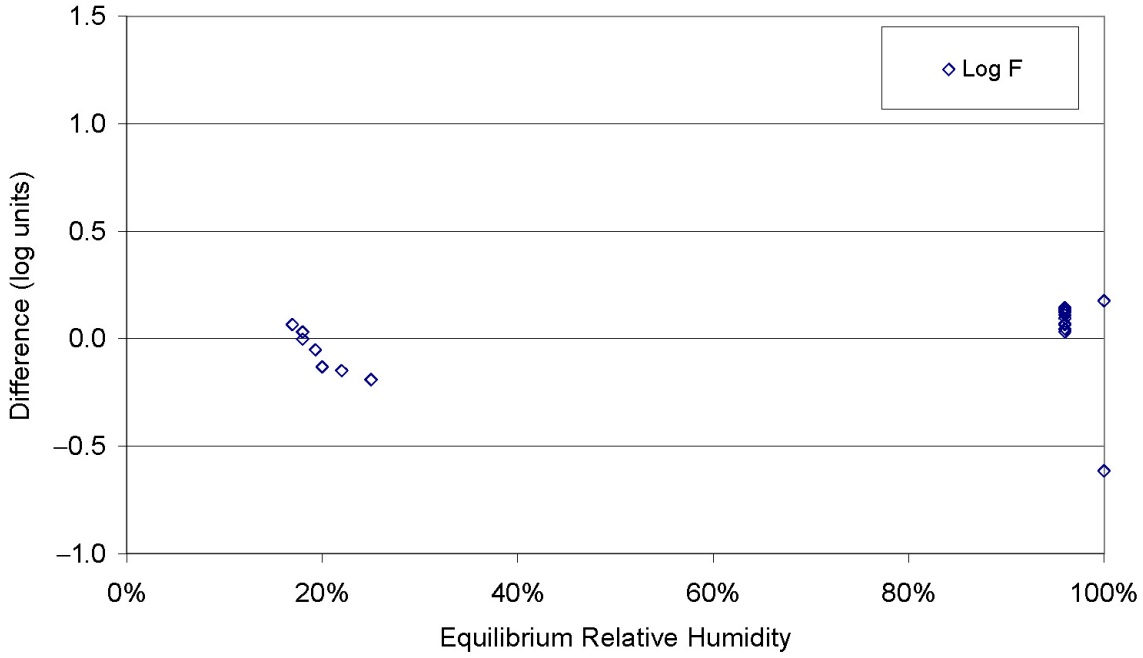

Output DTN: SN0611T0509206.007.

Figure 7-102. Differences between F Measurements and F Model Predictions

For the simple salt systems evaluated in Section 7.1, model predictions of F solubility were always within a factor of 10 and nearly always within a factor of 3 (Figures 7-1 and 7-2). The exception shown in Figure 7-102 is of a model underestimation of 0.6 log F molality in a solution saturated with sellaite (MgF_2) at 25°C (Lide 2000 [DIRS 162229], pp. 8-102 to 8-110). This difference is still within a factor of 5 of the F concentration derived from the MgF_2 solubility given by Lide (2000 [DIRS 162229]) which is equivalent to 0.0042 molal F. The model predicts a F concentration of 0.00102 molal for the same conditions. This difference may be partly the result of uncertainty in experimental determinations of sellaite solubility. For example, Fovet and Gal (2000 [DIRS 178481]) give a limiting solubility of MgF_2 of 0.00001 molar ($\cong$ 0.00001 molal) in a solution supersaturated with MgF_2 at 25°C. MgF_2 solubility is reported in the CRC handbook (Weast and Astle 1981 [DIRS 100833]) to be 0.0076 g/100cc. This solubility is equivalent to 0.0012 molal, implying a F concentration of 0.0024 molal.

In each of the J13 and 100× J13 multi-component evaporation experiments in Section 7.2, the total concentrations of F are predicted within a factor of 3 or less (Figures 7-68 and 7-72). The factor of 3 is readily confirmed in these figures because a line drawn at a factor of 3.16 would plot equidistantly between lines drawn at factors of 1 and 10 (i.e., $10^{1/2} = 3.16$).

The maximum differences in predictions and measurements for F in the J13 and 100× J13 evaporation data sets from Section 7.2 are less than 30% and are summarized in Table 7-9.

The estimated model uncertainties for F are presented in Table 7-10. With the exception of MgF_2 discussed above, model–data differences are within ±0.5 log molal F and do not have a distinct correlation with *RH*. These results support a triangular IDPS model uncertainty distribution with a most likely uncertainty of 0 and maximum and minimum uncertainties of ±0.5 log molal F for all *RH*.

INTENTIONALLY LEFT BLANK

8. CONCLUSIONS

Evaporation can have a profound effect on the chemical composition of water that could potentially seep into the repository. It can turn dilute ground water into a corrosive brine, and complete evaporation can result in the precipitation of hygroscopic salts. The in-drift precipitates/salts (IDPS) model is developed to predict the effects of evaporation on water composition and mineral precipitation in the repository for TSPA. This report documents the development, validation, use, limitations, and uncertainties of this model.

8.1 MODEL DESCRIPTION

In accordance with the purpose and scope of this modeling activity, a model is developed, validated, and documented to predict the effects of evaporation and deliquescence on the chemical evolution of potential aqueous solutions within the repository. The resulting model, called the IDPS model, is designed for the system containing Na-K-H-Mg-Ca-Al-Cl-F-NO_3-SO_4-Br-CO_3-SiO_2-CO_2-O_2-H_2O. This system encompasses the major ion chemistry output parameters potentially important to downstream models used to predict corrosion, colloid stability, degradation of EBS materials, dust deliquescence, and radionuclide transport. These output parameters include pH, ionic strength, total aqueous concentrations of chemical components, deliquescence relative humidity, aqueous concentrations of species that potentially contribute to acid-neutralizing capacity, and mineral precipitation. A full description of the model and its integration is provided in Section 6.

8.2 DEVELOPED OUTPUTS

The outputs developed in this report are listed in Table 8-1 along with references to their associated uncertainty. Titles and descriptions of outputs are modified in the table to improve readability. Actual titles can be found in Section 9. A more complete discussion of uncertainty is presented in Section 8.4.

Table 8-1. Developed Output

Output DTN	Output Description	Output Uncertainty
MO0701SPAPTZER.001 Pitzer database spreadsheets and EQ3/6 input/output files	Spreadsheet collection of thermodynamic data for Pitzer ion-interaction parameters and related EQ3/6 input/output files. Output used indirectly in TSPA calculations.	Output uncertainty is within model validation criteria specified in the TWP (SNL 2007 [DIRS 179287], Section 2.2.2), (Section 7).
SN0609T0502404.012[a] Pitzer thermodynamic database data0.yp2	The Pitzer thermodynamic database developed in Appendix I. Output used indirectly in TSPA calculations.	This database is validated for the intended use of the IDPS model by the results of the validation simulations. Model output predictions are within the uncertainty ranges specified in the validation criteria (Table 7-1).
LL031106231032.007 Solubility and vapor pressure data for aqueous systems containing single and multiple salts	Compilation and unit conversion of solubility and vapor pressure data in binary and ternary salt systems for a wide range of temperatures. Output used indirectly in TSPA calculations.	Uncertainty in these data are due to source uncertainty in original experiments and measurements.

Table 8-1. Developed Output (Continued)

Output DTN	Output Description	Output Uncertainty
SN0610T0509206.001 IDPS model template input files and base-case mineral suppressions	EQ3/6 input file templates for the IDPS model and a list of minerals typically suppressed in the IDPS model when using the Pitzer thermodynamic database. Output used indirectly in TSPA calculations.	The list of mineral suppressions is validated for the intended use of the IDPS model by the results of the validation simulations. Model output predictions are within the uncertainty ranges specified in the validation criteria (Table 7-1). Output uncertainty is not applicable to the EQ3/6 input file templates.
SN0702T0509206.008 Validation simulations of nonqualified evaporation experiments and comparison of results to alternate model simulation	EQ3/6 files resulting from IDPS model simulation of laboratory evaporation experiments in Sections 7.2.1, 7.2.2, and 7.2.3, and comparison of results to an alternate model simulation in Section 7.3. Output *not* used directly or indirectly in TSPA calculations.	Predictions for all model output parameters are within the uncertainty ranges specified in the validation criteria (Table 7-1).
SN0611T0509206.006 J-13 example abstraction simulations and example lookup tables	Example IDPS model EQ3/6 input/output files for in situ J-13 well water and example lookup tables. Output *not* used directly or indirectly in TSPA calculations.	Uncertainty in input values are not identified and propagated in this example application. Propagation of uncertainty is performed in downstream analyses that use the model. Uncertainty due to model uncertainty is estimated and summarized in Section 7.5.
MO0701EQ36IDPS.000 Validation simulations of qualified evaporation experiments, seawater evaporation, calcite and carbon dioxide solubility in simple systems, salt solubilities in binary and ternary systems, and deliquescence relative humidity in binary systems	EQ3/6 files and spreadsheets resulting from IDPS model simulation of qualified evaporation experiments, seawater evaporation, calcite and carbon dioxide solubility in simple systems, salt solubilities in binary and ternary systems, and deliquescence relative humidity in binary systems. Output *not* used directly or indirectly in TSPA calculations.	Uncertainty due to model uncertainty is estimated and summarized in Section 7.5.
SN0611T0509206.007 Estimated model uncertainties in IDPS model outputs	Estimated model uncertainties in pH, ionic strength, Cl concentration, F concentration, NO_3 concentration, Cl:NO_3 concentration ratio, and deliquescence relative humidity. Output used indirectly in TSPA calculations.	These estimates of uncertainties are justified and supported by the results of the model validation simulations, as explained in Section 7.5.

[a] A discrepancy was detected in the data block O2(aq) NH4+ SO4; the discrepancy is a very minor difference in the a1 value. The database has the value of 0, the actual value should be –0.028. This error was detected after all simulations were complete, thus the DTN was not superseded. Also, this data block was not used in any simulations completed in this document. Users of this database should be aware of the minor discrepancy and a note was added to the data block.

8.3 MODEL ABSTRACTION

The IDPS model can be used to generate lookup tables for downstream modeling and uncertainty analyses. The model is primarily designed to generate lookup tables for the incoming water compositions predicted by the thermal-hydrological-chemical model and for the deliquescence of dust. The resulting lookup tables are documented elsewhere, such as in *Engineered Barrier System: Physical and Chemical Environment* (BSC 2005 [DIRS 175083]).

IDPS model lookup tables provide model parameter outputs for a full range of equilibrium relative humidity values and steady-state relative evaporation rate values (Section 6.6.3.5). These tables are designed to define a response surface from which IDPS model outputs can be obtained or interpolated for given incoming water compositions.

8.4 UNCERTAINTY AND LIMITATIONS

The IDPS model has several uncertainties and limitations. Model uncertainties include uncertainties related to individual aspects of the IDPS model, such as the conceptual model, model equations, selected mineral suppressions, and constants in the thermodynamic database. Model limitations include simplifying assumptions and validation ranges.

The IDPS model is a simplification of the effects of evaporation and deliquescence on the chemistry and availability of liquid water within the drift. Use of the model is limited to the system containing Na-K-H-Mg-Ca-Al-Cl-F-NO_3-SO_4-Br-CO_3-SiO_2-CO_2-O_2-H_2O and temperatures between 20°C and 140°C. The temperature range is limited by the availability of independent validation data at high temperatures, the ability of the model to predict chemical behavior at high temperatures and ionic strengths, and by the temperature range needed for the IDPS model in *Engineered Barrier System: Physical and Chemical Environment* (BSC2005 [DIRS 175083]). This system implies oxidizing conditions at all times, which is defined in this report as maintaining an oxygen fugacity of at least 10^{-9} bars (Section 4.1.2). Two assumptions also limit the model. The aqueous solutions in the drift are assumed to have a flat air–water interface (Section 5.1), and chemical equilibrium conditions are assumed for all reactions except for certain minerals that are not allowed to precipitate (Section 5.2). Another exception to Assumption 5.2 is that the solution does not have to be at equilibrium with respect to relative humidity when necessary inputs are provided for steady-state predictions (Section 6.6.3.3).

With one exception, the IDPS model is validated for its intended use. The intended use of this model is to estimate and tabulate, within an appropriate level of confidence, the effects of evaporation, deliquescence, and potential environmental conditions on the pH, ionic strength, and chemical compositions of water and minerals on the drip shield or other location within the drift during the postclosure period for temperatures between 20°C and 140°C. The exception is the prediction of deliquescence relative humidity at *RH* below 40% and whenever $Mg(NO_3)_2$ is a major component of the brine at *RH* below 65%. Under these conditions, the deliquescence relative humidity predictions are often more than 20% in *RH* units below reported values. This difference exceeds both the ±10% (*RH* units) validation criterion adopted in Section 7 (Table 7-1) and the ±15% (*RH* units) validation criterion suggested in the TWP (SNL 2007 [DIRS 179287]). In this lower *RH* range, larger uncertainties in solute behavior result in larger differences between model predictions and reported measurements. Because the validation

criteria are exceeded for predicting deliquescence relative humidity when *RH* is below 40% and whenever $Mg(NO_3)_2$ is a major component of the brine at *RH* below 60%, any predictions of deliquescence relative humidity under these conditions will require information outside of this report.

There are several sources for model uncertainty. First, there is uncertainty associated with the conceptual model. To evaluate this uncertainty, a number of alternative conceptual models are considered (Section 6.5). Most are not utilized, however, because they either are not as realistic as the IDPS model, do not provide the types of outputs requested of the IDPS model, or do not cover the necessary ranges of applicability. The two conceptual models that are retained and incorporated into the IDPS model are the equilibrium model (Figure 6-1) and the steady-state alternative conceptual model (Figure 6-3). Both of these conceptual models are represented in the IDPS model output templates (Section 6.6.3.5).

Another model uncertainty is the choice of mineral suppressions. Not all minerals in the Pitzer database are expected to precipitate rapidly upon supersaturation under the temperature and pressure conditions anticipated in the repository. Because the IDPS model is used to produce model abstractions that are time-invariant, decisions must be made regarding which minerals are allowed and not allowed to precipitate in the repository. A methodology is developed in this report to aid in making these decisions (Section 6.6.2.6). For instances in which the decision is uncertain, uncertainty analyses are recommended.

Additional model uncertainties are uncertainties in the thermodynamic constants, such as equilibrium constants and Pitzer coefficients. The values of these constants control the interactions and solubilities of dissolved components, which ultimately control the evaporative evolution of a given input water and the deliquescence of a given salt assemblage.

The IDPS model uncertainties identified above are assessed as a whole in the model validation section by comparing model predictions to independent evaporation data, solubility data, and deliquescence relative humidity data (Section 7). This assessment is summarized in Section 7.5. Specifically, the validation involved comparisons of model predictions to:

- Five sets of evaporation data (synthetic average J-13 well water, synthetic average 100x J-13 well water, synthetic Topopah Spring Tuff pore water at 75°C, synthetic Topopah Spring Tuff pore water at 95°C, and seawater) (Section 7.2)
- Solubilities of 24 salts in binary systems at temperatures ranging from 20°C to 140°C (Sections 7.1.1.1.1 and 7.1.1.2.1)
- Solubilities of numerous salts in ternary salt systems at various temperatures (Section 7.1.2)
- Deliquescence relative humidity (RH_d) of numerous binary salt solutions at various temperatures (Sections 7.1.1.1.2 and 7.1.1.2.2)
- Evaporation predictions using the data0.ymp.R5 database up to an ionic strength of 1 molal (Section 7.3).

The results of the comparisons include the following:

- pH was always predicted within 0.79 pH units or less of reported measurements (Section 7.5.1 and Table 7-9).
- Ionic strength was always predicted within 50% or less (Section 7.5.2).
- Deliquescence relative humidity (RH_d) of single salt solutions was always (except for $Mg(NO_3)_2$) predicted within 10% of reported measurements (in *RH* units) when the predicted RH_d exceeded 40% (Section 7.5.3).
- Br, CO_3, Cl, F, Na, K, NO_3, and SO_4 concentrations were nearly always predicted within a factor of 3 or less (Section 7.5.4).
- Ca, Mg, and Si concentrations were predicted within a factor of approximately 100 or less (Section 7.5.5).

These observed differences between predictions and measurements are attributed to two types of uncertainties: model uncertainties and uncertainties in analytical measurements.

Uncertainties owing to model uncertainty alone are estimated for pH, ionic strength, Cl concentration, NO_3 concentration, the Cl:NO_3 ratio, F concentration, and RH_d, as presented in Table 7-10. These estimates are established as a function of *RH* because the uncertainties are highly correlated with *RH* (Figure 7-101). At high *RH* (i.e., dilute solutions), uncertainty is low because the evaporative evolution of the aqueous solution is undersaturated with respect to the major salt solubility boundaries that primarily control the concentrations of the major ions in the aqueous phase. At lower *RH*, ionic strength rises into the range where Pitzer interaction coefficients begin to control the chemical divides. In this lower *RH* range, uncertainties owing to Pitzer interaction coefficients, salt solubility products in the Pitzer database, and other model uncertainties result in larger differences between model predictions and reported measurements. The estimated model uncertainties are supported and justified by the validation in Section 7, as summarized in Section 7.5.

8.5 YUCCA MOUNTAIN REVIEW PLAN CRITERIA ASSESSMENT

This section provides responses to the YMRP acceptance criteria identified in the TWP as applicable to this report. The acceptance criteria for the quantity and chemistry of water contacting engineered barriers and waste forms are referenced from Section 2.2.1.3.3.3 of the YMRP (NRC 2003 [DIRS 163274]) and 10 CFR 63.114(a)-(c) and (e)-(g) [DIRS 173273].

8.5.1 Acceptance Criterion 1 – System Description and Model Integration Are Adequate

(1) Total system performance assessment adequately incorporates important design features, physical phenomena, and couplings, and uses consistent and appropriate assumptions throughout the quantity and chemistry of water contacting engineered barriers and waste forms abstraction process.

Development of the model documented in this report requires only qualitative design information and is based on physical phenomena expected within repository drifts (Section 6.4). Thermal-chemical coupled processes are incorporated in the model. Other coupled processes, in addition to thermal-chemical coupled processes, are primarily addressed in *Engineered Barrier System Features, Events, and Processes* (BSC 2005 [DIRS 175014]). Model assumptions are consistent and appropriate for the quantity and chemistry of water contacting engineered barriers and waste forms abstraction process (Section 5).

(2) The abstraction of the quantity and chemistry of water contacting engineered barriers and waste forms uses assumptions, technical bases, data, and models, that are appropriate and consistent with other related U.S. Department of Energy abstractions.

The model developed in this report uses the same technical bases and other information as are used in other TSPA supporting documents concerned with the chemistry of water contacting engineered barriers and waste forms. The conceptual model and assumptions that form the basis for this report are consistent with other system conceptual models and assumptions. One of the primary purposes of this model is to take abstracted output from the unsaturated zone thermal-hydrological-chemical model to predict in-drift water chemistry. These predictions are documented in *Engineered Barrier System: Physical and Chemical Environment* (BSC 2005 [DIRS 175083]). Input water fluxes are addressed in *Seepage Model for PA Including Drift Collapse* (BSC 2003 [DIRS 167652]).

(3) Important design features, such as waste package design and material selection, drip shield, ground support, thermal loading strategy, and degradation processes, are adequate to determine the initial and boundary conditions for calculations of the quantity and chemistry of water contacting engineered barriers and waste forms.

Initial and boundary conditions are taken from the predictions of the thermal-hydrological-chemical model. Design features of the engineered barrier systems affect the predictions of the thermal-hydrological-chemical model, which in turn adequately determine the initial and boundary conditions for the IDPS model. Input water fluxes are addressed in *Seepage Model for PA Including Drift Collapse* (BSC 2004 [DIRS 167652]).

(4) Spatial and temporal abstractions appropriately address physical couplings (thermal-hydrologic-mechanical-chemical). For example, the U.S. Department of Energy evaluates the potential for focusing of water flow into drifts, caused by coupled thermal-hydrologic-mechanical-chemical processes.

This report develops and validates a process model in support of TSPA. Abstractions using this model are documented in *Engineered Barrier System: Physical and Chemical Environment* (BSC 2005 [DIRS 175083]).

(5) Sufficient technical bases and justification are provided for total system performance assessment assumptions and approximations for modeling coupled thermal-hydrologic-mechanical-chemical effects on seepage and flow, the waste

package chemical environment, and the chemical environment for radionuclide release. The effects of distribution of flow on the amount of water contacting the engineered barriers and waste forms are consistently addressed, in all relevant abstractions.

Thermal-chemical effects are included in this model. Other coupled thermal-hydrological-mechanical-chemical effects, in addition to thermal-chemical coupled effects, are primarily discussed in *Engineered Barrier System Features, Events, and Processes* (BSC 2005 [DIRS 175014]). Distribution of flow within the drift is addressed in *Seepage Model for PA Including Drift Collapse* (BSC 2004 [DIRS 167652]).

(6) The expected ranges of environmental conditions within the waste package emplacement drifts, inside the breached waste packages, and contacting the waste forms and their evolution with time are identified.

The model is developed for the expected ranges of environmental conditions within the drifts, including temperature, relative humidity, redox conditions, fugacity of carbon dioxide, and relevant aqueous component concentrations (Section 4.1.2). The model is designed to predict the stability and composition of water contacting engineered barriers resulting from processes of evaporation, deliquescence, condensation, and chemical equilibria.

(8) Adequate technical bases are provided, including activities such as independent modeling, laboratory or field data, or sensitivity studies, for inclusion of any thermal-hydrologic-mechanical-chemical couplings and features, events, and processes.

Adequate technical bases are provided in Sections 6.4 and 6.6 for thermal-chemical couplings included in the IDPS model. Technical bases for features, events, and processes included in the model are provided in Sections 4.1.2, 5.2, 6.4, and 6.6.3.5, as summarized in Section 6.2. Technical bases for this model include laws of thermodynamics, conservation of mass, and chemical reaction data as a function of temperature.

(9) Performance-affecting processes that have been observed in thermal-hydrologic tests and experiments are included into the performance assessment.

The IDPS model incorporates processes of evaporation, deliquescence, condensation, and chemical equilibria to predict the chemical composition and presence of liquid water in the drift, which are potentially important to TSPA. The model is used in *Engineered Barrier System: Physical and Chemical Environment* (BSC 2005 [DIRS 175083]) to include these processes in the performance assessment. Water fluxes are addressed in *Seepage Model for PA Including Drift Collapse* (BSC 2004 [DIRS 167652]).

(10) Likely modes for container corrosion (see NRC 2003 [DIRS 163274], Section 2.2.1.3.1) are identified and considered in determining the quantity and chemistry of water entering the engineered barriers and contacting waste forms. For example, the model abstractions consistently address the role of parameters, such as pH, carbonate concentration, and the effect of corrosion on the quantity and chemistry of water contacting engineered barriers and waste forms.

The IDPS model addresses the roles of chemical and physical parameters on the chemical evolution and stability of water contacting engineered barriers. Abstractions using this model are documented in *Engineered Barrier System: Physical and Chemical Environment* (BSC 2005 [DIRS 175083]). Corrosion and its effects are addressed in *General Corrosion and Localized Corrosion of Waste Package Outer Barrier* (BSC 2004 [DIRS 169984]). Water fluxes are addressed in *Seepage Model for PA Including Drift Collapse* (BSC 2004 [DIRS 167652]).

(12) Guidance in NUREG–1297 (Altman et al. 1988 [DIRS 103597]) and NUREG–1298 (Altman et al. 1988 [DIRS 103750]), or other acceptable approaches, is followed.

Technical inputs were selected and documented according to applicable YMP procedures, which comply with NUREG-1298 (see Section 4.1).

8.5.2 Acceptance Criterion 2 – Data Are Sufficient for Model Justification

(1) Geological, hydrological, and geochemical values used in the license application are adequately justified. Adequate description of how the data were used, interpreted, and appropriately synthesized into the parameters is provided.

Sources of input data are contained in Section 4.1.2 and tabulated in DIRS. The thermodynamic data used in this model are internationally accepted (Appendix I) and other geochemical data are adequately justified (Sections 6 and 7). Site specific data are used to justify and validate the model (Sections 4.4 and 7.2). The data providing the basis for characterizing model uncertainty include laboratory evaporation data obtained from evaporation experiments of synthetic J-13 well water and Topopah Spring Tuff pore water (Sections 7.2.1 through 7.2.3), seawater evaporation data (Section 7.2.5), and salt solubility and vapor pressure data for binary and ternary salt solutions from chemistry handbooks and literature compilations (Section 7.1). Adequate description of how the data were used, interpreted, and synthesized are included in these sections.

(2) Sufficient data were collected on the characteristics of the natural system and engineered materials to establish initial and boundary conditions for conceptual models of thermal-hydrologic-mechanical-chemical coupled processes, that affect seepage and flow and the waste package chemical environment.

Data collected for this model are sufficient to establish initial and boundary conditions for the thermal-chemical coupled processes that affect the composition and chemical stability of seepage water in the drift chemical environment (Section 4.1). Abstractions using this model are documented in *Engineered Barrier System: Physical and Chemical Environment* (BSC 2005 [DIRS 175083]). Water fluxes are addressed in *Seepage Model for PA Including Drift Collapse* (BSC 2004 [DIRS 167652]).

(4) Sufficient information to formulate the conceptual approach(es) for analyzing water contact with the drip shield, engineered barriers, and waste forms is provided.

Sufficient information to formulate the conceptual approach for predicting the chemical evolution and chemical stability of water in contact with the drip shield and other engineered barriers is provided in Section 6.4. *In-Package Chemistry Abstraction* (BSC 2005 [DIRS 174583]) addresses water in contact with the waste form.

8.5.3 Acceptance Criterion 3 – Data Uncertainty Is Characterized and Propagated through the Model Abstraction

(1) Models use parameter values, assumed ranges, probability distributions, and bounding assumptions that are technically defensible, reasonably account for uncertainties and variabilities, and do not result in an under-representation of the risk estimate.

The parameter ranges and bounding assumptions of the model are defined in Sections 4.1.2 and 5 and are considered representative of the system. Although the model is designed for use in downstream abstractions, input parameters (Table 4-4) are developed in this report to be consistent with the expected ranges of values for upstream and downstream modeled systems. Values and ranges of these parameters are reasonable and do not result in under-representation of the risk estimate. Values for these parameters are determined in applications of the model, such as the TSPA application documented in *Engineered Barrier System: Physical and Chemical Environment* (BSC 2005 [DIRS 175083]).

(2) Parameter values, assumed ranges, probability distributions, and bounding assumptions used in the total system performance assessment calculations of quantity and chemistry of water contacting engineered barriers and waste forms are technically defensible and reasonable, based on data from the Yucca Mountain region (e.g., results from large block and drift-scale heater and niche tests), and a combination of techniques that may include laboratory experiments, field measurements, natural analog research, and process-level modeling studies.

Validation of this model uses data obtained in laboratory evaporation experiments in which the initial waters reflect water types observed at Yucca Mountain (Section 7.2). These experiments provide adequate data for justification of the model and its parameters for YMP applications.

(3) Input values used in the total system performance assessment calculations of quantity and chemistry of water contacting engineered barriers (e.g., drip shield and waste package) are consistent with the initial and boundary conditions and the assumptions of the conceptual models and design concepts for the Yucca Mountain site. Correlations between input values are appropriately established in the U.S. Department of Energy total system performance assessment. Parameters used to define initial conditions, boundary conditions, and computational domain in sensitivity analyses involving coupled thermal-hydrologic-mechanical-chemical effects on seepage and flow, the waste package chemical environment, and the chemical environment for radionuclide release, are consistent with available data. Correlations of uncertainties in IDPS model outputs are propagated in TSPA as discussed in Section 6.12 of *Engineered Barrier System:*

Physical and Chemical Environment (BSC 2005 [DIRS 175083]). Reasonable or conservative ranges of parameters or functional relations are established.

The ranges of parameters developed in this report are consistent with initial and boundary conditions common to other TSPA conceptual models and are compatible with design concepts. This report uses the same technical bases and other information as are used in other license application-supporting documents concerned with waste package and waste form performance, such as *General Corrosion and Localized Corrosion of Waste Package Outer Barrier* (BSC 2004 [DIRS 169984]) and *In-Package Chemistry Abstraction* (BSC 2005 [DIRS 174583] Section 4) and supporting documents. The conceptual model that forms the basis for this report is consistent with other engineered system models and repository design. Reasonable ranges of parameters are established in Section 4.1.2.

(4) Adequate representation of uncertainties in the characteristics of the natural system and engineered materials is provided in parameter development for conceptual models, process-level models, and alternative conceptual models. The U.S. Department of Energy may constrain these uncertainties using sensitivity analyses or conservative limits. For example, the U.S. Department of Energy demonstrates how parameters used to describe flow through the engineered barrier system bound the effects of excavation-induced changes.

Uncertainty in the natural system is adequately characterized in parameter development for conceptual models, process-level models, and alternative conceptual models. Model uncertainties are summarized in Sections 7.5 and 8.4. IDPS model uncertainty propagated into TSPA calculations includes the uncertainty characterized in the model validation. Uncertainties in natural system characteristics are further explored in *Engineered Barrier System: Physical and Chemical Environment* (BSC 2005 [DIRS 175083]).

8.5.4 Acceptance Criterion 4 – Model Uncertainty Is Characterized and Propagated through the Model Abstraction

(1) Alternative modeling approaches of features, events, and processes are considered and are consistent with available data and current scientific understanding, and the results and limitations are appropriately considered in the abstraction.

FEPs and alternative conceptual models specific to this document are discussed with their technical bases and limitations in Sections 6.2 and 6.5. They are consistent with available data and current scientific understanding.

(2) Alternative modeling approaches are considered and the selected modeling approach is consistent with available data and current scientific understanding. A description that includes a discussion of alternative modeling approaches not considered in the final analysis and the limitations and uncertainties of the chosen model is provided.

Alternative conceptual models along with their limitations and uncertainties are discussed in Section 6.5. Approaches not considered in the final analysis are also discussed in Section 6.5.

The selected modeling approach is consistent with available data and current scientific understanding.

(3) Consideration of conceptual model uncertainty is consistent with available site characterization data, laboratory experiments, field measurements, natural analog information and process-level modeling studies; and the treatment of conceptual model uncertainty does not result in an under-representation of the risk estimate.

Uncertainties in the conceptual model (Section 7.5) are based on natural analogues, model comparisons, and laboratory experiments (Sections 6.3 and 7). Model validation is consistent with these uncertainties. Treatment of conceptual model uncertainty does not result in a biased under-representation of the risk estimate (Section 7.5).

(4) Adequate consideration is given to effects of thermal-hydrologic-mechanical-chemical coupled processes in the assessment of alternative conceptual models.

Thermal-chemical processes and their effects are adequately considered in the assessment of alternative conceptual models (Section 6.2). The chosen modeling approach includes thermal-chemical processes of evaporation, deliquescence, condensation, and chemical equilibria (Section 6.4). Additional coupling of processes is addressed in *Engineered Barrier System: Physical and Chemical Environment* (BSC 2005 [DIRS 175083]) and in *Engineered Barrier System Features, Events, and Processes* (BSC 2005 [DIRS 175014]).

8.5.5 Acceptance Criterion 5 – Model Abstraction Output Is Supported by Objective Comparisons

(3) Accepted and well-documented procedures are used to construct and test the numerical models that simulate coupled thermal-hydrologic-mechanical-chemical effects on seepage and flow, waste package chemical environment, and the chemical environment for radionuclide release. Analytical and numerical models are appropriately supported. Abstracted model results are compared with different mathematical models, to judge robustness of results.

The Quality Assurance Program governing development of this report is discussed in Section 2. This model has been constructed and documented according to SCI-PRO-006. The model predicts the effects of thermal-chemical processes on the composition and stability of water in the drift. Validation complies with SCI-PRO-006 and applicable guidance. Qualified software codes are used in accordance with procedure to execute the model (Section 3). This report was generated according to the requirements of the TWP (SNL 2007 [DIRS 179287]) as directed by SCI-PRO-002. Model predictions are compared to ion association model results in Section 7.3 to judge robustness of results. They are also compared to laboratory evaporation data obtained from evaporation experiments of synthetic J-13 well water and Topopah Spring Tuff pore water (Sections 7.2.1 through 7.2.3), seawater evaporation data (Section 7.2.5), and salt solubility and vapor pressure data for binary and ternary salt solutions from chemistry handbooks and literature compilations (Section 7.1).

INTENTIONALLY LEFT BLANK

9. INPUTS AND REFERENCES

9.1 DOCUMENTS

176811 Alai, M.; Sutton, M.; and Carroll, S. 2005. "Evaporative Evolution of a Na–Cl–NO_3–K–Ca–SO_4–Mg–Si Brine at 95°C: Experiments and Modeling Relevant to Yucca Mountain, Nevada." *Geochemical Transactions, 6,* (2), 31-45. Melville, New York: American Institute of Physics. TIC: 258272.

103750 Altman, W.D.; Donnelly, J.P.; and Kennedy, J.E. 1988. *Qualification of Existing Data for High-Level Nuclear Waste Repositories: Generic Technical Position.* NUREG-1298. Washington, D.C.: U.S. Nuclear Regulatory Commission. TIC: 200652.

103597 Altman, W.D.; Donnelly, J.P.; and Kennedy, J.E. 1988. *Peer Review for High-Level Nuclear Waste Repositories: Generic Technical Position.* NUREG-1297. Washington, D.C.: U.S. Nuclear Regulatory Commission. TIC: 200651.

162064 Archer, D.G. 1999. "Thermodynamic Properties of the KCl + H_2O System." *Journal of Physical and Chemical Reference Data, 28,* (1), 1-17. New York, New York: American Chemical Society. TIC: 253882.

162065 Archer, D.G. 2000. "Thermodynamic Properties of the $NaNO_3$+H_2O System." *Journal of Physical and Chemical Reference Data, 29,* (5), 1141-1156. New York, New York: American Chemical Society. TIC: 253379.

100699 Arthur, R.C. and Murphy, W.M. 1989. "An Analysis of Gas-Water-Rock Interactions During Boiling in Partially Saturated Tuff." *Science Geology Bulletin, 42,* (4), 313-327. Strasbourg, France: Sciences Geologiques Bulletin Publisher Strasbourg, Universite Louis Pasteur de Strasbourg. TIC: 235013.

100702 Baes, C.F., Jr. and Mesmer, R.E. 1986. *The Hydrolysis of Cations.* Malabar, Florida: Krieger Publishing Company. TIC: 223481.

168318 Baes, C.F., Jr.; Reardon, E.J.; and Moyer, B.A. 1993. "Ion Interaction Model Applied to the $CuSO_4$-H_2SO_4-H_2O System at 25 °C." *Journal of Physical Chemistry, 97,* (47), 12343-12348. Washington, D.C.: American Chemical Society. TIC: 255756.

157865 Barin, I. and Platzki, G. 1995. *Thermochemical Data of Pure Substances.* 3rd Edition. Two volumes. New York, New York: VCH Publishers. TIC: 251934.

166051 Bates, R.G. 1973. *Determination of pH, Theory and Practice.* 2nd Edition. New York, New York: John Wiley & Sons. TIC: 245388.

162270 Bethke, C.M. 1996. *Geochemical Reaction Modeling, Concepts and Applications.* New York, New York: Oxford University Press. TIC: 252884.

178220 Birsoy, R. 2002. "Formation of Sepiolite-Palygorskite and Related Minerals From Solution." *Clays and Clay Minerals, 50,* (6), 736-745. Aurora, Colorado: The Clay Minerals Society.

162352 Bodine, M.W., Jr. and Jones, B.F. 1986. *The Salt Norm: A Quantitative Chemical—Mineralogical Characterization of Natural Waters.* Water Resources Investigations Report 86-4086. Reston, Virginia: U.S. Geological Survey. TIC: 254009.

156639 Borchardt, G. 1995. "Smectites." Chapter 14 of *Minerals in Soil Environments.* 2nd Edition. Dixon J.B. and Weed, S.B., eds. SSSA Book Series, No. 1. Madison, Wisconsin: Soil Science Society of America. TIC: 237222.

155640 BSC (Bechtel SAIC Company) 2001. *Environment on the Surfaces of the Drip Shield and Waste Package Outer Barrier.* ANL-EBS-MD-000001 REV 00 ICN 02. Las Vegas, Nevada: Bechtel SAIC Company. ACC: MOL.20010724.0082.

158966 BSC 2002. *The Enhanced Plan for Features, Events, and Processes (FEPs) at Yucca Mountain.* TDR-WIS-PA-000005 REV 00. Las Vegas, Nevada: Bechtel SAIC Company. ACC: MOL.20020417.0385.

169984 BSC 2004. *General Corrosion and Localized Corrosion of Waste Package Outer Barrier.* ANL-EBS-MD-000003 REV 02. Las Vegas, Nevada: Bechtel SAIC Company. ACC: DOC.20041004.0001.

169863 BSC 2004. *In-Drift Precipitates/Salts Model.* ANL-EBS-MD-000045 REV 02. Las Vegas, Nevada: Bechtel SAIC Company. ACC: DOC.20041111.0002.

167652 BSC 2004. *Seepage Model for PA Including Drift Collapse.* MDL-NBS-HS-000002 REV 03. Las Vegas, Nevada: Bechtel SAIC Company. ACC: DOC.20040922.0008; DOC.20051205.0001.

170025 BSC 2004. *Waste Form and In-Drift Colloids-Associated Radionuclide Concentrations: Abstraction and Summary.* MDL-EBS-PA-000004 REV 01. Las Vegas, Nevada: Bechtel SAIC Company. ACC: DOC.20041028.0007; DOC.20050425.0003.

172862 BSC 2005. *Drift-Scale THC Seepage Model.* MDL-NBS-HS-000001 REV 04. Las Vegas, Nevada: Bechtel SAIC Company. ACC: DOC.20050218.0001; DOC.20050801.0012.

175014 BSC 2005. *Engineered Barrier System Features, Events, and Processes.* ANL-WIS-PA-000002 REV 05. Las Vegas, Nevada: Bechtel SAIC Company. ACC: DOC.20050829.0003; DOC.20050830.0006.

175083 BSC 2005. *Engineered Barrier System: Physical and Chemical Environment.* ANL-EBS-MD-000033 REV 05. Las Vegas, Nevada: Bechtel SAIC Company. ACC: DOC.20050829.0008.

174583 BSC 2005. *In-Package Chemistry Abstraction.* ANL-EBS-MD-000037 REV 04. Las Vegas, Nevada: Bechtel SAIC Company. ACC: DOC.20050714.0003; DOC.20051130.0007.

177645 Busey, R.H. and Mesmer, R.E. 1977. "Ionization Equilibria of Silicic Acid and Polysilicate Formation in Aqueous Sodium Chloride Solutions to 300°C." *Inorganic Chemistry, 16,* (10), 2444-2450. Washington, D.C.: American Chemical Society. TIC: 258598.

166275 Canori, G.F. and Leitner, M.M. 2003. *Project Requirements Document.* TER-MGR-MD-000001 REV 02. Las Vegas, Nevada: Bechtel SAIC Company. ACC: DOC.20031222.0006.

105213 Carlos, B.A.; Chipera, S.J.; Bish, D.L.; and Raymond, R. 1995. "Distribution and Chemistry of Fracture-Lining Zeolites at Yucca Mountain, Nevada." *Natural Zeolites '93: Occurrence, Properties, Use, Proceedings of the 4th International Conference on the Occurrence, Properties, and Utilization of Natural Zeolites, June 20-28, 1993, Boise, Idaho.* Ming, D.W. and Mumpton, F.A., eds. Pages 547-563. Brockport, New York: International Committee on Natural Zeolites. TIC: 243086.

160453 Chen, C.-T.A. and Marshall, W.L. 1982. "Amorphous Silica Solubilities IV. Behavior in Pure Water and Aqueous Sodium Chloride, Sodium Sulfate, Magnesium Chloride, and Magnesium Sulfate Solutions up to 350°C." *Geochimica et Cosmochimica Acta, 46,* 279-287. New York, New York: Pergamon Press. TIC: 235346.

162066 Clarke, E.C.W. and Glew, D.N. 1985. "Evaluation of the Thermodynamic Functions for Aqueous Sodium Chloride from Equilibrium and Calorimetric Measurements below 154°C." *Journal of Physical and Chemical Reference Data, 14,* (2), 489-610. New York, New York: American Chemical Society. TIC: 253934.

162067 Clegg, S.L. and Brimblecombe, P. 1990. "Equilibrium Partial Pressures and Mean Activity and Osmotic Coefficients of 0–100% Nitric Acid as a Function of Temperature." *Journal of Physical Chemistry, 94,* (13), 5369-5380. Washington, D.C.: American Chemical Society. TIC: 253935.

159187 Clegg, S.L. and Brimblecombe, P. 1990. "Solubility of Volatile Electrolytes in Multicomponent Solutions with Atmospheric Applications." Chapter 5 of *Chemical Modeling of Aqueous Systems II.* Melchior, D.C. and Bassett, R.L., eds. ACS Symposium Series 416. Washington, D.C.: American Chemical Society. TIC: 241139.

162089 Clegg, S.L. and Brimblecombe, P. 1990. "The Solubility and Activity Coefficient of Oxygen in Salt Solutions and Brines." *Geochimica et Cosmochimica Acta, 54,* (12), 3315-3328. New York, New York: Pergamon Press. TIC: 253874.

162068 Clegg, S.L.; Milioto, S.; and Palmer, D.A. 1996. "Osmotic and Activity Coefficients of Aqueous $(NH_4)_2SO_4$ as a Function of Temperature, and Aqueous $(NH_4)_2SO_4$–H_2SO_4 Mixtures at 298.15 K and 323.15 K." *Journal of Chemical and Engineering Data, 41,* (3), 455-467. Washington, D.C.: American Chemical Society. TIC: 253389.

152734 Clegg, S.L.; Rard, J.A.; and Pitzer, K.S. 1994. "Thermodynamic Properties of 0–6 mol kg(–1) Aqueous Sulfuric Acid from 273.15 to 328.15 K." *Journal of the Chemical Society Faraday Transactions, 90,* (13), 1875–1894. Cambridge, England: Royal Society of Chemistry. TIC: 248984.

178211 Corti, H.R.; de Pablo, J.J.; and Prausnitz, J.M 1990. "Phase Equilibria for Aqueous Systems Containing Salts and Carbon Dioxide. Application of Pitzer's Theory for Electrolyte Solutions." *Journal of Physical Chemistry, 94,* 7876-7880. Easton, Pennsylvania: American Chemical Society.

100358 CRWMS M&O 1998. "Near-Field Geochemical Environment." Chapter 4 of *Total System Performance Assessment-Viability Assessment (TSPA-VA) Analyses Technical Basis Document.* B00000000-01717-4301-00004 REV 01. Las Vegas, Nevada: CRWMS M&O. ACC: MOL.19981008.0004.

153246 CRWMS M&O 2000. *Total System Performance Assessment for the Site Recommendation.* TDR-WIS-PA-000001 REV 00 ICN 01. Las Vegas, Nevada: CRWMS M&O. ACC: MOL.20001220.0045.

162110 de Lima, M.C.P. and Pitzer, K.S. 1983. "Thermodynamics of Saturated Electrolyte Mixtures of NaCl with Na_2SO_4 and with $MgCl_2$." *Journal of Solution Chemistry, 12,* (3), 187-199. New York, New York: Plenum Publishing Corporation. TIC: 253875.

100722 Dean, J.A. 1992. *Lange's Handbook of Chemistry.* 14th Edition. New York, New York: McGraw-Hill. TIC: 240690.

102773 Deer, W.A.; Howie, R.A.; and Zussman, J. 1966. *An Introduction to the Rock-Forming Minerals.* New York, New York: John Wiley & Sons. TIC: 245492.

166149 Dingemans, P. and Dijkgraaf, L.L. 1948. "The Vapour Pressure of Saturated Solutions of Sodium Nitrate in Water." *Recueil des Travaux Chimiques des Pays-Bas, 67,* 231-234. Leyden, The Netherlands: Société Chimique Neerlandaise. TIC: 255168.

118564 Drever, J.I. 1988. *The Geochemistry of Natural Waters.* 2nd Edition. Englewood Cliffs, New Jersey: Prentice-Hall. TIC: 242836.

178210 Duan, Z.; Moller, N.; Greenberg, J.; and Weare, J. 1992. "The Prediction of Methane Solubility in Natural Waters to High Ionic Strength From 0 to 250C and From 0 to 1600 Bar." *Geochimica et Cosmochimica Acta, 56,* 1451-1460. New York, New York: Pergamon Press Ltd..

166148 Dutrizac, J.E. 2002. "Calcium Sulphate Solubilities in Simulated Zinc Processing Solutions." *Hydrometallurgy, 65,* (2-3), 109-135. New York, New York: Elsevier. TIC: 255132.

177819 Ellis, A.J. 1963. "The Solubility of Calcite in Sodium Chloride Solutions at High Temperatures." *American Journal of Science, 261,* (3), 259-267. New Haven, Connecticut: Yale University. TIC: 258637.

100743 Eugster, H.P. and Hardie, L.A. 1978. "Saline Lakes." *Lakes, Chemistry, Geology, Physics.* Lerman, A., ed. Pages 237-293. New York, New York: Springer-Verlag. TIC: 240782.

123175 Eugster, H.P. and Jones, B.F. 1979. "Behavior of Major Solutes During Closed-Basin Brine Evolution." *American Journal of Science, 279,* 609-631. New Haven, Connecticut: Yale University, Kline Geology Laboratory. TIC: 234258.

162282 Faust, G.T. 1953. "Huntite, $Mg_3Ca(CO_3)_4$, a New Mineral." *American Mineralogist, 38,* (1-2), 4-24. Washington, D.C.: Mineralogical Society of America. TIC: 252888.

177660 Felmy, A.R. and MacLean, G.T. 2001. *Development of an Enhanced Thermodynamic Database for the Pitzer Model in ESP: The Fluoride and Phosphate Components.* PNWD-3120. Richland, Washington: Battelle Pacific Northwest Division. ACC: MOL.20060928.0081.

162112 Felmy, A.R.; Rustad, J.R.; Mason, M.J.; and de la Bretonne, R. 1994. *A Chemical Model for the Major Electrolyte Components of the Hanford Waste Tanks: The Binary Electrolytes in the System: Na-NO_3-NO_2-SO_4-CO_3-F-PO_4-OH-AI$(OH)_4$-H_2O.* PNL-SA-23952. Richland, Washington: Pacific Northwest Laboratory. TIC: 253271.

162111 Felmy, A.R.; Schroeder, C.C.; and Mason, M.J. 1994. *A Solubility Model for Amorphous Silica in Concentrated Electrolytes.* PNL-SA-25345. Richland, Washington: Pacific Northwest Laboratory. TIC: 253270.

162312 Fleischer, M. and Efremov, N. 1954. "New Mineral Names." *American Mineralogist, 39,* (3-4), 402-408. Washington, D.C.: Mineralogical Society of America. TIC: 252897.

162284 Fleischer, M. and Pabst, A. 1983. "New Mineral Names." *Journal of the Mineralogical Society of America, 68,* (1-2), 281-283. Washington, D.C.: Mineralogical Society of America. TIC: 252898.

178481 Fovet, Y. and Gal, J-Y. 2000. "Formation Constants Beta2 of Calcium and Magnesium Fluorides at 25C." *Talanta, 53,* 617-626. Montpellier Cedex 5, France: Elsevier. TIC 258930.

154365 Freeze, G.A.; Brodsky, N.S.; and Swift, P.N. 2001. *The Development of Information Catalogued in REV00 of the YMP FEP Database.* TDR-WIS-MD-000003 REV 00 ICN 01. Las Vegas, Nevada: Bechtel SAIC Company. ACC: MOL.20010301.0237.

101173 Freeze, R.A. and Cherry, J.A. 1979. *Groundwater.* Englewood Cliffs, New Jersey: Prentice-Hall. TIC: 217571.

144877 Garrels, R.M. and Christ, C.L. 1990. *Solutions, Minerals, and Equilibria.* Boston, Massachusetts: Jones and Bartlett Publishers. TIC: 223483.

123636 Garrels, R.M. and Mackenzie, F.T. 1967. "Origin of the Chemical Compositions of Some Springs and Lakes?" *Equilibrium Concepts in Natural Water Systems.* American Chemical Society Advances in Chemistry Series 67. Pages 222-242. Washington, D.C.: American Chemical Society. TIC: 246519.

100742 Glassley, W. 1997. *Chemical Composition of Water Before Contact with Repository Materials.* Milestone SPLA1M4, Rev. 1. Livermore, California: Lawrence Livermore National Laboratory. ACC: MOL.19971210.0031.

100741 Glassley, W.E. 1994. *Report on Near-Field Geochemistry: Water Composition Changes Due to Evaporation.* Milestone M0L26. Draft. Livermore, California: Lawrence Livermore National Laboratory. ACC: MOL.19950406.0153.

152684 Greenberg, J.P. and Moller, N. 1989. "The Prediction of Mineral Solubilities in Natural Waters: A Chemical Equilibrium Model for the Na-K-Ca-Cl-SO4-H2O System to High Concentration from 0 to 250°C." *Geochimica et Cosmochimica Acta, 53,* 2503–2518. New York, New York: Pergamon Press. TIC: 249020.

104945 Greenspan, L. 1977. "Humidity Fixed Points of Binary Saturated Aqueous Solutions." *Journal of Research of the National Bureau of Standards, 81A,* (1), 89-96. Washington, D.C.: U.S. Department of Commerce. TIC: 241138.

162069 Grønvold, F. and Meisingset, K.K. 1983. "Thermodynamic Properties and Phase Transitions of Salt Hydrates between 270 and 400 K. II. $Na_2CO_3 \cdot H_2O$ and $Na_2CO_3 \cdot 10H_2O$." *Journal of Chemical Thermodynamics, 15,* (9), 881-889. New York, New York: Academic Press. TIC: 253936.

176844 Gunnarsson, I.; Arnórsson, S.; and Jakobsson, S. 2005. "Precipitation of Poorly Crystalline Antigorite Under Hydrothermal Conditions." *Geochimica et Cosmochimica Acta, 69,* (11), 2813-2828. New York, New York: Elsevier. TIC: 258287.

176845 Gurevich, V.M.; Gorbunov, V.E.; Gavrichev, K.S.; and Khodakovskii, I.L. 1999. "A Calorimeter for Heat Capacity Measurements from 50 to 300 K: The Heat Capacities of Kogarkoite Na_3SO_4F(cr) at Low Temperatures." *Geochemistry International, 37,* (4), 367-377. Moscow, Russia: MAHK Nauka/Interperiodica. TIC: 258290.

100123 Hardin, E.L. 1998. *Near-Field/Altered-Zone Models Report.* UCRL-ID-129179. Livermore, California: Lawrence Livermore National Laboratory. ACC: MOL.19980630.0560.

100814 Harrar, J.E.; Carley, J.F.; Isherwood, W.F.; and Raber, E. 1990. *Report of the Committee to Review the Use of J-13 Well Water in Nevada Nuclear Waste Storage Investigations.* UCID-21867. Livermore, California: Lawrence Livermore National Laboratory. ACC: NNA.19910131.0274.

118163 Harvie, C.E.; Moller, N.; and Weare, J.H. 1984. "The Prediction of Mineral Solubilities in Natural Waters: The Na-K-Mg-Ca-H-Cl-SO_4-OH-HCO_3-CO_3-CO_2-H_2O System to High Ionic Strengths at 25°C." *Geochimica et Cosmochimica Acta, 48,* (4), 723-751. New York, New York: Pergamon Press. TIC: 239849.

105965 Hay, R.L. 1966. *Zeolites and Zeolitic Reactions in Sedimentary Rocks.* Special Paper 85. Boulder, Colorado: Geological Society of America. TIC: 238294.

162281 Hay, R.L. and Wiggins, B. 1980. "Pellets, Ooids, Sepiolite and Silica in Three Calcretes of the Southwestern United States." *Sedimentology, 27,* 559-576. Malden, Massachusetts: Blackwell Publishing. TIC: 222806.

162090 He, S. and Morse, J.W. 1993. "The Carbonic Acid System and Calcite Solubility in Aqueous Na-K-Ca-Mg-Cl-SO_4 Solutions from 0 to 90°C." *Geochimica et Cosmochimica Acta, 57,* (15), 3533-3554. New York, New York: Pergamon Press. TIC: 253894.

157904 Helgeson, H.C. and Kirkham, D.H. 1974. "Theoretical Prediction of the Thermodynamic Behavior of Aqueous Electrolytes at High Pressures and Temperatures: II. Debye-Hückel Parameters for Activity Coefficients and Relative Partial Molal Properties." *American Journal of Science, 274,* (7), 1199-1261. New Haven, Connecticut: Yale University, Kline Geology Laboratory. TIC: 240952.

106024 Helgeson, H.C.; Kirkham, D.H.; and Flowers, G.C. 1981. "Theoretical Prediction of the Thermodynamic Behavior of Aqueous Electrolytes at High Pressures and Temperatures: IV. Calculation of Activity Coefficients, Osmotic Coefficients, and Apparent Molal and Standard and Relative Partial Molal Properties to 600°C and 5 kb." *American Journal of Science, 281,* (10), 1249-1516. New Haven, Connecticut: Yale University, Kline Geology Laboratory. TIC: 238264.

162073 Holmes, H.F. and Mesmer, R.E. 1983. "Thermodynamic Properties of Aqueous Solutions of the Alkali Metal Chlorides to 250 °C." *Journal of Physical Chemistry, 87,* (7), 1242-1255. Washington, D.C.: American Chemical Society. TIC: 253375.

162074 Holmes, H.F. and Mesmer, R.E. 1986. "Thermodynamics of Aqueous Solutions of the Alkali Metal Sulfates." *Journal of Solution Chemistry, 15,* (6), 495-518. New York, New York: Plenum Press. TIC: 253633.

162076 Holmes, H.F. and Mesmer, R.E. 1992. "Isopiestic Studies of H_2SO_4(aq) at Elevated Temperatures, Thermodynamic Properties." *Journal of Chemical Thermodynamics, 24,* (3), 317-328. New York, New York: Academic Press. TIC: 253881.

162077 Holmes, H.F. and Mesmer, R.E. 1993. "Isopiestic Studies of $NaHSO_4$(aq) at Elevated Temperatures. Thermodynamic Properties." *Journal of Chemical Thermodynamics, 25,* (1), 99-110. New York, New York: Academic Press. TIC: 253937.

162078 Holmes, H.F. and Mesmer, R.E. 1994. "An Isopiestic Study of (1 – y)$NaHSO_4$ + yNa_2SO_4 (aq) at Elevated Temperatures." *Journal of Chemical Thermodynamics, 26,* (6), 581-594. New York, New York: Academic Press. TIC: 253880.

162083 Holmes, H.F. and Mesmer, R.E. 1998. "An Isopiestic Study of Aqueous Solutions of the Alkali Metal Bromides at Elevated Temperatures." *Journal of Chemical Thermodynamics, 30,* (6), 723-741. New York, New York: Academic Press. TIC: 253377.

162082 Holmes, H.F. and Mesmer, R.E. 1998. "Isopiestic Molalities for Aqueous Solutions of the Alkali Metal Hydroxides at Elevated Temperatures." *Journal of Chemical Thermodynamics, 30,* (3), 311-326. New York, New York: Academic Press. TIC: 253939.

162071 Holmes, H.F.; Baes, C.F., Jr.; and Mesmer, R.E. 1979. "Isopiestic Studies of Aqueous Solutions at Elevated Temperatures. II. NaCl + KCl Mixtures." *Journal of Chemical Thermodynamics, 11,* 1035-1050. New York, New York: Academic Press. TIC: 253876.

162072 Holmes, H.F.; Baes, C.F., Jr.; and Mesmer, R.E. 1981. "Isopiestic Studies of Aqueous Solutions at Elevated Temperatures. III. (1 - y)NaCl + y$CaCl_2$[a]." *Journal of Chemical Thermodynamics, 13,* 101-113. New York, New York: Academic Press. TIC: 253877.

162075 Holmes, H.F.; Busey, R.H.; Simonson, J.M.; Mesmer, R.E.; Archer, D.G.; and Wood, R.H. 1987. "The Enthalpy of Dilution of HCl(aq) to 648 K and 40 MPa, Thermodynamic Properties." *Journal of Chemical Thermodynamics, 19,* (7), 863-890. New York, New York: Academic Press. TIC: 253390.

162080 Holmes, H.F.; Simonson, J.M.; and Mesmer, R.E. 1997. "Aqueous Solutions of the Alkaline Earth Metal Chlorides. Corrected Constants for the Ion-Interaction Model." *Journal of Chemical Thermodynamics, 29,* (11), 1363-1373. New York, New York: Academic Press. TIC: 253938.

162331 Jones, B.F. 1983. "Occurrence of Clay Minerals in Surficial Deposits of Southwestern Nevada." *Sciences Géologiques, 2,* (72), 81-92. Strasbourg, France: Université Louis Pasteur de Strasbourg, Institut de Géologie. TIC: 254010.

123192 Jones, B.F.; Eugster, H.P.; and Rettig, S.L. 1977. "Hydrochemistry of the Lake Magadi Basin, Kenya." *Geochimica et Cosmochimica Acta, 41,* 53-72. New York, New York: Pergamon Press. TIC: 246224.

123170 Jones, B.F.; Rettig, S.L.; and Eugster, H.P. 1967. "Silica in Alkaline Brines." *Science, 158,* 1310-1314. Washington, D.C.: American Association for the Advancement of Science. TIC: 235387.

162345 Kent, D.B. and Kastner, M. 1985. "Mg $^{2+}$ Removal in the System Mg^{2+}—Amorphous SiO_2—H_2O by Adsorption and Mg-Hydroxysilicate Precipitation." *Geochimica et Cosmochimica Acta, 49,* 1123-1136. New York, New York: Pergamon Press. TIC: 253981.

161606 Kerr, P.F. 1977. *Optical Mineralogy.* 4th Edition. New York, New York: McGraw-Hill. TIC: 252886.

100769 Kinsman, D.J.J. 1976. "Evaporites: Relative Humidity Control of Primary Mineral Facies." *Journal of Sedimentary Petrology, 46,* 273-279. Tulsa, Oklahoma: Society of Economic Paleontologists and Mineralogists. TIC: 238672.

124293 Klein, C. and Hurlbut, C.S., Jr. 1999. *Manual of Mineralogy.* 21st Edition, Revised. New York, New York: John Wiley & Sons. TIC: 246258.

160184 Knauss, K.G. and Wolery, T.J. 1986. "Dependence of Albite Dissolution Kinetics on pH and Time at 25°C and 70°C." *Geochimica et Cosmochimica Acta, 50,* (11), 2481-2497. Elmsford, New York: Pergamon Journals. TIC: 221756.

133140 Knauss, K.G. and Wolery, T.J. 1988. "The Dissolution Kinetics of Quartz as a Function of pH and Time at 70°C." *Geochimica et Cosmochimica Acta, 52,* (1), 43-53. New York, New York: Pergamon Press. TIC: 203242.

143694 Knauss, K.G.; Beiriger, W.J.; and Peifer, D.W. 1985. *Hydrothermal Interaction of Crushed Topopah Spring Tuff and J-13 Water at 90, 150, and 250°C Using Dickson-Type, Gold-Bag Rocking Autoclaves.* UCRL-53630. Livermore, California: Lawrence Livermore National Laboratory. ACC: NNA.19931005.0010.

100150 Knauss, K.G.; Beiriger, W.J.; Peifer, D.W.; and Piwinskii, A.J. 1985. *Hydrothermal Interaction of Solid Wafers of Topopah Spring Tuff with J-13 Water and Distilled Water at 90, 150, and 250°C, Using Dickson-Type, Gold-Bag Rocking Autoclaves.* UCRL-53645. Livermore, California: Lawrence Livermore National Laboratory. ACC: NNA.19900207.0282.

166144 Knauss, K.G.; Wolery, T.J.; and Jackson, K.J. 1990. "A New Approach to Measuring pH in Brines and Other Concentrated Electrolytes." *Geochimica et Cosmochimica Acta, 54,* (5), 1519–1523. New York, New York: Pergamon. TIC: 253592.

162093 Königsberger, E. 2001. "Prediction of Electrolyte Solubilities from Minimal Thermodynamic Information." *Monatshefte für Chemie, 132,* 1363-1386. Vienna, Austria: Springer-Verlag. TIC: 253382.

168345 Königsberger, E.; Königsberger, L-C.; and Gamsjäger, H. 1999. "Low-Temperature Thermodynamic Model for the System Na_2CO_3-$MgCO_3$-$CaCO_3$-H_2O." *Geochimica et Cosmochimica Acta, 63,* (19-20), 3105-3119. New York, New York: Pergamon. TIC: 255783.

125329 Koorevaar, P.; Menelik, G.; and Dirksen, C. 1983. *Elements of Soil Physics.* Developments in Soil Science 13. New York, New York: Elsevier. TIC: 246286.

122125 Kracek, F.C. 1928. "P-T-X Relations for Systems of Two or More Components and Containing Two or More Phases (L-V, L_I-L_{II}-V and S-L-V Systems)." *International Critical Tables of Numerical Data, Physics, Chemistry and Technology.* Washburn, E.W., ed. Volume III. 1st Edition. New York, New York: McGraw-Hill. TIC: 243268.

105909 Krauskopf, K.B. 1979. *Introduction to Geochemistry.* 2nd Edition. New York, New York: McGraw-Hill. TIC: 242816.

101702 Krauskopf, K.B. and Bird, D.K. 1995. *Introduction to Geochemistry.* 3rd Edition. New York, New York: McGraw-Hill. TIC: 239316.

100051 Langmuir, D. 1997. *Aqueous Environmental Geochemistry.* Upper Saddle River, New Jersey: Prentice Hall. TIC: 237107.

159034 Li, G.; Peacor, D.R.; Coombs, D.S.; and Kawachi, Y. 1997. "Solid Solution in the Celadonite Family: The New Minerals Ferroceladonite, $K_2Fe^{2}_2+Fe^{3}_2+Si_8O_{20}(OH)_4$, and Ferroaluminoceladonite, $K_2Fe^{2}_2+Al_2Si_8O_{20}(OH)_4$." *American Mineralogist, 82,* (5-6), 503-511. Washington, D.C.: Mineralogical Society of America. TIC: 252472.

100771 Lichtner, P.C. and Seth, M. 1996. "Multiphase-Multicomponent Nonisothermal Reactive Transport in Partially Saturated Porous Media." *Proceedings of the 1996 International Conference on Deep Geological Disposal of Radioactive Waste, September 16-19, 1996, Winnipeg, Manitoba, Canada.* Toronto, Ontario, Canada: Canadian Nuclear Society. TIC: 233923.

162229 Lide, D.R., ed. 2000. *CRC Handbook of Chemistry and Physics.* 81st Edition. Boca Raton, Florida: CRC Press. TIC: 253056.

178081 Lide, D.R., ed. 2006. *CRC Handbook of Chemistry and Physics.* 87th Edition. Boca Raton, Florida: CRC Press. TIC: 258634.

166192 Linke, W.F. 1958. *Solubilities, Inorganic and Metal-Organic Compounds.* 4th Edition. Volume I, A–Ir. Washington, D.C.: American Chemical Society. TIC: 255159.

166191 Linke, W.F. 1965. *Solubilities, Inorganic and Metal-Organic Compounds.* 4th Edition. Volume II, K–Z. Washington, D.C.: American Chemical Society. TIC: 222176.

125331 Mahan, B.H. 1975. *University Chemistry.* 3rd Edition. Reading, Massachusetts: Addison-Wesley Publishing. TIC: 240721.

162085 Marshall, W.L. 1980. "Amorphous Silica Solubilities—I. Behavior in Aqueous Sodium Nitrate Solutions; 25–300°C, 0–6 Molal." *Geochimica et Cosmochimica Acta, 44,* (7), 907-913. New York, New York: Pergamon Press. TIC: 250701.

160481 Marshall, W.L. 1980. "Amorphous Silica Solubilities—III. Activity Coefficient Relations and Predictions of Solubility Behavior in Salt Solutions, 0-350°C." *Geochimica et Cosmochimica Acta, 44,* (7), 925-931. New York, New York: Pergamon Press. TIC: 250702.

162087 Marshall, W.L. and Chen, C-T.A. 1982. "Amorphous Silica Solubilities—V. Predictions of Solubility Behavior in Aqueous Mixed Electrolyte Solutions to 300°C." *Geochimica et Cosmochimica Acta, 46,* (2), 289-291. New York, New York: Pergamon Press. TIC: 250703.

162086 Marshall, W.L. and Chen, C-T.A. 1982. "Amorphous Silica Solubilities—VI. Postulated Sulfate-Silicic Acid Solution Complex." *Geochimica et Cosmochimica Acta, 46,* (3), 367-370. New York, New York: Pergamon Press. TIC: 250704.

160483 Marshall, W.L. and Warakomski, J.M. 1980. "Amorphous Silica Solubilities—II. Effect of Aqueous Salt Solutions at 25°C." *Geochimica et Cosmochimica Acta, 44,* (7), 915-924. New York, New York: Pergamon Press. TIC: 250705.

164481 McCaffrey, M.A.; Lazar, B.; and Holland, H.D. 1987. "The Evaporation Path of Seawater and the Coprecipitation of Br^- and K^+ with Halite." *Journal of Sedimentary Petrology, 57,* (5), 928-937. Tulsa, Oklahoma: Society of Economic Paleontologists and Mineralogists. TIC: 254627.

162094 Meisingset, K.K. and Grønvold, F. 1986. "Thermodynamic Properties and Phase Transitions of Salt Hydrates between 270 and 400 K. IV. $CaCl_2 \cdot 6H_2O$, $CaCl_2 \cdot 4H_2O$, $CaCl_2 \cdot 2H_2O$, and $FeCl_3 \cdot 6H_2O$." *Journal of Chemical Thermodynamics, 18,* 159-173. New York, New York: Academic Press. TIC: 253388.

166053 Mesmer, R.E. 1991. "Comments on 'A New Approach to Measuring pH in Brines and Other Concentrated Electrolytes' by K.G. Knauss, T.J. Wolery, and K.J. Jackson." *Geochimica et Cosmochimica Acta, 55,* (4), 1175-1176. New York, New York: Pergamon. TIC: 253594.

163594 Millero, F.J. and Pierrot, D. 1998. "A Chemical Equilibrium Model for Natural Waters." *Aquatic Geochemistry, 4,* (1), 153-199. New York, New York: Kluwer Academic Publishers. TIC: 254365.

152695 Moller, N. 1988. "The Prediction of Mineral Solubilities in Natural Waters: A Chemical Equilibrium Model for the Na-Ca-Cl-SO4-H2O System, to High Temperature and Concentration." *Geochimica et Cosmochimica Acta, 52,* 821–837. New York, New York: Pergamon Press. TIC: 248981.

177805 Møller, N.; Greenberg, J.P.; and Weare, J.H. 1998. "Computer Modeling for Geothermal Systems: Predicting Carbonate and Silica Scale Formation, CO_2 Breakout and H_2S Exchange." *Transport in Porous Media, 33,* 173-204. Amsterdam, The Netherlands: Kluwer Academic. TIC: 258638.

163593 Monnin, C. 1999. "A Thermodynamic Model for the Solubility of Barite and Celestite in Electrolyte Solutions and Seawater to 200°C and to 1 kBar." *Chemical Geology, 153,* (1-4), 187-209. New York, New York: Elsevier. TIC: 254364.

166150 Moore, R.C.; Mesmer, R.E.; and Simonson, J.M. 1997. "Solubility of Potassium Carbonate in Water between 384 and 529 K Measured Using the Synthetic Method." *Journal of Chemical Engineering Data, 42,* (6), 1078-1081. Washington, D.C.: American Chemical Society. TIC: 255169.

100804 Murphy, W.M. 1993. "Geochemical Models for Gas-Water-Rock Interactions in a Proposed Nuclear Waste Repository at Yucca Mountain." *Proceedings of the Topical Meeting on Site Characterization and Model Validation, FOCUS '93, September 26-29, 1993, Las Vegas, Nevada.* Pages 115-121. La Grange Park, Illinois: American Nuclear Society. TIC: 102245.

100805 Murphy, W.M. and Pabalan, R.T. 1994. *Geochemical Investigations Related to the Yucca Mountain Environment and Potential Nuclear Waste Repository.* NUREG/CR-6288. San Antonio, Texas: Southwest Research Institute. TIC: 227032.

178080 Neiburger, M.; Edinger, J.G.; and Bonner, W.D. 1982. *Understanding Our Atmospheric Environment.* 2nd Edition. San Francisco, California: W. H. Freeman and Company. TIC: 258635.

153965 Nordstrom, D.K. and Munoz, J.L. 1986. *Geochemical Thermodynamics.* Palo Alto, California: Blackwell Scientific Publications. TIC: 208228.

163274 NRC (U.S. Nuclear Regulatory Commission) 2003. *Yucca Mountain Review Plan, Final Report.* NUREG-1804, Rev. 2. Washington, D.C.: U.S. Nuclear Regulatory Commission, Office of Nuclear Material Safety and Safeguards. TIC: 254568.

178321 Nriagu, J.O. 1975. "Thermochemical Approximations for Clay Minerals." *American Mineralogist, 60,* (9 and 10), 834-839. Washington, D.C.: Mineralogical Society of America. TIC: 258820.

162102 Oakes, C.S.; Felmy, A.R.; and Sterner, S.M. 2000. "Thermodynamic Properties of Aqueous Calcium Nitrate $Ca(NO_3)_2$ to the Temperature 373 K Including New Enthalpy of Dilution Data." *Journal of Chemical Thermodynamics, 32,* (1), 29-54. New York, New York: Academic Press. TIC: 253509.

162096 Pabalan, R.T. and Pitzer, K.S. 1987. "Thermodynamics of Concentrated Electrolyte Mixtures and the Prediction of Mineral Solubilities to High Temperatures for Mixtures in the System Na-K-Mg-Cl-SO_4-OH-H_2O." *Geochimica et Cosmochimica Acta, 51,* (9), 2429-2443. New York, New York: Pergamon Journals. TIC: 253508.

162147 Pabalan, R.T. and Pitzer, K.S. 1987. "Thermodynamics of NaOH(aq) in Hydrothermal Solutions." *Geochimica et Cosmochimica Acta, 51,* (4), 829-837. New York, New York: Pergamon Press. TIC: 253383.

162280 Palache, C.; Berman, H.; and Frondel, C. 1951. *Halides, Nitrates, Borates, Carbonates, Sulfates, Phosphates, Arsenates, Tungstates, Molybdates, Etc.* Volume II of *The System of Mineralogy of James Dwight Dana and Edward Salisbury Dana, Yale University 1837–1892.* 7th Edition. New York, New York: John Wiley & Sons. TIC: 209332.

162274 Papke, K.G. 1976. *Evaporites and Brines in Nevada Playas.* Nevada Bureau of Mines and Geology Bulletin 87. Reno, Nevada: University of Nevada, Reno, and Mackay School of Mines. TIC: 211869.

162097 Peiper, J.C. and Pitzer, K.S. 1982. "Thermodynamics of Aqueous Carbonate Solutions Including Mixtures of Sodium Carbonate, Bicarbonate, and Chloride." *Journal of Chemical Thermodynamics, 14,* (7), 613-638. New York, New York: Academic Press. TIC: 240175.

162098 Phutela, R.C. and Pitzer, K.S. 1986. "Heat Capacity and Other Thermodynamic Properties of Aqueous Magnesium Sulfate to 473 K." *Journal of Physical Chemistry, 90,* (5), 895-901. Washington, D.C.: American Chemical Society. TIC: 253940.

152738 Pitzer, K.S. 1973. "Thermodynamics of Electrolytes. I. Theoretical Basis and General Equations." *Journal of Physical Chemistry, 77,* (2), 268–277. Washington, D.C.: American Chemical Society. TIC: 239503.

152709 Pitzer, K.S. 1991. "Ion Interaction Approach: Theory and Data Correlation." Chapter 3 of *Activity Coefficients in Electrolyte Solutions.* 2nd Edition. Pitzer, K.S., ed. Boca Raton, Florida: CRC Press. TIC: 251799.

123206 Pitzer, K.S. and Kim, J.J. 1974. "Thermodynamics of Electrolytes. IV. Activity and Osmotic Coefficients for Mixed Electrolytes." *Journal of the American Chemical Society, 96,* (18), 5701-5707. Washington, D.C.: American Chemical Society. TIC: 246223.

152742 Pitzer, K.S. and Mayorga, G. 1973. "Thermodynamics of Electrolytes. II. Activity and Osmotic Coefficients for Strong Electrolytes with One or Both Ions Univalent." *Journal of Physical Chemistry, 77,* (19), 2300–2308. Washington, D.C.: American Chemical Society. TIC: 249019.

163583 Pitzer, K.S. and Oakes, C.S. 1994. "Thermodynamics of Calcium Chloride in Concentrated Aqueous Solutions and in Crystals." *Journal of Chemical and Engineering Data, 39,* (3), 553-559. Washington, D.C.: American Chemical Society. TIC: 253384.

163582 Pitzer, K.S. and Shi, Y. 1993. "Thermodynamics of Calcium Chloride in Highly Concentrated Aqueous Solution and in Hydrated Crystals." *Journal of Solution Chemistry, 29,* (2), 99-105. New York, New York: Plenum Press. TIC: 253385.

162099 Pitzer, K.S.; Peiper, J.C.; and Busey, R.H. 1984. "Thermodynamic Properties of Aqueous Sodium Chloride Solutions." *Journal of Physical and Chemical Reference Data, 13,* (1), 1-102. Washington, D.C.: American Chemical Society. TIC: 253809.

101699 Pokrovskii, V.A. and Helgeson, H.C. 1995. "Thermodynamic Properties of Aqueous Species and the Solubilities of Minerals at High Pressures and Temperatures: The System Al_2O_3-H_2O-NaCl." *American Journal of Science, 295,* 1255-1342. New Haven, Connecticut: Yale University, Kline Geology Laboratory. TIC: 236803.

162101 Polya, D.A.; Woolley, E M.; Simonson, J.M.; and Mesmer, R.E. 2001. "The Enthalpy of Dilution and Thermodynamics of Na_2CO_3(aq) and $NaHCO_3$(aq) from T = 298 K to T = 523.15 K and Pressure of 40 MPa." *Journal of Chemical Thermodynamics, 33,* (2), 205-243. New York, New York: Academic Press. TIC: 253386.

162104 Rard, J.A. and Archer, D.G. 1995. "Isopiestic Investigation of the Osmotic and Activity Coefficients of Aqueous NaBr and the Solubility of $NaBr{\cdot}2H_2O$(cr) at 298.15 K: Thermodynamic Properties of the NaBr + H_2O System over Wide Ranges of Temperature and Pressure." *Journal of Chemical and Engineering Data, 40,* (1), 170-185. Washington, D.C.: American Chemical Society. TIC: 253941.

152759 Rard, J.A. and Clegg, S.L. 1997. "Critical Evaluation of the Thermodynamic Properties of Aqueous Calcium Chloride. 1. Osmotic and Activity Coefficients of 0–10.77 mol×kg(–1) Aqueous Calcium Chloride Solutions at 298.15 K and Correlation with Extended Pitzer Ion-Interaction Models." *Journal of Chemical & Engineering Data, 42,* (5), 819–849. Washington, D.C.: American Chemical Society. TIC: 249002.

152715 Rard, J.A. and Platford, R.F. 1991. "Experimental Methods: Isopiestic." *Activity Coefficients in Electrolyte Solutions.* 2nd Edition. Pitzer, K.S., ed. 209-277. Boca Raton, Florida: CRC Press. TIC: 251798.

162327 Rard, J.A. and Wijesinghe, A.M. 2003. "Conversion of Parameters Between Different Variants of Pitzer's Ion-Interaction Model, both With and Without Ionic Strength Dependent Higher-Order Terms." *Journal of Chemical Thermodynamics, 35,* (3), 439-473. New York, New York: Academic Press. TIC: 253943.

162105 Rard, J.A.; Clegg, S.L.; and Palmer, D.A. 2000. "Isopiestic Determination of the Osmotic Coefficients of Na_2SO_4(aq) at 25 and 50°C, and Representation with Ion-Interaction (Pitzer) and Mole Fraction Thermodynamic Models." *Journal of Solution Chemistry, 29,* (1), 1-49. New York, New York: Plenum. TIC: 253942.

173816 Rard, J.A.; Wijesinghe, A.M.; and Wolery, T.J. 2004. "Review of the Thermodynamic Properties of $Mg(NO_3)_2$(aq) and Their Representation with the Standard and Extended Ion-Interaction (Pitzer) Models at 298.15 K." *Journal of Chemical Engineering Data, 49,* (5), 1127-1140. Washington, D.C.: American Chemical Society. TIC: 257020.

153683 Robie, R.A. and Hemingway, B.S. 1995. *Thermodynamic Properties of Minerals and Related Substances at 298.15 K and 1 Bar (10^5 Pascals) Pressure and at Higher Temperatures.* Bulletin 2131. Reston, Virginia: U.S. Geological Survey. TIC: 249441.

108567 Robinson, R.A. and Stokes, R.H. 1965. *Electrolyte Solutions, The Measurement and Interpretation of Conductance, Chemical Potential and Diffusion in Solutions of Simple Electrolytes.* 2nd Edition (Revised). Washington, D.C.: Butterworth. TIC: 242575.

162107 Rogers, P.S.Z. and Pitzer, K.S. 1981. "High-Temperature Thermodynamic Properties of Aqueous Sodium Sulfate Solutions." *Journal of Physical Chemistry, 85,* (20), 2886-2895. Washington, D.C.: American Chemical Society. TIC: 253810.

125338 Rosenberg, N.D.; Knauss, K.G.; and Dibley, M.J. 1999. *Evaporation of J13 Water: Laboratory Experiments and Geochemical Modeling.* UCRL-ID-134852. Livermore, California: Lawrence Livermore National Laboratory. TIC: 246322.

125339 Rosenberg, N.D.; Knauss, K.G.; and Dibley, M.J. 1999. *Evaporation of Topopah Spring Tuff Pore Water.* UCRL-ID-135765. Livermore, California: Lawrence Livermore National Laboratory. TIC: 246231.

178223 Rumpf, B. and Maurer, G. 1993. "An Experimental and Theoretical Investigation on the Solubility of Carbon Dioxide in Aqueous Solutions of Strong Electrolytes." *Berichte der Bunsen-Gesellschaft fur Physikalische Chemie (An International Journal of Physical Chemistry), 97,* 85-97. Weinheim, Germany: VCH Verlagsgesellschaft mbH.

178222 Rumpf, B.; Nicolaisen, H.; Ocal, C.; and Maurer, G. 1994. "Solubility of Carbon Dioxide in Aqueous Solutions of Sodium Chloride: Experimental Results and Correlation." *Journal of Solution Chemistry, 23,* (3), 431-448. New York, New York: Plenum Publishing Corporation. TIC: 258825.

177381 Seward, T.M. 1974. "Determination of the First Ionization Constant of Silicic Acid from Quartz Solubility in Borate Buffer Solutions to 350°C." *Geochimica et Cosmochimica Acta, 38,* 1651-1664. New York, New York: Pergamon Press. TIC: 258509.

161602 Smith, W.R. and Missen, R.W. 1991. *Chemical Reaction Equilibrium Analysis: Theory and Algorithms.* Malabar, Florida: Krieger Publishing Company. TIC: 252885.

162494 SNL (Sandia National Laboratories) 2003. *Software User's Manual, EQ3/6, Version 8.0.* SDN: 10813-UM-8.0-00. Albuquerque, New Mexico: Sandia National Laboratories. ACC: MOL.20030312.0084.

179287 SNL 2007. *Technical Work Plan for: Revision of Model Reports for Near-Field and In-Drift Water Chemistry.* TWP-MGR-PA-000038 REV 02. Las Vegas, NV: Sandia National Laboratories. ACC: DOC.20070110.0004.

152713 Spencer, R.J.; Moller, N.; and Weare, J.H. 1990. "The Prediction of Mineral Solubilities in Natural Waters: A Chemical Equilibrium Model for the Na-K-Ca-Mg-Cl-SO_4-H_2O System at Temperatures Below 25°C." *Geochimica et Cosmochimica Acta, 54,* 575–590. New York, New York: Pergamon Press. TIC: 248999.

162116 Sterner, S.M.; Felmy, A.R.; Oakes, C.S.; and Pitzer, K.S. 1998. "Correlation of Thermodynamic Data for Aqueous Electrolyte Solutions to Very High Ionic Strength Using INSIGHT: Vapor Saturated Water Activity in the System $CaCl_2$-H_2O to 250°C and Solid Saturation." *International Journal of Thermophysics, 19,* (3), 761-770. New York, New York: Plenum Publishing. TIC: 253387.

125332 Stumm, W. and Morgan, J.J. 1996. *Aquatic Chemistry, Chemical Equilibria and Rates in Natural Waters.* 3rd Edition. New York, New York: John Wiley & Sons. TIC: 246296.

150775 Sverjensky, D.A.; Shock, E.L.; and Helgeson, H.C. 1997. "Prediction of the Thermodynamic Properties of Aqueous Metal Complexes to 1000°C and 5 kb." *Geochimica et Cosmochimica Acta, 61,* (7), 1359-1412. New York, New York: Elsevier. TIC: 248307.

162108 Thiessen, W.E. and Simonson, J.M. 1990. "Enthalpy of Dilution and the Thermodynamics of NH_4Cl(aq) to 523 K and 35 MPa." *Journal of Physical Chemistry, 94,* (20), 7794-7800. Washington, D.C.: American Chemical Society. TIC: 253883.

124334 Tsang, Y.W. 1999. *Yucca Mountain Single Heater Test Final Report.* Report 42537. Berkeley, California: Lawrence Berkeley National Laboratory. ACC: MOL.19990809.0191.

161603 Van Zeggeren, F. and Storey, S.H. 1970. *The Computation of Chemical Equilibria.* New York, New York: Cambridge University Press. TIC: 252891.

107066 Vaniman, D.T.; Ebinger, M.H.; Bish, D.L.; and Chipera, S. 1992. "Precipitation of Calcite, Dolomite, Sepiolite, and Silica from Evaporated Carbonate and Tuffaceous Waters of Southern Nevada, USA." *Proceedings of the 7th International Symposium on Water-Rock Interaction, Park City, Utah, July 13-18, 1992.* Kharaka, Y.K. and Maest, A., eds. *1,* 687-691. Brookfield, Vermont: A.A. Balkema. TIC: 208527.

162329 Wadley, S. and Buckley, C.A. 1997. *Chemical Speciation Self-Study Work Manual.* WRC Project No. K8/208. Durban, South Africa: University of Natal, Department of Chemical Engineering, Water Research Commission. TIC: 252923.

162283 Walling, E.M.; Rock, P.A.; and Casey, W.H. 1995. "The Gibbs Energy of Formation of Huntite, $CaMg_3(CO_3)_4$, at 298 K and 1 Bar from Electrochemical Cell Measurements." *American Mineralogist, 80,* (3-4), 355-360. Washington, D.C.: Mineralogical Society of America. TIC: 252890.

127454 Walton, J.C. 1994. "Influence of Evaporation on Waste Package Environment and Radionuclide Release from a Tuff Repository." *Water Resources Research, 30,* (12), 3479-3487. Washington, D.C.: American Geophysical Union. TIC: 246921.

162109 Wang, P.; Pitzer, K.S.; and Simonson, J.M. 1998. "Thermodynamic Properties of Aqueous Magnesium Chloride Solutions from 250 to 600 K and to 100 MPa." *Journal of Physical and Chemical Reference Data, 27,* (5), 971-991. Washington, D.C.: American Chemical Society. TIC: 249693.

100833 Weast, R.C. and Astle, M.J., eds. 1981. *CRC Handbook of Chemistry and Physics.* 62nd Edition. Boca Raton, Florida: CRC Press. TIC: 240722.

162148 Wesolowski, D.J. 1992. "Aluminum Speciation and Equilibria in Aqueous Solution: I. The Solubility of Gibbsite in the System Na-K-Cl-OH-$Al(OH)_4$ from 1 to 100°C." *Geochimica et Cosmochimica Acta, 56,* (3), 1065-1091. New York, New York: Pergamon Press. TIC: 253946.

176847 Wijesinghe, A.M. and Rard, J.A. 2005. "Conversion and Optimization of the Parameters from an Extended Form of the Ion-Interaction Model for $Ca(NO_3)_2$(aq) and $NaNO_3$(aq) to Those of the Standard Pitzer Model, and an Assessment of the Accuracy of the Parameter Temperature Representations." *Journal of Chemical Thermodynamics, 37,* 1196-1218. New York, New York: Elsevier. TIC: 258288.

100792 Wilder, D.G., ed. 1996. *Volume II: Near-Field and Altered-Zone Environment Report.* UCRL-LR-124998. Livermore, California: Lawrence Livermore National Laboratory. ACC: MOL.19961212.0121; MOL.19961212.0122.

100836 Wolery, T.J. 1992. *EQ3NR, A Computer Program for Geochemical Aqueous Speciation-Solubility Calculations: Theoretical Manual, User's Guide, and Related Documentation (Version 7.0).* UCRL-MA-110662 PT III. Livermore, California: Lawrence Livermore National Laboratory. ACC: MOL.19980717.0626.

177633 Wolf, M.; Breitkopf, O.; and Puk, R. 1989. "Solubility of Calcite in Different Electrolytes at Temperatures Between 10º and 60°C and at CO_2 Partial Pressures of About 1 kPa." *Chemical Geology, 76,* 291-301. Amsterdam, The Netherlands: Elsevier. TIC: 258562.

162340 Wollast, R.; Mackenzie, F.T.; and Bricker, O.P. 1968. "Experimental Precipitation and Genesis of Sepiolite at Earth-Surface Conditions." *American Mineralogist, 53,* 1645-1662. Washington, D.C.: Mineralogical Society of America. TIC: 253980.

9.2 CODES, STANDARDS, REGULATIONS, AND PROCEDURES

173273 10 CFR 63. 2005 Energy: Disposal of High-Level Radioactive Wastes in a Geologic Repository at Yucca Mountain, Nevada. ACC: MOL.20050405.0118.

IM-PRO-002, Rev. 0, ICN 0. *Control of the Electronic Management of Information*. Washington, D.C.: U.S. Department of Energy, Office of Civilian Radioactive Waste Management. ACC: DOC.20060927.0023

IM-PRO-003, Rev. 1, ICN 0. *Software Management.* Washington, D.C.: U.S. Department of Energy, Office of Civilian Radioactive Waste Management. ACC: DOC.20061113.0001.

SCI-PRO-006, Rev. 0, ICN 0. *Models*. Washington, D.C.: U.S. Department of Energy, Office of Civilian Radioactive Waste Management. ACC: DOC.20060928.0025.

SCI-PRO-003, Rev. 1, ICN 0. *Document Review.* Washington, D.C.: U.S. Department of Energy, Office of Civilian Radioactive Waste Management. ACC: DOC.20061113.0007.

SCI-PRO-002, Rev. 1, ICN 0. *Planning for Science Activities.* Washington, D.C.: U.S. Department of Energy, Office of Civilian Radioactive Waste Management. ACC: DOC.20070213.0012.

9.3 SOURCE DATA, LISTED BY TRACKING NUMBER

144913 LL000202905924.117. Environment on the Surfaces of the Drip Shield and Waste Package Outer Barrier. Submittal date: 02/18/2000.

177573 LL030106923121.018. Flask Evaporative Concentration Experiment # 13 (FEC 13) Solution Composition. Submittal date: 02/11/2003.

177574 LL030107023121.019. Flask Evaporative Concentration Experiment #9 (FEC 9) Solution Composition. Submittal date: 02/11/2003.

177575 LL030107123121.020. Evaporative Concentration Experiment (Flask Evaporative Concentration Testing) FEC 12. Submittal date: 02/10/2003.

177576 LL030408523121.028. Flask Evaporative Concentration Experiment #14 (FEC14). Submittal date: 06/03/2003.

120487 LL991008004241.041. Evaporation of Topopah Spring Tuff Pore Water. Submittal date: 10/21/1999.

120489 LL991008104241.042. Evaporation of J13 Water: Laboratory Experiments and Geochemical Modeling. Submittal date: 10/21/1999.

151029 MO0006J13WTRCM.000. Recommended Mean Values of Major Constituents in J-13 Well Water. Submittal date: 06/07/2000.

161756 MO0302SPATHDYN.000. Thermodynamic Data Input Files - Data0.YMP.R2. Submittal date: 02/05/2003.

170760 MO0407SEPFEPLA.000. LA FEP List. Submittal date: 07/20/2004.

162572 SN0302T0510102.002. Pitzer Thermodynamic Database (data0.ypf.r0, Formerly data0.ypf, Revision 1). Submittal date: 02/06/2003.

172759 SN0410T0510404.001. Corrections to Errors in the DATA0.YMP.R2 Thermodynamic Database. Submittal date: 11/01/2004.

172712 SN0410T0510404.002. Thermodynamic Database Input File for EQ3/6 - DATA0.YMP.R4. Submittal date: 11/01/2004.

173493 SN0504T0502404.011. Pitzer Thermodynamic Database for Some Actinide and Transition Metal Species (DATA0.YPF.F1). Submittal date: 04/19/2005.

178850 SN0612T0502404.014. Thermodynamic Database Input File for EQ3/6 - DATA0.YMP.R5. Submittal date: 12/15/2006.

9.4 OUTPUT DATA, LISTED BY DATA TRACKING NUMBER

LL031106231032.007. High Temperature Solubility and Vapor Pressure (Relative Humidity) Data for Aqueous Systems Containing Single and Multiple Salts. Submittal Date: 11/19/2003.

MO0701SPAPTZER.001. Pitzer Thermodynamic Database (DATA0.YPF.R2) Spreadsheets and EQ3/6 Input and Output Files. Submittal Date: 101/09/2007.

SN0609T0502404.012. Pitzer Thermodynamic Database (Data0.YP2). Submittal Date: 009/28/2006.

SN0610T0509206.001. In-Drift Precipitates/Salts (IDPS) Model EQ3/6 Input File Formats and List of Suppressed Minerals. Submittal Date: 10/30/2006.

SN0611T0509206.006. Example EQ3/6 In-Drift Precipitates/Salts Model Input/Output Files and Lookup Table for In Situ J-13 Well Water. Submittal Date: 11/20/2006.

SN0702T0509206.008. EQ3/6 Input/Output Files for In-Drift Precipitates/Salts Model Validation of Evaporation of J-13 Well Water and Topopah Springs Tuff Pore Water and Thermodynamic Database Comparison Validation. Submittal Date: 02/05/2007.

MO0701EQ36IDPS.000 . EQ3/6 Input and Output Files Used for IDPS Model Validation Simulations of Evaporation of Dilute Salt Solutions at 25C and 100C, Seawater, Binary and Ternary Salt Solutions, Synthetic Topopah Springs Tuff Pore Water at 95C and in the Carbonate System. Submittal Date: 01/16/2007

SN0611T0509206.007. Estimated Model Uncertainties in the IDPS Model Outputs. Submittal Date: 11/29/2006

9.5 SOFTWARE CODES

162228 EQ3/6 V. 8.0. 2003. WINDOWS 2000, WIN NT 4.0, WIN 98, WIN 95. STN: 10813-8.0-00.

161900 GetEQData V. 1.0.1. 2003. WINDOWS NT 4.0/98/95. STN: 10809-1.0.1-0

153218 SUPCRT92 VV1.0. 1999. PC w/Windows OS and MAC w/MAC OS. 10058-1.0-00.

APPENDIX I

PITZER DATABASE DEVELOPMENT: DESCRIPTION OF THE PITZER GEOCHEMICAL THERMODYNAMIC DATABASE (data0.ypf.R2)

CONTENTS

Page

CONTENTS (Continued)

Page

FIGURES

Page

INTENTIONALLY LEFT BLANK

TABLES

Page

TABLES (Continued)

Page

I.1 SCOPE

The Pitzer database data0.ypf.R0 (DTN: SN0302T0510102.002 [DIRS 162572]) was developed to calculate concentrations of electrolyte solutions resulting from the compositional evolution of waters from the unsaturated zone that are likely to seep into the waste emplacement drifts. These calculations are performed using the computer code EQ3/6 v8.0 (see Section 3.1.1), for which a Pitzer parameter database has been created. A subsequent version of this database (data0.ypf.R1; DTN: SN0504T0502404.011 [DIRS 173493]) was developed mainly to accommodate additions, updates, and corrections to parameter data relevant to actinides and transitions metal species. The current version of this report intends to qualify a new version of the Pitzer database, data0.ypf.R2 (Output DTN: SN0609T0502404.012), which includes updates in Pitzer and other thermodynamic parameter data. These updates, which include additions and corrections to data, are focused only on chemical species relevant to the IDPS model as described in the main body of this report.

As a result of above-ambient temperature conditions within the repository, water from the unsaturated zone undergoes evaporation to evolve into a concentrated electrolyte solution. These concentrated waters may accelerate degradation processes (e.g., metal corrosion), thereby affecting the integrity of Engineered Barrier System (EBS) components such as waste packages and drip shields. For this reason, electrolyte component concentrations under long-term evaporative conditions need to be estimated to provide input for downstream total system performance assessment (TSPA) models.

Geochemical modeling using data appropriate for dilute solutions, such as those data contained in the geochemical databases data0.ymp.R2 (DTN: MO0302SPATHDYN.000 [DIRS 161756]) and data0.ymp.R4 (DTN: SN0410T0510404.002 [DIRS 172712]) is not accurate or valid when applied to the concentrated (high ionic strength) solutions that result from the evaporation of seepage waters within the disposal drifts. As explained in Section I.3, the Pitzer database represents a more accurate way of predicting chemical behavior in concentrated aqueous electrolyte solutions. Modeling of water compositions associated with the in-drift physical and chemical environment under long-term evaporative repository conditions therefore relies upon this Pitzer database. Development and updating of this database involves a comprehensive compilation of Pitzer model parameters reported in the literature, focusing mostly on those functional at relatively elevated temperatures (i.e., above 25°C). Data above 25°C are needed, since for long periods of time the estimated temperature conditions in the repository will be above ambient temperatures.

The steps taken in the update and/or qualification of the new Pitzer database (data0.ypf.R2; Output DTN: SN0609T0502404.012) are as follows:

- Update of temperature-dependent Pitzer parameter for $CO_2(g)$ in aqueous saline systems up to a temperature of 250°C.
- Update of temperature-dependent Pitzer parameters for $CaCl_2$ up to a temperature of 250°C. This update also includes the addition of ion pairs consistent with the newly adopted Pitzer parameters.

- Update of temperature-dependent Pitzer parameter data for $NaNO_3$, and $Ca(NO_3)_2$. The update for $Mg(NO_3)_2$ is only valid at 25°C.

- Validation and testing of compiled Pitzer data to predict osmotic coefficients and therefore water activity when compared to source literature data. This also includes testing of the Pitzer parameter data in the prediction of phase solubility.

- Estimation and adjustment of solubility constants (i.e., log K values) for selected salt solids using tabulated thermodynamic and solubility data in concert with the estimated Pitzer parameters defining the activity model for the relevant salt system. This is done to bridge consistency between the compiled Pitzer electrolyte parameter data and the reported salt phase solubility reported in the scientific literature.

- Adjustment of log K values to fit calcite solubility to elevated temperatures.

- Incorporation of silicate mineral log K data from the recent thermodynamic data compilation *data0.ymp.R5* (DTN: SN0612T0502404.014 [DIRS 178850]) that include the phases amorphous sepiolite, kogarkoite, palygorskite, and "poorly crystalline antigorite."

I.2 INPUT DATA SELECTION

The Pitzer database was developed in this document using primary input data selected from a variety of published sources. The status of these input data is summarized in the Document Input Reference System. The primary sources for input data are the YMP-generated databases data0.ymp.R2 and data0.ymp.R4. Additional input data are selected from widely used handbook sources, and the remainder of the data used is selected from internationally recognized peer-reviewed journals. Data sources for Pitzer parameters are entirely restricted to peer-reviewed journals. The data sources for binary electrolyte solutions are listed in Table 4-2 of Section 4.1.1 of this report, and the data sources for ternary solutions are listed in Table 4-3 of that section. The rationale for the selection of these data is discussed in the subsections of Sections I.4.4 and I.4.5.

The most important rationale for adopting the Pitzer modeling approach and related parameter data is their wide acceptance by the scientific and international community. As documented below, this acceptance is comparable to that for scientific and technical handbooks. Since the early publications on the subject by Professor Kenneth S. Pitzer of the Department of Chemistry, the University of California at Berkeley (e.g., Pitzer 1973 [DIRS 152738]; Pitzer and Mayorga 1973 [DIRS 152742]; Pitzer and Kim 1974 [DIRS 123206]), Pitzer's approach to the thermodynamics of highly concentrated aqueous electrolytes has been widely accepted. This is evident not only by the large number of citations of publications by him (including co-authors) and citations of publications by other independent authors who used the same approach, but also by the range of organizations represented. Examples of this wide acceptance include use of the Pitzer approach by the staff at the University of California, San Diego (Møller 1988 [DIRS 152695]; Spencer et al. 1990 [DIRS 152713]); the Chemistry and Analytical Sciences Division, Oak Ridge National Laboratory (Holmes and Mesmer 1994 [DIRS 162078]); Lawrence Livermore National Laboratory (Rard and Wijesinghe 2003 [DIRS 162327]); Johns

Hopkins University (Eugster and Jones 1979 [DIRS 123175]; see the citations list in the body of this report); the Physical and Chemical Properties Division, National Institute of Standards and Technology (Archer 2000 [DIRS 162065]); Pacific Northwest National Laboratory in collaboration with Fluid Inclusion Technologies (Oakes et al. 2000 [DIRS 162102]); Plymouth Marine Laboratory, UK, in collaboration with the School of Environmental Sciences, University of East Anglia, UK (Clegg and Brimblecombe 1990 [DIRS 159187]); the Department of Chemistry, University of Coimbra, Portugal, in collaboration with the Department of Chemistry, the University of California at Berkeley (de Lima and Pitzer 1983 [DIRS 162110]); the Department of Geology, Texas A&M University (He and Morse 1993 [DIRS 162090]); the Department of Chemistry, Murdoch University, Australia (Königsberger 2001 [DIRS 162093]); the Department of Chemistry and Geochemistry, Colorado School of Mines (author was one of the first members of the Nuclear Waste Technical Review Board) (Langmuir 1997 [DIRS 100051], pp. 138-143; see the citations list in the body of this report); the Center for Nuclear Waste Regulatory Analyses (Pabalan and Pitzer 1987 [DIRS 162147]; Pabalan and Pitzer 1987 [DIRS 162096]); and others. The group at Oak Ridge National Laboratory (Holmes and Mesmer 1994 [DIRS 162078]) are well-known for producing high quality isopiestic data at elevated temperatures thanks to their considerable improvements on this experimental technique (see Rard and Platford 1991 [DIRS 152715], Section C, pp. 246 to 249). Isopiestic experiments on electrolytes provide osmotic coefficient data that are then used to obtain Pitzer parameter data. The studies by all these authors have been extensively cited and are therefore widely accepted, so much so as to indicate acceptance rather than rejection, as documented below in Sections I.4.4 through I.4.6 for individual ion doublets and triplets.

The Pitzer database data0.ypf.R2 (Output DTN: SN0609T0502404.012) is divided into four sections composed of data blocks containing thermodynamic data representing: (1) coefficient data for temperature-dependent interaction parameters defined in the Pitzer standard formulations in accord with the 3- to 4-term 25°C-centric parameter equation to describe temperature dependence (see Section I.3.2) and implemented in the code EQ3/6 v8.0; (2) selected log K's for ion pair speciation reactions; (3) log K's for solids obtained from existing thermodynamic data compilations except those salts for which log K values were obtained in the current effort; and (4) log K solubility data for selected gases also from existing data compilations.

A thorough evaluation of existing Pitzer parameter data is required for inclusion in the database. The criteria used for accepting data from a published source are as follows:

Criterion 1: Pitzer ion-interaction parameters for a specific electrolyte should be reproduced by the equations given by the source publication to express their temperature dependence. Failure to satisfy this criterion will result in either rejection of the data or refitting of the actual parameter if tabulated in the source. Parameter data given only at 25°C do not need to satisfy this criterion since they do not require refitting.

Criterion 2: Pitzer parameter data satisfying criterion 1 for a given range of temperatures and electrolyte concentrations will be used in the conversion (if necessary) and refitting procedures described in sections I.4.1, I.4.2, and I.4.3. Upon refitting to the temperature function embedded in EQ3/6 v8.0, the ion interaction parameters are compared to check that these closely match the input values obtained from the source. The comparison between refitted and input values of

osmotic coefficients or refitted Pitzer parameter should be a close match (see comparison analyses in Output DTN: MO0701SPAPTZER.001). Failure to satisfy this criterion will result in rejection of parameter data. Parameter data given only at 25°C do not need to satisfy this criterion since these do not need refitting.

Further tests in most of the fitted parameter data involve comparison of experimentally determined osmotic coefficients for specific electrolytes from alternate sources. Due to the limited amount of osmotic coefficient data available for many electrolytes of interest and their possible mixtures at the temperatures of interest, this comparison is not done on all binary parameters considered in this appendix. Nevertheless, it represents a robust validation of the predictive capabilities of the database. This test does not apply to parameter data obtained only at 25°C.

Most of the log K data for solids comes from data0.ymp.R2 (DTN: MO0302SPATHDYN.000 [DIRS 161756]) and data0.ymp.R4 (DTN: SN0410T0510404.002 [DIRS 172712]). Only a few log K values for salt solids are needed and these were obtained through a calibration method bound by tabulated salt solubilities and the compiled Pitzer activity model. Calibration of solubility constants or log Ks for the salt solids is achieved by fitting log K values to the salt saturation molality using the obtained Pitzer activity model. Saturation molalities for salt solids as a function of temperature are obtained from tabulated handbook data or peer-review journal articles. For comparison, the resulting log K values are then compared to those obtained by using tabulated standard Gibbs free-energy data (e.g., Robie and Hemingway 1995 [DIRS 153683]) when these data are available. The percent difference in log K values between those obtained through calibration and those from tabulated thermodynamic data should be less than ~15%. Percent differences exceeding the latter value should be regarded as unsatisfactory and will not be considered for inclusion in the database. However, exceptions to this rule may exist and justification for inclusion in the database is required. Most log K values obtained for the salt solids through the calibration method have percent differences of less than ~15% rendering the calibrated values as satisfactory within the predictive capabilities of the database.

I.3 PITZER ION-INTERACTION MODEL

The theory behind the development of Pitzer equations for describing the thermodynamic properties of electrolyte solutions is rather complex, and a detailed description goes beyond the scope needed for this thermodynamic database description. Consult the works of Pitzer (1973 [DIRS 152738]; 1991 [DIRS 152709] and references therein) for details on fundamental theoretical groundwork on the formalism and applications of this thermodynamic model as applied to concentrated aqueous electrolyte solutions. Basically, the Pitzer model is an extension of the Debye-Hückel model for ionic solutions. Ion interactions beyond the Debye-Hückel approximation are represented by a set of ion-interaction coefficients that form an integral feature of Pitzer semi-empirical equations. These equations are described in detail in *Software User's Manual, EQ3/6, Version 8.0* (SNL 2003 [DIRS 162494]). For completeness, the fundamental equations pertinent to pure aqueous electrolytes and mixtures will be briefly summarized here.

I.3.1 GENERAL PITZER ELECTROLYTE THEORY

The starting point for the formulation of Pitzer's model is the equation for the excess Gibbs free energy (G^{EX}) of the total solution:

$$G^{EX}/w_w = RT\sum_i m_i(1 - \phi + \ln\gamma_i) \quad \text{(Eq. I–1)}$$

where G^{EX} is the difference or "excess" in the Gibbs free energy between a real solution and an ideal solution defined on the molality composition scale, w_w is the mass of water in the solution in kilograms, m_i is the molality of the ith type of ion, ϕ is the molality-based osmotic coefficient of the solvent, and γ_i is the molality-based activity coefficient of the ith type of ion. R is the universal gas constant and T is the absolute temperature. Once an expression has been assumed for the dependence of G^{EX} on the ionic composition of the solution, the osmotic coefficient of the solvent and the activity coefficient of each ionic solute may be calculated by taking the appropriate partial derivatives:

$$\ln\gamma_i = [\partial\{G^{EX}/RTw_w\}/\partial m_i]_{n_w} \quad \text{(Eq. I-2)}$$

$$\phi = 1 - [\{\partial G^{EX}/RT\sum_i m_i\}/\partial w_w]_{n_i} \quad \text{(Eq. I-3)}$$

where n_w and n_i are the numbers of moles of water and of ion i, respectively. The osmotic coefficient is directly related to the water activity of the solution, a_w, by the relation:

$$\ln a_w = -(\sum_i m_i)\phi/\Omega \quad \text{(Eq. I-4)}$$

where the quantity $\Omega = (1\text{kg}/0.018015\ \text{kg}\cdot\text{mol}^{-1}) = 55.508\ \text{mol}\cdot\text{kg}^{-1}$ is the number of moles of water present in one kilogram of water.

Pitzer (1973 [DIRS 152738]) initially wrote his expression for G^{EX} in the following form (except for minor differences in notation):

$$G^{EX}/(RT) = w_w f^G(I) + (1/w_w)\sum_{ij}\lambda_{ij}(I)n_i n_j + (1/w_w^2)\sum_{ijk}\mu_{ijk}n_i n_j n_k \quad \text{(Eq. I-5)}$$

where $f^G(I)$ represents the total contribution of long-range electrostatic forces between ions, $\lambda_{ij}(I)$ represents the short-range specific interactions between pairs of ions i and j, and μ_{ijk} represents the short-range specific interactions between triplets of ions i, j, and k. The $f(I)$ and $\lambda_{ij}(I)$ are assumed to be functions of the ionic strength I. The ionic strength of the solution is defined on the molality concentration scale as:

$$I = (1/2)\sum_i m_i z_i^2 \quad \text{(Eq. I-6)}$$

where z_i is the valence of the ith ion. Pitzer tested two different variants of the Debye-Hückel equation for the long-range electrostatic term, and selected the Debye-Hückel "osmotic" function. For the osmotic coefficient, this function has the form:

$$f^{\phi}(I) = -A_{\phi}\sqrt{I}\,/(1 + b\sqrt{I}\,) \qquad \text{(Eq. I-7)}$$

where $f^{\phi}(I)$ depends only on the ionic strength I, and A_{ϕ} is the Debye-Hückel limiting law slope for the osmotic coefficient. Pitzer further selected $b = 1.2$ for all aqueous electrolytes, assumed that the λ_{ij} and μ_{ijk} functions are symmetrical in their indices, e.g. $\lambda_{ij} = \lambda_{ji}$, and noted that the ratios of moles of solute ion i to the number of kilograms of water yields the molality of that ion, i.e., $n_i/w_w = m_i$.

The corresponding equation for the Debye-Hückel "osmotic" function $f^{G}(I)$ for the excess Gibbs free energy is:

$$f^{G}(I) = -(4IA_{\phi}/b)\ln(1 + b\sqrt{I}\,) \qquad \text{(Eq. I-8)}$$

Similarly, Debye-Hückel "osmotic" function $f^{\gamma}(I)$ for the activity coefficient is:

$$f^{\gamma}(I) = -A_{\phi}\{\sqrt{I}\,/(1 + b\sqrt{I}\,) + (2/b)\ln(1 + b\sqrt{I}\,)\} \qquad \text{(Eq. I-9)}$$

I.3.1.1 Pitzer's Model for Aqueous Binary Electrolytes

Equation I–5 could be used as the starting point for deriving the expressions for the thermodynamic properties of the solvent and the solute ions. However, Pitzer (1973 [DIRS 152738]) rewrote his equations in terms of B_{MX} and C_{MX} functions which are now more commonly used, and which will be used in the subsequent discussion. Anyone interested in the explicit equations for ϕ and $\ln\gamma_i$ written in terms of the λ_{ij} and μ_{ijk} should consult Pitzer's (1973 [DIRS 152738]; 1991 [DIRS 152709]) publications and *Software User's Manual, EQ3/6, Version 8.0* (SNL 2003 [DIRS 162494]). The equations relating these two types of functions for a single aqueous electrolyte containing cation M and anion X are:

$$B^{\phi}_{MX}(I) = \lambda_{MX} + I\lambda_{MX}' + (\nu_M/2\nu_X)(\lambda_{MM} + I\lambda_{MM}') + (\nu_X/2\nu_M)(\lambda_{XX} + I\lambda_{XX}') \qquad \text{(Eq. I-10)}$$

and

$$C^{\phi}_{MX} = 3(\nu_M\mu_{MMX} + \nu_X\mu_{MXX})/\sqrt{\nu_M\nu_X} \qquad \text{(Eq. I-11)}$$

where the primes denote the derivative of a function with regard to the ionic strength (e.g., $\lambda_{MX}' = \partial\lambda_{MX}/\partial I$), ν_M is the stoichiometric number of cations formed by dissociation of one molecule of the solute, and ν_X is the stoichiometric number of anions formed by dissociation of one molecule of the solute.

Pitzer (1973 [DIRS 152738]) allowed the $B^{\phi}_{MX}(I)$ to vary with the ionic strength, but assumed that C^{ϕ}_{MX} could be approximated as a parameter that is independent of ionic strength but may vary with temperature and pressure. After testing two possible variants for the ionic-strength dependence of $B^{\phi}_{MX}(I)$, Pitzer (1973 [DIRS 152738]; 1991 [DIRS 152709]) chose the functional form:

$$B^{\phi}_{MX}(I) = \beta^{(0)}_{MX} + \beta^{(1)}_{MX}\cdot e^{-\alpha_1\sqrt{I}} + \beta^{(2)}_{MX}\cdot e^{-\alpha_2\sqrt{I}} \qquad \text{(Eq. I-12)}$$

The $\beta^{(2)}_{MX} \cdot e^{-\alpha_2\sqrt{I}}$ term is normally included only when modeling the thermodynamic properties of divalent metal sulfates and other high-valence electrolytes that exhibit significant association at low ionic strengths, but it is set equal to zero for strong electrolytes. The $\beta^{(0)}_{MX}$, $\beta^{(1)}_{MX}$, $\beta^{(2)}_{MX}$, and C^{ϕ}_{MX} coefficients are usually referred to as ion-interaction or Pitzer parameters. These Pitzer parameters may vary with temperature and pressure, but they do not depend on the ionic strength. The exponential coefficient α_1 is generally fixed at $\alpha_1 = 2.0$ for strong electrolytes, but for divalent metal sulfates and other 2:2 type electrolytes its value is usually fixed at $\alpha_1 = 1.4$ (Pitzer 1991 [DIRS 152709]). The value of α_2 for 2:2 type electrolytes is usually fixed at $\alpha_2 = 12.0$ at 25.0°C (298.15 K), but α_2 is either kept at this same value for all other temperatures or is assumed to vary with temperature as $\alpha_2 = k \cdot A_\phi$, where k is a constant (Pitzer 1991 [DIRS 152709]). By adjusting the α_1 parameter, Rard et al. (2004 [DIRS 173816]) and Rard and Wijesinghe (2005 [DIRS 176847]) optimized the parameter conversions for extended to the standard form of the Pitzer equations. This parameter adjustment improved the fit to experimental data and was considered for the updates in $NaNO_3$, $Mg(NO_3)_2$, and $Ca(NO_3)_2$ described in this report.

In terms of these ion-interaction parameters, the Pitzer equation for a binary electrolyte solution has the familiar form:

$$\phi = 1 - |z_M z_X| A_\phi \sqrt{I}/(1 + b\sqrt{I}) + \{2(\nu_M \nu_X)/\nu\} m \{\beta^{(0)}_{MX} + \beta^{(1)}_{MX} \cdot e^{-\alpha_1\sqrt{I}} + \beta^{(2)}_{MX} \cdot e^{-\alpha_2\sqrt{I}}\} + \{2(\nu_M \nu_X)^{3/2}/\nu\} m^2 \cdot C^{\phi}_{MX} \quad \text{(Eq. I–13)}$$

for the osmotic coefficient, where m denotes the stoichiometric molality of the solution. For the mean molal activity coefficient $\gamma_\pm$ of the electrolyte:

$$\ln \gamma_\pm = -|z_M z_X| A_\phi \{\sqrt{I}/(1 + b\sqrt{I}) + (2/b)\ln(1 + b\sqrt{I})\} + \{2(\nu_M \nu_X)/\nu\} m [2\beta^{(0)}_{MX} + 2\{\beta^{(1)}_{MX}/\alpha_1{}^2 I\}\{1 - (1 + \alpha_1\sqrt{I} - \alpha_1{}^2 I/2)e^{-\alpha_1\sqrt{I}}\} + 2\{\beta^{(2)}_{MX}/\alpha_2{}^2 I\}\{1 - (1 + \alpha_2\sqrt{I} - \alpha_2{}^2 I/2)e^{-\alpha_2\sqrt{I}}\}] + \{3(\nu_M \nu_X)^{3/2}/\nu\} m^2 \cdot C^{\phi}_{MX} \quad \text{(Eq. I-14)}$$

The corresponding expression for the excess Gibbs free energy is:

$$G^{EX}/(n_w RT) = -(4IA_\phi/b)\ln(1 + b\sqrt{I}) + (2\nu_M \nu_X) m^2 [\beta^{(0)}_{MX} + 2\{\beta^{(1)}_{MX}/\alpha_1{}^2 I\}\{1 - (1 + \alpha_1\sqrt{I})e^{-\alpha_1\sqrt{I}}\} + 2\{\beta^{(2)}_{MX}/\alpha_2{}^2 I\}\{1 - (1 + \alpha_2\sqrt{I})e^{-\alpha_2\sqrt{I}}\}] + (\nu_M z_M) m C_{MX} \quad \text{(Eq. I-15)}$$

where

$$C_{MX} = (C^{\phi}_{MX}/2\sqrt{|z_M z_X|}) \quad \text{(Eq. I-16)}$$

I.3.1.2 Pitzer's Model for Aqueous Electrolyte Mixtures

The corresponding Pitzer model equations for mixed electrolyte solutions of arbitrary complexity are more complicated, in part because they include mixing terms. For a system containing anions a and cations c (anions and cations chemically distinct from a and c are denoted with primes), the excess Gibbs free energy is given by:

$$G^{EX}/(w_w RT) = f^G(I) + 2\sum_c \sum_a m_c m_a [B_{ca} + (\sum_c m_c z_c) C_{ca}] + \sum_{c \neq c'} \sum m_c m_{c'} [2\Phi_{cc'} + \sum_a m_a \psi_{cc'a}] + \sum_{a \neq a'} \sum m_a m_{a'} [2\Phi_{aa'} + \sum_c m_c \psi_{caa'}] \quad \text{(Eq. I-17)}$$

where $f^G(I)$ was defined by equation (I–8), and C_{ca} is equivalent to C_{MX} defined by equation (I-16). The B_{ca} term is a function of the ion-interaction parameters and the ionic strength as given by:

$$B_{ca} = \beta_{ca}^{(0)} + 2\{\beta_{ca}^{(1)}/\alpha_1^2 I\}\{1 - (1 + \alpha_1\sqrt{I})e^{-\alpha_1\sqrt{I}}\} + 2\{\beta_{ca}^{(2)}/\alpha_2^2 I\}\{1 - (1 + \alpha_2\sqrt{I})e^{-\alpha_2\sqrt{I}}\} \quad \text{(Eq. I-18)}$$

The $\psi_{cc'a}$ and $\psi_{caa'}$ are mixing parameters for interactions among three distinct ions, two of which are of the same sign and the other of opposite sign, and the $\Phi_{cc'}$ and $\Phi_{aa'}$ are mixing functions for two different ions of the same sign. The $\Phi_{cc'}$ and $\Phi_{aa'}$ mixing functions will be described in more detail below.

The corresponding expression for the osmotic coefficient of the mixed electrolyte solutions of arbitrary complexity is given by (Pitzer 1991 [DIRS 152709]):

$$\phi = 1 - (2/\sum_i m_i)[-A_\phi I^{3/2}/(1 + b\sqrt{I}) + \sum_c \sum_a m_c m_a \{B_{ca}^\phi(I) + ZC_{ca}\} + \sum_{c \neq c'} \sum m_c m_{c'} [(\Phi_{cc'} + I\Phi_{cc'}') + \sum_a m_a \psi_{cc'a}] + \sum_{a \neq a'} \sum m_a m_{a'} [(\Phi_{aa'} + I\Phi_{aa'}') + \sum_c m_c \psi_{caa'}] \quad \text{(Eq. I-19)}$$

where

$$Z = \sum_i m_i |z_i| \quad \text{(Eq. I-20)}$$

is the total ionic molality. For a particular cation in this mixture, M, the ionic activity coefficient is given by:

$$\ln \gamma_M = z_M^2 F + \sum_a m_a (2B_{Ma} + ZC_{Ma}) + \sum_c m_c (2\Phi_{Mc} + \sum_a m_a \psi_{Mca}) + \sum_{a \neq a'} \sum m_a m_{a'} \psi_{Maa'} + z_M \sum_c \sum_a m_c m_a C_{ca} \quad \text{(Eq. I-21)}$$

and for a particular anion in this mixture, X, the ionic activity coefficient is given by:

$$\ln \gamma_X = z_X^2 F + \sum_c m_c(2B_{cX} + ZC_{cX}) + \sum_a m_a(2\Phi_{Xa} + \sum_c m_c\psi_{cXa})$$

$$+ \sum_{c \neq c'}\sum m_c m_{c'}\psi_{cc'X} + |z_X| \sum_c \sum_a m_c m_a C_c \qquad \text{(Eq. I-22)}$$

The quantity F that is present in both equations (Eq. I-21) and (Eq. I-22) includes the Debye-Hückel "osmotic" function $f^{\gamma}(I)$ along with several other terms:

$$F = f^{\gamma}(I) + \sum_c \sum_a m_c m_a B_{ca}' + \sum_{c \neq c'}\sum m_c m_{c'} \Phi_{cc'}' + \sum_{a \neq a'}\sum m_a m_{a'} \Phi_{aa'}' \qquad \text{(Eq. I-23)}$$

where $\Phi_{cc'}' = (\partial\Phi_{cc'}/\partial I)$, $\Phi_{aa'}' = (\partial\Phi_{aa'}/\partial I)$, and $B_{ca}' = (\partial B_{ca}/\partial I)$ are the ionic strength derivatives of the corresponding functions.

Equations I-17, I-19, and I-21 through I-23 contain the $\Phi_{cc'}$ and $\Phi_{aa'}$ and/or $\Phi_{cc'}'$ and $\Phi_{aa'}'$ mixing functions. For the ions *i* and *j* this function can be rewritten as:

$$\Phi_{ij} = {}^{S}\theta_{ij} + {}^{E}\theta_{ij}(I) \qquad \text{(Eq. I-24)}$$

The values of the high-order electrostatic function ${}^{E}\theta_{ij}(I)$ may be calculated from theory as described by Pitzer (1991 [DIRS 152709]). For ions of opposite charge, and for ions of the same sign and electrical charge, ${}^{E}\theta_{ij}(I) = 0$, the mixing function Φ_{ij} becomes equal to a simple (ionic strength independent) fitting parameter θ_{ij}. However, when the ions *i* and *j* are of the same sign but have different charges, then Equation I-24 should be used. Numerical analysis of integrals contributing to ${}^{E}\theta_{ij}(I)$ is discussed by Pitzer (1991 [DIRS 152709]). For further details, see *Software User's Manual, EQ3/6, Version 8.0* (SNL 2003 [DIRS 162494], Equations B–134 through B–147). The code EQ3/6 includes ${}^{E}\theta_{ij}(I)$ in the calculation of Φ_{ij} whenever appropriate.

According to Pitzer's model (Pitzer 1991 [DIRS 152709]), the thermodynamic properties of an electrolyte solution of arbitrary complexity may be represented using only the $\beta_{MX}^{(0)}$, $\beta_{MX}^{(1)}$, $\beta_{MX}^{(2)}$ (if needed), and C_{MX}^{ϕ} ion-interaction parameters for binary solutions, the two-ion ${}^{S}\theta_{MM'}$ and ${}^{S}\theta_{XX'}$ and the three-ion $\psi_{MM'X}$ and $\psi_{MXX'}$ mixing parameters. Within the framework of this model, the values of the mixing parameters are independent of the possible presence of other types of ions in solution, and once their values have been determined for a particular system, then the same values may be used with other systems. However, in a thermodynamically consistent database, it is essential that the same values of the mixing parameters be used for all systems containing those particular combinations of anions and cations.

I.3.1.3 Extension of Pitzer's Model to Include Dissolved Neutral Molecules

The equations given above apply to single electrolytes and to their mixtures. Neutral chemical species including dissolved gases such as O_2(aq), CO_2(aq), or NH_3(aq), and non-electrolytes such as SiO_2(aq), are often present at low concentrations in natural waters and brines. Pitzer's ion-interaction model can be modified to include the effects of neutral solutes, by adding terms arising from the interactions between different neutral species, terms for the interactions between neutral species and the cations, and terms for the interactions between neutral species and the

anions. For the excess Gibbs free energy, for example, Pitzer (1991 [DIRS 152709]) added interaction terms of the form $m_n m_c \lambda_{nc}$, $m_n m_a \lambda_{na}$, $m_n m_{n'} \lambda_{nn'}$, and $m_n^2 \lambda_{nn}$ for binary interactions, and terms of the form $m_n m_{n'} m_c \mu_{nn'c}$, $m_n m_{n'} m_a \mu_{nn'a}$, $m_n m_c m_a \mu_{nca}$, etc. for ternary interactions. Pitzer also defined two additional quantities, ζ_{nca} and $\eta_{ncc'}$, that are linear combinations of the μ_{ijk}. A detailed presentation of the equations for the interactions of neutral species and electrolytes is beyond the scope of this document, but detailed presentations are available in Appendix F of Pitzer's review (1991 [DIRS 152709]), in the article by Clegg and Brimblecombe (1990 [DIRS 159187]), and in *Software User's Manual, EQ3/6, Version 8.0* (SNL 2003 [DIRS 162494]).

I.3.1.4 Thermodynamic Data Used to Derive Parameters of Pitzer's Model

The ion-interaction parameters of Pitzer's model are empirical parameters. That is, they are obtained by fitting their values to best represent the experimental thermodynamic properties of aqueous electrolyte solutions. For most fairly soluble electrolytes, the types of thermodynamic data typically used to determine the Pitzer parameters are osmotic coefficients (generally obtained from isopiestic measurements), the emfs of reversible electrochemical cells, enthalpies of dilution, and heat capacities. Mixing parameters are frequently obtained for solutes of limited solubility by modeling the variation of solubility of that component with changes in the molalities of the other solutes. These less-soluble solutes include many important salts such as gypsum and calcite, $CaSO_4 \cdot 2H_2O(cr)$ and $CaCO_3(cr)$, and dissolved atmospheric gases such as $O_2(aq)$ and $CO_2(aq)$ that affect E_h and pH of solutions.

The Debye-Hückel limiting law slope used in Pitzer's model, A_ϕ, is that for the osmotic coefficient. Other authors sometimes present their equations in terms of the Debye-Hückel limiting law slope for activity coefficient, A_γ, where $A_\phi = A_\gamma/3$. Also, some values of A_γ reported in the literature may also differ by a factor of ln(10) = 2.302585, depending on whether the equations are written in terms of the natural logarithm of the activity coefficient or in terms of the decadic (base 10) logarithm of the activity coefficient. See Pitzer's (1973 [DIRS 152738] and 1991 [DIRS 152709]) works for a definition of A_ϕ in terms of fundamental constants and the properties of pure water.

I.3.2 TEMPERATURE FUNCTIONS FOR PITZER INTERACTION PARAMETERS

Extension of the Pitzer approach to temperatures above 25°C is necessary to expand its application to concentrated electrolyte solutions in many natural systems. The works of Møller (1988 [DIRS 152695]) and Greenberg and Møller (1989 [DIRS 152684]) exemplify such efforts by generating empirical functions that fit Pitzer interaction parameters as a function of both ionic strength (I) and temperature. Their approach utilizes a formulation containing eight fitting coefficients to describe the variations in the Pitzer interaction parameter as a function of temperature:

$$\chi(T) = a_1 + a_2 T + \frac{a_3}{T} + a_4 \ln T + \frac{a_5}{(T - 263)} + a_6 T^2 + \frac{a_7}{(680 - T)} + \frac{a_8}{(T - 227)} \qquad \text{(Eq. I-25)}$$

where χ represents any parameter of interest within the Pitzer model. Møller (1988 [DIRS 152695]) and Greenberg and Møller (1989 [DIRS 152684]) used "*P*" in their notation,

and T corresponds to the absolute temperature. a_1, a_2, a_3,…, a_8 are the coefficients used for fitting the temperature dependence of the parameter. Some parameters will generate relatively smooth curves with a very small number or no additional fitting coefficients. Therefore, not all seven or eight parameters will be needed. Sometimes a parameter will exhibit a different set of fitting terms between different temperature ranges, but this is rarely observed. When mixed electrolytes are modeled, then one must be cautious on how to approach the problem, checking always for internal consistency in the data being used and how it applies to the model.

Variations in Pitzer's equations have been developed to explain data for relatively simple experimental systems. These variations may include the use of non-customary values for the Pitzer alpha coefficients, addition of terms to temperature functions in order to fit data to very high temperatures, and including or excluding species such as ion pairs, complexes (along with their association constants) and partially dissociated acids. When combining results from these modified Pitzer models, these variations must be dealt with to obtain an internally consistent database.

Temperature functions have been developed to support the calculation of activity coefficients in geochemical models that are valid for the temperature ranges and chemical species considered. These will be compared with the functions used by Greenberg and Møller (1989 [DIRS 152684]) as well as with experimental data.

I.3.2.1 Models

All of the following models are suggested by the van't Hoff equation, the most common expression of which is (e.g., Garrels and Christ 1990 [DIRS 144877], Equation 9.100, p. 348):

$$\frac{\partial \ln K}{\partial T} = \frac{\Delta H_r^o}{RT^2} \qquad \text{(Eq. I-26)}$$

where K is an equilibrium constant, T is the absolute temperature, ΔH_r^o is the standard partial molar enthalpy of reaction, and R is the universal gas constant. This equation is often used as a basis for computing the temperature dependence of equilibrium constants. The general integrated form can be written as:

$$\ln K(T) = K(T_0) + \int_{T_0}^{T} \frac{\Delta H_r^0}{RT^2} dT \qquad \text{(Eq. I-27)}$$

where T_0 is normally 298.15K (25°C). As an example, the "constant enthalpy" approximation sometimes used in low-temperature geochemical modeling is given by:

$$\ln K(T) = \ln K(T_0) - \frac{\Delta H_r^0}{R}\left[\frac{1}{T} - \frac{1}{T_0}\right] \qquad \text{(Eq. I-28)}$$

More generally, it is recognized that ΔH_r^o is itself a function of temperature. A key relationship is:

$$\frac{\partial \Delta H_r^o}{\partial T} = \Delta C_{p,r}^o \quad \text{(Eq. I-29)}$$

where $\Delta C_{p,r}^o$ is the standard partial molar heat capacity (at constant pressure) of reaction. This in turn is given by:

$$\Delta C_{p,r}^o = \sum_i b_{ir} C_{p,i}^o \quad \text{(Eq. I-30)}$$

where the b_{ir} are reaction coefficients (defined as positive for products, negative for reactants) and $C_{p,i}^o$ is the standard molal heat capacity of the *i*th chemical species. Although the heat capacity of a species can be treated as a constant, usually it is represented by some temperature function, such as the Maier-Kelley formula (cf. Nordstrom and Munoz 1985 [DIRS 153965], p. 56) that is commonly applied to describe the heat capacities of solids:

$$C_{p,i}^o = a + bT - \frac{c}{T^2} \quad \text{(Eq. I-31)}$$

The van't Hoff relation can also be written as:

$$\frac{\partial (\Delta G_r^o / RT)}{\partial T} = \frac{-\Delta H_r^o}{RT^2} \quad \text{(Eq. I-32)}$$

(recall that $\Delta G_r^o = -RT \ln K$). A more general "van't Hoff" relationship is given by:

$$\frac{\partial (G / RT)}{\partial T} = \frac{-H}{RT^2} \quad \text{(Eq. I-33)}$$

where G is any type of Gibbs energy (for a reaction or a species, total, standard, ideal, or excess) and H is the corresponding enthalpy. Activity coefficients have a defining relationship with the excess Gibbs energy (cf. Pitzer 1973 [DIRS 152738]):

$$\ln \gamma_i = \frac{G_i^{EX}}{RT} \quad \text{(Eq. I-34)}$$

where γ_i is the activity coefficient of the *i*th chemical species and G_i^{EX} is the excess partial molar Gibbs energy of the same species (note that $G_i^{EX} = \partial G^{EX} / \partial n_i$, where G^{EX} is the excess Gibbs energy, and n_i is the number of moles of the *i*th species). The above two equations can be combined to yield:

$$\frac{\partial \ln \gamma_i}{\partial T} = \frac{-H_i^{EX}}{RT^2} \quad \text{(Eq. I-35)}$$

where H_i^{EX} is the excess partial molar enthalpy of the *i*th species. This equation can be viewed as the van't Hoff equation for activity coefficients.

In Pitzer's equations, $\ln\gamma_i$ depends on a series of terms that are linear with respect to the interaction coefficients. The dependence of the activity coefficient of an ion in solution on the second-order $\beta_{ij}^{(0)}$ parameter is expressed by:

$$\ln\gamma_i = \ldots + \beta_{ij}^{(0)} m_j + \ldots \quad \text{(Eq. I-36)}$$

(this parameter is second-order because in the equation for the total excess Gibbs energy of the solution, it appears multiplied by $m_i m_j$). This suggests the following van't Hoff equation for interaction parameters:

$$\frac{\partial\chi}{\partial T} = \frac{-\chi^{(H)}}{RT^2} \quad \text{(Eq. I-37)}$$

where χ is any interaction parameter (either second or third order; $\beta_{ij}^{(0)}$ $\beta_{ij}^{(1)}$, $\beta_{ij}^{(2)}$, C_{ijk}^{φ}, θ_{ij}, ψ_{ijk}, ζ_{ijn}, λ_{in}, or $\lambda_{nn'}$) and $\chi^{(H)}$ is the corresponding parameter appearing in the calculation of the excess partial molar enthalpy. It follows that:

$$\frac{\partial\chi^{(H)}}{\partial T} = \chi^{(C_p)} \quad \text{(Eq. I-38)}$$

where $\chi^{(C_p)}$ is the corresponding parameter appearing in the calculation of the excess partial molar heat capacity.

I.3.2.2 Constant Enthalpy

The simplest case is for the equivalent of constant enthalpy. Letting $b_1 = \chi^{(H)}$, one can write that:

$$\frac{\partial\chi}{\partial T} = \frac{-b_1}{RT^2} \quad \text{(Eq. I-39)}$$

Integration then yields:

$$\chi = b_0 + \frac{b_1}{R}\left[\frac{1}{T} - \frac{1}{T_0}\right] \quad \text{(Eq. I-40)}$$

where $b_0 = \chi(T_0)$. This can also be written as:

$$\chi = a_0 + \frac{a_1}{T} \quad \text{(Eq. I-41)}$$

where

$$a_0 = b_0 - \frac{b_1}{RT_0} \quad \text{(Eq. I-42)}$$

$$a_1 = \frac{b_1}{R} \quad \text{(Eq. I-43)}$$

Comparison of Equation I-41 with Equation I-25 shows that the former is a subset of the latter (allowing for a different system of numbering the coefficients). This suggests that the constant and $1/T$ terms in Equation I-25 are likely the most important, in terms of having a physical basis.

I.3.2.3 Constant Heat Capacity

Here one begins by writing $b_2 = \chi^{(C_p)}$. The first integration yields:

$$\chi^{(H)} = b_1 + b_2\left(T - T_0\right) \quad \text{(Eq. I-44)}$$

where $b_1 = \chi^{(H)}(T_0)$. The second integration, this time using the "van't Hoff relation," gives:

$$\chi = b_0 + \frac{\left(b_1 - b_2 T_0\right)}{R}\left[\frac{1}{T} - \frac{1}{T_0}\right] - \frac{b_2}{R}\left(\ln T - \ln T_0\right) \quad \text{(Eq. I-45)}$$

where once more $b_0 = \chi(T_0)$. This can also be written as:

$$\chi = a_0 + \frac{a_1}{T} + a_2 \ln T \quad \text{(Eq. I-46)}$$

where

$$a_0 = b_0 + \frac{b_2}{R} - \frac{b_1}{RT_0} + \frac{b_2}{R}\ln T_0 \quad \text{(Eq. I-47)}$$

$$a_1 = \frac{b_1 - b_2 T_0}{R} \quad \text{(Eq. I-48)}$$

$$a_2 = -\frac{b_2}{R} \quad \text{(Eq. I-49)}$$

Comparison of Equation I-46 with Equation I-25 will show that the former, like Equation I-41, is a subset of the latter (again allowing for a different system of numbering the coefficients). What this suggests is that after the constant and $1/T$ terms in Equation I-25, the term in ln T is likely the most important term with respect to having a physical basis.

I.3.2.4 Parabolic Heat Capacity

The standard partial molar heat capacity of aqueous electrolytes does not closely follow the Maier-Kelley form commonly exhibited by solids. Rather, it is described by temperature functions that appear parabolic, at least to a first order (cf. Helgeson et al. 1981 [DIRS 106024], pp. 1413 to 1426). Here it is assumed that $\chi^{(C_p)}$ will behave in a similar fashion. One may then write:

$$\chi^{(C_p)} = b_2 + b_3\left(T - T_x\right)^2 \qquad \text{(Eq. I-50)}$$

where $b_2 = \chi^{(C_p)}(T_0)$ and T_x is some temperature that may be unique for each distinct Pitzer interaction parameter. If that is so, then in effect a five-parameter model is obtained. Differentiation gives:

$$\frac{d\chi^{(C_p)}}{dT} = 2b_3\left(T - T_x\right) \qquad \text{(Eq. I-51)}$$

The extremis of the parabola occurs where this derivative is zero: that is, where $T = T_x$. Another step of differentiation gives:

$$\frac{d^2\chi^{(C_p)}}{dT^2} = 2b_3 \qquad \text{(Eq. I-52)}$$

The parabola will be convex up (the extremis will be a maximum) if b_3 is negative. Otherwise, it will be convex down (the extremis will be a minimum). Actual examples of the standard partial molar heat capacity of aqueous electrolytes are convex up, and the maximum of curves that visually resemble parabolas occurs at various different values of T (cf. Helgeson et al. 1981 [DIRS 106024], pp. 1413 to 1424). Thus, b_3 is expected to be a negative number.

The first integration yields:

$$\chi^{(H)} = b_1 + b_2\left(T - T_0\right) + b_3\left(\frac{\left(T^3 - T_0^3\right)}{3} - T_x\left(T^2 - T_0^2\right) + T_x^2\left(T - T_0\right)\right) \qquad \text{(Eq. I-53)}$$

where again $b_1 = \chi^{(H)}\left(T_0\right)$. Before continuing, it is convenient to rearrange this into terms organized by power of T:

$$\chi^{(H)} = \left[b_1 - b_2T_0 - b_3\left(T_x^2T_0 - T_xT_0^2 + \frac{T_0^3}{3}\right)\right] + \left[b_2 + b_3T_x^2\right]T - \left[b_3T_x\right]T^2 + \left[\frac{b_3}{3}\right]T^3 \qquad \text{(Eq. I-54)}$$

More simply, this can be written as:

$$\chi^{(H)} = c_1 + c_2T + c_3T^2 + c_4T^3 \qquad \text{(Eq. I-55)}$$

where c_1, c_2, c_3, and c_4 are given by the corresponding quantities in squared brackets in Equation I-54. The second integration, performed after substituting Equation I-55 into the "van't Hoff" relation, gives:

$$\chi = c_0 + \frac{c_1}{R}\left(\frac{1}{T} - \frac{1}{T_0}\right) - \frac{c_2}{R}\left(\ln T - \ln T_0\right) - \frac{c_3}{R}\left(T - T_0\right) - \frac{c_4}{2R}\left(T^2 - T_0^2\right) \qquad \text{(Eq. I-56)}$$

where $c_0 = \chi(T_0)$; in order to complete the relationships between the b and c coefficients, one may take that $c_0 = b_0$. Rearranging Equation I–56 into terms organized by power of T gives:

$$\chi = \left[c_0 - \frac{c_1}{RT_0} + \frac{c_2}{R}\ln T_0 + \frac{c_3}{R}T_0 + \frac{c_4}{2R}T_0^2\right] + \left[\frac{c_1}{R}\right]\frac{1}{T} + \left[\frac{-c_2}{R}\right]\ln T + \left[\frac{-c_3}{R}\right]T + \left[\frac{-c_4}{2R}\right]T^2 \qquad \text{(Eq. I-57)}$$

This can be written more simply as:

$$\chi = a_0 + \frac{a_1}{T} + a_2 \ln T + a_3 T + a_4 T^2 \qquad \text{(Eq. I-58)}$$

where a_0, a_1, a_2, a_3, and a_4 are given by the corresponding quantities in square brackets in Equation I-57. Equation I-58 as implemented in EQ3/6 v8.0 only takes into account up to the a_3 coefficient term. Also, the increasing order of coefficients is shifted by one as defined in the data0.ypf.R2 database (Output DTN: SN0609T0502404.012). That is, a_0 in Equation I-58 equals a_1 in the data.ypf.R2 database and so on. The T^2 term in Equation I-58 is not used in the data0.ypf.R2 database.

The additional terms in T and T^2 are also present in Equation I-25. The presence of T_x in the equation for the heat capacity interaction parameter has resulted in a five- rather than a four-parameter model, though T_x itself does not appear explicitly in the final result as represented by Equation I-58.

Note that the addition of a term linear in T to the equation for $\chi^{(C_p)}$ would not result in an additional term in the equivalent of Equation I-58. Adding such a term to Equation I-50 gives:

$$\chi^{(C_p)} = b_2 + b_3\left(T - T_x\right)^2 + b_4 T \qquad \text{(Eq. I-59)}$$

This would add a term in T^2 in the corresponding equation for $\chi^{(H)}$. Substitution of that result into the "van't Hoff" relation would just add to the constant term under the integral. After integration, this would result in additional contributions to a_0 and a_3 in Equation I-58, but no new term. Similarly, adding a term in T^2 to the equation for $\chi^{(C_p)}$ would result in no new term in the equivalent of Equation I-58.

I.3.2.5 Other Comments on Existing Temperature Functions

Recall that Equation I-25 is:

$$\chi(T) = a_1 + a_2 T + \frac{a_3}{T} + a_4 \ln T + \frac{a_5}{(T - 263)} + a_6 T^2 + \frac{a_7}{(680 - T)} + \frac{a_8}{(T - 227)}$$

The terms not suggested by the theoretical analysis given above are the fifth, seventh, and eighth. Each of these terms has the difference between T and some constant in the denominator, and thus a singularity. These occur at –10.15°C, 406.85°C, and –46.15°C, respectively. The fifth and seventh terms trace back to Rogers and Pitzer (1981 [DIRS 162107]). They have no theoretical origin, but were introduced as empirical devices to assist in fitting data for the system Na_2SO_4-H_2O over a wide range of temperatures. The eighth term is from Pitzer et al. (1984 [DIRS 162099]), who used it to fit data for the system NaCl-H_2O over a very wide temperature range. Again, the origin of the term was purely empirical. The singularity at 406.85°C (680 K) is well above the critical temperature of water.

Spencer et al.(1990 [DIRS 152713]) developed a model for the system Na-K-Ca-Mg-Cl-SO_4-H_2O for the temperature range –60°C to +25°C. They recognized the above-noted singularities (two of which were in their target range) and eliminated them by using a function of the form:

$$\chi(T) = a_1 + a_2 T + \frac{a_3}{T} + a_4 \ln T + a_6 T^2 + a_9 T^3 \qquad \text{(Eq. I-60)}$$

All but one of the terms in this equation carry forward from Equation I-25. The origin of the new term in T^3 is obscure. Spencer et al. (1990 [DIRS 152713]) do not discuss it, nor do they discuss the consequences of not including this term. They do use the new term universally in their model, applying it not only to Pitzer interaction coefficients, but also to the A^{φ} Debye-Hückel parameter and the dimensionless standard chemical potentials (μ^o/RT) of both aqueous species and minerals. This term would imply a term in T^2 in the equation for $\chi^{(H)}$ and one in T^3 in the equation for $\chi^{(C_p)}$.

I.4 EVALUATION, COMPILATION, AND CONVERSION OF PITZER INTERACTION PARAMETERS FROM PUBLISHED SOURCES

As part of the current effort to develop an internally consistent thermodynamic Pitzer parameter database for EQ3/6 v8.0, an extensive search for Pitzer interaction parameters and experimental data from the scientific literature was undertaken for ionic species of interest to the YMP. Because operating temperatures in the repository are expected to rise substantially above the boiling temperature of water, the primary focus of the work was on developing the Pitzer parameter database to higher temperatures up to 250°C. Unfortunately, high-temperature Pitzer parameter data are not available in the literature for all of the required chemical species, so that the data for certain ionic species included in the database are limited to lower temperature ranges. Some parameter data only applicable at 25°C are included in the database to extend the usefulness of the database to species that do not have high-temperature data but, nevertheless, are of interest to the YMP. A difficulty in the compilation of Pitzer binary and ternary parameters is

that some data at elevated temperatures and pressures are reported from variants and extensions of the original Pitzer formulations (Rard and Clegg 1997 [DIRS 152759]; Sterner et al. 1998 [DIRS 162116]; Archer 2000 [DIRS 162065]; Oakes et al. 2000 [DIRS 162102]; Rard et al. 2000 [DIRS 162105]) that are potentially more accurate than the standard Pitzer model, but which cannot be used directly with the standard Pitzer model.

Different authors have used different functions of temperature for the fitting of parameters to experimental data (see Section I.3.2). These different schemes make only minor differences in the goodness of fit, as stated by some of the authors themselves, and are documented for individual binary and ternary parameters in Sections I.4.4 through I.4.6. For the purposes of this report these refinements of the fits are unimportant. This is true even in the case of the ternary parameters (Section I.4.5), in which the percentage changes between one author and another are large, because the ternary interactions make only minor contributions to the calculation of the osmotic coefficients and activity coefficients. To develop an integrated database that encompasses the widest possible selection of ionic species with the smallest number of temperature coefficients, it is necessary to have a rational, thermodynamically motivated basis for selecting these temperature functions. To accomplish this, a comprehensive examination of the published Pitzer parameter data was undertaken to assess the accuracy and validity of the data and the associated temperature functions for each electrolyte of interest for a wide range of temperatures and ionic strength. On the basis of this assessment, a standard form of the temperature functions was developed. The standard Pitzer parameters for each electrolyte are either refitted in this standard form of the temperature functions, or nonstandard Pitzer model parameters are first converted to standard Pitzer model parameters and are then fitted to the standard form of the temperature functions. This last step requires refitting of the source Pitzer parameters to the temperature functions represented by a 4-parameter form of Equation I-58 that includes the constant, linear, inverse and logarithmic terms, but excludes the quadratic term.

To compile, analyze, validate, refit, and convert Pitzer parameters to a form usable by EQ3/6 v8.0, Microsoft Excel 2000 spreadsheets (see Tables I-1 and I-2) were developed. The temperature function fitting method and the conversion method documented in Rard and Wijesinghe (2003 [DIRS 162327]) are incorporated in most of the spreadsheets and are explained in subsequent sections. Most of the spreadsheets are used to refit standard Pitzer parameters without conversion from an extended Pitzer model. These spreadsheets are named "FitPitzerNC_Type_IonicSpecies.xls." A second type of spreadsheet involves the conversion of parameters from an extended Pitzer model to the parameters of the standard Pitzer model, followed by fitting new temperature functions of the standard form. This spreadsheet, named "ConPitzerNC_MX_(NH4)2SO4.xls," was prepared only for the electrolyte, for which source models were not available in the standard Pitzer form ($(NH_4)_2SO_4$). The Pitzer data defined in the *ConPitzerNC_MX_(NH4)2SO4.xls* spreadsheet is for a binary cation-anion parameters only. The spreadsheets named "FitPitzerNC_Int_Param_CFJC.xls" do not use the "FitPitzerNC" methodology but refit parameters using the regression tool in Excel (see Tables I-1 and I-2). In all spreadsheets, error analyses including parameter and osmotic coefficient plots, root mean square (RMS) errors, and Excel regression statistics are given in the "FitPitzer" and "Result Summary" worksheets or below the "SUMMARY OUTPUT" title within each worksheet. The "Int_Param" part of the spreadsheet name refers to the type of binary or ternary parameters consistent with the notation given by:

MX = Cation(M)-Anion(X) binary system parameters $\beta^{(0)}_{MX}$, $\beta^{(1)}_{MX}$, $\beta^{(2)}_{MX}$, C^{ϕ}_{MX}

MM = Cation(M1)-Cation(M2) ternary system parameter θ_{M1M2}

XX = Anion(X1)-Anion(X2) ternary system parameter θ_{X1X2}

MMX = Cation(M1)-Cation(M2)-Anion(X) ternary system parameter ψ_{M1M2X}

MXX = Cation(M)-Anion(X1)-Anion(X2) ternary system parameter ψ_{MX1X2}

NM = Neutral (N)-Cation (M) ternary system parameter λ_{NM}

NX = Neutral (N)-Anion (X) ternary system parameter λ_{NX}

NMX = Neutral (N)-Cation (M) -Anion (X) ternary system parameter ζ_{NMX}.

Only functions intrinsic to Excel were used in the calculations. The following sections describe the theoretical foundations of the Pitzer parameter fitting/conversion approaches mentioned above. Tables I-1 and I-2 summarize the types of parameters compiled for specific ions and the original sources of Pitzer parameter data.

The Debye-Hückel A_{φ} parameter, which depends on the electrostatic properties of pure liquid water, is an intrinsic part of any Pitzer model. This parameter is also treated by the use of a temperature function. The representation used in the IDPS model is based on that given by Greenberg and Møller (1989 [DIRS 152684]). However, the data were refitted to a different temperature function, the same one used in the IDPS model for the Pitzer interaction coefficients. This refitting of A_{φ} was done in *FitPitzerNC_MX_NaCl.xls* (first row of Table I-1). This refitting is repeated in analogous binary coefficient refitting spreadsheets (because the functionality was built into the template, not because it was necessary).

Table I-1. Catalog of Pitzer Ion-Interaction Parameter Spreadsheets

Ion Group	Spreadsheet File Name	Original Data Source	Type	T Range (°C)
Na_Cl	*FitPitzerNC_MX_NaCl.xls*	Greenberg and Møller 1989 [DIRS 152684]	MX	0–250
K_Cl	*FitPitzerNC_MX_KCl.xls*	Greenberg and Møller 1989 [DIRS 152684]	MX	0–250
Na_Br	*FitPitzerNC_MX_NaBr.xls*	Holmes and Mesmer 1998 [DIRS 162083]	MX	0–250
K_Br	*FitPitzerNC_MX_KBr.xls*	Holmes and Mesmer 1998 [DIRS 162083]	MX	0–250
Li_Cl	*FitPitzerNC_MX_LiCl.xls*	Holmes and Mesmer 1983 [DIRS 162073]	MX	0–250
Li_Br	*FitPitzerNC_MX_LiBr.xls*	Holmes and Mesmer 1998 [DIRS 162083]	MX	0–250
Cs_Cl	*FitPitzerNC_MX_CsCl.xls*	Holmes and Mesmer 1983 [DIRS 162073]	MX	0–250
Cs_Br	*FitPitzerNC_MX_CsBr.xls*	Holmes and Mesmer 1998 [DIRS 162083]	MX	0–250
Na_SO4	*FitPitzerNC_MX_Na2SO4.xls*	Greenberg and Møller 1989 [DIRS 152684]	MX	0–250
K_SO4	*FitPitzerNC_MX_K2SO4.xls*	Greenberg and Møller 1989 [DIRS 152684]	MX	0–250
Ca_SO4	*FitPitzerNC_MX_CaSO4.xls*	Greenberg and Møller 1989 [DIRS 152684]	MX	0–250
Mg_SO4	*FitPitzerNC_MX_MgSO4.xls*	Pabalan and Pitzer 1987 [DIRS 162096]	MX	0–250
Na_CO3	*FitPitzerNC_MX_Na2CO3.xls*	He and Morse 1993 [DIRS 162090]	MX	0–90
Ca_Cl	*FitPitzerNC_MX_CaCl_CFJC_Model3_Sterner_et_al_1998.xls*	Sterner et al. 1998 [DIRS 162116]	MX	0–250
CaCl_Cl	*FitPitzerNC_MX_CaCl_CFJC_Model3_Sterner_et_al_1998.xls*	Sterner et al. 1998 [DIRS 162116]	MX	0–250
Mg_Cl	*FitPitzerNC_MX_MgCl2.xls*	Pabalan and Pitzer 1987 [DIRS 162096]	MX	0–250
Na_HSO4	*FitPitzerNC_MX_NaHSO4.xls*	Holmes and Mesmer 1994 [DIRS 162078]	MX	25–220
Na_HCO3	*FitPitzerNC_MX_NaHCO3.xls*	He and Morse 1993 [DIRS 162090]	MX	0–90
Na_AlO2	*FitPitzerNC_MX_Na_AlO2.xls*[a]	Felmy et al. 1994 [DIRS 162112]	MX	0–250
Na_OH	*FitPitzerNC_MX_NaOH.xls*	Pabalan and Pitzer 1987 [DIRS 162147]	MX	0–250
H_SO4	*FitPitzerNC_MX_H2SO4.xls*	Holmes and Mesmer 1994 [DIRS 162078]	MX	25–200
H_HSO4	*FitPitzerNC_MX_HHSO4.xls*	Holmes and Mesmer 1994 [DIRS 162078]	MX	25–200
H_Cl	*FitPitzerNC_MX_HCl.xls*	Holmes et al. 1987 [DIRS 162075]	MX	0–250
Na_NO3	*FitPitzerNC_MX_NaNO3_CFJC.xls*	Wijesinghe and Rard 2005 [DIRS 176847]	MX	0–150

Table I-1. Catalog of Pitzer Ion-Interaction Parameter Spreadsheets (Continued)

Ion Group	Spreadsheet File Name	Original Data Source	Type	T Range (°C)
H_NO3	*FitPitzerNC_MX_H_NO3_CFJC.xls*[a]	Felmy et al. 1994 [DIRS 162111]; Clegg and Brimblecombe 1990 [DIRS 162067]	MX	25–100
Ca_NO3	*FitPitzerNC_MX_Ca(NO3)2_CFJC.xls*	Wijesinghe and Rard 2005 [DIRS 176847]	MX	25–150
NH4_SO4	*ConPitzerNC_MX_(NH4)2SO4.xls*	Clegg et al. 1996 [DIRS 162068]	MX	0–250
NH4_Cl	*FitPitzerNC_MX_NH4Cl.xls*	Thiessen and Simonson 1990 [DIRS 162108]	MX	25–250
Na_K	*FitPitzerNC_MM_Na_K.xls*	Greenberg and Møller 1989 [DIRS 152684]	MM	0–250
Na_Ca	*FitPitzerNC_MM_Na_Ca.xls*	Greenberg and Møller 1989 [DIRS 152684]	MM	0–250[b]
CaCl2(aq)_CaCl2(aq)	*FitPitzerNC_MX_CaCl_CFJC_Model3_Sterner_et_al_1998.xls*	Sterner et al. 1998 [DIRS 162116]	NX	0–250
K_Ca	*FitPitzerNC_MM_K_Ca.xls*	Greenberg and Møller 1989 [DIRS 152684]	MM	0–250[b]
Cl_SO4	*FitPitzerNC_XX_Cl_SO4.xls*	Greenberg and Møller 1989 [DIRS 152684]	XX	0–250[c]
HSO4_SO4	*FitPitzerNC_XX_HSO4_SO4.xls*	Holmes and Mesmer 1994 [DIRS 162078]	XX	25–200
Na_K_Cl	*FitPitzerNC_MMX_Na_K_Cl.xls*	Greenberg and Møller 1989 [DIRS 152684]	MMX	0–250
Na_K_SO4	*FitPitzerNC_MMX_Na_K_SO4.xls*	Greenberg and Møller 1989 [DIRS 152684]	MMX	0–250
Na_Ca_Cl	*FitPitzerNC_MMX_Na_Ca_Cl.xls*	Greenberg and Møller 1989 [DIRS 152684]	MMX	0–250[b]
Na_Ca_SO4	*FitPitzerNC_MMX_Na_Ca_SO4.xls*	Greenberg and Møller 1989 [DIRS 152684]	MMX	0–250[b]
K_Ca_Cl	*FitPitzerNC_MMX_K_Ca_Cl.xls*	Greenberg and Møller 1989 [DIRS 152684]	MMX	0–250
Na_Cl_SO4	*FitPitzerNC_MXX_Na_Cl_SO4.xls*	Greenberg and Møller 1989 [DIRS 152684]	MXX	0–250[c]
K_Cl_SO4	*FitPitzerNC_MXX_K_Cl_SO4.xls*	Greenberg and Møller 1989 [DIRS 152684]	MXX	0–250
Ca_Cl_SO4	*FitPitzerNC_MXX_Ca_Cl_SO4.xls*	Greenberg and Møller 1989 [DIRS 152684]	MXX	0–250[b]
H_HSO4_SO4	*FitPitzerNC_MXX_H_HSO4_SO4.xls*	Holmes and Mesmer 1994 [DIRS 162078]	MXX	25–200
Na_HSO4_SO4	*FitPitzerNC_MXX_Na_HSO4_SO4.xls*	Holmes and Mesmer 1994 [DIRS 162078]	MXX	25–225
CO2_Ca	F*itPitzerMX_Ca-HCO3_NMX_CO2_CFJC3.xls*[a]	Corti et al. 1990 [DIRS 178211]	NM	0–250
CO2_K	*FitPitzerMX_Ca-HCO3_NMX_CO2_CFJC3.xls*[a] (Same as CO2_Na)	Corti et al. 1990 [DIRS 178211]	NM	0–250
CO2_Mg	*FitPitzerMX_Ca-HCO3_NMX_CO2_CFJC3.xls*[a]	Corti et al. 1990 [DIRS 178211]	NM	0–250
CO2_Na	*FitPitzerMX_Ca-HCO3_NMX_CO2_CFJC3.xls*[a]	Corti et al. 1990 [DIRS 178211]	NM	0–250

Table I-1. Catalog of Pitzer Ion-Interaction Parameter Spreadsheets (Continued)

Ion Group	Spreadsheet File Name	Original Data Source	Type	T Range (°C)
CO2_H	No Spreadsheet	Conventionally defined as zero in Corti et al. 1990 [DIRS 178211]	NM	0–250
CO2_Cl	*FitPitzerMX_Ca-HCO3_NMX_CO2_CFJC3.xls*[a]	Corti et al. 1990 [DIRS 178211]	NX	0–250
CO2_SO4	*FitPitzerMX_Ca-HCO3_NMX_CO2_CFJC3.xls*[a]	Rumpf and Maurer 1993 [DIRS 178223]	NX	0–250
CO2_Na_Cl	*FitPitzerMX_Ca-HCO3_NMX_CO2_CFJC3.xls*[a]	Corti et al. 1990 [DIRS 178211]	NMX	0–250
CO2_Na_SO4	*FitPitzerMX_Ca-HCO3_NMX_CO2_CFJC3.xls*[a]	Corti et al. 1990 [DIRS 178211]	NMX	0–250
O2_Al	*FitPitzerNC_lambdas_zetas_O2_CFJC.xls*[a]	Clegg and Brimblecombe 1990 [DIRS 162089]	NM	25–100
O2_Ba	*FitPitzerNC_lambdas_zetas_O2_CFJC.xls*[a]	Clegg and Brimblecombe 1990 [DIRS 162089]	NM	25–100
O2_Ca	*FitPitzerNC_lambdas_zetas_O2_CFJC.xls*[a]	Clegg and Brimblecombe 1990 [DIRS 162089]	NM	25–100
O2_H	*FitPitzerNC_lambdas_zetas_O2_CFJC.xls*[a]	Clegg and Brimblecombe 1990 [DIRS 162089]	NM	25–100
O2_K	*FitPitzerNC_lambdas_zetas_O2_CFJC.xls*[a]	Clegg and Brimblecombe 1990 [DIRS 162089]	NM	25–100
O2_Li	*FitPitzerNC_lambdas_zetas_O2_CFJC.xls*[a]	Clegg and Brimblecombe 1990 [DIRS 162089]	NM	25–100
O2_Mg	*FitPitzerNC_lambdas_zetas_O2_CFJC.xls*[a]	Clegg and Brimblecombe 1990 [DIRS 162089]	NM	25–100
O2_Na	*FitPitzerNC_lambdas_zetas_O2_CFJC.xls*[a]	Clegg and Brimblecombe 1990 [DIRS 162089]	NM	25–100
O2_NH4	*FitPitzerNC_lambdas_zetas_O2_CFJC.xls*[a]	Clegg and Brimblecombe 1990 [DIRS 162089]	NM	25–100
O2_Cl	*FitPitzerNC_lambdas_zetas_O2_CFJC.xls*[a]	Clegg and Brimblecombe 1990 [DIRS 162089]	NX	25–100
O2_Br	*FitPitzerNC_lambdas_zetas_O2_CFJC.xls*[a]	Clegg and Brimblecombe 1990 [DIRS 162089]	NX	25–100
O2_CO3	*FitPitzerNC_lambdas_zetas_O2_CFJC.xls*[a]	Clegg and Brimblecombe 1990 [DIRS 162089]	NX	25–100
O2_HCO3	*FitPitzerNC_lambdas_zetas_O2_CFJC.xls*[a]	Clegg and Brimblecombe 1990 [DIRS 162089]	NX	25–100
O2_I	*FitPitzerNC_lambdas_zetas_O2_CFJC.xls*[a]	Clegg and Brimblecombe 1990 [DIRS 162089]	NX	25–100
O2_NO3	*FitPitzerNC_lambdas_zetas_O2_CFJC.xls*[a]	Clegg and Brimblecombe 1990 [DIRS 162089]	NX	25–100
O2_OH	*FitPitzerNC_lambdas_zetas_O2_CFJC.xls*[a]	Clegg and Brimblecombe 1990 [DIRS 162089]	NX	25–100
O2_SO4	*FitPitzerNC_lambdas_zetas_O2_CFJC.xls*[a]	Clegg and Brimblecombe 1990 [DIRS 162089]	NX	25–100
O2_Na_Cl	*FitPitzerNC_lambdas_zetas_O2_CFJC.xls*[a]	Clegg and Brimblecombe 1990 [DIRS 162089]	NMX	25–100
O2_Na_Br	*FitPitzerNC_lambdas_zetas_O2_CFJC.xls*[a]	Clegg and Brimblecombe 1990 [DIRS 162089]	NMX	25–100
O2_Na_NO3	*FitPitzerNC_lambdas_zetas_O2_CFJC.xls*[a]	Clegg and Brimblecombe 1990 [DIRS 162089]	NMX	25–100

Table I-1. Catalog of Pitzer Ion-Interaction Parameter Spreadsheets (Continued)

Ion Group	Spreadsheet File Name	Original Data Source	Type	T Range (°C)
O2_Na_OH	*FitPitzerNC_lambdas_zetas_O2_CFJC.xls*[a]	Clegg and Brimblecombe 1990 [DIRS 162089]	NMX	25–100
O2_Na_SO4	*FitPitzerNC_lambdas_zetas_O2_CFJC.xls*[a]	Clegg and Brimblecombe 1990 [DIRS 162089]	NMX	25–100
O2_K_Cl	*FitPitzerNC_lambdas_zetas_O2_CFJC.xls*[a]	Clegg and Brimblecombe 1990 [DIRS 162089]	NMX	25–100
O2_K_Br	*FitPitzerNC_lambdas_zetas_O2_CFJC.xls*[a]	Clegg and Brimblecombe 1990 [DIRS 162089]	NMX	25–100
O2_K_OH	*FitPitzerNC_lambdas_zetas_O2_CFJC.xls*[a]	Clegg and Brimblecombe 1990 [DIRS 162089]	NMX	25–100
O2_K_NO3	*FitPitzerNC_lambdas_zetas_O2_CFJC.xls*[a]	Clegg and Brimblecombe 1990 [DIRS 162089]	NMX	25–100
O2_K_SO4	*FitPitzerNC_lambdas_zetas_O2_CFJC.xls*[a]	Clegg and Brimblecombe 1990 [DIRS 162089]	NMX	25–100
O2_Mg_Cl	*FitPitzerNC_lambdas_zetas_O2_CFJC.xls*[a]	Clegg and Brimblecombe 1990 [DIRS 162089]	NMX	25–100
O2_Mg_SO4	*FitPitzerNC_lambdas_zetas_O2_CFJC.xls*[a]	Clegg and Brimblecombe 1990 [DIRS 162089]	NMX	25–100
O2_Ca_Cl	*FitPitzerNC_lambdas_zetas_O2_CFJC.xls*[a]	Clegg and Brimblecombe 1990 [DIRS 162089]	NMX	25–100
O2_Ca_NO3	*FitPitzerNC_lambdas_zetas_O2_CFJC.xls*[a]	Clegg and Brimblecombe 1990 [DIRS 162089]	NMX	25–100
O2_Al_Cl	*FitPitzerNC_lambdas_zetas_O2_CFJC.xls*[a]	Clegg and Brimblecombe 1990 [DIRS 162089]	NMX	25–100
O2_Al_SO4	*FitPitzerNC_lambdas_zetas_O2_CFJC.xls*[a]	Clegg and Brimblecombe 1990 [DIRS 162089]	NMX	25–100
O2_H_Cl	*FitPitzerNC_lambdas_zetas_O2_CFJC.xls*[a]	Clegg and Brimblecombe 1990 [DIRS 162089]	NMX	25–100
O2_Li_Cl	*FitPitzerNC_lambdas_zetas_O2_CFJC.xls*[a]	Clegg and Brimblecombe 1990 [DIRS 162089]	NMX	25–100
O2_Na_HCO3	*FitPitzerNC_lambdas_zetas_O2_CFJC.xls*[a]	Clegg and Brimblecombe 1990 [DIRS 162089]	NMX	25–100
O2_Na_CO3	*FitPitzerNC_lambdas_zetas_O2_CFJC.xls*[a]	Clegg and Brimblecombe 1990 [DIRS 162089]	NMX	25–100
O2_K_I	*FitPitzerNC_lambdas_zetas_O2_CFJC.xls*[a]	Clegg and Brimblecombe 1990 [DIRS 162089]	NMX	25–100
O2_NH4_SO4	*FitPitzerNC_lambdas_zetas_O2_CFJC.xls*[a]	Clegg and Brimblecombe 1990 [DIRS 162089]	NMX	25–100
O2_Ba_Cl	*FitPitzerNC_lambdas_zetas_O2_CFJC.xls*[a]	Clegg and Brimblecombe 1990 [DIRS 162089]	NMX	25–100
SiO2_H	*Pitzer_NMX_SiO2.xls*[a]	Felmy et al. 1994 [DIRS 162111]	NM	25–100
SiO2_Mg	*Pitzer_NMX_SiO2.xls*[a]	Felmy et al. 1994 [DIRS 162111]	NM	25–100
SiO2_Na	*Pitzer_NMX_SiO2.xls*[a]	Felmy et al. 1994 [DIRS 162111]	NM	25–100
SiO2_Cl	*Pitzer_NMX_SiO2.xls*[a]	Felmy et al. 1994 [DIRS 162111]	NX	25–100
SiO2_NO3	*Pitzer_NMX_SiO2.xls*[a]	Felmy et al. 1994 [DIRS 162111]	NX	25–100
SiO2_SO4	*Pitzer_NMX_SiO2.xls*[a]	Felmy et al. 1994 [DIRS 162111]	NX	25–100
SiO2_H_NO3	*Pitzer_NMX_SiO2.xls*[a]	Felmy et al. 1994 [DIRS 162111]	NMX	25–100

Table I-1. Catalog of Pitzer Ion-Interaction Parameter Spreadsheets (Continued)

Ion Group	Spreadsheet File Name	Original Data Source	Type	T Range (°C)
SiO2_Mg_Cl	*Pitzer_NMX_SiO2.xls*[a]	Felmy et al. 1994 [DIRS 162111]	NMX	25–100
SiO2_Na_Cl	*Pitzer_NMX_SiO2.xls*[a]	Felmy et al. 1994 [DIRS 162111]	NMX	25–100
Na_AlO2_NO3	No Spreadsheet	Felmy et al. 1994 [DIRS 162111]	MXX	0–250
Na_AlO2_OH	No Spreadsheet	Felmy et al. 1994 [DIRS 162111]	MXX	0–250
Na_Cl_OH	*Pabalan_icf_TJW.xls*	Pabalan and Pitzer 1987 [DIRS 162096]	MXX	0–250
K_Mg_Cl	*Pabalan_icf_TJW.xls*	Pabalan and Pitzer 1987 [DIRS 162096]	MMX	0–250
Na_Mg_Cl	*Pabalan_icf_TJW.xls*	Pabalan and Pitzer 1987 [DIRS 162096]	MMX	0–250
Mg_Na_Cl	*Pabalan_icf_TJW.xls*	Pabalan and Pitzer 1987 [DIRS 162096]	MMX	0–250
Mg_Cl_SO4	*Pabalan_icf_TJW.xls*	Pabalan and Pitzer 1987 [DIRS 162096]	MXX	0–250
Na_K_Cl	*Pabalan_icf_TJW.xls*	Pabalan and Pitzer 1987 [DIRS 162096]	MMX	0–250
Cl_OH_Na	*Pabalan_icf_TJW.xls*	Pabalan and Pitzer 1987 [DIRS 162096]	MMX	0–250
Na_OH_SO4	*Pabalan_icf_TJW.xls*	Pabalan and Pitzer 1987 [DIRS 162096]	MXX	0–250

Output DTN: MO0701SPAPTZER.001.

NOTE: For details on the valid composition salt range of these parameters, the user is referred to the corresponding sources.

[a] Spreadsheet refitting calculations do not entail the use of the "FitPitzerNC" methodology. Refitting of Pitzer parameters was conducted using the Excel regression function.

[b] The evaluation of these mixing parameters was based on the model and parameters of Greenberg and Møller (1989 [DIRS 152684]). Although these authors used a constant value for this parameter (rather than a temperature-dependent function), its value was chosen to represent solubilities over a wide temperature range, and thus it can be used over the indicated temperature range.

[c] The evaluation of these mixing parameters is based on the model and parameters of Greenberg and Møller (1989 [DIRS 152684]). These authors used a constant value for this parameter from 0°C to 150°C (rather than a temperature-dependent function), and then used a temperature-dependent function at higher temperatures. Since the constant value below 150°C was chosen to represent solubilities over a wide temperature range, it can be used over the indicated temperature range.

Table I-2. Pitzer Ion-Interaction Parameters Not Requiring Refitting (Values Only Valid at 25°C)

Ion Group	Spreadsheet File Name	Original Data Source	Type
Ca_Br	*Some2-1Salts25C_TJW.xls*	Pitzer 1991 [DIRS 152709]	MX
Ca_HCO3	*Some2-1Salts25C_TJW.xls*	Pitzer 1991 [DIRS 152709]	MX
Ca_HSO3	*Some2-1Salts25C_TJW.xls*	Pitzer 1991 [DIRS 152709]	MX
Ca_HSO4	*Some2-1Salts25C_TJW.xls*	Pitzer 1991 [DIRS 152709]	MX
Ca_I	*Some2-1Salts25C_TJW.xls*	Pitzer 1991 [DIRS 152709]	MX
Cl_HSO4	No Spreadsheet	Pitzer 1991 [DIRS 152709]	—
Cl_NO3	No Spreadsheet	Pitzer 1991 [DIRS 152709]	—
Cs_I	*Some1-1Salts25C_TJW.xls*	Pitzer 1991 [DIRS 152709]	MX
Cs_F	*Some1-1Salts25C_TJW.xls*	Pitzer 1991 [DIRS 152709]	MX
Cs_NO3	*Some2-1Salts25C_TJW.xls*	Pitzer 1991 [DIRS 152709]	MX
Cs_OH	*Some1-1Salts25C_TJW.xls*	Pitzer 1991 [DIRS 152709]	MX
Cs_SO4	*Some2-1Salts25C_TJW.xls*	Pitzer 1991 [DIRS 152709]	MX
Cu_HSO4	No Spreadsheet	Baes et al. 1993 [DIRS 168318], Table I, parameter set 11	MX
H_Br	*Some1-1Salts25C_TJW.xls*	Pitzer 1991 [DIRS 152709]	MX
H_I	*Some1-1Salts25C_TJW.xls*	Pitzer 1991 [DIRS 152709]	MX
K_CO3	*Some2-1Salts25C_TJW.xls*	Pitzer 1991 [DIRS 152709]	MX
K_HCO3	*Some2-1Salts25C_TJW.xls*	Pitzer 1991 [DIRS 152709]	MX
K_CrO4	*Some2-1Salts25C_TJW.xls*	Pitzer 1991 [DIRS 152709]	MX
K_F	*Some2-1Salts25C_TJW.xls*	Pitzer 1991 [DIRS 152709]	MX
K_HPO4	*Some2-1Salts25C_TJW.xls*	Pitzer 1991 [DIRS 152709]	MX
K_HSO4	*Some2-1Salts25C_TJW.xls*	Pitzer 1991 [DIRS 152709]	MX
K_I	*Some2-1Salts25C_TJW.xls*	Pitzer 1991 [DIRS 152709]	MX
K_NO3	*Some2-1Salts25C_TJW.xls*	Pitzer 1991 [DIRS 152709]	MX
K_OH	*Some2-1Salts25C_TJW.xls*	Pitzer 1991 [DIRS 152709]	MX
Li_I	*Some2-1Salts25C_TJW.xls*	Pitzer 1991 [DIRS 152709]	MX
Li_NO3	*Some2-1Salts25C_TJW.xls*	Pitzer 1991 [DIRS 152709]	MX
Li_OH	*Some2-1Salts25C_TJW.xls*	Pitzer 1991 [DIRS 152709]	MX
Li_SO4	*Some2-1Salts25C_TJW.xls*	Pitzer 1991 [DIRS 152709]	MX
Mg_Br	*Some2-1Salts25C_TJW.xls*	Pitzer 1991 [DIRS 152709]	MX
Mg_HCO3	*Some2-1Salts25C_TJW.xls*	Pitzer 1991 [DIRS 152709]	MX
Mg_HSO4	*Some2-1Salts25C_TJW.xls*	Pitzer 1991 [DIRS 152709]	MX
Mg_I	*Some2-1Salts25C_TJW.xls*	Pitzer 1991 [DIRS 152709]	MX
Mg_NO3	No Spreadsheet	Rard et al. 2004 [DIRS 173816]	MX
MgOH_Cl	*Some2-1Salts25C_TJW.xls*	Pitzer 1991 [DIRS 152709]	MX
Na_CrO4	*Some2-1Salts25C_TJW.xls*	Pitzer 1991 [DIRS 152709]	MX
Na_F	*Some2-1Salts25C_TJW.xls*	Pitzer 1991 [DIRS 152709]	MX
Na_HPO4	*Some2-1Salts25C_TJW.xls*	Pitzer 1991 [DIRS 152709]	MX
Na_I	*Some2-1Salts25C_TJW.xls*	Pitzer 1991 [DIRS 152709]	MX

Table I-2. Pitzer Ion-Interaction Parameters Not Requiring Refitting (Values Only Valid at 25°C) (Continued)

Ion Group	Spreadsheet File Name	Original Data Source	Type
NH4_Br	*Some2-1Salts25C_TJW.xls*	Pitzer 1991 [DIRS 152709]	MX
NH4_HCO3	*Some2-1Salts25C_TJW.xls*	Pitzer 1991 [DIRS 152709]	MX
NH4_I	*Some2-1Salts25C_TJW.xls*	Pitzer 1991 [DIRS 152709]	MX
NH4_NO3	*Some2-1Salts25C_TJW.xls*	Pitzer 1991 [DIRS 152709]	MX
Sr_Br	*Some2-1Salts25C_TJW.xls*	Pitzer 1991 [DIRS 152709]	MX
Sr_Cl	*Some2-1Salts25C_TJW.xls*	Pitzer 1991 [DIRS 152709]	MX
Sr_I	*Some2-1Salts25C_TJW.xls*	Pitzer 1991 [DIRS 152709]	MX
Sr_NO3	*Some2-1Salts25C_TJW.xls*	Pitzer 1991 [DIRS 152709]	MX
Br_Cl	No Spreadsheet	Pitzer 1991 [DIRS 152709]	MX
Br_OH	No Spreadsheet	Pitzer 1991 [DIRS 152709]	MX
Cl_HSO4	No Spreadsheet	Pitzer 1991 [DIRS 152709]	MX
Cl_NO3	No Spreadsheet	Pitzer 1991 [DIRS 152709]	MX
CO3_HCO3	No Spreadsheet	Pitzer 1991 [DIRS 152709]	MX
CO3_SO4	No Spreadsheet	Pitzer 1991 [DIRS 152709]	MX
CO3_OH	No Spreadsheet	Pitzer 1991 [DIRS 152709]	MX
HCO3_SO4	No Spreadsheet	Pitzer 1991 [DIRS 152709]	MX
Ca_H	No Spreadsheet	Pitzer 1991 [DIRS 152709]	MM
Ca_K	No Spreadsheet	Pitzer 1991 [DIRS 152709]	MM
Ca_Na	No Spreadsheet	Pitzer 1991 [DIRS 152709]	MM
Ca_Mg	No Spreadsheet	Pitzer 1991 [DIRS 152709]	MM
Cs_H	No Spreadsheet	Pitzer 1991 [DIRS 152709]	MM
Ca_HSO4	No Spreadsheet	Pitzer 1991 [DIRS 152709]	MX
Cs_K	No Spreadsheet	Pitzer 1991 [DIRS 152709]	MM
Cs_Li	No Spreadsheet	Pitzer 1991 [DIRS 152709]	MM
Cs_Na	No Spreadsheet	Pitzer 1991 [DIRS 152709]	MM
Cu_H	No Spreadsheet	Baes et al. 1993 [DIRS 168318], Table I, parameter set 11	MM
Cu_H_HSO4	No Spreadsheet	Baes et al. 1993 [DIRS 168318], Table I, parameter set 11	MMX
H_K	No Spreadsheet	Pitzer 1991 [DIRS 152709]	MM
H_Li	No Spreadsheet	Pitzer 1991 [DIRS 152709]	MM
H_Mg	No Spreadsheet	Pitzer 1991 [DIRS 152709]	MM
H_Na	No Spreadsheet	Pitzer 1991 [DIRS 152709]	MM
H_NH4	No Spreadsheet	Pitzer 1991 [DIRS 152709]	MM
H_Sr	No Spreadsheet	Pitzer 1991 [DIRS 152709]	MM
K_HSO4	No Spreadsheet	Pitzer 1991 [DIRS 152709]	MX
K_Li	No Spreadsheet	Pitzer 1991 [DIRS 152709]	MM
K_Mg	No Spreadsheet	Pabalan and Pitzer 1987 [DIRS 162096]	MM
Cl_CO3	No Spreadsheet	Peiper and Pitzer (1982 [DIRS 162097]	XX
Cl_HCO3	No Spreadsheet	Peiper and Pitzer (1982 [DIRS 162097]	XX

Table I-2. Pitzer Ion-Interaction Parameters Not Requiring Refitting (Values Only Valid at 25°C) (Continued)

Ion Group	Spreadsheet File Name	Original Data Source	Type
Na_Cl_HCO3	No Spreadsheet	Peiper and Pitzer 1982 [DIRS 162097], and Konigsberger et al. 1999 [DIRS 168345]	MXX
H_HSO4_SO4	No Spreadsheet	Baes et al. 1993 [DIRS 168318], Table I, parameter set 11	MXX
K_Na	No Spreadsheet	Pitzer 1991 [DIRS 152709]	MM
Li_Na	No Spreadsheet	Pitzer 1991 [DIRS 152709]	MM
Mg_HSO4	No Spreadsheet	Pitzer 1991 [DIRS 152709]	MM
Mg_Na	No Spreadsheet	Pabalan and Pitzer 1987 [DIRS 162096]	MM

Output DTN: MO0701SPAPTZER.001.

NOTE: "No Spreadsheet" means that values were taken directly from table(s) listed in the noted data sources.

I.4.1 FITPITZERNC METHODOLOGY

In the FitPitzerNC spreadsheets it is assumed that the Pitzer parameters are given as functions of the system temperature, *T*, and pressure, *P*. A new output temperature-pressure function *f(T,P)* is fitted to each Pitzer parameter that is defined in the source document in terms of a temperature-pressure function $f^0(T,P)$. Usually, both the input and output temperature-pressure functions are given as the sum of a finite series of numeric terms, each of which is the product of a constant coefficient (a_i , a^0_i), and a temperature-pressure interpolation basis function ($g_i(T,P)$, $g^0_i(T,P)$), as in:

$$f(T,P) = \sum_{i=1}^{i=n_f} a_i g_i(T,P) \qquad \text{(Eq. I-61)}$$

$$f^0(T,P) = \sum_{i=1}^{i=n^0_f} a^0_i g^0_i(T,P) \qquad \text{(Eq. I-62)}$$

where (n_f , n^0_f) are the numbers of terms in the two series. While the basis functions for the input model parameters are specified in the source document, the new basis functions of the output model parameters are selected by the user of the FitPitzerNC spreadsheets from a list of up to eight basis functions. It is important to note that the fitting coefficients $a_1,...,a_5$ specified in the "FitPitzerNC" and "ConPitzerNC_MX_(NH4)2SO4.xls" spreadsheets do not directly correspond to those specified for the data0.ypf.R2 database (Output DTN: SN0609T0502404.012). Table I-3 provides the actual correspondence between these parameters.

Table I-3. Fitting Coefficient Definitions for the 3- to 4-Term Parameter 25°C-Centric Equations Used in the FitPitzerNC/ConPitzerNC_MX_(NH4)2SO4.xls Spreadsheets and data0.ypf.R2 Database

FitPitzerNC/ConPitzerNC	data0.ypf.R2	Temperature Function
a_1	a_1	Constant
a_2	a_4	T
a_3	not used	T^2
a_4	a_2	1/T
a_5	a_3	ln T

Spreadsheets that do not use the "FitPitzerNC" or "ConPitzerNC_MX_(NH4)2SO4.xls" methodology express the fitting coefficients as in the data0.ypf.R2 database file (Output DTN: SN0609T0502404.012).

In the FitPitzerNC spreadsheets, it is assumed that a temperature-dependent standard system pressure $P(T)$ is equal to 1 atmosphere below 100°C, and is equal to the liquid-vapor saturation vapor pressure of pure water above 100°C. The reason for making this assumption is that this is the definition of system pressure used in *Software User's Manual, EQ3/6, Version 8.0* (SNL 2003 [DIRS 162494]). Consequently, the functional dependence of the output temperature-pressure functions of the Pitzer parameters can be simplified according to $g_i(T,P) = g_i(T,P(T)) = g_i(T)$, and expressed as functions of the temperature only.

On the basis of thermodynamic arguments, and parameter fitting accuracy considerations, the following set of eight functions for the output basis functions $g_i(T)$ was selected:

$$\begin{aligned} g_1(T) &= 1 \\ g_2(T) &= T \\ g_3(T) &= T^2 \\ g_4(T) &= T^{-1} \\ g_5(T) &= \ln(T) \\ g_6(T) &= T^3 \\ g_7(T) &= T^{-2} \\ g_8(T) &= T^{-3} \end{aligned} \qquad \text{(Eq. I-63)}$$

This series of basis functions not only spans the entire sequence of powers of the temperature T increasing from –3 to +2 (i.e., T^{-3}, T^{-2}, T^{-1}, T^{-k} $(k<<1)$, T^0, $T^k(k<<1)$, T^1, T^2), but it also incorporates as subsets important temperature function forms for the Pitzer parameters that can be justified on the basis of fundamental thermodynamic considerations.

It is convenient for parameter data verification purposes to directly represent the coefficient a_1 of the constant basis function $g_1(T)$ as the value of the fitted parameter at some reference absolute temperature T_{ref}, usually 298.15 K. This can be achieved by redefining the basis functions $g_i(T)$ as:

$$
\begin{aligned}
g_1(T) &= 1 \\
g_2(T) &= T - T_{\text{ref}} \\
g_3(T) &= T^2 - T_{\text{ref}}^2 \\
g_4(T) &= T^{-1} - T_{\text{ref}}^{-1} \\
g_5(T) &= \ln\left(\frac{T}{T_{\text{ref}}}\right) \\
g_6(T) &= T^3 - T_{\text{ref}}^3 \\
g_7(T) &= T^{-2} - T_{\text{ref}}^{-2} \\
g_8(T) &= T^{-3} - T_{\text{ref}}^{-3}
\end{aligned}
\qquad \text{(Eq. I-64)}
$$

In the FitPitzerNC spreadsheet, this feature for centering the fitted functions at any specified absolute reference temperature T_{ref} has been implemented and can be selected as an option.

I.4.2 PROCEDURE FOR FITTING TEMPERATURE FUNCTIONS TO PITZER PARAMETERS

A least-squares error minimization method was devised for fitting the new temperature functions to the input source functions with minimum error by first defining a measure $E^2(a_i)$ of the cumulative square error between the fitted function $f(T)$ and the input function $f^0(T,P)$ over the desired temperature range (T_{min}, T_{max}) by:

$$E^2(a_i) = \frac{1}{n_T}\sum_{j=1}^{j=n_T}\left\{f(T_j) - f^0(T_j, P_j)\right\}^2 \qquad \text{(Eq. I-65)}$$

where T_j are the n_T discrete temperatures at which the parameters are evaluated, $T_1 = T_{min}$, $T_2 = T_{max}$, and $P_j = P(T_j)$.

Setting the partial derivatives of E with respect to the output temperature coefficients a_i equal to zero now minimizes the error measure:

$$\frac{\partial E^2}{\partial a_i} = \frac{2}{n_T}\sum_{j=1}^{j=n_T}\frac{\partial f}{\partial a_i}\left\{f(T_j) - f^0(T_j, P_j)\right\} = 0 \qquad \text{(Eq. I-66)}$$

Substituting the series representations for the temperature function given by Equations I-61 and I-62 into equation I-66, and re-arranging the terms, yields the equation:

$$\sum_{k=1}^{k=n_f}\sum_{j=1}^{j=n_T} g_i(T_j)g_k(T_j)a_k = \sum_{j=1}^{j=n_T} g_i(T_j)f^0(T_j, P_j) \qquad \text{(Eq. I-67)}$$

Equation I-67 can be recast in a more compact and transparent form as the matrix equations:

$$[A_{ik}](a_k) = (b_i) \quad ; \quad i,k = 1...n_f \qquad \text{(Eq. I-68)}$$

$$A_{ik} \equiv \sum_{j=1}^{j=n_T} g_i(T_j) g_k(T_j) \quad \text{(Eq. I-69)}$$

$$b_i \equiv \sum_{j=1}^{j=n_T} g_i(T_j) f^0(T_j, P_j) \quad \text{(Eq. I-70)}$$

The matrix Equations I-68 through I-70 can be solved by standard matrix equation solution methods for the unknown vector of temperature coefficients (a_k) in terms of the known right-hand-side vector (b_i), and known interpolation function matrix $[A_{ik}]$.

When the temperature coefficients a_i have been determined by solving equation I-68 in this way, the input and fitted parameters $f^0(T_j)$ and $f(T_j)$ are evaluated using the values of the determined coefficients in the temperature function representations of Equation I-62. The binary and ternary system osmotic coefficients can then be calculated by substituting the input and fitted parameter values evaluated as a function of temperature in Equations I-13 and I-14, respectively.

This mathematical procedure has been implemented in each FitPitzerNC worksheet to fit new temperature functions to the source Pitzer parameters.

I.4.2.1 FitPitzerNC Worksheet Implementation

The full set of temperature basis functions given by Equations I-63 and I-64 spans the entire sequence of powers of the temperature T increasing from –3 to +2 (i.e., T^{-3}, T^{-2}, T^{-1}, T^k $(k<<1)$, T^0, $T^k(k<<1)$, T^1, T^2). However, when implementing the FitPitzerNC methodology, it is necessary to allow for the fact that only a subset of the full set of basis functions may be activated, or chosen, for a particular Pitzer parameter database. A spreadsheet that does not treat each choice as a special case can be developed, by solving for all temperature coefficients in a way that forces the de-activated temperature coefficients a_k to be equal to zero. In this no-code version of the FitPitzer spreadsheet, this feature is implemented using only spreadsheet macro functions in the following way.

An activation-index vector IA_i (row 22 in RunSettings Worksheet) is first set up to reflect the user's choice of temperature basis functions such that:

$$LA_i \equiv 1 \quad ; \quad a_i \neq 0; \quad i = 1,2...8 \quad \text{(Eq. I-71)}$$

$$LA_i \equiv 0 \quad ; \quad a_i = 0; \quad i = 1,2...8 \quad \text{(Eq. I-72)}$$

The matrix equation to be solved for the unknown temperature coefficients is then given by:

$$[A_{ik}](a_k^p) = (b_i^p) \quad ; \quad i,k = 1...n_f \quad \text{(Eq. I-73)}$$

$$A_{ik} \equiv A_{ik}^0 . IAM_{ik}; \quad i,k = 1...n_f \quad \text{(Eq. I-74)}$$

$$b_i^p \equiv b_i^{0p} . IA_i; \quad i = 1...n_f \quad \text{(Eq. I-75)}$$

where p is the parameter index. The activation-index matrix IAM_{ij} is defined in terms of the activation-index vector IA_i by:

$$IAM_{ij} \equiv 1 \quad ; \quad i = j \tag{Eq. I-76}$$

$$IAM_{ij} \equiv IA_i.IA_j \quad ; \quad i \neq j \tag{Eq. I-77}$$

In this way, the correct matrix coefficients and right-hand side vector values for the set of activated temperature coefficients are retrieved, while forcing the deactivated temperature coefficients to be equal to zero. All matrix–vector and matrix–matrix multiplications are performed using the MMULT and TRANSPOSE spreadsheet functions, inversion of the matrix equation I-73 is performed using the MINVERSE spreadsheet function, and the individual elements of the vector and matrix arrays are accessed using the INDEX function. These spreadsheet functions are standard intrinsic features of Microsoft Excel 2000 (and above).

I.4.2.2 Example Calculation for FitPitzerNC_MX_NaCl.xls Workbook

For the purpose of illustrating the specific manner in which these calculations are carried out, the sequence of calculations performed in the *FitPitzerNC_MX_NaCl.xls* workbook (located in Output DTN: MO0701SPAPTZER.001) are presented below:

1. CoverPage worksheet: On this worksheet, software identification information and spreadsheet checker review comments are first presented. Next, spreadsheet user information on a contents roadmap, an overview of methodology and data sources, protection of data and computational integrity and manner of presentation of results, are given.

2. Directions worksheet: This worksheet gives directions for fitting different temperature functions selected by the user.

3. RunSettings worksheet: Select the desired temperature basis functions.

4. RunSettings worksheet: Select, if desired, Temperature centering and Reference Temperature.

5. FitPitzerNC worksheet: Constant input (Archer) and output (standard Pitzer) model parameters are defined in cells A13:L13 and A14:L14.

6. FitPitzerNC worksheet: The input standard Pitzer model temperature coefficients are set in cells B17:I20, and for the Aphi Debye-Hückel parameter in cells B21:I21.

7. FitPitzerNC worksheet: The input standard Pitzer model parameters and the Aphi Debye-Hückel parameter are calculated as functions of temperature in cells B31:AB35.

8. FitPitzerNC worksheet: The matrix array, $G_{ij} = g_i(T_j)$, is calculated in accordance with Equations I-64 or I-78 (along with the option chosen for the Tref switch), and the

results placed in the range of cells, B78:AB85. The corresponding A^0_{ik} matrix is calculated according to Equation I-69 (or Equation I-79 below), specifically, MMULT(G,TRANSPOSE(G))/27, and the results placed in the range of cells, B88:I95. Division by 27 is convenient for keeping the entry for $A^0(1,1)$ the same as that for g-1 at 0°C:

$$G = \$B\$78 : \$AB\$85 \quad \text{(Eq. I-78)}$$

$$A^0 = MMULT(G, TRANSPOSE(G)) = \$B\$88 : \$I95 \quad \text{(Eq. I-79)}$$

9. FitPitzerNC worksheet: The input parameter function matrix array, $F^{0p}_i = f^{0p}(T_i)$, where p stands for the parameter index and i signifies the temperature value index, is calculated in accordance with Equation I-62 (entered as Equation I-80 below), and the results placed in the range of cells, B31:AB34. The corresponding B^{0p}_i matrix is calculated according to Equation I-70 (or Equation I-81 below), specifically, MMULT(G,TRANSPOSE(F^0))/27, and the results placed in the range of cells, B128:E135. Division by 27 is needed to keep both sides of Equation I-68 compatible:

$$F^0 = \$B\$31 : \$AB\$34 \quad \text{(Eq. I-80)}$$

$$B^0 = MMULT(G, TRANSPOSE(F^0)) = \$B\$128 : \$E\$135 \quad \text{(Eq. I-81)}$$

10. FitPitzerNC worksheet: The temperature basis function activation vector IA_i and activation matrix IAM_{ij} are set up according to Equations I-82 (or Equation I-76) and I-83 (or Equation I-77), respectively:

$$IA = \$B\$24 : \$I\$24 \quad \text{(Eq. I-82)}$$

$$IAM = \$B\$98 : \$I\$105 \quad \text{(Eq. I-83)}$$

11. FitPitzerNC worksheet: The modified coefficient matrix A_{ik} and the modified matrix of right-hand side vectors B^p_i are calculated according to Equations I-84 (or Equation I-74) and I-85 (or Equation I-75), respectively:

$$A = \$B\$108 : \$I\$115 \quad \text{(Eq. I-84)}$$

$$B = \$B\$138 : \$I\$E145 \quad \text{(Eq. I-85)}$$

12. FitPitzerNC worksheet: Equation I-73 is solved to obtain the desired matrix of temperature coefficient vectors $CoefFIT = a^p_i$ by inverting the coefficient matrix A to obtain its inverse $AINV$ and then multiplying the inverse matrix by the modified matrix of right-hand-side vectors B^p_i :

$$AINV = MINVERSE(A) = \$B\$118 : \$I\$125 \quad \text{(Eq. I-86)}$$

$$CoefFIT = MMULT(AINV, B) = \$B\$25 : \$I\$28 \quad \text{(Eq. I-87)}$$

13. FitPitzerNC worksheet: The input standard Pitzer model parameters, and the fitted parameters for the same model, are calculated as functions of temperature according to Equations I-88 and I-89, respectively:

$$ParamDAT = \$B\$31:\$AB\$34 \quad \text{(Eq. I-88)}$$

$$ParamFIT = MMULT(TRANSPOSE(CoefFIT), G) = \$B\$38:\$AB\$41 \quad \text{(Eq. I-89)}$$

14. FitPitzerNC worksheet: The ionic strength dependent factors in the Debye-Hückel and exponential Beta-parameter terms in the equation for the osmotic coefficient are calculated and stored as follows:

$$DHDAT = \$D\$148:\$D\$153 \quad \text{(Eq. I-90)}$$

$$DHFIT = \$D\$156:\$D\$161 \quad \text{(Eq. I-91)}$$

$$PFuncDAT = \$E\$148:\$H\$153 \quad \text{(Eq. I-92)}$$

$$PFuncFIT = \$E\$156:\$H\$161 \quad \text{(Eq. I-93)}$$

15. FitPitzerNC worksheet: The osmotic coefficient from the Debye-Hückel and Beta-parameter terms are calculated according to the equations:

$$APhi = \$B\$35:\$AB\$35 \quad \text{(Eq. I-94)}$$

$$PhiM1DAT = MMULT(DHDAT, APhi) + MMULT(PFuncDAT, ParamDAT);$$
$$PhiM1FIT = MMULT(DHFIT, APhi) + MMULT(PFuncFIT, ParamFIT) \quad \text{(Eq. I-95)}$$

$$PhiDAT = 1 + PhiM1DAT = \$B\$50:\$AB\$55 \quad \text{(Eq. I-96)}$$

$$PhiFIT = 1 + PhiM1FIT = \$B\$58:\$AB\$63 \quad \text{(Eq. I-97)}$$

16. FitPitzerNC worksheet: This completes the fitting of new temperature functions to the input standard Pitzer model parameters, the calculation of the input and fitted Pitzer parameters as functions of temperature, and the computation of the osmotic coefficient as a function of ionic strength and temperature from the input and fitted Pitzer parameter values at each temperature. These are used to evaluate the accuracy of fitting the standard Pitzer parameters.

17. FitPitzerNC worksheet: The temperature function fitting error in the osmotic coefficient is calculated as the difference between the osmotic coefficients from the input and fitted standard Pitzer models in cells B67:AB72 as a function of temperature and ionic strength. The RMS error (cells AC67:AC72) and the average, maximum and minimum values of the osmotic coefficient are also calculated for the two models in cells AD50:AF55 and AD58:AF63, respectively.

18. FitPitzerNC worksheet: Pitzer parameters, osmotic coefficients and their errors, calculated from the input and fitted standard Pitzer models, are plotted in charts on the extreme right-hand side of each FitPitzerNC worksheet.

19. ResultsSummary worksheet: The input and fitted temperature coefficients for the standard Pitzer model are summarized in cells B17:I21 and B25:I28, respectively.

20. ResultsSummary worksheet: The RMS errors, average, maximum, and minimum values of the Pitzer parameters (B31:E34), and osmotic coefficients (A37:E42) calculated from the input and fitted standard Pitzer models are summarized here. These statistics enable the errors incurred in temperature function fitting to be assessed.

I.4.3 CONPITZERNC METHODOLOGY

In the spreadsheet *ConPitzerNC_MX_(NH4)2SO4.xls* (Output DTN: MO0701SPAPTZER.001), the parameters are given as a function of temperature for an extended Pitzer model in the data source document and are converted to the parameters of the standard Pitzer model. Temperature coefficients for a user specified temperature function are then fit to these standard parameters in the "FitPitzerNC" worksheet of the *ConPitzerNC_MX_(NH4)2SO4.xls* spreadsheet as described above.

This section summarizes the procedure developed by Rard and Wijesinghe (2003 [DIRS 162327]) used in the "ConPitzerNC" worksheet in *ConPitzerNC_MX_(NH4)2SO4.xls* for converting parameters between the parameter (i.e., $\beta^{(0)}_{MX}(T,P)$, $\beta^{(1)}_{MX}(T,P)$, $\beta^{(2)}_{MX}(T,P)$, $C^{\phi}_{MX}(T,P)$) standard Pitzer model presented in Section I-3, and the 6-parameter (i.e., $\beta^{(0)}_{MX}(T,P)$, $\beta^{(1)}_{MX}(T,P)$, $\beta^{(2)}_{MX}(T,P)$, $C^{(0)}_{MX}(T,P)$, $C^{(1)}_{MX}(T,P)$, $C^{(2)}_{MX}(T,P)$) extended Pitzer model developed by Archer (2000 [DIRS 162065]) and extended by Oakes et al. (2000 [DIRS 162102]).

The expression for the osmotic coefficient in the 4-parameter standard Pitzer model, denoted by the superscript *P*, is given by:

$$\phi^{P} = 1 - \frac{|z_M z_X| A_\phi I^{1/2}}{(1 + bI^{1/2})} + \left(\frac{2\nu_M \nu_X m}{\nu_M + \nu_X} \right) \left\{ B^{\phi,P}_{MX} + m(\nu_M \nu_X)^{1/2} C^{\phi,P}_{MX} \right\} \qquad \text{(Eq. I-98)}$$

where

$$B^{\phi,P}_{MX}(I,T,P) \equiv \beta^{(0,P)}_{MX}(T,P) + \beta^{(1,P)}_{MX}(T,P) e^{-\alpha_1 \sqrt{I}} + \beta^{(2,P)}_{MX}(T,P) e^{-\alpha_2 \sqrt{I}} \qquad \text{(Eq. I-99)}$$

and $C^{\phi,P}_{MX}$ is a function of *(T,P)* only. The expression for the osmotic coefficient in the 6-parameter extended Archer model (see Rard and Wijesinghe 2003 [DIRS 162327] for more details), denoted by the superscript *EA*, is given by:

$$\phi^{EA} = 1 - \frac{|z_M z_X| A_\phi I^{1/2}}{(1 + bI^{1/2})} + \left(\frac{2\nu_M \nu_X m}{\nu_M + \nu_X} \right) \left\{ B^{\phi,EA}_{MX} + m(\nu_M \nu_X)^{1/2} C^{EA}_{MX} \right\} \qquad \text{(Eq. I-100)}$$

where

$$B_{MX}^{\phi,EA}(I,T,P) \equiv \beta_{MX}^{(0,EA)}(T,P) + \beta_{MX}^{(1,EA)}(T,P)e^{-\alpha_1\sqrt{I}} + \beta_{MX}^{(2,EA)}(T,P)e^{-\alpha_2\sqrt{I}} \quad \text{(Eq. I-101)}$$

$$C_{MX}^{EA}(I,T,P) \equiv C_{MX}^{(0,EA)}(T,P) + C_{MX}^{(1,EA)}(T,P)e^{-\omega_1\sqrt{I}} + C_{MX}^{(2,EA)}(T,P)e^{-\omega_2\sqrt{I}} \quad \text{(Eq. I-102)}$$

ω_1 and ω_2 are constant coefficients for $C_{MX}^{(1,EA)}$ and $C_{MX}^{(2,EA)}$ parameters, respectively, as defined in the Archer model (see Rard and Wijesinghe 2003 [DIRS 162327]). In contrast to $C^{\phi,P}{}_{MX}$ in the standard Pitzer model, the $C_{MX}{}^{EA}$ is a function of ionic strength in addition to temperature and pressure, and is expressed as the sum of an ionic strength-dependent parameter and two terms that decay exponentially with the square root of ionic strength. Equation I-101 is the analogue of Equation I-99 for the standard Pitzer model with the same values assigned to exponents of the terms that decay exponentially with increasing ionic strength. It is important to note here that the coefficient of these functions in Equations I-98 and I-100 are not equal.

I.4.3.1 Procedure for Determining Standard Pitzer Model Parameters from Archer Model Parameters

A least-squares error minimization method was devised for determining with minimum error the set of standard Pitzer model parameters $X_i^P = \{\beta^{(0,P)}{}_{MX}(T,P)\ ,\ \beta^{(1,P)}{}_{MX}(T,P)\ ,\ \beta^{(2,P)}{}_{MX}(T,P),\ C^{\phi,P}{}_{MX}(T,P)\}$ from the set of Archer model parameters $X_j^{EA} = \{\beta^{(0,EA)}{}_{MX}(T,P)\ ,\ \beta^{(1,EA)}{}_{MX}(T,P)\ ,\ \beta^{(2,EA)}{}_{MX}(T,P),\ C^{(0,EA)}{}_{MX}(T,P),\ C^{(1,EA)}{}_{MX}(T,P),\ C^{(2,EA)}{}_{MX}(T,P\ )\}$ by first defining a measure $E^2(X_i^P,\ X_j^{EA}\ )$ of the cumulative square error $(\phi^P - \phi^{EA})$ between the osmotic coefficient in the two models over the desired ionic strength range $(0,\ I_{max})$:

$$E^2(X_i^P, X_j^{EA}) = \frac{1}{2}\int_0^{I_{\max}} \{\phi^P(I, X_i^P) - \phi^{EA}(I, X_j^{EA})\}^2\, dI \quad \text{(Eq. I-103)}$$

The subsequent mathematical expressions can be simplified considerably, by recasting the difference between the errors in osmotic coefficient in terms of the differences in the model parameters as follows:

$$\begin{aligned}\phi^P - \phi^{EA} &= I\Delta\beta_{MX}^{(0)} + Ie^{-\alpha_1 I^{1/2}}\Delta\beta_{MX}^{(1)} + Ie^{-\alpha_2 I^{1/2}}\Delta\beta_{MX}^{(2)} \\ &+ I^2\Delta C_{MX}^{(0)} - \left(\frac{4\nu_M}{(\nu_M+\nu_X)|z_M|}\right)\left\{I^2 e^{-\varpi_1 I^{1/2}} C_{MX}^{(1,EA)} + I^2 e^{-\varpi_2 I^{1/2}} C_{MX}^{(2,EA)}\right\}\end{aligned} \quad \text{(Eq. I-104)}$$

where

$$\Delta X_1 \equiv \Delta\beta_{MX}^{(0)} \equiv \beta_{MX}^{(0,P)} - \beta_{MX}^{(0,EA)} \quad \text{(Eq. I-105)}$$

$$\Delta X_2 \equiv \Delta\beta_{MX}^{(1)} \equiv \beta_{MX}^{(1,P)} - \beta_{MX}^{(1,EA)} \quad \text{(Eq. I-106)}$$

$$\Delta X_3 \equiv \Delta\beta_{MX}^{(2)} \equiv \beta_{MX}^{(2,P)} - \beta_{MX}^{(2,EA)} \quad \text{(Eq. I-107)}$$

$$\Delta X_4 \equiv \Delta C_{MX}^{(0)} \equiv \left(\frac{2(v_M v_X)^{1/2}}{(v_M + v_X) \mid z_M z_X \mid} \right) C_{MX}^{(\phi,P)} - \left(\frac{4v_M}{(v_M + v_X) \mid z_X \mid} \right) C_{MX}^{(0,EA)} \quad \text{(Eq. I-108)}$$

The error measure E is now minimized by setting the partial derivatives of E with respect to the unknown parameter differences ΔX_i equal to zero:

$$\frac{\partial E^2}{\partial \Delta X_i} = \int_0^{I_{\max}} \frac{\partial(\phi^P - \phi^{EA})}{\partial \Delta X_i} (\phi^P - \phi^{EA}) dI = 0 \quad \text{(Eq. I-109)}$$

Substituting for the osmotic coefficient error from Equation I-104 in Equation I-109, and re-arranging the terms, yields the matrix equation:

$$[A_{ik}](\Delta X_k) = (B_i) \quad ; \quad i,k = 1...4 \quad \text{(Eq. I-110)}$$

where

$$A_{ik} \equiv \int_0^{I_{\max}} \frac{\partial(\phi^P - \phi^{EA})}{\partial \Delta X_i} \frac{\partial(\phi^P - \phi^{EA})}{\partial \Delta X_k} dI \quad \text{(Eq. I-111)}$$

$$B_i \equiv \left(\frac{4v_M}{(v_M + v_X) \mid z_X \mid} \right) \int_0^{I_{\max}} \frac{\partial(\phi^P - \phi^{EA})}{\partial \Delta X_i} \{ I^2 . e^{-\omega_1 I^{1/2}} C_{MX}^{(1,EA)} + I2 . e^{-\omega_2 I^{1/2}} C_{MX}^{(2,EA)} \} dI \quad \text{(Eq. I-112)}$$

and

$$\frac{\partial\left(\phi^P - \phi^{EA}\right)}{\partial \Delta X_i} = \left\{ I, Ie^{-\alpha_1 I^{1/2}}, Ie^{-\alpha_2 I^{1/2}}, I^2 \right\} \quad \text{(Eq. I-113)}$$

The integrals in the definitions above (Equations I-111 and I-112 can be evaluated in closed form as analytical expressions and are given in the study by Rard and Wijesinghe (2003 [DIRS 162327]). The matrix Equation I-110 can be solved by standard matrix equation solution methods for the unknown parameter differences ΔX_i . The unknown standard Pitzer model parameters can then be evaluated using these parameter differences and the known Archer model parameters from Equations I-105 through I-108 recast as follows:

$$\beta_{MX}^{(0,P)} = \Delta X_1 + \beta_{MX}^{(0,EA)} = \Delta \beta_{MX}^{(0)} + \beta_{MX}^{(0,EA)} \quad \text{(Eq. I-114)}$$

$$\beta_{MX}^{(1,P)} = \Delta X_2 + \beta_{MX}^{(1,EA)} = \Delta \beta_{MX}^{(1)} + \beta_{MX}^{(1,EA)} \quad \text{(Eq. I-115)}$$

$$\beta_{MX}^{(2,P)} = \Delta X_3 + \beta_{MX}^{(2,EA)} = \Delta \beta_{MX}^{(2)} + \beta_{MX}^{(2,EA)} \quad \text{(Eq. I-116)}$$

$$C_{MX}^{(\phi,P)} = \left(\frac{(v_M + v_X \mid z_M z_X \mid)}{2(v_M v_X)^{1/2}}\right)\left(\Delta X 4 + \left(\frac{4v_M}{(v_M + v_X) \mid z_X \mid}\right) C_{MX}^{(0,EA)}\right)$$
$$= \left(\frac{v_M + v_X \mid z_M z_X \mid}{2(v_M v_X)^{1/2}}\right)\left(\Delta C_{MX}^{(0)} + \left(\frac{4v_M}{(v_M + v_X) \mid z_X \mid}\right) C_{MX}^{(0,EA)}\right) \quad \text{(Eq. I-117)}$$

This mathematical procedure has been implemented in the "ConPitzerNC" worksheet in *ConPitzerNC_MX_(NH4)2SO4.xls* (Output DTN: MO0701SPAPTZER.001), to determine the standard Pitzer model parameters from the Archer model Parameters at each temperature and pressure. The Pitzer parameter values at each temperature determined in this way are then used by the "FitPitzerNC" worksheet in *ConPitzerNC_MX_(NH4)2SO4.xls* to fit new temperature functions and determine the corresponding temperature coefficients.

I.4.3.2 ConPitzerNC Workbook Implementation

The "ConPitzerNC" workbooks are designed to first compute the standard Pitzer model parameters from Archer model parameters in *ConPitzerNC_MX_(NH4)2SO4.xls* (Output DTN: MO0701SPAPTZER.001) and then fit new temperature functions to these values using a FitPitzerNC-type worksheet. The FitPitzerNC worksheet methodology and implementation are the same as that described in Section I.3, and will not be discussed further in this section. The only user-specifiable parameters in *ConPitzerNC_MX_(NH4)2SO4.xls* are the values IDmax and DImax used to specify the method of imposing the upper limit I_{max} of the range of ionic strength over which the parameter conversion between models is valid. They are used together to implement three different options, as follows:

1. IDmax=1. Maximum Ionic Strength Limit I_{max} = DImax, a user assigned value.

2. IDmax=2. Maximum Ionic Strength Limit I_{max} = Solubility Limit as a function of temperature.

3. IDmax=3. Maximum Ionic Strength Limit I_{max} = Smaller of (DImax, Solubility Limit).

I.4.3.3 Example Calculation for ConPitzerNC_MX_(NH4)2SO4.xls Workbook

For the purpose of illustrating the specific manner in which these calculations are carried out, the sequence of calculations performed in *ConPitzerNC_MX_(NH4)2SO4.xls* (located in Output DTN: MO0701SPAPTZER.001) is presented below:

1. CoverPage worksheet: On this worksheet, software identification information and spreadsheet checker review comments are first presented. Next, spreadsheet user information on a contents roadmap, an overview of methodology and data sources, protection of data and computational integrity and manner of presentation of results, are given.

2. Directions worksheet: This worksheet gives directions for converting parameters from Archer to standard Pitzer models and fitting different temperature functions selected by the user to the converted parameters.

3. RunSettings worksheet: Select the desired temperature basis functions.

4. RunSettings worksheet: Select, if desired, Temperature centering and Reference Temperature.

5. RunSettings worksheet: Select Maximum Ionic Strength Option and Maximum Ionic Strength Cut-off Value.

6. ConPitzerNC worksheet: Constant input (Archer) and output (standard Pitzer) model parameters are defined in lines B13:L13 and B14:L14.

7. ConPitzerNC worksheet: The input Archer model temperature coefficients are set in cells B17:I21 and for the Aphi Debye-Hückel parameter in cells B22:I22.

8. ConPitzerNC worksheet: The input Archer parameters and the Aphi Debye-Hückel parameter are calculated as functions of temperature in cells B32:AB37.

9. ConPitzerNC worksheet: Solubilities as a function of temperature are defined on lines B37:AB37 (molality) and B38:AB38 (ionic strength).

10. ConPitzerNC worksheet: Maximum Ionic Strength is calculated as a function of temperature according to the selected option in cells B81:AB81.

11. ConPitzerNC worksheet: The least-squares coefficient matrix A is calculated at each temperature in cells B87:AB95.

12. ConPitzerNC worksheet: The right-hand-side vector B is calculated at each temperature in cells B96:AB98.

13. ConPitzerNC worksheet: The matrix equation solution is carried out at each temperature in cells B99:AB105 and the final solution for parameter differences is calculated in cells B106:AB108.

14. ConPitzerNC worksheet: The standard Pitzer model parameters are calculated from the parameter differences obtained in Step 11, and entered in cells B42:AB45.

15. ConPitzerNC worksheet: The osmotic coefficient is calculated for the Archer model in cells B54:AB59 as a function of temperature and ionic strength.

16. ConPitzerNC worksheet: The osmotic coefficient is calculated for the standard Pitzer model in cells B62:AB67 as a function of temperature and ionic strength.

17. ConPitzerNC worksheet: The model conversion error in the osmotic coefficient is calculated as the difference between the osmotic coefficients from the standard Pitzer and Archer models in cells B71:AB76 as a function of temperature and ionic strength.

18. The RMS error (cells AC71:AC76) and the average, maximum, and minimum values of the osmotic coefficient are also calculated for the two models in cells AD54:AF59 and AD62:AF67, respectively.

19. ConPitzerNC worksheet: Pitzer parameters, osmotic coefficients, and their errors, calculated from the two models, are plotted in charts on the extreme right-hand side of each ConPitzerNC worksheet.

20. FitPitzerNC worksheet: standard Pitzer model parameters are accessed from cells B42:AB45 and are used to fit the temperature coefficients displayed in cells B25:I28. The implementation is the same as previously described in Section I.3.

21. FitPitzerNC worksheet: Pitzer parameters, osmotic coefficients, and their errors, calculated from the input standard Pitzer model parameters and the temperature functions fitted to the same model, are plotted in charts on the extreme right-hand side of the FitPitzerNC worksheet of the ConPitzerNC workbook.

22. ResultsSummary worksheet: The fitted temperature coefficients for the standard Pitzer model are summarized in cells B25:I28.

23. ResultsSummary worksheet: The RMS errors, average, maximum, and minimum values of the osmotic coefficients calculated from the output standard Pitzer model and the input Archer model are summarized here separately for the model conversion and temperature function steps. These statistics enable the errors incurred in the model conversion and temperature function fitting steps to be separately assessed.

The testing and validation of the Pitzer parameters involves the comparison of computed osmotic coefficients from the binary (MX*)* and ternary (MMX, MXX) spreadsheets with the predictions obtained between different Pitzer models reported in the literature sources in order to examine the accuracy of the conversion. This process also includes evaluation of the accuracy of temperature functions of the refitted parameters. Pitzer parameters obtained through the refitting of reported values will be discussed individually in the following section. Parameters obtained for 25°C only will be summarized in a single section since those did not require refitting.

I.4.4 BINARY PITZER INTERACTION PARAMETERS

In this section, the selected Pitzer ion interaction parameters for major salt constituents included in the data0.ypf.R2 database will be described. All these parameters and associated spreadsheets are listed in Tables I-1 and I-2 as Type MX. The discussions on the compilation of parameter data are focused on those that needed refitting due to their temperature dependence. Many parameters did not require any refitting since the gathered values are only valid at 25°C. For these, only simple conversions were necessary.

The user is advised of the limited ranges listed in Table I-1 for several Pitzer parameters. The user must consult the original sources for more information on the permissible physico-chemical conditions for which the parameters are valid. Use of these parameters outside their respective ranges of validation is inadvisable and is not permitted for applications on the Yucca Mountain Project unless specific justification is provided.

I.4.4.1 Ions: Ca^{2+} - Cl^- and $CaCl^+$ - Cl^-

Associated Spreadsheet: *FitPitzerNC_MX_CaCl_CFJC_Model3_Sterner_et_al_1998.xls* (Output DTN: MO0701SPAPTZER.001)

Source: Sterner et al. 1998 [DIRS 162116].

Description: Input parameters and equations from Sterner et al. (1998 [DIRS 162116], Model 3 in Table II) in the FitPitzerNC model parameter fitting worksheet were verified for $\beta^{(0)}_{MX}$, $\beta^{(1)}_{MX}$, and C^{ϕ}, termed Beta(0), Beta(1), and C(phi), respectively, in the spreadsheet for Ca^{2+} - Cl^- and $CaCl^+$ - Cl^-. Sterner et al. (1998 [DIRS 162116]) did not report tabulated values of the osmotic coefficients calculated using their Model 3, but these are depicted in Figure 3 of their study. The standard Pitzer model parameters $\beta^{(0)}_{MX}$, $\beta^{(1)}_{MX}$, and C^{ϕ} were obtained from Table II of the source (Sterner et al. 1998 [DIRS 162116]). The temperature coefficients for the standard form of Pitzer model parameters $\beta^{(0)}_{MX}$, $\beta^{(1)}_{MX}$, and C^{ϕ} are calculated in the FitPitzerNC worksheet using the parameter values computed as a function of temperature from the input temperature function and coefficients in accord with Model 3 of Sterner et al. (1998 [DIRS 162116]) and refitted to the 3- to 4-term temperature function used in the code EQ3/6. The temperature coefficient fitting errors are acceptable for this database and negligible compared to the model parameter conversion errors. It should be noted that Sterner et al.'s Model 3, valid from 25°C to 250°C, also has ternary interaction parameters for $CaCl_2$(aq)-$CaCl_2$(aq) interactions.. In addition to these, the model also incorporates the use of the ion pairs $CaCl^+$ and $CaCl_2$(aq) in the form of log K values for the ion-pairing reactions as a function of temperature. It is expected that the present fitted model for a wide range of ionic strengths (I = 0–45 mol/kg) should yield more accurate solubility predictions than the model presented for $CaCl_2$ by Greenberg and Møller (1989 [DIRS 152684]), which had not been developed for such high ionic strengths. This version of the model yields better results than the previous refit of Model 2 from the same authors, particularly at lower temperatures. Table I-4 compares the current model's 3 to 4 term stoichiometric osmotic coefficients computed using the code EQ3/6 to experimental results from Robinson and Stokes (1965 [DIRS 108567]) at 25°C. The model predictions were computed using all the binary and higher-order parameters plus the ion pairs intrinsic to Model 3 using the computer code EQ3/6. Notice that the 3- to 4-term model prediction at 25°C is very close to the tabulated values of Robinson and Stokes (1965 [DIRS 108567]) up to 6 molal $CaCl_2$ with maximum differences in the neighborhood of 0.7% to 1.7%.

Table I-4. Comparison of Stoichiometric Osmotic Coefficients (ϕ) from the 3- to 4-Term Fit to Those Measured for $CaCl_2$ at 25°C

Molality of $CaCl_2$	3- to 4-Term Fit	Measurements	Difference (%)
1.0	1.0379	1.046	0.77
3.0	1.7396	1.779	2.21
6.0	2.9397	2.891	1.68

NOTE: Measurements taken from Robinson and Stokes 1965 [DIRS 108567], Appendix 8.5, Table 1, p. 478.

I.4.4.2 Ions: Ca^{2+} - NO_3^- and Mg^{2+} - NO_3

Associated Spreadsheet: *FitPitzerNC_MX_Ca(NO3)2_CFJC.xls*
(Output DTN: MO0701SPAPTZER.001)

Source: Wijesinghe and Rard 2005 [DIRS 176847]; Rard et al. 2004 [DIRS 173816]; Rard and Wijesinghe 2003 [DIRS 162327].

Description: For Ca^{2+} - NO_3^-, input parameters and equations from Wijesinghe and Rard (2005 [DIRS 176847], Table 7 and Equation 45) in the FitPitzerNC model parameter worksheet were verified for $\beta_{MX}^{(0)}$, $\beta_{MX}^{(1)}$, and C^{ϕ} (termed Beta(0), Beta(1), and C(phi), respectively, in the spreadsheets). Wijesinghe and Rard (2005 [DIRS 176847]) presented a "7-term" fitting temperature function refitted here to a 3 to 4 term temperature function used in the code EQ3/6. Wijesinghe and Rard (2005 [DIRS 176847]) demonstrated that the osmotic coefficient data from the extended Archer model given by Oakes et al. (2000 [DIRS 162102]) model parameters calculated at selected temperatures and molalities agreed almost exactly within the bounds of relatively small rounding errors. In the work of Wijesinghe and Rard (2005 [DIRS 176847]), the standard Pitzer model parameters $\beta_{MX}^{(0)}$, $\beta_{MX}^{(1)}$, and C^{ϕ} were determined from the Oakes et al. (2000 [DIRS 162102]) model parameters using the methodology presented by Rard and Wijesinghe (2003 [DIRS 162327]). This methodology incorporates the adjustment of the α_1 parameter (denoted as "alpha1" in the worksheet) in the standard Pitzer formulation to optimize the representation of osmotic coefficient data from Wijesinghe and Rard (2005 [DIRS 176847]). This parameter was customarily treated as a constant as originally given by Pitzer (1973 [DIRS 152738]) and in many applications of the Pitzer formulations thereafter. The refitted Pitzer parameters from a "7-term" to 3- to 4-term temperature function indicate a strong agreement with fitting errors in the order of ~10^{-5} to ~10^{-3}. It should be noted that the original model in the study by Oakes et al. (2000 [DIRS 162102]) was claimed to be valid from 25°C to 100°C, so that the results presented in this spreadsheet outside this temperature range represent extrapolations beyond the confirmed range of validity.

For Mg^{2+} - NO_3^-, input parameters from Rard et al. (2004 [DIRS 173816]) consistent with the standard form of Pitzer equations (i.e., $\beta_{MX}^{(0)}$, $\beta_{MX}^{(1)}$, C^{ϕ}, and α_1) were obtained directly from Table 2 and are valid for T=298.15 K. Rard et al. (2004 [DIRS 173816]) conducted a comprehensive evaluation of experimental data for $Mg(NO_3)(aq)$ that includes osmotic coefficient, relative apparent molar enthalpies, and apparent molar heat capacities. These data were then used to evaluate Pitzer parameters consistent with the standard form and the Archer variant of the Pitzer model in a somewhat similar way done for Ca^{2+} - NO_3^- as described above. In this case, the fit optimization to the data is done as a function of ionic strength at a single temperature. The quality of the fits to the experimental data as a result of optimizing the α_1 parameter in both the standard form of Pitzer and Archer type formulations is very similar for both forms of the Pitzer equations. Therefore, the authors recommend the standard form of the Pitzer equations given its simpler form.

I.4.4.3 Ions: Cs^+ - Cl^-

Associated Spreadsheet: *FitPitzerNC_MX_CsCl.xls*
(Output DTN: MO0701SPAPTZER.001)

Source: Holmes and Mesmer 1983 [DIRS 162073].

Description: Input parameters and equations from Holmes and Mesmer (1983 [DIRS 162073], Table V and Equation 25) were verified for $\beta_{MX}^{(0)}$, $\beta_{MX}^{(1)}$, and C^{ϕ}. Calculated values of the osmotic coefficient from this spreadsheet were compared with those listed in a supplement to the data source paper by Holmes and Mesmer (1983 [DIRS 162073], Supplementary Material). There was nearly exact agreement with values calculated in this spreadsheet, with a maximum difference of less than 0.001 over the full range of molality and temperature given in the spreadsheet. This agreement is a confirmation of the validity of the osmotic coefficient calculations reported in this spreadsheet. Additionally, Table I-5 contains a comparison of osmotic coefficients from the 3- to 4-term fitting to experimental results (Robinson and Stokes 1965 [DIRS 108567], Appendix 8.10, Table 3, p 485), with excellent agreement achieved (≤0.5% difference).

Table I-5. Comparison of Osmotic Coefficients (ϕ) from the 3- to 4-Term Fit to Those Measured for CsCl at 25°C

Molality of CsCl	3- to 4-Term Fit	Measurements	Difference (%)
0.1	0.916	0.917	0.1
0.5	0.872	0.869	0.3
1.0	0.861	0.857	0.5
3.0	0.881	0.880	0.1
6.0	0.950	0.945	0.5

NOTE: Measurements taken from Robinson and Stokes 1965 [DIRS 108567], Appendix 8.10, Table 3, p. 485.

I.4.4.4 Ions: H^+ - Cl^-

Associated Spreadsheet: *FitPitzerNC_MX_HCl.xls*
(Output DTN: MO0701SPAPTZER.001)

Source: Holmes et al. 1987 [DIRS 162075].

Description: Input parameters and equation from Holmes et al. (1987 [DIRS 162075], Table 3 (first column) and Equation 31) were verified for $\beta_{MX}^{(0)}$, $\beta_{MX}^{(1)}$, C^{ϕ}, and A^{ϕ}. The RMS error in the osmotic coefficient over the fitted temperature range (see spreadsheet tab "Results Summary") for the 3- to 4-term conversion was >0.001. Calculated values of the osmotic coefficient from this spreadsheet were compared with those listed at 25°C in the extensive tables from Robinson and Stokes (1965 [DIRS 108567], Table 1, Appendix 8.10, p. 483). There was very good agreement with the spreadsheet values at 25°C as shown in Table I-6, with a maximum difference of 0.006 at I = 3 mol/kg. Model I of Holmes et al. (1987 [DIRS 162075], Table 3 and text p. 876) is stated to be valid up to an ionic strength of 7.0 mol/kg. This agreement is considered to be sufficient confirmation of the validity of the osmotic coefficient calculations reported in the spreadsheet.

Table I-6. Comparison of Osmotic Coefficients (ϕ) from the 3- to 4-Term Fit to Those Measured for HCl at 25°C

Molality of HCl	3- to 4-Term Fit	Measurements	Difference (%)
0.1	0.944	0.943	0.1
0.5	0.974	0.974	<0.1
1.0	1.039	1.039	<0.1
3.0	1.342	1.348	0.4
6.0	1.844	1.845	<0.1

NOTE: Measurements taken from Robinson and Stokes 1965 [DIRS 108567], Appendix 8.10, Table 1, p. 483.

I.4.4.5 Ions: H^+ - HSO_4^-

Associated Spreadsheet: *FitPitzerNC_MX_HHSO4.xls*
(Output DTN: MO0701SPAPTZER.001)

Source: Holmes and Mesmer 1994 [DIRS 162078].

Description: Input parameters and equation from Holmes and Mesmer (1994 [DIRS 162078], Table 4 and Equation 28) were verified for $\beta_{MX}^{(0)}$, $\beta_{MX}^{(1)}$, and C^{ϕ}. Note that there is an error in Table 4 of the source document (Holmes and Mesmer 1994 [DIRS 162078]); it gives incorrect p1 parameter values that are too large by a factor of 1,000. Calculated values of the hypothetical fully dissociated binary osmotic coefficient from this spreadsheet cannot be compared with any experimental values because experimentally determined values include the effects of partial dissociation into H^+, HSO_4^-, and SO_4^{2-} ions rather than H^+ and HSO_4^- ions only. However, the values of the calculated osmotic coefficient are reasonable for a fully dissociated 1-1 electrolyte, except at the highest ionic strengths where the source parameters are not constrained by experimental measurements and are larger than expected for an electrolyte of this charge type. The binary parameters for H^+ and HSO_4^- should only be used in combination with the H^+ and SO_4^{2-} parameters and the mixing parameters (θ, ψ) should be taken from the same source document. The only exception is the inclusion of ternary interactions (ψ) for H^+-HSO_4^--SO_4^{2-} determined by Baes et al. (1993 [DIRS 168318]) in their study of the cupric sulfate system. It was noted that the presence of this parameter with a non-zero value in the database did not generate any discrepancies in computed osmotic coefficients or activity coefficients. It should also be noted that the higher-order electrostatic interactions represented by the ${}^{E}\theta$ and ${}^{E}\theta'$ third order terms of the Pitzer model were taken into account in this source document. In an earlier study (Holmes and Mesmer 1992 [DIRS 162076]), the authors did not account for these interactions. Holmes and Mesmer (1994 [DIRS 162078]) demonstrate that their new fits result in calculations that agree well with the experimental measurements over a range of conditions that include different degrees of dissociation of HSO_4^-. In fact, they found that the earlier models also result in acceptable fits.

I.4.4.6 Ions: H^+ - SO_4^{2-}

Associated Spreadsheet: *FitPitzerNC_MX_H2SO4.xls*
(Output DTN: MO0701SPAPTZER.001)

Source: Holmes and Mesmer 1994 [DIRS 162078].

Description: Input parameters and equation from Holmes and Mesmer (1994 [DIRS 162078], Table 4 and Equation 28) were verified for $\beta_{MX}^{(0)}$, $\beta_{MX}^{(1)}$, and C^{ϕ}. Calculated values of the hypothetical fully dissociated binary osmotic coefficient from this spreadsheet cannot be compared with any experimental values because experimentally determined values include the effects of partial dissociation into H^+, HSO_4^-, and SO_4^{2-} ions rather than H^+ and SO_4^{2-} ions only. However, the values of the calculated osmotic coefficient are reasonable for a fully dissociated 1-2 electrolyte, except at the highest ionic strengths where the source parameters are not constrained by experimental measurements and are unrealistically large. The binary parameters for H^+ and SO_4^{2-} should only be used in combination with the H^+ and HSO_4^- parameters and the mixing parameters (θ, ψ) should be taken from the same source document. The only exception is the inclusion of ternary interactions (ψ) for H^+-HSO_4^--SO_4^{2-} determined by Baes et al. (1993 [DIRS 168318]) in their study of the cupric sulfate system. It was noted that the presence of this parameter with a non-zero value in the database did not generate any discrepancies in computed osmotic coefficients or activity coefficients. In addition, several values of C^{ϕ} were independently calculated using the input source data and underlying equations, and exact agreement was obtained with the values calculated in the spreadsheet. It should also be noted that the higher-order electrostatic interactions represented by the ${}^{E}\theta$ and ${}^{E}\theta'$ third-order terms of the Pitzer model were taken into account in this source document. In an earlier study (Holmes and Mesmer 1992 [DIRS 162076]), the authors did not account for these interactions. Holmes and Mesmer (1994 [DIRS 162078]) demonstrate that their new fits result in calculations that agree well with the experimental measurements over a range of conditions that include different degrees of dissociation of HSO_4^-. In fact, they found that the earlier models also result in acceptable fits.

I.4.4.7 Ions: H^+ - NO_3^-

Associated Spreadsheet: *FitPitzerNC_MX_H_NO3_CFJC.xls*
(Output DTN: MO0701SPAPTZER.001)

Source: Felmy et al. 1994 [DIRS 162111]; Clegg and Brimblecombe 1990 [DIRS 162067].

Description: The binary parameters $\beta_{MX}^{(0)}$, $\beta_{MX}^{(1)}$, and C^{ϕ} listed by Clegg and Brimblecombe (1990 [DIRS 162067], Table X) at 298.15 K were compared to the values generated with the coefficients reported by Felmy et al. (1994 [DIRS 162111], Table 1 with Equation 2), who used the former source for derivation of Pitzer temperature-dependent parameter data. Unlike the previous FitPitzerNC spreadsheets, the binary parameters were refitted using the standard regression function in Excel. The reproducibility of the refitted binary parameters when compared with those tabulated from Clegg and Brimblecombe (1990 [DIRS 162067], Table 10, p. 5378) at 298.15 K was identical. Visual comparison of mean activity and rational osmotic coefficients (Clegg and Brimblecombe 1990 [DIRS 162067], Figures 1 and 9) calculated using

these binary parameters indicate a strong agreement with those given by Clegg and Brimblecombe (1990 [DIRS 162067]) up to an HNO_3 concentration of ~6 molal. These favorable comparisons demonstrate the acceptability of these coefficients for this database. The Clegg and Brimblecombe model (1990 [DIRS 162067]) is mole-fraction based, and these authors suggested this upper concentration value for the binary parameters they report for the Pitzer model that is molality based.

I.4.4.8 Ions: K^+ - Br^-

Associated Spreadsheet: *FitPitzerNC_MX_KBr.xls*
(Output DTN: MO0701SPAPTZER.001)

Source: Holmes and Mesmer 1998 [DIRS 162083].

Description: Input parameters and equation from Holmes and Mesmer (1998 [DIRS 162083], Table 4 and Equation 14) were verified for $\beta_{MX}^{(0)}$, $\beta_{MX}^{(1)}$, and C^{ϕ}. The RMS error in the osmotic coefficient over the fitted temperature range (see spreadsheet tab "Results Summary") from the 3- to 4-term conversion is typically $\Delta\phi$ ~0.001, except at higher ionic strengths where the deviation becomes 0.005 and 0.026 at I = 3 and 6 mol/kg, respectively. Values of the osmotic coefficient calculated using the source equation were compared with experimental values listed at 25°C by Robinson and Stokes (1965 [DIRS 108567], Appendix 8.10, Table 2, p. 484) and at 200°C in the source document (Holmes and Mesmer 1998 [DIRS 162083], Table 1, p. 728). Results of the comparison at 25 °C are shown in Table I-7; there was good agreement with the 3- to 4-term values calculated in this spreadsheet, with a maximum difference of 0.005 at I = 3.0 mol/kg. Good agreement is also obtained at 200°C up to high ionic strengths (e.g., at I = 6.097 mol/kg, ϕ = 1.0264), while in Holmes and Mesmer (1998 [DIRS 162083], Table 1, p. 728) at I = 6 mol/kg, the value of ϕ = 1.0258. It should be noted that there are two errors in Equation 14 of Holmes and Mesmer (1998 [DIRS 162083], p. 734) in the functional formula of the temperature function, and in the reference temperature T_r that was incorrectly reported as 413.15 K instead of 298.15 K. The correct version of this equation is given in the spreadsheet cover page, and it is equivalent to the equation as originally derived by Holmes and Mesmer (1983 [DIRS 162073], Equation 25).

Table I-7. Comparison of Osmotic Coefficients (ϕ) from the 3- to 4-Term Fit to Those Measured for KBr at 25°C

Molality of KBr	3- to 4-Term Fit	Measurements	Difference (%)
0.1	0.928	0.928	0.0
0.5	0.905	0.904	0.1
1.0	0.907	0.907	<0.0
3.0	0.960	0.955	0.5

NOTE: Measurements taken from Robinson and Stokes 1965 [DIRS 108567], Appendix 8.10, Table 2, p. 484.

I.4.4.9 Ions: K^+ - Cl^-

Associated Spreadsheet: *FitPitzerNC_MX_KCl.xls*
(Output DTN: MO0701SPAPTZER.001)

Source: Greenberg and Møller 1989 [DIRS 152684].

Description: Input parameters and equation from Greenberg and Møller (1989 [DIRS 152684], Tables 1 and 3, Equation 3) were verified for $\beta_{MX}^{(0)}$, $\beta_{MX}^{(1)}$, C^{ϕ}, and A^{ϕ}. The RMS error in the osmotic coefficient over the fitted temperature range (see spreadsheet tab "Results Summary") for source to 3- to 4-term conversion was $\Delta\phi < 0.001$. In addition, several values of $\beta_{MX}^{(0)}$ were independently calculated using the input source data and underlying equations, and exact agreement was obtained with the values calculated in the spreadsheet. Calculated values of the osmotic coefficient from this spreadsheet were compared with those from the recent critical review of Archer (1999 [DIRS 162064], Table 7). There was good agreement with values calculated in this spreadsheet, with a maximum difference of 0.006, but with much better agreement at most temperatures and molalities. Direct comparison at 25°C and 100°C is shown in Table I-8 below. These minor differences most likely arise from the differences in the underlying data sources. This agreement is considered sufficient confirmation of the validity of the osmotic coefficient calculations reported in this spreadsheet.

Table I-8. Comparison of Osmotic Coefficients (ϕ) Values from the 3- to 4-Term Fit to Those Measured for KCl at 25°C and 100°C

25°C			
Molality of KCl	**3- to 4-Term Fit**	**Measurements**	**Difference (%)**
0.1	0.926	0.9261	<0.1
0.5	0.900	0.9000	0.1
1.0	0.898	0.8992	0.1
100°C			
0.1	0.918	0.9168	0.1
0.5	0.895	0.8939	0.1
1.0	0.899	0.8984	0.1
6.0	1.032	1.0341	0.2

NOTE: Measurements taken from Archer 1999 [DIRS 162064], Table 7.

I.4.4.10 Ions: K^+ - SO_4^{2-}

Associated Spreadsheet: *FitPitzerNC_MX_K2SO4.xls*
(Output DTN: MO0701SPAPTZER.001)

Source: Greenberg and Møller 1989 [DIRS 152684].

Description: Input parameters and equation from Greenberg and Møller (1989 [DIRS 152684], Tables 1 and 3, Equation 3) were verified for $\beta_{MX}^{(0)}$, $\beta_{MX}^{(1)}$, C^{ϕ}, and A^{ϕ}. The RMS error in the osmotic coefficient over the fitted temperature range (see spreadsheet tab "Results Summary") for the 3- to 4-term fitting conversion was negligible ($<10^{-10}$). In addition, several values of

$\beta^{(0)}_{MX}$, $\beta^{(1)}_{MX}$, and C^{ϕ} were independently calculated using the input source data and underlying equations, and exact agreement was obtained with the values calculated in the spreadsheet. In Table I-9 below, calculated values of the osmotic coefficient from this spreadsheet were compared with those listed by Holmes and Mesmer (1986 [DIRS 162074], Table V). There was reasonable agreement of the values reported in this study with values calculated in the spreadsheet (differences in osmotic coefficient, $\Delta\phi \leq 0.02$), except at 200°C where the error was relatively high ($\Delta\phi_{max} = 0.11$). Because the available data do not extend beyond I = 2 mol/kg at low temperatures and I = 7 mol/kg at high temperatures, and due to solubility limitations, the values calculated in this spreadsheet at the higher ionic strengths are not physically relevant. The agreement at lower ionic strengths and temperatures is confirmation of the validity of the osmotic coefficient calculations reported in this spreadsheet.

Table I-9. Comparison of Osmotic Coefficients (ϕ) Values from the 3- to 4-Term Fit to Those Measured for K_2SO_4 at 25°C and 150°C.

25°C			
Molality of K_2SO_4	**3- to 4-Term Fit**	**Measurements**	**Difference (%)**
0.1	0.784	0.779	0.6
0.5	0.686	0.690	0.6
1.0	0.631	0.651	3.1
150°C			
0.1	0.743	0.726	2.3
0.5	0.652	0.646	1.2
1.0	0.616	0.613	0.5

NOTE: Measurements taken from Holmes and Mesmer 1986 [DIRS 162074], Table V.

I.4.4.11 Ions: Cs^+ - Br^-

Associated Spreadsheet: *FitPitzerNC_MX_CsBr.xls*
(Output DTN: MO0701SPAPTZER.001)

Source: Holmes and Mesmer 1998 [DIRS 162083].

Description: Input parameters and equations from Holmes and Mesmer (1998 [DIRS 162083], Table 4 and Equation 14) were verified for $\beta^{(0)}_{MX}$, $\beta^{(1)}_{MX}$, and C^{ϕ}. The RMS fitting errors over the corresponding fitted temperatures between Holmes and Mesmer's (1998 [DIRS 162083]) Equation 14 and the spreadsheet's 3- to 4-term fit were mostly $\Delta\phi < 0.001$, with the exception at I = 6 mol/kg where $\Delta\phi = 0.0045$. Values of the osmotic coefficient calculated using the source equation were compared with experimental values listed in the source document at 200°C (Holmes and Mesmer 1998 [DIRS 162083], Table 1), and at 25°C against Robinson and Stokes (1965 [DIRS 108567], Appendix 8.10, Table 3, p. 485). At 25°C, there was good agreement with values calculated in this spreadsheet, with a maximum difference of $\Delta\phi_{max} = 0.003$ at I =0.1 mol/kg as shown in Table I-10. At 200°C, good agreement is also obtained with $\Delta\phi = 0.055$ at ~6 mol/kg. It should be noted that there are two errors in Equation 14 of Holmes and Mesmer (1998 [DIRS 162083], p. 734): (1) an error in the formula of the temperature function; and (2) an error in the reference temperature T_r, which was incorrectly reported as 413.15 K instead

of 298.15 K. The corrected version of this equation is given on the spreadsheet cover page and is equivalent to the correct form of the equation as originally derived by Holmes and Mesmer (1983 [DIRS 162073], Equation 25).

Table I-10. Comparison of Source Osmotic Coefficients (ϕ) to Those Measured for CsBr at 25°C

Molality of CsBr	Source Equation	Measurements	Difference (%)
0.1	0.914	0.917	0.3
0.5	0.867	0.865	0.2
1.0	0.852	0.850	0.2
3.0	0.866	0.866	0.0

NOTE: Measurements taken from Robinson and Stokes 1965 [DIRS 108567], Appendix 8.10, Table 3, p. 485.

I.4.4.12 Ions: Li^+ - Br^-

Associated Spreadsheet: *FitPitzerNC_MX_LiBr.xls*
(Output DTN: MO0701SPAPTZER.001)

Source: Holmes and Mesmer 1998 [DIRS 162083].

Description: Input parameters and equations from Table 4 and Equation 14 of Holmes and Mesmer (1998 [DIRS 162083], pp. 737 and 734, respectively) were verified for $\beta_{MX}^{(0)}$, $\beta_{MX}^{(1)}$, and C^{ϕ}. The RMS error in the osmotic coefficient over the fitted temperature range (see spreadsheet tab "Results Summary") for the 3- to 4-term conversion is typically $\Delta\phi$ ~0.001, except towards higher ionic strengths (e.g., deviations approach 0.02 at I = 6 mol/kg). Values of the osmotic coefficient calculated using the source equation were compared with experimental values listed by Holmes and Mesmer (1998 [DIRS 162083], Table 1, p. 728) at 200°C and at 25°C against Robinson and Stokes (1965 [DIRS 108567], Appendix 8.10, Table 3). For 25°C, the comparison is shown in Table I-11; there was good agreement with values calculated in this spreadsheet, with a maximum difference of $\Delta\phi_{max} = 0.007$ at I = 3.0 mol/kg, increasing to $\Delta\phi_{max} = 0.01$ at I = 6.0 mol/kg. Good agreement is also obtained at 200°C, e.g., $\phi = 1.146$ at 3.07 molality (Holmes and Mesmer 1998 [DIRS 162083], Table 1, p. 728), compared with $\phi = 1.138$ from the source equation at exactly 3.0 molality. It should be noted that there are two errors in Equation 14 of Holmes and Mesmer (1998 [DIRS 162083], p. 734) for the functional formula of the temperature function, and an error in the reference temperature T_r, which was incorrectly reported as 413.15 K instead of 298.15 K. The correct version of this equation is given in the spreadsheet cover page and is equivalent to the correct form of the equation as originally derived by Holmes and Mesmer (1983 [DIRS 162073], Equation 25).

Table I-11. Comparison of Source Osmotic Coefficients (ϕ) to Those Measured for LiBr at 25°C

Molality of LiBr	Source Equation	Measurements	Difference (%)
0.1	0.942	0.943	0.1
0.5	0.972	0.970	0.2
1.0	1.038	1.035	0.3
3.0	1.373	1.364	0.7
6.0	1.999	1.989	0.5

NOTE: Measurements taken from Robinson and Stokes 1965 [DIRS 108567], Appendix 8.10, Table 1, p. 483.

I.4.4.13 Ions: Li^+ - Cl^-

Associated Spreadsheet: *FitPitzerNC_MX_LiCl.xls*
(Output DTN: MO0701SPAPTZER.001)

Source: Holmes and Mesmer 1983 [DIRS 162073].

Description: Input parameters and equation from the source document were verified for $\beta^{(0)}_{MX}$, $\beta^{(1)}_{MX}$, and C^{ϕ} data from Holmes and Mesmer (1983 [DIRS 162073], Table V, Equation 25). Fitting errors between the source and spreadsheet 3- to 4-term equation were negligible and resulted in osmotic coefficient differences of $<10^{-5}$. Values of the osmotic coefficient at ~1.0 mol/kg calculated using the source equation (Holmes and Mesmer 1983 [DIRS 162073], Equation 25) were compared with experimental values listed in the source document (Table III) at 250°C at ϕ = 0.8292 and 0.825, respectively. For the comparison at 25°C against Robinson and Stokes (1965 [DIRS 108567], Appendix 8.10, Table 1, p. 483), there is good agreement with values calculated in this spreadsheet, with a maximum difference of Δϕ = 0.004 at I = 6.0 mol/kg as shown in Table I-12 below.

Table I-12. Comparison of Source Osmotic Coefficients (ϕ) to Those Measured for LiCl at 25°C

Molality of LiCl	Source Equation	Measurements	Difference (%)
0.1	0.941	0.939	0.2
0.5	0.963	0.963	0.0
1.0	1.016	1.018	0.2
3.0	1.287	1.286	0.1
6.0	1.795	1.791	0.2

NOTE: Measurements taken from Robinson and Stokes 1965 [DIRS 108567], Appendix 8.10, Table 1, p. 483.

I.4.4.14 Ions: Mg^{2+} - Cl^-

Associated Spreadsheet: *FitPitzerNC_MX_MgCl2.xls*
Output DTN: MO0701SPAPTZER.001

Source: Pabalan and Pitzer 1987 [DIRS 162096].

Description: Input parameters and equations from the source document by Pabalan and Pitzer (1987 [DIRS 162096], Appendix, p. 2442) were verified for $\beta^{(0)}_{MX}$, $\beta^{(1)}_{MX}$, and C^{ϕ} by

independently calculating these parameters, using the input source data and the underlying equations, and agreement was obtained with the values calculated in the spreadsheet. The RMS error in the osmotic coefficient over the fitted temperature range (see spreadsheet tab "Results Summary") for the 3- to 4-term conversion is typically $\Delta\phi$ <0.001, except at I = 18 mol/kg, when it is 0.0015. In addition, osmotic coefficients were calculated from the source equation (Pabalan and Pitzer 1987 [DIRS 162096], Appendix, p. 2442) and compared with those listed in the tables from Holmes et al. (1997 [DIRS 162080], Table 2) and Wang et al. (1998 [DIRS 162109], Table 4). There was fair agreement with values calculated in this spreadsheet, within 0.013 at 25°C (see Table I-13), within 0.2 at 100°C (see Table I-14), within 0.25 at 150°C, and within 0.2 at 200°C. These larger differences at higher temperatures arise from the differences in the data used to calculate the values in these two papers and the generally lower accuracy in high temperature thermodynamic measurements.

Table I-13. Comparison of Source Osmotic Coefficients (ϕ) to Those Measured for $MgCl_2$ at 25°C

Molality of $MgCl_2$	Source Equation	Measurements	Difference (%)
0.1	0.8618	0.8606	0.14
0.5	0.9439	0.9439	0.00
1.0	1.1088	1.1100	0.11
3.0	2.0205	2.0070	0.67

NOTE: Measurements taken from Holmes et al. 1997 [DIRS 162080], Table 2, p. 1369.

Table I-14. Comparison of Source Osmotic Coefficients (ϕ) to Those Measured for $MgCl_2$ at 100°C

Molality of $MgCl_2$	Source Equation	Measurements	Difference (%)
0.05	0.8429	0.8460	0.4
0.1	0.8324	0.8332	0.1
0.5	0.8737	0.8628	1.3
1.0	0.9856	0.9921	0.7
3.0	1.6634	1.6891	1.5
6.0	2.8450	3.0357	6.3

NOTE: Measurements taken from Wang et al. 1998 [DIRS 162109], Table 4, p. 979.

I.4.4.15 Ions: Mg^{2+} - SO_4^{2-}

Associated Spreadsheet: *FitPitzerNC_MX_MgSO4.xls*
(Output DTN: MO0701SPAPTZER.001)

Source: Pabalan and Pitzer 1987 [DIRS 162096].

Description: Input parameters and equations from Pabalan and Pitzer (1987 [DIRS 162096], Appendix, p. 2443) were verified for $\beta^{(0)}_{MX}$, $\beta^{(1)}_{MX}$, and C^{ϕ}. The RMS error in the osmotic coefficient over the fitted temperature range (see spreadsheet tab "Results Summary") for the 3- to 4-term conversion is typically $\Delta\phi$ <0.01, except at very high ionic strengths: e.g., at I = 12 and 24 mol/kg, then $\Delta\phi$ = 0.014 and 0.132, respectively. Calculated values of the osmotic coefficient from this spreadsheet were compared with those listed in the Table V of Phutela and Pitzer (1986 [DIRS 162097]), which is the original source of the temperature coefficients used

by Pabalan and Pitzer (1987 [DIRS 162096]). There is good agreement with source equation values calculated in this spreadsheet, with a maximum difference of ~0.001. The minor differences that exist most likely arise from differences in the Debye-Hückel A^{φ}(phi) coefficient. In the original source paper by Phutela and Pitzer (1986 [DIRS 162098]), models with both constant and temperature-dependent α_2 parameters were mentioned, but the model from which the listed osmotic coefficient results were generated was not clearly specified. However, Pabalan and Pitzer (1987 [DIRS 162096]) implied the use of a constant alpha2 parameter, and this was confirmed by the good agreement with the calculations in this spreadsheet. It should be noted that the highest ionic strengths, for which unrealistic osmotic coefficients are calculated in this spreadsheet, greatly exceed the concentration range for which the model was parameterized. The model should provide reasonably accurate results at ionic strengths below the solubility limit. This is supported by a comparison with experimental measurements at 25°C in Table I-15 below, where the 3- to 4-term fitted results are compared to the experiments at 25°C and 100°C with a $\Delta\phi_{max} = 0.012$.

Table I-15. Comparison of 3- to 4-Term Fitting Osmotic Coefficients (ϕ) to Those Measured for $MgSO_4$ at 25°C and 100°C

25°C			
Molality of $MgSO_4$	**3- to 4-Term Fit**	**Measurements**	**Difference (%)**
0.1	0.597	0.596	0.2
0.5	0.530	0.527	0.6
1.0	0.531	0.527	0.8
3.0	0.915	0.925	1.1
100°C			
0.1	0.527	0.529	0.4
0.5	0.438	0.444	1.3
1.0	0.412	0.419	1.7
3.0	0.646	0.634	1.9

NOTE: Measurements taken from Phutela and Pitzer 1986 [DIRS 162098], Table V, p. 899.

I.4.4.16 Ions: Na^+ - Br^-

Associated Spreadsheet: *FitPitzerNC_MX_NaBr.xls*
(Output DTN: MO0701SPAPTZER.001)

Source: Holmes and Mesmer 1998 [DIRS 162083].

Description: Input parameters and equations from Table 4 and Equation 14 of Holmes and Mesmer (1998 [DIRS 162083], pp. 737 and 734, respectively) were verified for $\beta^{(0)}_{MX}$, $\beta^{(1)}_{MX}$, and C^{ϕ}. The average of the RMS error in the osmotic coefficient over the fitted temperature range (see spreadsheet tab "Results Summary") for the 3- to 4-term conversion was 0.0013, with a $\Delta\phi_{max} = 0.0023$. Values of the osmotic coefficient calculated using the source equation were compared with experimental values listed by Holmes and Mesmer (1998 [DIRS 162083], Table 1, p. 728) at 200°C, and at 25°C against both Robinson and Stokes (1965 [DIRS 108567]) and Rard and Archer (1995 [DIRS 162104]). Comparison at 25°C is shown in Table I-16, where there was good agreement with values calculated in this spreadsheet, with a maximum difference

of 0.008 at I = 6.0 mol/kg. At 200°C, good agreement is obtained over this range of molalities as seen in Table I-17. It should be noted that there are two errors in Equation 14 of Holmes and Mesmer (1998 [DIRS 162083], p. 734) for the formula of the temperature function, and an error in the reference temperature T_r, which was incorrectly reported as 413.15 K instead of 298.15 K. The correct version of this equation is given in the spreadsheet cover page and is equivalent to the correct form of the equation as originally derived by Holmes and Mesmer (1983 [DIRS 162073], Equation 25).

Table I-16. Comparison of Source Osmotic Coefficients (ϕ) to Those Measured for NaBr at 25°C

Molality of NaBr	Source Equation	Measurements	Difference (%)
0.1	0.935	0.934[a]	0.1
0.5	0.933	0.933[a]	0.0
1.0	0.959	0.958[a]	0.1
3.0	1.109	1.107[a]	0.2
6.0	1.381	1.389[b]	0.6

[a] Taken from Robinson and Stokes 1965 [DIRS 108567], Appendix 8.10, Table 1, p. 483.
[b] Taken from Rard and Archer 1995 [DIRS 162104], Table 3; ϕ at 6.0 mol/kg was linearly interpolated from 5.9151 and 6.1073 mol/kg values.

Table I-17. Comparison of Source Osmotic Coefficients (ϕ) to Those Measured for NaBr at 200°C

Spreadsheet Calculated Values		Experimental Values	
Molality of NaBr	Source Equation	Molality of NaBr	Measured
1.0	0.921	0.9814	0.9225
3.0	1.049	2.8264	1.0431
6.0	1.234	6.1392	1.2401

NOTE: Experimental values taken from Holmes and Mesmer 1998 [DIRS 162083], Table1, p.728.

I.4.4.17 Ions: Na^+ - NO_3^-

Associated Spreadsheet: *FitPitzerNC_MX_NaNO3_CFJC.xls*
(Output DTN: MO0701SPAPTZER.001)

Source: Wijesinghe and Rard 2005 [DIRS 176847]; Archer 2000 [DIRS 162065].

Description: Input parameters and equations from Wijesinghe and Rard (2005 [DIRS 176847], Table 7 and Equation 49) in the FitPitzerNC model parameter worksheet were verified for $\beta_{MX}^{(0)}$, $\beta_{MX}^{(1)}$, and C^{ϕ} (termed Beta(0), Beta(1), and C(phi), respectively, in the spreadsheets). Wijesinghe and Rard (2005 [DIRS 176847]) presented a "7-term" fitting temperature function refitted here to a 3- to 4-term temperature function to be consistent with that used in the computer code EQ3/6. They demonstrated that the osmotic coefficient data from the extended model given by Archer (2000 [DIRS 162065]) model parameters for $NaNO_3$ calculated at selected temperatures and molalities agreed almost exactly within the bounds of relatively small rounding errors. In the work of Wijesinghe and Rard (2005 [DIRS 176847]), the standard Pitzer model parameters $\beta_{MX}^{(0)}$, $\beta_{MX}^{(1)}$, and C^{ϕ} were determined from the Archer (2000 [DIRS 162065]) model parameters using the methodology presented by Rard and Wijesinghe (2003

[DIRS 162327]). This methodology incorporates the adjustment of the α_1 parameter (denoted as "alpha1" in the worksheet) in the standard Pitzer formulation to optimize the representation of osmotic coefficient data in the study by Wijesinghe and Rard (2005 [DIRS 176847]). This parameter was customarily treated as a constant as originally given by Pitzer (1973 [DIRS 152738]) and in many applications of the Pitzer formulations thereafter. The refitted Pitzer parameters from a "7-term" to 3- to 4-term temperature function indicate a strong agreement with fitting errors in the order of ~10^{-5} to ~10^{-3} (Figure I-1). It should be noted that Archer's original model was claimed to be valid from –37°C to 152°C, so that the results presented in this spreadsheet at higher temperatures represent an extrapolation beyond the confirmed range of validity of the source model.

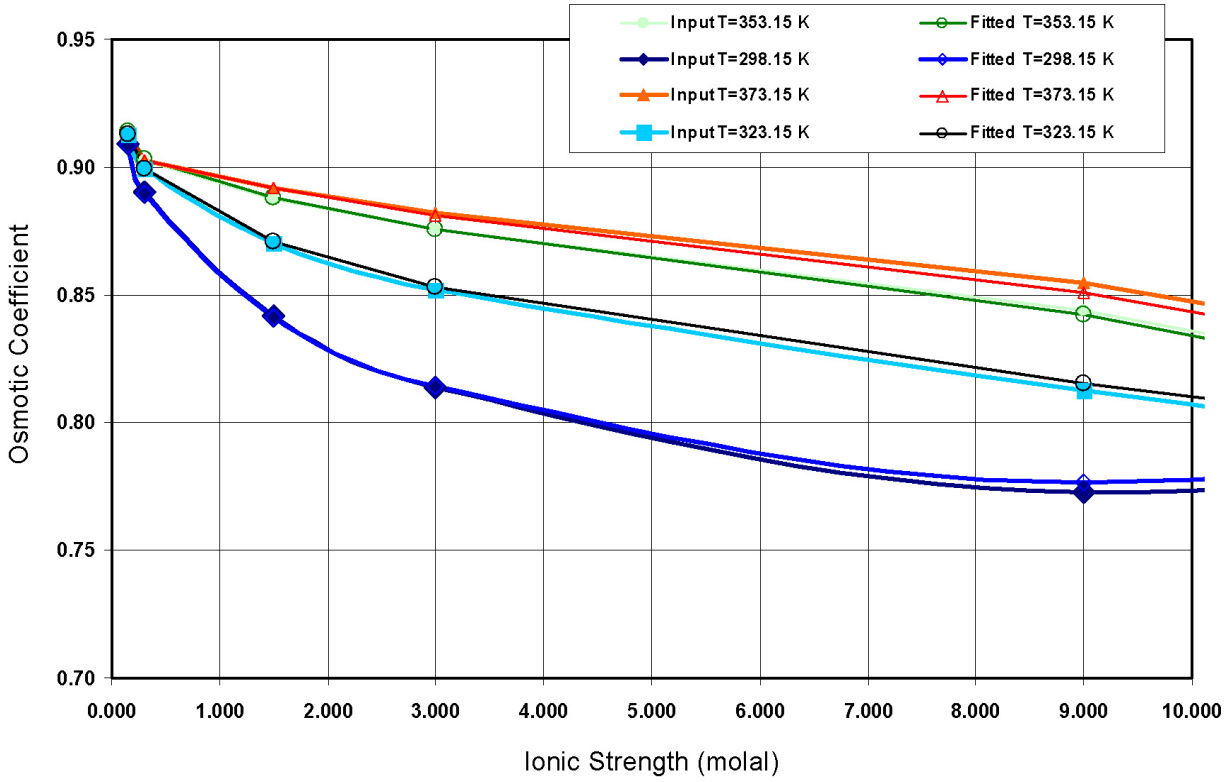

Output DTN: MO0701SPAPTZER.001.

Source: Archer 2000 [DIRS 162065].

Figure I-1. Calculated Osmotic Coefficients from the Input "7-term" Temperature Function Compared to the 3- to 4-Term Fit

I.4.4.18 Ions: Na^+ - SO_4^{2-}

Associated Spreadsheet: *FitPitzerNC_MX_Na2SO4.xls*
(Output DTN: MO0701SPAPTZER.001)

Source: Greenberg and Møller 1989 [DIRS 152684].

Description: Input parameters and equation from Greenberg and Møller (1989 [DIRS 152684], Tables 1 and 3, Equation 3) were verified for $\beta_{MX}^{(0)}$, $\beta_{MX}^{(1)}$, C^{ϕ}, and A^{ϕ}. The average of the RMS errors in the osmotic coefficient over the fitted temperature range (see spreadsheet tab "Results Summary") for the 3- to 4-term conversion was 0.012, with $\Delta\phi_{max} = 0.0436$ at I = 18 mol/kg, which is well above the solubility limit and not physically relevant. Calculated values of the osmotic coefficient from this spreadsheet were also compared with those listed by Holmes and Mesmer (1986 [DIRS 162074], Table IV) and by Rard et al. (2000 [DIRS 162105], Table XI). There was reasonable agreement of the values reported in these two papers with values calculated in this spreadsheet, as indicated in the summary on the associated spreadsheet cover page, and specifically as shown in Table I-18 comparing the spreadsheet results to those of Rard et al. (2000 [DIRS 162105]) at 25°C and 100°C. The differences between the values in the two papers arise from differences in the underlying data sources. Also note that because the solubility does not extend to I = 18 mol/kg, the reported values in this spreadsheet at this high ionic strength are not physically relevant. This agreement is considered to be sufficient confirmation of the validity of the osmotic coefficient calculations reported in this spreadsheet. In addition, several values of $\beta_{MX}^{(0)}$, $\beta_{MX}^{(1)}$, and C^{ϕ} were independently calculated using the input source data and underlying equations, and exact agreement was obtained with the values calculated in the spreadsheet.

Table I-18. Comparison of Fitted Osmotic Coefficients (ϕ) to Those Measured for Na_2SO_4 at 25°C and 100°C

25°C Comparison			
Molality of Na_2SO_4	**Fitted Equation**	**Measurements**	**Difference (%)**
0.05	0.8281	0.8260	0.3
0.1	0.7927	0.7902	0.3
0.5	0.6871	0.6931	0.9
1.0	0.6345	0.6451	1.6
3.0	0.6602	0.6700	1.5
100°C Comparison			
0.05	0.8041	0.8036	0.1
0.1	0.7686	0.7682	0.1
0.5	0.6860	0.6917	0.8
1.0	0.6591	0.6595	0.1
3.0	0.6380	0.6387	0.1

NOTE: Measurements taken from Rard et al. 2000 [DIRS 162105], Table XI.

I.4.4.19 Ions: Na^+ - Cl^-

Associated Spreadsheet: *FitPitzerNC_MX_NaCl.xls*
(Output DTN: MO0701SPAPTZER.001)

Source: Greenberg and Møller 1989 [DIRS 152684].

Description: Input parameters and equations from Greenberg and Møller (1989 [DIRS 152684], Tables 1 and 3, and Equation 3) were verified for $\beta_{MX}^{(0)}$, $\beta_{MX}^{(1)}$, C^{ϕ}, and A^{ϕ}. The RMS error in the osmotic coefficient over the fitted temperature range (see spreadsheet tab "Results Summary")

for the 3- to 4-term conversion was $\Delta\phi < 0.001$. Calculated values of the osmotic coefficient from this spreadsheet were compared with those listed in the extensive tables from Clarke and Glew (1985 [DIRS 162066], Table 19A). There was good agreement with values calculated in this spreadsheet, with a maximum difference of 0.005, but with much better agreement at most temperatures and molalities; this is shown in Table I-19. These minor differences most likely arise from the differences in the underlying data sources. This agreement is considered to be sufficient confirmation of the validity of the osmotic coefficient calculations reported in this spreadsheet. In addition, several values of $\beta_{MX}^{(1)}$ parameters were independently calculated using the input source data and underlying equations, and exact agreement was obtained with the values calculated in the spreadsheet.

Table I-19. Comparison of Fitted Osmotic Coefficients (ϕ) to Those Measured for NaCl at 25°C and 100°C

25°C Comparison			
Molality of NaCl	**Fitted Equation**	**Measurements**	**Difference (%)**
0.05	0.9435	0.9436	<0.1
0.1	0.9324	0.9325	<0.1
0.5	0.9214	0.9222	<0.1
1.0	0.9354	0.9373	0.2
3.0	1.0431	1.0485	0.5
6.0	1.2716	1.2688	0.2
100°C Comparison			
0.05	0.9345	0.9346	<0.1
0.1	0.9222	0.9223	<0.1
0.5	0.9139	0.9142	<0.1
1.0	0.9332	0.9341	0.1
3.0	1.0439	1.0458	0.2
6.0	1.2108	1.2083	0.2

NOTE: Measurements taken from Clarke and Glew 1985 [DIRS 162066], Table 19A, pp. 525 and 526.

I.4.4.20 Ions: Na^+ - OH^-

Associated Spreadsheet: *FitPitzerNC_MX_NaOH.xls*
(Output DTN: MO0701SPAPTZER.001)

Source: Pabalan and Pitzer 1987 [DIRS 162147].

Description: Input parameters and equations from Pabalan and Pitzer (1987 [DIRS 162147], Table 3 and Equations 28 through 30) were verified for $\beta_{MX}^{(0)}$, $\beta_{MX}^{(1)}$, C^{ϕ}, and A^{ϕ}. The average of the RMS errors in the osmotic coefficient over the fitted temperature range (see spreadsheet tab "Results Summary") for the 3- to 4-term conversion was 0.002 (~0.2%). In addition, several values of $\beta_{MX}^{(0)}$, $\beta_{MX}^{(1)}$, and C^{ϕ} were independently calculated using the input source data and underlying equations, and exact agreement was obtained with the values calculated in the spreadsheet. Calculated values of the osmotic coefficient from this spreadsheet are compared in Table I-20 below, against those listed for 25°C by Robinson and Stokes (1965 [DIRS 108567], Appendix 8.10, Table 1, p. 483). There was good agreement with the fitted spreadsheet values at

25°C, with a maximum difference of 1.3%. There was also good agreement over 110°C to 170°C with the osmotic coefficient values reported by Holmes and Mesmer (1998 [DIRS 162082]). The direct comparison is shown at 170°C below in Table I-21. These comparisons are considered to be sufficient confirmation of the validity of the osmotic coefficient calculations reported in this spreadsheet.

Table I-20. Comparison of Fitted 3- to 4-Term Osmotic Coefficients (ϕ) to Those Measured for NaOH at 25°C

Molality of NaOH	3- to 4-Term Fit	Measurements	Difference (%)
0.1	0.932	0.925	0.8
0.5	0.925	0.937	1.3
1.0	0.947	0.958	1.1
3.0	1.104	1.094	0.9
6.0	1.442	1.434	0.6

NOTE: Measurements taken from Robinson and Stokes 1965 [DIRS 108567], Appendix 8.10, Table 1, p. 483.

Table I-21. Comparison of Fitted 3- to 4-Term Osmotic Coefficients (ϕ) to Those Measured for NaOH at 170°C

Spreadsheet Calculated Values		Experimental Values	
Molality of NaOH	Fitted 3- to 4-Term ϕ	Molality of NaOH	Measured ϕ
1.0	0.875	1.0495	0.8547
3.0	0.906	3.0341	0.8922
6.0	1.001	6.0[a]	1.0126

[a] Linearly interpolated from the average results between 5.6 and 6.4 molality.

NOTE: Experimental values taken from Holmes and Mesmer 1998 [DIRS 162082], Table1, p.315.

I.4.4.21 Ions: $NH_4^+ - SO_4^{2-}$

Associated Spreadsheet: *ConPitzerNC_MX_(NH4)2SO4.xls*
(Output DTN: MO0701SPAPTZER.001)

Source: Clegg et al. 1996 [DIRS 162068].

Description: Input temperature coefficients and equation from Clegg et al. (1996 [DIRS 162068], Table 5, equation therein) in the ConPitzerNC model parameter conversion worksheet were verified for $\beta_{MX}^{(0)}$, $\beta_{MX}^{(1)}$, $C_{MX}^{(0)}$, and $C_{MX}^{(1)}$ input parameters. The model used by Clegg et al. (1996 [DIRS 162068]) is an Archer-type extended Pitzer model with four parameters, for which conversion of model data to the standard Pitzer model was presented by Rard and Wijesinghe (2003 [DIRS 162327]). The osmotic coefficient calculated at selected molalities using the input model in the worksheet agreed exactly with the values given by Clegg et al. (1996 [DIRS 162068], Table 7) at 25°C. The 3- to 4-term fitting results differed from those osmotic coefficient values by less than $\Delta\phi = 0.0009$ over the 0°C to 100°C range. Values presented in the worksheet above 100°C also agree well with those calculated using the input model, but these extrapolations are beyond the range of validity claimed for the input model. The 3- to 4-term calculated values of the osmotic coefficient from this spreadsheet are compared

with those listed at 25°C and 100°C in the study by Clegg et al. (1996 [DIRS 162068], Table 7) in Table I-22. There was very good agreement with the spreadsheet values at 25°C with a maximum difference of 0.9%, and reasonable agreement over the 100°C range with an RMS difference of 2.3%. The model conversion errors for the osmotic coefficient, in going from a 4-parameter Archer-type input model to the 3-parameter standard Pitzer model, as a function of temperature ranged from 0.0010 to 0.0256 from 0°C to 100°C, respectively (see spreadsheet cover page). The model conversion error can be as large as 0.06 at higher temperatures, but this is beyond the range of validity of the input model. Generally, the model conversion errors are much larger than the temperature coefficient fitting errors.

Table I-22. Comparison of Fitted 3- to 4-Term Osmotic Coefficients (ϕ) to Those Measured for $(NH_4)_2SO_4$ at 25°C and 100°C

25°C			
Molality of $(NH_4)_2SO_4$	**3- to 4-Term Fit**	**Measurements**	**Difference (%)**
0.05	0.8160	0.8127	0.4
0.1	0.7760	0.7723	0.5
0.5	0.6756	0.6774	0.2
1.0	0.6379	0.6420	0.9
3.0	0.6398	0.6382	0.3
6.0	0.7177	0.7138	0.6
100°C			
0.05	0.7902	0.7687	2.8
0.1	0.7466	0.7198	3.7
0.5	0.6358	0.6316	0.7
1.0	0.5923	0.6027	1.7
3.0	0.5832	0.5810	0.4
6.0	0.6036	0.6202	2.7

NOTE: Measurements taken from Clegg et al. 1996 [DIRS 162068], Table 7.

I.4.4.22 Ions: NH_4^+ - Cl^-

Associated Spreadsheet: *FitPitzerNC_MX_NH4Cl.xls*
(Output DTN: MO0701SPAPTZER.001)

Source: Thiessen and Simonson 1990 [DIRS 162108].

Description: Input parameters and equations from Thiessen and Simonson (1990 [DIRS 162108], Table IV and Equation 24) were verified for $\beta_{MX}^{(0)}$, $\beta_{MX}^{(1)}$, and C^{ϕ}. Calculated values of the parameter term coefficients in the spreadsheet agreed well with the values reported by the authors, with near exact agreement in most cases but with an occasional difference of 0.001 to 0.002. Each osmotic coefficient RMS error over the fitted temperature range (as shown on "Results Summary" spreadsheet) was below 0.0004, with a maximum individual difference of $\Delta\phi$ = 0.0007. This is considered to be excellent agreement, with the minor differences attributable to the A^{ϕ} parameter and the water saturation vapor pressure equation used to establish the system pressure. Calculated values of the osmotic coefficient from this spreadsheet were compared with those listed for 25°C in the extensive tables from Robinson and Stokes

(1965 [DIRS 108567], Appendix 8.10, Table 3, p. 485). There was good agreement with the final fitted spreadsheet values at 25°C, with $\Delta\phi_{max} = 0.002$ (Table I-23).

Table I-23. Comparison of 3- to 4-Term Fitted Osmotic Coefficients (ϕ) to Measured for NH_4Cl at 25°C

Molality of NH_4Cl	3- to 4-Term Fitting	Measurements	Difference (%)
0.1	0.925	0.927	0.2
0.5	0.899	0.899	<0.1
1.0	0.897	0.897	<0.1
3.0	0.927	0.926	0.1
6.0	0.969	0.969	<0.1

NOTE: Measurements taken from Robinson and Stokes 1965 [DIRS 108567], Appendix 8.10, Table 3, p. 485.

I.4.4.23 Ions: Na^+ - HCO_3^-

Associated Spreadsheet: *FitPitzerNC_MX_NaHCO3.xls*
(Output DTN: MO0701SPAPTZER.001)

Source: He and Morse 1993 [DIRS 162090].

Description: Input parameters and equation from He and Morse (1993 [DIRS 162090], Table 7 and the Equation on p. 3548) were verified for $\beta_{MX}^{(0)}$, $\beta_{MX}^{(1)}$, and C^{ϕ}. The RMS error in the osmotic coefficient over the fitted temperature range (see spreadsheet tab "Results Summary") for source to 3- to 4-term conversion is zero (to within calculation precision) as both use the same functional form. Calculated values of these coefficients at 25°C from this spreadsheet agreed with the values reported by Peiper and Pitzer (1982 [DIRS 162097], Table 1). The source document used Pitzer parameter values at 25°C from this paper to determine the temperature coefficients. The osmotic coefficients calculated from the input parameters were compared with those listed in tables from Peiper and Pitzer (1982 [DIRS 162097], Table 6, pp. 631 to 636). There was good agreement with values calculated in this spreadsheet, with a maximum difference raging from $\Delta\phi = 0.001$ to 0.002 over 0 to 1.0 mol/kg ionic strength at 25°C and 45°C as seen in Table I-24. This agreement is considered sufficient for the validity of the osmotic coefficient calculations reported in this spreadsheet. Pitzer parameter values over a wider temperature range than 0°C to 90°C have been reported in the literature, but these are limited to narrower ranges of concentration. For example, the Pitzer parameter data given by Polya et al. (2001 [DIRS 162101]) are limited to an ionic strength range of 0 to 4.5 mol/kg for Na_2CO_3, and 0 to 1.0 mol/kg for $NaHCO_3$. Furthermore, reproduction of the results of Polya et al. (2001 [DIRS 162101]) using their equations was unsuccessful. Also, the uncertainties in their study could not be resolved. The model of He and Morse (1993 [DIRS 162090]), although it is limited to 0°C to 90°C, was parameterized to very high ionic strengths and is therefore suitable for calculation of Na_2CO_3 solubility.

Table I-24. Comparison of Fitted 3- to 4-Term Osmotic Coefficients (ϕ) to Those Measured for $NaHCO_3$ at 25°C and 45°C

25°C			
Molality of $NaHCO_3$	**3- to 4-Term Fit**	**Measurements**	**Difference (%)**
0.05	0.934	0.933	0.1
0.1	0.915	0.914	0.1
1.0	0.856	0.854	0.2
45°C			
0.05	0.932[a]	0.931	0.1
0.1	0.914[a]	0.913	0.1
1.0	0.865[a]	0.864	0.1

[a] Linearly interpolated by hand from spreadsheet data between 40°C and 50°C.

NOTE: Measurements taken from Peiper and Pitzer 1982 [DIRS 162097], Table 6, pp. 631 to 636.

I.4.4.24 Ions: Na^+ - CO_3^{2-}

Associated Spreadsheet: *FitPitzerNC_MX_Na2CO3.xls*
(Output DTN: MO0701SPAPTZER.001)

Source: He and Morse 1993 [DIRS 162090].

Description: Input parameters and equations from He and Morse (1993 [DIRS 162090], Table 7 and the Equation on p. 3548) were verified for $\beta_{MX}^{(0)}$, $\beta_{MX}^{(1)}$, and C^{ϕ}. The RMS error in the osmotic coefficient over the fitted temperature range (see spreadsheet tab "Results Summary") for the 3 to 4 term conversion is $\Delta\phi$ = zero (to within calculation precision) as both use the same functional form. Calculated values of these coefficients at 25°C from this spreadsheet agreed with the values reported by Peiper and Pitzer (1982 [DIRS 162097], Table 1). The source document used the Pitzer parameter values at 25°C from this paper to determine the temperature coefficients. The osmotic coefficients calculated from the input parameters were compared with those listed by Peiper and Pitzer (1982 [DIRS 162097], Table 6) and shown in Table I-25 at 25°C and 45°C. There was good agreement with values calculated in this spreadsheet, with a maximum difference ranging from 0.002 to 0.01 over 0 to 9 mol/kg ionic strength. This agreement is considered sufficient confirmation of the validity of the osmotic coefficient calculations reported in this spreadsheet. Just like the $NaHCO_3$, Pitzer parameter values over a wider temperature range than 0°C to 90°C have been reported for Na_2CO_3 in the literature, but these are limited to narrower ranges of concentration. For example, the Pitzer data given by Polya et al. (2001 [DIRS 162101]) are limited to an ionic strength range of 0 to 4.5 mol/kg for Na_2CO_3, and 0 to 1.0 mol/kg for $NaHCO_3$. Furthermore, reproduction of the results of Polya et al. (2001 [DIRS 162101]) using their equations was not possible. In addition, the uncertainties in their study could not be resolved. The solubility of Na_2CO_3 above 25°C exceeds the ionic strength range of the model at high temperatures, and as was shown by Königsberger (2001 [DIRS 162093]), does not yield reliable solubility predictions above about 50°C. The model of He and Morse (1993 [DIRS 162090]), although limited to 0°C to 90°C, was parameterized to very high ionic strengths and is suitable for calculation of solubility.

Table I-25. Comparison of Fitted 3- to 4-Term Osmotic Coefficients (ϕ) to Measured for Na_2CO_3 at 25°C and 45°C

25°C			
Molality of Na_2CO_3	**3- to 4-Term Fit**	**Measurements**	**Difference (%)**
0.05	0.842	0.847	0.6
0.1	0.814	0.817	0.4
1.0	0.681	0.683	0.3
3.0	0.737	0.739	0.3
45°C			
0.05	0.835[a]	0.845	1.2
0.1	0.806[a]	0.815	1.1
1.0	0.698[a]	0.704	0.9

[a] Linearly interpolated by hand from spreadsheet data between 40°C and 50°C.

NOTE: Measurements taken from Peiper and Pitzer 1982 [DIRS 162097], Table 6, pp. 631 to 636.

I.4.4.25 Ions: Na^+ - HSO_4^-

Associated Spreadsheet: *FitPitzerNC_MX_NaHSO4.xls*
(Output DTN: MO0701SPAPTZER.001)

Source: Holmes and Mesmer 1994 [DIRS 162078].

Description: Input parameters and equations from Holmes and Mesmer (1994 [DIRS 162078], Table 4 and Equation 28) were verified for $\beta_{MX}^{(0)}$, $\beta_{MX}^{(1)}$, and C^{ϕ}, and A^{ϕ}. Calculated values of the osmotic coefficient for the fully dissociated binary electrolyte from this spreadsheet cannot be compared with any experimental values because experimentally determined values include the effects of partial dissociation into Na^+, H^+, HSO_4^-, and SO_4^{2-} ions rather than Na^+ and HSO_4^- ions only. However, the values of the calculated osmotic coefficient are reasonable for a fully dissociated 1-1 electrolyte. The binary parameters for Na^+ and HSO_4^- should only be used in combination with the mixing parameters (θ and ψ) from the same document. Furthermore, to be consistent, these parameters should only be used in combination with the binary and mixing parameters for HSO_4^- and SO_4^{2-} ions given in the source document, and for Na_2SO_4 in the study by Holmes and Mesmer (1986 [DIRS 162074]). Of the two models given in the latter paper, Model I with alpha1 = 1.4 (instead of 2) should be used for Na_2SO_4. Note that there is an error in Table 4 of the source document (Holmes and Mesmer 1994 [DIRS 162078]); it gives incorrect p1 parameter values that are too large by a factor of 1,000. There is an exception for the inclusion of ternary interactions (ψ) for H^+-HSO_4^--SO_4^{2-} determined by Baes et al. (1993 [DIRS 168318]) in their study of the cupric sulfate system. It was noted that the presence of this parameter with a non-zero value in the database did not generate any discrepancies in computed osmotic coefficients or activity coefficients. It should also be noted that the higher order electrostatic interactions represented by the ${}^{E}\theta$ and ${}^{E}\theta'$ third order terms of the Pitzer model were taken into account in this source document. In an earlier paper by Holmes and Mesmer (1993 [DIRS 162077]), the authors did not account for these interactions. Note that there is an error in Table 2 of this document for isothermal fits; it gives incorrect C^{ϕ} values that are too large by a factor of 1,000.

I.4.4.26 Ions: Na^+ - AlO_2^- (equivalent to Na^+ - $Al(OH)_4^-$)

Associated Spreadsheet: *FitPitzerNC_MX_Na_AlO2.xls*
(Output DTN: MO0701SPAPTZER.001)

Source: Felmy et al. 1994 [DIRS 162112].

Description: The binary parameters $\beta_{MX}^{(0)}$, $\beta_{MX}^{(1)}$, and C^{ϕ} generated with the coefficients and equations reported by Felmy et al. (1994 [DIRS 162112], Table 1 and Equation 1) were examined and compared with the data reported by Wesolowski (1992 [DIRS 162148], Table 13) based on gibbsite solubility at alkaline conditions. Unlike previous FitPitzerNC spreadsheets, the binary parameters were refitted using the regression function intrinsic to Excel. The conventions used for representing aqueous aluminate ion as AlO_2^- instead of $Al(OH)_4^-$ are different from those reported by Felmy et al. (1994 [DIRS 162112]) and Wesolowski (1992 [DIRS 162148]). The convention used to denote the aluminate ion AlO_2^- is equivalent to $Al(OH)_4^-$ in the two latter studies and thermodynamically consistent with the chemical reactions for aqueous and solid species in the current data0.ypf.R2 or Pitzer database and those obtained from the data0.ymp.R4 database (see Pokrovskii and Helgeson 1995 [DIRS 101699] for more details on the adopted convention).

The binary parameter values obtained after refitting agree with those generated by Felmy et al. (1994 [DIRS 162112]), depending on temperature. Comparison of generated parameter values with those reported by Wesolowski (1992 [DIRS 162148], Table 13, p.1087) for a temperature range of 25°C to 100°C are also in good agreement. Somewhat larger differences are observed for the $\beta_{MX}^{(1)}$ values, but in general these are considered reasonable when all parametric differences are taken as a whole. An error in table 1 of Felmy et al. (1994 [DIRS 162112]) was detected for the $\beta_{MX}^{(0)}$ parameter where the listed a3 coefficient is actually a4 in the fitting equation used by the authors. When the fitting coefficient is corrected, the $\beta_{MX}^{(0)}$ values obtained are nearly identical to those reported by Wesolowski (1992 [DIRS 162148], Table 13).

Felmy et al. (1994 [DIRS 162112]) conducted a gibbsite solubility study at ambient temperature and noticed that in order to model the effect of $NaNO_3$ concentration in NaOH solutions, two additional ternary parameters (θ and ψ; see Felmy et al. 1994 [DIRS 162112]) were needed. These were modified by Felmy et al. (1994 [DIRS 162112]) to fit their solubility data for a mixed Na-OH-NO_3-H_2O electrolyte. A further test of these parameters was the prediction of the equilibrium solubility for gibbsite in a concentrated NaOH solution at 70°C with the code EQ3/6 v8.0 for a total Na concentration of 3.045 molal. The log K value for gibbsite was taken from the data0.ymp.R2 database (DTN: MO0302SPATHDYN.000 [DIRS 161756]). The calculated total Al (equivalent to AlO_2^- or $Al(OH)_4^-$) was nearly identical to that in the study by Wesolowski (1992 [DIRS 162148], Table 4) for the same Na^+ concentration (See EQ3NR output file *gibbs_weso_sol.3o* in Output DTN: MO0611SPATZER.000).

I.4.4.27 Ions: Ca^{2+} - SO_4^{2-}

Associated Spreadsheet: No Spreadsheet

Source: Møller 1988 [DIRS 152695]; Greenberg and Møller 1989 [DIRS 152684].

Description: Binary parameters from Greenberg and Møller (1989 [DIRS 152684]) were verified for $\beta_{MX}^{(0)}$, $\beta_{MX}^{(1)}$, and C^{ϕ} given without any temperature dependence. It appears from the work of Greenberg and Møller (1989 [DIRS 152684]) that an explicit $CaSO_4$(aq) ion pair constant was used to fit a temperature range above 50°C. The explicit use of this ion pair is what actually brings the temperature dependence to the model. As incorporated in the data0.ypf.R2 database, the $\beta_{MX}^{(2)}$ term is set to zero, and the $CaSO_4$(aq) ion pair represented in the log K data block for aqueous species is used all throughout the valid temperature range. It is suspected that the ion pair was not actually used by Greenberg and Møller (1989 [DIRS 152684]) at temperatures less than 50°C and extrapolation to this lower temperature range might add some additional error. Even though the ion pair is used and $\beta_{MX}^{(2)}$ is not, it appears that an α_1 value of 1.4 was retained. A corrected value of "a1" for $\beta_{MX}^{(0)}$ was used after noticing that it differs from the original source of Møller (1988 [DIRS 152695]). Møller (1988 [DIRS 152695]) reports a value of 0.15 for the "a1" coefficient instead of 0.015 as reported by Greenberg and Møller (1989 [DIRS 152684]). Millero and Pierrot (1998 [DIRS 163594]) and Monnin (1999 [DIRS 163593]) adopted a value of 0.15 for this coefficient in their Pitzer models. Monnin (1999 [DIRS 163593]) states in his study that the value of 0.015 reported by Greenberg and Møller (1989 [DIRS 152684]) appears to be incorrect since it yields significant discrepancies. Therefore, a corrected value of 0.15 is adopted in his study (Monnin 1999 [DIRS 163593], Table 3, footnote f). The solubility of gypsum in water (Figure I-2) was calculated using the Pitzer parameters and compared to the curve given by Møller (1988 [DIRS 152695], Figure 3, p. 827). The computed solubility by the code is in excellent agreement with the values depicted in Figure 3 of Møller (1988 [DIRS 152695]) with a slight underestimation at 25°C of ~5%. The predicted solubilities were also compared to those given in the more recent review by Dutrizac (2002 [DIRS 166148]) showing a good agreement with the reported solubility curve up to 100°C.

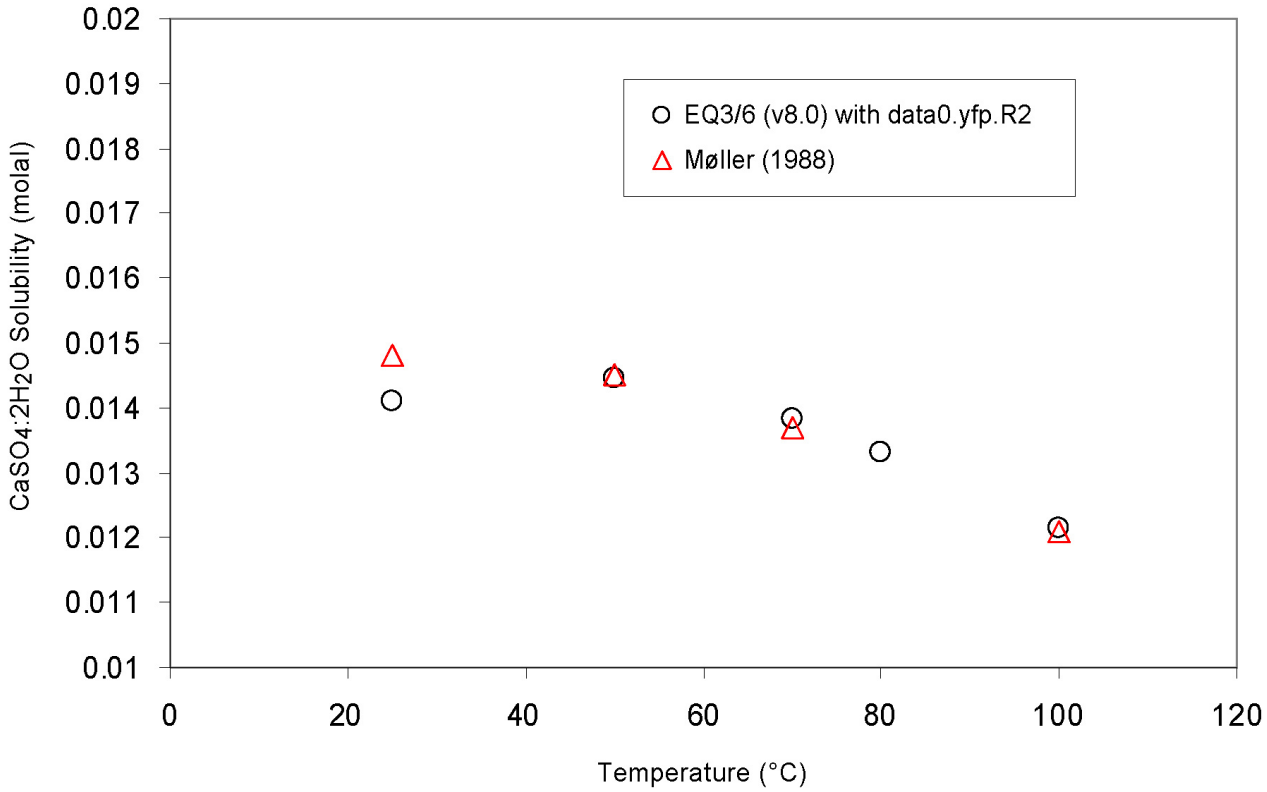

NOTE: Predicted m_{sat} values (Output DTN: MO0701SPAPTZER.001) were computed using data0.ypf.R2 and EQ3/6 Version 8.0. The saturation molalities for gypsum were obtained from Figure 3 in the study by Møller (1988 [DIRS 152695]).

Figure I-2. Comparison of Saturation Molalities for Gypsum

I.4.5 TERNARY PITZER INTERACTION PARAMETERS

In this section, the selected ternary Pitzer ion interaction parameters for major salt constituents included in the developed data0.ypf.R2 database (Output DTN: SN0609T0502404.012) for EQ3/6 v8.0 (See Section 3.1.1) will be described. All these parameters and associated spreadsheets are listed in Tables I-1 and I-2 as "Types other than MX." Remarks on the refitting and reproducibility of gathered Pitzer parameter data will be discussed here and on the associated spreadsheet cover pages. Discussions of parameter data are focused on the parameters that needed refitting due to their temperature dependence. Many parameters did not require any refitting since the gathered values are only valid at 25°C and were obtained directly from tabulated data. For these, only simple conversions were necessary. The reader is reminded that ternary interaction parameters make relatively small contributions to the calculation of osmotic coefficients and activity coefficients. Thus, even large percentage differences in the values used by different authors make only small differences in the final results. For details, see the individual papers cited, which generally evaluate the magnitude of these differences.

Significant limitations exist for the application of the parameters discussed in the following subsections. Most have been determined only at 25°C and many only for relatively simple systems. For more complex systems, such as for most groundwater and other temperatures,

refitting of the parameters to the changed conditions may be necessary to obtain accurate results. Failure to make such adjustments can lead to significant errors in some applications (e.g., modeling of evaporation of a water to near dryness), because of the accumulation of small deviations of the model from the actual chemistry. To mitigate this problem, data were taken from consistent or single sources to the extent possible. For example, many parameters were taken from Greenberg and Møller (1989 [DIRS 152684]), who studied the rather complex Na-K-Ca-Cl-SO_4-H_2O system. Still, this study lacked some important constituents, notably Mg and carbonate, present in most natural waters, and did not fit the Ca-depleted portion of the system well. For some applications, Al and Si need to be included and, less often, other elements that are generally present in groundwater in minor to trace amounts. Thus, in spite of qualification of these data from the point of view that they generally suffice to reproduce individual details of the experimental results well, they need to be viewed with caution in respect to modeling chemical processes that change the composition of the solution.

I.4.5.1 Ions: Ca^{2+} - K^+

Associated Spreadsheet: *FitPitzerNC_MM_K_Ca.xls*
(Output DTN: MO0701SPAPTZER.001)

Source: Greenberg and Møller 1989 [DIRS 152684].

Description: Input parameters and equations from Greenberg and Møller (1989 [DIRS 152684]) were verified for θ and A^{ϕ}. The authors used a constant value of θ for all temperatures. At 25°C, Pitzer and Kim (1974 [DIRS 123206]) reported values of $\theta = -0.040$ and $\psi = -0.015$ for the K-Ca-Cl system, compared to $\theta = 0.1156$ and $\psi = -0.04319$ from the spreadsheet, and $\theta = 0.032$ and $\psi = -0.025$ reported by Pitzer (1991 [DIRS 152709]). Unlike the calculations of both Pitzer and this spreadsheet, Pitzer and Kim (1974 [DIRS 123206]) did not account for the higher order electrostatic terms ${}^{E}\theta$ and ${}^{E}\theta'$ in their model. Therefore, the evaluation of θ is dominated by the differences in the models used by different authors. In particular, Pitzer and Kim (1974 [DIRS 123206]) based their parameter evaluations using isopiestic data. Although Greenberg and Møller (1989 [DIRS 152684]) also considered this isopiestic data, they adjusted the mixing parameters to better represent solubility of sylvite (KCl) in mixed KCl-$CaCl_2$ solutions.

I.4.5.2 Ions: Ca^{2+} - Na^+

Associated Spreadsheet: *FitPitzerNC_MM_Na_Ca.xls*
(Output DTN: MO0701SPAPTZER.001)

Source: Greenberg and Møller 1989 [DIRS 152684].

Description: Input parameters and equations from Greenberg and Møller (1989 [DIRS 152684]) were verified for θ and A^{ϕ}. The authors used a constant value of θ for all temperatures. There are no independent studies of this θ parameter reported in the literature that would enable a meaningful comparison. In the study by Holmes et al. (1981 [DIRS 162072]), the authors represent θ from isopiestic data by the equation $\theta = (10.7/T) - 0.0316$. Holmes et al. (1981 [DIRS 162072]) state that the osmotic coefficients could be represented reproduced to 0.5% or better even without mixing parameters, which indicates that mixing effects are small. The

equation given by Holmes et al. (1981 [DIRS 162072]) yields values that vary from 0.0043 to –0.0090 kg/mol over the temperature range 25°C to 201°C. Because θ has only a small influence on the osmotic coefficient of the system, the evaluation of this parameter is dominated by differences in the models used by different authors. These differences include neglecting of the higher-order electrostatic terms ${}^{E}\theta$ and ${}^{E}\theta'$. Greenberg and Møller (1989 [DIRS 152684]), for example, included these terms while Holmes et al. (1981 [DIRS 162072]) did not include them. Therefore, the adequacy of this θ parameter estimate should be assessed in combination with other binary and ternary parameters by examining the accuracy of the osmotic coefficients calculated in the MMX-type ternary parameter spreadsheets for the Na-Ca ion combination.

I.4.5.3 Ions: K^+ - Na^+

Associated Spreadsheet: *FitPitzerNC_MM_Na_K.xls*
(Output DTN: MO0701SPAPTZER.001)

Source: Greenberg and Møller 1989 [DIRS 152684].

Description: Input parameters and equations from Greenberg and Møller (1989 [DIRS 152684]) were verified for θ and A^{ϕ}. There are no independent studies of this θ parameter reported in the literature that would enable a meaningful comparison. Holmes et al. (1979 [DIRS 162071], p. 1044) represent θ from isopiestic data by the equation $\theta = -(6.726/T) + 0.0039$, whereas Greenberg and Møller (1989 [DIRS 152684]) give the expression $\theta = (14.021314/T) - 0.0502312$ for 0°C to 250°C. Greenberg and Møller (1989 [DIRS 152684]) used the same basic model and experimental data as Holmes et al. (1979 [DIRS 162071]), but adjusted the mixing parameter θ to better represent solubility data for the NaCl-KCl-H_2O system at temperatures above 150°C. Holmes et al. (1979 [DIRS 162071]) state that the osmotic coefficients could be reproduced to within 1% or better even without mixing parameters, which indicates that mixing effects are small. The equation given by Holmes et al. (1979 [DIRS 162071]) yields values that vary from −0.01866 to −0.01032 kg/mol over 25°C to 200°C whereas the corresponding values from Greenberg and Møller (1989 [DIRS 152684]) vary from –0.00320 to –0.02060 mol/kg. Because θ has only a very small influence on the osmotic coefficient of the system, its evaluation is sensitive to differences in the models used by the different authors. Therefore, the adequacy of this estimate of the θ parameter should be assessed in combination with other binary and ternary parameters by examining the accuracy of the osmotic coefficients calculated in the MMX-type ternary parameter spreadsheets for the Na-K ion combination.

I.4.5.4 Ions: Cl^- - SO_4^{2-}

Associated Spreadsheet: *FitPitzerNC_XX_Cl_SO4.xls*
(Output DTN: MO0701SPAPTZER.001)

Source: Greenberg and Møller 1989 [DIRS 152684].

Description: Input parameters and equations from Greenberg and Møller (1989 [DIRS 152684]) were verified for θ and A^{ϕ}. The temperature function given in the source document for θ has a discontinuity in slope at 150°C. This discontinuity is not accurately accommodated by the fitted continuous temperature function, causing the largest error in θ (about 10%) to occur in the

immediate vicinity of 150°C. De Lima and Pitzer (1983 [DIRS 162110]) fitted the Na-Cl-SO_4 system solubilities from 25°C to 100°C with θ = -0.02 and ψ = 0.004 taken from an earlier evaluation by Pitzer at 25°C. Both of these studies imply that ternary mixing contributions to the osmotic coefficient are small.

I.4.5.5 Ions: HSO_4^- - SO_4^{2-}

Associated Spreadsheet: *FitPitzerNC_XX_HSO4_SO4.xls*
(Output DTN: MO0701SPAPTZER.001)

Source: Holmes and Mesmer 1994 [DIRS 162078].

Description: Input parameters and equations from Holmes and Mesmer (1994 [DIRS 162078]) were verified for the parameter θ. These authors regressed the model parameters simultaneously for the H-HSO_4-SO_4 and Na-HSO_4-SO_4 systems, including the ${}^{E}\theta$ and ${}^{E}\theta'$ higher-order electrostatic interactions. Clegg et al. (1994 [DIRS 152734]) were able to fit the thermodynamic properties of sulfuric acid without including either θ or ψ Pitzer mixing parameters, but with an additional C(1) extended binary parameter and the ${}^{E}\theta$ and ${}^{E}\theta'$ higher-order electrostatic interaction parameters. Clegg et al. (1994 [DIRS 152734]) found that these model enhancements were significant in improving the accuracy of the fit at concentrations much lower than those considered by Holmes and Mesmer (1994 [DIRS 162078]). Both of these studies imply that the contributions of the ternary mixing parameters are negligible in the H-HSO_4-SO_4 system, but not always negligible in the Na-HSO_4-SO_4 system. In an earlier paper by Holmes and Mesmer (1992 [DIRS 162076]), the authors did not account for these interactions.

I.4.5.6 Ions: K^+ - Ca^{2+} - Cl^-

Associated Spreadsheet: *FitPitzerNC_MMX_K_Ca_Cl.xls*
(Output DTN: MO0701SPAPTZER.001)

Source: Greenberg and Møller 1989 [DIRS 152684].

Description: Input parameters and equations from Greenberg and Møller (1989 [DIRS 152684]) were verified for the θ ternary Pitzer parameter and A^{ϕ}. At 25°C, Pitzer and Kim (1974 [DIRS 123206]) reported values of $\theta = -0.040$ and $\psi = -0.015$ for the K-Ca-Cl system compared to $\theta = 0.1156$ and $\psi = -0.04319$ from the spreadsheet, and $\theta = 0.032$ and $\psi = -0.025$ reported by Pitzer (1991 [DIRS 152709]). Unlike the calculations by Pitzer and those presented in this spreadsheet, Pitzer and Kim (1974 [DIRS 123206]) did not account for the higher-order electrostatic terms ${}^{E}\theta$ and ${}^{E}\theta'$ in their model. Therefore, the evaluation of θ is dominated by the differences in the models used by different authors. In particular, Pitzer and Kim (1974 [DIRS 123206]) based their parameter evaluations using these isopiestic data. Although Greenberg and Møller (1989 [DIRS 152684]) also considered this isopiestic data they adjusted the mixing parameters to better represent solubility of sylvite (KCl) in mixed KCl-$CaCl_2$ solutions. It should be noted that the osmotic coefficient values presented in the spreadsheet for an ionic strength of I = 18 mol/kg are not realistic because they fall outside the range of validity of the model parameters, especially for potassium-rich solutions at low temperatures. Exact agreement was obtained between the osmotic coefficients for the limiting binary solutions,

KCl(aq) and $CaCl_2$(aq), calculated by the ternary and the binary spreadsheets, for both input and fitted Pitzer parameters.

I.4.5.7 Ions: Na^+ - Ca^{2+} - Cl^-

Associated Spreadsheet: *FitPitzerNC_MMX_Na_Ca_Cl.xls*
(Output DTN: MO0701SPAPTZER.001)

Source: Greenberg and Møller 1989 [DIRS 152684].

Description: Input parameters and equations from Greenberg and Møller (1989 [DIRS 152684]) were verified for ψ and A^{ϕ}. Holmes et al. (1981 [DIRS 162072]) found that the osmotic coefficients could be reproduced to within 0.5% or better even without mixing parameters, which indicates that mixing effects are small. Holmes et al. (1981 [DIRS 162072]) also found that while using the θ mixing parameter improved the standard deviation for isothermal fits by a factor of 2, including both θ and ψ did not yield a significant improvement over using θ alone. θ varied between 0.0056 and –0.0081 over 25°C to 201°C. Because ψ has only a very small influence on the osmotic coefficient of the system, its value is dominated by differences in the models used by the different authors. These differences include the neglect of the higher order electrostatic terms ${}^{E}\theta$ and ${}^{E}\theta'$. Greenberg and Møller (1989 [DIRS 152684]), for example, included these terms while Holmes et al. (1981 [DIRS 162072]) did not. Therefore, the adequacy of this estimate of the ψ parameter should be assessed in combination with other binary and ternary parameters by examining the accuracy of the osmotic coefficients calculated in the MMX-type ternary parameter spreadsheets for the Na-Ca ion combination. Exact agreement was obtained between the osmotic coefficients for the limiting binary solutions, NaCl(aq) and $CaCl_2$(aq), calculated by the ternary and the binary spreadsheets, for both input and fitted Pitzer parameters.

I.4.5.8 Ions: Na^+ - Ca^{2+} - SO_4^{2-}

Associated Spreadsheet: *FitPitzerNC_MMX_Na_Ca_SO4.xls*
(Output DTN: MO0701SPAPTZER.001)

Source: Greenberg and Møller 1989 [DIRS 152684].

Description: Input parameters and equations from Greenberg and Møller (1989 [DIRS 152684]) were verified for the θ ternary Pitzer parameter and A^{ϕ}. The authors used constant values of θ and ψ for all temperatures. At 25°C, Pitzer (1991 [DIRS 152709]) used the values $\theta = 0.07$ and $\psi = -0.055$ compared to $\theta = 0.05$ and $\psi = -0.012$ calculated from the correlation of Greenberg and Møller (1989 [DIRS 152684]). Both sets of values account for the higher order terms θ and ${}^{E}\theta'$. At low temperatures, the calculated values of the osmotic coefficient from this spreadsheet are plausible, but, for $CaSO_4$-rich solutions, they become unrealistic in magnitude at temperatures beyond 100°C to 150°C. Because of the relatively low solubility of $CaSO_4$, the high concentrations cannot be achieved experimentally. The parameters were designed to represent solubility in mixed electrolyte solutions and are inadequate for representing the properties of the hypothetical pure $CaSO_4$(aq) solutions. Exact agreement was obtained between

the osmotic coefficients for the limiting binary solutions, Na_2SO_4(aq) and $CaSO_4$(aq), calculated by the ternary and the binary spreadsheets, for both input and fitted Pitzer parameters.

I.4.5.9 Ions: Na^+ - K^+ - Cl^-

Associated Spreadsheet: *FitPitzerNC_MMX_Na_K_Cl.xls*
(Output DTN: MO0701SPAPTZER.001)

Source: Greenberg and Møller 1989 [DIRS 152684].

Description: Input parameters and equations from Greenberg and Møller (1989 [DIRS 152684]) were verified for ψ and A^{ϕ}. In the study by Holmes et al. (1979 [DIRS 162071]), the authors state that the osmotic coefficients could be reproduced to within 1% or better even without mixing parameters, which indicates that mixing effects are small. However, Holmes et al. (1979 [DIRS 162071]) found that including the θ mixing parameter caused a significant improvement in the accuracy of representing the data with the standard deviation for isothermal fits decreasing by a factor of 2 to 4. Including both θ and ψ resulted in no further improvement, and the authors recommended using θ only in the Pitzer model. Greenberg and Møller (1989 [DIRS 152684]) used the same basic model and experimental data as Holmes et al. (1979 [DIRS 162071]) but adjusted the mixing parameter θ to better represent the solubility data for the NaCl-KCl-H_2O system at temperatures above 150°C. Because ψ has only a small influence on the osmotic coefficient of the system, its evaluation is sensitive to differences in the models used by the different authors. Therefore, the adequacy of the ψ parameter estimation should be assessed in combination with other binary and ternary parameters by examining the accuracy of the osmotic coefficients calculated in the MMX-type ternary parameter spreadsheets for the Na-K ion combination. Exact agreement was obtained between the osmotic coefficients for the limiting binary solutions, NaCl(aq) and KCl(aq), calculated by the ternary and the binary spreadsheets, for both input and fitted Pitzer parameters.

I.4.5.10 Ions: Na^+ - K^+ - SO_4^{2-}

Associated Spreadsheet: *FitPitzerNC_MMX_Na_K_SO4.xls*
(Output DTN: MO0701SPAPTZER.001)

Source: Greenberg and Møller 1989 [DIRS 152684].

Description: Input parameters and equations from Greenberg and Møller (1989 [DIRS 152684]) were verified for the ψ ternary Pitzer parameter and A^{ϕ}. Greenberg and Møller (1989 [DIRS 152684]) used a 2-term temperature function for ψ with different sets of parameters from 0°C to 150°C and 150°C to 250°C. The value of ψ was optimized using both osmotic coefficient and solubility data. Table 18 of the study by Pitzer (1991 [DIRS 152709]) includes the values of $\theta = -0.012$ and $\psi = -0.010$ at 25°C taken from the original paper by Pitzer and Kim (1974 [DIRS 123206]). This should be compared with the values of $\theta = -0.0032$ and $\psi = 0.0073$ at 25°C calculated from Greenberg and Møller's (1989 [DIRS 152684]) correlations. Both of these studies imply that ternary mixing contributions to the osmotic coefficient are small, but that the mixing parameter values should always be evaluated in combination with the binary and other ternary parameters for the electrolyte system. It should be noted here that the osmotic coefficient

values presented in the spreadsheet for an ionic strength of I = 18 mol/kg are not realistic because they fall outside the range of validity of the model parameters. Exact agreement was obtained between the osmotic coefficients for the limiting binary solutions, Na_2SO_4(aq) and K_2SO_4(aq), calculated by the ternary and the binary spreadsheets, for both input and fitted Pitzer parameters.

I.4.5.11 Ions: Ca^{2+} - Cl^- - SO_4^{2-}

Associated Spreadsheet: *FitPitzerNC_MXX_Ca_Cl_SO4.xls*
(Output DTN: MO0701SPAPTZER.001)

Source: Greenberg and Møller 1989 [DIRS 152684].

Description: Input parameters and equations from Greenberg and Møller (1989 [DIRS 152684]) were verified for the ψ ternary Pitzer parameter and A^{ϕ}. The authors used a constant value of ψ for all temperatures. At 25°C, Pitzer (1991 [DIRS 152709]) used the values of $\theta = 0.030$ and $\psi = -0.002$, compared to $\theta = 0.070$ and $\psi = -0.018$ calculated from the correlation of Greenberg and Møller (1989 [DIRS 152684]). Both sets of values account for the higher order terms θ and ${}^{E}\theta'$. At low temperatures, the calculated values of the osmotic coefficient from this spreadsheet are plausible, but, for $CaSO_4$-rich solutions, they become unrealistic in magnitude at temperatures beyond 100°C to 150°C. Because of the low solubility of $CaSO_4$, the high concentrations cannot be achieved experimentally. The parameters were designed to represent solubility in mixed electrolyte solutions and are inadequate for representing the properties of the hypothetical pure $CaSO_4$(aq) solutions. Exact agreement was obtained between the osmotic coefficients for the limiting binary solutions, $CaCl_2$(aq) and $CaSO_4$(aq), calculated by the ternary and the binary spreadsheets, for both input and fitted Pitzer parameters.

I.4.5.12 Ions: K^+ - Cl^- - SO_4^{2-}

Associated Spreadsheet: *FitPitzerNC_MXX_K_Cl_SO4.xls*
(Output DTN: MO0701SPAPTZER.001)

Source: Greenberg and Møller 1989 [DIRS 152684].

Description: Input parameters and equations from Greenberg and Møller (1989 [DIRS 152684]) were verified for ψ and A^{ϕ}. At 25°C, Pitzer and Kim (1974 [DIRS 123206]) reported values of $\theta = -0.035$ and $\psi = 0$, compared to $\theta = 0.07$ and $\psi = -0.0016152$ from the spreadsheet. In the study by Pitzer (1991 [DIRS 152709]), the higher-order interaction terms were included with $\theta = 0.030$ and $\psi = -0.005$ at 25°C. These differences arise from differences in the binary parameters as well as model differences such as inclusion of the higher order electrostatic parameters ${}^{E}\theta$ and ${}^{E}\theta'$ in the spreadsheet. Therefore, the adequacy of this estimate of the ψ parameter should be assessed in combination with other binary and ternary parameters by examining the accuracy of the osmotic coefficients calculated in the MXX-type ternary parameter spreadsheets for the Cl-SO_4 ion combination. Because of the limited solubility of potassium sulfate, the calculated osmotic coefficients in the spreadsheet at certain high ionic strengths will exceed the range of validity of the model and may not be realistic. Exact agreement was obtained between the osmotic coefficients for the limiting binary solutions,

KCl(aq) and K_2SO_4(aq), calculated by the ternary and the binary spreadsheets, for both input and fitted Pitzer parameters.

I.4.5.13 Ions: Na^+ - Cl^- - SO_4^{2-}

Associated Spreadsheet: *FitPitzerNC_MXX_Na_Cl_SO4.xls*
(Output DTN: MO0701SPAPTZER.001)

Source: Greenberg and Møller 1989 [DIRS 152684].

Description: Input parameters and equations from Greenberg and Møller (1989 [DIRS 152684]) were verified for ψ and A^{ϕ}. Greenberg and Møller (1989 [DIRS 152684]) use $\theta = 0.07$ for 0°C to 150°C and $\psi = -0.009$ for 0°C to 250°C. De Lima and Pitzer (1983 [DIRS 162110]) fitted the Na-Cl-SO_4 system solubilities from 25°C to 100°C with $\theta = -0.02$ and $\psi = 0.004$ taken from an earlier evaluation by Pitzer at 25°C (Pitzer 1979 [DIRS 152738]). In the latter model, higher-order electrostatic interaction terms ${}^{E}\theta$ and ${}^{E}\theta'$ were not included. In another study by Pitzer (1991 [DIRS 152709]), the higher-order interaction terms were included, with $\theta = 0.030$ and $\psi = 0.0$ at 25°C. Both of these studies imply that ternary mixing contributions to the osmotic coefficient are small, but that the mixing parameter values should always be evaluated in combination with the binary and other ternary parameters for the electrolyte system. It should be noted here that the osmotic coefficient values presented in the spreadsheet for an ionic strength of I = 18 mol/kg may not be realistic because they fall outside the range of validity of the model parameters. The input temperature function given by Greenberg and Møller (1989 [DIRS 152684]) for the ψ parameter is discontinuous, with a constant value assigned from 0°C to 150°C and with varying values over the temperature range of 150°C to 250°C. Since a single continuous output function was adopted over the entire 0°C to 250°C range, the fitting equation loses accuracy around 150°C, resulting in a maximum error of about 20% at this temperature. Exact agreement was obtained between the osmotic coefficients for the limiting binary solutions, NaCl(aq) and Na_2SO_4(aq), calculated by the ternary and the binary spreadsheets, for both input and fitted Pitzer parameters.

I.4.5.14 Ions: Na^+ - HSO_4^- - SO_4^{2-}

Associated Spreadsheet: *FitPitzerNC_MXX_Na_HSO4_SO4.xls*
(Output DTN: MO0701SPAPTZER.001)

Source: Holmes and Mesmer 1994 [DIRS 162078].

Description: Input parameters and equations from Holmes and Mesmer (1994 [DIRS 162078]) were verified for ψ. They regressed the model parameters simultaneously for the H-HSO_4-SO_4 and Na-HSO_4-SO_4 systems, including the ${}^{E}\theta$ and ${}^{E}\theta'$ higher-order electrostatic interactions. Clegg et al. (1994 [DIRS 152734]) were able to fit the properties of sulfuric acid without including both the θ and ψ Pitzer mixing parameters, but with an additional C(1) extended binary ion-interaction parameter and the ${}^{E}\theta$ and ${}^{E}\theta'$ higher-order electrostatic interaction parameters. It was found by Clegg et al. (1994 [DIRS 152734]) that these model enhancements were significant in improving the accuracy of the fit at concentrations much lower than those considered by Holmes and Mesmer (1994 [DIRS 162078]). Both of these studies imply that the

contributions of the ternary mixing parameters are negligible in the H-HSO_4-SO_4 system, but are not always negligible in the Na-HSO_4-SO_4 system. In an earlier paper by Holmes and Mesmer (1993 [DIRS 162077]), the authors did not account for these higher order electrostatic interactions. Still, the ternary mixing parameters (ψ) for H-HSO_4-SO_4 given by Baes et al. (1993 [DIRS 168318]) in their study of the cupric sulfate system were included in data0.ypf.R2. It was noted that the presence of this parameter with a non-zero value in the database did not generate any discrepancies in computed osmotic coefficients or activity coefficients in agreement with the assertion about their negligible contributions implied by Clegg et al. (1994 [DIRS 152734]) and Holmes and Mesmer (1994 [DIRS 162078]). Exact agreement was obtained between the osmotic coefficients for the limiting binary solutions, $NaHSO_4$(aq) and Na_2SO_4(aq), calculated by the ternary and the binary spreadsheets, for both input and fitted Pitzer parameters. The osmotic coefficients were calculated for arbitrary speciations that range from one pure component to the other, but under real conditions the equilibrium ionic concentrations would be determined by iterative speciation calculations. The Na-H-HSO_4-SO_4 system ionic strength differs from stoichiometric value because of incomplete disassociation of hydrogen ions from the bisulfate ions. The dependence of the actual ionic strength of the solution on the degree of dissociation of the bisulfate ion leads to a strong dependence of the ionic strength on the molality and temperature of the solution. The osmotic coefficients calculated at certain high ionic strengths, especially for solutions with high molality fractions of Na_2SO_4, fall outside the valid range of ionic strengths for their model. The temperature range of 0°C to 250°C also falls outside the range (25°C to 225°C) of parameterization of the model.

I.4.5.15 Neutral Species: Doublets and Triplets Parameters among SiO_2(aq), CO_2(aq), and O_2(aq)

See Table I-1 for a listing of doublets and triplets parameters among SiO_2(aq), CO_2(aq), and O_2(aq).

Associated Spreadsheets: *FitPitzerNC_lambdas_zetas_O2_CFJC.xls*
Pitzer_NMX_SiO2.xls
FitPitzerMX_Ca-HCO3_NMX_CO2_CFJC3.xls
Cp_Solids_j_Kogarkoite_TJW_2.xls
Solids_j_Kogarkoite_TJW.xls
FitPitzerNC_MX_CaCl_CFJC_Model3_Sterner_et_al_1998.xls
(Output DTN: MO0701SPAPTZER.001)

Source: Corti et al. 1990 [DIRS 178211]; Rumpf and Maurer 1993 [DIRS 178223]; Rumpf et al. 1994 [DIRS 178222]; Clegg and Brimblecombe 1990 [DIRS 162089]; Felmy et al. 1994 [DIRS 162111].

Description: Two types of updates in Pitzer parameters for the carbonate systems were conducted on this Pitzer database revision: CO_2(aq)-cation, and CO_2(aq)-anion binary parameters. An update of Pitzer parameter data for CO_2(aq) based on work by He and Morse (1993 [DIRS 162090]) is needed due to the breakdown of the temperature function when parameters are extrapolated beyond the validity limit of 90°C. For this reason, Pitzer interaction parameters for CO_2(aq) at elevated temperatures were obtained from Corti et al. (1990 [DIRS 178211]) and Rumpf and Maurer (1993 [DIRS 178223]) for NaCl and Na_2SO_4,

respectively. Those obtained for CO_2 solubility in NaCl by Corti et al. (1990 [DIRS 178211]) are compared to those determined by Rumpf et al. (1994 [DIRS 178222]). Since the latter source does not reference Corti et al. (1990 [DIRS 178211]), it is assumed that the studies are independent of each other. The parameters given by Rumpf et al. (1994 [DIRS 178222]) are based on experimental data. The work by Corti et al. (1990 [DIRS 178211]) is based on a compilation of CO_2 solubility data from multiple sources. The Pitzer parameters from Corti et al. (1990 [DIRS 178211]) are selected for inclusion in the updated Pitzer database because of their validity up to a temperature of 250°C and their strong agreement with those given by Rumpf et al. (1994 [DIRS 178222]), which are valid at somewhat lower temperatures. Pitzer formulations describing interaction parameters for neutral species are explained in detail in Section F and given in Appendix F of Pitzer's (1991 [DIRS 152709]) report. The Pitzer expression of neutral solute interactions is less involved than those for charged species since it involves simplifications in the number of terms needed to represent such interactions. Pitzer (1991 [DIRS 152709], Equation 75) suggested the following equation for the activity coefficient of the neutral species (γ_N) only including second-order terms:

$$\ln \gamma_N = 2\sum_c m_c \lambda_{Nc} + 2\sum_a m_a \lambda_{Na} + 2\sum_n m_n \lambda_{Nn} \quad \text{(Eq. I-118)}$$

where the summation symbols represent the sum of all cations (c), anions (a), and neutral species (n) in the electrolyte. m_c, m_a, and m_n are the molalities of the cation, anions, and neutral aqueous species, respectively. λ_{Nc}, λ_{Na}, and λ_{Nn} denote the Pitzer interaction parameters for neutral–cation, neutral–anion, and neutral–neutral aqueous species, respectively. In this case, $N = n$ in λ_{Nn} and delineates solute–solute interactions in solutions with no salts (i.e., pure water). Notice that Equation I-118 does not include the third-order terms of Equation F-9 in the study by Pitzer (1991 [DIRS 152709]). However, Pitzer (1991 [DIRS 152709]) suggested that these can be included in the above equation if necessary. In fact, Corti et al. (1990 [DIRS 178211]) and Rumpf et al. (1994 [DIRS 178222]) incorporate a third-order term in their equations to fit their data. By convention, the parameter λ_{Nc} for $CO_2(aq)$-H^+ is usually set to zero (see Pitzer 1991 [DIRS 152709]). Since independent determination of the parameters λ_{Nc} and λ_{Na} in single salt solutions is not possible, it's often convenient to set one of the parameters to zero. In this case, the λ_{Na} for $CO_2(aq)$-Cl^- is also set to zero (see Pitzer 1991 [DIRS 152709]). Corti et al. (1990 [DIRS 178211]) and Rumpf and Maurer (1993 [DIRS 178223]) utilize Pitzer formulations that are consistent with Pitzer (1991 [DIRS 152709]) but use somewhat different symbols for the Pitzer parameter notations in their expressions. For the sake of parameter definition and tractability to the standard form of Pitzer equations, general explanations concerning the differences in notation will be discussed below.

In the study by Corti et al. (1990 [DIRS 178211]), the second Λ_{12} (or Λ_{nc}, to be consistent with the above subscript notation) and third-order Γ_{122} (or Γ_{Nca}) terms in the activity coefficient expression for $\ln \gamma_1$ (Corti et al. 1990 [DIRS 178211], Equation 14) are given by:

$$\Lambda_{nc} = (\upsilon_+ \lambda_{Nc} + \upsilon_- \lambda_{Na}) \quad \text{(Eq. I-119)}$$

and

$$\Gamma_{Nca} = \left(2\tau_{nca} + \left|\frac{z_-}{z_+}\right|\tau_{ncc} + \left|\frac{z_+}{z_-}\right|\tau_{naa} \right) \quad \text{(Eq. I-120)}$$

where υ_+ and υ_- denote the salt stoichiometry for the cations and anions in the electrolyte, respectively. z_+ and z_- are the respective charge of the cation and anions in the electrolyte. Although the Pitzer expressions in the study by Corti et al. (1990 [DIRS 178211]) look somewhat different from those given by Pitzer (1991 [DIRS 152709]) due to the use of different symbols, these are indeed consistent with Pitzer standard formulations. For example, the parameter τ_{nca} corresponds to μ_{nca} for neutral-cation-anion interactions in Equation F-3 of Pitzer's (1991 [DIRS 152709]) study, and so on. For the sake of clarity, the relevant equations defining the neutral-cation-anion interactions given by Pitzer (1991 [DIRS 152709]) will be given along with the algebraic manipulations to establish the correspondence with Equation I-120 above. Pitzer (1991 [DIRS 152709], Equation F-3) defines the parameter for the neutral-cation-anion interactions (ζ_{Nca}) as:

$$\zeta_{Nca} = 6\mu_{nca} + 3\left|\frac{Z_a}{Z_c}\right|\mu_{ncc} + 3\left|\frac{Z_c}{Z_a}\right|\mu_{naa} \quad \text{(Eq. I-121)}$$

which can be simplified to

$$\zeta_{Nca} = 3\left(2\mu_{nca} + \left|\frac{Z_a}{Z_c}\right|\mu_{ncc} + \left|\frac{Z_c}{Z_a}\right|\mu_{naa} \right) \quad \text{(Eq. I-122)}$$

In Equation I-122, substituting Z_c and Z_a for z_+ and z_-, and μ_{nca}, μ_{ncc}, and μ_{naa} for τ_{nca}, τ_{ncc}, and τ_{naa}, respectively, will yield the relationship between Γ_{Nca} and ζ_{Nca} as:

$$\frac{1}{3}\zeta_{Nca} = \Gamma_{Nca} \quad \text{(Eq. I-123)}$$

Replacing Equation I-123 in Equation 14 of Corti et al. (1990 [DIRS 178211]), plus recasting the molality term $m_2^2\upsilon_+\upsilon_-$ in this equation as $m_c m_a$ by the relations $m_c = \upsilon_+ m_2$ and $m_a = \upsilon_- m_2$ (see Pitzer 1991 [DIRS 152709], p. 86) where m_2 (or m in Pitzer 1991 [DIRS 152709]) delineates the salt molality in the electrolyte yields the same third-order term (i.e., ζ_{Nca}) found in Equation F-9 of Pitzer (1991 [DIRS 152709]).

The Pitzer parameter entries in the thermodynamic database are based on the formulations and symbol definitions given by Pitzer (1991 [DIRS 152709]), so the above conversion of parameter values from Corti et al. (1990 [DIRS 178211]) and Rumpf and Maurer (1993 [DIRS 178223]) to those in the database are needed. The Pitzer expressions of Rumpf and Maurer (1993 [DIRS 178223]) and Rumpf et al. (1994 [DIRS 178222]) are somewhat similar to those adopted by Corti et al. (1990 [DIRS 178211]) except in some cases for the symbol notation. For

example, second-order interaction parameters in Equation 6 of Rumpf and Maurer (1993 [DIRS 178223]) are identical to those in Equation 10 of Corti et al. (1990 [DIRS 178211]), except for the Λ and λ symbols in the latter, which are equivalent to B and β in the former. The considered third-order parameters (i.e., Γ_{Nca}) in Equation 7 of Rumpf and Maurer (1993 [DIRS 178223]) are equivalent to those in Equation 12 of Corti et al. (1990 [DIRS 178211]). The equivalent equations from these authors look different, but by doing some algebraic manipulation of Equation 12 of Corti et al. (1990 [DIRS 178211]) using the electrical neutrality relation $z_+\upsilon_+ = |z_-|\upsilon_-$ and the designations of salt and ion molalities as defined above and given by Pitzer (1991 [DIRS 152709]), the equations end up being equivalent and consistent with Pitzer's standard formulations. This is shown by taking Equation 7 of Rumpf and Maurer (1993 [DIRS 178223]) or Equation 6 of Rumpf et al. (1994 [DIRS 178222]) given as:

$$\Gamma_{G,CA,CA} = \left(\upsilon_+^2\tau_{G,C,C} + 2\upsilon_+\upsilon_-\tau_{G,C,A} + \upsilon_-^2\tau_{G,A,A}\right) \quad \text{(Eq. I-124)}$$

or recast as

$$\Gamma_{G,CA,CA} = \upsilon_+\upsilon_-\left(\frac{\upsilon_+}{\upsilon_-}\tau_{G,C,C} + 2\tau_{G,C,A} + \frac{\upsilon_-}{\upsilon_+}\tau_{G,A,A}\right) \quad \text{(Eq. I-125)}$$

where $\Gamma_{G,CA,CA}$, $\tau_{G,C,C}$, $\tau_{G,C,A}$, and $\tau_{G,A,A}$ correspond to Γ_{Nca}, τ_{nca}, τ_{ncc}, and τ_{naa}, respectively, in Equation I-120 above. Substituting the relation $z_+\upsilon_+ = |z_-|\upsilon_-$ (see Pitzer 1991 [DIRS 152709]) in Equation I-125 yields:

$$\Gamma_{G,CA,CA} = \upsilon_+\upsilon_-\left(\left|\frac{z_-}{z_+}\right|\tau_{G,C,C} + 2\tau_{G,C,A} + \left|\frac{z_+}{z_-}\right|\tau_{G,A,A}\right) \quad \text{(Eq. I-126)}$$

which when substituted in the appropriate term in Equation 5 of Rumpf and Maurer (1993 [DIRS 178223]) or Equation 3 of Rumpf et al. (1994 [DIRS 178222]) yields the same third term as that in the activity coefficient expression defined by Equation 14 in the study by Corti et al. (1990 [DIRS 178211]). Therefore, the equivalent third virial term expressions of Corti et al. (1990 [DIRS 178211]), Rumpf and Maurer (1993 [DIRS 178223]), and Rumpf et al. (1994 [DIRS 178222]) for neutral-cation-anion interactions can be related to that given by Pitzer (1991 [DIRS 152709]) by:

$$\frac{1}{3}\upsilon_+\upsilon_-\zeta_{Nca} = \Gamma_{Nca} = \Gamma_{G,CA,CA} \quad \text{(Eq. I-127)}$$

The parameter $\lambda_{CO_2(aq)-SO_4^{--}}$ was calculated from the equation and parameter data given by Rumpf and Maurer (1993 [DIRS 178223]):

$$B^{(0)}_{G,MX,MX} = (\upsilon_+\beta^{(0)}_{G,M} + \upsilon_-\beta^{(0)}_{G,X}) \quad \text{(Eq. I-128)}$$

where $B^{(0)}_{G,MX,MX}$, $\beta^{(0)}_{G,M}$ and $\beta^{(0)}_{G,X}$ correspond to Λ_{nc}, λ_{Nc}, and λ_{Na} in Equation I-119, respectively. It should be noted that the parameters $\beta^{(0)}_{G,M}$ and $\beta^{(0)}_{G,X}$ in Equation I-128 should not be confused with the standard notation used by Pitzer of $\beta^{(0)}$ to designate binary interactions between cations and anions. To obtain the value of $\lambda_{CO_2(aq)-SO_4^{--}}$, the value of $\lambda_{CO_2(aq)-Na^+}$ must be known. In this case, the values for $\lambda_{CO_2(aq)-Na^+}$ from Corti et al. (1990 [DIRS 178211]) were adopted to be consistent with other Pitzer parameter data from these authors as these were considered for inclusion into the database. For further explanations on these equations, the user is referred to the original authors' articles.

The data fitting to the EQ3/6 temperature function was done using the regression tool in Excel. Instructions on the fitting are given in the tab "Direction" in the file *FitPitzerMX_Ca-HCO3_NMX_CO2_CFJC3.xls*, located in Output DTN: MO0701SPAPTZER.001. Notice that the ζ_{Nca} parameter from Corti et al. (1990 [DIRS 178211]) was fitted using only one term of the EQ3/6 temperature function since it changes little with temperature. The single variable term chosen for this fitting is $(T - T_r)$ where T_r is the reference temperature at 298.158 K. An almost identical fit can be obtained using the $\left(\frac{1}{T} - \frac{1}{T_r}\right)$ term and is given in the tab "Corti et al. CO2-Na" in the spreadsheet *FitPitzerMX_Ca-HCO3_NMX_CO2_ CFJC3.xls*, located in Output DTN: MO0701SPAPTZER.001 for comparison. The worksheets containing the data from He and Morse (1993 [DIRS 162098]) parameters are also included for comparison.

In the tab "Corti et al. CO2-Na," there are also parameters for $\lambda_{CO_2(aq)-Ca^{++}}$ and $\lambda_{CO_2(aq)-Mg^{++}}$, which are approximated by multiplying $\lambda_{CO_2(aq)-Na^+}$ by 2. This approximation approach has been used before by Duan et al. (1992 [DIRS 178210]) for methane solubility as a function of ionic strength using Pitzer equations. This approximation assumes that ternary interactions are negligible.

Input parameters and equations for the ion-pair reactions for $CaCl^+$, $CaCl_2$(aq) and CaCl2(aq)-CaCl2(aq) are from the data source (Sterner et al. 1998 [DIRS 162116], Model 3 in Table I and Table II). Model 3 of Sterner et al. (1998 [DIRS 162116]) uses binary parameters for CaCl and CaCl-Cl, and binary neutral parameters for $CaCl_2$(aq)-$CaCl_2$(aq) interactions. The model also incorporates the use of the ion pairs $CaCl^+$ and $CaCl_2$(aq) (see Section I.4.4.1) in the form of ln K values for the ion-pairing reactions as a function of temperature. The temperature function of Sterner et al. (1998 [DIRS 162116], Equation 4) and associated model parameters for these two reactions are entered in the spreadsheet *FitPitzerNC_MX_CaCl_CFJC_Model3_Sterner_ et_al_1998.xls* (Output DTN: MO0701SPAPTZER.001). The ln K values representing the association reactions in the form given by Sterner et al. (1998 [DIRS 162116]) are transformed in the spreadsheet to log K (dividing by the ln(10)). The sign is reversed to designate a dissociation reaction. Temperature values corresponding to the EQ3/6 temperature grid are then incorporated in the data0.ypf.R2 database. Input parameters for the binary neutral-neutral parameters (λ_{NN}) for $CaCl_2$(aq)-$CaCl_2$(aq) interactions were fitted to the EQ3/6 temperature function using the regression tool in Excel, yielding a fit (see spreadsheet *FitPitzerNC_MX_*

CaCl_CFJC_ Model3_Sterner_et_al_1998.xls, worksheet "lambda-lambda-CaCl2," in Output DTN: MO0701SPAPTZER.001.

O_2 solubility parameters representing binary neutral-cation (NM and NX), (λ_{NM}, λ_{NX}), and ternary neutral-cation-anion (NMX) (ζ_{NMX}) interactions were obtained from the source equations and compared to data parameters reported by Clegg and Brimblecombe (1990 [DIRS 162089]). The authors used O_2 solubility data from multiple sources. The generated parameters were refitted to almost the exact value reported by the authors. Visual comparison of reported activity coefficients at 298.15 K for O_2(aq) depicted in Clegg and Brimblecombe (1990 [DIRS 162089]) indicate a strong agreement with computed values using EQ3/6 v8.0. This was in the presence of various salts such as $NaNO_3$, NaCl, and $MgCl_2$ at relatively high concentration. Due to the manner in which the authors treated their model (i.e., selection of solubility data from different origins and, in many cases, applying density conversions), a straightforward comparison or corroboration with alternate data sources was not possible. The authors parameterized the model up to 100°C but many of the ion parameters for some doublets and triplets do not have temperature dependence and are given only at 298.15 K.

SiO_2(aq) parameters representing binary neutral-cation and neutral-anion (NM and NX) (λ_{NM} and λ_{NX}) and ternary neutral-cation-anion (NMX) (ζ_{NMX}) interactions were obtained from the relevant source equations and compared with those reported by Felmy et al. (1994 [DIRS 162111]). The parameter fitting was based on experimental data on amorphous silica solubility at elevated temperatures as a function electrolyte type and concentration as reported by Marshall (1980 [DIRS 162085]; 1980 [DIRS 160481]), Marshall and Warakomski (1980 [DIRS 160483]), Marshall and Chen (1982 [DIRS 162086]; 1982 [DIRS 162087]), and Chen and Marshall (1982 [DIRS 160453]). In some cases, the authors needed to vary not only the parameter but also the standard chemical potential defining the equilibrium between solution and solid phase. According to Felmy et al. (1994 [DIRS 162111]), the standard chemical potential of amorphous silica was one of the most difficult parameters to fix for the ion interaction parameter fitting. As explained by Felmy et al. (1994 [DIRS 162111]) and Marshall (1980 [DIRS 162085]), the complex nature and ill-defined particle size of this phase, together with experimental difficulties, could create significant variability in solubility data under different temperatures and electrolyte concentrations. Another possible source for discrepancies is the use of different Pitzer parameters for some binary salts other than those used by Felmy et al. (1994 [DIRS 162111]). Further, the log K values for amorphous silica in the current data0.ypf.R2 database are taken from the data0.ymp.R2 database (DTN: MO0302SPATHDYN.000 [DIRS 161756]. Therefore, differences between calculated amorphous silica solubility and that reported by Felmy et al. (1994 [DIRS 162111]) are expected. Due to the apparent variability in reported values for this phase, no attempt was made to fit amorphous silica solubility or to reproduce the values presented by Felmy et al. (1994 [DIRS 162111]). Nevertheless, a validation test involving a visual comparison of the prediction of amorphous silica as a function of $NaNO_3$ at 25°C with the Felmy et al. (1994 [DIRS 162111], Figure 3a) model, suggests differences that are approximately 2% to 15% of those reported in their study. At 100°C (Felmy et al. 1994 [DIRS 162111], Figure 3b), the differences are slightly smaller at low $NaNO_3$ concentrations, but they increase significantly at concentrations larger than 2 molal. Prediction of amorphous silica solubility in other electrolytes shows approximately the same magnitude of uncertainties. Overall, these differences appear to be reasonable given the plausible existence of uncertainties in the amorphous silica solubility data and the different log K values used in the

calculations to represent the equilibrium solubility of this phase. The parameters for SiO_2(aq) are valid only for neutral to acid conditions, in keeping with the studied experimental conditions.

The log K values for $NaHSiO_3$(aq), $HSiO_3^-$, $CaHSiO_3^+$, and $MgHSiO_3^+$ are from the thermodynamic analysis of Sverjensky et al. (1997 [DIRS 150775]). It was noted that the log K obtained by these authors mainly in the temperature range of 25°C to a 100°C has a consistent discrepancy of ~0.2 log units. It was also noted that the log K values in the previous release of the Pitzer database called data0.ypf.R0 (DTN: SN0302T0510102.002 [DIRS 162572]) are consistent with the Sverjensky et al. (1997 [DIRS 150775]) source, and are inconsistent with the "Rimstidt paradigm" for SiO_2(aq) adopted in this database. Interestingly, recalculating the log K temperature grid with the SiO_2(aq) values from the Rimstidt paradigm using the computer code SUPCRT92 v1.0 (see Section 3.1.3) and the associated database file *speq06.dat* yields values that are in good agreement with those obtained experimentally by Busey and Mesmer (1977 [DIRS 177645]) and Seward (1974 [DIRS 177381]) in the temperature range from 25°C to 300°C. In fact, the revised values offer a much better representation of the experimental data depicted in Figure 5 of Sverjensky et al. (1997 [DIRS 150775]), particularly in the low temperature range. For the species $NaHSiO_3$(aq), $CaHSiO_3^+$, and $MgHSiO_3^+$, the log K values need to be recalculated using the SiO_2(aq) values from the Rimstidt paradigm, since the source expressions for the solubility reactions are written on the basis of $HSiO_3^-$ and not SiO_2(aq). Therefore, for consistency with the SiO_2(aq) thermodynamic data in the current database, the log K values for this aqueous species were recalculated using SUPCRT92 v1.0. A check on the predicted log K at 200°C and 300°C indicates a very close match to the experimental data depicted in Figure 15 of Sverjensky et al. (1997 [DIRS 150775]).

The phase kogarkoite (Na_3SO_4F) has been identified as a product of the experimental evaporation of synthetic seepage solutions. Thermodynamic properties for this phase have been determined by Gurevich et al. (1999 [DIRS 176845]). This source provides enthalpy, standard entropy, and heat capacity coefficient data. The Gibbs energy of formation was based on a solubility evaluation study by Felmy and MacLean (2001 [DIRS 177660]). These authors provide a value for the dimensionless parameter standard chemical potential $\left(\frac{\mu^\circ}{RT}\right)$ which can be converted to Gibbs energy of formation of the solid. However, this parameter was determined in the source by using on the basis of $\frac{\mu^\circ}{RT}$ of the dissolution reaction. Therefore, thermodynamic consistency of this value with respect to the solid needs to be consistent with thermodynamic for the basis aqueous species in the current database. From all the relevant chemical species in the reaction (Na^+, SO_4^{2-}, and F^-), only F^- shows a large discrepancy of the Gibbs energy of reaction. Thus, the Gibbs energy of reaction needs to be recalculated for database consistency to then obtain the Gibbs energy of formation of the solid. The spreadsheet *Solids_j_Kogarkoite_TJW.xls* (Output DTN: MO0701SPAPTZER.001) shows all pertinent calculations for the determination of the Gibbs energy of reaction and Gibbs energy of formation of the solid consistent with the F^- thermodynamic data in the current database. Because the heat capacity data for kogarkoite extend only up to about 25°C, the fit was done using data in the range −75°C to +25°C. Kogarkoite solubility needs to be calculated at higher temperatures (e.g., ~110°C). The extrapolation error in extrapolating the fit based on lower temperature data to higher temperature was examined by comparing the fitted equation over the range −75°C to 200°C against

stoichiometrically equivalent sums of heat capacities for NaF + Na_2SO_4 using data for three forms of Na_2SO_4. The "Na_2SO_4" form thenardite may be the most relevant here, as it is the stable form over most of the temperature range of interest. According to Gurevich et al. (1999 [DIRS 176845]), the data for kogarkoite in the temperature range of their study closely corresponded with the stoichiometric sum of heat capacities for NaF and Na_2SO_4. The Na_2SO_4 phase referenced in their work is assumed to be the "Na_2SO_4" thenardite considered here. The heat capacity data for NaF and the Na_2SO_4 phases were taken from the spreadsheet *Cp_Solids_j_Na_TJW_1.xls* (Output DTN: MO0701SPAPTZER.001). The comparisons shown on the spreadsheet *Cp_Solids_j_Kogarkoite_TJW_2.xls* (worksheet "Test – Kogarkoite" in Output DTN: MO0701SPAPTZER.001) suggest that the extrapolated heat capacity of kogarkoite might be slightly high, by about 20 joule/mol-K at 200°C, 10 joule/mol-K at 125°C, and 7 joule/mol-K at 100°C. These estimates were obtained by the differences in heat capacity (i.e., Cp(T) − Cp(25°C)) for the various solids and then comparing the differences in those for kogarkoite versus those for its stoichiometric equivalent (NaF + Na_2SO_4). This is equivalent to looking at the heat capacity differences that would be obtained if one were to adjust the stoichiometric equivalent NaF + Na_2SO_4 data to exactly match the kogarkoite data at 25°C. The numbers quoted above are for "Na_2SO_4" equating to the mineral thenardite. Somewhat different numbers are obtained using two other forms of "Na_2SO_4."

Data for amorphous sepiolite (sepiolite(am)) is based on the solubility study of Wollast et al. (1968 [DIRS 162340]). The log K value provided by the source is only for 25°C. However, log K values other than 25°C are reported in the data block provided to a temperature of 100°C. This value was added to the database as part of a validation analysis in the IDPS model (Section 7.1.3). The log K values other than those at 25°C are fictive in the sense that these represent a constant increment in log K relative to that of crystalline sepiolite. The constant increment corresponds to the difference between the log K value for "Sepiolite(am)" and "Sepiolite" at 25°C in the database. This difference (or Δ log K) is 7.1161. So all the log K values other than those at 25°C for "Sepiolite(am)" equal the log K value of "Sepiolite" at the temperature of interest plus 7.1161. The report explains the use of "Sepiolite(am)" in the validation analysis. The phase palygorskite was also added to the database and the log K value is based on estimated the Gibbs energy of formation for the phase stoichiometry $Mg_{2.84}Al_{1.8}Si_{7.73}O_{20}(OH)_2{:}4H_2O$ after the method of Birsoy (2002 [DIRS 178220]). Birsoy (2002 [DIRS 178220]) uses the formulation by Nriagu (1975 [DIRS 178321]) to estimate the $\Delta G^{\circ}_{f,298}$ of the solid. The reaction representing the formation of palygorskite as given by Birsoy (2002 [DIRS 178220]) is given as:

$$\mathrm{Mg_{2.84}Al_{1.8}Si_{7.73}O_{20}(OH)_2(OH_2)_4\,H_2O = 2.84\,Mg(OH)_2 + 1.8\,Al(OH)_3 + 7.73\,Si(OH)_4 + 3.46\,H_2O} \quad \text{(Eq. I-129)}$$

The expression for the estimation of $\Delta G^{\circ}_{f,298}$ based on Nriagu (1975 [DIRS 178321]) delineating the formation of palygorskite is given by Birsoy (2002 [DIRS 178220]) as:

$$\Delta G^{\circ}_{f,298,paly} = \sum n_i \Delta G^{\circ}_{f,298,(hydroxide)} - \left(\sum n_i z_i - 30\right)\Delta G^{\circ}_{f,298,(H_2O)} - \left[0.39(n_i z_i - 30)\right] \quad \text{(Eq. I-130)}$$

where n_i is the stoichiometric coefficient of the mass balance reaction of the hydroxide phase i and z_i refers to the charge of the cation. The reaction representing the formation of palygorskite is similar to that by Birsoy (2002 [DIRS 178220]) but consistent with the use of SiO_2(qtz) instead of $Si(OH)_4$. This is given as:

$$Mg_{2.84}Al_{1.8}Si_{7.73}O_{20}(OH)_2(OH_2)_4 \;\; H_2O + 12H_2O = 2.84\,Mg(OH)_2 + 1.8\,Al(OH)_3 + 7.73\,Si(OH)_4$$

(Eq. I-131)

The $\Delta G^{\circ}_{f,298}$ estimated from Equation I-130 based on the palygorskite formation reaction given by Equation I-131 using thermodynamic data from data0.ymp.R4 can be expressed as:

$$\Delta G^{\circ}_{f,298,paly} = (2.84(-835318.86) + 1.8(-1155486.91) + 7.73(-856280.70) + 3.46(-237181.38)$$
$$+ ([0.39 * 4.184 * 1000](3.46)) = -11911460.55 \text{ J/mol}$$

(Eq. I-132)

Notice that the factor "0.39" in the equation above (see also Birsoy 2002 [DIRS 178220]) needs to be scaled as well when converting from kcal/mol to J/mol. The value estimated using the thermodynamic database data0.ymp.R4 is different from that given by Birsoy (2002 [DIRS 178220]); the difference is 32855.45 J/mol. These calculations are given in *Solids_j_Mg_Silicates_CFJC_KBH1.xls* (Output DTN: MO0701SPAPTZER.001).

Thermodynamic data for the phase "Antigorite(am)" or "poorly crystalline antigorite" was obtained from the study by Gunnarsson et al. (2005 [DIRS 176844]). The authors used the formula $Mg_3Si_2O_5(OH)_4$ instead of antigorite ($Mg_{48}Si_{34}O_{85}(OH)_{62}$) which correspond to Mg-silicates of the serpentine group of minerals such as chrysotile. The authors appeared to have assigned this stoichiometry to the precipitated phase in their experiments on the basis of Mg/Si ratio (i.e., 3/2) of sampled solutions and the infrared spectra of the poorly crystalline solid (Gunnarsson et al. 2005 [DIRS 176844]). Notice that the Mg/Si ratio of antigorite is slightly smaller than that of "Antigorite(am)." The Gibbs energy of formation for "Antigorite(am)" was estimated by matching the log K value obtained from Equation 3 of Gunnarsson et al. (2005 [DIRS 176844]). This calculation is presented in the spreadsheet *Solids_j_Mg_Silicates_CFJC_KBH1.xls* (Output DTN: MO0701SPAPTZER.001).

I.4.5.16 Ions: MMX Ternary Parameters in the System Na-K-Mg-Cl-OH-SO_4

See Table I-1 for MMX ternary parameters in the system Na-K-Mg-Cl-OH-SO_4.

Associated Spreadsheet: *Pabalan_icf_TJW.xls*
(Output DTN: MO0701SPAPTZER.001)

Source: Pabalan and Pitzer 1987 [DIRS 162096].

Description: Some ternary parameters encompassing cation(M), cation(M), and anion(X) (ψ_{M1M2X}) in the system Na-K-Mg-Cl-OH-SO_4 were refitted from equations and data by Pabalan and Pitzer (1987 [DIRS 162096]). Some of these parameters are expressed as constants and do not need refitting.

I.4.6 VARIOUS MX AND MM PARAMETERS FROM TABLE I-2 AT 25°C THAT DO NOT REQUIRE REFITTING

Associated Spreadsheets: *Some2-1Salts25C_TJW.xls*
Some1-1Salts25C_TJW.xls
(Output DTN: MO0701SPAPTZER.001)

Source: Pitzer 1991 [DIRS 152709] ("No Spreadsheet" in Table I-2 means that values were taken directly from the tables in this source).

Description: Binary and ternary parameters reported at 25°C in the study by Pitzer (1991 [DIRS 152709]) were also incorporated in the data0.ypf.R2 database. These parameters did not require any refitting but are expressed in the source as the product of the parameter multiplied by constant factors. The associated spreadsheets recalculate the parameter value without the multipliers so these can be incorporated in the data0.ypf.R2 database file.

I.5 DATA FOR SOLID PHASES, AQUEOUS SPECIES, AND GASES

The majority of solid phases included in the data0.ypf.R2 database in the form of log K data to represent solubility are taken from the data0.ymp.R4 database (DTN: SN0410T0510404.002 [DIRS 172712]; see Table I-27) or derived from thermodynamic data for solids reported by Barin and Platzki (1995 [DIRS 157865]). Log K data for most salt phases are taken from various sources such as Harvie et al. (1984 [DIRS 118163]), Greenberg and Møller (1989 [DIRS 152684]), and Pabalan and Pitzer (1987 [DIRS 162096]) which are in many cases given in the form of standard chemical potentials (see Table I-28 for spreadsheets *Minerals_gmo.xls* and *Minerals_hmw.xls*). For a few salts ($CaCl_2$, Na_2CO_3:H_2O, and $NaNO_3$), solubility data in the literature were scant and log K values for the salt dissolution reactions were estimated from combined sources of thermodynamic data such as heat capacity and standard enthalpy. For these few salts, these data were used with the code SUPCRT92 v1.0 by addition to the SUPCRT92 thermodynamic database. The SUPCRT92 configuration run file (*liqvap.con*) and output files used for the Windows NT (*suptest.tab* in *supcrt92test_Yueting_Chen.zip*) and Windows 2000 (*nano3_soda_niter.tab*, *thermonatrite.tab*, *cacl2_solub.tab*) runs are included in the Output DTN: MO0701SPAPTZER.001. Also included in this DTN is the input file *supcrt_runs.rxn*, which describes the input reactions for salt dissolution as used in all SUPCRT92 runs. The modified SUPCRT92 thermodynamic database (*sprons96_mod2.dat* and *dprons96_mod2.dat*) is included in Output DTN: MO0701SPAPTZER.001. In a similar fashion, Excel spreadsheet calculations were used to calculate the many log K's for reactions denoting salt solubility using this type of thermodynamic data as a source. Either approach allowed for the initial estimates of log K values, which were then modified and fitted to the Pitzer activity model of the relevant system to predict the reported salt saturation molality values obtained from recognized sources such as the report by Linke (1965 [DIRS 166191]), among others. This is done to bridge consistency between the activity model and salt solubility within the bounds of model applicability to accurately predict saturation molalities for the relevant salt. This type of fitting

and optimization approach is necessary given the multiple sources of data obtained in different ways (e.g., calorimetry vs. solubility). The resulting differences in log K's before and after fitting were reasonable given the associated uncertainties. Information on the fitting procedure and results is detailed in the corresponding Excel spreadsheets given in Table I-28. Only information on salt log K's that required fitting, the $CaCl_2$ hydrates, thermonatrite (Na_2CO_3:H_2O), and soda niter ($NaNO_3$), will be summarized below. As mentioned above, log K values for other salt solids were obtained from Greenberg and Møller (1989 [DIRS 152684]) and Pabalan and Pitzer (1987 [DIRS 162096]) where no solubility constant fitting/optimization was needed due to their self-consistency with the Pitzer activity model of salt components adopted in this database development. Log K's of aqueous species were also taken from the data0.ymp.R2 and data0.ymp.R4 databases (see Tables I-29 and I-30) except for $CaSO_4$(aq), which was taken directly from Greenberg and Møller (1989 [DIRS 152684]) to be consistent with their activity model. Data for two redox-related auxiliary species (NH_4^+ and NO_2^-) were also derived from data0.ymp.R2 but were obtained through a combination of reaction log K's to generate the values incorporated in data0.ypf.R2. The log K values for the gases were also obtained from the data0.ymp.R2 database. Tables I-27 through I-31 below show a list of solid phases, aqueous species, and gases plus relevant spreadsheets where calculations of log K's were performed.

Table I-27. Solid Minerals Sourced from the data0.ymp.R2 or data0.ymp.R4 Databases

Solid Mineral	Molecular Formula
Albite	$NaAlSi_3O_8$
Alunite	$KAl_3(OH)_6(SO_4)_2$
Amesite-7A	$Mg_2Al_2SiO_5(OH)_4$
Amesite-14A	$Mg_4Al_4Si_2O_{10}(OH)_8$
Analcime	$Na_{0.96}Al_{0.96}Si_{2.04}O_6$:$H_2O$
Analcime-dehy	$Na_{0.96}Al_{0.96}Si_{2.04}O_6$
Aragonite	$CaCO_3$
Artinite	$Mg_2CO_3(OH)_2$:$3H_2O$
Beidellite-Mg	$Mg_{0.165}Al_{2.33}Si_{3.67}O_{10}(OH)_2$
Beidellite-Ca	$Ca_{0.165}Al_{2.33}Si_{3.67}O_{10}(OH)_2$
Beidellite-K	$K_{0.33}Al_{2.33}Si_{3.67}O_{10}(OH)_2$
Beidellite-Na	$Na_{0.33}Al_{2.33}Si_{3.67}O_{10}(OH)_2$
Beidellite-H	$H_{0.33}Al_{2.33}Si_{3.67}O_{10}(OH)_2$
Boehmite	AlOOH
Brucite	$Mg(OH)_2$
Calcite	$CaCO_3$
Celadonite	$KMgAlSi_4O_{10}(OH)_2$
Celestite	$SrSO_4$
Chabazite	$K_{0.6}Na_{0.2}Ca_{1.55}Al_{3.8}Si_{8.2}O_{24}$:$10H_2O$
Chamosite-7A	$Fe_2Al_2SiO_5(OH)_4$
Clinoptilolite	$Na_{0.954}K_{0.543}Ca_{0.761}Mg_{0.124}Sr_{0.036}Ba_{0.062}Mn_{0.002}Al_{3.45}F$
Clinoptilolite-dehy	$Sr_{0.036}Mg_{0.124}Ca_{0.761}Mn_{0.002}Ba_{0.062}K_{0.543}Na_{0.954}Al_{3.45}F$
Clinoptilolite-Ca	$Ca_{1.7335}Al_{3.45}Fe_{0.017}Si_{14.533}O_{36}$:$10.922H_2O$
Clinoptilolite-Cs	$Ca_{3.467}Al_{3.45}Fe_{0.017}Si_{14.533}O_{36}$:$10.922H_2O$
Clinoptilolite-K	$K_{3.467}Al_{3.45}Fe_{0.017}Si_{14.533}O_{36}$:$10.922H_2O$
Clinoptilolite-NH4	$(NH_4)_{3.467}Al_{3.45}Fe_{0.017}Si_{14.533}O_{36}$:$10.922H_2O$

Table I-27. Solid Minerals Sourced from the data0.ymp.R2 or data0.ymp.R4 Databases (Continued)

Solid Mineral	Molecular Formula
Clinoptilolite-Na	$Na_{3.467}Al_{3.45}Fe_{0.017}Si_{14.533}O_{36}:10.922H_2O$
Clinoptilolite-Sr	$Sr_{1.7335}Al_{3.45}Fe_{0.017}Si_{14.533}O_{36}:10.922H_2O$
Corundum	Al_2O_3
Cristobalite(alpha)	SiO_2
Cronstedtite-7A	$Fe_2Fe_2SiO_5(OH)_4$
Daphnite-14A	$Fe_5AlAlSi_3O_{10}(OH)_8$
Daphnite-7A	$Fe_5AlAlSi_3O_{10}(OH)_8$
Dawsonite	$NaAlCO_3(OH)_2$
Dolomite	$CaMg(CO_3)_2$
Erionite	$K_{1.5}Na_{0.9}Ca_{0.9}Al_{4.2}Si_{13.8}O_{36}:13H_2O$
Ferroaluminoceladonite	$KFeAlSi_4O_{10}(OH)_2$
Ferroceladonite	$KFeFeSi_4O_{10}(OH)_2$
Fe2(MoO4)3	$Fe_2(MoO_4)_3$
FeF3	FeF_3
Fe(OH)3	$Fe(OH)_3$
Fe2(SO4)3	$Fe_2(SO_4)_3$
Fluorapatite	$Ca_5(PO_4)_3F$
Fluorite	CaF_2
Gibbsite	$Al(OH)_3$
Goethite	FeOOH
Greenalite	$Fe_3Si_2O_5(OH)_4$
Hematite	Fe_2O_3
Heulandite	$Ba_{0.065}Sr_{0.175}Ca_{0.585}K_{0.132}Na_{0.383}Al_{2.165}Si_{6.835}O_{18}:6H_2O$
Huntite	$CaMg_3(CO_3)_4$
Hydroxylapatite	$Ca_5(OH)(PO_4)_3$
Hydromagnesite	$Mg_5(CO_3)_4(OH)_2:4H_2O$
Illite	$K_{0.6}Mg_{0.25}Al_{1.8}Al_{0.5}Si_{3.5}O_{10}(OH)_2$
Jarosite	$KFe_3(SO_4)_2(OH)_6$
Jarosite-Na	$NaFe_3(SO_4)_2(OH)_6$
K-Feldspar	$KAlSi_3O_8$
K2CO3:1.5H2O	$K_2CO_3:1.5H_2O$
Kaolinite	$Al_2Si_2O_5(OH)_4$
KMgCl3:2H2O	$KMgCl_3:2H_2O$
Lansfordite	$MgCO_3:5H_2O$
Laumontite	$K_{0.2}Na_{0.2}Ca_{1.8}Al_4Si_{8.0}O_{24}:8H_2O$
Lime	CaO
Magnesite	$MgCO_3$
Maximum Microcline	$KAlSi_3O_8$
Mesolite	$Na_{0.676}Ca_{0.657}Al_{1.99}Si_{3.01}O_{10}:2.647H_2O$
Minnesotaite	$Fe_3Si_4O_{10}(OH)_2$
MoO2Cl2	MoO_2Cl_2
Molysite	$FeCl_3$

Table I-27. Solid Minerals Sourced from the data0.ymp.R2 or data0.ymp.R4 Databases (Continued)

Solid Mineral	Molecular Formula
Montmorillonite-H	$H_{0.33}Mg_{0.33}Al_{1.67}Si_4O_{10}(OH)_2$
Montmorillonite-Na	$Na_{0.33}Mg_{0.33}Al_{1.67}Si_4O_{10}(OH)_2$
Montmorillonite-K	$K_{0.33}Mg_{0.33}Al_{1.67}Si_4O_{10}(OH)_2$
Montmorillonite-Ca	$K_{0.165}Mg_{0.33}Al_{1.67}Si_4O_{10}(OH)_2$
Montmorillonite-Mg	$Mg_{0.495}Al_{1.67}Si_4O_{10}(OH)_2$
Mordenite	$Ca_{0.2895}Na_{0.361}Al_{0.94}Si_{5.06}O_{12}:3.468H_2O$
Natrolite	$Na_2Al_2Si_3O_{10}:2H_2O$
Nesquehonite	$MgCO_3:3H_2O$
Nontronite-Mg	$Mg_{0.165}Fe_2Al_{0.33}Si_{3.67}H_2O_{12}$
Nontronite-Ca	$Ca_{0.165}Fe_2Al_{0.33}Si_{3.67}H_2O_{12}$
Nontronite-K	$K_{0.33}Fe_2Al_{0.33}Si_{3.67}H_2O_{12}$
Nontronite-Na	$Na_{0.33}Fe_2Al_{0.33}Si_{3.67}H_2O_{12}$
Nontronite-H	$H_{0.33}Fe_2Al_{0.33}Si_{3.67}H_2O_{12}$
Phillipsite	$K_{0.7}Na_{0.7}Ca_{1.1}Al_{3.6}Si_{12.4}O_{32}:12.6H_2O$
Portlandite	$Ca(OH)_2$
Pyrolusite	MnO_2
Pyrophyllite	$Al_2Si_4O_{10}(OH)_2$
Quartz	SiO_2
Ripidolite-7A	$Mg_3Fe_2Al_2Si_3O_{10}(OH)_8$
Ripidolite-14A	$Mg_3Fe_2Al_2Si_3O_{10}(OH)_8$
Saponite-H	$H_{0.33}Mg_3Al_{0.33}Si_{3.67}O_{10}(OH)_2$
Saponite-Na	$Na_{0.33}Mg_3Al_{0.33}Si_{3.67}O_{10}(OH)_2$
Saponite-K	$K_{0.33}Mg_3Al_{0.33}Si_{3.67}O_{10}(OH)_2$
Saponite-Ca	$Ca_{0.165}Mg_3Al_{0.33}Si_{3.67}O_{10}(OH)_2$
Saponite-Mg	$Mg_{0.165}Mg_3Al_{0.33}Si_{3.67}O_{10}(OH)_2$
Scolecite	$CaAl_2Si_3O_{10}:3H_2O$
Sepiolite	$Mg_4Si_6O_{15}(OH)_2:6H_2O$
SiO2(am)	SiO_2
Smectite-high-Fe-Mg	$Ca_{0.025}Na_{0.1}K_{0.2}Fe^{++}_{0.5}Fe^{+++}_{0.2}Mg_{1.15}Al_{1.25}Si_{3.5}H_2O_{12}$
Smectite-high-Fe-Mg	$Ca_{0.02}Na_{0.15}K_{0.2}Fe^{++}_{0.29}Fe^{+++}_{0.16}Mg_{0.9}Al_{1.25}Si_{3.75}H_2O_{12}$
Stellerite	$Ca_2Al_4Si_{14}O_{36}:14H_2O$
Stilbite	$Ca_{1.019}Na_{0.136}K_{0.006}Al_{2.18}Si_{6.82}O_{18}:7.33H_2O$
Strontianite	$SrCO_3$
Talc	$Mg_3Si_4O_{10}(OH)_2$
Whitlockite	$Ca_3(PO_4)_2$

Source: DTNs: MO0302SPATHDYN.000 [DIRS 161756] and SN0410T0510404.002 [DIRS 172712].

Table I-28. Salt Solids Sourced from Various Spreadsheets

Solid Mineral	Molecular Formula	Spreadsheet File in Output DTN: MO0701SPAPTZER.001
Anhydrite	$CaSO_4$	*Minerals_gmo.xls*
Antarcticite	$CaCl_2:6H_2O$	*cacl2_hydrates_min_cal_CFJC2.xls*
Antigorite(am)	$Mg_3Si_2O_5(OH)_4$	*Solids_j_Mg_Silicates_CFJC_KBH1.xls*
Arcanite	K_2SO_4	*Minerals_gmo.xls*
Bischofite	$MgCl_2:6H_2O$	*Solids_j_Pabalan_TJW_1.xls*
Bloedite	$Na_2Mg(SO_4)_2:4H_2O$	*Minerals_hmw.xls*
Brushite	$CaHPO_4:2H_2O$	*Solids_j_Ca_TJW_1.xls*
Burkeite	$Na_6CO_3(SO_4)_2$	*Minerals_hmw.xls*
CaBr2	$CaBr_2$	*Solids_j_Ca_TJW_1.xls*
Ca2Cl2(OH)2:H2O	$Ca_2Cl_2(OH)_2:H_2O$	*Minerals_hmw.xls*
Ca4Cl2(OH)6:13H2O	$Ca_4Cl_2(OH)_6:13H_2O$	*Minerals_hmw.xls*
CaCl2	$CaCl_2$	*cacl2_solub.tab* (this is not an Excel spreadsheet)
CaCl2:2H2O	$CaCl_2:2H_2O$	*cacl2_hydrates_min_cal_CFJC2.xls*
CaCl2:4H2O	$CaCl_2:4H_2O$	*cacl2_hydrates_min_cal_CFJC2.xls*
CaI2	CaI_2	*Solids_j_Ca_TJW_1.xls*
Ca(NO3)2	$Ca(NO_3)_2$	*Solids_j_Ca_TJW_1.xls*
Ca(NO3)2:2H2O	$Ca(NO_3)_2:2H_2O$	*Solids_j_Ca_TJW_1.xls*
Ca(NO3)2:3H2O	$Ca(NO_3)_2:3H_2O$	*Solids_j_Ca_TJW_1.xls*
Ca(NO3)2:4H2O	$Ca(NO_3)_2:4H_2O$	*Solids_j_Ca_TJW_1.xls*
CaOHCl	CaOHCl	*Solids_j_Misc_1_TJW_11.xls*
Carnallite	$KMgCl_3:6H_2O$	*Solids_j_Pabalan_TJW_1.xls*
Carobbite	KF	*Solids_j_K_TJW_1.xls*
CaWO4	$CaWO_4$	*Solids_j_Ca_TJW_1.xls*
Chloromagnesite	$MgCl_2$	*Solids_j_Pabalan_TJW_1.xls*
Cryolite	Na_3AlF_6	*Solids_j_Na_TJW_1.xls*
$CuSO_4:5H_2O$	$CuSO_4:5H_2O$	No Spreadsheet (Baes et al. 1993 [DIRS 168318], Table VI, set 11)
Darapskite	$Na_3SO_4NO_3$:H2O	*Solids_j_Misc_1_TJW_11.xls*
Epsomite	$MgSO_4:7H_2O$	*Solids_j_Pabalan_TJW_1.xls*
Gaylussite	$CaNa_2(CO_3)_2:5H_2O$	*Minerals_hmw.xls*
Glaserite	$NaK_3(SO_4)_2$	*Minerals_hmw.xls*
Glauberite	$Na_2Ca(SO_4)_2$	*Minerals_gmo.xls*
Gypsum	$CaSO_4:2H_2O$	*Minerals_gmo.xls*
Halite	NaCl	*Minerals_gmo.xls*
Hemihydrate	$CaSO_4:0.5H_2O$	*Minerals_gmo.xls*
Hexahydrite	$MgSO_4:6H_2O$	*Solids_j_Pabalan_TJW_1.xls*
K2CO3	K_2CO_3	*Solids_j_K_TJW_1.xls*
K2O	K_2O	*Solids_j_K_TJW_1.xls*
K2Si4O9	$K_2Si_4O_9$	*Solids_j_K_TJW_1.xls*
K3H(SO4)2	$K_3H(SO_4)_2$	*Minerals_hmw.xls*

Table I-28. Salt Solids Sourced from Various Spreadsheets (Continued)

Solid Mineral	Molecular Formula	Spreadsheet File in Output DTN: MO0701SPAPTZER.001
K8H4(CO3)6:3H2O	$K_8H_4(CO_3)_6:3H_2O$	*Minerals_hmw.xls*
Kainite	$KmgClSO_4:3H_2O$	*Minerals_hmw.xls*
KAlCl4	$KAlCl_4$	*Solids_j_K_TJW_1.xls*
K2HPO4	K_2HPO_4	*Solids_j_K_TJW_1.xls*
K3AlCl6	K_3AlCl_6	*Solids_j_K_TJW_1.xls*
K3AlF6	K_3AlF_6	*Solids_j_K_TJW_1.xls*
K3PO4	K_3PO_4	*Solids_j_K_TJW_1.xls*
Kalicinite	$KHCO_3$	*Minerals_hmw.xls*
KAl(SO4)2	$KAl(SO_4)_2$	*Solids_j_K_TJW_1.xls*
KAl(SO4)2:3H2O	$KAl(SO_4)_2:3H_2O$	*Solids_j_K_TJW_1.xls*
KAl(SO4)2:12H2O	$KAl(SO_4)_2:12H_2O$	*Solids_j_K_TJW_1.xls*
KBr	KBr	*Solids_j_K_TJW_1.xls*
KClO4	$KClO_4$	*Solids_j_K_TJW_1.xls*
KH2PO4	KH_2PO_4	*Solids_j_K_TJW_1.xls*
KI	KI	*Solids_j_K_TJW_1.xls*
Kieserite	$MgSO_4:H_2O$	*Solids_j_Pabalan_TJW_1.xls*
KNaCO3:6H2O	$KNaCO_3:6H_2O$	*Minerals_hmw.xls*
Kogarkoite	Na_3SO_4F	*Cp_Solids_j_Kogarkoite_TJW_2.xls* and *Solids_j_Kogarkoite_TJW.xls*
KOH	KOH	*Solids_j_K_TJW_1.xls*
Labile_Salt	$Na_2Ca_5(SO_4)_6:3H_2O$	*Minerals_gmo.xls*
Leonhardtite	$MgSO_4:4H_2O$	*Solids_j_Pabalan_TJW_1.xls*
Leonite	$K_2Mg(SO_4)_2:4H_2O$	*Minerals_hmw.xls*
Mercallite	$KHSO_4$	*Minerals_hmw.xls*
MgBr2	$MgBr_2$	*Solids_j_Mg_TJW_1.xls*
MgCl2:H2O	$MgCl_2:H_2O$	*Solids_j_Pabalan_TJW_1.xls*
MgCl2:2H2O	$MgCl_2:2H_2O$	*Solids_j_Pabalan_TJW_1.xls*
MgCl2:4H2O	$MgCl_2:4H_2O$	*Solids_j_Pabalan_TJW_1.xls*
MgI2	MgI_2	*Solids_j_Mg_TJW_1.xls*
MgMoO4	$MgMoO_4$	*Solids_j_Mg_TJW_1.xls*
Mg(NO3)2	$Mg(NO_3)_2$	*Solids_j_Mg_TJW_1.xls*
MgOHCl	MgOHCl	*Solids_j_Mg_TJW_1.xls*
MgSO4	$MgSO_4$	*Solids_j_Pabalan_TJW_1.xls*
MgWO4	$MgWO_4$	*Solids_j_Mg_TJW_1.xls*
Mirabilite	$Na_2SO_4:10H_2O$	*Minerals_gmo.xls*
Misenite	$K_8H_6(SO_4)_7$	*Minerals_hmw.xls*
NaBr	NaBr	*Solids_j_Na_TJW_1.xls*
NaClO4	$NaClO_4$	*Solids_j_Na_TJW_1.xls*
NaI	NaI	*Solids_j_Na_TJW_1.xls*
NaNO2	$NaNO_2$	*Solids_j_Na_TJW_1.xls*
NaOH	NaOH	*Solids_j_Na_TJW_1.xls*

Table I-28. Salt Solids Sourced from Various Spreadsheets (Continued)

Solid Mineral	Molecular Formula	Spreadsheet File in Output DTN: MO0701SPAPTZER.001
Na2CO3:7H2O	$Na_2CO_3:7H_2O$	*Minerals_hmw.xls*
Na2CrO4	Na_2CrO_4	*Solids_j_Na_TJW_1.xls*
Na2MoO4	Na_2MoO_4	*Solids_j_Na_TJW_1.xls*
Na2WO4	Na_2WO_4	*Solids_j_Na_TJW_1.xls*
Na2O	Na_2O	*Solids_j_Na_TJW_1.xls*
Na2SO4(Sol-3)	Na_2SO_4	*Solids_j_Na_TJW_1.xls*
Na3H(SO4)2	$Na_3H(SO_4)_2$	*Minerals_hmw.xls*
Na4Ca(SO4)3:2H2O	$Na_4Ca(SO_4)_3:2H_2O$	*Minerals_hmw.xls*
Nahcolite	$NaHCO_3$	*Solids_j_Na_TJW_1.xls*
Natrite	Na_2CO_3	*Solids_j_Na_TJW_1.xls*
Natron	Na_2CO_3	*Minerals_hmw.xls*
NH4Cl	NH_4Cl	*Solids_j_NH4_TJW_1.xls*
NH4ClO4	NH_4ClO_4	*Solids_j_NH4_TJW_1.xls*
NH4I	NH_4I	*Solids_j_NH4_TJW_1.xls*
(NH4)2SO4	$(NH_4)_2SO_4$	*Solids_j_NH4_TJW_1.xls*
Niter	KNO_3	*Solids_j_K_TJW_1.xls*
Oxychloride-Mg	$Mg_2Cl(OH)_3:4H_2O$	*Minerals_hmw.xls*
Palygorskite	$Mg_{2.84}Al_{1.8}Si_{7.73}O_{20}(OH)_2:4H_2O$	*Solids_j_Mg_Silicates_CFJC_KBH1.xls*
Pentahydrite	$MgSO_4:5H_2O$	*Solids_j_Pabalan_TJW_1.xls*
Pentasalt	$K_2Ca_5(SO_4)_6:H_2O$	*Minerals_gmo.xls*
Periclase	MgO	*Solids_j_Mg_TJW_1.xls*
Picromerite	$K_2Mg(SO_4)_2:6H_2O$	*Minerals_hmw.xls*
Pirssonite	$Na_2Ca(CO_3)_2:2H_2O$	*Minerals_hmw.xls*
Polyhalite	$K_2MgCa_2(SO_4)_4:2H_2O$	*Minerals_hmw.xls*
Powellite	$CaMoO_4$	*Solids_j_Ca_TJW_1.xls*
Sellaite	MgF_2	*Solids_j_Mg_TJW_1.xls*
Sepiolite(am)	$Mg_4Si_6O_{15}(OH)_2:6H_2O$	No Spreadsheet
Soda Niter	$NaNO_3$	*NaNO3_min_cal_CFJC2.xls*
SrBr2	$SrBr_2$	*Solids_j_Sr_TJW_1.xls*
SrCl2	$SrCl_2$	*Solids_j_Sr_TJW_1.xls*
SrF2	SrF_2	*Solids_j_Sr_TJW_1.xls*
SrI2	SrI_2	*Solids_j_Sr_TJW_1.xls*
SrMoO4	$SrMoO_4$	*Solids_j_Sr_TJW_1.xls*
SrO	SrO	*Solids_j_Sr_TJW_1.xls*
Sr(OH)2	$Sr(OH)_2$	*Solids_j_Sr_TJW_1.xls*
SrWO4	$SrWO_4$	*Solids_j_Sr_TJW_1.xls*
Sylvite	KCl	*Minerals_gmo.xls*
Syngenite	$K_2Ca(SO_4)_2:H_2O$	*Minerals_gmo.xls*
Tachyhydrite	$Mg_2CaCl_6:12H_2O$	*Minerals_hmw.xls*
Tarapacaite	K_2CrO_4	*Solids_j_K_TJW_1.xls*
Thenardite	Na_2SO_4	*Minerals_gmo.xls*

Table I-28. Salt Solids Sourced from Various Spreadsheets (Continued)

Solid Mineral	Molecular Formula	Spreadsheet File in Output DTN: MO0701SPAPTZER.001
Thermonatrite	$Na_2CO_3:H_2O$	*thermonatrite_solubility_CFJC2.xls*
Trona	$Na_3H(CO_3)_2:2H_2O$	*Minerals_hmw.xls*
Trona-K	$K_2NaH(CO_3)_2:2H_2O$	*Minerals_hmw.xls*
Villiaumite	NaF	*Solids_j_Na_TJW_1.xls*

Source: Output DTN: MO0701SPAPTZER.001.

Table I-29. Auxiliary Basis Aqueous Species Data Sources

Aqueous Species	Molecular Formula	Source
ClO4-	ClO_4^-	DTN: SN0410T0510404.002 [DIRS 172712]
Fe+++	Fe^{3+}	DTN: SN0410T0510404.002 [DIRS 172712]
H2(aq)	H_2(aq)	DTN: SN0410T0510404.002 [DIRS 172712]
NH4+	NH_4^+	*AuxBasisSpecies.xls* in Output DTN: MO0701SPAPTZER.001
NO2-	NO_2^-	*AuxBasisSpecies.xls* in Output DTN: MO0701SPAPTZER.001
O2(aq)	O_2(aq)	DTN: SN0410T0510404.002 [DIRS 172712]

Table I-30. Aqueous Species Data Sources

Aqueous Species	Molecular Formula	Source
AlO2-	AlO_2^-	DTN: SN0410T0510404.002 [DIRS 172712]
AlOH++	$AlOH^{2+}$	DTN: SN0410T0510404.002 [DIRS 172712]
AlO+	AlO^+	DTN: SN0410T0510404.002 [DIRS 172712]
CaCl+	CaCl+	*FitPitzerNC_MX_CaCl_CFJC_Model3_Sterner_et_al_1998.xls* in Output DTN: MO0701SPAPTZER.001
CaCl2(aq)	CaCl2(aq)	*FitPitzerNC_MX_CaCl_CFJC Model3_Sterner_et_al_1998.xls* in Output DTN: MO0701SPAPTZER.001
CaCO3(aq)	$CaCO_3$(aq)	DTN: SN0410T0510404.002 [DIRS 172712]
CaHCO3+	$CaHCO_3^+$	DTN: SN0410T0510404.002 [DIRS 172712]
CaHSiO3+	CaHSiO3+	*Silicic_Acid_spreadsheet.xls* in Output DTN: MO0701SPAPTZER.001
CaOH+	$CaOH^+$	DTN: SN0410T0510404.002 [DIRS 172712]
CaSO4(aq)	$CaSO_4$(aq)	*Minerals_gmo.xls* in Output DTN: MO0701SPAPTZER.001
CO2(aq)	CO_2(aq)	DTN: SN0410T0510404.002 [DIRS 172712]
CO3--	CO_3^{2-}	DTN: SN0410T0510404.002 [DIRS 172712]
HSO4-	HSO_4^-	DTN: SN0410T0510404.002 [DIRS 172712]
HSiO3-	$HSiO_3^-$	DTN: SN0410T0510404.002 [DIRS 172712]
H2PO4-	$H_2PO_4^-$	DTN: SN0410T0510404.002 [DIRS 172712]
H3PO4(aq)	H_3PO_4(aq)	DTN: SN0410T0510404.002 [DIRS 172712]
MgCO3(aq)	$MgCO_3$(aq)	DTN: SN0410T0510404.002 [DIRS 172712]
MgHCO3+	$MgHCO_3^+$	DTN: SN0410T0510404.002 [DIRS 172712]

Table I-30. Aqueous Species Data Sources (Continued)

Aqueous Species	Molecular Formula	Source
MgHSiO3+	MgHSiO3+	*Silicic_Acid_spreadsheet.xls* in Output DTN: MO0701SPAPTZER.001
MgOH+	$MgOH^+$	DTN: SN0410T0510404.002 [DIRS 172712]
NaHSiO3(aq)	NaHSiO3(aq)	*Silicic_Acid_spreadsheet.xls* in Output DTN: MO0701SPAPTZER.001
NH3(aq)	NH_3(aq)	DTN: SN0410T0510404.002 [DIRS 172712]
NaF(aq)	NaF(aq)	DTN: SN0410T0510404.002 [DIRS 172712]
OH-	OH^-	DTN: SN0410T0510404.002 [DIRS 172712]
PO4---	PO_4^{3-}	DTN: SN0410T0510404.002 [DIRS 172712]

Table I-31. Gas Data Sources

Gases	Molecular Formula	Source
CO2(g)	CO_2	DTN: SN0410T0510404.002 [DIRS 172712]
H2(g)	H_2	DTN: SN0410T0510404.002 [DIRS 172712]
H2O(g)	H_2O	DTN: SN0410T0510404.002 [DIRS 172712]
HBr(g)	HBr	DTN: SN0410T0510404.002 [DIRS 172712]
HCl(g)	HCl	DTN: SN0410T0510404.002 [DIRS 172712]
HF(g)	HF	DTN: SN0410T0510404.002 [DIRS 172712]
HNO3(g)	HNO_3	DTN: SN0410T0510404.002 [DIRS 172712]
N2O5(g)	N_2O_5	DTN: SN0410T0510404.002 [DIRS 172712]
NO3(g)	NO_3	DTN: SN0410T0510404.002 [DIRS 172712]
O2(g)	O_2	*Gases_j_TJW_2.xls* in Output DTN: MO0701SPAPTZER.001

I.5.1 $CACL_2$ HYDRATES ($CACL_2$•NH_2O WHERE N EQUALS 2, 4, AND 6)

Associated Spreadsheets: *cacl2_hydrates_min_cal_CFJC2.xls*
Solids_j_CaCl2hydrates_TJW_1.xls
Cp_Solids_j_CaCl2hydrates_TJW_1.xls
(all located in Output DTN: MO0701SPAPTZER.001)

Source: Meisingset and Grønvold 1986 [DIRS 162094]; Pitzer and Shi 1993 [DIRS 163582]; Pitzer and Oakes 1994 [DIRS 163583]; Robie and Hemingway 1995 [DIRS 153683], pp. 23 and 53.

Description: Solubilities of $CaCl_2$ hydrates ($CaCl_2 \cdot nH_2O$ where n equals 2, 4, and 6) were estimated for a temperature range of 25°C to 150°C within the valid range of the activity model to generate bounding saturation molalities for the stable phases. Standard state thermodynamic properties were obtained from Pitzer and Shi (1993 [DIRS 163582]) and Pitzer and Oakes (1994 [DIRS 163583]) along with their reported saturation molality values of the corresponding $CaCl_2$ hydrate phases. Calculations of initial log K's were conducted in the spreadsheet *Solids_j_CaCl2hydrates_TJW_1.xls* using heat capacity data from Meisingset and Grønvold (1986 [DIRS 162094]). Log K values for dehydrated $CaCl_2$ were obtained from thermodynamic

data reported by Robie and Hemingway (1995 [DIRS 153683], pp. 23 and 53) and using SUPCRT92 v1.0 (see file *cacl2_solub.tab* in Output DTN: MO0701SPAPTZER.001). Because the stability range of dehydrated $CaCl_2$ with respect to temperature exceeds the validity range of the activity model to predict $CaCl_2 \cdot 2H_2O$ solubility, it was not considered in the fitting but was added to the database for the sake of completeness. Initial log K values for the dissolution of the hydrated phases were obtained using the spreadsheet *Solids_j_CaCl2hydrates_TJW_1.xls* and tested for prediction of solid solubility using the Pitzer parameters from Model 3 of Sterner et al. (1998 [DIRS 162116]). The log K values were then modified to fit saturation molalities of the $CaCl_2$ hydrates given by Pitzer and Shi (1993 [DIRS 163582]) and Pitzer and Oakes (1994 [DIRS 163583]) within their estimated temperature range of stability. The resulting log K values plus their relative differences from the initial values determined using the spreadsheet *Solids_j_CaCl2hydrates_TJW_1.xls* are given in Table I-32 below.

Table I-32. Comparison of Initial and Fitted log K Values for $CaCl_2$ Hydrates Used in the data0.ypf.R2 Database

T(°C)	$CaCl_2 \cdot nH_2O$	log K for $CaCl_2$ Hydrate from Data Provided by Pitzer and Shi (1993) and Pitzer and Oakes (1994)	Fitted Log K to Fit Saturation Molality	% Difference in log K
0	$CaCl_2:6H_2O$	—	3.4916	—
25	$CaCl_2:6H_2O$	3.8293	4.0875	−6.32
60	$CaCl_2:6H_2O$	4.1076	4.1676	−1.44
25	$CaCl_2:4H_2O$	5.3425	5.7588	−11.91
60	$CaCl_2:4H_2O$	5.0728	5.9465	−14.69
25	$CaCl_2:2H_2O$	7.4163	8.1163	−8.62
60	$CaCl_2:2H_2O$	6.5028	7.6115	−14.57
100	$CaCl_2:2H_2O$	5.4969	6.4875	−15.27
150	$CaCl_2:H_2O$	4.2688	4.9255	−13.33

Source: Pitzer and Shi 1993 [DIRS 163582]; Pitzer and Oakes 1994 [DIRS 163583].

As shown in the above table, the relative differences in log K computed from tabulated thermodynamic data and the fitted saturation molalities at 25°C, 60°C, and 150°C are on the order of 1.4% up to ~15.3% depending on the phase and the temperature. Fitting solubility data for $CaCl_2 \cdot 2H_2O$ above ~45°C was satisfactory up to a temperature of 150°C. The model was not tested beyond this temperature. It should be emphasized that some of the EQ3/6 runs used to determined the optimal log K value in fitting the experimental data for $CaCl_2:2H_2O$ did not meet the criterion for saturation (i.e., "Log Q/K" = 0.00000) before the code run began to show problems in the reaction path calculations. To attain a saturation value representative of equilibrium, values of "Log Q/K" in the range of −0.00018 to 0.00013 were considered characteristic of equilibrium phase saturation for this solid. The optimal value for the phase saturation molality by adjustment of the log K consistent with experimental solubilities was obtained through an iterative process between multiple EQ3/6 runs at various temperatures. Given the closeness to zero (or to the equilibrium criterion) and the inherent uncertainty present in solubility measurements, the log K values obtained using this approach are deemed to be representative of equilibrium. This is demonstrated by the overall agreement of the predicted saturation molalities and those reported in the literature for the $CaCl_2$ hydrates considered in the

database (see Figure I-3 below). Note also that these $CaCl_2$ hydrates undergo phase transitions to less hydrated forms with increasing temperature.

Log K values are entered in the data0.ypf.R2 database (Output DTN: SN0609T0502404.012) only at specific temperatures, namely, 0°C, 25°C, 60°C, 100°C, 150°C, 200°C, 250°C, and 300°C. For other temperatures, EQ3/6 uses a polynomial fit, either to the log K's at the four lower temperatures, or to the five upper ones. (Thus, the fits match at 100°C.) This means that, if a phase transition occurs between 25°C and 60°C, there will be only two points, those at 0°C and 25°C, available for fitting log K's to the phase stable below the transition temperature. In other words, the fit of log K against temperature will be linear. The same situation applies to the phase stable above the transition; namely, only the points for 60°C and 100°C are available. If data for metastable equilibria, or heat capacity data, were available for these phases outside their stability ranges better fits could of course be obtained. Specifically, $CaCl_2 \cdot 6H_2O$ (antarcticite) appears to be the stable phase from temperatures below 25°C up to ~30°C based on the reported solubility and thermodynamic data; above 30°C $CaCl_2 \cdot 4H_2O$ becomes stable. Above ~45°C, $CaCl_2 \cdot 2H_2O$ is the dominant phase. Saturation molalities were calculated using EQ3/6 runs at several temperatures to obtain the curve shown in Figure I-3 for these three solids. These curves indicate the approximate transition temperatures of the calculated solubility curves. In general, m_{sat} predictions in the lower temperature range seem to fit the data acceptably. When one considers the inherent uncertainties of the $CaCl_2$ activity model, and the collective uncertainties from utilizing multiple data sources and that present in the data, the fitted values for log K result in satisfactory predictions for the solubility of this binary salt system (Figure I-4).

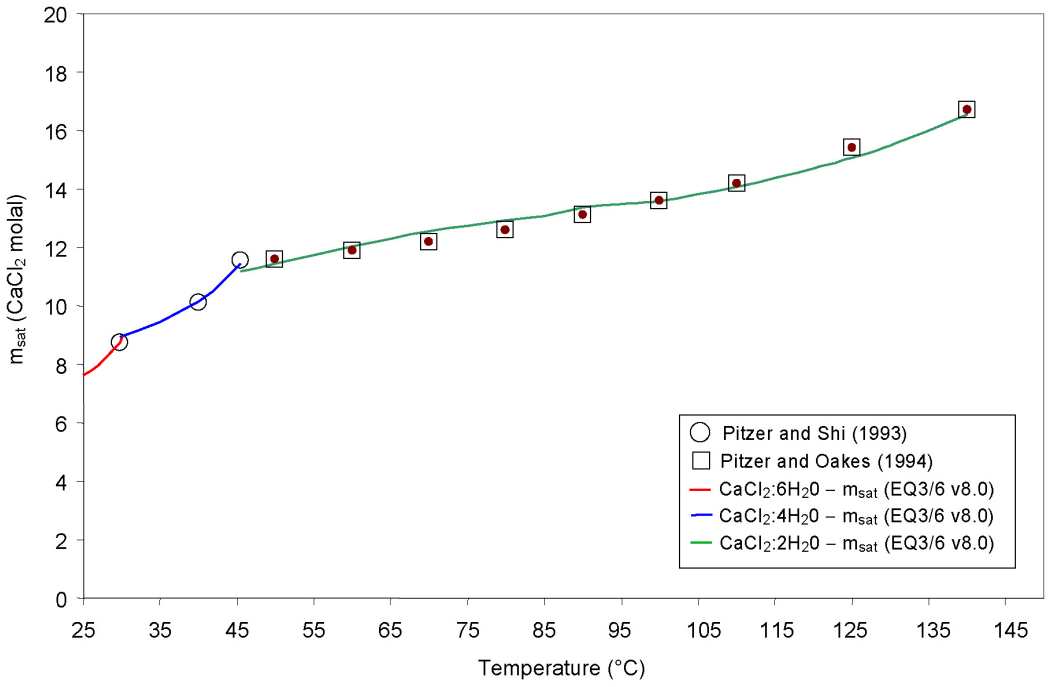

Output DTN: MO0701SPAPTZER.001, file: *cacl2_hydrates_min_cal_CFJC2.xls*.

NOTE: Predicted msat values were computed using data0.ypf.R2 and EQ3/6 v8.0.

Figure I-3. Comparison of Predicted and Compiled Saturation Molalities (m_{sat}) for $CaCl_2$ Hydrates

I.5.2 THERMONATRITE (Na_2CO_3:H_2O)

Associated Spreadsheet: *thermonatrite_solubility_CFJC2.xls*
(Output DTN: MO0701SPAPTZER.001)

Source: Grønvold and Mesingset 1983 [DIRS 162069]; Robie and Hemingway 1995 [DIRS 153683], pp. 26 and 55; Linke 1965 [DIRS 166191], p. 915.

Description: Solubility of thermonatrite ($Na_2CO_3 \cdot H_2O$) as predicted using the activity model of He and Morse (1993 [DIRS 162090]) and Corti et al. (1990 [DIRS 178211]) for the carbonate system and bounded by saturation molalities reported by Linke (1965 [DIRS 166191], p. 915) was estimated for a temperature of 25°C to 109°C using the computer code EQ3/6. Initial log K's were determined by SUPCRT92 v1.0 (Output DTN: MO0701SPAPTZER.001) using thermodynamic data from Grønvold and Mesingset (1983 [DIRS 162069]) and Robie and Hemingway (1995 [DIRS 153683], pp. 26 and 55). Heat capacities reported by Grønvold and Mesingset (1983 [DIRS 162069]) are those listed by Robie and Hemingway (1995 [DIRS 153683]). It should be emphasized that the log K's generated by SUPCRT92 are only used either as initial reference values or for comparison purposes only. That is, these are not used as direct data inputs. The resulting fit of these initial log K's to fit Linke (1965 [DIRS 166191]) saturation molalities shows that the difference between initial and fitted log K's is on the order of ~±1.9%. Figure I-4 below shows a comparison of initial and modified log K's for the EQ3/6 temperature grid up to a temperature of 150°C. The log K value at this latter temperature should be considered as fictive since the upper stability temperature for this phase is around 109°C. That is, this 150°C value was modified to fit the saturation molality at 109°C. As shown in the figure, the fitted log K values are in good agreement with those obtained with SUPCRT92 up to a temperature of 100°C.

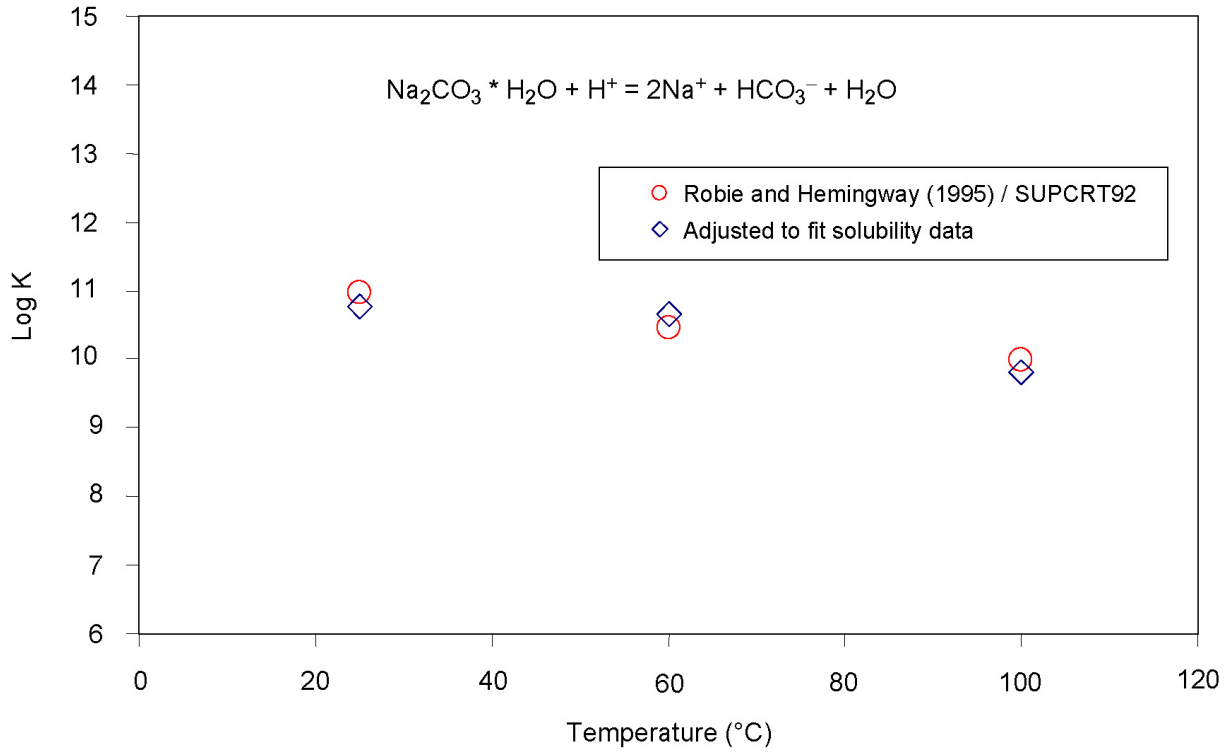

Output DTN: MO0701SPAPTZER.001, file: *thermonatrite_solubility_CFJC2.xls*.

NOTE: Initial values were obtained from thermodynamic data reported by Robie and Hemingway (1995 [DIRS 153683]) and the code SUPCRT92 v1.0. Notice the relatively small difference between initial and fitted values modified in conjunction with Pitzer parameter data from Corti et al. (1990 [DIRS 178211]) and He and Morse (1993 [DIRS 162090]) for the carbonate system. Saturation molalities for thermonatrite are those reported by Linke (1965 [DIRS 166191]).

Figure I-4. Comparison of Initial and Fitted log K Values for the Reaction Describing Thermonatrite Solubility as Implemented in the data0.ypf.R2 Database

Figure I-5 depicts the saturation molalities obtained with the use of modified log K values to fit the thermonatrite solubility given by Linke (1965 [DIRS 166191]). Notice that the resulting saturation molalities strongly conform to the reported solubility values up to the upper stability temperature limit of 109°C. The strong agreement in predicted saturation molalities and the relatively minimal change in log K values are viewed as a robust validation of the Pitzer activity model given the different data sources used to constrain the model. The thermodynamic data obtained by fitting to the Linke (1965 [DIRS 166191], p. 915) solubility data were those actually adopted for the IDPS model (Figure I-5). The cited data based on Grønvold and Meisingset (1983 [DIRS 162069]) and Robie and Hemingway (1995 [DIRS 153683]) constitutes the validation.

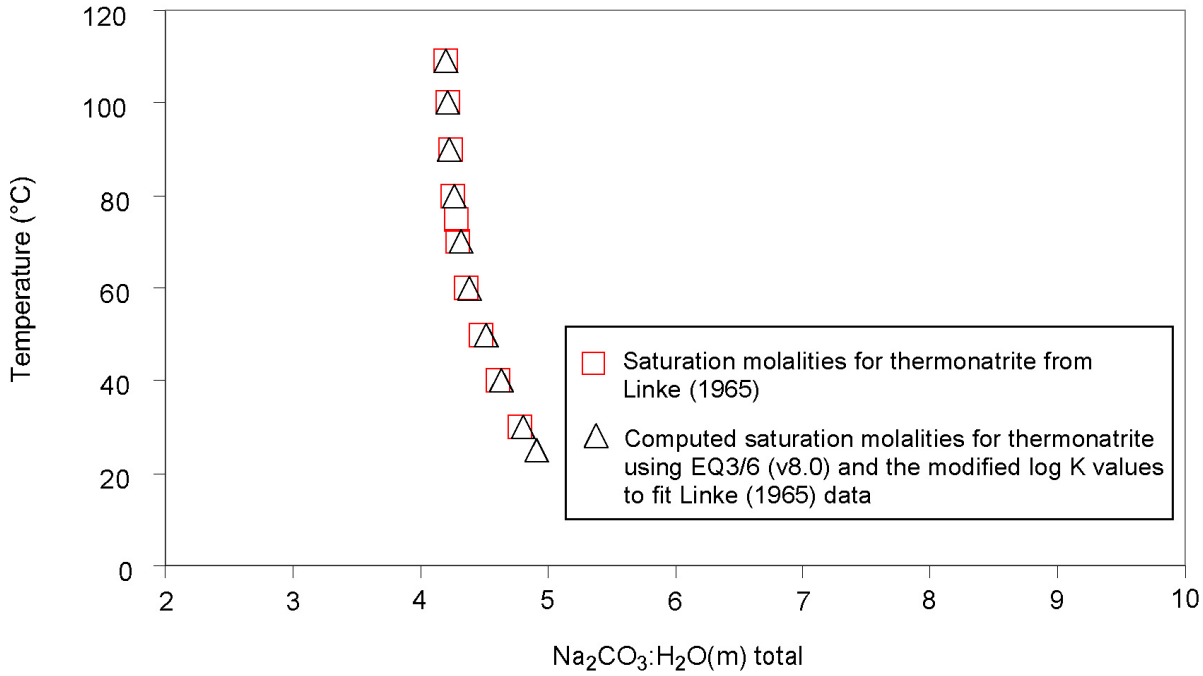

Output DTN: MO0701SPAPTZER.001, file: *thermonatrite_solubility_CFJC2.xls*.

NOTE: The fitted log K values used in data0.ypf.R2 are those modified to fit Linke (1965 [DIRS 166191]) thermonatrite solubility data using Corti et al. (1990 [DIRS178211]) and He and Morse (1993 [DIRS 162090]) Pitzer parameters.

Figure I-5. Comparison of Predicted Saturation Molalities for Thermonatrite Using EQ3/6 (v8.0) and data0.ypf.R2 to Those Reported by Linke

I.5.3 SODA NITER ($NANO_3$)

Associated Spreadsheet: *NaNO3_min_cal_CFJC2.xls*
(Output DTN: MO0701SPAPTZER.001)

Source: Robie and Hemingway 1995 [DIRS 153683], pp. 27 and 55; Barin and Platzki 1995 [DIRS 157865]; Archer 2000 [DIRS 162065].

Description: The solubility of soda niter ($NaNO_3$) was modeled using the recent thermodynamic model and Pitzer parameters of Archer (2000 [DIRS 162065]) up to a temperature of 119°C. The Pitzer parameters were converted to a standard Pitzer form as described by Wijesinghe and Rard (2005 [DIRS 176847]). The temperature of 119°C represents the approximate maximum temperature for which solubility data are reported in Figure 10 of Archer (2000 [DIRS 162065], p. 1153). Accurate log K fits were only obtained from 0°C to 100°C since saturation molality values compiled by Archer (2000 [DIRS 162065]) are only tabulated in this temperature range. The log K value at 150°C in the data0.ypf.R2 data block for this phase is fictive since it was fitted to obtain an approximate bounding saturation molality value of ~24.1 at 119°C. Figure I-6 shows a comparison between log K values obtained from: (1) combined data from Robie and Hemingway (1995 [DIRS 153683], pp. 27 and 55) and Archer (2000 [DIRS 162065]) incorporated into the modified database for SUPCRT92 v1.0 (Output DTN: MO0701SPAPTZER.001); (2) data from Barin and Platzki (1995 [DIRS 157865]) (see

spreadsheet *Solids_j_Na_TJW_1.xls*); and (3) log K values fitted to saturation molalities reported by Archer (2000 [DIRS 162065]). It should be emphasized that the log K's generated by SUPCRT92 or the Excel spreadsheet using data from Barin and Platzki (1995 [DIRS 157865]) are only used either as initial reference values or for comparison purposes. That is, these are not used as direct data inputs. As shown in the figure, the differences in log K values between different data sets are relatively minor. Figure I-7 shows the predicted saturation molalities for soda niter from 0°C to 100°C indicating nearly identical values to those reported by Archer (2000 [DIRS 162065]). The close agreement of log K values from multiple sources and those obtained in the fitting, together with the prediction of saturation molalities in Archer (2000 [DIRS 162065]) validates the Pitzer activity model for $NaNO_3$.

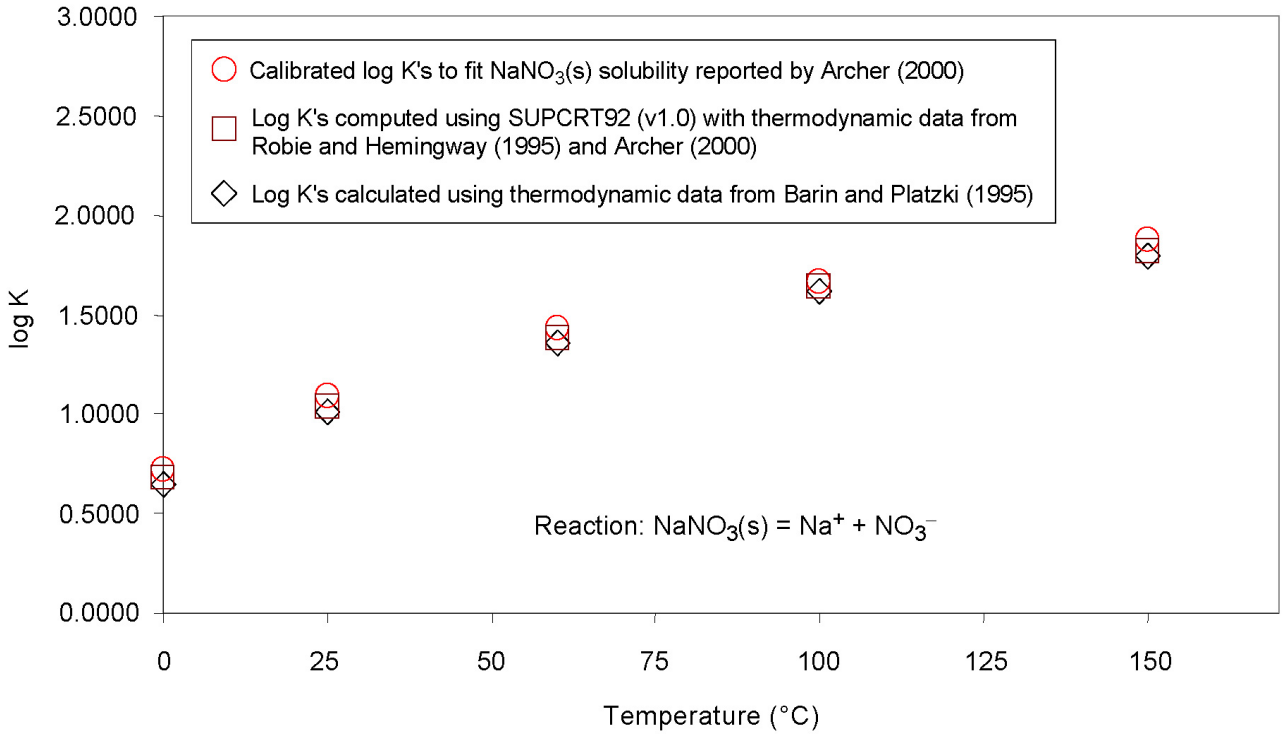

Output DTN: MO0701SPAPTZER.001, file: *NaNO3_min_cal_CFJC2.xls*.

Source: Archer 2000 [DIRS 162065].

Figure I-6. Comparison of log K Values for Soda Niter ($NaNO_3$(s)) Dissolution from Various Sources and Those Obtained by Fitting Saturation Molalities Reported by Archer

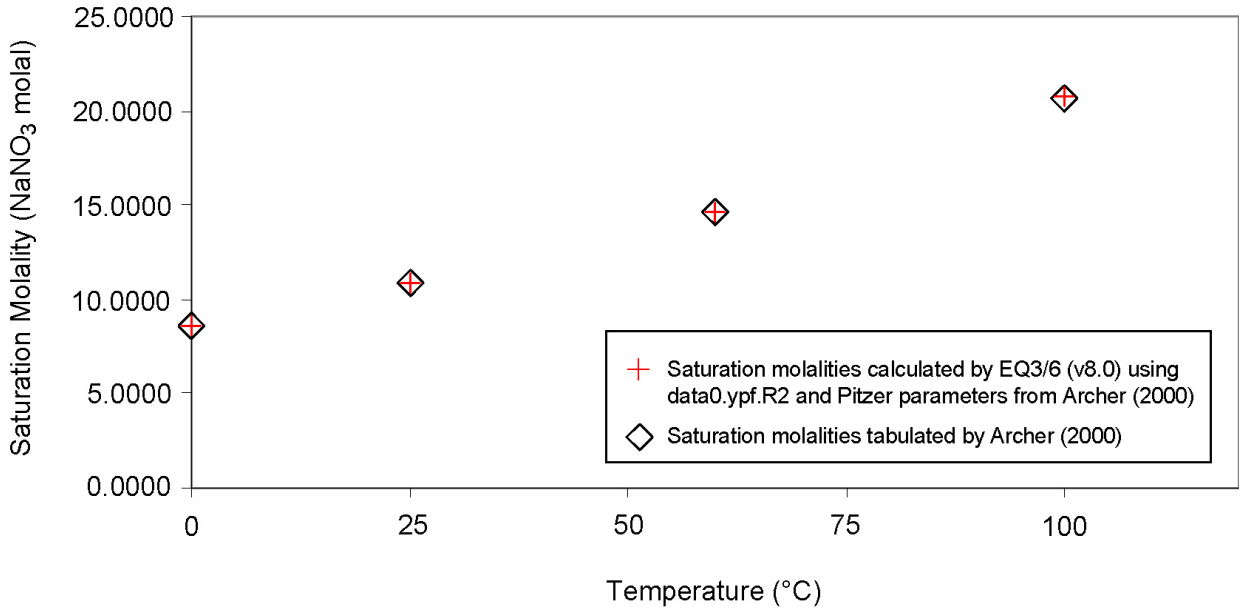

Output DTN: MO0701SPAPTZER.001, file: *NaNO3_min_cal_CFJC2.xls*.

Source: Archer 2000 [DIRS 162065].

Figure I-7. Comparison of Saturation Molalities for Soda Niter ($NaNO_3$(s)) Predicted by EQ3/6 v8.0 Using data0.ypf.R2 and Fitted log K to Those from Archer to a Temperature of 100°C

I.5.4 CALCITE ($CACO_3$)

Associated Spreadsheet: *Calcite_Solubility_CFJC2.xls*
(Output DTN: MO0701SPAPTZER.001)

Source: data0.ymp.R4 database (DTN: SN0410T0510404.002 [DIRS 172712]); Ellis 1963 [DIRS 177819]; Wolf et al. 1989 [DIRS 177633]; Møller et al. 1998 [DIRS 177805].

Description: The solubility of calcite ($CaCO_3$) was modeled using the Pitzer model parameters for the system Na-Ca-Cl-CO_3-HCO_3-CO_2-H_2O of Peiper and Pitzer (1982 [DIRS 162097]), Corti et al. (1990 [DIRS 178211]), He and Morse (1993 [DIRS 162090]), and Konigsberger et al. (1999 [DIRS 168345]) to a temperature of 300°C. Previous sections describe the treatment of the relevant Pitzer parameters to this system and their implementation into the thermodynamic database for use with the code EQ3/6. For the most part, the log K values for the calcite solubility reaction were mainly fitted to experimental solubility data at temperatures from 25°C to 300°C in NaCl solutions at various ionic strengths. It should be noted that the choice of $CaCl_2$ Pitzer parameter data has a significant effect on predicted calcite solubility as a function of ionic strength and temperature. Figure I-8 indicates that the log K values obtained through fitting of experimental data are in good agreement with those in data0.ymp.R4 (DTN: SN0410T0510404.002 [DIRS 172712]) to a temperature of approximately 100°C. Above this temperature, there is an evident divergence from the log K data in data0.ymp.R4 trending towards smaller values. This adjustment was necessary in order to fit the bulk of high temperature solubility data reported by Ellis (1963 [DIRS 177819]) and Møller et al. (1998 [DIRS 177805]). This change in trend coincides with the predominance of the ion pair $CaCl^+$,

which according to log K data becomes progressively more stable with increasing temperature. The calcite solubility data utilized in the log K calibration is mainly from experiments involving NaCl solutions with concentrations spanning from 0.2 to 1 molal and CO_2 partial pressures in excess of 1 atmosphere. Since these adjusted log K values are consistent with the Pitzer activity coefficient model in this database, it should be emphasized that their use with other data or other thermodynamic databases is not recommended. At this point, there are no unambiguous reasons for why there is such a divergence from the log K values in data0.ymp.R4 at temperatures above 100°C. One possible explanation is the limitation in the Pitzer model for the Na-carbonate system from He and Morse (1993 [DIRS 162090]), which is valid only up to 90°C. It has been noted that extrapolations of other Pitzer parameter data using this model beyond this temperature limit produces results that to a large extent differ from those generated by other Pitzer models valid at higher temperatures. Most of the other relevant Pitzer parameters for species relevant to calcite equilibria in NaCl solutions (e.g., CO_2(aq)) are valid at temperatures up to 250°C.

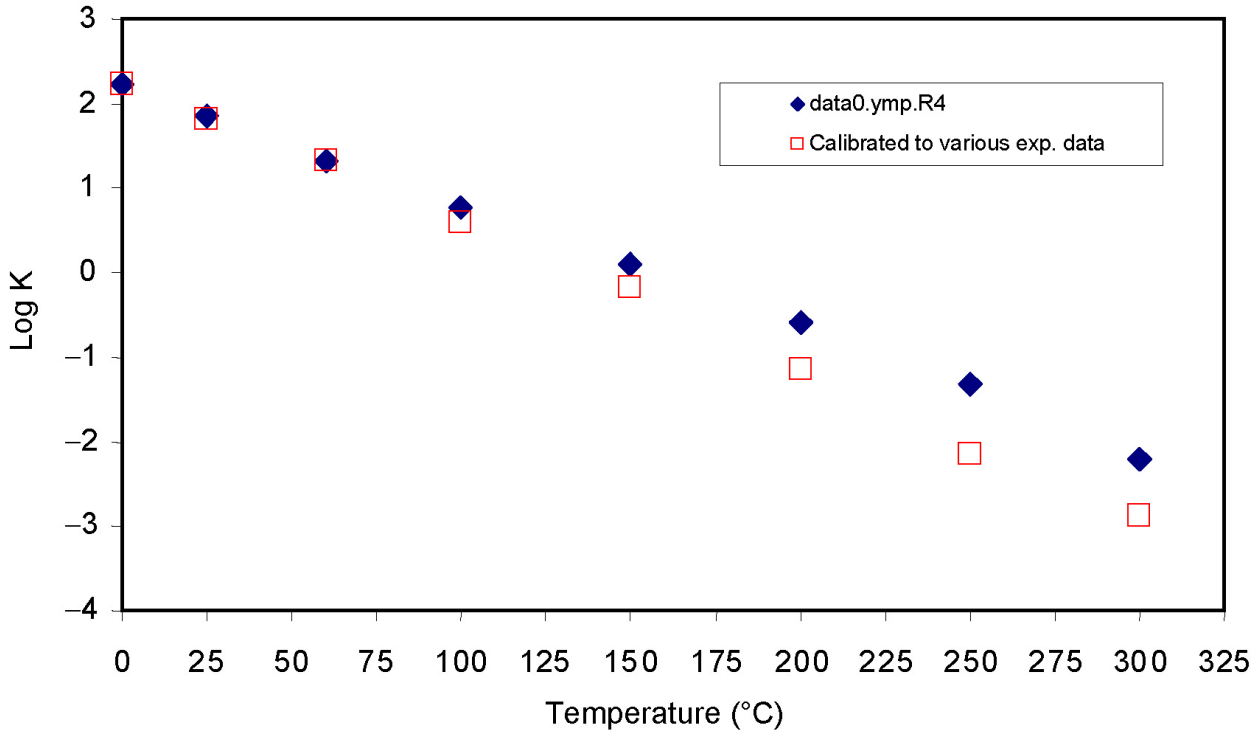

Output DTN: MO0701SPAPTZER.001, file: *Calcite_Solubility_CFJC2.xls*.

Source: data0.ymp.R4 (DTN: SN0410T0510404.002 [DIRS 172712]).

Figure I-8. Comparison of log K Values for Calcite ($CaCO_3$(s)) Dissolution from data0.ymp.R4 and Those Obtained by Fitting Saturation Molalities Reported by Archer

APPENDIX II

EXAMPLE IDPS EVAPORATION LOOKUP TABLE

Table II-1 is an example IDPS model lookup table for the example evaporation of average in situ J-13 well water. For this example, the rows below *RH* 56 percent have been truncated. The full lookup table is documented in DTN: SN0611T0509206.006, file j13c3t7e.xls.

Table II-1. Example IDPS Model Evaporation Lookup Table for Average In Situ J-13 Well Water

Calculations			RH Calc.	Temperature and Gas Fugacities				Total Elemental Aqueous Co	
			RH rel. humid.	log Xi log react. progr.	Temp. (C)	O2(g) fug.	CO2(g) fug.	log Xi log react. progr.	Pitzer pH
				11/8/2006 User: Sara Arthur EQ3/6,				11/8/2006 User: Sara Arthur EQ3/6,	
CF=1/DF	Qe/Qs	1-Qe/Qs=DF	RH	log Xi - j13c3t7e.6o	Temp (C) - j13c3t7e.6o	O2(g) Fugacity	CO2(g) Fugacity	log Xi - j13c3t7e.6o	Pitzer pH
1.0	0.0000	1.0000	99.990%	-99999.0000	70.0000	0.1995	0.0010	-99999	8.247
1.0	0.0057	0.9943	99.990%	-0.4987	70.0000	0.1995	0.0010	-0.4987	8.248
1.1	0.0901	0.9099	99.989%	0.6990	70.0000	0.1995	0.0010	0.69897	8.269
1.2	0.1802	0.8199	99.989%	1.0000	70.0000	0.1995	0.0010	1	8.295
1.4	0.2702	0.7298	99.987%	1.1761	70.0000	0.1995	0.0010	1.17609	8.326
1.6	0.3603	0.6397	99.986%	1.3010	70.0000	0.1995	0.0010	1.30103	8.364
1.8	0.4504	0.5496	99.984%	1.3979	70.0000	0.1995	0.0010	1.39794	8.410
2.2	0.5405	0.4596	99.981%	1.4771	70.0000	0.1995	0.0010	1.47712	8.466
2.7	0.6305	0.3695	99.977%	1.5441	70.0000	0.1995	0.0010	1.54407	8.537
3.6	0.7206	0.2794	99.970%	1.6021	70.0000	0.1995	0.0010	1.60206	8.627
5.3	0.8107	0.1893	99.957%	1.6532	70.0000	0.1995	0.0010	1.65321	8.748
6.6	0.8490	0.1510	99.947%	1.6733	70.0000	0.1995	0.0010	1.67327	8.815
6.8	0.8528	0.1472	99.946%	1.6752	70.0000	0.1995	0.0010	1.6752	8.824
10.1	0.9008	0.0992	99.925%	1.6990	70.0000	0.1995	0.0010	1.69897	8.960
109.0	0.9908	0.0092	99.388%	1.7404	70.0000	0.1995	0.0010	1.74036	9.543
405.0	0.9975	0.0025	98.001%	1.7433	70.0000	0.1995	0.0010	1.74329	9.695
862.9	0.9988	0.0012	95.999%	1.7439	70.0000	0.1995	0.0010	1.74386	9.745
1087.1	0.9991	0.0009	95.016%	1.7440	70.0000	0.1995	0.0010	1.74397	9.759
1261.9	0.9992	0.0008	94.247%	1.7440	70.0000	0.1995	0.0010	1.74402	9.771
1317.1	0.9992	0.0008	94.000%	1.7440	70.0000	0.1995	0.0010	1.74404	9.774
1748.6	0.9994	0.0006	92.000%	1.7441	70.0000	0.1995	0.0010	1.74412	9.802
2150.4	0.9995	0.0005	90.000%	1.7442	70.0000	0.1995	0.0010	1.74416	9.830
2345.4	0.9996	0.0004	88.979%	1.7442	70.0000	0.1995	0.0010	1.74418	9.845
2345.4	0.9996	0.0004	88.978%	1.7442	70.0000	0.1995	0.0010	1.74418	9.845
2596.3	0.9996	0.0004	88.407%	1.7442	70.0000	0.1995	0.0010	1.7442	9.859
2596.3	0.9996	0.0004	88.407%	1.7442	70.0000	0.1995	0.0010	1.7442	9.859
2706.7	0.9996	0.0004	88.000%	1.7442	70.0000	0.1995	0.0010	1.74421	9.867
3210.0	0.9997	0.0003	86.000%	1.7442	70.0000	0.1995	0.0010	1.74423	9.903
3660.6	0.9997	0.0003	84.000%	1.7443	70.0000	0.1995	0.0010	1.74425	9.936
4071.3	0.9998	0.0002	82.000%	1.7443	70.0000	0.1995	0.0010	1.74426	9.968
4129.7	0.9998	0.0002	81.706%	1.7443	70.0000	0.1995	0.0010	1.74426	9.973
4129.8	0.9998	0.0002	81.706%	1.7443	70.0000	0.1995	0.0010	1.74426	9.973
4228.3	0.9998	0.0002	81.626%	1.7443	70.0000	0.1995	0.0010	1.74426	9.972
6158.0	0.9998	0.0002	80.000%	1.7443	70.0000	0.1995	0.0010	1.7443	9.954
8388.6	0.9999	0.0001	78.001%	1.7443	70.0000	0.1995	0.0010	1.74431	9.933
10492.0	0.9999	0.0001	76.035%	1.7443	70.0000	0.1995	0.0010	1.74433	9.914
10540.2	0.9999	0.0001	76.000%	1.7443	70.0000	0.1995	0.0010	1.74433	9.914
13258.7	0.9999	0.0001	74.000%	1.7443	70.0000	0.1995	0.0010	1.74433	9.898
15926.0	0.9999	0.0001	72.000%	1.7443	70.0000	0.1995	0.0010	1.74434	9.883
18554.8	0.9999	0.0001	70.000%	1.7443	70.0000	0.1995	0.0010	1.74434	9.870
21159.8	1.0000	0.0000	67.999%	1.7444	70.0000	0.1995	0.0010	1.74435	9.858
23751.4	1.0000	0.0000	66.000%	1.7444	70.0000	0.1995	0.0010	1.74435	9.847
26099.2	1.0000	0.0000	64.196%	1.7444	70.0000	0.1995	0.0010	1.74435	9.838
26848.9	1.0000	0.0000	64.001%	1.7444	70.0000	0.1995	0.0010	1.74435	9.841
34586.3	1.0000	0.0000	62.001%	1.7444	70.0000	0.1995	0.0010	1.74435	9.868
41881.8	1.0000	0.0000	60.000%	1.7444	70.0000	0.1995	0.0010	1.74436	9.891
47758.0	1.0000	0.0000	57.999%	1.7444	70.0000	0.1995	0.0010	1.74436	9.907
49772.0	1.0000	0.0000	56.740%	1.7444	70.0000	0.1995	0.0010	1.74436	9.909
49788.6	1.0000	0.0000	56.703%	1.7444	70.0000	0.1995	0.0010	1.74436	9.909
49795.8	1.0000	0.0000	56.683%	1.7444	70.0000	0.1995	0.0010	1.74436	9.909
49799.8	1.0000	0.0000	56.671%	1.7444	70.0000	0.1995	0.0010	1.74436	9.909
49802.3	1.0000	0.0000	56.663%	1.7444	70.0000	0.1995	0.0010	1.74436	9.909
49803.3	1.0000	0.0000	56.658%	1.7444	70.0000	0.1995	0.0010	1.74436	9.909
49804.5	1.0000	0.0000	56.654%	1.7444	70.0000	0.1995	0.0010	1.74436	9.909
49805.5	1.0000	0.0000	56.649%	1.7444	70.0000	0.1995	0.0010	1.74436	9.909
49806.7	1.0000	0.0000	56.644%	1.7444	70.0000	0.1995	0.0010	1.74436	9.909
49806.7	1.0000	0.0000	56.643%	1.7444	70.0000	0.1995	0.0010	1.74436	9.909

Table II-1. Example IDPS Model Evaporation Lookup Table for Average In Situ J-13 Well Water (Continued)

RH rel. humid.	IS ionic strength	H2O (kg) (m)	Al aluminum	C carbon	Ca calcium	Cl chlorine	F fluorine	K potassium	Mg magnesium	N nitrogen
a(w) - j13c3t7e.6o	(I) - j13c3t7e.6o	Mass Solvent (kg) - j13c3t7e.6o	Al Moles/kg. H2O	C Moles/kg. H2O	Ca Moles/kg. H2O	Cl Moles/kg. H2O	F Moles/kg. H2O	K Moles/kg. H2O	Mg Moles/kg. H2O	N Moles/kg. H2O
1.000	2.773E-03	1.000E+00	2.132E-14	1.454E-03	9.320E-05	2.014E-04	1.147E-04	1.279E-04	6.493E-05	1.416E-04
1.000	2.783E-03	9.943E-01	2.086E-14	1.458E-03	9.275E-05	2.026E-04	1.154E-04	1.286E-04	6.440E-05	1.424E-04
1.000	2.957E-03	9.099E-01	1.489E-14	1.531E-03	8.583E-05	2.213E-04	1.261E-04	1.405E-04	5.642E-05	1.556E-04
1.000	3.191E-03	8.199E-01	9.985E-15	1.630E-03	7.784E-05	2.456E-04	1.400E-04	1.560E-04	4.792E-05	1.727E-04
1.000	3.495E-03	7.298E-01	6.374E-15	1.757E-03	6.933E-05	2.760E-04	1.572E-04	1.752E-04	3.958E-05	1.940E-04
1.000	3.898E-03	6.397E-01	3.829E-15	1.926E-03	6.041E-05	3.148E-04	1.794E-04	1.999E-04	3.160E-05	2.214E-04
1.000	4.453E-03	5.496E-01	2.130E-15	2.155E-03	5.130E-05	3.664E-04	2.088E-04	2.326E-04	2.420E-05	2.576E-04
1.000	5.250E-03	4.596E-01	1.071E-15	2.477E-03	4.228E-05	4.382E-04	2.497E-04	2.782E-04	1.759E-05	3.081E-04
1.000	6.465E-03	3.695E-01	4.672E-16	2.953E-03	3.368E-05	5.451E-04	3.106E-04	3.461E-04	1.197E-05	3.833E-04
1.000	8.507E-03	2.794E-01	1.647E-16	3.711E-03	2.581E-05	7.208E-04	4.107E-04	4.577E-04	7.450E-06	5.068E-04
1.000	1.256E-02	1.893E-01	4.020E-17	5.093E-03	1.897E-05	1.064E-03	6.061E-04	6.754E-04	4.069E-06	7.479E-04
0.999	1.578E-02	1.510E-01	1.819E-17	6.103E-03	1.643E-05	1.334E-03	7.599E-04	8.468E-04	2.966E-06	9.378E-04
0.999	1.620E-02	1.472E-01	1.779E-17	6.254E-03	1.612E-05	1.368E-03	7.794E-04	8.686E-04	2.887E-06	9.619E-04
0.999	2.428E-02	9.924E-02	1.265E-17	9.115E-03	1.263E-05	2.029E-03	1.156E-03	1.288E-03	1.995E-06	1.427E-03
0.994	2.925E-01	9.173E-03	1.947E-18	8.361E-02	8.465E-06	2.196E-02	1.251E-02	1.394E-02	9.103E-07	1.544E-02
0.980	1.138E+00	2.469E-03	7.732E-19	2.850E-01	9.101E-06	8.156E-02	4.647E-02	5.178E-02	1.051E-06	5.735E-02
0.960	2.468E+00	1.159E-03	4.572E-19	5.857E-01	1.039E-05	1.738E-01	9.901E-02	1.103E-01	1.322E-06	1.222E-01
0.950	3.122E+00	9.199E-04	3.864E-19	7.314E-01	1.095E-05	2.189E-01	1.247E-01	1.390E-01	1.428E-06	1.539E-01
0.942	3.638E+00	7.924E-04	3.443E-19	8.506E-01	1.130E-05	2.541E-01	1.330E-01	1.614E-01	1.490E-06	1.787E-01
0.940	3.801E+00	7.592E-04	3.327E-19	8.882E-01	1.141E-05	2.653E-01	1.356E-01	1.684E-01	1.507E-06	1.865E-01
0.920	5.077E+00	5.719E-04	2.614E-19	1.182E+00	1.198E-05	3.521E-01	1.542E-01	2.236E-01	1.585E-06	2.476E-01
0.900	6.266E+00	4.650E-04	2.148E-19	1.456E+00	1.219E-05	4.331E-01	1.708E-01	2.750E-01	1.586E-06	3.045E-01
0.890	6.843E+00	4.264E-04	1.966E-19	1.589E+00	1.220E-05	4.724E-01	1.789E-01	2.999E-01	1.568E-06	3.321E-01
0.890	6.843E+00	4.264E-04	1.966E-19	1.589E+00	1.220E-05	4.724E-01	1.789E-01	2.999E-01	1.568E-06	3.321E-01
0.884	7.080E+00	3.852E-04	1.761E-19	1.706E+00	1.216E-05	5.229E-01	1.842E-01	3.320E-01	1.573E-06	3.676E-01
0.884	7.080E+00	3.852E-04	1.761E-19	1.706E+00	1.216E-05	5.229E-01	1.842E-01	3.320E-01	1.573E-06	3.676E-01
0.880	7.298E+00	3.695E-04	1.678E-19	1.777E+00	1.213E-05	5.451E-01	1.707E-01	3.461E-01	1.565E-06	3.833E-01
0.860	8.323E+00	3.115E-04	1.384E-19	2.102E+00	1.189E-05	6.465E-01	1.168E-01	4.105E-01	1.511E-06	4.545E-01
0.840	9.285E+00	2.732E-04	1.188E-19	2.393E+00	1.157E-05	7.372E-01	7.979E-02	4.681E-01	1.446E-06	5.183E-01
0.820	1.020E+01	2.456E-04	1.043E-19	2.658E+00	1.122E-05	8.200E-01	5.457E-02	5.206E-01	1.377E-06	5.765E-01
0.817	1.033E+01	2.422E-04	1.025E-19	2.695E+00	1.117E-05	8.317E-01	5.162E-02	5.281E-01	1.367E-06	5.848E-01
0.817	1.033E+01	2.421E-04	1.025E-19	2.695E+00	1.117E-05	8.317E-01	5.162E-02	5.281E-01	1.367E-06	5.848E-01
0.816	1.034E+01	2.365E-04	1.003E-19	2.681E+00	1.109E-05	8.516E-01	5.027E-02	5.407E-01	1.352E-06	5.987E-01
0.800	1.063E+01	1.624E-04	7.170E-20	2.428E+00	9.872E-06	1.240E+00	3.098E-02	7.874E-01	1.121E-06	8.720E-01
0.780	1.106E+01	1.192E-04	5.504E-20	2.149E+00	8.997E-06	1.689E+00	1.915E-02	1.073E+00	9.696E-07	1.188E+00
0.760	1.153E+01	9.531E-05	4.582E-20	1.905E+00	8.490E-06	2.113E+00	1.298E-02	1.342E+00	8.945E-07	1.486E+00
0.760	1.153E+01	9.488E-05	4.564E-20	1.902E+00	8.481E-06	2.123E+00	1.295E-02	1.348E+00	8.936E-07	1.493E+00
0.740	1.179E+01	7.542E-05	3.747E-20	1.733E+00	8.093E-06	2.670E+00	1.135E-02	1.695E+00	8.567E-07	1.877E+00
0.720	1.212E+01	6.279E-05	3.211E-20	1.575E+00	7.842E-06	3.207E+00	1.000E-02	2.036E+00	8.410E-07	2.255E+00
0.700	1.250E+01	5.389E-05	2.827E-20	1.428E+00	7.675E-06	3.737E+00	8.859E-03	2.373E+00	8.388E-07	2.627E+00
0.680	1.293E+01	4.726E-05	2.536E-20	1.292E+00	7.561E-06	4.261E+00	7.887E-03	2.706E+00	8.455E-07	2.996E+00
0.660	1.342E+01	4.210E-05	2.306E-20	1.164E+00	7.482E-06	4.783E+00	7.056E-03	3.037E+00	8.586E-07	3.363E+00
0.642	1.392E+01	3.832E-05	2.134E-20	1.055E+00	7.429E-06	5.254E+00	6.407E-03	3.337E+00	8.744E-07	3.696E+00
0.640	1.406E+01	3.725E-05	2.093E-20	1.049E+00	7.422E-06	5.261E+00	6.345E-03	3.433E+00	8.752E-07	3.802E+00
0.620	1.557E+01	2.891E-05	1.752E-20	9.683E-01	7.360E-06	5.364E+00	5.713E-03	4.422E+00	8.868E-07	4.897E+00
0.600	1.724E+01	2.388E-05	1.519E-20	8.580E-01	7.321E-06	5.534E+00	5.129E-03	5.355E+00	9.040E-07	5.931E+00
0.580	1.918E+01	2.094E-05	1.379E-20	7.139E-01	7.300E-06	5.814E+00	4.641E-03	6.107E+00	9.273E-07	6.763E+00
0.567	2.076E+01	2.009E-05	1.367E-20	5.939E-01	7.294E-06	6.108E+00	4.419E-03	6.364E+00	9.477E-07	7.048E+00
0.567	2.082E+01	2.008E-05	1.368E-20	5.896E-01	7.294E-06	6.119E+00	4.415E-03	6.366E+00	9.485E-07	7.050E+00
0.567	2.085E+01	2.008E-05	1.369E-20	5.874E-01	7.294E-06	6.126E+00	4.412E-03	6.367E+00	9.489E-07	7.051E+00
0.567	2.087E+01	2.008E-05	1.370E-20	5.860E-01	7.294E-06	6.129E+00	4.411E-03	6.368E+00	9.491E-07	7.052E+00
0.567	2.088E+01	2.008E-05	1.370E-20	5.850E-01	7.294E-06	6.132E+00	4.410E-03	6.368E+00	9.493E-07	7.052E+00
0.567	2.089E+01	2.008E-05	1.370E-20	5.845E-01	7.294E-06	6.134E+00	4.409E-03	6.368E+00	9.494E-07	7.052E+00
0.567	2.090E+01	2.008E-05	1.370E-20	5.839E-01	7.294E-06	6.135E+00	4.409E-03	6.368E+00	9.495E-07	7.052E+00
0.566	2.091E+01	2.008E-05	1.371E-20	5.834E-01	7.294E-06	6.137E+00	4.408E-03	6.369E+00	9.496E-07	7.053E+00
0.566	2.091E+01	2.008E-05	1.371E-20	5.828E-01	7.294E-06	6.138E+00	4.408E-03	6.369E+00	9.497E-07	7.053E+00
0.566	2.091E+01	2.008E-05	1.371E-20	5.827E-01	7.294E-06	6.138E+00	4.408E-03	6.369E+00	9.497E-07	7.053E+00

Table II-1. Example IDPS Model Evaporation Lookup Table for Average In Situ J-13 Well Water (Continued)

			ANC species concentrations								
Na sodium	**S** sulfur	**Si** silicon	**log Xi** log react. progr.	**H2O (kg)**	**HCO3-**	**CO3--**	**OH-**	**H+**		**CaCO3(aq)**	**CaOH+**
			11/8/2006 User: Sara Arthur EQ3/6,								
Na Moles/kg. H2O	**S Moles/kg. H2O**	**Si Moles/kg. H2O**	**log Xi - j13c3t7e.6o**	**Mass Solvent (kg) - j13c3t7e.6o**	**HCO3- Molality**	**CO3-- Molality**	**OH- Molality**	**H+ Molality**		**CaCO3(aq) Molality**	**CaOH+ Molality**
1.992E-03	1.915E-04	9.999E-04	-1.000E+05	1.000E+00	1.406E-03	2.364E-05	2.926E-05	6.039E-09		7.141E-06	1.039E-07
2.004E-03	1.926E-04	1.005E-03	-4.987E-01	9.943E-01	1.410E-03	2.379E-05	2.935E-05	6.023E-09		7.141E-06	1.036E-07
2.189E-03	2.105E-04	1.089E-03	6.990E-01	9.099E-01	1.481E-03	2.634E-05	3.082E-05	5.756E-09		7.141E-06	9.904E-08
2.430E-03	2.336E-04	1.199E-03	1.000E+00	8.199E-01	1.576E-03	2.996E-05	3.279E-05	5.436E-09		7.141E-06	9.353E-08
2.730E-03	2.625E-04	1.337E-03	1.176E+00	7.298E-01	1.699E-03	3.501E-05	3.534E-05	5.074E-09		7.141E-06	8.731E-08
3.114E-03	2.994E-04	1.517E-03	1.301E+00	6.397E-01	1.860E-03	4.229E-05	3.869E-05	4.669E-09		7.141E-06	8.035E-08
3.625E-03	3.485E-04	1.757E-03	1.398E+00	5.496E-01	2.079E-03	5.329E-05	4.321E-05	4.220E-09		7.141E-06	7.264E-08
4.335E-03	4.168E-04	2.093E-03	1.477E+00	4.596E-01	2.383E-03	7.092E-05	4.952E-05	3.729E-09		7.141E-06	6.420E-08
5.392E-03	5.184E-04	2.597E-03	1.544E+00	3.695E-01	2.828E-03	1.016E-04	5.873E-05	3.199E-09		7.141E-06	5.508E-08
7.130E-03	6.855E-04	3.429E-03	1.602E+00	2.794E-01	3.526E-03	1.618E-04	7.314E-05	2.634E-09		7.141E-06	4.537E-08
1.052E-02	1.012E-03	5.056E-03	1.653E+00	1.893E-01	4.763E-03	3.070E-04	9.860E-05	2.035E-09		7.141E-06	3.509E-08
1.319E-02	1.268E-03	6.331E-03	1.673E+00	1.510E-01	5.640E-03	4.414E-04	1.166E-04	1.769E-09		7.141E-06	3.051E-08
1.353E-02	1.301E-03	6.373E-03	1.675E+00	1.472E-01	5.768E-03	4.632E-04	1.192E-04	1.735E-09		7.141E-06	2.994E-08
2.007E-02	1.930E-03	7.155E-03	1.699E+00	9.924E-02	8.127E-03	9.658E-04	1.673E-04	1.306E-09		7.141E-06	2.255E-08
2.172E-01	2.088E-02	1.914E-02	1.740E+00	9.173E-03	4.312E-02	4.047E-02	8.154E-04	4.568E-10		7.141E-06	8.187E-09
8.068E-01	7.757E-02	3.452E-02	1.743E+00	2.469E-03	8.288E-02	2.021E-01	1.328E-03	4.076E-10		7.141E-06	8.004E-09
1.719E+00	1.653E-01	4.858E-02	1.744E+00	1.159E-03	1.123E-01	4.733E-01	1.482E-03	4.046E-10		7.141E-06	9.038E-09
2.166E+00	2.082E-01	5.421E-02	1.744E+00	9.199E-04	1.222E-01	6.092E-01	1.478E-03	3.975E-10		7.141E-06	9.440E-09
2.514E+00	2.417E-01	5.860E-02	1.744E+00	7.924E-04	1.295E-01	7.210E-01	1.464E-03	3.881E-10		7.141E-06	9.667E-09
2.624E+00	2.523E-01	5.996E-02	1.744E+00	7.592E-04	1.317E-01	7.565E-01	1.457E-03	3.848E-10		7.141E-06	9.728E-09
3.483E+00	3.349E-01	7.043E-02	1.744E+00	5.719E-04	1.472E-01	1.035E+00	1.382E-03	3.534E-10		7.141E-06	1.004E-08
4.284E+00	4.119E-01	8.032E-02	1.744E+00	4.650E-04	1.603E-01	1.296E+00	1.293E-03	3.188E-10		7.141E-06	1.010E-08
4.672E+00	4.490E-01	8.527E-02	1.744E+00	4.264E-04	1.665E-01	1.422E+00	1.248E-03	3.012E-10		7.141E-06	1.005E-08
4.672E+00	4.490E-01	8.527E-02	1.744E+00	4.264E-04	1.665E-01	1.422E+00	1.248E-03	3.012E-10		7.141E-06	1.005E-08
4.831E+00	3.836E-01	8.856E-02	1.744E+00	3.852E-04	1.726E-01	1.533E+00	1.223E-03	2.858E-10		7.141E-06	9.838E-09
4.831E+00	3.836E-01	8.856E-02	1.744E+00	3.852E-04	1.726E-01	1.533E+00	1.223E-03	2.858E-10		7.141E-06	9.838E-09
4.972E+00	3.785E-01	9.097E-02	1.744E+00	3.695E-04	1.764E-01	1.601E+00	1.207E-03	2.776E-10		7.141E-06	9.757E-09
5.640E+00	3.633E-01	1.024E-01	1.744E+00	3.115E-04	1.935E-01	1.908E+00	1.126E-03	2.418E-10		7.141E-06	9.380E-09
6.272E+00	3.609E-01	1.133E-01	1.744E+00	2.732E-04	2.090E-01	2.184E+00	1.047E-03	2.120E-10		7.141E-06	9.012E-09
6.873E+00	3.672E-01	1.241E-01	1.744E+00	2.456E-04	2.235E-01	2.434E+00	9.740E-04	1.865E-10		7.141E-06	8.640E-09
6.959E+00	3.688E-01	1.257E-01	1.744E+00	2.422E-04	2.256E-01	2.469E+00	9.639E-04	1.831E-10		7.141E-06	8.586E-09
6.959E+00	3.688E-01	1.257E-01	1.744E+00	2.421E-04	2.256E-01	2.469E+00	9.639E-04	1.831E-10		7.141E-06	8.586E-09
6.966E+00	3.750E-01	1.252E-01	1.744E+00	2.365E-04	2.246E-01	2.457E+00	9.608E-04	1.813E-10		7.141E-06	8.607E-09
7.122E+00	5.039E-01	1.164E-01	1.744E+00	1.624E-04	2.067E-01	2.221E+00	8.989E-04	1.500E-10		7.141E-06	9.051E-09
7.362E+00	6.633E-01	1.074E-01	1.744E+00	1.192E-04	1.880E-01	1.961E+00	8.244E-04	1.201E-10		7.141E-06	9.608E-09
7.639E+00	8.178E-01	9.989E-02	1.744E+00	9.531E-05	1.728E-01	1.733E+00	7.540E-04	9.712E-11		7.141E-06	1.017E-08
7.641E+00	8.167E-01	9.974E-02	1.744E+00	9.488E-05	1.726E-01	1.730E+00	7.526E-04	9.669E-11		7.141E-06	1.017E-08
7.770E+00	7.578E-01	9.187E-02	1.744E+00	7.542E-05	1.617E-01	1.571E+00	6.744E-04	7.532E-11		7.141E-06	1.062E-08
7.943E+00	7.139E-01	8.514E-02	1.744E+00	6.279E-05	1.523E-01	1.423E+00	6.030E-04	5.882E-11		7.141E-06	1.108E-08
8.156E+00	6.834E-01	7.936E-02	1.744E+00	5.389E-05	1.445E-01	1.284E+00	5.383E-04	4.600E-11		7.141E-06	1.155E-08
8.407E+00	6.652E-01	7.439E-02	1.744E+00	4.726E-05	1.382E-01	1.153E+00	4.799E-04	3.595E-11		7.141E-06	1.202E-08
8.697E+00	6.593E-01	7.015E-02	1.744E+00	4.210E-05	1.334E-01	1.030E+00	4.273E-04	2.803E-11		7.141E-06	1.249E-08
8.994E+00	6.654E-01	6.688E-02	1.744E+00	3.832E-05	1.303E-01	9.252E-01	3.844E-04	2.230E-11		7.141E-06	1.289E-08
9.029E+00	6.805E-01	6.722E-02	1.744E+00	3.725E-05	1.313E-01	9.178E-01	3.757E-04	2.153E-11		7.141E-06	1.285E-08
9.447E+00	8.693E-01	7.089E-02	1.744E+00	2.891E-05	1.413E-01	8.270E-01	2.957E-04	1.475E-11		7.141E-06	1.248E-08
1.004E+01	1.142E+00	7.456E-02	1.744E+00	2.388E-05	1.514E-01	7.066E-01	2.328E-04	9.918E-12		7.141E-06	1.219E-08
1.095E+01	1.567E+00	7.789E-02	1.744E+00	2.094E-05	1.610E-01	5.530E-01	1.870E-04	6.542E-12		7.141E-06	1.213E-08
1.195E+01	2.026E+00	7.979E-02	1.744E+00	2.009E-05	1.674E-01	4.264E-01	1.675E-04	4.863E-12		7.141E-06	1.236E-08
1.199E+01	2.045E+00	7.984E-02	1.744E+00	2.008E-05	1.677E-01	4.220E-01	1.670E-04	4.815E-12		7.141E-06	1.237E-08
1.201E+01	2.055E+00	7.987E-02	1.744E+00	2.008E-05	1.678E-01	4.196E-01	1.668E-04	4.789E-12		7.141E-06	1.238E-08
1.202E+01	2.061E+00	7.989E-02	1.744E+00	2.008E-05	1.679E-01	4.181E-01	1.667E-04	4.774E-12		7.141E-06	1.239E-08
1.203E+01	2.066E+00	7.990E-02	1.744E+00	2.008E-05	1.679E-01	4.170E-01	1.666E-04	4.763E-12		7.141E-06	1.239E-08
1.204E+01	2.068E+00	7.991E-02	1.744E+00	2.008E-05	1.679E-01	4.165E-01	1.665E-04	4.757E-12		7.141E-06	1.239E-08
1.204E+01	2.071E+00	7.992E-02	1.744E+00	2.008E-05	1.680E-01	4.160E-01	1.665E-04	4.751E-12		7.141E-06	1.239E-08
1.205E+01	2.073E+00	7.993E-02	1.744E+00	2.008E-05	1.680E-01	4.154E-01	1.664E-04	4.745E-12		7.141E-06	1.240E-08
1.205E+01	2.076E+00	7.993E-02	1.744E+00	2.008E-05	1.680E-01	4.147E-01	1.664E-04	4.739E-12		7.141E-06	1.240E-08
1.206E+01	2.076E+00	7.993E-02	1.744E+00	2.008E-05	1.680E-01	4.147E-01	1.664E-04	4.738E-12		7.141E-06	1.240E-08

Table II-1. Example IDPS Model Evaporation Lookup Table for Average In Situ J-13 Well Water (Continued)

HSiO3-	Ca++	Mg++	MgHCO3+	MgOH+	HSO4-	Mineral Precipitation log react. progr.	H2O (kg)	Antigorite(am)	Calcite	Celadonite
						11/8/2006 User: Sara Arthur EQ3/6,				
HSiO3- Molality	Ca++ Molality	Mg++ Molality	MgHCO3+ Molality	MgOH+ Molality	HSO4- Molality	log Xi - j13c3t7e.6o	Mass Solvent (kg) - j13c3t7e.6o	Antigorite(am) Moles	Calcite Moles	Celadonite Moles
9.361E-05	8.418E-05	6.167E-05	1.096E-06	5.531E-07	3.328E-10	-99999	1	5.5753E-06	0.00023117	1.0377E-06
9.435E-05	8.373E-05	6.115E-05	1.089E-06	5.498E-07	3.337E-10	-0.4987	0.99429	5.8772E-06	0.00023215	1.0377E-06
1.069E-04	7.684E-05	5.341E-05	9.898E-07	4.997E-07	3.464E-10	0.69897	0.90993	1.0106E-05	0.00024627	1.0377E-06
1.244E-04	6.890E-05	4.516E-05	8.804E-07	4.445E-07	3.601E-10	1	0.81985	1.4124E-05	0.00026055	1.0377E-06
1.484E-04	6.045E-05	3.708E-05	7.683E-07	3.878E-07	3.737E-10	1.17609	0.72978	1.7592E-05	0.00027377	1.0377E-06
1.823E-04	5.163E-05	2.937E-05	6.547E-07	3.305E-07	3.870E-10	1.30103	0.6397	2.0482E-05	0.00028572	1.0377E-06
2.327E-04	4.265E-05	2.224E-05	5.417E-07	2.734E-07	3.999E-10	1.39794	0.54962	2.2787E-05	0.00029617	1.0377E-06
3.119E-04	3.378E-05	1.592E-05	4.314E-07	2.177E-07	4.125E-10	1.47712	0.45955	2.4525E-05	0.00030494	1.0377E-06
4.469E-04	2.535E-05	1.057E-05	3.266E-07	1.647E-07	4.253E-10	1.54407	0.36947	2.5746E-05	0.00031193	1.0377E-06
7.057E-04	1.769E-05	6.329E-06	2.298E-07	1.159E-07	4.403E-10	1.60206	0.2794	2.6527E-05	0.00031716	1.0377E-06
1.311E-03	1.107E-05	3.226E-06	1.438E-07	7.242E-08	4.623E-10	1.65321	0.18932	2.6964E-05	0.00032078	1.0377E-06
1.856E-03	8.623E-06	2.242E-06	1.110E-07	5.590E-08	4.768E-10	1.67327	0.151	2.7071E-05	0.00032189	1.0377E-06
1.898E-03	8.330E-06	2.167E-06	1.090E-07	5.484E-08	4.767E-10	1.6752	0.14721	2.7079E-05	0.00032199	1.0377E-06
2.678E-03	5.023E-06	1.315E-06	8.210E-08	4.126E-08	4.763E-10	1.69897	0.099244	2.7154E-05	0.00032311	1.0377E-06
1.459E-02	1.202E-06	3.070E-07	2.991E-08	1.463E-08	6.119E-10	1.74036	0.0091726	2.7218E-05	0.00032429	1.0377E-06
2.972E-02	1.865E-06	4.433E-07	2.952E-08	1.406E-08	8.052E-10	1.74329	0.0024693	0.00002722	0.00032435	1.0377E-06
4.338E-02	3.156E-06	7.006E-07	3.379E-08	1.606E-08	9.313E-10	1.74386	0.0011589	0.00002722	0.00032436	1.0377E-06
4.879E-02	3.712E-06	7.999E-07	3.554E-08	1.696E-08	9.658E-10	1.74397	0.00091985	0.00002722	0.00032433	1.0377E-06
5.301E-02	4.071E-06	8.573E-07	3.659E-08	1.753E-08	9.827E-10	1.74402	0.00079244	0.00002722	0.0003197	1.0377E-06
5.432E-02	4.173E-06	8.722E-07	3.688E-08	1.770E-08	9.871E-10	1.74404	0.00075922	0.00002722	0.00031845	1.0377E-06
6.432E-02	4.751E-06	9.388E-07	3.862E-08	1.879E-08	1.008E-09	1.74412	0.0005719	0.00002722	0.00031108	1.0377E-06
7.374E-02	4.962E-06	9.304E-07	3.940E-08	1.944E-08	1.008E-09	1.74416	0.00046504	0.00002722	0.00030671	1.0377E-06
7.845E-02	4.966E-06	9.074E-07	3.953E-08	1.965E-08	1.002E-09	1.74418	0.00042637	0.00002722	0.00030518	1.0377E-06
7.845E-02	4.966E-06	9.074E-07	3.953E-08	1.965E-08	1.002E-09	1.74418	0.00042636	0.00002722	0.00030518	1.0377E-06
8.160E-02	4.946E-06	9.111E-07	3.886E-08	1.936E-08	8.105E-10	1.7442	0.00038516	0.00002722	0.00032436	1.0377E-06
8.160E-02	4.946E-06	9.111E-07	3.886E-08	1.936E-08	8.105E-10	1.7442	0.00038516	0.00002722	0.00032436	1.0377E-06
8.392E-02	4.914E-06	9.006E-07	3.866E-08	1.931E-08	7.712E-10	1.74421	0.00036946	0.00002722	0.00032436	1.0377E-06
9.480E-02	4.687E-06	8.385E-07	3.774E-08	1.913E-08	6.305E-10	1.74423	0.00031153	0.00002722	0.00032436	1.0377E-06
1.052E-01	4.380E-06	7.651E-07	3.683E-08	1.894E-08	5.443E-10	1.74425	0.00027318	0.00002722	0.00032436	1.0377E-06
1.155E-01	4.032E-06	6.876E-07	3.588E-08	1.872E-08	4.873E-10	1.74426	0.00024562	0.00002722	0.00032436	1.0377E-06
1.170E-01	3.979E-06	6.761E-07	3.574E-08	1.869E-08	4.806E-10	1.74426	0.00024215	0.00002722	0.00032436	1.0377E-06
1.170E-01	3.979E-06	6.761E-07	3.574E-08	1.869E-08	4.806E-10	1.74426	0.00024214	0.00002722	0.00032436	1.0377E-06
1.166E-01	3.900E-06	6.602E-07	3.585E-08	1.876E-08	4.890E-10	1.74426	0.0002365	0.00002722	0.00032436	1.0377E-06
1.089E-01	2.667E-06	4.162E-07	3.821E-08	2.043E-08	6.594E-10	1.7443	0.00016239	0.00002722	0.00032437	1.0377E-06
1.009E-01	1.771E-06	2.489E-07	4.126E-08	2.274E-08	8.594E-10	1.74431	0.00011921	0.00002722	0.00032437	1.0377E-06
9.420E-02	1.241E-06	1.568E-07	4.440E-08	2.532E-08	1.035E-09	1.74433	9.53105E-05	0.00002722	0.00032437	1.0377E-06
9.407E-02	1.233E-06	1.556E-07	4.444E-08	2.537E-08	1.033E-09	1.74433	9.48751E-05	0.00002722	0.00032437	1.0377E-06
8.700E-02	8.455E-07	1.013E-07	4.722E-08	2.804E-08	9.415E-10	1.74433	7.54219E-05	0.00002722	0.00032437	1.0377E-06
8.090E-02	5.955E-07	6.693E-08	5.018E-08	3.114E-08	8.595E-10	1.74434	6.27903E-05	0.00002722	0.00032437	1.0377E-06
7.565E-02	4.296E-07	4.483E-08	5.331E-08	3.475E-08	7.863E-10	1.74434	5.38945E-05	0.00002722	0.00032437	1.0377E-06
7.112E-02	3.164E-07	3.034E-08	5.657E-08	3.893E-08	7.211E-10	1.74435	4.72594E-05	0.00002722	0.00032437	1.0377E-06
6.724E-02	2.373E-07	2.069E-08	5.994E-08	4.380E-08	6.630E-10	1.74435	4.21028E-05	0.00002722	0.00032437	1.0377E-06
6.424E-02	1.856E-07	1.470E-08	6.303E-08	4.886E-08	6.162E-10	1.74435	3.83153E-05	0.00002722	0.00032437	1.0377E-06
6.463E-02	1.781E-07	1.377E-08	6.297E-08	4.914E-08	6.186E-10	1.74435	3.72455E-05	0.00002722	0.00032437	1.0377E-06
6.874E-02	1.164E-07	6.821E-09	6.242E-08	5.216E-08	6.400E-10	1.74435	2.89132E-05	0.00002722	0.00032437	1.0377E-06
7.275E-02	7.802E-08	3.299E-09	6.234E-08	5.602E-08	6.508E-10	1.74436	2.38767E-05	0.00002722	0.00032437	1.0377E-06
7.628E-02	5.707E-08	1.624E-09	6.345E-08	6.208E-08	6.408E-10	1.74436	2.09389E-05	0.00002722	0.00032437	1.0377E-06
7.817E-02	5.212E-08	1.058E-09	6.561E-08	6.908E-08	6.140E-10	1.74436	2.00916E-05	0.00002722	0.00032437	1.0377E-06
7.823E-02	5.212E-08	1.045E-09	6.572E-08	6.938E-08	6.128E-10	1.74436	2.00849E-05	0.00002722	0.00032437	1.0377E-06
7.825E-02	5.212E-08	1.039E-09	6.577E-08	6.954E-08	6.121E-10	1.74436	0.000020082	0.00002722	0.00032437	1.0377E-06
7.827E-02	5.213E-08	1.034E-09	6.581E-08	6.964E-08	6.117E-10	1.74436	2.00804E-05	0.00002722	0.00032437	1.0377E-06
7.828E-02	5.213E-08	1.031E-09	6.583E-08	6.971E-08	6.114E-10	1.74436	2.00794E-05	0.00002722	0.00032437	1.0377E-06
7.829E-02	5.214E-08	1.030E-09	6.584E-08	6.974E-08	6.112E-10	1.74436	0.000020079	0.00002722	0.00032437	1.0377E-06
7.830E-02	5.214E-08	1.028E-09	6.586E-08	6.978E-08	6.110E-10	1.74436	2.00785E-05	0.00002722	0.00032437	1.0377E-06
7.830E-02	5.214E-08	1.027E-09	6.587E-08	6.982E-08	6.109E-10	1.74436	2.00781E-05	0.00002722	0.00032437	1.0377E-06
7.831E-02	5.215E-08	1.025E-09	6.588E-08	6.987E-08	6.107E-10	1.74436	2.00776E-05	0.00002722	0.00032437	1.0377E-06
7.831E-02	5.215E-08	1.025E-09	6.589E-08	6.987E-08	6.107E-10	1.74436	2.00776E-05	0.00002722	0.00032437	1.0377E-06

Table II-1. Example IDPS Model Evaporation Lookup Table for Average In Situ J-13 Well Water (Continued)

Fluorite	Halite	Kogarkoite	Natrite	SiO2(am)	Thenardite
Fluorite Moles	Halite Moles	Kogarkoite Moles	Natrite Moles	SiO2(am) Moles	Thenardite Moles
				9.8665E-07	
				1.8674E-05	
				0.00024667	
				0.00078106	
				0.00087142	
				0.00090035	
2.8227E-08				0.00090679	
4.6617E-06				0.00091022	
5.9118E-06				0.00091113	
1.3277E-05				0.00091637	
1.7656E-05				0.0009193	
1.9184E-05		1.1821E-07		0.00092029	
1.9181E-05		1.2469E-07		0.00092029	
1.0664E-13		4.3784E-05		0.00092254	
		4.3784E-05		0.00092254	
		5.1694E-05		0.00092304	
		7.8348E-05		0.00092476	
		0.00009295		0.0009257	
		0.00010134		0.00092617	
		0.00010225	1.5353E-07	0.00092622	
		0.00010225	1.6242E-07	0.00092622	
		0.00010286	0.00001811	0.00092704	
		0.00010972	0.00025324	0.00093774	
		0.00011246	0.00038858	0.00094385	
		0.00011351	0.00046173	0.00094713	8.1808E-08
		0.00011352	0.00046283	0.00094719	5.4138E-07
		0.00011389	0.00051174	0.00094972	2.0498E-05
		0.00011412	0.00054295	0.0009513	3.2594E-05
		0.00011427	0.00056448	0.00095237	0.00004044
		0.00011437	0.00058015	0.00095313	0.00004573
		0.00011445	0.000592	0.0009537	4.9334E-05
	1.0258E-07	0.0001145	0.00060044	0.00095409	5.1544E-05
	5.4504E-06	0.00011451	0.00060178	0.00095414	5.1683E-05
	0.00004631	0.00011458	0.00061267	0.0009546	5.1823E-05
	0.00006926	0.00011462	0.00062007	0.00095487	4.9641E-05
	0.00007965	0.00011465	0.00062555	0.00095502	4.4088E-05
	7.8677E-05	0.00011466	0.00062858	0.00095505	3.6181E-05
	7.8487E-05	0.00011466	0.00062867	0.00095504	3.5813E-05
	7.8381E-05	0.00011466	0.00062872	0.00095504	3.5614E-05
	7.8314E-05	0.00011466	0.00062875	0.00095504	0.00003549
	7.8264E-05	0.00011466	0.00062877	0.00095504	0.0000354
	7.8239E-05	0.00011466	0.00062878	0.00095504	3.5355E-05
	7.8213E-05	0.00011466	0.00062879	0.00095504	3.5308E-05
	7.8185E-05	0.00011466	0.0006288	0.00095504	3.5257E-05
	7.8155E-05	0.00011466	0.00062882	0.00095504	3.5202E-05
	7.8151E-05	0.00011466	0.00062882	0.00095504	3.5197E-05

INTENTIONALLY LEFT BLANK

APPENDIX III

INDEPENDENT TECHNICAL REVIEW

An independent technical review by David Sassani (SNL) was performed in accordance with SCI-PRO-006, Attachment 4, as a model validation method per *Technical Work Plan for: Revision of Model Reports for Near-Field and In-Drift Water Chemistry* (SNL 2007 [DIRS 179287]). The group manager for the Near-Field Environment (NFE) team (Geoff Freeze) directed the review, as part of the NFE manager's determination regarding the adequacy of model validation. The reviewer was selected by the NFE manager, and is independent of the development, checking, and review of the IDPS model documentation, including documents providing inputs to the IDPS model.

The review criteria were specified by the NFE manager and included the following:

- The technical approach described in the IDPS model report captures all physical and chemical processes that are significant to the intended use of the model for representing in-drift water chemistry.

- Modeling assumptions are clearly defined and justified as appropriate for the intended use of the model.

- Uncertainties in model parameters, process representation, and assumptions are sufficiently described, and impacts of these uncertainties on model confidence and model output, as appropriate for the intended use of the model, are adequately discussed. The overall technical credibility of the approach, including assumptions, parameters, equations, and numerical implementation, is appropriate for the intended use of the model.

A facsimile of the independent technical review letter addressing these criteria is attached below.

Sandia National Laboratories

Operated for the U.S. Department of Energy by
Sandia Corporation

Albuquerque, New Mexico 87185-

date: February 26, 2007

to: Geoffrey A. Freeze **QA/QA**

from: David Sassani 2/26/2007

subject: INDEPENDENT TECHNICAL REVIEW FOR MODEL VALIDATION OF THE IN-DRIFT PRECIPITATES/SALTS MODEL

The purpose of this memo is to document my independent technical review of the *In-Drift Precipitates/Salts Model* (ANL-EBS-MD-000045 Rev 03C; i.e., the IDPS model) conducted using the criteria provided for the review within Section 2.2.2.4 of *Technical Work Plan for: Revision of Model Reports for Near-Field and In-Drift Water Chemistry* (TWP-MGR-PA-000038 Revision 02; i.e., the TWP) and following the instructions given in Attachment 4 of procedure SCI-PRO-006 Revision 1. As indicated in the Attachment 4 and in the TWP, the goal of this review is to assess whether the model as developed is appropriate for its intended use. In this manner, this independent technical review provides input to the Manager of the work being evaluated so that the Manager may make a determination on the adequacy of model validation. Based on my evaluation of the IDPS model approach and implementation, I find that the conceptual aspects of the system are well covered, the geochemical system is comprehensively represented, and assumptions are appropriately justified. The representation of uncertainty is generally appropriate for the intended use of the model, but some potential for improvement in that area is possible as a means to eliminate potentially unrealistic water compositions to result from application of the uncertainty as constrained. It is my conclusion that the IDPS model is appropriate for its intended use.

Purpose/Intended Use of the IDPS model

The purpose/intended use of the IDPS model is given in the TWP (Sec. 2.1.1) as

> *The IDPS report develops the thermodynamic model for evaluating the evaporative evolution of water chemistry in the emplacement drifts, including validation and evaluation of uncertainties. The revised IDPS model will be implemented to generate the results used to construct the abstraction models described in Revision 06 of the P&CE report (see below) to represent the composition of in-drift waters and chemical conditions on the waste package surface, for TSPA.*

This is further elaborated upon in the TWP (Sec. 2.1.2.2)

> *The IDPS model is a geochemical model designed to predict the postclosure effects of evaporation and deliquescence on the chemical composition of water within the EBS in support of TSPA. The model is developed and validated in the IDPS report and is applied in the P&CE report (Section 2.1.2.3).*

Exceptional Service in the National Interest

07_365_YMP-LL_02-26-2007

Geoffrey A. Freeze - 2 - February 26, 2007

The intended use of the model is to estimate and tabulate, within an appropriate level of confidence, the effects of evaporation, deliquescence, and potential environmental conditions on the pH, ionic strength, and chemical compositions of water and minerals on the drip shield or other location within the drift during the postclosure period. The IDPS model is independent of the length of the postclosure period considered, and requires no modifications for extension to peak dose time intervals.

The intended use of the IDPS model is reasonably straightforward in terms of the geochemical phenomena being represented. It is especially central that it is intended to be used to generate abstraction models for evaluating postclosure conditions within the TSPA, this latter being a stochastic analysis of potential future performance that is focused on capturing the range of possible behavior with explicit representation of uncertainty. This usage is distinct from application of a complex geochemical model to make a deterministic prediction (i.e., to find the single most accurate outcome) of the future evolution of an individual specific spatial point in a system. As such, the IDPS model would be appropriate for its intended use as long as it captures the major conceptual behaviors of the geochemical system, as well as having appropriate representation of the possible range of behavior given consideration of the uncertainties within the model itself.

Within the approach of the IDPS model development, the TWP provides the specific portions undergoing change regarding this current revision (Sec. 2.1.2.2)

The first task for this revision is to evaluate the effects of the revised Pitzer database on IDPS model predictions, validation, and uncertainty. Each model validation simulation in the IDPS report will be rerun using the revised Pitzer database. Differences between model predictions and experimental data will be plotted, tabulated, and analyzed in the same or similar manner as Revision 02. Corrections to experimental evaporation data, where justifiable, will be made prior to model simulations. For example, it can be shown that reported concentration factors in studies by Rosenberg et al. (1999 [DIRS 125338]; 1999 [DIRS 125339]) are overestimated based on the concentration factors of nonreactive dissolved salts in solution. Instead of using the reported concentration factors, obtained from an inferior method of measurement, the concentration factors of the nonreactive dissolved salts will be used for comparisons of model predictions to experimental data. Justification for such treatment of data will be fully documented in the report. The Rosenberg et al. source documents are available from the TIC, and the data are available from the TDMS.

***Additional Validation Data**—New validation simulations will be performed to evaluate the ability of the IDPS model to predict aqueous concentrations and pH values observed in a new evaporation experiment performed at Lawrence Livermore National Laboratory and published by Alai et al. (2005 [DIRS 176811]). This source is available from the TIC, and the data are available from the TDMS. In addition, results of new simulations will be compared to additional solubility data found in the literature relevant to the IDPS model. Additional solubility data will include the solubility of carbon dioxide and calcite for temperatures between 25°C and 140°C. Differences between model predictions and experimental data will be plotted, tabulated, and analyzed in a similar manner as Revision 02. These results will be included in the overall model validation and*

07_365_YMP-LL_02-26-2007

uncertainty analyses. Validation will be assessed based on the criteria established in Section 2.2.2 of this TWP.

***Re-evaluation of Model Uncertainty Estimates**—Model uncertainties will be evaluated in a similar manner as in Revision 02. Additional evaluation will involve consideration of uncertainty correlation, covariance, and ratio of conservative components to better define and preserve the relationships between output parameters.*

It is clear from this description, and from the IDPS model itself, that the focus of this last revision has been strengthening the confidence by accounting for revisions in the fundamental thermochemical data being used, further assessing uncertainties in some data sets used to test the model, by adding some additional test cases that allow for some new evaluations of the model, and by more detailed consideration of the uncertainty in the model.

Level of Validation Required and Confidence Building Activities During and After Model Development

The TWP provides in Section 2.2.2.2 the following description of the Level of Validation Requirements, and the activities used within the IDPS model report to achieve this:

According to SCI-PRO-002 (Attachment 3) the criteria for Level II validation include listed criteria (1) through (6) during development, and two post-development model validation methods (as described in SCI-PRO-006, Section 6.3.2). Honoring the requirements defined in SCI-PRO-002, the following steps are adopted for building confidence into the models in the THC seepage report.

Confidence Building during Model Development

The development of the model will be documented addressing the following requirements:

• Selection of appropriate input parameters and/or input data, assumptions, simplifications, and physical principles, consistent with the intended use of the model, and discussion of how the selections build model confidence.

• Description of important future state (aleatory), parameter (epistemic), and alternative model uncertainties and how they are represented, commensurate with the intended use of the model.

• Demonstration that model predictions adequately represent the range of possible outcomes, consistent with important uncertainties and modeling assumptions, conceptualizations, and implementation.
• Documentation of steps taken to ensure that chosen simulation conditions span the range of intended use, and that such conditions avoid inconsistent results, or that any inconsistencies are adequately explained and demonstrated to have little impact on results.

07_365_YMP-LL_02-26-2007

> *Model confidence will be obtained by thorough discussion of model inputs including thermodynamic data, boundary conditions for chemical modeling (i.e., temperature, humidity, and gas chemistry), and the nature of chemical heterogeneity (i.e., presence of mineral precipitates) likely to exist in the repository emplacement drift environment.*

In Section 2.2.2.3, The TWP provides the specific direction to this independent technical reviewer regarding this during development model validation activity.

> *The independent technical review will ensure that these aspects are brought together into a technically complete and adequate presentation using appropriate data and with appropriate description of uncertainty.*

The discussion of inputs for this model is quite extensive both in its detail and in the compositional space that it covers. Section 4.1.1 of the IDPS model report covers an overview of the Pitzer database developed for the system Na-K-H-Mg-Ca-Al-Cl-F-NO_3-SO_4-Br-CO_3-SiO_2-CO_2-O_2-H_2O. This encompasses most of the elements that may play a dominant role in groundwater evolution. In addition the discussion indicates that the database is developed to be used up to 200°C, however it clearly provides the constraint that the IDPS model itself is only appropriate for usage up to 140°C. This latter limitation results primarily from divergence with available data at the higher temperature range for Cl-NO_3 solutions (as shown in Section 7 of the IDPS model report). Further work on solution data at these higher temperatures may allow an enhanced application range of this model.

In the IDPS model report, the database development discussion is provided in detail in Appendix I where the evaluations of the data sets used to construct this database are given. This has in general good description of the uncertainties in the data sets and how these affect the constructed Pitzer database. For example, Section I.5.4 on calcite solubility (see Figure I-8) examines the divergence between calculated equilibrium constants for calcite solubility with other direct data based on measurements from the literature. This magnitude of divergence is on the order of two tenths of a log unit (at 100-150°C) to two-thirds of a log unit (at 300°C). It is stated in the text that this may be related to limitations for the Pitzer data used for the Na-carbonate system. This provides an excellent level of detailed coverage of the source information and the level of mismatch that is covered is well within the tolerance of the intended use of the IDPS model. This is supported even more by the post-development validation corroborations provided within the document as discussed below.

The major assumptions are adequately justified within the IDPS model. In particular, the discussion regarding mineral suppression (Section 6.6.2.6) provides a rational, reasonably justified approach for the major exceptions taken to the equilibrium assumption, which is applied as would be expected to solid phases that may be possible to precipitate. Alternative conceptual models are covered in Section 6.5 and although the discussion of these is a bit on the light side, it appears to be sufficient given the extensive sets of post-development corroboration provided for the IDPS model. The boundary conditions are discussed in the context of the conceptual aspects of the model, but because the IDPS model report does not perform the actual post-closure analyses, the specific boundary conditions and the assurance that the analyses span the needed range are appropriately to be found in the downstream documentation where the analyses are executed.

Further in Section 2.2.2.2, the TWP provides the following description of the post-development activities used within the IDPS model report to build confidence:

Confidence Building after Model Development

After development, the IDPS model will achieve the required validation by the following methods:

- *Corroboration of model results with data acquired from the laboratory, field experiments, analog studies, or other relevant observations, not previously used to develop or calibrate the model (SCI-PRO-006, Section 6.3.2, 1st bullet).*

- *Corroboration of model results with relevant information published in refereed journals or literature (SCI-PRO-006, Section 6.3.2, 3rd bullet).*

- *Technical review, planned in this TWP (SCI-PRO-006, Section 6.3.2, 5th bullet).*

The first two bullets above are corroboration activities where model results are compared against data sets to evaluate how well the model is approximating what is known. The last of the three bullets above is this independent technical review itself. The version of the IDPS model report being reviewed here (rev. 03C) had not yet been fully updated to include this independent technical review in the list it contained in Section 7. Furthermore, that list in the IDPS model report contained an additional activity given as:

> *(2) SCI-PRO-006, Section 6.3.2, (2nd bullet), Corroboration of model results with other model results (alternative model) obtained from the implementation of other independent mathematical models developed for similar or comparable intended use/purpose.*

In Section 2.2.2.3, The TWP provides the specific direction to this independent technical reviewer regarding the post-development model validation activity. That section states that:

> *The independent technical review will ensure that these aspects are brought together into a technically complete and adequate presentation using appropriate data and with appropriate description of uncertainty.*

What follows here is a brief overview and assessment regarding the three above activities that represent the corroboration activities conducted post-development for the IDPS model. It should be stated directly that the detailed comparisons made to a variety of data sets using this model represent a very persuasive set of evidence to this reviewer. This stems from primarily that the comparisons span a wide compositional spectrum, cover about five orders of magnitude in concentration, allow direct evaluation of deliquescence relative humidity (RH) down to 40%, and go to temperatures well above the stated limitation (140°C) for the model itself. The last two limitations are set by the most constraining portions of the system, within the nitrate-chloride system that is central to evaluation of brines at the Yucca Mountain site. That there are 100 figures representing these comparisons speaks to the high level of effort put into determining confidence in the IDPS model. The corroborative agreement being sought for dissolved concentrations is within about 1 order of magnitude in general (or 1 pH unit), except in the case of some alkaline earth cations (e.g., Ca^{+2}) in the evaporation experiments. For the deliquescence RH (DRH), an absolute 10% RH is used as the criterion. Both phase solubility and deliquescence RH are evaluated using the IDPS model.

07_365_YMP-LL_02-26-2007

Section 7.1.1 of the IDPS model report evaluates corroborating data for binary salt systems. Figs 7.1 and 7.2 demonstrate good agreement with handbook data for salts solubilities at low and high temperatures with concentrations ranging from about 0.0002 molal to ~30 molal. Table 7-4 provides the comparison of calculated DRH with handbook values, all of which are within the criterion. Figures 7-3 through 7-24 provide corroborations for solubility and DRH for binary salts from literature sources other than handbooks. As stated in the IDPS model report, solubility is generally within a factor of 2 and DRH generally within 5%. There are some exceptions to this and there are cases where the approach does not necessarily result in an actual solubility limit being reached (generally for salts that have DRH <60%). The discussion of how these issues are handled indicates that the value at the lowest DRH is taken as a proxy for solubility which appears to be a reasonable approach based on examining the figures. It is pointed out that the comparisons are always within the factor of 10 for solubility. The DRH is off at higher temperatures particularly for K-nitrate and Mg-nitrate systems (see Figs 7-22 and 7-24, respectively).

Section 7.1.2 covers similar corroborations for ternary salt systems as shown in Figures 7-25 through 7-53. Although the agreement here is slightly less tight than for the binary salts, it is still generally within the level needed. Some larger divergences occur at the higher temperatures (for Na-K-Nitrate in Fig. 7-26 and for Na-Ca-nitrate in Fig. 7-40) or at higher concentrations (like for Na-Cl-nitrate in Fig. 7-29). The system Mg-Cl-nitrate appears to have large discrepancies that are noted in the report, but the estimated values of solubility are always within the needed validation factor. Given the intended usage of the IDPS model, these corroborations provide strong confidence in the model.
Section 7.1.3 covers corroboration of the IDPS model to calcite solubility data to evaluate the connection between this major carbonate mineral and the evaluation of CO_2 gas interaction with minerals and the aqueous solution (i.e., pH effects). Comparison with handbook data on CO_2 gas solubility shows excellent agreement. Figures 7-55 through 7-65 provide corroboration of calcite solubility in a number of different brine compositions and up to higher temperature (~100°C) that demonstrate the model is well within the criteria for validation.

Section 7.2 covers corroboration with empirical data for evaporation of three different water compositions, average J-13 well water (Figs. 7-66 through 7-72), Topopah Spring Tuff pore water (Figs. 7-73 through 7-92), and Inagua Seawater (Figs. 7-93 through 7-96). In general these corroborations show good agreement, well within the criteria, over large degrees of evaporation. The largest discrepancies are for Ca and Mg at low concentrations for some of the J-13 type results (e.g., see Fig. 6-68) and this drives the need for a 2 order of magnitude band for those elements. However, it should be noted that this large relative uncertainty at low concentration almost surely would not apply to high concentrations where other physical-chemical principles would work to limit uncertainties, especially on the high concentration side. Because these empirical studies are actually capturing the evaporative process, these corroborations provide very strong confidence that the IDPS model is representing those within the needed level of efficacy.

Section 7.3 provides corroboration of the IDPS model by comparing results at lower ionic strength (<1 molal) with results using a different solution model that has a different mathematical implementation. The comparisons using the IDPS model to those model results using an ion association model for dissolved species show good agreement in the Figs. 7-97 through 7-100 and provide additional support that the IDPS model is properly representing the processes.

07_365_YMP-LL_02-26-2007

Section 7.5 provides a thorough overview of the validation activities as they relate to the various output parameters of the IDPS model (pH, ionic strength, Cl^-, F^-, NO_3^-, Cl^-/NO_3^- ratio, DRH). In addition, a discussion of the uncertainties provides the basis for quantification is provided that is adequate. The one place that I could suggest for improvement would be the application of uncertainties. These are given for each output within Table 7-10 as functions of the RH range (as proxy for ionic strength). However, there is no explicit temperature dependence to the uncertainty, which is definitely seen within the corroborations. Because the RH is a property that convolves the temperature this may not be too significant of an issue. However, the uncertainties are given as constant relative uncertainties that can lead to unrealistic results being generated for conditions that are in the high concentration range. Some consideration should be given to having uncertainty bands that may represent large absolute uncertainties but realistic ones (in the relative sense) at high concentrations, particularly with smaller relative uncertainties on the high concentration side of the estimates.

Evaluation of the IDPS Model against the MV ITR Criteria

The TWP states that (Section 2.2.2.4):

> *The independent technical review will be performed in accordance with SCI-PRO-006, Attachment 4. The group manager for the NFE team will direct the review, as part of the manager's determination regarding the adequacy of model validation. The reviewer will be selected by the NFE manager, and will be independent of the development, checking, and review of the IDPS model documentation, including documents providing inputs to the IDPS model. The NFE manager will provide the subject matter expertise and qualifications for the reviewer and establish selection criteria to ensure that the review addresses the important elements of the model. Documentation of the selection of the reviewers shall be included as an appendix to the IDPS model report. The review criteria will be specified by the NFE manager, and will include the following as a minimum:*
>
> *•The technical approach described in the IDPS model report captures all physical and chemical processes that are significant to the intended use of the model for representing in-drift water chemistry.*
>
> *• Modeling assumptions are clearly defined and justified as appropriate for the intended use of the model.*
>
> *• Uncertainties in model parameters, process representation, and assumptions are sufficiently described, and impacts of these uncertainties on model confidence and model output, as appropriate for the intended use of the model, are adequately discussed.*
>
> *• The overall technical credibility of the approach, including assumptions, parameters, equations, and numerical implementation, is appropriate for the intended use of the model.*

As discussed above in detail, the IDPS model has abundant validation activities demonstrating its usefulness for estimating water compositions within systems that are heated where water is evaporating, or conversely in cooling systems where salts would be deliquescing to form brines. The mathematical description of the model is straightforward (the Pitzer parameter for activity coefficients is more

complex than the description of evaporation and species concentration) and its implementation in the EQ3/6 code package is entirely appropriate. The conceptual aspects of the system are well covered, the geochemical system is comprehensively represented, and assumptions are appropriately justified. The representation of uncertainty is generally appropriate for the intended use of the model, but some potential for improvement in that area is possible as a means to eliminate potentially unrealistic water compositions to result from application of the uncertainty as constrained. It is my conclusion that the IDPS model is appropriate for its intended use.

07_365_YMP-LL_02-26-2007

INTENTIONALLY LEFT BLANK